TECHNISCHE UNIVERSITÄT MÜNCHEN

Fakultät für Chemie

WACKER-Lehrstuhl für Makromolekulare Chemie

From C-H Bond Activation to Function: Diversification of Smart Materials Generated via Rare Earth Metal-Mediated Group Transfer Polymerization

Andreas Friedrich Josef Schaffer

Vollständiger Abdruck der von der Fakultät für Chemie der Technischen Universität München zur Erlangung des akademischen Grades eines

Doktors der Naturwissenschaften

genehmigten Dissertation.

Vorsitzender:	Prof. Dr.-Ing. Kai-Olaf Martin Hinrichsen
Prüfer der Dissertation:	1. Prof. Dr. Dr. h.c. Bernhard Rieger
	2. apl. Prof. Dr. Wolfgang Eisenreich
	3. Prof. Dr. Ralf Huss

Die Dissertation wurde am 25.01.2021 bei der Technischen Universität München eingereicht und durch die Fakultät für Chemie am 12.04.2021 angenommen.

„Somehow, I thought it would be really nice…

…but it was really bad.“

Lucas Stieglitz‘ indirekte Zusammenfassung
des Laboralltags eines Chemikers.
Aber: Niemals aufgeben! Das wird schon!

Die vorliegende Arbeit wurde in der Zeit von Oktober 2017 bis Dezember 2020 am WACKER-Lehrstuhl für Makromolekulare Chemie, Technische Universität München, unter Betreuung von Herrn Prof. Dr. Dr. h.c. Bernhard Rieger angefertigt.

Acknowledgements

Ein bisschen mehr als drei Jahre sind nun vergangenen, seitdem ich meine Promotion gestartet habe. Und auf einmal ist der Zeitpunkt da, an dem die Promotion mehr oder weniger plötzlich vorbei ist. In diesem Zeitraum trifft man auf eine Menge Leute, die einem auf seinem Weg mal länger, mal kürzer begleiten.

In diesem Sinne gebührt Ihnen, Professor Rieger, zuerst mein Dank, weil Sie mir dir Chance und ihr Vertrauen geschenkt haben, an ihrem Lehrstuhl meine Promotion durchführen zu können. Als Chef waren Sie stets ein starker Unterstützer, wenn es mal nicht so lief und konnten immer mit neuen Impulsen aufwarten. Gleichzeitig geben Sie ihren Leuten ein großes Maß an Freiheit, um eigene Ideen zu verfolgen. Gerade dies erlaubte es mir, mich fachlich wie persönlich stark zu entwickeln.

Carsten möchte in seiner Funktion als „Gute Seele des Lehrstuhls“ danken, da du für die alltäglichen Schwierigkeiten immer ein offenes Ohr hattest und man dich immer mit technischen Problemen behelligen konnte. Wir können uns glücklich schätzen, dass wir dank dir einen wirklich gut organisierten Lehrstuhl haben. Man schaue bloß auf die Getränkeliste (und Bestellungen, Geräte, Grillen, IT, etc.). In der Hinsicht auch vielen Dank für die mehr als faire Kaffee-Flat! 😊 Werde ich sehr vermissen! In dem Zusammenhang muss natürlich auch Sergei erwähnt werden: Dich konnte man genauso wegen jedem Problemchen ansprechen. Aber insbesondere was dein chemisches Wissen angeht, macht dir niemand etwas vor. Bei jeder Angelegenheit kannst du eine valide Aussage treffen oder neue Ideen einbringen. Danke! Zu guter Letzt darf Frau Bauer nicht vergessen werden! Gefühlt bei jedem bürokratischen Problem wussten Sie wie es gelöst wird, egal ob es um Reisekosten, Verträge oder Termine ging. Sie mach(t)en uns das Doktorandenleben damit sehr viel einfacher und wahrscheinlich auch um einiges stressfreier. Danke dafür!

Darüber hinaus möchte ich allen ehemaligen wie auch aktuellen Lehrstuhlkollegen und -freunden für die tolle gemeinsame Zeit danken. Ein bisschen war das Promovieren für mich wie zur Schule zu gehen, da ich hier jeden Tag Freunde treffen konnte.

Hier möchte ich erst mal Christina, hervorheben, da du mir mit der Masterarbeit bei dir den Weg in den Lehrstuhl geebnet hast. Außerdem habe ich mir von dir Einiges abgeschaut– gerade dein Denken („Wie würde Christina das jetzt machen?“ 😉). Mit Christina habt ihr – Kerstin (Meine Nachfolgerin! Deine Süßigkeitenkiste war sehr fein! 😊), Alina, Marina, Chris, Erwin (leider im Silicium-Institut verschollen), Basti, Markus, Sophia, Rike, Martin (Waren leider nur drei Monate dann noch. Deine alte Line ist immer noch top!), Lucas, Jonas, Asad, Philipp, Toni (Waren leider auch nur ein paar Wochen), Jakob (Trainier weiter Junge!) und Marius – in der Makro-Nord immer für eine sehr entspannte und witzige Laboratmosphäre gesorgt. 😊 Dazu möchte ich noch allen danken, die mich in chemischen Diskussionen (z.B. Moritz, etc.), beim Korrekturlesen (z.B. Moritz, Jonas, Chris, Alina, etc.) und mir damit beim erfolgreichen Publizieren unterstützt haben!

Mit euch (eigentlich allen) konnte man immer eine gute Zeit haben, sei’s in den (Kaffee)pausen, beim Grillen, Feiern und auch so privat. Schade, dass 2020 so von Corona verhagelt wurde…

Einen weiteren Dank möchte ich noch all meinen Studenten aussprechen. Ihr alle, also Simone (Du hast sogar Bachelorarbeit und Forschungspraktikum bei mir durchgezogen!), Laura, Amelie, Theresa, Eva, Dario und Fabio, wart wirklich zuverlässig und habt mich toll unterstützt. Einiges von euren Daten konnte ich auch in einigen Papern

unterbringen! Also war eure Zeit hier nicht ganz umsonst. Außerdem hoffe ich, dass ich euch ein bisschen was mitgeben konnte und ihr was gelernt habt bei mir!

Zum Schluss noch meine Familie: Mama, Papa und Thomas: Chemie ist jetzt nicht eure größte Stärke, aber das ist auch gar nicht wichtig. Wichtig ist, und dafür bin ich euch dankbar, dass ich mich bis zum heutigen Tag auf euch verlassen konnte und ihr mich auf meinem Weg immer unterstützt habt. Auch jetzt immer noch während der Promotion. Das ist nicht selbstverständlich! Aber es ist sehr beruhigend, dass immer jemand da ist, auf den man sich zurückfallen könnte, wenn nichts mehr geht. Schön, dass es euch gibt!!

List of Abbreviations

2VP	2-Vinylpyridine
Å	Angstrom; 10^{-10} m
AIBN	Azobis(isobutyronitrile)
ATRP	Atom-transfer radical polymerization
a.u.	Arbitrary unit
BYP	2-(But-3-yn-1-yloxy)-2-oxo-1,3,2-dioxaphospholane
CuAAC	Copper-catalyzed azide-alkyne click reaction
cat.	Catalyst
CMC	Critical micelle concentration
Cp	Cyclopentadienyl
Đ	Polydisperity index
DAVP	Dialkyl vinylphsophonate
DAlVP	Diallyl vinylphosphonate
DEEP	Diethyl ethylphosphonate
DEVP	Diethyl vinylphosphonate
DIVP	Diisopropyl vinylphosphonate
DMPA	2,2-Dimethoxy-2-phenylacetophenone
DMVP	Dimethyl vinylphosphonate
DPVP	Di-*n*-propyl vinylphosphonate
DNA	Deoxyribonucleic acid
DLS	Dynamic light scattering
DOSY	Diffusion Ordered Spectroscopy
DOX	Doxorubicin
DPE	1,1-Diphenylethylene
DSC	Dynamic scanning calorimetry
εCL	ε-Caprolactone
ESI-MS	Electrospray ionization mass spectrometry
equiv.	Equivalent
FCS	Fetal calf serum
FTIR	Fourier transform infrared
GPC	Gel permeation chromatography
Grubbs I catalyst	Benzylidene-bis(tricyclohexylphosphino)-dichlororuthenium
HeLa	Henrietta Lacks – breast cancer cell line
IE	Initiator efficiency
IPOx	2-Isoprenyl-2-oxazoline
it-PAMA	Isotactic poly(allyl methacrylate)
Karstedt's catalyst	$Pt_2[(Me_2SiCH{=}CH_2)_2O]_3$
LCST	Lower critical solution temperature

List of Abbreviations

LLA	L-lactic acid
MALS	Multi-angle light scattering
MCF-7	Michigan cancer foundation-7 – breast cancer cell line
MeCN	Acetonitrile
MFI	Mean fluorescence intensity
MMA	Methyl methacrylate
M_n	Number average molecular weight
n-BuLi	*n*-Butyllithium
NMR	Nuclear magnetic resonance
P2VP	Poly(2-vinylpyridine)
PA12	Polyamide-12
PBS	Phosphate-buffered saline
PDAVP	Poly(dialkyl vinylphosphonate)
PDEVP	Poly(diethyl vinylphosphonate)
PDIVP	Poly(diisopropyl vinylphosphonate)
PDMS	Poly(dimethylsiloxane)
PDMVP	Poly(dimethyl vinylphosphonate)
PεCL	Poly(ε-caprolactone)
PLLA	Poly(L-lactic acid)
PMMA	Poly(methyl methacrylate)
PPE	Polyphosphoester
ppm	parts per million
PS	Polystyrene
PVPA	Poly(vinylphosphonic acid)
REM-GTP	Rare earth metal-mediated group transfer polymerization
RNA	Ribonucleic acid
ROP	Ring-opening polymerization
SKA-GTP	Silyl ketene acetal-initiated group transfer polymerization
TBAF	Tetrabutylammonium fluoride
TBDMS	*tert*-Butyldimethylsilyl-
TEM	Transmission electron microscopy
THF	Tetrahydrofuran
TMPy	2,3,5,6-Tetramethylpyrazine
TMS	Trimethylsilyl- or tetramethylsilane
TMSBr	Trimethylsilyl bromide
TOF	Turnover frequency
Tol	Toluene
UV	Ultraviolet light
Vis	Visible light

Publication List

- A. Schaffer, M. Weger, B. Rieger*, *Eur. Polym. J.* **2020**, *122*, 109385 „From Lanthanide-mediated, High-Precision Group Transfer Polymerization of *Michael*-type Monomers, to Intelligent, Functional Materials.“
- A. Schaffer, M. Kränzlein, B. Rieger*, *Macromolecules* **2020**, *53*, 4345-4354. „Synthesis and Application of Functional Group-Bearing Pyridyl-Based Initiators in Rare Earth Metal-Mediated Group Transfer Polymerization.“
- A. Schaffer, M. Kränzlein, B. Rieger*, *Macromolecules* **2020**, *53*, 8382–8392 „Precise Synthesis of Poly(dimethylsiloxane) Copolymers through C-H Bond Activated Macroinitiators in the Yttrium-Mediated Group Transfer Polymerization and Ring-Opening Polymerization.“
- A. Saurwein,‡ A. Schaffer,‡ C. Wieser, B. Rieger*, *RSC Adv.* **2021**, *11*, 1586–1594. „ Synthesis, Characterisation and Functionalisation of BAB-based Dual-Responsive Nanocarriers for Targeted Drug Delivery: Evolution of Nanoparticles based on 2-Vinylpyridine and Diethyl Vinylphosphonate.“

Publications beyond the Scope of this Thesis

- C. Schwarzenböck, A. Schaffer, P. Pahl, P. J. Nelson, R. Huss, B. Rieger*, *Polym. Chem*. **2018**, *9*, 284-290, rewarded with cover page. „Precise Synthesis of Thermoresponsive Polyvinylphosphonate-Biomolecule Conjugates via Thiol-Ene Click Chemistry.“
- C. Schwarzenböck, A. Schaffer, E. Nößner, P. J. Nelson, R. Huss, B. Rieger*, *Chem. Eur. J.* **2018,** *24*, 2584-2587. „Fluorescent Polyvinylphosphonate Bioconjugates for Selective Cellular Delivery.“
- A. Denk,‡ S. Kernbichl,‡ A. Schaffer, M. Kränzlein, T. Pehl, B. Rieger*, *ACS Macro Lett.* **2020**, *9*, 571-575. „Heteronuclear, Monomer-Selective Zn/Y Catalyst Combines Copolymerization of Epoxides and CO_2 with Group-Transfer Polymerization of *Michael*-Type Monomers.“
- T. Pehl,‡ M. Kränzlein,‡ F. Adams,‡ A. Schaffer, B. Rieger*, *Catalysts* **2020**, *10*, 448. „C–H Bond Activation of Silyl-Substituted Pyridines with Bis(Phenolate)Yttrium Catalysts as a Facile Tool towards Hydroxyl-Terminated Michael-Type Polymers.“
- K. Halama,‡ A. Schaffer,‡ B. Rieger*, *manuscript in preparation*. „Allyl Group-Containing Polyvinylphosphonates as a Flexible Platform for the Selective Introduction of Functional Groups via Polymer-Analogous Transformations.“

‡These authors contributed equally. *Corresponding authors.

Conference Contribution

- A. Schaffer, C. Schwarzenböck, B. Rieger*, Biennial Meeting of the GDCh-Division of Macromolecular Chemistry **2018**, Karlsruhe, poster presentation. “Precise Synthesis of Well-Defined Thermoresponsive Polyvinylphosphonate-Biomolecule Conjugates for Selective Cellular Delivery.”

Table of Contents

List of Abbreviations V
Publication List VII
1 Introduction 1
2 Theoretical Background 3
2.1 Synthesis and Properties of Poly(vinylphosphonate)s 3
2.1.1 Radical and Anionic Synthesis of Poly(vinylphosphonate)s 4
2.1.2 Rare Earth Metal-Mediated Group Transfer Polymerization 5
2.1.3 C-H Bond Activation with Rare Earth Metal Complexes 10
2.2 GTP-Polymers as Functional Materials 13
2.2.1 Post-Polymerization Functionalization of Poly(vinylphosphonate)s 13
2.2.2 Thermoresponsive Behavior of Poly(vinylphosphonate)s 20
2.2.3 Application of Poly(vinylphosphonate)s in Drug Delivery 22
2.2.4 Copolymers derived from Poly(dimethylsiloxane)-based Macroinitiators 25
3 Aim of this Thesis 28
4 From Lanthanide-mediated, High-Precision Group Transfer Polymerization of *Michael*-type Monomers, to Intelligent, Functional Materials 32
4.1 Bibliographic Data 32
4.2 Summary 33
4.3 Manuscript 34
4.4 Reprint Permission Copyrighted Content 47
5 Synthesis and Application of Functional Group-Bearing Pyridyl-Based Initiators in Rare Earth Metal-Mediated Group Transfer Polymerization 48
5.1 Bibliographic Data 48
5.2 Summary 49
5.3 Manuscript 50
5.4 Reprint Permission Copyrighted Content 60
6 Precise Synthesis of Poly(dimethylsiloxane) Copolymers through C-H Bond Activated Macroinitiators in the Yttrium-mediated Group Transfer Polymerization and Ring-Opening Polymerization 61
6.1 Bibliographic Data 61
6.2 Summary 62
6.3 Manuscript 63
6.4 Reprint Permission Copyrighted Content 74
7 Synthesis, Characterisation and Functionalisation of BAB-type Dual-Responsive Nanocarriers for Targeted Drug Delivery: Evolution of Nanoparticles based on 2-Vinylpyridine and Diethyl Vinylphosphonate 75
7.1 Bibliographic Data 75
7.2 Summary 76

7.3 Manuscript 77
7.4 Reprint Permission Copyrighted Content 86
8 Excursus: Synthesis of Poly(vinylphosphonate)-based Hydrogels 87
8.1 Polymerization 87
8.2 Formation of the Hydrogels 88
8.3 Characterization of the Swelling Behavior and Stability 91
9 Summary and Outlook 94
10 Zusammenfassung und Ausblick 99
11 Publications Beyond the Scope of this Thesis 104
11.1 Precise Synthesis of Thermoresponsive Polyvinylphosphonate-Biomolecule Conjugates via Thiol-Ene Click Chemistry 104
11.2 Fluorescent Polyvinylphosphonate Bioconjugates for Selective Cellular Delivery 106
11.3 Heteronuclear, Monomer-Selective Zn/Y Catalyst Combines Copolymerization of Epoxides and CO_2 with Group-Transfer Polymerization of *Michael*-Type Monomers 108
11.4 C–H Bond Activation of Silyl-Substituted Pyridines with Bis(Phenolate)Yttrium Catalysts as a Facile Tool towards Hydroxyl-Terminated Michael-Type Polymers 110
11.5 Allyl Group-Containing Polyvinylphosphonates as a Flexible Platform for the Selective Introduction of Functional Groups via Polymer-Analogous Transformations 112
12 Appendix 113
12.1 Supporting Information of the Manuscript “Synthesis and Application of Functional Group-Bearing Pyridyl-Based Initiators in Rare Earth Metal-Mediated Group Transfer Polymerization” 113
12.2 Supporting Information of the Manuscript “Precise Synthesis of Poly(dimethylsiloxane) Copolymers through C-H Bond Activated Macroinitiators in the Yttrium-Mediated Group Transfer Polymerization and Ring-Opening Polymerization” 154
12.3 Supporting Information of the Manuscript “Synthesis, Characterisation and Functionalisation of BAB-based Dual-Responsive Nanocarriers for Targeted Drug Delivery: Evolution of Nanoparticles based on 2-Vinylpyridine and Diethyl Vinylphosphonate” 201
12.4 Experimental Section for Chapter 8 238
13 Copyright Licenses 241
14 References 250

1 Introduction

Historically macromolecular materials have always been ubiquitous. In a societal context naturally occurring materials such as fibers made from cellulose (cotton or flax)[1] or proteins (wool and silk)[2] are known for a long time. With upcoming of the 19th century, scientist steadily advanced the material science of plastics and discovered new materials such as nitrocellulose through *Christian Schönbein*[3] or *Bakelite* through *Leo Baekland*.[4] However, scientists still lacked a basic understanding in the microscopic structure of the macromolecules and appropriate characterization methods, which led to some tremendous misinterpretations of the polymer features. Yet, the understanding for these materials had to remain fragmentary until *Hermann Staudinger* pioneered the field of polymer chemistry in the early 20th century.[5] Already in the year 1922 he postulated macromolecules to be long-chained molecules that are connected via covalent bonds[6, 7] and established a set of new theories as well as a basic understanding for the material properties which was awarded with the Nobel prize in 1953 and still represent the foundation for modern polymer chemistry.[7, 8] Since then plastics became omnipresent in the society and are used as engineering materials in the automotive industry, in lifestyle products such as electronics and cosmetics, packaging materials, textiles, adhesives, coatings and many more parts of everyday life (Figure 1.1).[9]

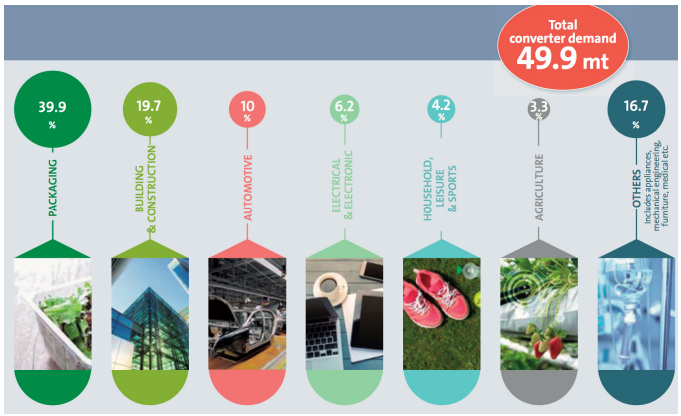

Figure 1.1. Application fields of polymeric materials in Europe sorted by the demand of the respective converter sectors.[9]

Economical-wise, the polymer field emerged to be one of the largest production sectors in the chemical industry and took up approximately 20% of the total production value in Germany in 2018 according to the *Verband der Chemischen Industrie e.V.* (VCI) (Figure 1.2).[10] The global market size reached a value of USD 568.9 billion in 2019.[11]

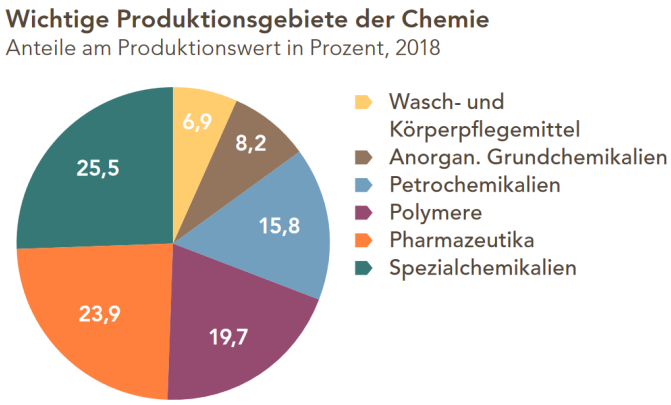

Figure 1.2. Most important production sectors in chemistry in 2018: Washing and body care products (yellow), inorganic basic chemicals (brown), petrochemicals (blue), polymers (purple), pharmaceuticals (orange) and special chemicals (dark green).[10]

Consequently, the production of plastics has increased continuously over the course of the last two decades and reached a production volume of $359 \cdot 10^6$ metric tons in 2018. However, the production of plastics in Europe stagnates at approximately $62 \cdot 10^6$ metric tons.[12] With respect to their production volume, the material properties and hence the resulting market prize plastics can be distinguished into three different subtypes that include the so-called commodities as well as engineering and high-performance plastics (Figure 1.3).[13, 14]

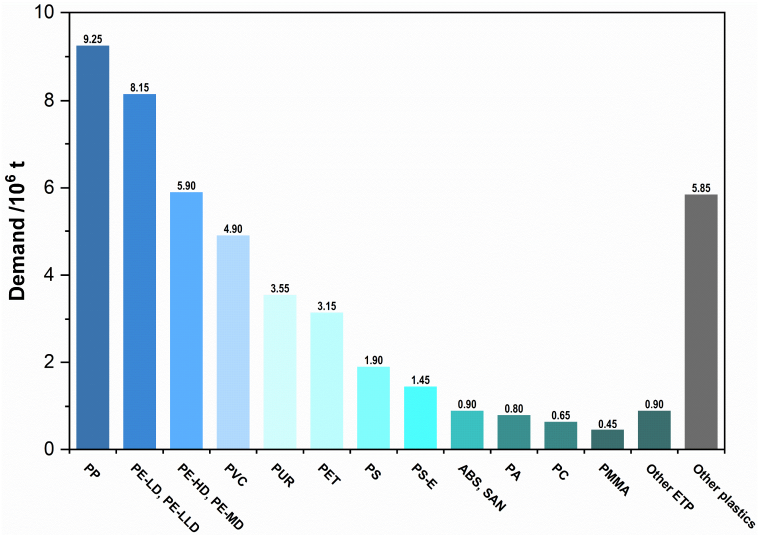

Figure 1.3. Illustrations of common plastics according to their production volume in Europe in 2015.[13] Adopted from ref. [13].

The group of stimuli-sensitive polymers are associated with these high-performance plastics and are often referred to as *smart materials*. Materials based on such kinds of polymers are able to respond to external stimuli which can be changes in the surrounding temperature, changes of the pH-environment, irradiation of the polymer or mechanical stress.[15, 16] The phosphorous-containing poly(vinylphosphonate)s belong to this group of intelligent materials and exhibit a thermoresponsive behavior which is characterized by their lower critical solution temperature (LCST).[17]

2 Theoretical Background

2.1 Synthesis and Properties of Poly(vinylphosphonate)s

Phosphorous-containing polymers are an abundant form of macromolecules in nature and are most prominently found as deoxyribonucleic acid (DNA) or ribonucleic acid (RNA) in living organisms. These polymers consist of nucleoside units which are connected by phosphate groups.[18] However, the generation of these types of polymers via synthetic chemistry proves to be difficult because of the sensitivity of the phosphate linkages towards hydrolysis. As a result, the functional groups in synthetic, phosphorous-containing polymers are usually located remotely to the main chain which can be either accomplished by the ring-opening polymerization (ROP) of cyclic monomers (Figure 2.1, a) or through the chain growth polymerization olefinic monomers (Figure 2.1, b).[17]

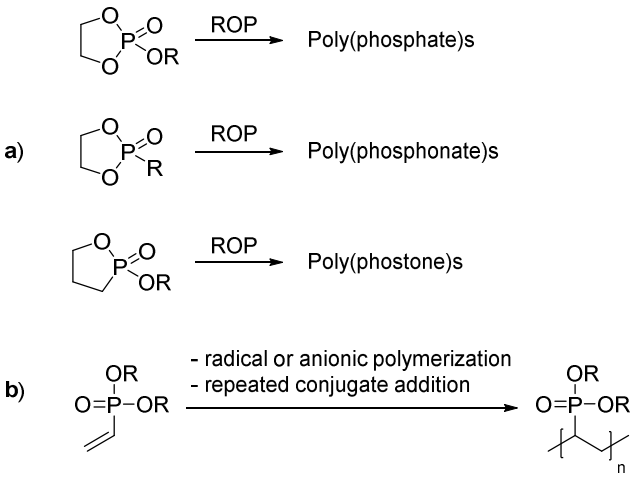

Figure 2.1. Generation of phosphorous-containing polymers via a) ring-opening polymerization of polar phosphates, phosphonates or phostones and b) chain-growth polymerization of unsaturated monomers.[17] Adapted with permission from Ref. [17]. Copyright 2016 American Chemical Society.

By synthetic means the use of cyclic monomers is most widespread and enables the generation of phosphorous-containing polymers. Cyclic phosphate esters which are derived from condensation of 2-chloro-1,3,2-dixoaphospholane-2-oxide with a plethora of alcohols set the foundation for numerous macromolecular substances.[17, 19-23] In this research field the group of *Wurm* achieved great progress in the polymerization of phosphonates and phosphates via ROP,[24, 25] olefin metathesis,[26-29] and ring-opening metathesis polymerization.[30] Additionally, the group expanded this field by a substance class called poly(phostone)s which proved to have a greater stability towards hydrolysis than the analogue poly(phosphate)s and poly(phosphonate)s.[25] Materials that are obtained from vinylphosphonates are structurally related to polymers such as poly(methyl methacrylate) (PMMA) with a stable backbone. Similarly, they comprise repeated C-C bonds and the phosphonate ester as side groups adjacent to the main chain. These ester functions also remain stable up to temperatures between 240 and 280 °C. However, the generation of poly(dialkyl vinylphosphonate)s (PDAVP) remains a complex task.[17]

2.1.1 Radical and Anionic Synthesis of Poly(vinylphosphonate)s

Naturally, monomers with olefinic groups are commonly available through radical or ionic polymerization techniques. However, only few studies exist that solely focus on the radical or ionic polymerization of vinylphosphonates. In case of the radical polymerization the formation of stable radical species results in very low propagation rates and is accompanied by chain transfer reactions to the monomer and other polymeric species, which prevent the reaction from reaching full conversion and leads to materials with low molecular weights.[31] This side reaction is characterized by an intramolecular hydrogen transfer from the phosphonate ester to the primary vinyl radical. The novel radical can insert into a new monomer and an unstable P-O-C motif is formed over the course of the reaction. Eventually, the polymer chain is cleaved at the position of the thermally labile P-O-C bond (Scheme 2.1).[17]

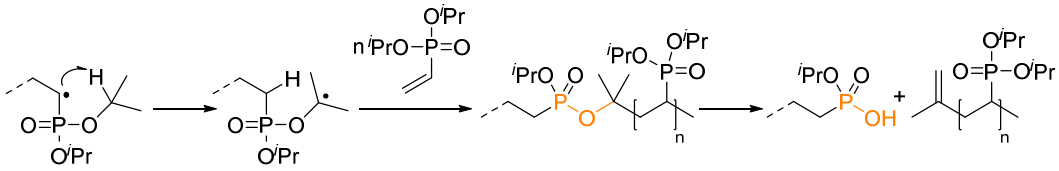

Scheme 2.1. Radical-induced generation of a labile P-O-C bond mediated by an intramolecular hydrogen transfer and subsequent chain scission of the poly(vinylphosphonate).[17] Adapted with permission from Ref. [17]. Copyright 2016 American Chemical Society.

To date diethyl vinylphosphonate (DEVP) has to be copolymerized with other vinylic monomers, i. e. styrene,[32-34] which is the most frequently used co-monomer in the conversion of DEVP, or acrylic monomers such as methyl methacrylate (MMA), vinyl acetate, acrylonitrile, or acrylamide. [34, 35] However, only low amounts of the phosphonate are incorporated in the copolymer during this process and, therefore, influence the material properties marginally. The approach of *Jin et al*. used cyclic ketene acetals to form copolymers from caprolactone and vinylphosphonic acid or dimethyl vinylphosphonate (DMVP), respectively.[36] At a first glance, the anionic polymerization turned out to be a more appropriate polymerization approach for this monomer class. It showed higher activities which resulted in better monomer conversions and polymers with higher molecular weights but does not come without limitations. The main issue for the anionic polymerization can be narrowed down to the presence of an acidic proton in the α-vinylic position which concludes in side and termination reactions with organolithium, magnesium, or aluminum compounds (Scheme 2.2).[17, 37]

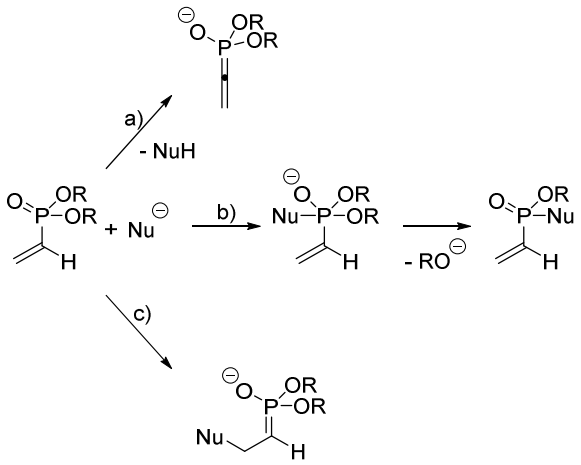

Scheme 2.2. Side reactions occurring during the anionic polymerization of vinylphosphonates: a) Deprotonation of the α-vinylic acidic proton. b) Nucleophilic substitution of a phosphonate-bound alcoholate. c) Nucleophilic attack at the β-vinylic position.[37] Reprinted with permission from Ref. [37]. Copyright 2012 John Wiley and Sons.

Copolymerization attempts of the α-masked monomer dimethyl 1-methylvinylphosphonate with styrene were reported to be not successful using *n*-butyllithium (*n*-BuLi). The application of sodium naphthalene as initiator though facilitated the incorporation of the monomer in the polystyrene (PS) copolymer to some extent.[38] Back in 2008, *Jannasch* and co-workers were able to graft PDEVP on polysulfones in the presence of *n*-BuLi and 1,1-diphenylethylene (DPE) as co-initiator.[39] This co-initiator appears to be essential as the polymerization results of *Leute* and *Bingöl* were drastically improved by this approach because DPE reduces the nucleophilicity as well as the basicity of the initiator.[40, 41] The application of DPE also benefited the production of PS-*b*-PDEVP block copolymers via sequential anionic polymerization since the absence of DPE rendered both the co- and homopolymerization impossible.[42] These observations coincide with the polymerization results of DMVP and diisopropyl vinylphosphonate (DIVP) of similar studies.[43] Although many improvements were achieved in past decades, the anionic polymerization is still limited to low degrees of polymerization and broad molecular weight distributions ($Đ > 3$).[40, 43] The rare earth metal-mediated group transfer polymerization (REM-GTP) proved to be a much more efficient approach in the synthesis of poly(vinylphosphonate)s.

2.1.2 Rare Earth Metal-Mediated Group Transfer Polymerization

REM-GTP combines the beneficial properties of ionic and coordinative polymerization techniques, gives access to highly functional polymers, and allows the introduction of polymer chain-end groups.[17] Due to its living character REM-GTP exhibits a linear increase of the average molecular weight and yields well-defined materials with very narrow polydispersities ($Đ < 1.1$). This polymerization method derived its origin from the so-called silyl ketene acetal-initiated group transfer polymerization (SKA-GTP) which was established by *Webster* and co-workers at *DuPont* in the 1980s.[44] This living-type polymerization is characterized by a linear increase of the molecular weights with the monomer conversion and gives access to block copolymers by sequential addition of the *Michael*-type monomers.[17] In 1992 this concluded in the work of *Yasuda* and *Collins* and *Ward* who used metallocene catalysts in the polymerization of MMA in independent publications and, hence, defined the general framework for REM-GTP.[45, 46] While *Yasuda* used neutral samarocenes like $[(C_5Me_5)_2SmH]_2$, *Collins* and *Ward* employed an isoelectronic zirconocene catalyst. Such catalyst motifs enabled the generation of highly syndiotactic,

high-molecular-weight PMMA with a very narrow molecular weight distribution ($Đ < 1.05$).[46, 47] Crystallographic analysis of the samarocene-MMA adduct [$(C_5Me_5)Sm(MMA)_2H$] confirmed a propagation via an ester enolate and corroborated mechanistic proposals which suggested a repeated conjugate addition.[45] In a first step the hydrido-bridged dimer dissociates upon the coordination of one MMA molecule (Scheme 2.3, a). After formation of the ester enolate through a 1,4-addition of the hydride to MMA, the free coordination site is occupied by a new monomer. The ester enolate inserts into the new monomer again via a 1,4 addition under formation of an eight-membered transition state (Scheme 2.3, b). Subsequently, the coordinating ester is repeatedly replaced by a new MMA molecule and inserted via the same reaction mechanism resulting in the eight-membered transition state again (Scheme 2.3, c).[17]

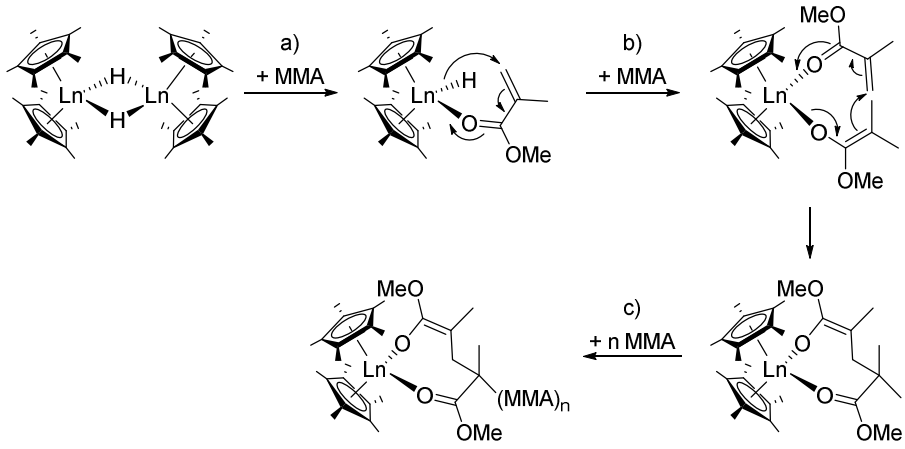

Scheme 2.3. *Yasuda*-type REM-GTP of MMA: a) Dissociation and coordination of MMA. b) Hydride transfer to MMA and formation of the eight-membered transition state. c) Repeated conjugate addition of MMA.[17] Adapted with permission from Ref. [17]. Copyright 2016 American Chemical Society.

The cationic zirconocene catalysts follow the same propagation pathway but also require co-catalysts which can affect the polymerization activity and stereoselectivity.[46, 48, 49] For the polymerization of (meth)acrylates trivalent rare earth metals in the oxidation state +III are usually preferred because complexes based on these metal centers are reasonably stable, show high activities and are able to initiate the polymerization by a nucleophilic attack on the acrylic monomer. As described the formation of defined poly(vinylphosphonate)s by classical radical and anionic polymerization strategies remained an unresolved task. However, vinylphosphonates such as DEVP strongly resembles other *Michael*-acceptor monomers (i. e. MMA, 2-vinylpyridne (2VP), or 2-isopropenyl-2-oxazoline (IPOx)) in structure as well as in their electronic properties (Figure 2.2).[17]

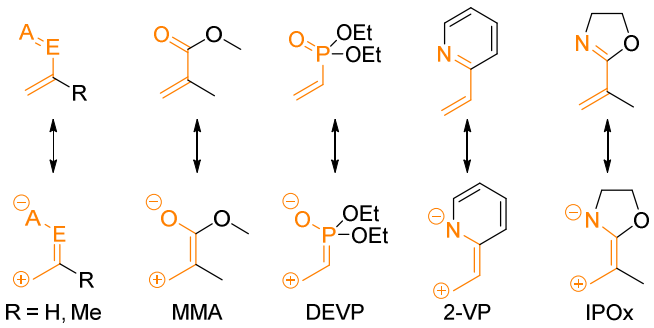

Figure 2.2. General structure and examples for typical *Michael*-type monomers and corresponding zwitterionic resonance structure.[17]

Rieger and co-workers took advantage of this resemblance and were able to generate high-molecular-weight PDEVP in a very controlled fashion with rare earth metallocenes of the type Cp_2LnX (Ln = Gd-Lu; X = Cp, Me, CH_2TMS, Cl).[50, 51] Copolymerization attempts with DEVP and MMA substantiated a GTP-type polymerization mechanism. For the initiation, a nucleophilic transfer of a η^1-coordinated Cp ligand to vinyl group at the β-position was proposed. In a similar fashion to the GTP of MMA, the free coordination site can be occupied by DEVP and then inserted via a conjugate addition during the propagation step (Scheme 2.4).[50, 51]

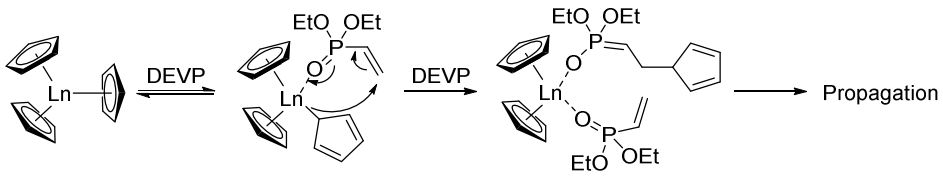

Scheme 2.4. Postulated mechanism for the polymerization of DEVP with Cp_3Ln.[51] Reprinted with permission from Ref. [51]. Copyright 2011 American Chemical Society.

As expected, the REM-GTP of dialkyl vinylphsophonates (DAVP) showed a living behavior and led to products with much higher degrees of polymerization and narrow molecular weight distributions. These initial studies have already reported a strong influence of the metal center on the polymerization characteristics. Hence, decreasing ionic radii (Dy > Tm > Yb > Lu) were beneficial for the polymerization rate and led to higher initiator efficiencies as well as lower polydispersities. Therefore, the polymerization mechanism with special focus on the initiation, kinetic aspects of the polymerization, the influence of the central metal atom, and the surrounding ligand sphere were studied in-depth.

Peculiarly, chlorido ligands are able to initiate the polymerization of DAVPs which is impossible in the REM-GTP of other *Michael*-type monomers due to their low nucleophilicity. Moreover, a complex reaction network is caused by the interaction of the strongly basic ligands with the α-acidic proton. As a result, nucleophilic transfers, deprotonation of the α-acidic hydrogen, or ligand exchanges can start the polymerization (Scheme 2.5).[52]

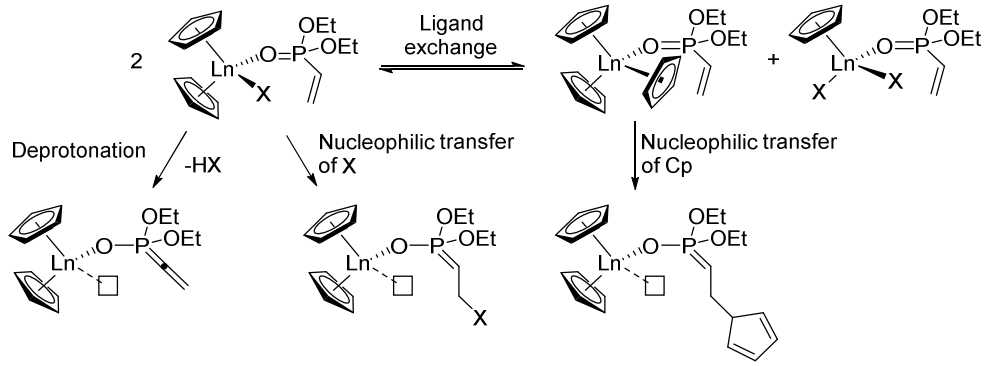

Scheme 2.5. Complex initiation network of Cp_2LnX complexes in the REM-GTP of DAVP.[52] Adapted with permission from Ref. [52]. Copyright 2013 American Chemical Society.

To obtain a more cohesive view on the initiation process, Cp_2LnX complexes were treated with diethyl ethylphosphonate (DEEP) which was used as a surrogate for DEVP since it had a similar steric demand but is not polymerizable due to the absence of the olefinic group. These experiments showed a monomer-induced ligand exchange which led to an equilibrium between the original species Cp_2LnX(DEEP), Cp_3Ln(DEEP), and

$CpLnX_2(DEEP)_n$ (Scheme 2.6). Furthermore, the $Cp_3Y(DEEP)$ complex as well as $Cp_2LnCl(DEVP)$ species were isolated and analyzed by crystallography. The crystal structures showed a coordination via the oxygen and not the vinyl group of the monomer. In case of the DEVP adduct a S-*cis* conformation with a pronounced π-overlap (torsion angles O=P-C=C of -10.14° and 10.47°) was retained.[52] These structural characteristics meet the key feature for the polymerizability of a *Michael*-type monomer by a repeated conjugate addition or GTP, respectively.[48, 50]

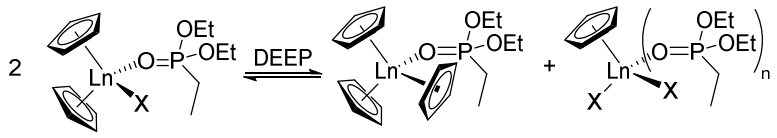

Scheme 2.6. Equilibrium of the DEEP-induced ligand exchange starting from $Cp_2LnX(DEEP)$.[52] Reprinted with permission from Ref. [52]. Copyright 2013 American Chemical Society.

The kinetic investigations with DEVP were performed with Cp_3Tm to determine the reaction order of the polymerization. $[Cp_2Y(S^tBu)]_2$ was used as catalyst for the investigation of the sterically more demanding DIVP. In both cases the reaction orders of the catalyst as well as of the monomer were determined to be n = 1 which means that the propagation mechanism is independent from the steric demand of the monomer.[52] However, these experiments did not explain the strong dependence between the ionic radii of the metal centers and the polymerization activity. As mentioned earlier, a reduction of the radius of the central metal atom was accompanied by an increase in activity and better initiator efficiencies. Consequently, temperature-dependent kinetic studies were performed to determine the activation enthalpy $\Delta H^{\ddagger}$ and entropy $\Delta S^{\ddagger}$. These experiments demonstrated that $\Delta H^{\ddagger}$ is not affected by the metal center. Hence, $\Delta H^{\ddagger}$ is neither influenced by the Lewis acidity of the central metal atom and the corresponding strength of the Ln-(O=P) bond nor by the size of the lanthanide and the effective ring strain of the eight-membered metallacycle.[17, 52] As a consequence, the activation barrier $\Delta G^{\ddagger}$ results from a change in the entropy term $-T\Delta S^{\ddagger}$ which behaves proportional to the ionic radii of the respective lanthanides. Therefore, changes of the steric demand of the side chains and the crowding at the metal center within the pentacoordinated intermediate define the activation entropy. It was observed that smaller metal centers led to a more constraint eight-membered metallacycle (shorter Ln-Cp, Ln-(O-P), and Ln-(O=P) bonds) and thus a destabilization of the propagation ground state and a longer Ln-(O=P) phosphonate. Furthermore, the GTP activity is mainly influenced from the steric demand of the growing polymer chain, which destabilizes the transition state by entropic and also enthalpic effects.[52, 53] Ultimately, these studies concluded a *Yasuda*-type, monometallic propagation for the REM-GTP of vinylphosphonates with rare earth metal complexes as catalysts. The rate-determining step of this reaction is the associative exchange of the coordinating polyphosphonate ester with a new monomer (Scheme 2.7).[17, 52]

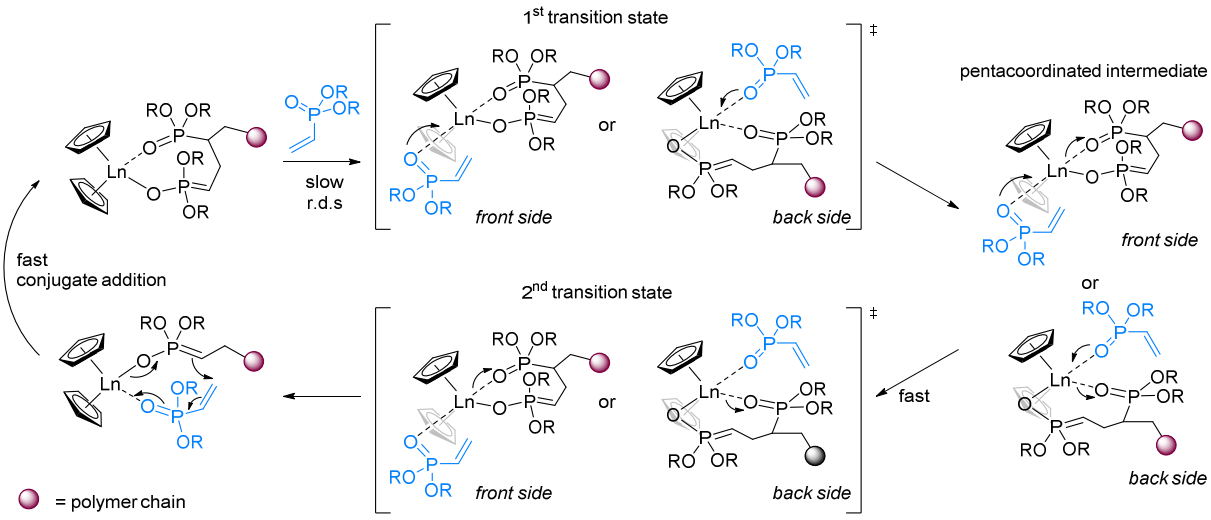

Scheme 2.7. Mechanism for the propagation of DAVPs via REM-GTP.[52] Adapted with permission from Ref. [52]. Copyright 2013 American Chemical Society.

To that date, only non-metallocenes of the type $Ln(NSiHMe_2)_3(THF)_2$ were explored in the polymerization of DEVP, but obtained materials with high $Đ$'s at low conversions.[40] Consequently, in-depth studies on the steric influence of the ligand sphere gave advanced insights into this topic. First experiments with Cp_3Y and $(C_5MeH_4)_3Y(THF)$ already showed strong improvements in terms of the initiation period, polymerization time and initiator efficiency. The structural analogue $(C_5H_4TMS)_3Y$ is also able to start the REM-GTP of DEVP without an initiation delay. However, it exhibited a lower activity which was explained by the higher steric demand of the TMS group. The densely crowded complex $(C_5Me_4H)_3Y$ showed the best initiator efficiency (*IE*) (86%) and the lowest polydispersity ($Đ = 1.05$).[54] These basic experiments were complemented by studies on the thermodynamic parameters $\Delta H^‡$ and $\Delta S^‡$. Surprisingly, the complexes $(C_5MeH_4)_3Y(THF)$ and $(C_5H_4TMS)_3Y$ shared the same activation enthalpy $\Delta H^‡$. Hence, deviations in activity were accounted to entropic reasons due to changes in the substitution pattern of the Cp ligands. This observation was explained with the high rotational freedom of the mono-substituted cyclopentadienyl group which has to be oriented with the highest spacious distance to compensate the steric demand of the crowded pentacoordinated intermediate (Figure 2.3, left).[54] Temperature-dependent activity measurements with $(C_5Me_4H)_3Ln$ (Ln = Sm, Tb, Y) showed an increase of the activation enthalpy since the tetramethyl-substituted ligands are unable to rearrange with maximum distance to the active center. This leads to prolonged Ln-(O-P) and Ln-(O=P) bonds to counteract the steric demand of the ligands towards the eight-membered metallacycle (Figure 2.3, right).[54]

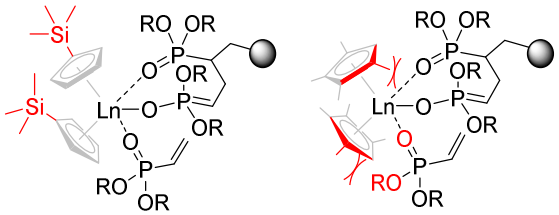

Figure 2.3. Orientation of the trimethylsilyl- and the tetramethyl-substituted Cp ligand of a rare earth metal complex during the pentacoordinated intermediate.[54] Adapted with permission from Ref. [54]. Copyright 2016 American Chemical Society.

2.1.3 C-H Bond Activation with Rare Earth Metal Complexes

As depicted in Scheme 2.5 the initiation step of the GTP of DAVPs proceeds via a complex reaction network consisting of different, competing reactions (deprotonation, nucleophilic transfer and ligand exchanges) and delay the initial monomer insertion. Studies of *Collins* and co-workers investigated ester enolates in the zirconocene-mediated GTP to improve initiator efficiencies and reduce the initiation delay which were observed with alkyl initiators.[55] Accordingly, *Rieger et al.* followed a similar approach and envisioned ester- and enamide-based rare earth metallocenes for REM-GTP to have the desired properties for the initiation. However, these complexes were inaccessible by protonolysis with a variety of α-CH acidic reagents. Even at elevated temperatures no controlled formation was observed which was attributed to a strong kinetic limitation.[56] Beyond that rare earth metals as well as transition metals with a d^0 electron configuration are prevented from forming new bonds via an oxidative addition due to a lack of electrons. In spite of that, σ-bond metathesis represents an attractive approach to generate new bonding motifs via intramolecular C-H bond activations of suitable substrates while the oxidation state of the metal is retained.[57, 58] Generally speaking, H-H (hydrogen), C-H, and C-C bonds are able to be activated by hydrogenolysis or alkanolysis, respectively. The reaction proceeds as a (2_σ+2_σ) cycloaddition via a four-membered transition state whereby a concerted exchange of a metal ligand and the substrate σ-bond takes place (Scheme 2.8).[59, 60]

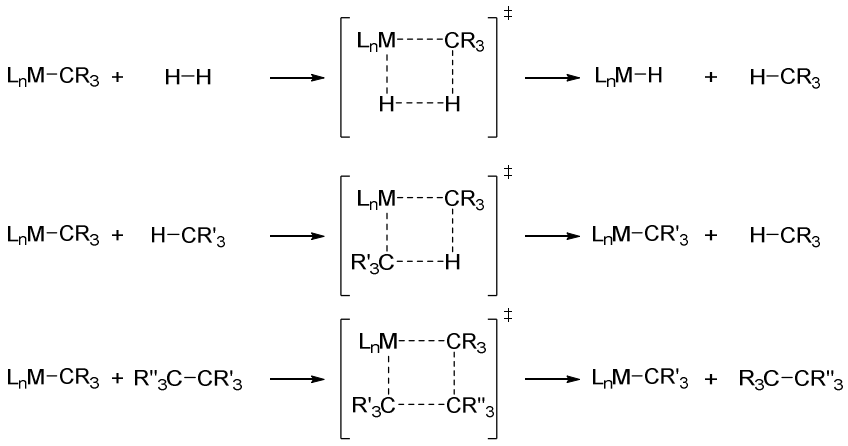

Scheme 2.8. Hydrogenolysis and alkanolysis through σ-bond metathesis.[59]

As shown by *Teuben et al*., group 3 elements show high activity in the σ-bond metathesis and C-H bond activation experiments were successfully performed with pyridines, other heteronuclear compounds, and internal alkynes.[61] *Mashima* and co-workers used this approach for the introduction of chain end moieties in the polymerization of 2VP. In their work, alkylyttrium compounds facilitated the C-H bond activation of non-classical CH-acidic substrates such as 2,4,6-trimethylpyridine (*sym*-collidine) (**1**), phenylpyridine or 1-trimethylsilyl-1-propyne.[62]

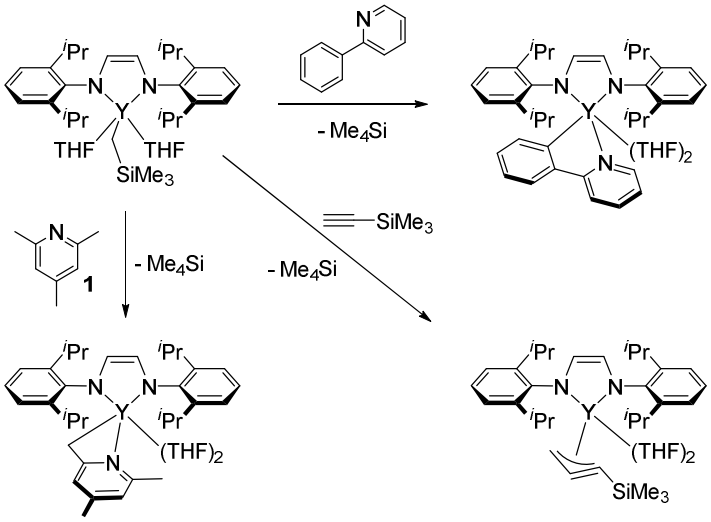

Scheme 2.9. C-H bond activation of various, non-classical CH-acidic compounds using alkylyttrium complexes by *Mashima et al*.[62] Adapted with permission from Ref. [62]. Copyright 2011 American Chemical Society.

The applicability of this approach with rare earth metallocenes was successfully verified by treating $Cp_2Y(CH_2TMS)(THF)$ (**2**) with *sym*-collidine (**1**) which yielded the desired complex $Cp_2Y(CH_2(C_5H_2Me_2N))$ (**3**) after only 30 minutes in quantitative yield (Scheme 2.10).[56] Both, the *in situ* generated as well as the isolated complex showed the same high activity and molecular weights in the REM-GTP of DEVP. In the same fashion, the lutetium complex was treated with initiator **1** but required a prolonged reaction time of 24 hours and purification by recrystallization rendering the *in situ* approach inadequate for the smaller lutetium center.[17, 56]

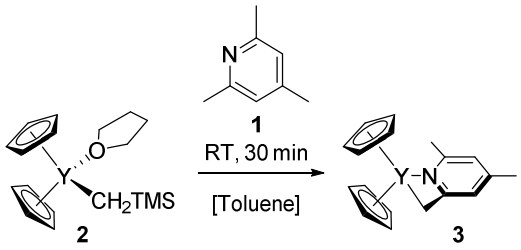

Scheme 2.10. C-H bond activation of *sym*-collidine (**1**) with $Cp_2Y(CH_2TMS)(THF)$ (**2**).[56] Reprinted with permission from Ref. [56]. Copyright 2015 American Chemical Society.

The polymerization with the highly active $Cp_2Y(CH_2(C_5H_2Me_2N))$ (**3**) exhibited a living character, a linear growth of the molecular weight with the conversion and good initiator efficiencies. PDEVP produced with **3** showed narrow molecular weight distributions ($Đ$ = 1.05).[17, 56]

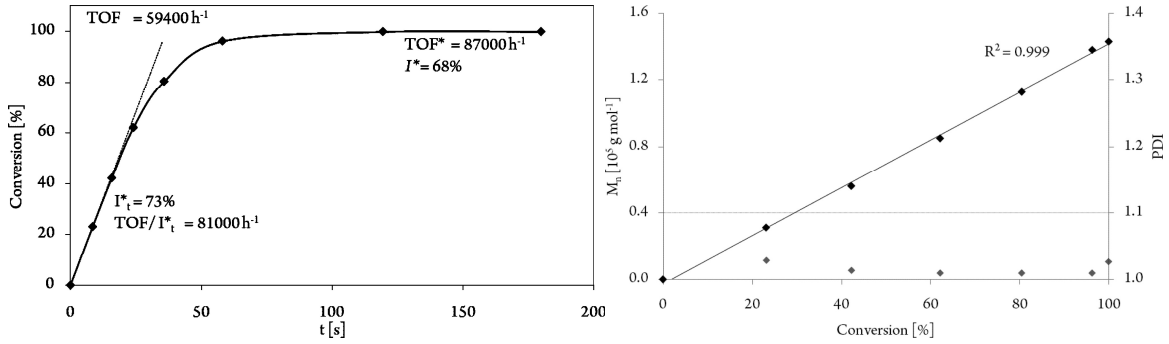

Figure 2.4. Conversion-time plot of the REM-GTP of DEVP with catalyst **3** (left) and conversion-dependent plot of the molecular weights M_n and corresponding polydispersites *Đ* (right).[56] Reprinted with permission from Ref. [56]. Copyright 2015 American Chemical Society.

Moreover, the kinetic study ruled out the presence of an initiation delay. Likewise, the lutetium catalyst showed no initiation period but a considerably lower *IE*, which was led back to the formation of a stable dimer. End-group analysis by electrospray ionization mass spectrometry (ESI-MS) of DEVP oligomers further confirmed the selective incorporation of the initiator at the chain end of the polymer and ruled out competing reactions, i.e. deprotonation. Crystallographic analysis of $Cp_2Y(CH_2(C_5H_2Me_2N))$ (**3**) revealed a partial double bond character of the methylene group. Therefore, the pyridyl ligand can coordinate via a carbanion or an enamine (Figure 2.5).[56]

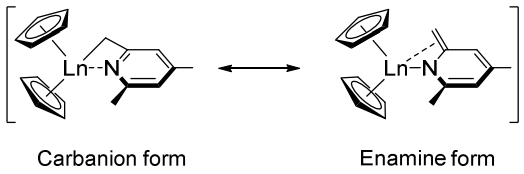

Figure 2.5. Mesomeric structures of the carbanionic and the enamine form.[56] Adapted with permission from Ref. [56]. Copyright 2015 American Chemical Society.

Mechanistic considerations on the initiation process propose a nucleophilic transfer of the pyridine ligand which is in accordance with the experimental data. The insertion of the first monomer may proceed via a six-membered or an eight-membered transition state (Scheme 2.11).[56]

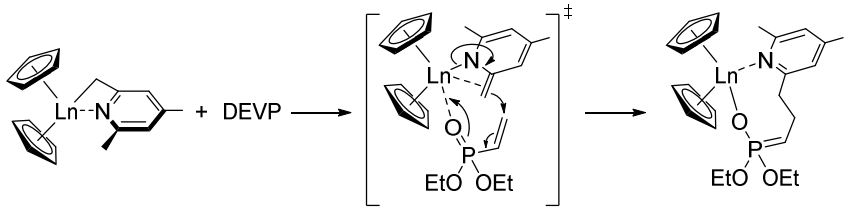

Scheme 2.11. Proposed initiation mechanism for DEVP using species **3**.[56] Adapted with permission from Ref. [56]. Copyright 2015 American Chemical Society.

As a result of the high flexibility of this activation approach, rapid progress was made in this field and polymers with selectively introduced, functional end-groups as well as new polymer topologies were accessible. In specific, bipyridine-based initiators were used in the synthesis of AB block copolymers (A: 2VP, B: DEVP) and later functionalized with $Re(CO)_5Cl$ for the reduction of CO_2 to CO.[63] Moreover, the binuclear initiator 2,3,5,6-

tetramethylpyrazine (TMPy) enabled the synthesis of BAB block copolymers which formed defined micelles in aqueous solution and proved to be promising candidates for drug delivery.[64] Besides, the C-H bond activation of multinuclear initiators with complex **2** also gave access to novel, functional three-arm star-shaped polymers generated from IPOx and DEVP.[65]

2.2 GTP-Polymers as Functional Materials

2.2.1 Post-Polymerization Functionalization of Poly(vinylphosphonate)s

The application of these C-H bond activated catalysts in REM-GTP not only allows to control the (co)polymer architecture but also the introduction of reactive groups that can be selectively modified via post-polymerization functionalization. One efficient approach, which was explored by our group, focused on the end-group functionalization of PDEVP via thiol-ene click chemistry.

2.2.1.1 Thiol-Ene Click Chemistry

Among many other reactions, the conversion of thiols with unsaturated carbon-carbon bonds to respective thioethers is one example for the so-called click chemistry. Being efficient transformations with a high atom economy and often quantitative yields, good regio- and stereospecificity, and a high resistance towards oxygen and moisture are typical features of click reactions. Besides, click reactions are performed under mild conditions and are often orthogonal to other organic transformations. These reasons rendered click reactions to be a potent tool in (bio-)organic and pharmaceutical chemistry because they allow the introduction of new functional moieties and formation of new bonding motifs, respectively, in usually highly complex target molecules.[66-68] The term click chemistry is most prominently attributed to the Cu(I) catalyzed 1,3-dipolar cycloaddition of azides and alkynes, also known as copper-catalyzed azide-alkyne click reaction or CuAAC and was established by *Sharpless* and co-workers. The CuAAC leads to the formation of 1,2,3-triazols and emerged originally from the work of *Rolf Huisgen* on 1,3-dipolar cycloadditions.[66, 67, 69] Besides, Diels-Alder reactions are also considered to be click reactions and were used in the functionalization of surfaces and polymers.[68, 69]

Consequently, thiol-ene click reactions attracted great attention in the past years because of being efficient and fast reactions.[68, 70] Because S-H bonds are comparatively weak, thiol-ene reactions can be initiated easily and performed under mild conditions. Generally, the reaction is distinguished into the free radical type and the *thia-Michael*-type addition to electron-poor olefins. The radical-induced reaction can be either initiated thermally via the degradation of initiators such as azobis(isobutyronitrile) (AIBN) or photochemically by irradiation of photoinitiators, i.e. benzophenone or 2,2-dimethoxy-2-phenylacetophenone (DMPA). According to mechanistic studies the thioether formation proceeds via an alternating, two-step process which starts with the abstraction of a hydrogen atom from the mercapto group (Scheme 2.12). During the propagation step the thiyl radical adds to the unsaturated bond resulting in the sulfur-carbon bond. In the final step the product is generated by the abstraction of a hydrogen atom from a new thiol molecule initiating the reaction cycle again.[66, 68]

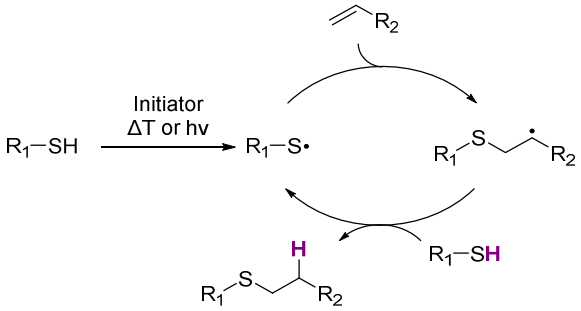

Scheme 2.12. Reaction cycle of the radical-induced thiol-ene reaction.[68]

Thiol-ene reactions are exotherm and highly selective towards the thioether formation since no homopolymerizations of the olefinic monomers were observed. Moreover, a strong relation with the steric demand of the used olefin and thiol was detected. Hence, 1,2-disubstituted olefins were found to have a reduced reaction rate and showed a reversible addition of thiyl radical to the olefin. For less reactive olefins the propagation step is slower and becomes rate-determining.[66, 71]

In general, acceptor-substituted olefines are not favored in the radical thiol-ene chemistry due to a lower reactivity related to electron deficiency of the substrate and the stabilization of the radical.[68] *Michael*-acceptors, however, are convertible through the *thia-Michael* variation. For this reaction, either weak bases such as triethylamine or nucleophilic catalysts, usually phosphines, are suitable to promote high conversions. In case of the base-mediated route the thiolate anion is formed which then attacks the acceptor-olefin at the β-position of the double bond resulting in the respective enolate. The related carbanion deprotonates a thiol again which yields the product or the ammonium ion releasing the base in the course (Scheme 2.13, a). Employing phosphines the olefin is directly transferred into the carbanion and able to deprotonate the thiol (Scheme 2.13, b).[66, 68]

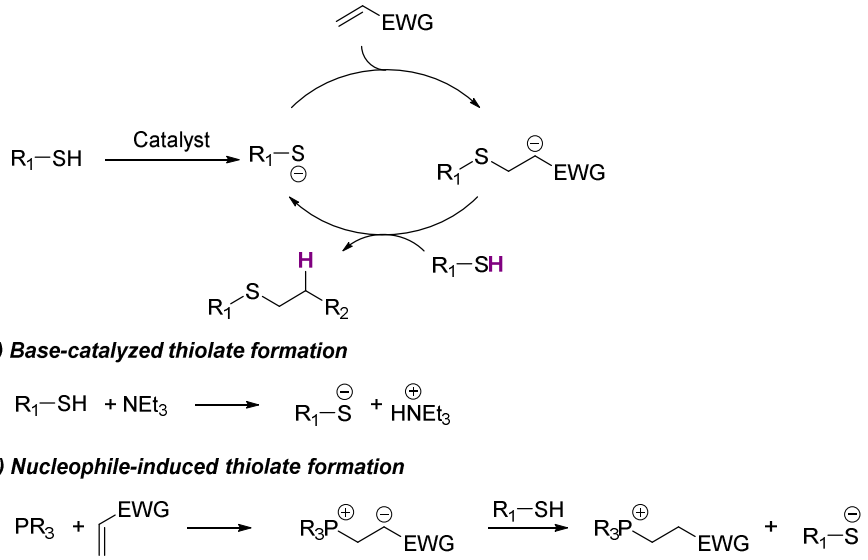

Scheme 2.13. Reaction cycle of the base- or nucleophile-mediated thiol-ene reaction. Initiation via deprotonation of thiol or addition of a phosphine to acceptor olefin.[68]

2.2.1.2 Polymer Functionalization via Thiol-Ene Click Chemistry

In the literature a plurality of studies can be found that take advantage of the positive characteristics of these click reactions. Some of these are exemplarily presented in the following section to give an impression of the scope for the polymer functionalization via thiol-ene click chemistry. *Campos et al*. used the orthogonality of the CuAAC towards the thiol-ene chemistry to their advantage. Prior to the functionalization styrene was polymerized via atom-transfer radical polymerization (ATRP) using an alkyne-functionalized ATRP-initiator. Afterwards, the bromo function was substituted with sodium azide to obtain the asymmetrically chain-end functionalized polystyrene. This substrate was treated in a photo-radical thiol-ene reaction with thioglycolic acid followed by the conversion of the azide with propargyl alcohol. The same reaction was also successfully performed in the opposite order (Scheme 2.14).[72]

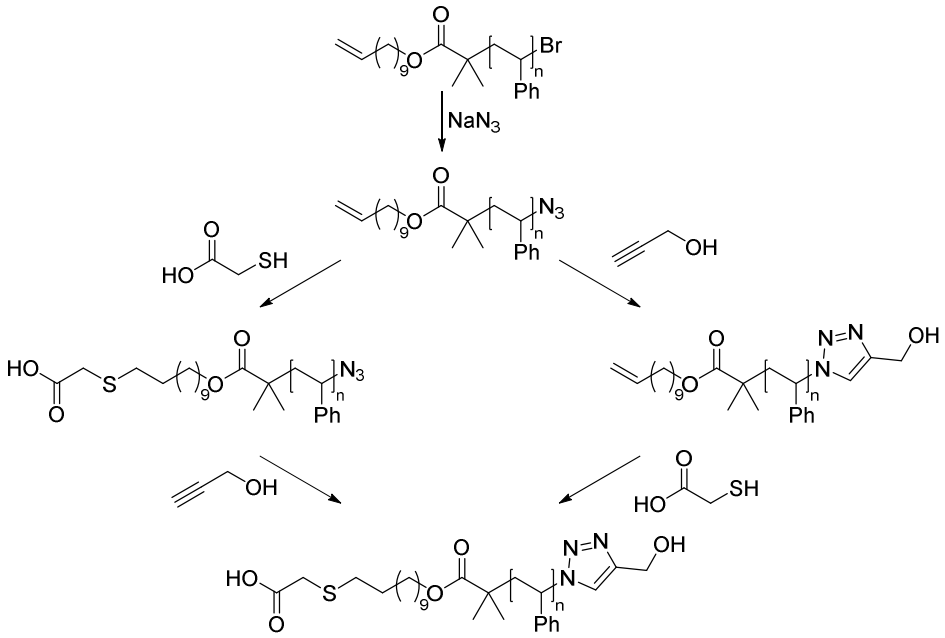

Scheme 2.14. Two pathways for the formation of telechelic polystyrene by use of the orthogonal thiol-ene coupling of thioglycolic acid and CuAAC with propargyl alcohol.[72]

Hvilsted and co-workers tested a similar approach in the functionalization of telechelic poly(ε-caprolactone) (PεCL) which consisted of an alkene and an alkyne end-group. The ROP of εCL was performed with hex-5-yn-1-ol in the presence of $Sn(Oct)_2$ as catalyst. The hydroxyl chain-end was masked with 4-pentonic acid to insert the alkene end-group. First the alkynyl group was converted via CuAAC and followed by the photochemically-induced conversion of the double bond with thiocholesterol and DMPA (Scheme 2.15).[73]

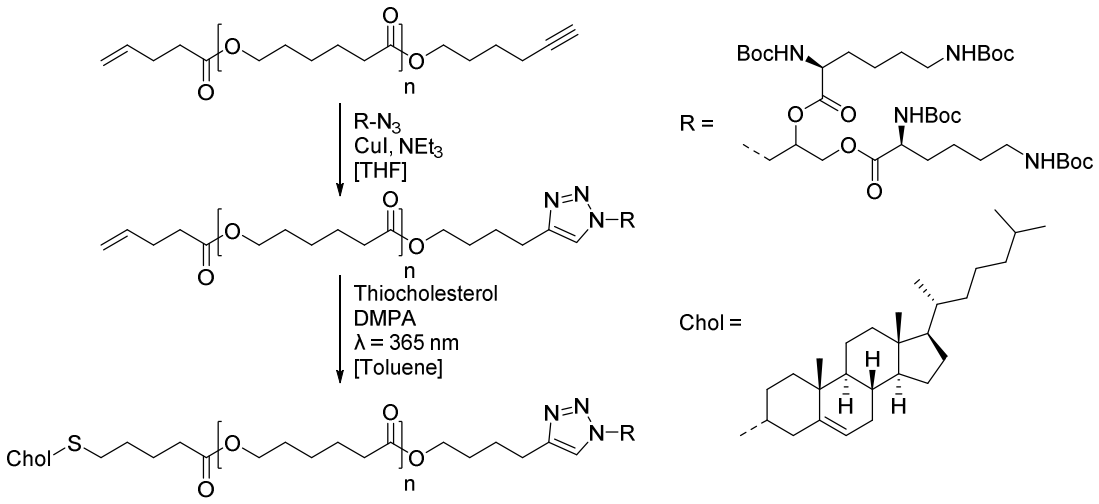

Scheme 2.15. Generation of telechelic PεCL via orthogonal CuAAC and subsequent conjugation of thiocholesterol.[73]

A tailor-made initiator was designed by *Rieger et al.* who used 2,6-dimethyl-4-(4-vinylphenyl)pyridine (**4**) in the C-H bond activation with $Cp_2Y(CH_2TMS)(THF)$ (**2**). In the same fashion as *sym*-collidine, the *in situ* activated complex (**5**) polymerized DEVP via REM-GTP in a controlled way ($Đ$ = 1.01-1.09) and incorporated the vinyl group-bearing initiator in the polymer chain which was confirmed by ESI-MS. In the following, the obtained polymers were coupled with thiocholesterol and cysteamine-hydrochloride at the terminal double bond and in case of the cysteamine conjugate further modified with folic acid to form the polymer-biomolecule conjugate (Scheme 2.16).[74]

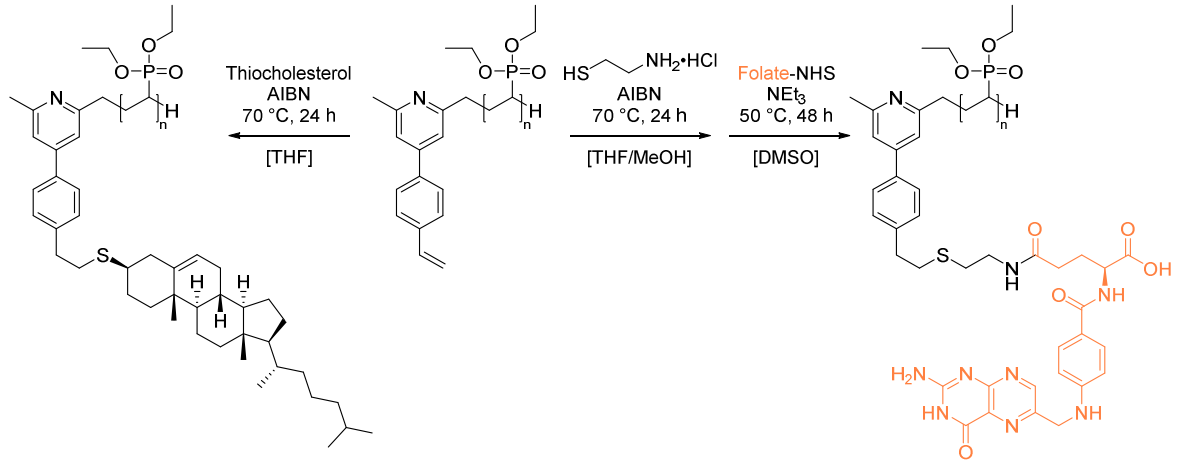

Scheme 2.16. Formation of biomolecule-polymer conjugates from end-group functionalized PDEVP with thiocholesterol or cysteamine and activated folic acid.[74] Adapted with permission from Ref. [74]. Copyright 2018 The Royal Society of Chemistry.

Obviously, this reaction is not limited to chain-end modifications but also side group transformations. On that score *Chen* and co-workers generated highly isotactic poly(allyl methacrylate) (*it*-PAMA) with chiral, ethylene-bridged *ansa*-zirconocences. Irradiation at λ = 350 nm in the presence of DMPA facilitated the conversion of *it*-PAMA with 1-adamantanethiol or 4-*tert*-butylbenzyl mercaptan. Additionally, *it*-PAMA was cross-linked with 1,6-hexanedithiol to yield a flexible, translucent material (Scheme 2.17).[75]

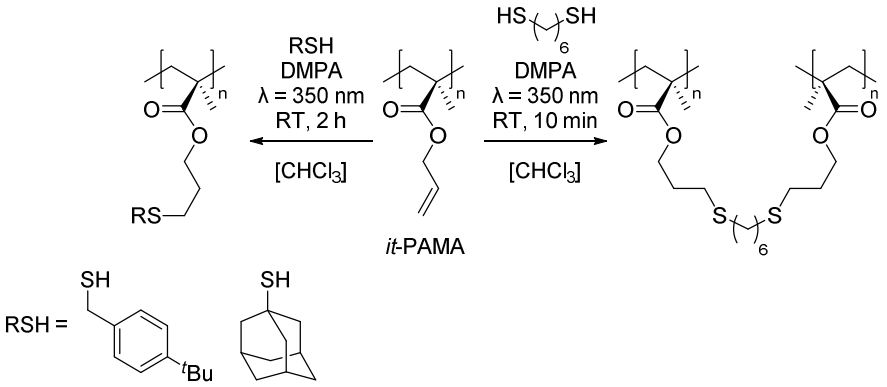

Scheme 2.17. Side-group modification and cross-linking with 1,6-dithiohexane of *it*-PAMA by thiol-ene click chemistry.[75]

Wooley and co-workers synthesized block copolymers with a polyphosphoester (PPE) block consisting of alkyne side groups and poly(L-lactic acid) (PLLA) by sequential ring-opening polymerization of 2-(but-3-yn-1-yloxy)-2-oxo-1,3,2-dioxaphospholane (BYP) and L-lactic acid (Scheme 2.18, top). These precursors were employed in the thiol-yne reactions with either 3-mercaptopropanoic acid or cysteamine-hydrochloride to yield anionic or cationic PPE-*b*-PLLA, respectively (Scheme 2.18, bottom).[19] The biodegradable, anionic copolymers formed well-defined, spherical micelles in aqueous solution and were able to be loaded with silver-based antimicrobials. Release studies were performed *in vitro* to evaluate these novel carriers regarding their antimicrobial activity.[76]

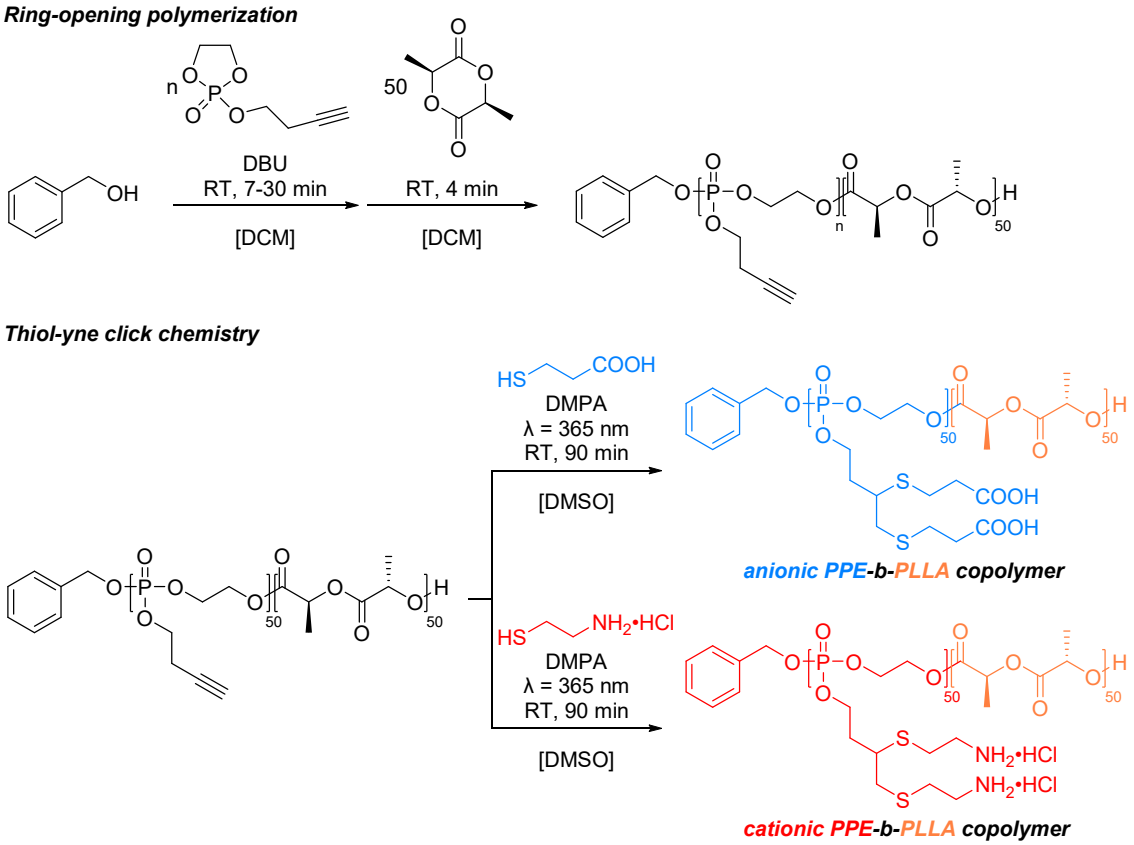

Scheme 2.18. Sequential ring-opening polymerization of BYP and LLA (top) and post-polymerization functionalization via photo-induced thiol-yne chemistry with 3-mercaptopropanoic acid or cysteamine-hydrochloride (bottom).[19, 76]

In a similar fashion these studies were complemented with bifunctional AB block PPEs which were generated from BYP and 2-ethylbutyl phospholane. Likewise, the resulting copolymers were modified via thiol-yne chemistry with different, charged and non-charged thiols. The amphiphilic copolymers were able to form micelles featuring predefined surface charge types.[23]

2.2.1.3 Side Group Functionalization of Poly(vinylphosphonate)s

This kind of side group functionalization was also utilized in the generation of defined, stable nanospheres from ABB'-type block copolymers for the application as drug delivery carriers. REM-GTP enabled the sequential polymerization of 2VP (A), DEVP (B) and diallyl vinylphosphonate (DAlVP) (B') and, hence, allowed the selective introduction of allyl moieties. The dual-responsive nanocarriers were obtained via shell cross-linking of the DAlVP block with 3,6-dioxa-1,8-octanedithiol (**6**) via a thermally induced thiol-ene reaction (Scheme 2.19) and exhibited diameters of 35-66 nm according to analysis by dynamic light scattering (DLS). Besides, the nanocarriers formed independently from concentration effects and did not exhibit a critical micelle concentration (CMC) as the micellar pendants.[77]

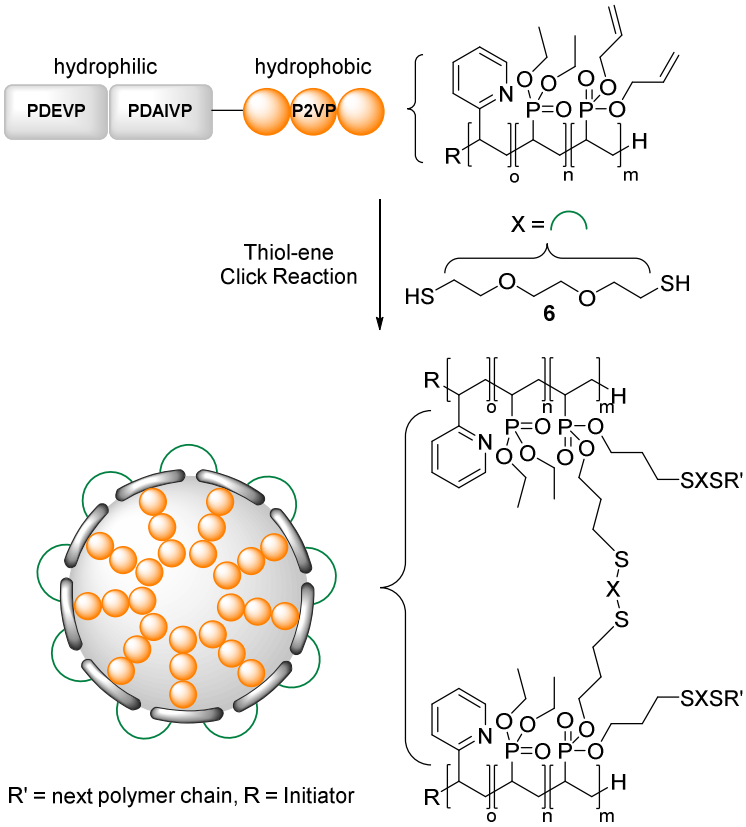

Scheme 2.19. Cross-linking of ABB' block copolymers (A: 2VP, B: DEVP, B': DAlVP) via thiol-ene click reaction with 3,6-dioxa-1,8-octanedithiol (**6**).[77] Reprinted with permission from Ref. [77]. Copyright 2018 The Royal Society of Chemistry.

Interestingly, the particle size showed strong dependence on the P2VP block length but was not affected by the PDEVP block.[77] The initial motivation and potential of poly(vinylphosphonate)-based delivery vehicles will be discussed in detail in section 2.2.3, as these nanoparticles represent the latest iteration of our nanocarriers.

Apart from thiol-ene chemistry, it is also feasible to perform polymer-analogous reactions with the phosphonate esters. Early studies of our group focused on the generation of poly(vinylphosphonic acid) (PVPA), which evidently is inaccessible via REM-GTP due to its acidic nature of the vinylphosphonic acid. One simple approach was the thermal treatment of both PDEVP and PDIVP which facilitated the cleavage of the ester functions (Scheme 2.20, top).[51] At 280-340 °C a sharp transition was found for PDEVP by thermogravimetric analysis with a mass loss that corresponds well to the release of ethylene as elimination product. Traces of ethanol and diethyl ether were detected by mass spectrometry as well. For PDIVP such a transition was observed after reaching a temperature of 245-270 °C, with propylene being the only cleavage product. Further heating to temperatures above 460-520 °C indicated the degradation of the polymer backbone. Hence, tempering of PDEVP and PDIVP at 350 °C for 30 minutes yielded PVPA.[51]

One alternative approach by *Wagner et al.* utilized trimethylsilyl bromide (TMSBr) as a mild cleaving agent in the saponification of PDIVP.[43] Accordingly, the approach was adopted for PDEVP: In a two-step process the ethyl ester was transferred into its TMS equivalent with TMSBr and subsequently hydrolyzed with acidified methanol to yield PVPA in high conversions. Moreover, it was possible to transesterify the silyl ester in the presence of tetrabutylammonium fluoride (TBAF) and an alkyl halide (Scheme 2.20, bottom).[51]

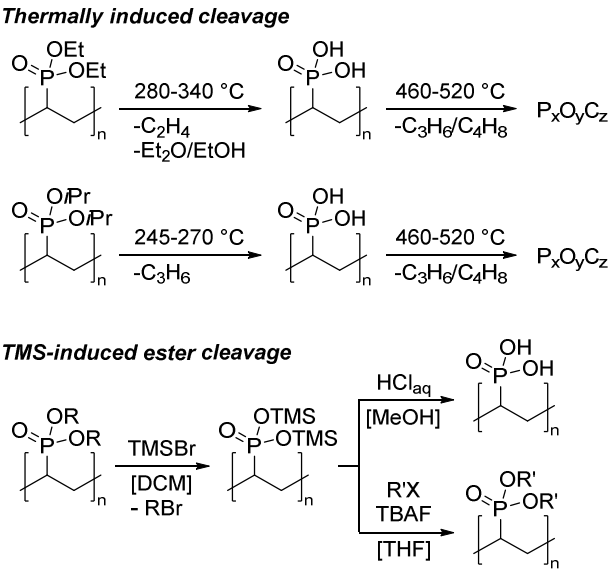

Scheme 2.20. Thermal treatment of PDEVP and PDIVP to PVPA and TMSBr-mediated formation of PVPA by hydrolysis or transesterification with TBAF and an alkyl halide.[51]

However, this route appeared impractical for a quantitative conversion of the ester functions as TBAF had to be added in stochiometric amounts relative to the ester motifs rendering the consecutive purification impossible.[51] Nevertheless, partial transesterification of the side chains with TMSBr, TBAF, and 1-(bromomethyl)pyrene proved to be a viable route towards fluorescent poly(diethyl vinylphosphonate)s (Scheme 2.21) with the polymerizations of these being initiated with 2,6-dimethyl-4-(4-vinylphenyl)pyridine (**4**). In the same fashion as described in chapter 2.2.1.2, the fluorescent derivatives were modified with thiocholesterol or folic acid and characterized with respect to their photophysical properties. Moreover, *in vitro* localization studies with the endothelial cell line HMEC-1 detected the conjugates at different positions in cells. While the folic acid conjugate was internalized into the cell, the cholesterol conjugate was found in the cell membrane.[78]

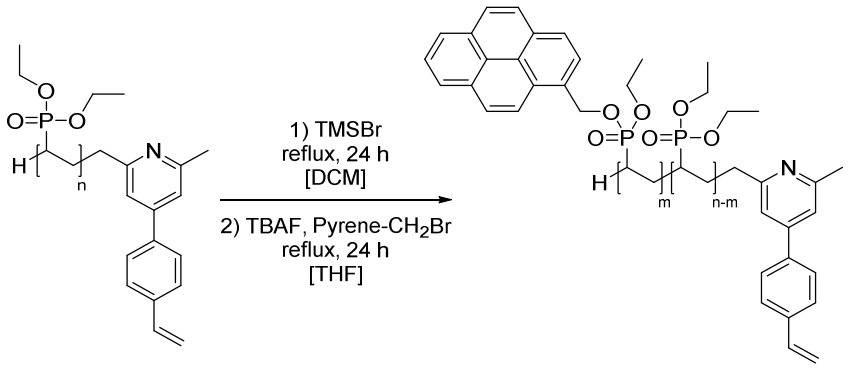

Scheme 2.21. Synthesis of fluorescent PDEVP via partial transesterification of the ethyl esters with TMSBr, TBAF, and 1-(bromomethyl)pyrene.[78] Reprinted with permission from Ref. [78]. Copyright 2018 John Wiley and Sons.

2.2.2 Thermoresponsive Behavior of Poly(vinylphosphonate)s

In combination with this set of different organic transformations, REM-GTP manifests as a facile method for the tailoring of complex materials with intrinsic material properties such as the pH-sensitivity of P2VP or the temperature-responsive behavior of PDEVP and complex biological moieties introduced by post-polymerization functionalization.

Basically, the complexity of the poly(vinylphosphonate)s is already reflected in their solution properties. While the hydrophilic poly(dimethyl vinylphosphonate) (PDMVP) dissolves almost exclusively in water, poly(di-*iso*-propyl vinylphosphonate) (PDIVP) favors organic solvents because of its hydrophobic *iso*-propyl groups. Between these two extremes PDEVP stands out due to its amphiphilic behavior and shows good solubility in both, water and organic solvents. As a result, PDEVP features a temperature-dependent solubility in aqueous media which is represented by its lower critical solution temperature (LCST). Upon reaching the cloud point T_c = 40-46 °C aqueous solutions of PDEVP exhibit a sharp and reversible transition.[17, 51, 53]

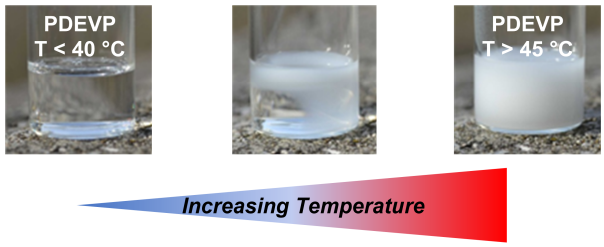

Figure 2.6. Phase transition of an aqueous PDEVP solution upon heating.[51]

The LCST of PDEVP can be affected by varying parameter such as the polymer concentration or the molecular weight. Higher concentrations result in a lower T_c and sharper phase transitions. Likewise, an increase of the molecular weight is accompanied by a decrease of the LCST.[51] Moreover, the cloud points of the poly(vinylphosphonate) can be precisely tuned in a temperature range from 5-92 °C via the statistical copolymerization of DEVP with DMVP or di-*n*-propyl vinylphosphonate (DPVP) in order to increase or decrease the LCST, respectively. Copolymers with DMVP as hydrophilic component result in higher cloud points while the incorporation of hydrophobic DPVP shows the opposing trend (Figure 2.7).[53]

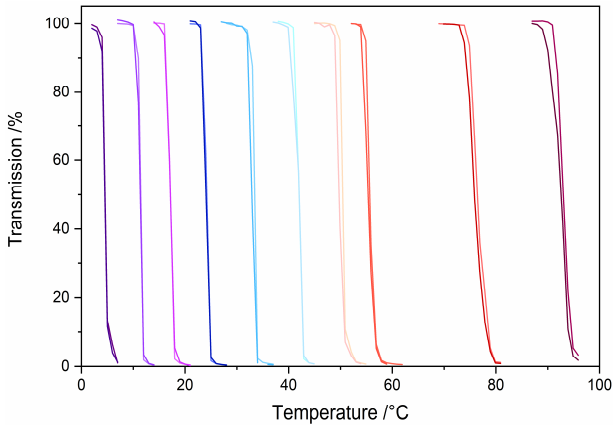

Figure 2.7. Determination of the cloud points of P(DEVP-DPVP) (0-35 °C), PDEVP (42 °C), and P(DEVP-DMVP) (50-95 °C) copolymers in aqueous solution (1.0 wt%).[17] Adapted with permission from Ref. [17]. Copyright 2016 American Chemical Society.

Interestingly, the hydrophobic as well as the hydrophilic copolymers showed a linear correlation between the measured LCST and the copolymer composition (Figure 2.8).[53]

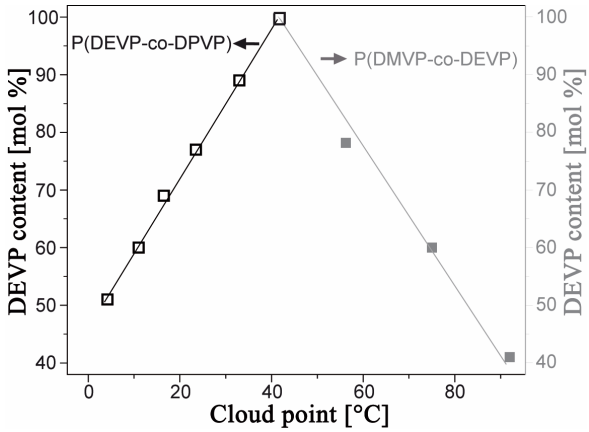

Figure 2.8. Linear dependence of the LCST from the polymer composition of P(DEVP-*co*-DPVP) and P(DEVP-*co*-DMVP).[53] Reprinted with permission from Ref. [53]. Copyright 2012 American Chemical Society.

A follow-up study took advantage of this dependence and generated micelles with a tunable LCST. In the same fashion as above, a hydrophobic P2VP section was combined with a thermoresponsive DAVP block for which DEVP was either copolymerized with DIVP or DMVP.[79]

This solution-dependent behavior can be explained by understanding the events that are taking place on the microscopic level. Below its cloud point the polymer chains exist as random coils in aqueous solution and are solvated by water. Upon reaching the cloud point the macromolecules perform a so-called coil-to-globule transition and precipitate in form of compact particles due to the release of the hydrating water molecules (Figure 2.9).[80]

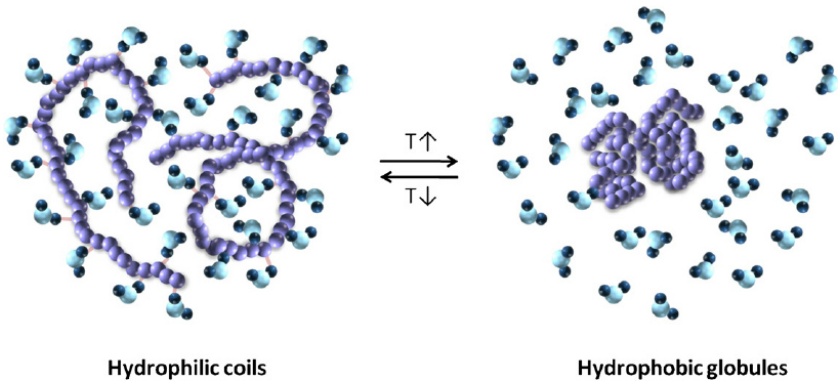

Figure 2.9. Illustration of the coil-to-globule transition of a thermoresponsive polymer.[80] Reprinted with permission from Ref. [80]. Copyright 2012 Elsevier.

Characterization of concentrated solutions of PDEVP in water (30 wt%) via dynamic scanning calorimetry (DSC) corroborated such a transition. During heating a pronounced endothermic transition was observed which was associated with a break-up of the hydrogen bonds between water and the solubilized polymers. On the contrary, cooling of the polymer solution was accompanied with an exothermic process.[53]

With respect to a potential application of poly(vinylphosphonate)s in biological and biomedical areas the solubilizing media (blood plasma, cell media) usually contain salts and buffers as additives. Hence, the phase transition of P(DEVP$_{0.89}$-*co*-DPVP$_{0.11}$) was investigated in the presence of either phosphate-buffered saline (PBS), fetal calf serum (FCS) or sodium chloride and calcium chloride. Exemplarily for sodium chloride, a decreased cloud point T_c was observed which originates from a salting-out effect because the polymer chains are partially dehydrated leading to a decrease by as much as 3 °C (c_{NaCl} = 0-10 mg mL^{-1}).[53, 81]

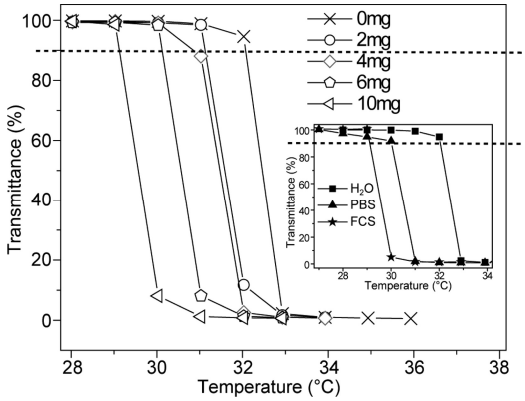

Figure 2.10. Determination of the LCST of P(DEVP$_{0.89}$-co-DPVP$_{0.11}$) (1.0 wt%) in aqueous solution at different NaCl concentration upon heating. Inset: Determination of the cloud points of P(DEVP$_{0.89}$-co-DPVP$_{0.11}$) (1.0 wt%) in deionized water, PBS, and FCS medium upon heating.[53] Reprinted with permission from Ref. [53]. Copyright 2012 American Chemical Society.

2.2.3 Application of Poly(vinylphosphonate)s in Drug Delivery

In this context it seemed natural to incorporate poly(vinylphosphonate)s in stimuli-responsive drug delivery vehicles. With the motivation to create such multi-responsive nanocarriers our group took advantage of the living character of REM-GTP and developed novel BAB block copolymers from 2VP and DEVP.[64] Intriguingly, these copolymers formed stable and highly defined micelles in water as shown by DLS and transmission electron

microscopy (TEM). The loaded micelles also revealed a strong response towards a lower pH and elevated temperatures in release experiments with fluorescein (Figure 2.11, left) and proved to be very attractive for the delivery of anti-cancer agents. Due to that reason the uptake of the micellar carriers into HeLa cells was conducted. Incubation of the cells with Nile red-loaded micelles gave proof for the internalization and the cargo release from the micelles as these experiments demonstrated a cytosol-located fluorescence (Figure 2.11, right) which was caused by the interaction of Nile red with free cytosolic lipids.[64, 82]

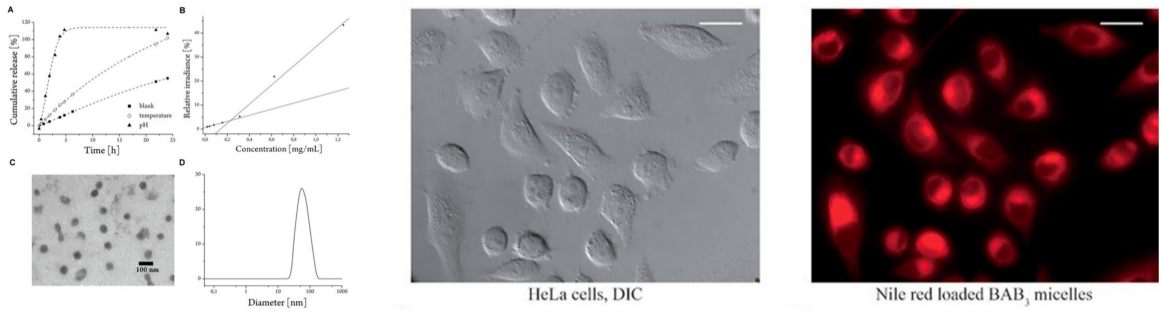

Figure 2.11. Exemplary illustration of the micelle properties (cumulative release under varying conditions, determination of the CMC, TEM image and DLS measurement) (left) and studies on the cellular uptake of Nile red-loaded micelles (right).[64] Reprinted with permission from Ref. [64]. Copyright 2016 John Wiley and Sons.

Moreover, cell viabilities studies substantiated the micelles to be highly biocompatible even at a concentration of 1 mg mL^{-1} of the non-loaded micelles. In subsequent localization studies HeLa cells were treated with doxorubicin (DOX)-loaded micelles and revealed the doxorubicin-associated fluorescence in the cytosol. After longer incubation times doxorubicin was also co-localized in the nuclei (Figure 2.12, left). Cell viability assays with DOX-loaded micelles corroborated these findings since considerably lower cell viabilities were observed for the DOX-loaded carriers compared to non-encapsulated doxorubicin (Figure 2.12, right).[64]

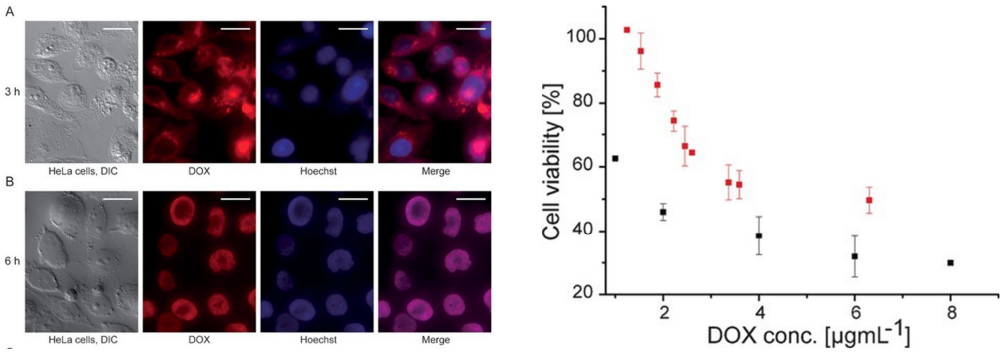

Figure 2.12. Co-localization studies of DOX-loaded micelles after 3 h and 6 h of incubation with HeLa cells (left) and cell viabilities of DOX-loaded micelles (■) in comparison to non-encapsulated doxorubicin (■) (right).[64] Reprinted with permission from Ref. [64]. Copyright 2016 John Wiley and Sons.

As a matter of fact, micelles form in a concentration-dependent manner and might lose their therapeutic efficacy as they are subjected to a high dilution after intravenous injection. Consequently, the micellar carriers can degrade and release their cargo prior to reaching the site of disease.[83, 84] To avoid such an issue our group designed covalently cross-linked nanocarriers. For that purpose, DAlVP as a third block was introduced which enabled a transformation of the unimers to stable, monodisperse particles (compare chapter 2.2.1.3, Scheme 2.19). In a

similar manner to the BAB micelles, release studies were performed with the nanoparticles under varying pH and temperature levels. The cumulative release of fluorescein from the carrier vehicles was improved significantly compared to neutral conditions at room temperature.

Cell viability assays with MCF-7 and HeLa cell lines tested the toxicity of unloaded carriers as control experiments and their DOX-loaded equivalents. For each cell type a composition-dependent toxicity was observed as the nanoparticles featuring a 1:1 ratio (2VP/DEVP = 1/1) were less toxic than the nanoparticles comprising a 1:2 ratio (2VP/DEVP = 1/2). The treatment of the cells with the DOX-loaded carriers substantially decreased the cell growth at higher levels of doxorubicin (Figure 2.13).[77]

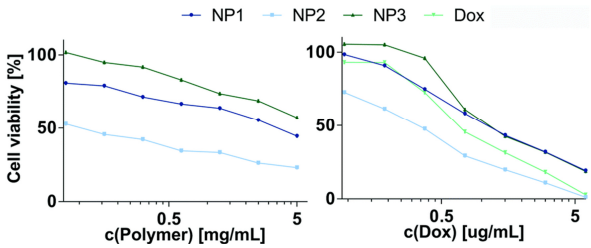

Figure 2.13. Cell viability of MCF-7 cells after 24 h of incubation with the non-loaded (left; 0.08-5.00 mg mL^{-1}) and the DOX-loaded samples (right; 0.09-6.00 µg mL^{-1}).[77] Reprinted with permission from Ref. [77]. Copyright 2018 The Royal Society of Chemistry.

Fluorescence microscopy imaging localized the loaded nanocarriers at the nucleus of the MCF-7 cells after only one hour (Figure 2.14, A). Same results were also obtained with HeLa cells. Additionally, both cell lines were incubated with PBS, free doxorubicin or the loaded carriers and analyzed via fluorescence activated cell sorting (FACS) to obtain a statistical insight on the uptake dynamics. Already after 10 minutes a slight shift of the fluorescence curves was seen which indicated the successful uptake of the nanoparticles by the cells (Figure 2.14, B). Flow cytometry measurements including a three-hour incubation period detected an elevated uptake level according to the increases in the doxorubicin fluorescence.[77] For MCF-7 cells the uptake level of the nanoparticles after 10 minutes and three hours is illustrated in Figure 2.14, C.

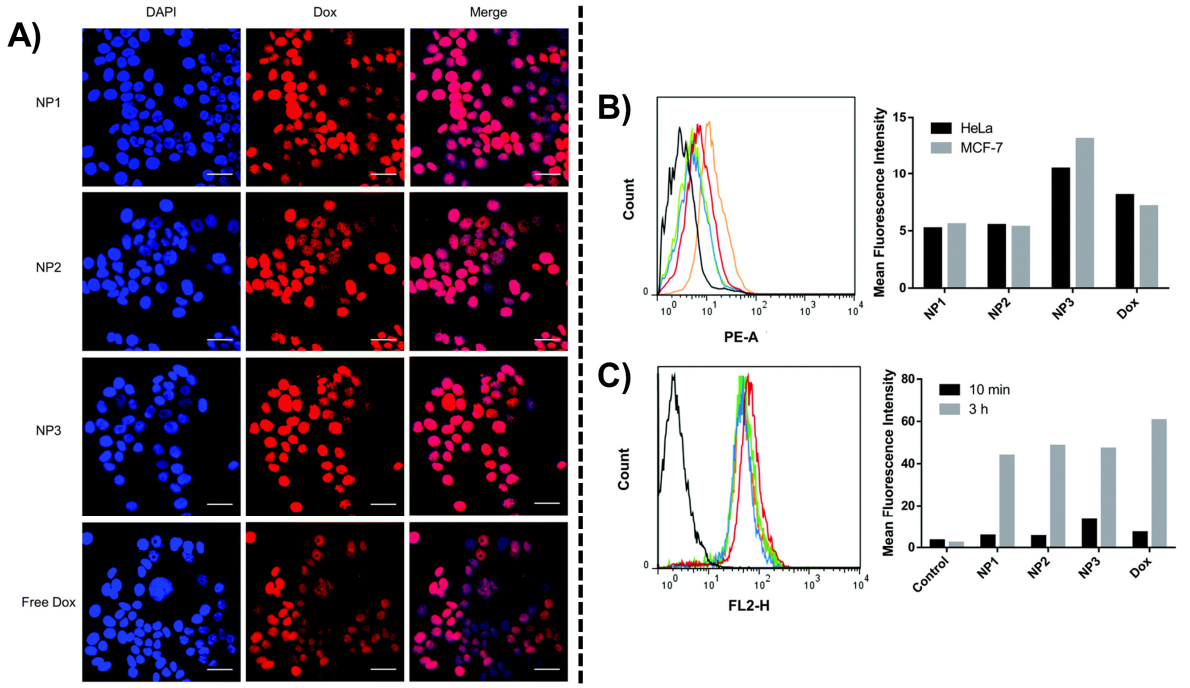

Figure 2.14. Images of MCF-7 cells after incubation with the loaded nanoparticles and DOX for 1 h at 37 °C taken by fluorescence microscopy (left). Mean fluorescence intensities (MFI) of MCF-7 cells incubated with PBS (black), DOX (red) and the loaded nanoparticles (blue, green, orange) and a comparison of MFIs of HeLa and MCF-7 cells after incubation for 10 minutes at 37 °C (right).[77] Reprinted with permission from Ref. [77]. Copyright 2018 The Royal Society of Chemistry.

2.2.4 Copolymers derived from Poly(dimethylsiloxane)-based Macroinitiators

As presented in chapter 2.2.3, REM-GTP represents a facile tool to form defined block copolymers but is limited to the application of α,β-acceptor-type monomers. However, the incorporation of non-*Michael*-type polymers such as poly(dimethylsiloxane) (PDMS) might yield novel materials with unprecedented properties as PDMS itself features a set of unique qualities due to its Si-O-Si linkage.[85] A high bond energy of 452 kJ mol^{-1} adds to an impressive thermal stability and renders silicone networks chemically inert.[86] Silicones exhibit low glass transitions temperatures T_g and very flexible polymer chains as the Si-O bond length (1.64 Å) is increased (compared to the C-O analogue (1.43 Å)). Moreover, a low torsion potential as well as an elevated Si-O-Si bond angle of 143° are experimentally verified.[85, 87] On a macroscopic scale these properties translate into a high hydrophobicity,[88, 89] unparalleled surface-active properties,[85, 87, 90] and a good biocompatibility.[88, 91] Hence, a diversity of application fields emerged, ranging from antifoaming agents[92] and medicinal uses,[93, 94] to soft lithography[95, 96] and the use in microfluidic devices.[97]

Driven by these positive characteristics, a plurality of studies reports on the incorporation of PDMS into novel copolymers. This can be achieved, e.g. via polymer-polymer conjugations or with PDMS used as a macroinitiator for polymerization reactions. Polymer-polymer conjugations on the one hand can be performed by using efficient reactions such as thiol-ene click reactions,[98, 99] copper-free azide alkyne click couplings,[100] or hydrosilylation.[101, 102] On the other hand, ATRP represents the most widely used approach for which PDMS is usually functionalized with 2-bromo-2-methylpropanoyl bromide via condensation (Scheme 2.22, top).[103, 104] The modification of H-terminated PDMS via a hydrosilylation reaction represents a viable route as well (Scheme 2.22, bottom).[105]

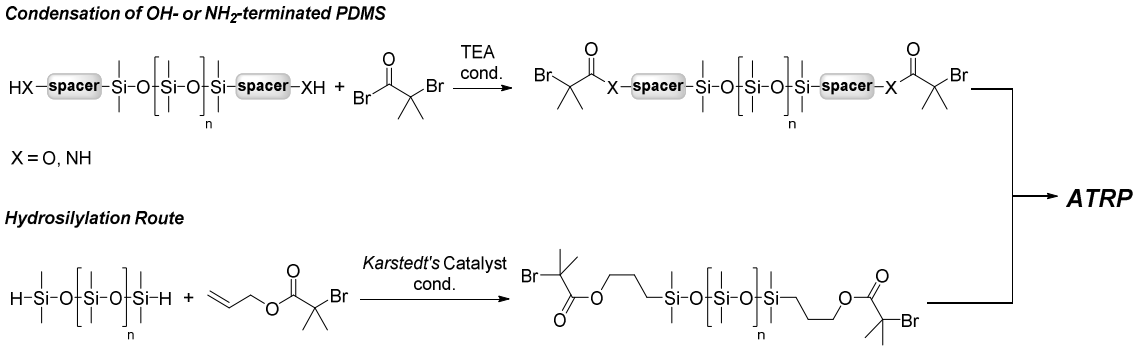

Scheme 2.22. Preparation of PDMS macroinitiators for ATRP via condensation (top) or hydrosilylation (bottom).[103-105]

Khoshdel et al. used this approach to generate copolymers from MMA, which exhibited microphase separation, or 2-dimethylaminoethyl methacrylate, that resulted in water-dispersible PDMS,[105] while the group of *Soucek* polymerized 2-hydroxyethyl methacrylate to form macromolecules with a controlled microstructure.[103] *He* and co-workers generated defined triblock copolymers via ATRP of *N*,*N*-dimethylacrylamide. Modification of these copolymers with allylamine allowed the cross-linking with Si-H-bearing PDMS yielding amphiphilic co-networks with an excellent oxygen permeability and a good water uptake, thus being promising candidates for coatings for islet encapsulation.[106] *Lyall et al*. were able to generate diblock copolymers comprising a PEG-fluoroalkyl-modified polystyrene compound to produce fluorine-containing coatings and evaluate their performance regarding fouling release with *Ulva linza* macroalgae.[107] Apart from ATRP other polymerization techniques are equally viable. *Gonsalves et al.* simply employed α,ω-hydroxypropyl-terminated PDMS in the ROP of L-lactide with $Sn(Oct)_2$.[108] Moreover, the controlled copolymer synthesis via ROP of ε-caprolactone using triethylaluminum as catalyst was possible. Depending on the structure of the PDMS substrate used a variety of copolymer topologies were realized.[109] A rather exotic approach was taken by *Pla* and co-workers who developed a synthetic strategy towards PA12-*b*-PDMS-*b*-PA12 copolymers (Scheme 2.23). Hydroxyl-terminated PDMS was converted with 4,4'-methylene diphenyl diisocyanate into the respective PDMS-diisocyanate and reacted with two equivalents of ε-caprolactam.[110] This macroinitiator was used in the anionic ROP of lauryl lactam to produce a variety of block copolymers. It was shown that the content of the soft and the hard block affected the thermal properties drastically.

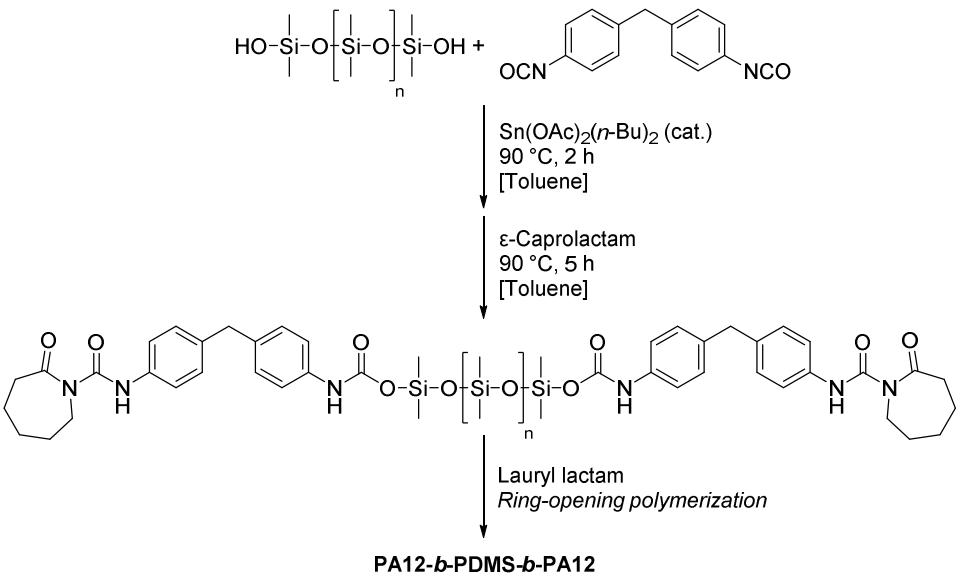

Scheme 2.23. Synthesis of the PDMS macroinitiator modified with terminal ε-caprolactam motifs for the generation of PA12-*b*-PDMS-*b*-PA12 copolymers.[110]

By turning PDMS into the respective silyl ketene acetal, also GTP becomes accessible (Scheme 2.24).[111] Exemplarily, *Johnston et al*. used such an initiator in the GTP of *tert*-butyl methacrylate which was hydrolyzed into the free methacrylic acid derivative. These copolymers were investigated as stabilizing agent for dispersion polymerizations in supercritical CO_2.[112]

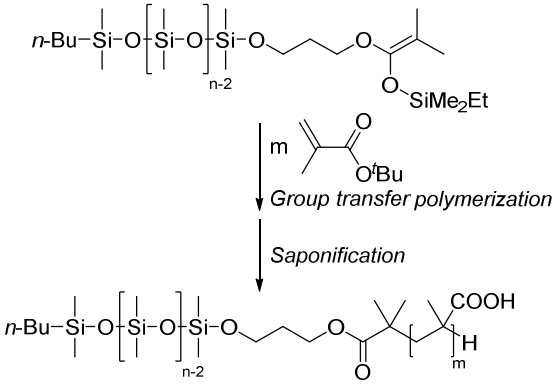

Scheme 2.24. Synthesis of a PDMS-poly(methacrylic acid) block copolymer starting from a GTP macroinitiator.[111]

3 Aim of this Thesis

In 2010 *Rieger* and co-workers succeeded in the generation of high molecular-weight PDEVP via REM-GTP using lanthanide-based polymerization catalysts.[50] Since this breakthrough, the polymerization process of vinylphosphonates[51, 52, 54, 56] as well as their material properties were investigated in detail.[53] Through the knowledge gained in these studies, more application-oriented studies were performed as poly(vinylphosphonate)s exhibit intriguing material features. Hence, their application was tested in form of particular drug delivery vehicles,[64, 77, 79] flame-retardants,[113] for surface modifications[114, 115] or macromolecular delivery probes.[74, 78] The latter studies focused on the functionalization of the poly(vinylphosphonate)s with thiocholesterol and folic acid to facilitate the selective delivery of the polymer conjugates to certain cell compartments. This was achieved by the incorporation of a tailored initiator, resulting in PDEVP with a terminal vinyl group. However, this functionalization approach was limited to thiol-ene chemistry which is why several target structures were envisioned as potential initiating substrates to make this functionalization approach more versatile (Figure 3.1). Therefore, the introduction of hydroxyl, amino or thiol groups via the initiator is targeted. However, since lanthanide complexes used in the REM-GTP show high sensitivity towards protic moieties, the initiators **7-9** need to bear protective groups. Hence, *tert*-butyldimethylsilyl (TBDMS) (**7**), trityl (**8**), and 2,5-dimethylpyrrole (**9**) motifs are chosen for the masking of the reactive moieties because simple deprotection procedures are reported for these groups (Figure 3.1).

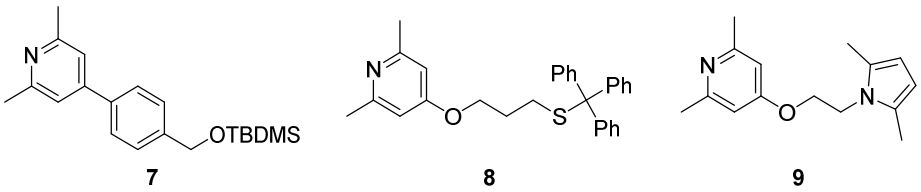

Figure 3.1. Target structures of the functional group-bearing initiators **7-9**.

These structures shall first be investigated as C-H bond activation substrates with $Cp_2Y(CH_2TMS)(THF)$ (**2**) and subsequently be employed in the polymerization of DEVP to obtain PDEVP with the respective end-group (Figure 3.2). A careful evaluation of the C-H bond activation and the initiators' capabilities in REM-GTP is then required to ensure a selective incorporation of the initiator as end-group and the formation of defined polymers.

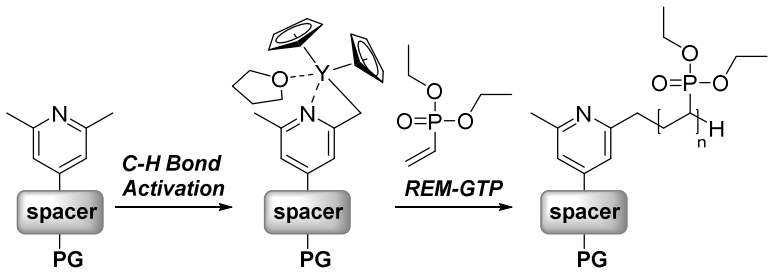

Figure 3.2. Schematic illustration of the C-H bond activation of the functional initiators and REM-GTP of DEVP.

As presented in Figure 3.3 the end-groups need to be deprotected to release the reactive OH, SH or NH_2 moieties for the use in the post-polymerization functionalizations. Hence, the reaction conditions must be optimized to ensure a quantitative removal of the protective groups followed by a detailed analysis of the polymer integrity. Eventually, it is the goal to modify these polymers with model compounds such as cholesteryl chloroformate or *N*-phenyl maleimide. Consequently, the covalent linkage of the polymers and the small electrophiles has to be evaluated to prove the availability of this synthetic strategy.

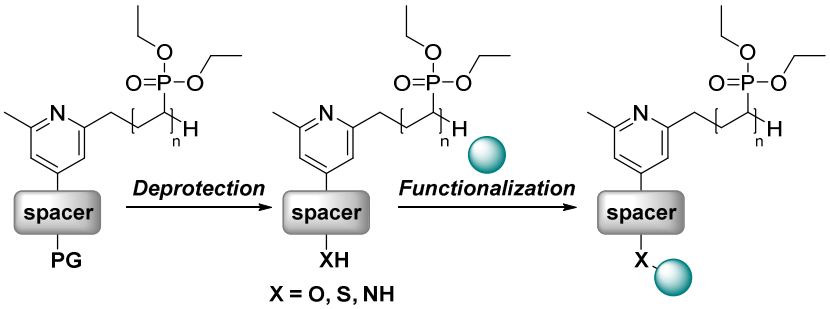

Figure 3.3. Strategy for the functionalization of PDEVP by removing the protection groups and re-functionalization with an electrophilic test substrate.

In case that the C-H bond activation process turns out be resilient towards these kinds of functional groups, a follow up study aims for the application of macromolecule-sized initiators because the initiating process of REM-GTP has only been studied with low-molecular weight substrates so far. Since PDEVP represents a hydrophilic polymer type, the combination with PDMS as hydrophobic counterpart appears especially attractive as such a copolymer system might feature a set of unprecedented surface-active properties. Moreover, PDMS is already a frequently used component in biomedical applications. Hence, to accomplish this task, the PDMS substrates have to be made accessible to σ-bond metathesis. Therefore, it is planned to modify commercially available Si-H-bearing PDMS with 4-(allyloxy)-2,6-dimethylpyridine (**10**) via hydrosilylation (Figure 3.4). These substrates shall then be employed in the C-H bond activation experiments with $Cp_2Y(CH_2TMS)(THF)$ (**2**). Afterwards a detailed analysis of the reaction products is required to verify the conversion of the initiating units and the selectivity of this process (Figure 3.4).

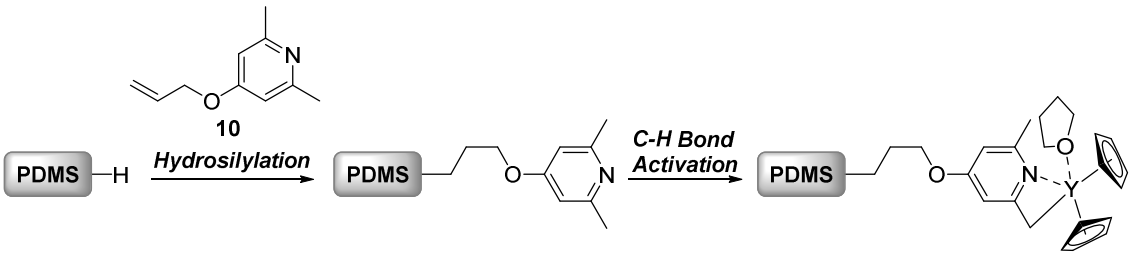

Figure 3.4. Generation of the macro-sized initiators using H-terminated PDMS and precursor (**10**) and investigation of these substrates in the C-H bond activation with $Cp_2Y(CH_2TMS)(THF)$ (**2**).

The subsequent polymerization experiments with the macroinitiators shall generate a library of copolymers. Hence, various PDMS feedstocks are employed to adjust the length of the hydrophobic core as well as the copolymer topology and different monomer feeds of DEVP. Moreover, the versatility is investigated by using 2VP as an alternative *Michael*-type monomer and by performing the ring-opening polymerization of εCL (Figure 3.5).

These new materials have to be examined with respect to their solution behavior as well as their thermal properties to obtain basic insights into the material features.

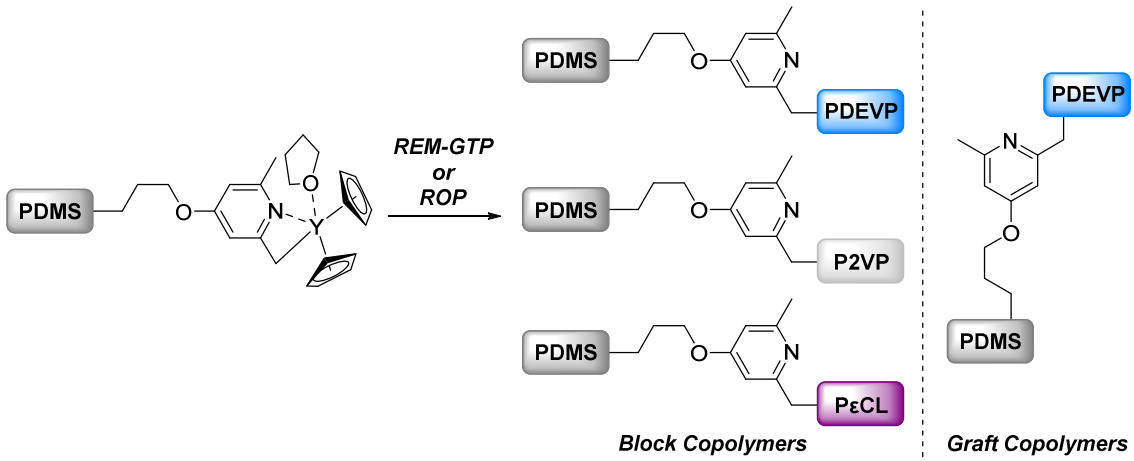

Figure 3.5. Application of the activated macroinitiators in the REM-GTP of DEVP or 2VP and ROP of εCL.

Likewise to PDEVP-*b*-P2VP-*b*-PDEVP, PDEVP-*b*-PDMS-*b*-PDEVP copolymers are suspected to form micelles in water. Initial studies by our group substantiated these P2VP-based copolymers to be promising candidates as delivery vehicles of anti-cancer agents.[64] But owing to the fact that micelle formation occurs in a concentration-dependent manner, an unspecific cargo release is highly probable upon an intravenous injection. To optimize these carriers for systemic applications, this foundation concluded in the generation of stable nanoparticles based on ABB' (A: 2VP; B: DEVP; B': DAlVP) block copolymers.[77] The introduction of an additional DAlVP block allowed the cross-linking of the allyl shell with a dithiol via thiol-ene click chemistry. Initial characterizations of the products by DLS, TEM and surface tension measurements corroborated stable, monodisperse nanoparticles. Subsequent release studies with fluorescein concluded a considerably faster release at elevated temperature and pH levels compared to standard conditions. The positive characteristics were underlined by good cell viabilities for MCF-7 cells after incubation with the non-loaded particles. Accordingly, the cell viabilities decreased tremendously after treatment of the MCF-7 cell lines with doxorubicin-loaded particles. Imaging by fluorescence microscopy supported these observations since the loaded nanocarriers were localized in the cell interior after incubation. In addition, FACS analysis provided a statistical view on the cell uptake of the loaded particles.

Hence, it seems logical to unite both main features, the BAB copolymer architecture and the shell cross-linking, in one carrier system. To guarantee a better comparability of the ABB' nanoparticles, which were produced with the mononuclear species **3**, with the desired B'BABB' pendants a binuclear Cp_2Y-based catalyst **11** has to be used. Accordingly, the activation of TMPy has to be evaluated with respect to its kinetic behavior (TOF), initiator efficiencies *IE*, and the selective formation of a binuclear species. With a properly defined catalyst a plethora of copolymers comprising different feed compositions will be generated to control the particle size and the cross-linking density (Figure 3.6).

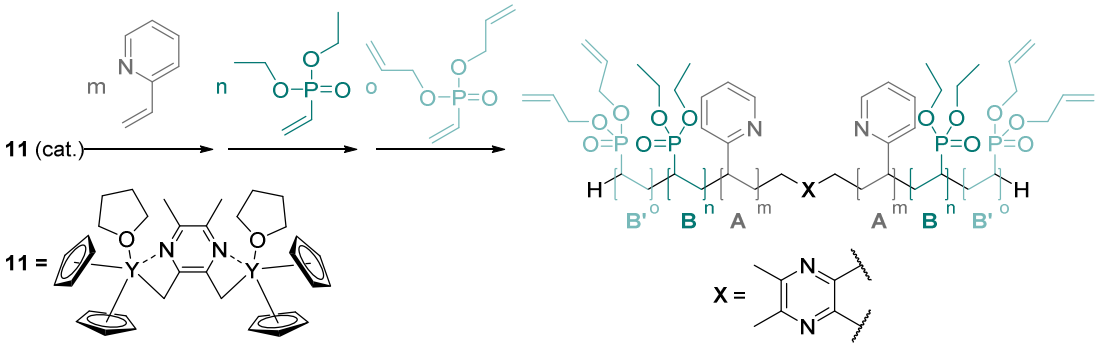

Figure 3.6. Synthesis of B'BABB' block copolymers (A: 2VP; B: DEVP; B': DAlVP) with binuclear catalyst **11**.

After determination of the fundamental polymer properties like the molecular weights M_n and the corresponding mass distributions $Đ$, the copolymers are subjected to the shell cross-linking procedure in the next step via thiol-ene click chemistry (Figure 3.7, left pathway).

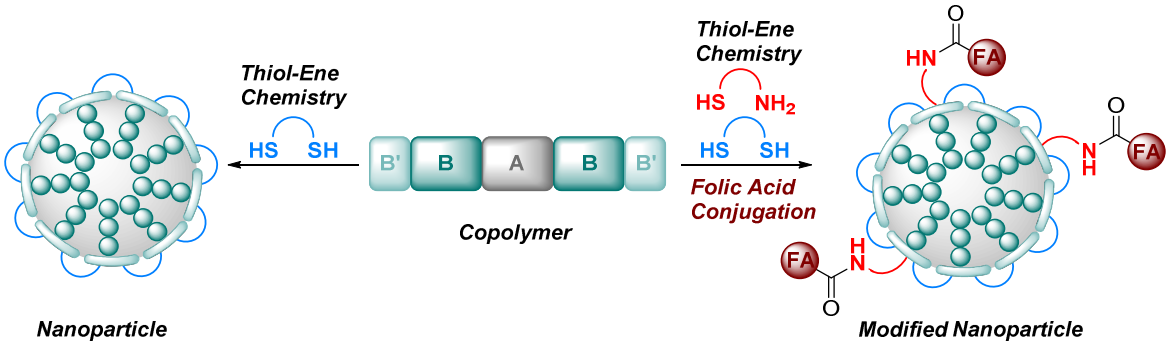

Figure 3.7. Cross-linking of the B'BABB' block copolymers with dithiols and synthetic route towards folic acid modified nanoparticles.

Because a significant influence of the zeta potential ζ on the pharmacokinetics is reported in the literature, three dithiols with varying polarities are tested to potentially tune ζ. All nanoparticles have then to be evaluated according to their spatial features, stability in solution, and their release behavior under varying conditions. Taking into account that these nanocarriers are passive drug delivery vehicles, a synthetic strategy shall be envisioned to introduce targeting ligands selectively and develop a system for active drug delivery. This complex task can be accomplished by turning the cross-linking procedure into a two-step process by coupling cysteamine first followed by the saturation of the remaining allyl groups with the dithiol (Figure 3.7, right pathway). In theory, the superficial amino groups can be reacted with an activated folic acid derivative. Besides the size-related characterization, it is of utmost importance to confirm the covalent conjugation of folic acid to the particle.

On the basis of these studies a comprehensive view on the versatility of the initiation process as well as a diversification of the existing post-polymerization functionalization strategies of GTP-polymer can be achieved.

4 From Lanthanide-mediated, High-Precision Group Transfer Polymerization of *Michael*-type Monomers, to Intelligent, Functional Materials

4.1 Bibliographic Data

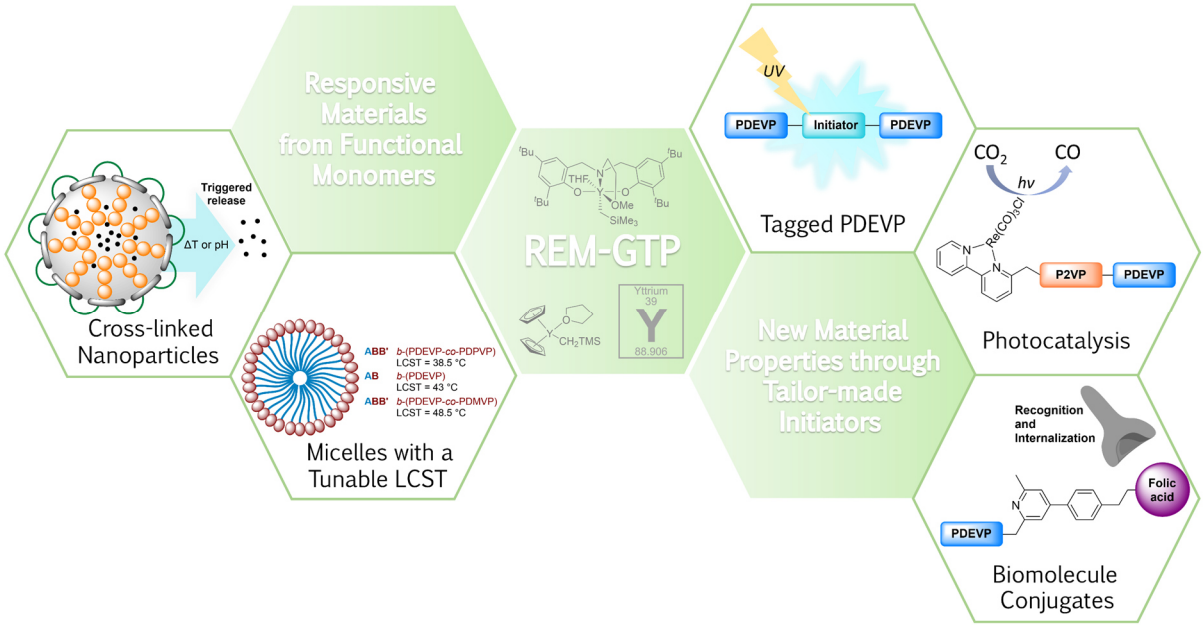

Title: "From Lanthanide-mediated, High-Precision Group Transfer Polymerization of *Michael*-type Monomers, to Intelligent, Functional Materials"

Status: Feature article, accepted 22nd November 2019

Journal: European Polymer Journal, 2020, 122, 109385

Publisher: Elsevier

Link/DOI: https://www.sciencedirect.com/science/article/pii/S0014305719313023

Authors: Andreas Schaffer, Michael Weger, and Bernhard Rieger[a]

[a]Andreas Schaffer conceptualized the structure and content of the article. Andreas Schaffer and Michael Weger wrote the manuscript. All work was carried out under supervision of Bernhard Rieger.

4.2 Summary

Smart polymers are increasingly attracting notice in the scientific community as these materials are able to respond to a set of external stimuli, such as changes in temperature or pH, irradiation with light or mechanical stress. Many of these materials are based on functional α,β-unsaturated monomers. For the precise polymerization of these substrates a wide range of catalytic systems has already been established. In this feature article, special notice was put on the rare earth metal-mediated group transfer polymerization (REM-GTP) which is a well-known polymerization technique for the fast and controlled conversion of (meth)acrylates. *Rieger* and co-workers were able to expand the scope of this method towards new *Michael*-type monomers, like the temperature-responsive DEVP but also 2VP with new rare earth metal-based complexes.

With this foundation of REM-GTP catalysts, the synthesis of defined macromolecular materials with newly introduced smart functions as well as the combination of different functional monomers were rendered possible.

Copolymers comprising 2VP and DEVP were found to be promising candidates as dual-responsive drug-delivery vehicles, while exhibiting high biocompatibility during cytotoxicity screenings and *in vitro* studies. Moreover, a novel initiation approach allowed the post-polymerization functionalization of PDEVPs and gave access to polymer-biomolecule conjugates which were studied as polymeric fluorescent markers. These two features were combined in the generation of P(DEVP-*co*-2VP) with a tailor-made bipyridine initiator. This end-group facilitated the complexation of $Re(CO)_5Cl$, resulting in a photocatalytically-active copolymer.

4.3 Manuscript

European Polymer Journal 122 (2020) 109385

Contents lists available at ScienceDirect

European Polymer Journal

journal homepage: www.elsevier.com/locate/europolj

From lanthanide-mediated, high-precision group transfer polymerization of *Michael*-type monomers, to intelligent, functional materials

Andreas Schaffer, Michael Weger, Bernhard Rieger*

Wacker Chair of Macromolecular Chemistry – Technical University of Munich, Lichtenbergstrasse 4, 85748 Garching, Germany

ARTICLE INFO

Keywords:
REM-GTP
Smart materials
Poly(vinylphosphonates)
Drug delivery
Polymer functionalization
Photocatalysis

ABSTRACT

A wide range of catalytic systems is already established for the precise polymerization of functional α,β unsaturated monomers. The rare earth metal-mediated group transfer polymerization (REM-GTP) represents a well-known method which not only enables the fast and controlled conversion of (meth)acrylates, but also of other *Michael*-type monomers, like the stimuli-responsive 2–vinylpyridine (2VP) and dialkyl vinylphosphonates (DAVP). The next step is to connect and combine the defined macromolecules with smart functions. This feature article is focused on the recent application-oriented advances in the fields of 2VP/DAVP (co)polymers synthesized with REM-GTP catalysts. On the one hand, these copolymers function as dual-responsive drug-delivery vehicles, while exhibiting high biocompatibility during cytotoxicity screenings and *in vitro* studies. On the other hand, post-polymerization functionalization of PDAVPs allows access to polymer-biomolecule conjugates and polymeric fluorescent markers. Combing these two features, p(DEVP-*co*-2VP), polymerized with a tailor-made initiator, facilitated the complexation of a rhenium compound, resulting in a photocatalytically-active copolymer.

1. Introduction

Functional polymers form - due their specific chemical groups - the basis for new and smart materials with enhanced properties. Synthesizing these types of polymers requires the precision and control with regard to composition, microstructure and molecular weight. Among several approaches, the group transfer polymerization (GTP), a subgroup of the coordinative-anionic type, is a predestined method for the precise and efficient (co)polymerization of functional α,β unsaturated monomers. The silyl ketene acetal (SKA)-initiated GTP including an additional catalyst was discovered back in 1983 by *DuPont* scientists [1]. The name originates from the initially-postulated associative propagation mechanism which was more recently questioned with different key experimental evidences while maintaining the term [2–4]. About ten years later, *Yasuda et al.* presented neutral trivalent samarocenes for the polymerization of methyl methacrylate (MMA) acting as both initiator and catalyst [5]. The dimeric $[Cp^*_2SmH]_2$ is broken up by the coordination of the first monomer molecule, and initiates the polymerization process through a nucleophilic transfer of the hydride onto the C—C double bond of MMA. This is followed by the conjugate addition of the resulting ester enolate to a second MMA coordinated to the samarium center, giving rise to the eight-membered-chelate propagating species which was confirmed by an X-ray crystal structure. In this way, the so-called "rare earth metal-mediated" (REM) GTP was constituted, and this forms our focus in this feature article.

As the living behavior of the REM-GTP enables the synthesis of high-molecular weight and well-defined (co)polymers, a wide range of further lanthanide catalysts was established after the seminal work of *Yasuda et al.* These non-bridged lanthanocenes, with varying ligand design and central metals, extended the scope of monomers and polymer architectures [6–13]. The synthesis of the applied lanthanide compounds can be achieved by a salt metathesis route, which is the classical strategy in metalorganic chemistry (Scheme 1). Additionally, lanthanide complexes can undergo C—H bond activation which is a convenient pathway, less prone to side reactions [14]. This [2σ + 2σ] cycloaddition permits to incorporate alkynes and heteroaromatic compounds which render improved initiator efficiencies, multiblock copolymers and star-shaped polymers [12,15–17].

To address the stereospecificity of the REM-GTP, bridged lanthanocenes were introduced to the REM-GTP. A well-chosen ligand design leads to the production of highly syndio- as well as isotactic poly(meth) acrylates [18–21]. Furthermore, non-metallocenes have attracted more and more attention since lanthanocenes displayed insufficient activity towards other *Michael*-type monomers like 2-vinylpyridine (2VP) [16,22,23]. With newly developed (bisphenolate) yttrium catalysts, it was possible to achieve a high degree of isotacticity for P2VP [24–26].

* Corresponding author.
E-mail address: rieger@tum.de (B. Rieger).

https://doi.org/10.1016/j.eurpolymj.2019.109385
Received 27 June 2019; Received in revised form 20 November 2019; Accepted 22 November 2019
Available online 27 November 2019
0014-3057/

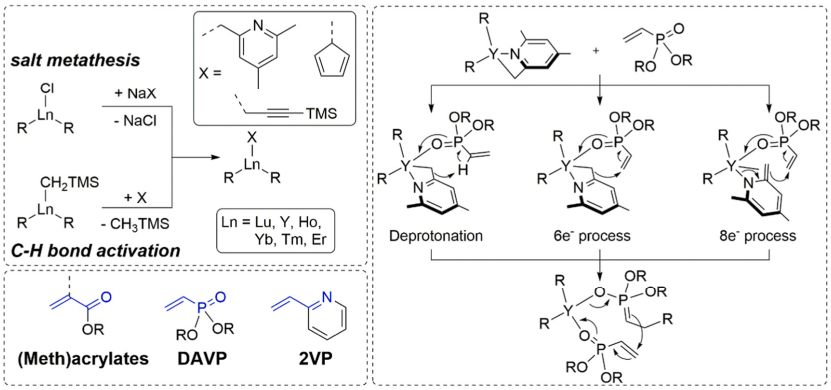

Scheme 1. Overview of the possible synthesis routes for lanthanide GTP catalysts (top left), the structural analogy of DAVP and 2VP to (meth)acrylates (bottom left) and the GTP mechanism by the example of a yttrium(*sym*-collidinyl) catalyst and DAVP (right).

2VP, as well as dialkyl vinylphosphonates (DAVP), are very interesting monomers for the synthesis of functional materials, due to the stimuli-responsivity of their polymers. The hydrophobic P2VP demonstrates a pH-dependent solubility, whereas the hydrophilic PDAVPs are known for their thermoresponsive behavior with a widely tunable lower critical solution temperature (LCST) in water [27,28]. The precise polymerization of these monomers is an indispensable requirement for the synthesis of functional materials. Hence, the initiation - as well as the propagation mechanism and the influence of metal center and ligand on the REM-GTP of DAVP - was investigated in greater detail [14,29,30]. The studies revealed that the initiation reaction occurs through a six- or eight-electron nucleophilic addition of the initiator ligand or through unwanted deprotonation of the α-acidic monomers while the propagation follows a *Yasuda*-type monometallic and living process (Scheme 1). Additional copolymerization investigations determined the relative coordination strength to the lanthanide center of DEVP to be stronger than for 2VP [31]. Based on this preliminary work, drug delivery vehicles consisting of 2VP/DAVP copolymers and new methods for the post-polymerization functionalization of PDAVPs were developed in our group, which we would like to highlight here.

2. Smart materials based on high-precision polymers

2.1. Drug delivery vehicles

Conventional cancer therapies such as radiation or chemotherapeutic approaches are usually accompanied by adverse effects causing damage to healthy tissue, and toxicity to the patient [32,33]. Drug delivery vehicles in the form of engineered nanoparticles emerge as promising candidates to overcome these issues. The incorporation of pharmacologically active agents in such nanosized drug carriers can substantially increase the bioavailability and prevent clearance via liver and/or kidneys. The delivery of encapsulated drugs can furthermore benefit from the enhanced permeability and retention (EPR) effect, resulting in reduced toxicity and higher drug concentrations at the site of the disease. While oral administration is hampered due to reduced absorption, intravenous administration of the hydrophobic agent also requires formulation with solubilizing agents such as ethanol, causing additional toxic side effects. Both issues can be addressed by incorporation of these agents in a nanoparticular system [32–36]. Additionally, the protection of the drug from harsh environments leading to prolonged circulation times should be mentioned, controlled release of the cargo and co-delivery of multiple drugs [32,37].

In the following we want to focus on polymer-based drug carriers that can be generated from copolymers comprising a block structure (AB diblock or BAB triblock copolymer) with a hydrophilic shell and a hydrophobic core. They usually manifest as micelles, since these polymers are able to self-assemble into micellar structures in an aqueous environment [35]. Recent advancements in this field have established stimuli-sensitive polymers for more sophisticated nanocarriers, enabling the triggered release of the encapsulated cargo caused by external stimuli. Consequently, stimuli-sensitive carriers could exploit naturally occurring gradients in diseased tissue compared to healthy tissue, such as variations in the pH values (healthy tissue: pH = 7.4; extracellular environment of solid tumors: pH = 6.5–6.8) or local temperature variations due to pathological conditions (tumor, inflammation or infection), thus permitting to hyperthermia therapies (T_{tissue} > 37 °C) [32,38–40]. A pH-dependent release can be triggered by variations in structure or hydrophobicity upon (de)protonation, leading to extension or a collapse of the polymer chains caused by electrostatic interactions [32]. In one example, a pH-triggered release was induced by a membrane-rupture of the related PEG-*b*-P2VP polymersomes due to the pH-sensitivity of P2VP [41]. The temperature-responsive class polymers which are characterized by a lower or upper critical solution temperature (LCST and UCST) comprise poly(N-isopropylacrylamide) (PNIPAam), poly(*N*,*N*-diethylacrylamide) (PDEAAm) and poly(methyl vinylether) (PMVE), among many other examples [32,42,43].

2.2. Micelles as drug carriers based on 2VP-DEVP block copolymers

In 2016 our group reported on the preparation of block copolymers made from 2VP and DEVP via REM-GTP, which showed intriguing potential for their application as drug delivery vehicles in cancer therapy [17]. Initially we decided to generate copolymers with a BAB block structure (A: hydrophobic block; B: hydrophilic block) since the received micelles proved to be more stable with respect to their lower critical micelle concentration, compared to their inversed analogues [44–47]. To achieve such a copolymer architecture, 2-methoxyethylamino-bis(phenolate)-yttrium catalyst **1** was employed in the C—H bond activation of 2,3,5,6-tetramethylpyrazine (TMPy), to yield compound **2** (Scheme 2) [22].

In the illustrated case, the application of TMPy as a binuclear initiator is crucial for the generation of a species with two active sites as starting point for the polymerization, in order to obtain the desired triblock architecture (Scheme 2). Single-crystal XRD further corroborated the activation of both opposing methyl groups adjacent to the same nitrogen atom, and therefore the formation of a binuclear species.

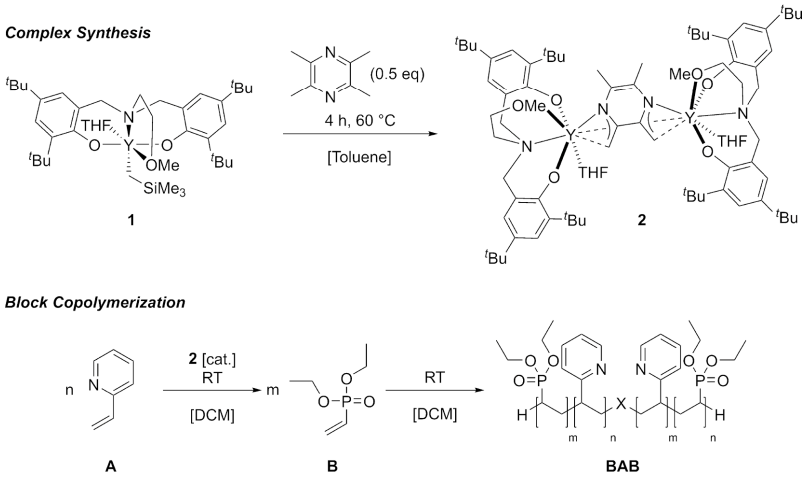

Scheme 2. Formation of catalyst **2** via C–H bond activation of 2,3,5,6-tetramethylpyrazine with complex **1** (top). Block copolymerization of 2VP and DEVP via REM-GTP with catalyst **2** in DCM at room temperature (bottom). (Redrawn with permission from Ref. [17]. Copyright 2016 John Wiley and Sons.)

Prior to the copolymerization experiments, the incorporation of the initiator into the polymer chain was proven via ESI-MS studies with 2VP oligomers that gave evidence for the insertion of a monomer into a Y–C bond during the initial polymerization step. Subsequent block copolymerization was achieved with a constant 2VP feed of 200 equivalents and varying amounts of DEVP (200–400 equivalents), yielding three defined copolymers with composition ratios between 1/0.8 and 1/2.1. Gel permeation chromatography attributed very narrow molecular weight distributions ($Đ \leq 1.20$) as it is expected for REM-GTP. Moreover, the molecular weights of the copolymers exceeded 40 kDa, which is the threshold for renal clearance [48,49].

Due to the BAB block structure, all polymers self-assembled to micelles in aqueous solution above the determined critical micelle concentration (CMC) of 0.1–0.2 mg mL^{-1}. Characterization using dynamic light scattering (DLS) revealed the particle diameters to be between 54 and 88 nm, corresponding to the literature reports postulating a diameter of 30–100 nm as prerequisite for the application of polymer-based drug delivery vehicles [50]. Imaging via transmission electron microscopy (TEM) confirmed the uniformity and spherical shape of the micellar structures. Studies on the thermoresponsive behavior showed a temperature-dependent phase transition above a temperature of 43 °C. Temperature-dependent DLS measurements also showed the collapse and formation of the micelles above and below the LCST. In addition, a salting-out effect was observed for LCST measurements in a phosphate buffer solution (PBS) and *Dulbecco's Modified Eagle's medium* (DMEM).

Preliminary release studies were rendered with fluorescein as a drug surrogate. With respect to the dual-responsive character, the release was evaluated at room temperature in a neutral medium, and compared to samples in an acidic environment (pH = 4.5) and at an elevated temperatures (44 °C) as a trigger condition. In summary, copolymer BAB_3 ($2VP_{200}DEVP_{400}$) proved to be most promising since it showed strongest response to temperature and pH, resulting in quantitative releases within the observation period (Fig. 1).

For the subsequent *in vitro* studies, the micelles were loaded with *Nile red* to evaluate their potential as delivery vehicles. Consecutive *HeLa* cells were treated with the loaded micelles, and conducted to light microscopy. As illustrated in Fig. 2 *Nile red* was detected in the cytosol of the cancer cells. For further studies on the cell viability, *HeLa* cells were incubated with increasing concentrations of the non-loaded micelles. Ultimately the cell viability assays gave no evidence of growth-inhibition effects, even at a concentration of 1 mg mL^1, suggesting high biocompatibility and great potential in biomedical applications.

In additional *in vitro* studies, the internalization of DOX-loaded micelles based on copolymer BAB_3 were compared to the uptake of free doxorubicin. For that reason, the nuclei of *Hela* Cells were stained with *Hoechst 33342,* resulting in a blue fluorescence allowing a clear distinction from the autofluorescence of doxorubicin. These experiments showed the successful internalization of DOX-loaded micelles into *HeLa* cells as Fig. 3 indicates, given a complete overlap of the images with doxorubicin and *Hoechst 33342*. Moreover, a transfer of doxorubicin into the nucleus was indicated by fluorescence microscopy over time (see Fig. 3).

2.3. Micelles with tuneable LCST

Encouraged by these promising results, it seemed natural to investigate the tuneability of the temperature-sensitivity of the micelles to optimize possible *hyperthermia* therapies [51]. Our group could already evidence the precise adjustment of the LCST of PDEVP via the incorporation of hydrophobic and hydrophilic vinyl phosphonate, resulting in a decrease or an increase in the LCST [28]. Consequently, in the course of this study, a set of AB-type and ABB'-type block copolymers were synthesized via sequential REM-GTP of 2VP and DAVP. The statistic character of the (BB') block was accomplished via prior mixing of DEVP and the respective monomer DPVP and DMVP (Scheme 3).

Characterization by GPC-MALS once again attributed defined copolymer structures with narrow molecular weight distributions ($Đ < 1.15$). Furthermore, due to the extraordinary initiator efficiency of 99% no unreacted catalyst complexes remained in the reaction mixture that could lead to the formation of PDAVP-homopolymers [22]. These beneficial attributes of REM-GTP are of great interest for the potential application of these copolymers in biomedical fields, since unimodal block copolymers exhibit the same composition, ultimately leading to the formation of identical micelles. The composition of the AB-type copolymers, as well as the composition of B/B' [DEVP/DPVP, DMVP] of the statistical blocks, was also calculated from ^{1}H NMR and ^{31}P NMR data [28].

The determination revealed a polyvinylphosphonate block consisting of 5% DPVP for $A(BB')^1$ while in the case of $A(BB')^2$ almost 10% of DMVP were incorporated (Fig. 4). The CMC of the corresponding

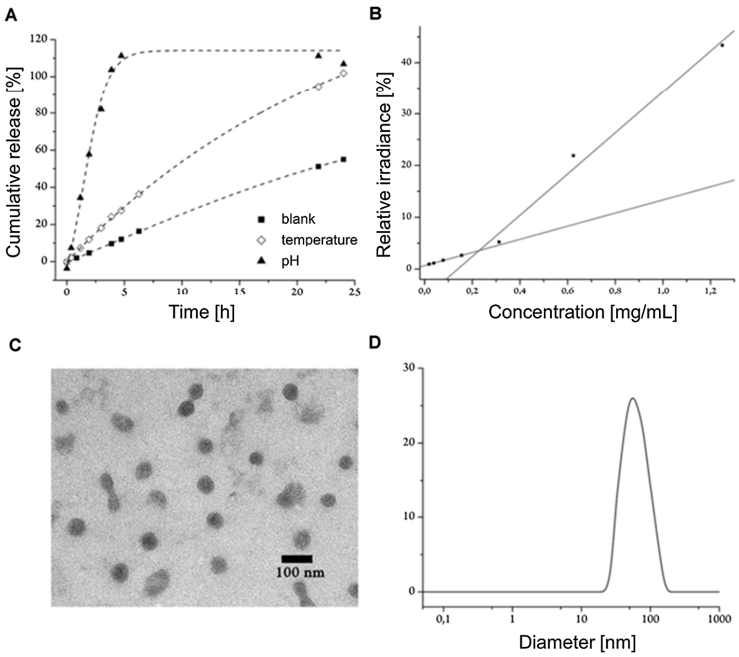

Fig. 1. (A) Cumulative release of fluorescein from loaded micelle BAB_3 ($2VP_{200}DEVP_{400}$) – untriggered, pH- (pH 4.5 buffer solution) and temperature-triggered (44 °C). (B) Determination of the CMC with Nile red. (C) TEM image of the BAB_3 micelle. (D) Light-scattering measurement of micelle (2.5 mg mL^{-1}) in water. (Modified reproduction with permission from Ref. [17]. Copyright 2016 John Wiley and Sons.) (For interpretation of the references to color in this figure legend, the reader is referred to the web version of this article.)

micelles was determined as 0.13 mg mL^{-1}.

DLS measurements once more confirmed the unimodal size distribution of these polymer-based micelles. Interestingly, only block copolymer compositions with a DAVP content exceeding the 2VP content of 50 eq. allowed micellization. Adjustment of a 100/100 ratio between the 2VP and DEVP blocks enabled the formation of stable and perfectly sized micelles. Furthermore, dissolution experiments with 0.1 M hydrogen chloride solution revealed an increase in solubility at a pH = 4.5 which is in agreement with literature values [27,41,52,53].

As mentioned, a major focus of this study was the investigation of the thermoresponsive behavior of the micelles. Consequently, a LCST of 43–43.5 °C was measured for micelles build from the standard block copolymers merely consisting 2VP and DEVP. The statistical incorporation of small amounts of hydrophilic DMVP or hydrophobic DPVP (3–10 eq.) into the DEVP block allowed the precise shift of the cloud points [28]. As a result, DMVP led to an increase of the LCST up to 48.5 °C while DPVP decreased the LCST of the A(BB′) block copolymers to 38.5 °C (Fig. 5).

The presence of P2VP and the variation of the PDEVP block length had no measurable influence on the cloud points compared to other polymers such as PNIPAam and PEG which show a strong correlation between LCST behavior and chain length [44,54].

2.4. Cross-linked nanoparticles

Though polymeric micelles exhibit very low CMCs and show therefore high stability in aqueous solutions, it has to be taken into account that micelles and free polymer chains are in an equilibrium state [35,39]. Since micelle-based carriers are exposed to high dissolution upon injection in the human body, the equilibrium might be shifted towards a state favouring the free unimers. Consequently, micellar carriers might degrade before they reach the diseased area and therefore lack therapeutic efficacy, due to the loss of their cargo [55]. To avoid this issue, we refined the concept of the micellar carriers through the extension of the block copolymer architecture with the monomer diallyl vinylphosphonate (DAlVP) (Scheme 4).

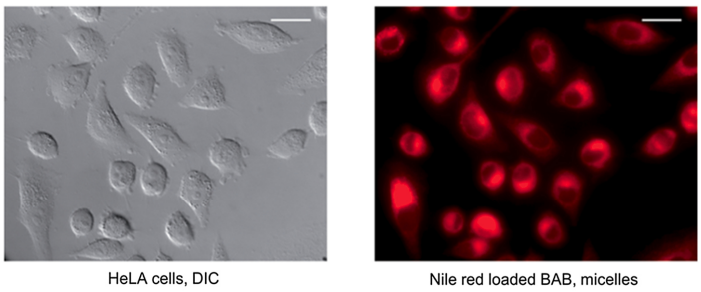

Fig. 2. Studies on the cellular uptake of loaded micelles (BAB_3) into HeLa cells. Light microscopy images of HeLa cells incubated with Nile red-loaded micelles (BAB_3). Scale bar: 25 μm. Images were taken 3 h after treatment with Nile-red-loaded micelles. (Modified reproduction with permission from Ref. [17]. Copyright 2016 John Wiley and Sons.) (For interpretation of the references to color in this figure legend, the reader is referred to the web version of this article.)

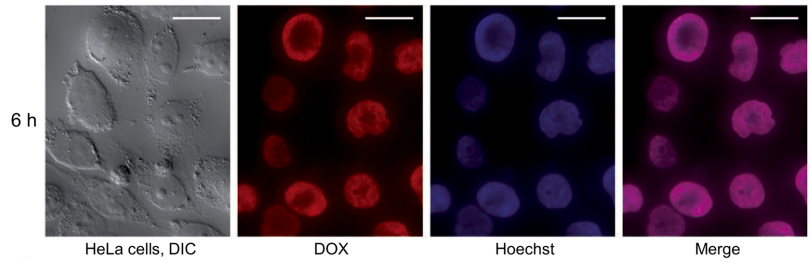

Fig. 3. Localization studies of intracellular doxorubicin release of DOX-loaded micelles (BAB_3) and non-encapsulated DOX, followed by fluorescence microscopy: Images of *HeLa* cells treated with DOX-loaded micelles (BAB_3) after 6 h. Experiments were performed at a concentration of 3 μg mL^{-1}. Left to right: Images depict brightfield *HeLa* cells captured by differential interference contrast (DIC) microscopy, DOX fluorescence in cells (red), nuclei stained with Hoechst 33342 (blue), and overlays of the fluorescence images (scale bar: 25 μm). (Modified reproduction with permission from Ref. [17]. Copyright 2016 John Wiley and Sons.) (For interpretation of the references to color in this figure legend, the reader is referred to the web version of this article.)

Analogously to the previous described micelles, the incorporation of DAlVP was rendered via sequential copolymerization in order to achieve a triblock structure ABB′ (A = 2VP, B = DEVP, B′ = DAlVP). As expected, the copolymerization experiments resulted in well-defined copolymers with low polydispersities ($Đ$ = 1.10–1.17) and desired molecular masses larger than 40 kDa (M_n = 4.1–7.9 × 10^4 g/mol) since carriers of such mass show beneficial properties regarding selective accumulation and extended retention durations in tumor tissue [49]. The subsequent formation of the nanoparticles was rendered via radical-induced thiol-ene click chemistry, using 3,6-dioxa-1,8-octanedithiol as a cross-linking agent (Scheme 5).

Monitoring of the cross-linking process could be achieved via ^{1}H NMR spectroscopy by observing the consumption of the allylic proton signals between 4.50 and 6.20 ppm. Thus, it was possible to link single-polymer chains over the allyl functions, to obtain defined core-shell-type nanoparticles. Characterization by DLS measurements and imaging via TEM confirmed the generation of uniform and spherically shaped particles with particle diameters of 35 and 66 nm, whereby size was mainly dependent on the length of the P2VP block. By way of example, Fig. 6 illustrates the results of the DLS and TEM measurements of nanoparticle NP1 generated from copolymer ABB'1 ($2VP_{100}DEVP_{100}DAlVP_5$).

Surface-tension measurements of the copolymers and their respective nanoparticles with varying dilution grades were conducted to negate a concentration-dependant particle formation. Eventually all nanoparticles were missing an inflexion point, verifying the stability of the particles after cross-linking. Release experiments with the synthesized nanoparticles using fluorescein clearly showed that temperature can trigger the release, as well as the exposure of the loaded particles to an acidic environment. The best results in this respect were obtained at a temperature of 44 °C and a pH of 4.3.

Interestingly, it appears that the composition of the respective copolymer has a major impact on the cell viability. Cytotoxicity experiments with *MCF-7* cells exhibited good cell viabilities after incubation with solutions of the unloaded nanoparticles NP1 ($2VP_{100}DEVP_{100}DAlVP_5$) and NP3 ($2VP_{200}DEVP_{200}DAlVP_5$) while NP2 ($2VP_{100}DEVP_{200}DAlVP_5$) was found to be more harmful to the cells. In all experiments, DOX-loaded nanocarriers led to decreasing cell viabilities with increasing amounts of doxorubicin. Accordingly, *HeLa* and *MCF-7* cells were subjected to fluorescence microscopy to prove the internalization of the loaded nanoparticles or likewise of doxorubicin. Here, the cells were stained with the nuclear dye *DAPI* and treated with DOX-loaded particles. Merging of the *DAPI*- and DOX-fluorescence-based images demonstrates that doxorubicin reaches the nucleus after just one hour.

Lastly, fluorescence-assisted cell sorting (FACS) enabled a statistical perspective to be obtained on the uptake of the Dox-loaded particles in *MCF-7* cells. As depicted in Fig. 7, a remarkable increase of the mean fluorescence intensity can be observed after prolonged incubation times. This means that the elevated doxorubicin fluorescence levels correspond to an increased uptake of the DOX-loaded particles as well as of doxorubicin itself.

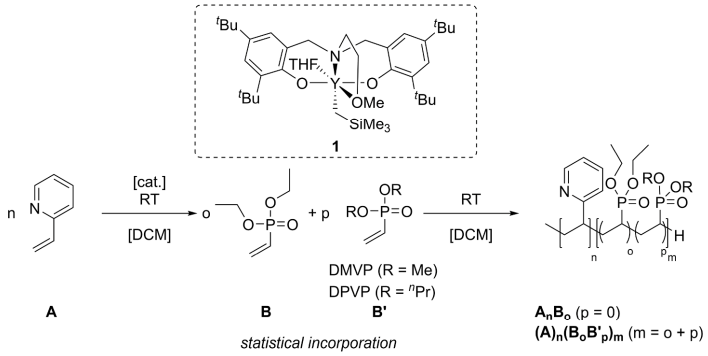

Scheme 3. Copolymerization of 2VP and DAVP (DEVP, DMVP, DPVP) via REM-GTP with catalyst **1** at room temperature to obtain AB and A(BB') polymers. (Redrawn with permission from Ref. [51]. Copyright 2016 Royal Society of Chemistry.)

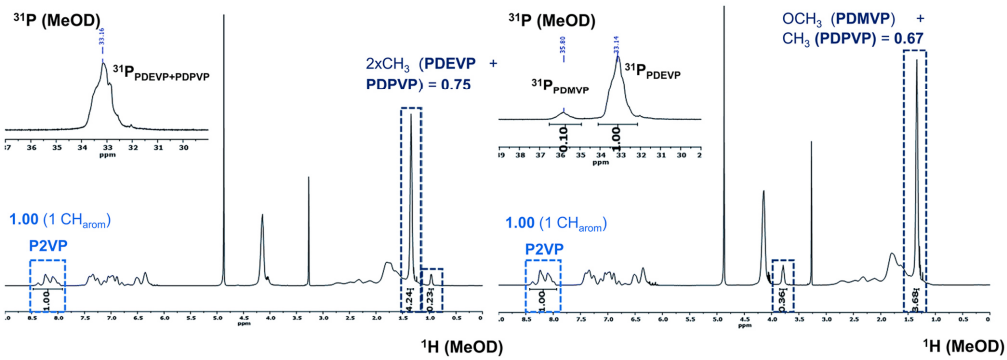

Fig. 4. ^{1}H- and ^{31}P NMR spectrum of A(BB')^{1} ($2VP_{100}/DEVP_{97}/DPVP_{3}$) and A(BB')^{2} ($2VP_{100}/DEVP_{90}/DMVP_{10}$) in MeOD at 298 K. Assignment of the protons according to *Rieger et al.* overlapping of PDEVP and PDPVP-^{31}P-signal.[28] (Reprinted with permission from Ref. [51]. Copyright 2016 Royal Society of Chemistry.)

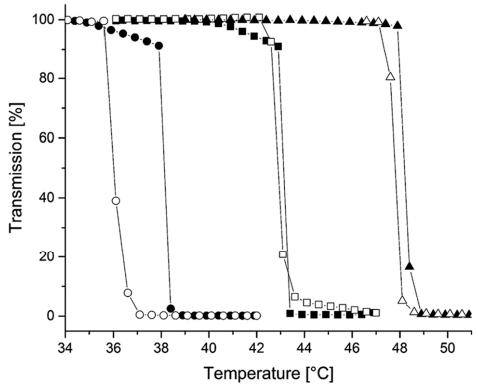

Fig. 5. Determination of the cloud points of copolymers AB (squares), A(BB')^{1} (circles) and A(BB')^{2} (triangles). The cloud point was determined at 10% decrease of transmittance for 2.5 wt-% aqueous polymer solution. (Reprinted with permission from Ref. [51]. Copyright 2016 Royal Society of Chemistry.)

3. Tailoring the initiator of REM-GTP catalysts for post-polymerization functionalization of poly(vinylphosphonates)

The stimuli-responsive behavior of the nanocarriers described above rests on the intrinsic properties of the respective polymer block. Thus, the temperature response results from the PDEVP block while the pH-sensitivity is introduced by the P2VP block, due to basic nature of the pyridyl groups. Further advancement of our nanoparticular systems would require the introduction of superficial targeting ligands. Such a modification could shift these delivery systems from vehicles for passive targeting towards more specific nanocarriers allowing active targeting [56]. Intriguingly, we are already able to introduce new functions selectively via post-polymerization functionalization. This can be achieved either via transesterification of the phosphonate esters, or with pyridyl-based initiators that are incorporated into the polymer chain during the initial step of the polymerization [10,14].

3.1. Polyvinylphosphonate-biomolecule-conjugates

With the knowledge that pyridyl-type compounds such as *sym*-collidine or 2,3,5,6-TMPy facilitate REM-GTP with high initiator efficiencies, we developed a new initiator **3** bearing a vinyl moiety [57]. This gave us the opportunity to functionalize PDEVP after the polymerization process via the highly efficient click reaction between thiols and olefinic groups. Initially starting from 2,6-lutidine, the initiator structure of **3** was built up by a *Suzuki* cross-coupling and a *Wittig* olefination.

Before the new initiator was subjected to initial polymerization attempts, it was extensively investigated regarding its applicability as a substrate for the C—H bond activation (Scheme 6). A characterization of the resulting complex by elemental analysis and NMR spectroscopy proved the transformation of one methyl groups into a methylene group via σ-bond metathesis.

Kinetic investigation gave evidence of the linear growth of the molecular weights proving the living-type character of the polymerization, while all samples exhibit low polydispersities ($Đ \approx 1.20$). In addition, the polymerization proceeds extremely fast, featuring an initial TOF of almost 70,000 h^{-1} and is consequently even outperforming the gold standard *sym*-collidine with a TOF of 59,400 h^{-1} [14]. Also, the initial initiator efficiency I^{*}_{t} of 94% was found to be

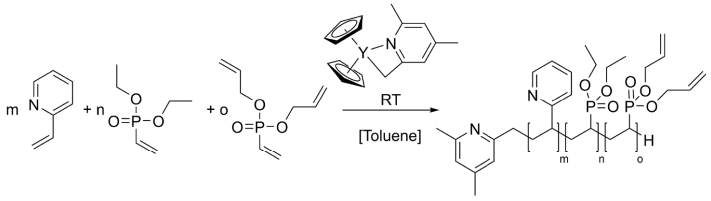

Scheme 4. Block copolymerisation of 2VP, DEVP and the new diallyl vinylphosphonate (DAlVP) at room temperature with $Cp_2Y(CH_2(C_5H_2Me_2N))$ as catalyst. (Redrawn with permission from Ref. [48]. Copyright 2018 Royal Society of Chemistry.)

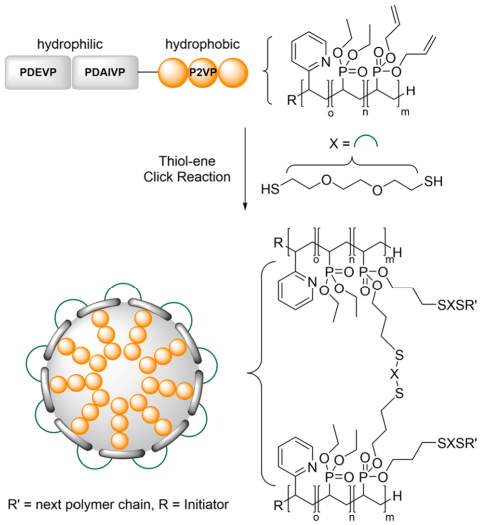

Scheme 5. Thiol–ene click reaction with 3,6-dioxa-1,8-octanedithiol towards cross-linked P2VP-PDEVP-PDAlVP nanoparticles. (Redrawn with permission from Ref. [48]. Copyright 2018 Royal Society of Chemistry.)

higher than the one determined for *sym*-collidine (I^*_t = 73%). Lastly, ESI-MS analysis confirmed the covalent integration of the initiator moiety into DEVP oligomers. Hence the novel initiator was employed in the generation of two polymeric materials with different chain lengths (100 and 600 eq. DEVP) (Scheme 6).

Afterwards, the PDEVP substrates were subjected to the functionalization attempts in order to obtain the polymer-biomolecule conjugates. Here, we focused on two compounds: On the one hand cholesterol, an important component of the cellular membrane, was directly coupled in the form of thiocholesterol via radical-induced thiol-ene click chemistry (Scheme 7) [58,59]. On the other hand folic acid was chosen since the related folate receptor is overexpressed on many cancer types and therefore makes it an intensely examined ligand in cancer-related research fields [60–64]. Folic acid was conjugated in a two-step process, introducing cysteamine hydrochloride as a linker unit via a thiol-ene reaction and was subsequently reacted with the NHS-ester of folic acid at the terminal amino group (Scheme 7).

Quantitative conversion of the vinyl group was determined via ^{1}H NMR exhibiting the complete disappearance of the vinylic protons between 5.30 ppm and 6.90 ppm (Fig. 8; after reaction with thiocholesterol).

In the next phase of this study localization studies, of the PDEVP bioconjugates were planned. Since the detection via confocal microscopy requires the use of fluorescent substrates, we aimed for the introduction of pyrene groups by the partial transesterification of the ethyl esters (Scheme 8), as earlier studies by our group corroborated that the ester side groups of polyvinylphosphonates can be cleaved with trimethylsilyl bromide [10,65]. After the introduction of the pyrene groups, functionalization degrees ranged between 0.38% and 1.13%.

Likewise, the fluorescent substrates obtained in this reaction were coupled with cholesterol and folic acid as illustrated in Scheme 7 and characterized with regard to their thermoresponsive and their photophysical properties. With exception of two fluorescent samples, all the non-fluorescent and the fluorescent polymers as well as the respective bioconjugates showed a thermoresponsive behavior in water and more intriguingly under complex conditions in a medium/phosphate buffer saline solution containing 1% antibiotics (PS) and 10% fetal bovine serum (FBS). The photophysical properties were investigated via UV/Vis and photoluminescence measurements to determine absorbance and emission characteristics. Typical absorbance bands of pyrene were determined within 200 and 450 nm (Fig. 9, left). Under excitation at 365 nm, the emission maxima were determined between 450 and 500 nm, corresponding to a light blue fluorescence of the pyrene groups (Fig. 9, right).

In the last phase of this study, the polymer bioconjugates were biologically evaluated. One major aspect was the investigation of the cytotoxicity of the polymer-biomolecule conjugates via the colorimetric 3-(4,5-dimethylthiazol-2-yl)-2,5-diphenyltetrazolium bromide (MTT) assay with *HEK-293* and *HMEC-1* cells. In the case of the non-fluorescent samples, the cell viabilities were – apart from a few instances - determined to be above 50%, even after the incubation of highly concentrated polymer solutions (up to 5 mg mL^{-1}). In some cases, data points surpassed 100% probably due to beneficial properties of the PDEVP samples for cell growth. HOwever, both cell lines showed comparatively reduced viabilities after treatment with the fluorescent samples, due to intrinsic toxicity of pyrene and its metabolites [66,67]. With respect to the reduced cell viabilities, localization studies could be rendered with endothelial *HMEC-1* cells under optimized conditions (1.25 mg mL^{-1} and incubation for four hours) and were assayed by imaging using confocal microscopy. Thus, a cross-section through the cell (region of interest – ROI analysis) was analyzed by comparing the local intensities of polymer-related fluorescence and the fluorescent plasma membrane stain (*W6/32-RRX*). Our studies revealed that the substrates could be localized at different compartments of the cell. While PDEVP without anchor and folate-bearing PDEVP showed direct uptake into the cell, cholesterol functionalized PDEVP was localized in the plasma membrane (Fig. 10).

These results give grounds for the conjugation of biologically active functions permitting the direction of PDEVP-substrates to different cell compartments.

In this context it should be mentioned that fluorescence labelling of

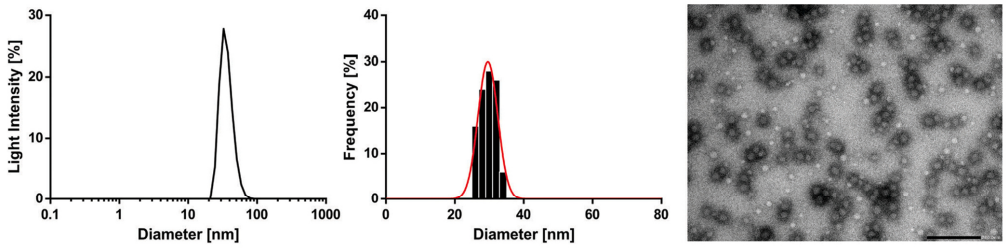

Fig. 6. Size distribution of NP1 determined via DLS measurements at a concentration of 2.5 mg mL^{-1} in water (left); histogram plot with a *Gaussian* regression fit (middle); and a TEM image of NP1 (right) with a scale bar of 200 nm. (Reprinted with permission from Ref. [48]. Copyright 2018 Royal Society of Chemistry.)

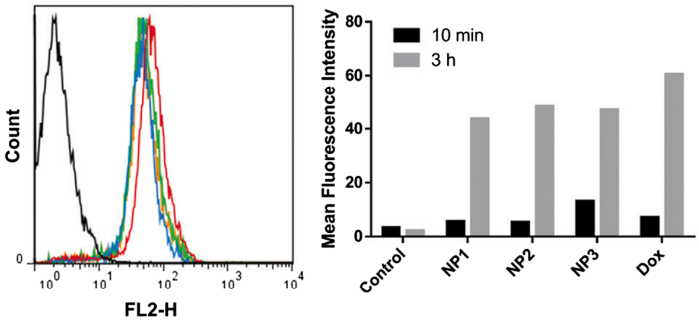

Fig. 7. Mean fluorescence intensities of *MCF-7* cells incubated with PBS (black), NP1 (blue), NP2 (green), NP3 (orange) and doxorubicin (red) for 3 h at 37 °C (left). Comparison of DOX uptake after 10 min and 3 h (right). (Reprinted with permission from Ref. [48]. Copyright 2018 Royal Society of Chemistry.) (For interpretation of the references to color in this figure legend, the reader is referred to the web version of this article.)

PDEVP can be achieved by using specially designed initiators [68]. The binuclear initiator **4** was used in the C—H bond activation of $Cp_2Y(CH_2TMS)(THF)$ and the activated catalyst **5** enabled to obtain fluorescently tagged PDEVP (Scheme 9).

The solubility of the polymerization products depended greatly on the reaction temperature. Consequently, at room temperature and 50 °C, only insoluble gels were obtained, while polymerization at 100 °C resulted in a soluble product with a comparatively broad polydispersity of $Đ = 2$ due to a more pronounced chain termination/catalyst decomposition. Hence the initiator efficiencies range between 7 and 13%.

The tagged PDEVP samples exhibited an emission maximum at around 490 nm upon excitation at 365 nm, which reflected in a very strong blue-green photoluminescence. The biocompatibility of these substrates was determined by MTT assays using *HEK-293* and *HMEC-1* cells that showed very good cell viabilities even after incubation times longer than 48 h, and treatment with polymer solutions with concentrations up to 5 mg mL.

3.2. Application of AB block copolymer micelles as support for Rhenium-based photocatalysis

Another study by our group focused on the introduction of bipyridines as a polymer end-group due to the broad applicability of these type of ligands in coordination chemistry with a variety of transition metals [Pd, Pt, Fe, Co, Ni, Cu, Zn] [69–76]. In the homogenous photocatalytic reduction of CO_2 to CO, bipyridines are used to form $[Re(CO)_3(Bpy)Cl]$ from $Re(CO)_5Cl$. Unfortunately, this catalyst class lacks sufficient stability for industrial applications. To overcome this issue, rhenium-species were, for example, incorporated into polymer brush ion gels (PS-PEO-PS) or introduced in charged and neutral norbornenyl-based polymeric frameworks [77,78]. Here, the bipyridine motif was introduced in the form of an initiator for REM-GTP to synthesize P2VP-PDEVP-block copolymers. Initially, two bipyridines were tested with $(ONOO)^tBuY(CH_2TMS)(THF)$ (**1**) in C—H bond activation experiments. Treatment of complex **1** with 6-Me_2bpy gave the respective catalyst in a 28% yield while complex **6** could be isolated with 62% yield after C—H bond activation of 6-Mebpy. Beforehand, oligomers generated using both catalysts were clearly analyzed by ESI-MS clearly and revealed the incorporation of the initiator into the oligomer chain. Furthermore, the complexes were investigated regarding their kinetic behavior. Compared to the literature standard **1**, both catalysts demonstrated lower TOFs due to a reduced initiator efficiency (24–54% vs. 99% with CH_2TMS) [22]. Hereafter, block copolymerizations were performed with catalyst **6** due to its superior initiator efficiency. As described in the previous examples, 2VP was first polymerized to generate the hydrophobic block and was extended with DEVP (Scheme 10). Next, characterization via GPC and NMR spectroscopy DLS measurements was performed. Depending on the length of the P2VP block, micelles with diameters of around 36–66 nm were obtained.

After purification of the copolymer, the post-polymerization functionalization of the copolymers with $Re(CO)_5Cl$ resulted in the rhenium-containing AB block copolymers (Scheme 10). This was strongly indicated by the comparison of the rhenium-containing polymer and the analogue $[Re(CO)_3(6\text{-}Mebpy)Cl]$ complex (**7**) using UV/Vis and PL-spectroscopy. With both methods, an identical absorption (maxima at 325 and 365 nm) and emission (620 nm) behavior in DMF could be observed, while the non-modified polymers did not exhibit these characteristic bands (Fig. 11).

In addition, complexation experiments with 2VP-DEVP-block copolymers lacking a bipyridine end-group gave no indication for the incorporation of rhenium, since PL- and UV/Vis spectra showed no related emission and absorption bands. Furthermore, the photophysical properties were also observed in aqueous solution after micelle formation.

As $[Re(CO)_3(bpy)Cl]$ is a well-known motif for the homogenous

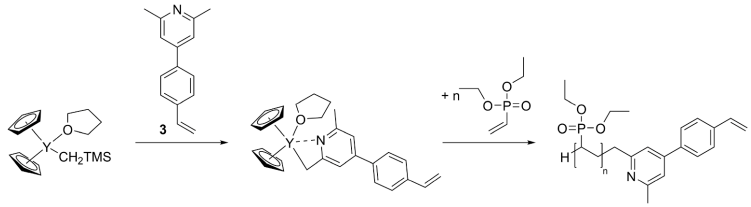

Scheme 6. C—H bond activation of **3** with $Cp_2Y(CH_2TMS)(THF)$ followed by polymerization of DEVP. (Redrawn with permission from Ref. [57]. Copyright 2018 Royal Society of Chemistry.)

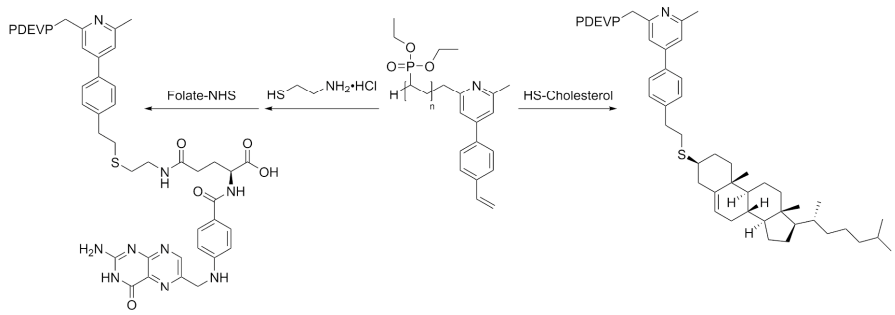

Scheme 7. Conjugation of the activated biomolecules cholesterol and folic acid to PDEVP. (Redrawn with permission from Ref. [57]. Copyright 2018 Royal Society of Chemistry.)

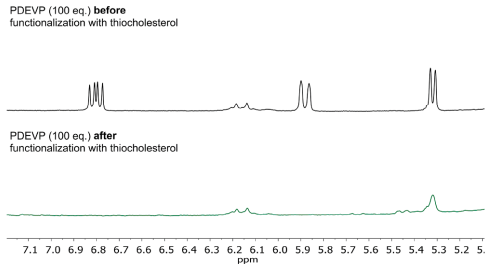

Fig. 8. ^{1}H NMR spectra in MeOD of PDEVP (100 eq.) before (black) and after (green) functionalization with thiocholesterol. (Reprinted with permission from Ref. [57]. Copyright 2018 Royal Society of Chemistry.) (For interpretation of the references to color in this figure legend, the reader is referred to the web version of this article.)

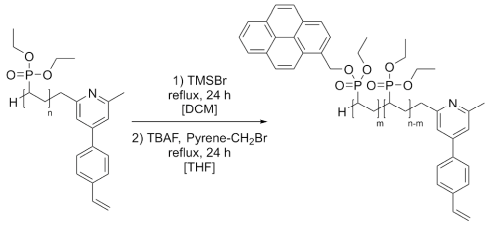

Scheme 8. Partial transesterification of the side chain groups of poly(diethyl vinylphosphonate) to introduce fluorescent pyrene groups. (Redrawn with permission from Ref. [66]. Copyright 2018 John Wiley and Sons.)

photocatalytic reduction of CO_2 the newly synthesized rhenium-block copolymers were investigated in this reaction as well. In this study the Re-containing copolymers were compared to model complex **7** possessing an analogue ligand sphere. As depicted in Fig. 12, the catalytic activity correlates with polymer length, showing increasing TONs with growing chain lengths. Interestingly, the TONs achieved with polymeric photocatalysts are higher than the one determined with the free complex **7**. This might be attributed to a shielding or prohibition effect of the polymer chain preventing, the rhenium-core from the negative effects of free radicals and deactivation processes. Corresponding DLS data suggests that no micelles are formed in DMF. Gas chromatographic analysis showed exclusively the formation of CO while ^{1}H NMR of the solution gave no hint of any methanol, formic acid or formaldehyde generated during the reaction. Moreover, no side reactions involving the block copolymer occurred.

Unfortunately, the CO_2 reduction cannot be observed in aqueous systems. In pure water, no conversion of CO_2 was detected. Only the addition of DMF in sufficient amounts allowed the formation of CO but prohibited the formation of micelles.

4. Conclusion and outlook

In summary REM-GTP is an efficient polymerization method, enabling the synthesis of defined functional homo- and block copolymers using functional *Michael*-type monomers. The living nature of REM-GTP allows the generation of precisely defined block copolymers. Dual-responsive 2VP-DEVP-based micelles exhibited promising properties as drug delivery vehicles with pH-dependent and temperature-triggered release, good results in the cytotoxicity screenings and - most importantly - were internalized into cells, as corresponding *in vitro* studies have proven. Furthermore, it was demonstrated that via the incorporation of DMVP and DPVP, the LCST of the micelles can be tuned to optimize the window of the temperature-triggered release. Recently, nanoparticles were developed from the micellar carriers by introducing DAlVP as third block. Hence, the copolymers could be cross-linked using thiol-ene chemistry, yielding stable nanoparticles which once again showed very good stimuli-responsive release behavior. *In vitro* studies attributed biocompatibility of the non-loaded particles while DOX-loaded nanocarriers released their cargo, resulting in drastically reduced cell viabilities. These carriers were also internalized into the cells, as fluorescence microscopy and FACS studies demonstrated. Currently we are working on the synthetic procedures to bind superficial targeting ligands to the nanocarriers. These modifications will lead to more specific nanocarriers for more sophisticated applications in the future, shifting our nanosized carriers from passive targeting to actively targeting vehicles.

The affinity of the used rare earth metals towards C—H bond activation of pyridyl-type substrates revealed an elegant approach in order to introduce additional material features or reactive functional groups that allow post-polymerization functionalizations. In this context, we showed that the introduction of a vinyl-group bearing initiator allowed the formation of polymer-biomolecule conjugates with cholesterol and folic acid. Localization studies with these substrates revealed a strong dependence if the polymer was internalized into the cell or located in

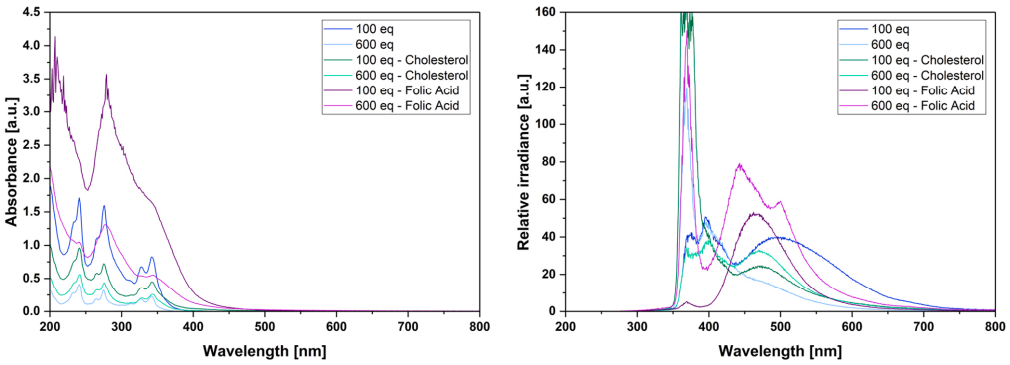

Fig. 9. UV/Vis spectra of the fluorescent polymers in aqueous solution (2.5 mg mL^{-1}) (left). Photoluminescence spectra of the fluorescent polymers in aqueous solution (2.5 mg mL^{-1}) (right). (Reprinted and rearranged with permission from Ref. [66]. Copyright 2018 John Wiley and Sons.)

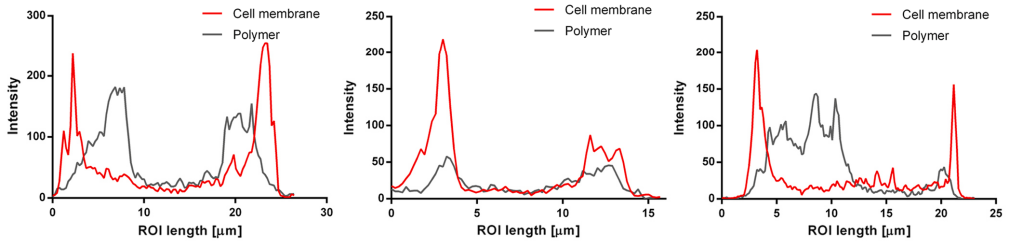

Fig. 10. Region of interest (ROI) analysis of *HMEC-1* cells treated with polymer without anchor (left), polymer with cholesterol (middle) and polymer with folic acid (right). Red curves represent intensity of the cell membrane stain. Grey curves illustrate the intensity of the fluorescent polymer sample. (Modified reproduction from Ref. [66], copyright 2018 John Wiley and Sons). (For interpretation of the references to color in this figure legend, the reader is referred to the web version of this article.)

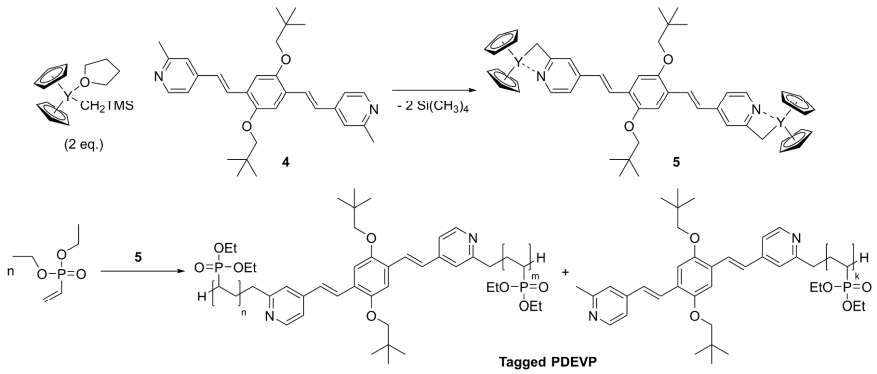

Scheme 9. C–H bond activation of the novel chromophoric initiator **4** and polymerization of DEVP with catalyst **5**. (Redrawn with permission from Ref. [68]. Copyright 2018 John Wiley and Sons.)

the cell membrane. Furthermore, C–H bond activation with a specially designed highly fluorescent initiator allows the synthesis of tagged, biocompatible PDEVP circumventing the need to of toxic fluorophores like pyrenes as an imaging probe. In a final study, a bipyridine-based initiator was used for the complexation of rhenium, in order to obtain photocatalytically active copolymers. Interestingly, these rhenium-containing polymers showed superior activities in the reduction of CO_2 compared to the free, analog complex. Unfortunately, the copolymers remained inactive in water and showed no micellization in DMF, potentially protecting the rhenium core from deactivation processes. The

From Lanthanide-mediated, High-Precision Group Transfer Polymerization of Michael-type Monomers, to Intelligent, Functional Materials

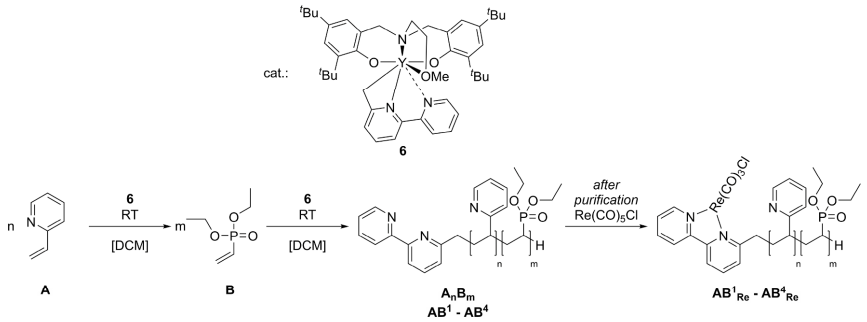

Scheme 10. Preparation of AB-block copolymers (A = P2VP; B = PDEVP) using catalyst **6**. Subsequent complexation of the rhenium-precursor $[Re(CO)_5Cl]$ to purified block copolymer. (Redrawn with permission from Ref. [76]. Copyright 2018 John Wiley and Sons.)

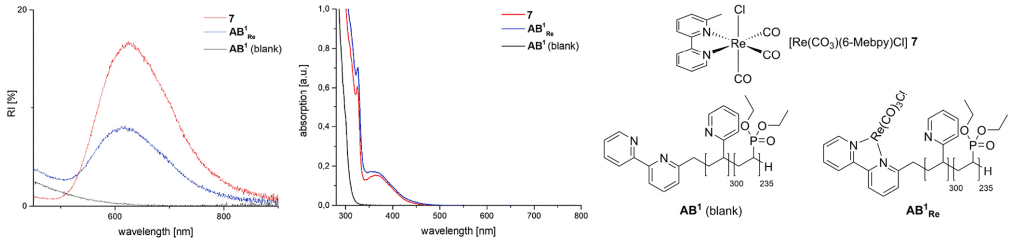

Fig. 11. PL-spectra of catalyst **7** (0.15 mM; red), AB^1 (3.20 mg in 2 mL dmf; black) and AB^1_{Re}. (3.24 mg in 2 mL DMF; blue) (left). UV/Vis-spectra of catalyst **7** (red), AB^1 (black) and AB^1_{Re} (middle). The same samples are used for PL and UV/VIS-measurements. Illustration of catalyst **7**, AB^1 and AB^1_{Re} (right). (Modified reproduction from Ref. [76]. Copyright 2018 John Wiley and Sons.) (For interpretation of the references to color in this figure legend, the reader is referred to the web version of this article.)

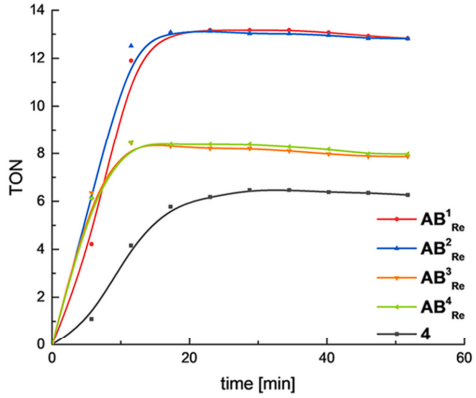

Fig. 12. TON (CO) development during photocatalytic reduction of CO_2 using AB^1_{Re}–AB^4_{Re} (AB1: $2VP_{300}DEVP_{235}$, AB2: $2VP_{220}DEVP_{275}$, AB3: $2VP_{110}DEVP_{80}$, AB4: $2VP_{90}DEVP_{170}$) and catalyst **7**. Reaction conditions: Irradiation of CO_2-saturated DMF/TEOA ([TEOA] = 1.2 M) solution containing a 0.1 mM catalyst using an LED light source (λ = 450 nm). (Reprinted with permission from Ref. [76]. Copyright 2018 John Wiley and Sons.)

introduction of functional groups via the initiator now give the opportunity for the conjugation of a plurality of small molecules, but also biopolymers such as RNA and polypeptides, via a modular synthetic strategy. Moreover, the flexibility of the C–H bond activation might also facilitate the generation of completely new copolymers using "orthogonal" polymerization types in future work.

Declaration of Competing Interest

There are no conflicts to declare.

Acknowledgements

Michael Weger is grateful for a generous scholarship from the Studienstiftung des deutschen Volkes.

Data availability

The raw data required to reproduce these findings are available to download from the publications referenced in the literature section below.

References

[1] O.W. Webster, W.R. Hertler, D.Y. Sogah, W.B. Farnham, T.V. RajanBabu, Group-transfer polymerization. 1. A new concept for addition polymerization with organosilicon initiators, J. Am. Chem. Soc. 105 (17) (1983) 5706–5708, https://doi.org/10.1021/ja00355a039.
[2] A.H.E. Müller, G. Litvinenko, D. Yan, Kinetic analysis of "living" polymerization systems exhibiting slow equilibria. 4. "Dissociative" mechanism of group transfer polymerization and generation of free ions in cationic polymerization, Macromolecules 29 (7) (1996) 2346–2353, https://doi.org/10.1021/ma950928p.
[3] R.P. Quirk, G.P. Bidinger, Mechanistic role of enolate ions in "group transfer polymerization", Polym. Bull. 22 (1) (1989) 63–70, https://doi.org/10.1007/BF00283285.
[4] R.P. Quirk, J.-S. Kim, Mechanistic aspects of silicon-mediated polymerization (group transfer polymerization) of methyl methacrylate with ester enolate anions as

From Lanthanide-mediated, High-Precision Group Transfer Polymerization of Michael-type Monomers, to Intelligent, Functional Materials

nucleophilic catalysts, J. Phys. Org. Chem. 8 (4) (1995) 242–248, https://doi.org/10.1002/poc.610080407.
[5] H. Yasuda, H. Yamamoto, K. Yokota, S. Miyake, A. Nakamura, Synthesis of monodispersed high molecular weight polymers and isolation of an organolanthanide(III) intermediate coordinated by a penultimate poly(MMA) unit, J. Am. Chem. Soc. 114 (12) (1992) 4908–4910, https://doi.org/10.1021/ja00038a069.
[6] L.S. Boffa, B.M. Novak, Bimetallic Samarium(III) initiators for the living polymerization of methacrylates and lactones. A new route into telechelic, triblock, and "link-functionalized", Polymers, Macromolecules 27 (23) (1994) 6993–6995, https://doi.org/10.1021/ma00101a044.
[7] Y. Wang, Q. Shen, F. Xue, K. Yu, Heteroleptic diphenylamido complexes of ytterbium: syntheses and molecular structures of (MeC5H4)2YbNPh2(THF) and (C5Me5)2YbNPh2, J. Organomet. Chem. 598 (2) (2000) 359–364, https://doi.org/10.1016/S0022-328X(99)00735-4.
[8] Y. Satoh, N. Ikitake, Y. Nakayama, S. Okuno, H. Yasuda, Syntheses of bis- and tetra (trimethylsilyl) substituted lanthanocene methyl complexes and their catalyses for polymerizations of methyl methacrylate, ε-caprolactone and l-lactide, J. Organomet. Chem. 667 (1) (2003) 42–52, https://doi.org/10.1016/S0022-328X(02)02124-1.
[9] N. Barros, M. Schappacher, P. Dessuge, L. Maron, S.M. Guillaume, New insights into the polymerization of methyl methacrylate initiated by rare-earth borohydride complexes: a combined experimental and computational approach, Chem. – Eur. J. 14 (6) (2008) 1881–1890, https://doi.org/10.1002/chem.200701438.
[10] S. Salzinger, U.B. Seemann, A. Plikhta, B. Rieger, Poly(vinylphosphonate)s synthesized by trivalent cyclopentadienyl lanthanide-induced group transfer polymerization, Macromolecules 44 (15) (2011) 5920–5927, https://doi.org/10.1021/ma200752d.
[11] U.B. Seemann, J.E. Dengler, B. Rieger, High-molecular-weight poly(vinylphosphonate)s by single-component living polymerization initiated by rare-earth-metal complexes, Angew. Chem. 122 (20) (2010) 3567–3569, https://doi.org/10.1002/anie.201000804.
[12] P. Pahl, C. Schwarzenböck, F.A.D. Herz, B.S. Soller, C. Jandl, B. Rieger, Core-first synthesis of three-armed star-shaped polymers by rare earth metal-mediated group transfer polymerization, Macromolecules 50 (17) (2017) 6569–6576, https://doi.org/10.1021/acs.macromol.7b01007.
[13] M. Nodono, T. Tokimitsu, S. Tone, T. Makino, A. Yanagase, Chain transfer polymerization of methyl methacrylate initiated by organolanthanide complexes, Macromol. Chem. Phys. 201 (17) (2000) 2282–2288, https://doi.org/10.1002/1521-3935(20001101)201:17<2282::AID-MACP2282>3.0.CO;2-K.
[14] B.S. Soller, S. Salzinger, C. Jandl, A. Pöthig, B. Rieger, C-H bond activation by σ-bond metathesis as a versatile route toward highly efficient initiators for the catalytic precision polymerization of polar monomers, Organometallics 34 (11) (2015) 2703–2706, https://doi.org/10.1021/om501173r.
[15] H. Kaneko, H. Nagae, H. Tsurugi, K. Mashima, End-functionalized polymerization of 2-vinylpyridine through initial C-H bond activation of N-heteroaromatics and internal alkynes by yttrium ene-diamido complexes, J. Am. Chem. Soc. 133 (49) (2011) 19626–19629, https://doi.org/10.1021/ja208293h.
[16] F. Adams, M.R. Machat, P.T. Altenbuchner, J. Ehrmaier, A. Pöthig, T.N.V. Karsili, B. Rieger, Toolbox of nonmetallocene lanthanides: multifunctional catalysts in group-transfer polymerization, Inorg. Chem. 56 (16) (2017) 9754–9764, https://doi.org/10.1021/acs.inorgchem.7b01261.
[17] P.T. Altenbuchner, P.D.L. Werz, P. Schöppner, F. Adams, A. Kronast, C. Schwarzenböck, A. Pöthig, C. Jandl, M. Haslbeck, B. Rieger, Next generation multiresponsive nanocarriers for targeted drug delivery to cancer cells, Chem. – Eur. J. 22 (41) (2016) 14576–14584, https://doi.org/10.1002/chem.201601822.
[18] M.A. Giardello, Y. Yamamoto, L. Brard, T.J. Marks, Stereocontrol in the polymerization of methyl methacrylate mediated by chiral organolanthanide metallocenes, J. Am. Chem. Soc. 117 (11) (1995) 3276–3277, https://doi.org/10.1021/ja00116a034.
[19] E. Kirillov, C.W. Lehmann, A. Razavi, J.-F. Carpentier, Synthesis, structure, and polymerization activity of neutral halide, alkyl, and hydrido yttrium complexes of isopropylidene-bridged cyclopentadienyl-fluorenyl ligands, Organometallics 23 (11) (2004) 2768–2777, https://doi.org/10.1021/om049902p.
[20] C. Qian, W. Nie, J. Sun, Cs-symmetric ansa-lanthanocenes designed for stereospecific polymerization of methyl methacrylate synthesis and structural characterization of silylene-bridged fluorenyl cyclopentadienyl lanthanide halides, amides, and hydrocarbyls, Organometallics 19 (20) (2000) 4134–4140, https://doi.org/10.1021/om000276f.
[21] C. Qian, G. Zou, W. Jiang, Y. Chen, J. Sun, N. Li, Selective synthesis, structure, and catalytic behavior of meso-divalent 1,1'-(3-oxapentamethylene)-bridged bis(indenyl)lanthanidocenes, Organometallics 23 (21) (2004) 4980–4986, https://doi.org/10.1021/om049753a.
[22] P.T. Altenbuchner, B.S. Soller, S. Kissling, T. Bachmann, A. Kronast, S.I. Vagin, B. Rieger, Versatile 2-methoxyethylaminobis(phenolate)yttrium catalysts: catalytic precision polymerization of polar monomers via rare earth metal-mediated group transfer polymerization, Macromolecules 47 (22) (2014) 7742–7749, https://doi.org/10.1021/ma501754u.
[23] C.-X. Cai, L. Toupet, C.W. Lehmann, J.-F. Carpentier, Synthesis, structure and reactivity of new yttrium bis(dimethylsilyl)amido and bis(trimethylsilyl)methyl complexes of a tetradentate bis(phenoxide) ligand, J. Organomet. Chem. 683 (1) (2003) 131–136, https://doi.org/10.1016/S0022-328X(03)00513-8.
[24] P.T. Altenbuchner, F. Adams, A. Kronast, E. Herdtweck, A. Pöthig, B. Rieger, Stereospecific catalytic precision polymerization of 2-vinylpyridine via rare earth metal-mediated group transfer polymerization with 2-methoxyethylamino-bis (phenolate)-yttrium complexes, Polym. Chem. 6 (38) (2015) 6796–6801, https://doi.org/10.1039/C5PY01146A.
[25] T. Xu, J. Liu, X.-B. Lu, Highly active half-metallocene yttrium catalysts for living and chemoselective polymerization of allyl methacrylate, Macromolecules 48 (20) (2015) 7428–7434, https://doi.org/10.1021/acs.macromol.5b01517.
[26] A. Kronast, D. Reiter, P.T. Altenbuchner, S.I. Vagin, B. Rieger, 2-Methoxyethylamino-bis(phenolate)yttrium catalysts for the synthesis of highly isotactic poly(2-vinylpyridine) by rare-earth metal-mediated group transfer polymerization, Macromolecules 49 (17) (2016) 6260–6267, https://doi.org/10.1021/acs.macromol.6b01179.
[27] T.J. Martin, K. Procházka, P. Munk, S.E. Webber, pH-Dependent micellization of poly(2-vinylpyridine)-block-poly(ethylene oxide), Macromolecules 29 (18) (1996) 6071–6073, https://doi.org/10.1021/ma960629f.
[28] N. Zhang, S. Salzinger, B. Rieger, Poly(vinylphosphonate)s with widely tunable LCST: a promising alternative to conventional thermoresponsive polymers, Macromolecules 45 (24) (2012) 9751–9758, https://doi.org/10.1021/ma3019014.
[29] B.S. Soller, Q. Sun, S. Salzinger, C. Jandl, A. Pöthig, B. Rieger, Ligand Induced steric crowding in rare earth metal-mediated group transfer polymerization of vinylphosphonates: does enthalpy matter? Macromolecules 49 (5) (2016) 1582–1589, https://doi.org/10.1021/acs.macromol.5b01937.
[30] S. Salzinger, B.S. Soller, A. Plikhta, U.B. Seemann, E. Herdtweck, B. Rieger, Mechanistic studies on initiation and propagation of rare earth metal-mediated group transfer polymerization of vinylphosphonates, J. Am. Chem. Soc. 135 (35) (2013) 13030–13040, https://doi.org/10.1021/ja404457f.
[31] N. Zhang, S. Salzinger, B.S. Soller, B. Rieger, Rare earth metal-mediated group-transfer polymerization: from defined polymer microstructures to high-precision nano-scaled objects, J. Am. Chem. Soc. 135 (24) (2013) 8810–8813, https://doi.org/10.1021/ja4036175.
[32] T. Sun, Y.S. Zhang, B. Pang, D.C. Hyun, M. Yang, Y. Xia, Engineered nanoparticles for drug delivery in cancer therapy, Angew. Chem. Int. Ed. 53 (46) (2014) 12320–12364, https://doi.org/10.1002/anie.201403036.
[33] C. Oerlemans, W. Bult, M. Bos, G. Storm, J.F.W. Nijsen, W.E. Hennink, Polymeric micelles in anticancer therapy: targeting, imaging and triggered release, Pharm. Res. 27 (12) (2010) 2569–2589, https://doi.org/10.1007/s11095-010-0233-4.
[34] H. Maeda, J. Wu, T. Sawa, Y. Matsumura, K. Hori, Tumor vascular permeability and the EPR effect in macromolecular therapeutics: a review, J. Control. Release 65 (1) (2000) 271–284, https://doi.org/10.1016/S0168-3659(99)00248-5.
[35] V.P. Torchilin, Micellar nanocarriers: pharmaceutical perspectives, Pharm. Res. 24 (1) (2006) 1, https://doi.org/10.1007/s11095-006-9132-0.
[36] R.B. Weiss, R.C. Donehower, P.H. Wiernik, T. Ohnuma, R.J. Gralla, D.L. Trump, J.R. Baker, D.A. Van Echo, D.D. Von Hoff, B. Leyland-Jones, Hypersensitivity reactions from taxol, J. Clin. Oncol. 8 (7) (1990) 1263–1268, https://doi.org/10.1200/jco.1990.8.7.1263.
[37] D.A. LaVan, T. McGuire, R. Langer, Small-scale systems for in vivo drug delivery, Nat. Biotechnol. 21 (10) (2003) 1184–1191, https://doi.org/10.1038/nbt876.
[38] S. Mura, J. Nicolas, P. Couvreur, Stimuli-responsive nanocarriers for drug delivery, Nat. Mater. 12 (2013) 991, https://doi.org/10.1038/nmat3776.
[39] A.V. Ambade, E.N. Savariar, S. Thayumanavan, Dendrimeric micelles for controlled drug release and targeted delivery, Mol. Pharm. 2 (4) (2005) 264–272, https://doi.org/10.1021/mp050020d.
[40] P. Bawa, V. Pillay, Y.E. Choonara, L.C. du Toit, Stimuli-responsive polymers and their applications in drug delivery, Biomed. Mater. 4 (2) (2009) 022001, , https://doi.org/10.1088/1748-6041/4/2/022001.
[41] U. Borchert, U. Lipprandt, M. Bilang, A. Kimpfler, A. Rank, R. Peschka-Süss, R. Schubert, P. Lindner, S. Förster, pH-induced release from P2VP – PEO block copolymer vesicles, Langmuir 22 (13) (2006) 5843–5847, https://doi.org/10.1021/la060227t.
[42] T. Tanaka, Dynamics of critical concentration fluctuations in gels, Phys. Rev. A 17 (2) (1978) 763–766, https://doi.org/10.1103/PhysRevA.17.763.
[43] C. Weber, R. Hoogenboom, U.S. Schubert, Temperature responsive bio-compatible polymers based on poly(ethylene oxide) and poly(2-oxazoline)s, Prog. Polym. Sci. 37 (5) (2012) 686–714, https://doi.org/10.1016/j.progpolymsci.2011.10.002.
[44] X. Zhao, W. Liu, D. Chen, X. Lin, W.W. Lu, Effect of block order of ABA- and BAB-type NIPAAm/HEMA triblock copolymers on thermoresponsive behavior of solutions, Macromol. Chem. Phys. 208 (16) (2007) 1773–1781, https://doi.org/10.1002/macp.200700155.
[45] N.P. Balsara, M. Tirrell, T.P. Lodge, Micelle formation of BAB triblock copolymers in solvents that preferentially dissolve the A block, Macromolecules 24 (8) (1991) 1975–1986, https://doi.org/10.1021/ma00008a040.
[46] S.H. Kim, W.H. Jo, A Monte Carlo simulation for the micellization of ABA- and BAB-type triblock copolymers in a selective solvent. II. Effects of the block composition, J. Chem. Phys. 117 (18) (2002) 8565–8572, https://doi.org/10.1063/1.1512646.
[47] A.J. de Graaf, K.W.M. Boere, J. Kemmink, R.G. Fokkink, C.F. van Nostrum, D.T.S. Rijkers, J. van der Gucht, H. Wienk, M. Baldus, E. Mastrobattista, T. Vermonden, W.E. Hennink, Looped structure of flowerlike micelles revealed by 1H NMR relaxometry and light scattering, Langmuir 27 (16) (2011) 9843–9848, https://doi.org/10.1021/la2019605.
[48] C. Schwarzenböck, P.J. Nelson, R. Huss, B. Rieger, Synthesis of next generation dual-responsive cross-linked nanoparticles and their application to anti-cancer drug delivery, Nanoscale 10 (34) (2018) 16062–16068, https://doi.org/10.1039/C8NR04760J.
[49] J. Fang, H. Nakamura, H. Maeda, The EPR effect: unique features of tumor blood vessels for drug delivery, factors involved, and limitations and augmentation of the effect, Adv. Drug Deliv. Rev. 63 (3) (2011) 136–151, https://doi.org/10.1016/j.addr.2010.04.009.
[50] J. Wang, W. Mao, L.L. Lock, J. Tang, M. Sui, W. Sun, H. Cui, D. Xu, Y. Shen, The role of micelle size in tumor accumulation, penetration, and treatment, ACS Nano 9 (7) (2015) 7195–7206, https://doi.org/10.1021/acsnano.5b02017.

From Lanthanide-mediated, High-Precision Group Transfer Polymerization of Michael-type Monomers, to Intelligent, Functional Materials

[51] F. Adams, P.T. Altenbuchner, P.D.L. Werz, B. Rieger, Multiresponsive micellar block copolymers from 2-vinylpyridine and dialkylvinylphosphonates with a tunable lower critical solution temperature, RSC Adv. 6 (82) (2016) 78750–78754, https://doi.org/10.1039/C6RA17160E.

[52] L.I. Atanase, G. Riess, Micellization of pH-stimulable poly(2-vinylpyridine)-b-poly (ethylene oxide) copolymers and their complexation with anionic surfactants, J. Colloid Interface Sci. 395 (2013) 190–197, https://doi.org/10.1016/j.jcis.2012.12.058.

[53] C. Tsitsilianis, D. Voulgaris, M. Štěpánek, K. Podhájecká, K. Procházka, Z. Tuzar, W. Brown, Polystyrene/poly(2-vinylpyridine) heteroarm star copolymer micelles in aqueous media and onion type micelles stabilized by diblock copolymers, Langmuir 16 (17) (2000) 6868–6876, https://doi.org/10.1021/la000176e.

[54] Y. Yu, D. Hong, Z. Liu, F. Jia, Y. Zhou, C. Leng, Controllable preparation and characterization of the thermosensitive block polymers, J. Polym. Res. 20 (9) (2013) 235, https://doi.org/10.1007/s10965-013-0235-0.

[55] C.F. van Nostrum, Covalently cross-linked amphiphilic block copolymer micelles, Soft Matter 7 (7) (2011) 3246–3259, https://doi.org/10.1039/C0SM00999G.

[56] P. Galvin, D. Thompson, K.B. Ryan, A. McCarthy, A.C. Moore, C.S. Burke, M. Dyson, B.D. MacCraith, Y.K. Gun'ko, M.T. Byrne, Y. Volkov, C. Keely, E. Keehan, M. Howe, C. Duffy, R. MacLoughlin, Nanoparticle-based drug delivery: case studies for cancer and cardiovascular applications, Cell. Mol. Life Sci. 69 (3) (2012) 389–404, https://doi.org/10.1007/s00018-011-0856-6.

[57] C. Schwarzenbock, A. Schaffer, P. Pahl, P.J. Nelson, R. Huss, B. Rieger, Precise synthesis of thermoresponsive polyvinylphosphonate-biomolecule conjugates via thiol-ene click chemistry, Polym. Chem. 9 (3) (2018) 284–290, https://doi.org/10.1039/C7PY01796K.

[58] E. Ikonen, Cellular cholesterol trafficking and compartmentalization, Nat. Rev. Mol. Cell Biol. 9 (2) (2008) 125–138, https://doi.org/10.1038/nrm2336.

[59] K. Simons, W.L. Vaz, Model systems, lipid rafts, and cell membranes 1, Annu. Rev. Biophys. Biomol. Struct. 33 (2004) 269–295, https://doi.org/10.1146/annurev.biophys.32.110601.141803.

[60] C. Chen, J. Ke, X.E. Zhou, W. Yi, J.S. Brunzelle, J. Li, E.-L. Yong, H.E. Xu, K. Melcher, Structural basis for molecular recognition of folic acid by folate receptors, Nature 500 (7463) (2013) 486–489, https://doi.org/10.1038/nature12327.

[61] C.M. Alexander, K.L. Hamner, M.M. Maye, J.C. Dabrowiak, Multifunctional DNA-gold nanoparticles for targeted doxorubicin delivery, Bioconjug. Chem. 25 (7) (2014) 1261–1271, https://doi.org/10.1021/bc500136r.

[62] B. Stella, S. Arpicco, M.T. Peracchia, D. Desmaële, J. Hoebeke, M. Renoir, J. D'Angelo, L. Cattel, P. Couvreur, Design of folic acid-conjugated nanoparticles for drug targeting, J. Pharm. Sci. 89 (11) (2000) 1452–1464, https://doi.org/10.1002/1520-6017(200011)89:11<1452::AID-JPS8>3.0.CO;2-P.

[63] X. Qiang, T. Wu, J. Fan, J. Wang, F. Song, S. Sun, J. Jiang, X. Peng, Preparation and folic acid conjugation of fluorescent polymer nanoparticles for cancer cell targeting, J. Mater. Chem. 22 (31) (2012) 16078–16083, https://doi.org/10.1039/C2JM30618B.

[64] S. Dong, H.J. Cho, Y.W. Lee, M. Roman, Synthesis and cellular uptake of folic acid-conjugated cellulose nanocrystals for cancer targeting, Biomacromolecules 15 (5) (2014) 1560–1567, https://doi.org/10.1021/bm401593n.

[65] T. Wagner, A. Manhart, N. Deniz, A. Kaltbeitzel, M. Wagner, G. Brunklaus, W.H. Meyer, Vinylphosphonic acid homo- and block copolymers, Macromol. Chem. Phys. 210 (22) (2009) 1903–1914, https://doi.org/10.1002/macp.200900284.

[66] C. Schwarzenböck, A. Schaffer, E. Nößner, P.J. Nelson, R. Huss, B. Rieger, Fluorescent polyvinylphosphonate bioconjugates for selective cellular delivery, Chem. – Eur. J. 24 (11) (2018) 2584–2587, https://doi.org/10.1002/chem.201706034.

[67] T. Yoshikawa, L.P. Ruhr, W. Flory, D. Giamalva, D.F. Church, W.A. Pryor, Toxicity of polycyclic aromatic hydrocarbons: I. Effect of phenanthrene, pyrene, and their ozonized products on blood chemistry in rats, Toxicol. Appl. Pharmacol. 79 (2) (1985) 218–226, https://doi.org/10.1016/0041-008X(85)90343-6.

[68] C. Schwarzenböck, S.I. Vagin, W.R. Heinz, P.J. Nelson, B. Rieger, Studies on the biocompatibility of poly(diethyl vinyl-phosphonate) with a new fluorescent marker, Macromol. Rapid Commun. 39 (15) (2018) 1800259, https://doi.org/10.1002/marc.201800259.

[69] A. Canty, B. Skelton, P. Traill, A. White, Structural chemistry of the platinum group-metals: MCl < sub > 2 < /sub > (bpy) (M = Pd, Pt, bpy = 2,2′-Bipyridine), Aust. J. Chem. 45 (2) (1992) 417–422, https://doi.org/10.1071/CH9920417.

[70] C. Kaes, A. Katz, M.W. Hosseini, Bipyridine: the most widely used ligand. A review of molecules comprising at least two 2,2'-bipyridine units, Chem. Rev. 100 (10) (2000) 3553–3590, https://doi.org/10.1021/cr990376z.

[71] J. Komoschinski, E. Steckhan, Efficient indirect electrochemical in situ regeneration of NAD+ and NADP+ for enzymatic oxidations using iron bipyridine and phenanthroline complexes as redox catalysts, Tetrahedron Lett. 29 (27) (1988) 3299–3300, https://doi.org/10.1016/0040-4039(88)85145-1.

[72] M.T. Carter, M. Rodriguez, A.J. Bard, Voltammetric studies of the interaction of metal chelates with DNA. 2. Tris-chelated complexes of cobalt(III) and iron(II) with 1,10-phenanthroline and 2,2'-bipyridine, J. Am. Chem. Soc. 111 (24) (1989) 8901–8911, https://doi.org/10.1021/ja00206a020.

[73] S. Derien, E. Dunach, J. Perichon, From stoichiometry to catalysis: electroreductive coupling of alkynes and carbon dioxide with nickel-bipyridine complexes. Magnesium ions as the key for catalysis, J. Am. Chem. Soc. 113 (22) (1991) 8447–8454, https://doi.org/10.1021/ja00022a037.

[74] R.G. Inskeep, Infra-red spectra of metal complex ions below 600 cm − 1—I: The spectra of the tris complexes of 1, 10-phenanthroline and 2,2′-bipyridine with the transition metals iron(II) through zinc(II), J. Inorg. Nucl. Chem. 24 (7) (1962) 763–776, https://doi.org/10.1016/0022-1902(62)80096-7.

[75] S.M. Barnett, K.I. Goldberg, J.M. Mayer, A soluble copper–bipyridine water-oxidation electrocatalyst, Nat. Chem. 4 (2012) 498, https://doi.org/10.1038/nchem.1350.

[76] F. Adams, M. Pschenitza, B. Rieger, Yttrium-catalyzed synthesis of bipyridine-functionalized AB-block copolymers: micellar support for photocatalytic active rhenium-complexes, ChemCatChem 10 (19) (2018) 4309–4316, https://doi.org/10.1002/cctc.201801009.

[77] B.J. McNicholas, J.D. Blakemore, A.B. Chang, C.M. Bates, W.W. Kramer, R.II. Grubbs, II.B. Gray, Electrocatalysis of CO2 reduction in brush polymer ion gels, J. Am. Chem. Soc. 138 (35) (2016) 11160–11163, https://doi.org/10.1021/jacs.6b08795.

[78] S. Sahu, P.L. Cheung, C.W. Machan, S.A. Chabolla, C.P. Kubiak, N.C. Gianneschi, Charged macromolecular rhenium bipyridine catalysts with tunable CO2 reduction potentials, Chem. – Eur. J. 23 (36) (2017) 8619–8622, https://doi.org/10.1002/chem.201701901.

Andreas Schaffer studied chemistry at the Technische Universität München and received his M.Sc. degree in 2017. In 2016, he carried out an internship at EOS Electro Optical Systems GmbH in Krailling (Germany) focusing on the preparation and characterization of novel polymer materials for the 3D-printing process. During his master's thesis in the group of Bernhard Rieger he developed novel polymer-conjugates via coupling of biomolecules to polyvinylphosphonates and enabled their detection via introduction of fluorescent moieties. Since 2017 he is continuing his scientific career as a Ph.D. candidate with the group of Prof. Rieger. His work includes the development of novel materials containing polyvinylphosphonates, synthesis of novel initiators for REM-GTP and the post-polymerization functionalization of this exciting polymer class.

Michael Weger received his B.Sc. (2014) and his M.Sc. degree (2016) in chemistry from the Technische Universität München under the guidance of Prof. Bernhard Rieger. He is currently doing his Ph.D. work in the group of Prof. Rieger for which he received a scholarship of the Studienstiftung des deutschen Volkes. The key goal of his research interests is to establish a main group element-mediated group transfer polymerization based on the readily available aluminum. The catalysts are intended for the (co)polymerization of polar monomers, especially for the synthesis of polyacrylonitrile, the most important precursor for carbon fibers.

Bernhard Rieger studied chemistry at the Ludwig-Maximilians-Universität München (LMU) and received his Ph.D. in 1988. After research at the University of Massachusetts at Amherst and in the plastics laboratory of BASF SE, he received his habilitation in 1995 at the University of Tübingen. In 1996, he became professor at the Department Materials and Catalysis at the University of Ulm. Since 2006, he has been professor at the Technische Universität München at the WACKER-Chair of Macromolecular Chemistry and director of the Institute of Silicon Chemistry. He is a fellow of the National Academy of Science and Engineering "acatech" (2013), a member of the European Academy of Science (2011), a member of the Finnish Academy of Science and Letters (2008), and an Honorary Doctor Dr. h.c. phil. of the University of Helsinki (2007). In 2013, he was awarded the Wöhler Prize for Sustainable Chemistry and holds a Philip Morris Award. Since 2015 he is the spokesperson of IRTG 2022 "ATUMS" - Alberta/TUM International Graduate School for Functional Hybrid Materials.

4.4 Reprint Permission Copyrighted Content

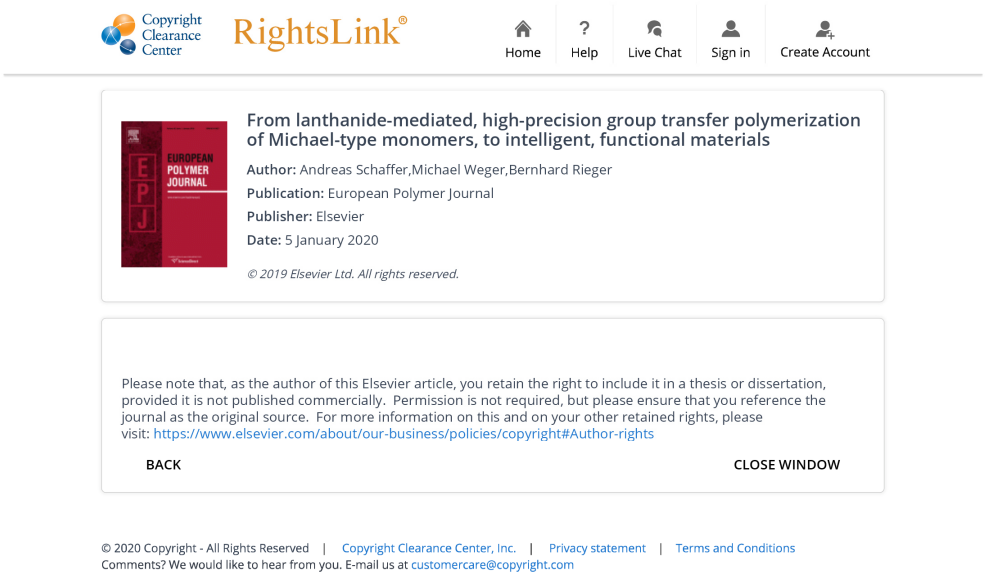

5 Synthesis and Application of Functional Group-Bearing Pyridyl-Based Initiators in Rare Earth Metal-Mediated Group Transfer Polymerization

5.1 Bibliographic Data

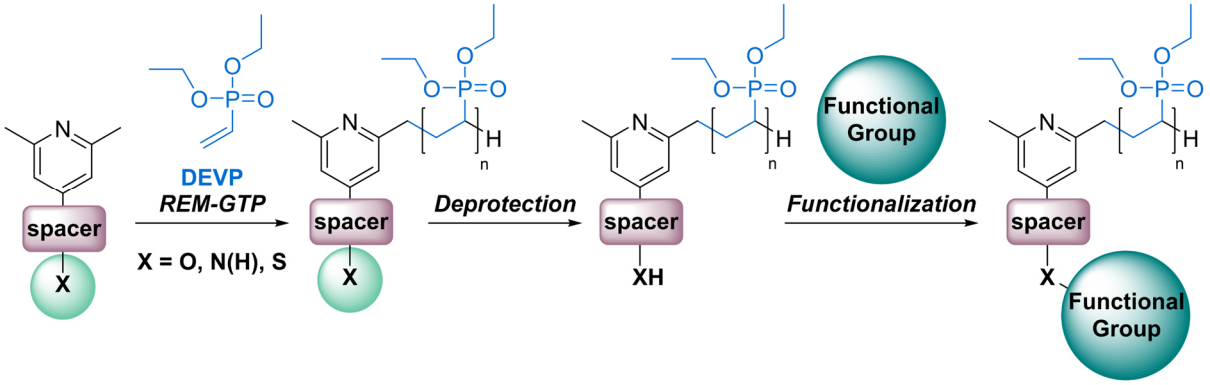

Title: "Synthesis and Application of Functional Group-Bearing Pyridyl-Based Initiators in Rare Earth Metal-Mediated Group Transfer Polymerization"

Status: Full paper, published online 28th May 2020

Journal: Macromolecules 2020, 53, 11, 4345–4354

Publisher: American Chemical Society

Link/DOI: https://pubs.acs.org/doi/10.1021/acs.macromol.0c00642

Authors: Andreas Schaffer, Moritz Kränzlein, and Bernhard Rieger[a]

[a]Andreas Schaffer had the initial idea, executed most of the experiments and wrote the manuscript. Moritz Kränzlein synthesized one initiator and contributed with fruitful ideas. All work was carried out under supervision of Bernhard Rieger.

5.2 Summary

Due to their high biocompatibility, a thermoresponsive behavior and an option for the selective end-group modification with biologically relevant functions polyvinylphosphonates are considered ideal candidates for (bio)medical applications. The latter one was initially achieved via C-H bond activation of 2,6-dimethyl-4-(4-vinylphenyl)pyridine with $Cp_2Y(CH_2TMS)(THF)$ which facilitated the introduction of a terminal vinyl group in PDEVP. However, an efficient conversion of the terminal olefin was limited to thiol group containing substrates which potentially require a complex modification strategy prior to the conjugation step. Consequently, novel initiator motifs were designed to expand this synthetic platform. Hence, the group tolerance of $Cp_2Y(CH_2TMS)(THF)$ was investigated in the C-H bond activation of three initiators which comprised protected functional groups (OH – O-*tert*-butyldimethylsilyl; NH_2 – 2,5-dimethylpyrrole; SH – STrityl). These experiments were found to be successful and all activated species were characterized in detail by ^{1}H and ^{13}C nuclear magnetic resonance (NMR) spectroscopy. The incorporation of the individual moieties was confirmed through ESI-MS and diffusion ordered spectroscopy (DOSY). Following this, DEVP was polymerized by employing these initiators in the REM-GTP. All obtained polymers were characterized by ^{1}H-, ^{31}P- and DOSY-NMR as well as gel permeation chromatography multi-angle light scattering (GPC-MALS). Hereafter, the polymers were deprotected to release the reactive motifs. Analysis of the deprotected substrates via ^{1}H-, ^{31}P-NMR and GPC-MALS verified the integrity of the polymers. Post-polymerization functionalization with either cholesteryl chloroformate or *N*-phenyl maleimide proved this approach to be viable for the formation of the respective polymer conjugates. One more time, NMR spectroscopy confirmed the covalent coupling of the small molecules to PDEVP.

As the C-H bond activation showed high flexibility towards the initiator structure, this synthetic strategy is able to establish a foundation for sophisticated polymer conjugates comprising complex and highly functional molecules.

5.3 Manuscript

Macromolecules

pubs.acs.org/Macromolecules Article

Synthesis and Application of Functional Group-Bearing Pyridyl-Based Initiators in Rare Earth Metal-Mediated Group Transfer Polymerization

Andreas Schaffer, Moritz Kränzlein, and Bernhard Rieger*

Cite This: Macromolecules 2020, 53, 4345−4354 Read Online

ACCESS | Metrics & More | Article Recommendations | Supporting Information

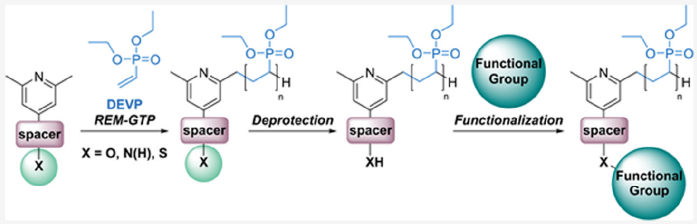

ABSTRACT: The polymer class of poly(vinylphosphonates) offers a wide array of attractive features such as high biocompatibility, thermoresponsive behavior, and the option for the directed introduction of small molecules at the initial step of the polymerization. Through the latter, polymer conjugates consisting of targeting ligands, fluorophores, or pharmacologically active substances become feasible. However, the modification of such compounds for the utilization in postpolymerization functionalization is usually cumbersome due to their structural complexity. In this study, we considered this factor and envisioned a flexible platform of functional polymers via the introduction of initiators comprising reactive functionalities. Hence, a series of customized initiators with protected functional groups (O-*tert*-butyldimethylsilyl, 2,5-dimethylpyrrole, and STrityl) were synthesized and studied in the C−H bond activation with $Cp_2Y(CH_2TMS)(THF)$. The positive outcome of the activation experiments allowed the use of these initiators in the rare earth metal-mediated group transfer polymerization (REM-GTP). The versatility of this approach was demonstrated by end-group analysis using electrospray ionization mass spectrometry (ESI-MS) and DOSY-NMR, confirming the incorporation of the individual end group in poly(diethyl vinylphosphonate) (PDEVP). On this basis, PDEVP with varying feed concentrations was generated and the protection groups were removed to release the reactive motif. Doing so eventually enabled the successful coupling of model compounds, namely, cholesteryl chloroformate and *N*-phenyl maleimide, which established a foundation in the direction of more sophisticated polymer conjugates involving complex and highly functional compounds.

■ INTRODUCTION

Stimuli-responsive polymers have aroused a broad interest during recent years because these kinds of polymers add a new level of complexity to the material, allowing control of the polymer properties upon reaching certain trigger conditions.[1−3] Their stimulus response enables their application in a variety of fields, i.e., (bio)sensing,[3−6] drug delivery,[7−10] responsive coatings targeting for adhesive surfaces,[10−12] and bioseparation.[3,13−15] These polymers can be sensitive to changes in temperature and pH or show conformational changes upon irradiation when light-sensitive moieties are present.[1,2] Among these, the best-studied group is the thermoresponsive polymers. These polymers exhibit a lower or an upper critical solution temperature (LCST and UCST), transitioning from a homogeneous solution to a heterogeneous phase upon reaching the cloud point T_c.[16,17] A broad diversity of polymers is known that features such a behavior, ranging from poly(*N*,*N*-diethylacrylamide),[8] derivatives of 2-oxazoline,[16] to poly(phosphonate)s[18] and, most prominently, poly(*N*-isopropylacrylamide) (PNIPAam), which offers a phase transition at 30−35 °C, being close to the physiological body temperature.[16] The rather new class of poly(vinylphosphonates) is complementing these thermoresponsive substrates. Poly(vinylphosphonates) feature a sharp and tunable phase transition (T_{LCST} = 5−92 °C) in aqueous solution, as well as high biocompatibility toward HEK-293 and HMEC-1 cells.[19,20] Polymerization of the α,β-unsaturated

Received: March 19, 2020
Revised: May 4, 2020
Published: May 28, 2020

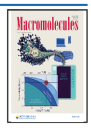

https://dx.doi.org/10.1021/acs.macromol.0c00642
Macromolecules 2020, 53, 4345−4354

Scheme 1. Overview on the Synthetic Pathways Toward the Initiator Structures 1−3

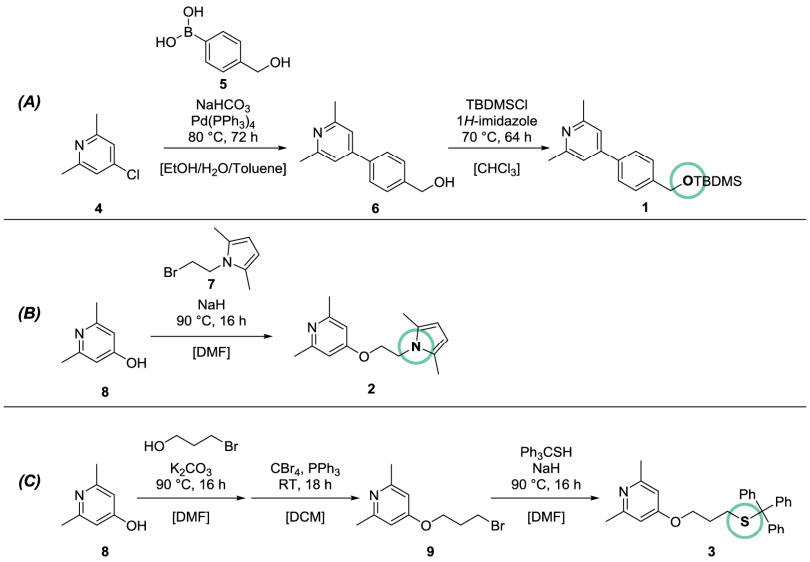

vinylphosphonates is performed via the so-called rare earth metal-mediated group transfer polymerization (REM-GTP), which is based on the pioneering work of Webster and colleagues, who, for the first time, employed the concept of GTP with organosilicon initiators.[21] Yasuda et al. refined this approach by using neutral samarocenes in the defined polymerization of methyl methacrylate (MMA),[22,23] whereas Collins and Ward focused on the application of cationic zirconocenes.[24] Consequently, lanthanide metallocenes proved to be highly efficient catalysts for the polymerization of diethyl vinylphosphonate (DEVP). In 2010, our group was successful in the generation of high-molecular-weight poly(diethyl vinylphosphonate) (PDEVP) by using Cp_2YbMe as a catalyst.[25] After this breakthrough, a variety of complexes with different metal centers and ligand spheres were explored regarding their catalytic activity and were investigated to gain deeper insights into the polymerization mechanism.[26−28] However, these studies revealed a complex initiation network leading to an inefficient and slow initiation process.[27,29] Nevertheless, lanthanides also show a high affinity toward σ-bond metathesis, which is why C−H bond activation was envisioned as an elegant workaround for this issue. This approach was already successfully investigated by the Mashima group, which treated yttrium−ene diamido complexes with 2,4,6-trimethylpyridine (*sym*-collidine), and Ł'euben et al., who employed 2-methylpyridine in the C−H bond activation.[30−32] Based on this work, $Cp_2Y(CH_2TMS)(THF)$ (**10**) was converted with *sym*-collidine into a highly active species allowing to polymerize DEVP without an initiation delay.[29] Moreover, this procedure renders the incorporation of reactive end groups in the polymer chain possible, which was demonstrated in the C−H bond activation of a novel vinyl group-bearing initiator that facilitated the synthesis of (fluorescent) polymer−biomolecule conjugates. The formation of photocatalytically active AB block copolymers through the introduction of terminal bipyridines, as well as the synthesis of star-shaped polymers using multifunctional initiators, was also possible.[20,33−35]

Given the indicated flexibility of the C−H bond activation process, we were motivated to push toward initiator motifs with a higher level of complexity. In this study, we aimed for the linkage of a protected hydroxyl (OH—O-*tert*-butyldimethylsilyl (TBDMS)), amine (NH_2−pyrrole), and thiol group (SH—STrityl) to the initiators and investigated these novel structures in the σ-bond metathesis with $Cp_2Y(CH_2TMS)(THF)$ (**10**). Moreover, the behavior of the activated complexes in the polymerization of DEVP was also studied. Eventually, both the removability of the protective groups from the obtained polymers and the (re)functionalization of the released groups were investigated.

■ RESULTS AND DISCUSSION

Initiator Syntheses. To introduce the desired functional groups, we had to consider the sensitivity of the rare earth metal complex toward protic motifs since this sensitivity results in the degradation of the complex. As a result, the hydroxyl, amine, and thiol groups are needed to be masked by adequate protection groups. In addition, these protective groups should not interfere with the C−H bond activation process, e.g., through blocking of the metal center or side reactions induced by the metal atom. Therefore, silyl, pyrrole, and trityl groups appeared to be best suited for the target structures **1**−**3** (Scheme 1).

The synthesis of the hydroxyl group-bearing initiator **1** was realized by a Suzuki cross-coupling in the first instance, starting from 4-chloro-2,6-dimethylpyridine (**4**) and boronic acid **5** to form intermediate **6** in high yields. The two-step synthesis of organohalide **4** followed procedures from the literature.[35] A

https://dx.doi.org/10.1021/acs.macromol.0c00642
Macromolecules 2020, 53, 4345−4354

coupling product **6** was then reacted with *tert*-butyldimethylsilyl chloride and 1*H*-imidazole to yield the desired structure **1** (Scheme 1A). Since two acidic protons had to be protected in the case of initiator **2**, standard protection groups such as Boc, Fmoc, or CBz were inappropriate. Eventually, 2,5-dimethylpyrrole manifested as the group of choice, making it possible to mask the amine group in a stable heterocycle. Hence, it was necessary to prepare 1-(2-bromoethyl)-2,5-dimethyl-1*H*-pyrrole (**7**) from 2,5-hexanedione and 2-bromoethylamine, which was achieved by a published procedure.[36] Subsequently, initiator **2** was formed in a reaction between bromide **7** and alcohol **8** (Scheme 1B). The trityl-group-bearing initiator **3** could be obtained via a three-step approach. Thus, the alcohol 3-((2,6-dimethylpyridin-4-yl)oxy)propan-1-ol known from the literature was prepared from 2,6-dimethyl-4-hydroxypyridine (**8**) and 3-bromopropanol[37] followed by an Appel reaction to yield the corresponding organobromide **9**.[38] Eventually, thioether **3** was generated by using triphenylmethanethiol (Scheme 1C). All novel initiator motifs were fully characterized by elemental analysis, ^{1}H, ^{13}C, and ^{29}Si NMR spectroscopy, as well as electrospray ionization mass spectrometry (ESI-MS).

C−H Bond Activation. As shown in the literature, transition metals comprising a d^0 electron configuration are prone to σ-bond metathesis,[31] which is beneficial for the C−H bond activation of 2,6-dimethylpyridyl motifs. Consequently, the novel initiators were investigated regarding their ability to be activated in such C−H bond activations. Therefore, equal amounts of the initiator and $Cp_2Y(CH_2TMS)(THF)$ (**10**) were dissolved in dry benzene-d_6, which immediately resulted in yellow- to orange-colored solutions after mixing both components, which already indicated a successful activation process (Scheme 2).

Scheme 2. Overview of the C−H Bond Activation Experiments with Initiators 1−3 Toward the Activated Species 11−13

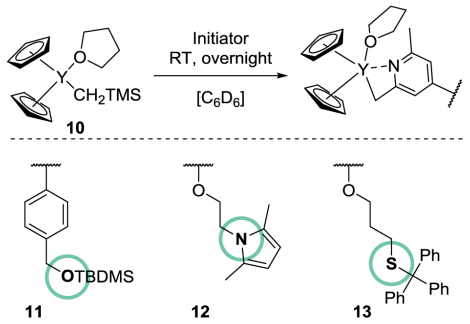

All in situ-generated catalysts were analyzed using ^{1}H NMR, thus revealing the conversion of one pyridyl-bound methyl group. An overview of all three activation products is given in Figure 1 along with the significant regions of the ^{1}H NMR (1.70−4.00 ppm) and ^{13}C NMR (28.0−44.0 ppm) spectra. For a better understanding of the activation process, the spectra of *sym*-collidine are illustrated in black.[29]

For complex **11** (blue), the yttrium-attached CH_2 group (2.40 ppm, 2H) and the remaining CH_3 group (2.12 ppm, 3H) are clearly visible. Moreover, the CH_2O signal of tetrahydrofuran (THF) is slightly shifted to 3.41 ppm compared to that of free THF in benzene-d_6, indicating that THF is still coordinating to the yttrium center. Looking more closely at the respective section in the ^{13}C NMR, a duplet of the C−Y bond (42.4 ppm) with a coupling constant of J_{CY} = 11.0 Hz can be assigned, which is in accordance with the activation process utilizing *sym*-collidine. Moving to the activation product **12** (green), the methylene group can be attributed to the peak at 2.27 ppm (2H), while the signals of the free methyl group and both methyl groups of the pyrrole ring are overlapping at 2.02 ppm (9H). Similar to **11**, a duplet at 41.5 ppm (J_{CY} = 11.6 Hz) is visible in the ^{13}C NMR, confirming the presence of the C−Y bond. In the case of compound **13** (orange), the original CH_3 signals are again split into the CH_2Y signal (2.27 ppm, 2H) and the remaining CH_3 group (2.03 ppm, 3H). Likewise, the ^{13}C NMR exhibits a duplet at 41.2 ppm (J_{CY} = 12.0 Hz) corresponding to the C−Y bond. Additionally, as found for **11**, both complexes **12** and **13** exhibit a slight upfield shift of the THF signals. In conclusion, the comparative analysis of initiators **1**−**3** with *sym*-collidine by NMR clearly proved the successful C−H bond activation using $Cp_2YCH_2TMS(THF)$ (**10**). Unfortunately, reasonable stability for all activated complexes could only be guaranteed in solution. Removal of the solvent under reduced pressure or freeze-drying resulted in the degradation of the complexes, as ^{1}H NMR spectroscopy revealed, preventing the characterization by elemental analysis. Presumably, this might be a result of the comparably large protecting groups and flexible orientation of the linkage, both of which inhibit an ordered assembly in a solid state.

End-Group Analysis. Encouraged by the generally positive outcome of the C−H bond activation, end-group analysis was performed via ESI-MS to verify the incorporation of the initiator in the polymer chain. For this purpose, catalysts **11**−**13** were treated with a small amount of DEVP (5 equiv) to form the respective oligomers. Furthermore, polymers **P1**, **P3**, and **P5** (compare Table 1) were analyzed by diffusion-ordered spectroscopy (DOSY)-NMR to corroborate the results from the ESI measurements. By way of example, Figure 2 illustrates the oligomer pattern of PDEVP generated from complex **11** and the related DOSY-NMR of polymer **P1**.

In Figure 2, the oligomer pattern received by ESI-MS analysis corroborates the covalent linkage of initiator **1**. The *m*/*z* values found can be attributed to the sole initiator **1** ionized with H^+ (328 u) and the respective oligomer signals ionized with H^+ as well (657, 821, and 985 u) (Figure 3, left, and Figure S7). In the ^{1}H NMR, the characteristic signals of the TBDMS group can be assigned to the signals at 0.14 and 0.97 ppm (Figure 2, right, and Figure S12). These signals share the same diffusion coefficient in DOSY-NMR as the polymer signals at 1.38 ppm ($POCH_2CH_3$) and 4.18 ppm ($POCH_2$), which substantiates a covalent linkage of the initiator and polymer (Figure 2, right, and Figure S13). The same analytic approach was rendered for initiators **2** and **3**. The corresponding ESI-MS measurement with pyrrole-containing initiator **2** revealed two oligomer patterns. One was ionized with H^+, indicating initiator **2** (245 u) and the oligomer signals (573, 738, 902, and 1066 u), while the second row was ionized with NH_4^+, presumably forming an adduct with acetonitrile (631, 798, and 960 u). Interestingly, **2** seemed to form dimers indicated by the signals at 261 and 275 u (Figure S8). Likewise, **P2** was analyzed via DOSY-NMR, proving that the characteristic pyrrole singlet at 5.65 ppm can be assigned to the

https://dx.doi.org/10.1021/acs.macromol.0c00642
Macromolecules 2020, 53, 4345−4354

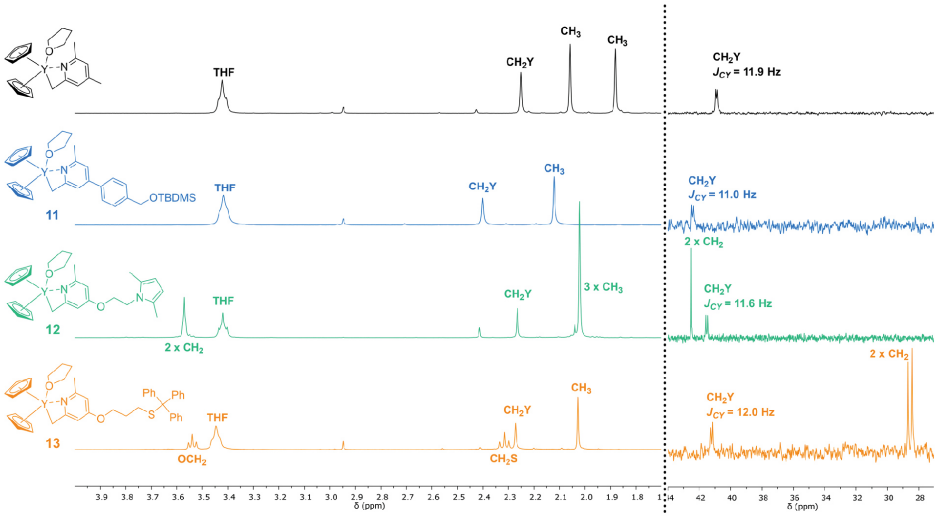

Figure 1. Comparison of the significant regions of the ^{1}H NMR (left) and ^{13}C NMR (right) spectra of *sym*-collidine (top) and the activated complexes **11**−**13** in C_6D_6.

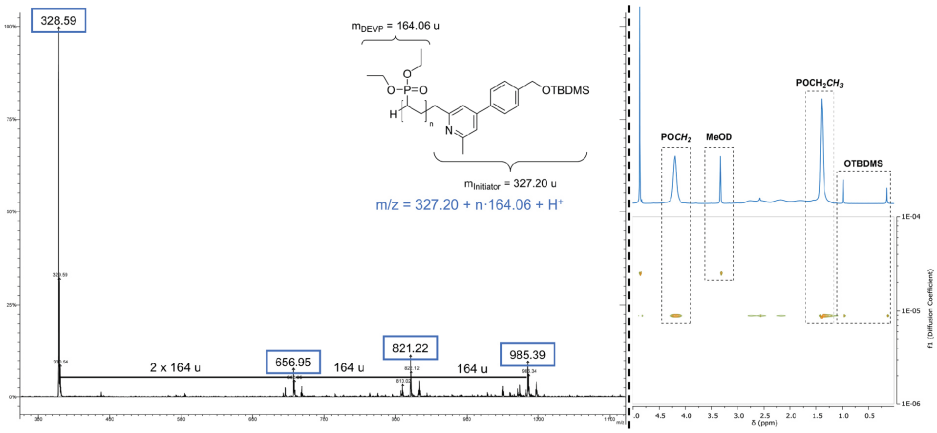

Figure 2. ESI-MS spectrum of the PDEVP oligomers generated with species **11** measured in acetonitrile (left) and the corresponding DOSY-NMR section of polymer **P1** in MeOD (right).

polymer (Figures S17 and S18) and verifying a covalent bond between **2** and the polymer. Finally, oligomeric PDEVP was generated using **13**. Similar to the findings for **12**, two patterns were assigned in the respective ESI-MS spectrum (Figure S9). When again ionized with H^+, initiator **3** (440 u) and the respective oligomer signals (604, 769, 933, and 1097 u) were identified. Moreover, oligomer signals ionized with NH_4^+ (662, 827, and 991 u, adduct with acetonitrile) were also able to be matched. ^{1}H and DOSY-NMR strongly supported the results of the ESI-MS measurements (Figures S22 and S23) since only one polymeric species was present. In summary, the combination of mass spectrometry and DOSY-NMR clearly confirms the presence of the initiating group at the chain end in the cases of all three initiators **1**−**3**.

Polymerization Studies with Complexes 11−13. To fully characterize the new complexes for REM-GTP, compounds **11**−**13** were investigated in time-dependent polymerization experiments. The samples acquired in these experiments were analyzed via ^{31}P NMR to produce a time-dependent plot of the DEVP conversion and by gel permeation chromatography to verify the living character of the polymerizations. The results for the polymerization of DEVP (600 equiv) with complex **11** are illustrated in Figure 3 by a

https://dx.doi.org/10.1021/acs.macromol.0c00642
Macromolecules 2020, 53, 4345−4354

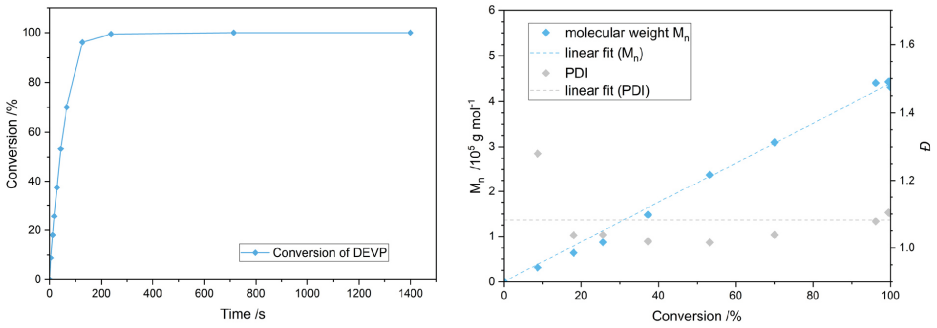

Figure 3. Conversion−time plot (left) and corresponding molecular weights M_n and the polydispersities $Đ$ of PDEVP generated from DEVP (600 equiv) with species **11** (right).

Scheme 3. Polymerization of DEVP with Catalysts 11−13

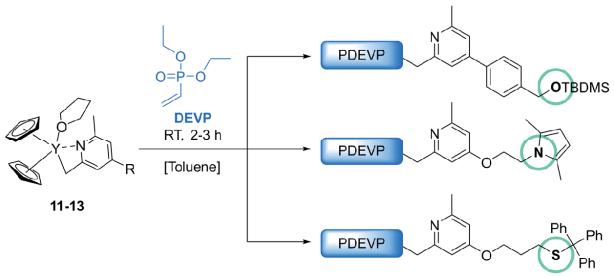

Table 1. Feed Ratio, Molecular Weights M_n, Polydispersities $Đ$, Initiator Efficiencies IE, and Cloud Points T_c of PDEVP in Aqueous Solution

entry	product	catalyst	$[M]_0/[cat]_0$	$M_{n,NMR}$[a]/kg mol^{-1}	$M_{n,GPC}$[b]/kg mol^{-1}	$Đ$[c]	IE[d]/%	T_c/°C
1	**P1**	**11**	25	7.20	10.9	1.13	41	33.0
2	**P2**	**11**	100	23.7	20.3	1.05	82	47.5
3	**P3**	**12**	25	7.50	13.2	1.18	33	41.5
4	**P4**	**12**	100	25.3	27.5	1.34	61	44.0
5	**P5**	**13**	25	7.70	10.8	1.13	42	35.0
6	**P6**	**13**	100	23.0	25.6	1.05	66	47.0

[a] $M_{n,NMR} = M_{Initiator} + (I_{POCH_2}/4) \times M_{DEVP}$. The integral of the $POCH_2$ signal was determined by normalization to a characteristic signal of the initiator. [b] Absolute determination of the molecular weight by gel permeation chromatography multiangle light scattering (GPC-MALS) in THF/H_2O. [c] Polydispersity index $Đ$ (averaged over the entire peak). [d] $I^* = M_{n,theo}/M_{n,GPC} \times 100\%$ with $M_{n,theo} = M_{Initiator} \times$ equivalents $\times M_{DEVP}$.

conversion−time plot (left) and the conversion-dependent plot of the molecular weights M_n (right).

As expected for DEVP, the polymerization using **11** proceeded very fast and was completed after only 240 s (Figure 3, left). Moreover, no initiation delay was detected, meaning that the polymerization starts immediately upon injection of the monomer, which is typical for the application of a pyridyl-type initiator in the REM-GTP of DEVP.[20,29] In addition, analysis of the aliquots via gel permeation chromatography multiangle light scattering (GPC-MALS) verified the living character of the polymerization, as indicated by the linear increase of molecular weights M_n, while simultaneously exhibiting low polydispersities (PDI) $Đ$ ($Đ$ = 1.04−1.28) (Figure 3, right). The same observations were made for the model polymerization of DEVP using species **12** and **13** (Figures S10 and S11). Here, too, the progression of the polymerization led to a linear growth of the molecular weights while exhibiting low polydispersities (complex **12**: $Đ$ = 1.09−1.21; complex **13**: $Đ$ = 1.06−1.15). Concerning the time-dependent plots of the DEVP conversion, a very short delay of approximately 5 seconds was observable, which might be attributed to the flexible linkage of the functional groups in **12** and **13** that are shielding the active center from the coordination of DEVP. The polymerization reached full conversion after 60 s in both cases. Upon verification of the living-type character of the DEVP polymerization, a multitude of polymerizations were rendered for the latter deprotection experiments using two different feed concentrations (25 and 100 equiv) (Scheme 3 and Table 1).

https://dx.doi.org/10.1021/acs.macromol.0c00642
Macromolecules 2020, 53, 4345−4354

Scheme 4. Cleavage of the Protection Groups (P1−P2: TBDMS, Left; P3−P4: Pyrrole, Middle; P5−P6: Trityl, Right) and Corresponding ^{1}H NMR Spectra in MeOD with the Significant Regions Before and After Deprotection (Bottom)

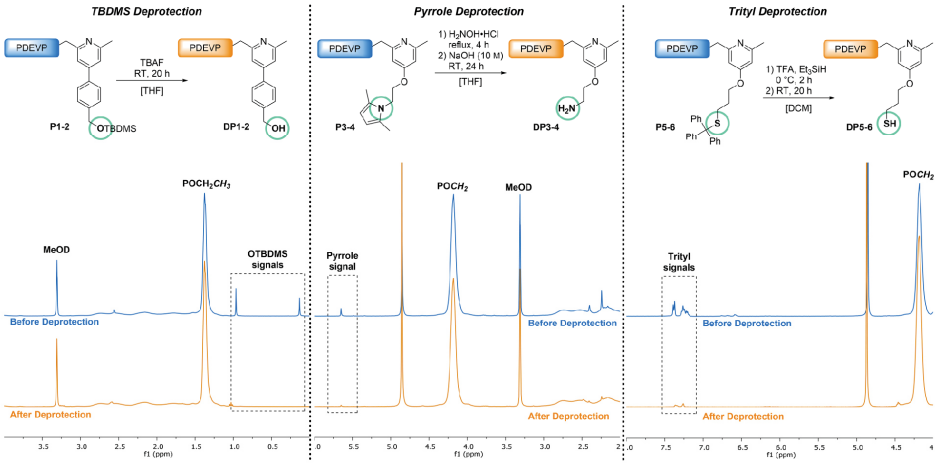

Table 2. Conversion of the Deprotection Reactions, Molecular Weights M_n Before and After Deprotection, Polydispersities $Đ$, and Cloud Points T_c of the Deprotected PDEVP in Aqueous Solution

entry	product	substrate	conversion[a]/%	$M_{n,GPC}$[b] (before)/kg mol^{-1}	$M_{n,GPC}$[b] (after)/kg mol^{-1}	$Đ$[c]	T_c/°C
1	**DP1**	**P1**	quant.	10.9	8.00	1.26	61.5
2	**DP2**	**P2**	quant.	20.3	22.8	1.05	52.5
3	**DP3**	**P3**	80	13.2	13.2	1.39	41.5
4	**DP4**	**P4**	quant.	27.5	30.5	1.38	48.5
5	**DP5**	**P5**	quant.	10.8	13.5	1.19	63.5
6	**DP6**	**P6**	quant.	25.6	35.2	1.16	48.5

[a]Calculated by comparison of the respective ^{1}H NMR spectra. [b]Absolute determination of the molecular weight by GPC-MALS in THF/H_2O. [c]Polydispersity index $Đ$ (averaged over the entire peak).

Molecular weights M_n and polydispersity indices $Đ$ were determined via GPC-MALS and validated by ^{1}H NMR for comparison. As noted in Table 1, all polymers show low PDIs ($Đ \leq 1.20$), with the exception of entry 4, in which case, a PDI of 1.34 was calculated for **P4**, which is slightly higher than expected for the polymers generated via REM-GTP. The higher polydispersity of **P4** can be attributed to a shoulder visible in the respective GPC trace (trace recorded by the MALS detector) (Figure S21). This shoulder was also observed for **P3**, indicating a polymeric species with lower molecular weight (Figure S19). This behavior seemed to correspond to the solution properties of **12**. Since ESI-MS indicated a dimer formation for initiator **2** (Figure S8), we also assumed a similar behavior for **12**, because **12** precipitated partially at higher concentrations but was dissolved after the addition of DEVP. Consequently, the initiation with the previously undissolved complexes started with a delay, yielding the shoulders visible in the GPC traces. Furthermore, all molecular weights M_n calculated via ^{1}H NMR are in good accordance with the values determined by GPC-MALS. Turbidity measurements were conducted to analyze the thermoresponsive behavior of the polymers. The respective cloud points (T_c) were defined as the temperature corresponding to a 10% decrease in optical transmittance. Interestingly, polymers **P1**, **P3**, and **P5** exhibited comparatively low cloud points (T_c = 33−41.5 °C). Especially in the case of the TBDMS and the trityl group, the hydrophobic nature of these moieties might have a significant effect on the enthalpy of mixing ΔH_{mix}, resulting in lower LCSTs. **P2**, **P4**, and **P6** themselves showed expected LCSTs between 44 and 47.5 °C.

Deprotection Experiments with PDEVP. In the next step of this study, we investigated the removal of the protection groups from the polymer end groups (Scheme 4).

Since silyl ethers can be easily cleaved under mild conditions using fluoride-donating reagents, treatment of the TBDMS-containing polymers **P1**−**P2** with 1 M tetrabutylammonium fluoride (TBAF) solution facilitated a quantitative deprotection (Scheme 4, left),[39] yielding PDEVP **DP1** (25 equiv DEVP; Figure S28) as well as **DP2** (100 equiv DEVP; Figure S30). Monitoring by ^{1}H NMR confirmed the complete disappearance of the TBDMS singlets (Scheme 4, left). The GPC results of the deprotected products were also in good agreement with the data of **P1**−**P2** (Table 1, entries 1 and 2). Both the molecular weights M_n and the polydispersity indices remained at the same level (Table 2, entries 1 and 2), meaning that the polymers stayed intact after the deprotection. The LCST of **DP1** showed an increase to 62.5 °C after the loss of the TBDMS group, supporting the assumption that the end group affects the solubilization in water.

https://dx.doi.org/10.1021/acs.macromol.0c00642
Macromolecules 2020, 53, 4345−4354

Scheme 5. Conversion of the Deprotected PDEVP Substrates DP1, DP3, and DP5 with Cholesteryl Chloroformate (Top, Middle) or *N*-Phenyl Maleimide (Bottom)

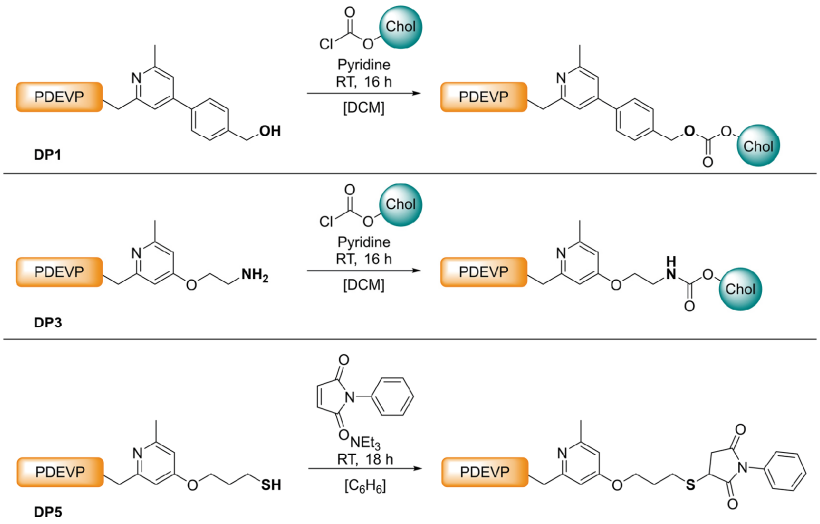

The decomposition of the pyrrole ring was imitated from a procedure found in the literature and requires more complex reaction conditions, in which case polymers **P3**−**P4** were refluxed in the presence of hydroxylamine and treated with 10 M sodium hydroxide solution later on to yield the free amine group (Scheme 4, center).[40] Also in this case, the reaction was monitored by ^{1}H NMR and it revealed a significant reduction of the pyrrole signal (Scheme 4, center). Comparison of the signal intensities concluded a conversion of 80% from **P3** to **DP3** (25 equiv DEVP), while the pyrrole signal vanished completely in the case of **P4** (100 equiv DEVP) (Figure S34). The molecular weight and PDI values of **DP3**−**DP4** determined by GPC-MALS (Table 2, entries 3 and 4) were in the same region as those of the corresponding polymers **P3**−**P4** (Table 1, entries 3 and 4). However, **DP4** showed an increased molecular weight of 30.5 kg mol^{-1}. It is possible that the exposed amine group led to an interaction with the column material and, therefore, deviations in the retention times. The cloud point of **DP4** increased by 4.5−48.5 °C, while the LCST of **DP3** remained constant at 41.5 °C. Usually, **DP4** should exhibit a lower LCST than **DP3**, because the LCST decreases with increasing molecular weights.[19] However, we assume that the cloud point of **DP3** was affected by the presence of polymer **P3** (80% conversion; compare Table 2, entry 3). Additionally, a salting-out effect appeared possible that was caused by inorganic residues of the deprotection agent.

Eventually, the deprotection experiments were performed with the trityl-group-bearing polymers **P5** and **P6** (Scheme 4, right). In this case, the conversion of **P5** and **P6** with trifluoroacetic acid (TFA) and triethylsilane yielded the fully deprotected species **DP5**−**DP6**, as revealed by ^{1}H NMR spectroscopy (Scheme 4, right, and Figure S39). Interestingly, the shift of the aromatic protons of the pyridyl unit moved downfield from approximately 6.75 to 7.25 ppm, which might be explained by the protonation of the pyridine motif by TFA.

In addition to the NMR analysis, the free thiol group in **DP5** was detected via UV−vis spectroscopy using Ellman's reagent (5,5′-dithiobis-(2-nitrobenzoic acid), DTNB). 2-Nitro-5-thiobenzoate (TNB) is released through the cleavage of the disulfide bond of DTNB during the reaction with a free thiol. Under neutral and basic conditions, the corresponding anion is formed, featuring a yellow color with an absorption maximum at around 412 nm (Figure S38).[41] Comparing the molecular weights and mass distributions of **DP5**−**DP6** with their precursors **P5**−**P6**, a similar trend can be noted. As stated for **DP3**−**DP4**, GPC analysis attributed an increase of the molecular weights to 13.5 and 35.2 kg mol^{-1} (Table 2, entries 5 and 6), which again might be explained by the interaction of the free thiol group with the column material. The LCST of **DP6** drastically increased from 35 to 63.5 °C. For a better overview, all important results of the deprotection experiments discussed above are summarized in Table 2.

Functionalization of the Released Moieties with Model Compounds. The final step of the study comprised the functionalization of the polymers **DP1**, **DP3**, and **DP5** (Table 2, entries 1, 3, and 5) with model compounds to prove their accessibility in the formation of polymer conjugates (Scheme 5).

With regard to the hydroxy and amino groups, we decided to choose cholesterol chloroformate as an electrophile to form the corresponding carbonate with **DP1** (Scheme 5, top) or to form carbamate from **DP3** (Scheme 5, middle). The formation of the cholesterol conjugate could be observed in both cases, revealing the cholesterol-associated methyl groups in the corresponding ^{1}H NMR spectra between 0.72 and 1.02 ppm (Figures S42 and S44). Additionally, the presence of a single polymeric species was confirmed by DOSY-NMR measurements (Figures S43 and S45). However, this approach needs some improvement for possible future applications because the coupling efficiency of the cholesterol substrate ranged between

https://dx.doi.org/10.1021/acs.macromol.0c00642
Macromolecules 2020, 53, 4345−4354

49% for **DP1** and 30% for **DP3** (calculated from proton NMR). We further decided to examine the Michael addition of a maleimide with a mercaptan species inspired from coupling reactions, as performed in bioconjugations or protein modifications.[42−44] In this specific case, we aimed for the conjugation of *N*-phenyl maleimide to the polymer **DP5** (Scheme 4, bottom). In the corresponding proton NMR, the newly introduced phenyl group was clearly visible in the region from 7.16 to 7.61 ppm (Figure S46). Likewise, DOSY-NMR of the product concluded a successful conjugation since the newly introduced phenyl group and the PDEVP signals share the same diffusion coefficient (Figure S47). The conversion calculated by ^{1}H NMR reaches a moderate value of 41%.

■ CONCLUSIONS

In summary, three novel initiator structures with masked functional groups (OH—O-*tert*-butyldimethylsilyl, NH_2—2,5-dimethylpyrrole, and SH—STrityl) were synthesized and successfully employed in the REM-GTP of DEVP. The 2,6-dimethylpyridyl motif allowed the selective C−H bond activation of these compounds with $Cp_2Y(CH_2TMS)(THF)$ (**10**) and enabled the precise polymerization of DEVP, initially incorporating these structures in the polymer chain. The covalent attachment of the novel groups was proofed by ESI-MS analysis and DOSY-NMR, revealing exclusively a single polymeric species in all three cases. Subsequent deprotection experiments resulted in the quantitative cleavage of the respective protection groups. Only in the case of the pyrrole-bearing PDEVP with a feed of 25 equiv DEVP was the conversion limited to 80%. The release of these functional groups allowed the conjugation of model substances, namely, cholesterol chloroformate and *N*-phenyl maleimide, to the polymer. With this work, we have demonstrated the group tolerance of the Cp_2Y system regarding the σ-bond metathesis and the ability to extend the scope of coupling partners for potential polymer conjugates. Consequently, the conjugation is not limited to thiols in the first place (as showcased with 2,6-dimethyl-4-(4-vinylphenyl)pyridine), but rather also renders the coupling of electrophilic substrates possible, allowing the formation of classical ester or amide linkages. This particular approach takes the often complex, structural nature of such highly functional coupling partners into account, e.g., targeting ligands (folic acid, peptides, or carbohydrates), imaging probes (fluorescein, rhodamine), or pharmacologically active agents (doxorubicin, paclitaxel). Moreover, the use of the deprotected polymers in orthogonal modification routes becomes plausible if, for example, the respective functional groups are present as side chains. This would allow the generation of even more complex conjugates such as polymer−drug conjugates consisting of targeting ligands and therapeutic agents.

■ EXPERIMENTAL SECTION

General. All reactions with air- and moisture-sensitive substances were carried out under an argon atmosphere using standard Schlenk techniques or in a glovebox. Prior to use, all glassware was heat-dried under a vacuum. Unless otherwise stated, all chemicals were purchased from Sigma-Aldrich, ABCR, or TCI Europe and used without further purification. Toluene, THF, and dichloromethane (DCM) were dried using an MBraun SPS-800 solvent purification system and stored over 3 Å molecular sieves. Liquid chromatography−mass spectrometry (LC−MS)-grade acetonitrile and methanol were purchased from VWR. The precursor complexes $Y(CH_2Si(CH_3)_3)_3(THF)_2$ and $LiCH_2TMS$ and the catalyst $Cp_2Y(CH_2TMS)(THF)$ (**10**) were prepared according to procedures found in the literature.[27,45−47] Diethyl vinylphosphonate was synthesized according to procedures from the literature, dried over calcium hydride, and distilled prior to use.[48] 4-Chloro-2,6-dimethylpyridine (**4**) was also prepared according to a procedure found in the literature.[35]

NMR spectra were recorded on a Bruker AV-400HD and an AVIII-500 Cryo spectrometer. ^{1}H and ^{13}C NMR spectroscopic chemical shifts δ were reported in ppm relative to the residual proton signal of the solvent. δ (^{1}H) was calibrated to the residual proton signal and δ (^{13}C) to the carbon signal of the solvent. Unless otherwise stated, coupling constants J were the averaged values and refer to couplings between two protons. All deuterated solvents (C_6D_6, $CDCl_3$, MeOD-d_4) were obtained from Sigma-Aldrich. For the analysis of C−H bond activation products, C_6D_6 was dried and stored over 3 Å molecular sieves in a glovebox. DOSY-NMR measurements were performed for the characterization of polymer conjugates.

ESI-MS spectra were measured on a Varian 500-MS spectrometer in acetonitrile or methanol. Elemental analyses were measured on a Vario EL (Elementar) at the Laboratory for Microanalysis at the Institute of Inorganic Chemistry at the Technical University of Munich.

Turbidity measurements were performed on a Cary 50 UV−vis spectrophotometer (Varian). The cloud point of the aqueous polymer solutions was determined by spectrophotometric detection of the changes in transmittance at λ = 500 nm. The samples were heated/cooled at a rate of 1.0 K min^{-1} in steps of 1 K followed by a 5 min period at a constant temperature to ensure equilibration. The cloud point was defined as the temperature corresponding to a 10% decrease in optical transmittance.

Molecular Weight Determination. Gel permeation chromatography was performed with samples of 5 mg mL^{-1} on a combination of a Shimadzu LC-10ADVP with a DGU-3A as degasser (Shimadzu) and a column thermostat CTO-10A (Shimadzu) equipped with two PL Polargel-M or two PL Polargel-L columns. The eluent used was a mixture of 50% THF and 50% water, treated with tetrabutylammonium bromide (TBAB) (9 g L^{-1}) and 340 mg L^{-1} 3,5-di-*tert*-butyl-4-hydroxytoluene (BHT) as a stabilizing agent. Absolute molecular weights were determined by multiangle light scattering (MALS) analysis using a Wyatt Dawn Heleos II in combination with a Wyatt Optilab rEX as the concentration source. The dn/dc of PDEVP was determined experimentally (dn/dc = 0.0922 mL g^{-1}) at 40 °C.

C−H Bond Activation. The procedure for the C−H bond activation of 2,6-dimethylpyridyl-based initiators was adopted from our previous work.[20] The respective initiator (26.4 μmol, 1.00 equiv) was dissolved in C_6D_6 (550 μL) at room temperature and added to $Cp_2Y(CH_2TMS)(THF)$ (**10**) (10.0 mg, 26.4 μmol, 1.00 equiv). Immediately after mixing, the solution showed an instant yellow to orange coloring, depending on the initiator used. The reaction was monitored by ^{1}H NMR spectroscopy until full conversion was detected. The compounds generated in situ were analyzed by ^{1}H NMR and ^{13}C NMR spectroscopy. Characterization by elemental analyses was not feasible due to the instability of the compounds outside the liquid phase.

Oligomerization. To verify the incorporation of initiators **1**−**3**, oligomeric PDEVP was generated for the end-group analysis via ESI-MS measurements. A solution of $Cp_2Y(CH_2TMS)(THF)$ (**10**) (46.1 mg, 122 μmol, 1.00 equiv) in dry toluene (1.00 mL) was mixed with a solution of the respective initiator (122 μmol, 1.00 equiv) in toluene (1.00 mL). After the quantitative conversion was determined via ^{1}H NMR spectroscopy, the solution was diluted with dry toluene (3.00 mL), and a total of 5.00 equiv of DEVP (100 mg, 609 μmol) was added. Full conversion of DEVP was confirmed by ^{31}P NMR spectroscopy after 3 h. The mixture was quenched by the addition of 0.50 mL methanol (LC−MS grade). The oligomer samples for the analysis by ESI-MS were taken from the crude solution without further purification.

General Polymerization Procedure. A solution of the respective initiator (60.9 μmol, 1.00 equiv) in absolute toluene (1.00 mL) was added to a solution of $Cp_2Y(CH_2TMS)(THF)$ (**10**) (23.1 mg, 60.9 μmol, 1.00 equiv) in absolute toluene (1.00 mL), resulting in the instant coloration of the reaction mixture. After

https://dx.doi.org/10.1021/acs.macromol.0c00642
Macromolecules 2020, 53, 4345−4354

stirring at room temperature overnight, full conversion was verified by proton NMR, and the mixture was diluted with additional toluene (8.00 mL). DEVP (1.00 g, 6.09 mmol, 100 equiv) was then added to the solution in one portion. After 3 hours, the completion of the polymerization was detected by ^{31}P NMR spectroscopy. The reaction was quenched by the addition of MeOH (500 μL), and the polymer was precipitated in pentane. The supernatant solvent was decanted off, and the residual polymer was dissolved in water and freeze-dried to yield the pure polymer as a colorless solid. Polymerizations with a feed of 25 equiv were performed in a similar manner by increasing the initial amount of the initiator and $Cp_2Y(CH_2TMS)(THF)$ (**10**).

■ ASSOCIATED CONTENT

Supporting Information

The Supporting Information is available free of charge at https://pubs.acs.org/doi/10.1021/acs.macromol.0c00642.

Detailed experimental procedures and analytical data for initiators **1**−**3** and the respective precursors; ^{1}H and ^{31}C NMR spectra of the C−H bond activation products; ESI-MS spectra for end-group analysis; polymerization procedures for the time-dependent polymerization of DEVP and ^{1}H, ^{31}P, and DOSY-NMR spectra; GPC traces and LCST curves of polymers **P1**−**P6**; deprotection procedures and ^{1}H and ^{31}P NMR spectra; GPC traces and LCST curves of polymers **DP1**−**DP6**; UV/vis spectrum of **DP5** after treatment with DTNB; and coupling procedures and ^{1}H, ^{31}P, and DOSY-NMR spectra of the conjugation products (PDF)

■ AUTHOR INFORMATION

Corresponding Author

Bernhard Rieger − *WACKER-Chair of Macromolecular Chemistry, Technical University of Munich, 85748 Garching near Munich, Germany*; orcid.org/0000-0002-0023-884X; Email: rieger@tum.de

Authors

Andreas Schaffer − *WACKER-Chair of Macromolecular Chemistry, Technical University of Munich, 85748 Garching near Munich, Germany*

Moritz Kränzlein − *WACKER-Chair of Macromolecular Chemistry, Technical University of Munich, 85748 Garching near Munich, Germany*

Complete contact information is available at: https://pubs.acs.org/10.1021/acs.macromol.0c00642

Author Contributions

The manuscript was written through the contributions of all authors. All authors have given approval to the final version of the manuscript.

Notes

The authors declare no competing financial interest.

■ ACKNOWLEDGMENTS

The authors thank Simone Poprawa and Eva Krois for their support in performing the reactions and Sebastian Kernbichl for revising the manuscript.

■ REFERENCES

(1) Wei, M.; Gao, Y.; Li, X.; Serpe, M. J. Stimuli-responsive polymers and their applications. *Polym. Chem.* **2017**, *8*, 127−143.

(2) Larson, N.; Ghandehari, H. Polymeric Conjugates for Drug Delivery. *Chem. Mater.* **2012**, *24*, 840−853.

(3) Stuart, M. A. C.; Huck, W. T. S.; Genzer, J.; Müller, M.; Ober, C.; Stamm, M.; Sukhorukov, G. B.; Szleifer, I.; Tsukruk, V. V.; Urban, M.; Winnik, F.; Zauscher, S.; Luzinov, I.; Minko, S. Emerging applications of stimuli-responsive polymer materials. *Nat. Mater.* **2010**, *9*, 101−113.

(4) Maji, S.; Cesur, B.; Zhang, Z.; De Geest, B. G.; Hoogenboom, R. Poly(N-isopropylacrylamide) coated gold nanoparticles as colourimetric temperature and salt sensors. *Polym. Chem.* **2016**, *7*, 1705−1710.

(5) Ma, Y.; Promthaveepong, K.; Li, N. CO2-Responsive Polymer-Functionalized Au Nanoparticles for CO2 Sensor. *Anal. Chem.* **2016**, *88*, 8289−8293.

(6) Chiappelli, M. C.; Hayward, R. C. Photonic Multilayer Sensors from Photo-Crosslinkable Polymer Films. *Adv. Mater.* **2012**, *24*, 6100−6104.

(7) Mura, S.; Nicolas, J.; Couvreur, P. Stimuli-responsive nanocarriers for drug delivery. *Nat. Mater.* **2013**, *12*, 991.

(8) Sun, T.; Zhang, Y. S.; Pang, B.; Hyun, D. C.; Yang, M.; Xia, Y. Engineered Nanoparticles for Drug Delivery in Cancer Therapy. *Angew. Chem., Int. Ed.* **2014**, *53*, 12320−12364.

(9) Blum, A. P.; Kammeyer, J. K.; Rush, A. M.; Callmann, C. E.; Hahn, M. E.; Gianneschi, N. C. Stimuli-Responsive Nanomaterials for Biomedical Applications. *J. Am. Chem. Soc.* **2015**, *137*, 2140−2154.

(10) De las Heras Alarcón, C.; Pennadam, S.; Alexander, C. Stimuli responsive polymers for biomedical applications. *Chem. Soc. Rev.* **2005**, *34*, 276−285.

(11) Kwon, O. H.; Kikuchi, A.; Yamato, M.; Sakurai, Y.; Okano, T. Rapid cell sheet detachment from Poly(N-isopropylacrylamide)-grafted porous cell culture membranes. *J. Biomed. Mater. Res.* **2000**, *50*, 82−89.

(12) Ista, L. K.; Mendez, S.; Pérez-Luna, V. H.; López, G. P. Synthesis of Poly(N-isopropylacrylamide) on Initiator-Modified Self-Assembled Monolayers. *Langmuir* **2001**, *17*, 2552−2555.

(13) Wong, V. N.; Fernando, G.; Wagner, A. R.; Zhang, J.; Kinsel, G. R.; Zauscher, S.; Dyer, D. J. Separation of Peptides with Polyionic Nanosponges for MALDI-MS Analysis. *Langmuir* **2009**, *25*, 1459−1465.

(14) Nagase, K.; Kobayashi, J.; Kikuchi, A.; Akiyama, Y.; Kanazawa, H.; Okano, T. Effects of Graft Densities and Chain Lengths on Separation of Bioactive Compounds by Nanolayered Thermoresponsive Polymer Brush Surfaces. *Langmuir* **2008**, *24*, 511−517.

(15) Ebara, M.; Yamato, M.; Aoyagi, T.; Kikuchi, A.; Sakai, K.; Okano, T. Temperature-Responsive Cell Culture Surfaces Enable "On−Off" Affinity Control between Cell Integrins and RGDS Ligands. *Biomacromolecules* **2004**, *5*, 505−510.

(16) Kim, Y.-J.; Matsunaga, Y. T. Thermo-responsive polymers and their application as smart biomaterials. *J. Mater. Chem. B* **2017**, *5*, 4307−4321.

(17) Weber, C.; Hoogenboom, R.; Schubert, U. S. Temperature responsive bio-compatible polymers based on poly(ethylene oxide) and poly(2-oxazoline)s. *Prog. Polym. Sci.* **2012**, *37*, 686−714.

(18) Wolf, T.; Hunold, J.; Simon, J.; Rosenauer, C.; Hinderberger, D.; Wurm, F. R. Temperature responsive poly(phosphonate) copolymers: from single chains to macroscopic coacervates. *Polym. Chem.* **2018**, *9*, 490−498.

(19) Zhang, N.; Salzinger, S.; Rieger, B. Poly(vinylphosphonate)s with Widely Tunable LCST: A Promising Alternative to Conventional Thermoresponsive Polymers. *Macromolecules* **2012**, *45*, 9751−9758.

(20) Schwarzenböck, C.; Schaffer, A.; Pahl, P.; Nelson, P. J.; Huss, R.; Rieger, B. Precise synthesis of thermoresponsive polyvinylphosphonate-biomolecule conjugates via thiol-ene click chemistry. *Polym. Chem.* **2018**, *9*, 284−290.

(21) Webster, O. W.; Hertler, W. R.; Sogah, D. Y.; Farnham, W. B.; RajanBabu, T. V. Group-transfer polymerization. 1. A new concept for addition polymerization with organosilicon initiators. *J. Am. Chem. Soc.* **1983**, *105*, 5706−5708.

(22) Yasuda, H.; Yamamoto, H.; Yokota, K.; Miyake, S.; Nakamura, A. Synthesis of monodispersed high molecular weight polymers and isolation of an organolanthanide(III) intermediate coordinated by a

penultimate poly(MMA) unit. *J. Am. Chem. Soc.* **1992**, *114*, 4908−4910.
(23) Yasuda, H.; Yamamoto, H.; Yamashita, M.; Yokota, K.; Nakamura, A.; Miyake, S.; Kai, Y.; Kanehisa, N. Synthesis of high molecular weight poly(methyl methacrylate) with extremely low polydispersity by the unique function of organolanthanide(III) complexes. *Macromolecules* **1993**, *26*, 7134−7143.
(24) Collins, S.; Ward, D. G. Group-transfer polymerization using cationic zirconocene compounds. *J. Am. Chem. Soc.* **1992**, *114*, 5460−5462.
(25) Seemann, U. B.; Dengler, J. E.; Rieger, B. High-Molecular-Weight Poly(vinylphosphonate)s by Single-Component Living Polymerization Initiated by Rare-Earth-Metal Complexes. *Angew. Chem.* **2010**, *122*, 3567−3569.
(26) Salzinger, S.; Seemann, U. B.; Plikhta, A.; Rieger, B. Poly(vinylphosphonate)s Synthesized by Trivalent Cyclopentadienyl Lanthanide-Induced Group Transfer Polymerization. *Macromolecules* **2011**, *44*, 5920−5927.
(27) Salzinger, S.; Soller, B. S.; Plikhta, A.; Seemann, U. B.; Herdtweck, E.; Rieger, B. Mechanistic Studies on Initiation and Propagation of Rare Earth Metal-Mediated Group Transfer Polymerization of Vinylphosphonates. *J. Am. Chem. Soc.* **2013**, *135*, 13030−13040.
(28) Soller, B. S.; Sun, Q.; Salzinger, S.; Jandl, C.; Pöthig, A.; Rieger, B. Ligand Induced Steric Crowding in Rare Earth Metal-Mediated Group Transfer Polymerization of Vinylphosphonates: Does Enthalpy Matter? *Macromolecules* **2016**, *49*, 1582−1589.
(29) Soller, B. S.; Salzinger, S.; Jandl, C.; Pöthig, A.; Rieger, B. C−H Bond Activation by σ-Bond Metathesis as a Versatile Route toward Highly Efficient Initiators for the Catalytic Precision Polymerization of Polar Monomers. *Organometallics* **2015**, *34*, 2703−2706.
(30) Kaneko, H.; Nagae, H.; Tsurugi, H.; Mashima, K. End-Functionalized Polymerization of 2-Vinylpyridine through Initial C−H Bond Activation of N-Heteroaromatics and Internal Alkynes by Yttrium Ene−Diamido Complexes. *J. Am. Chem. Soc.* **2011**, *133*, 19626−19629.
(31) Waterman, R. σ-Bond Metathesis: A 30-Year Retrospective. *Organometallics* **2013**, *32*, 7249−7263.
(32) Duchateau, R.; van Wee, C. T.; Teuben, J. H. Insertion and C−H Bond Activation of Unsaturated Substrates by Bis(benzamidinato) yttrium Alkyl, [PhC(NSiMe3)2]2YR (R = CH2Ph·THF, CH(SiMe3)2), and Hydrido, {[PhC(NSiMe3)2]2Y(μ-H)}2, Compounds. *Organometallics* **1996**, *15*, 2291−2302.
(33) Schwarzenböck, C.; Schaffer, A.; Nößner, E.; Nelson, P. J.; Huss, R.; Rieger, B. Fluorescent Polyvinylphosphonate Bioconjugates for Selective Cellular Delivery. *Chem. - Eur. J.* **2018**, *24*, 2584−2587.
(34) Adams, F.; Pschenitza, M.; Rieger, B. Yttrium-Catalyzed Synthesis of Bipyridine-Functionalized AB-Block Copolymers: Micellar Support for Photocatalytic Active Rhenium Complexes. *ChemCatChem* **2018**, *10*, 4309−4316.
(35) Pahl, P.; Schwarzenböck, C.; Herz, F. A. D.; Soller, B. S.; Jandl, C.; Rieger, B. Core-First Synthesis of Three-Armed Star-Shaped Polymers by Rare Earth Metal-Mediated Group Transfer Polymerization. *Macromolecules* **2017**, *50*, 6569−6576.
(36) Jacobi, N.; Lindel, T. Assembly of the Bis(imidazolyl)propene Core of Nagelamides C and S by Double Grignard Reaction. *Eur. J. Org. Chem.* **2010**, *2010*, 5415−5425.
(37) Wang, Q.; Chen, S.; Liang, Y.; Dong, D.; Zhang, N. Bottle-Brush Brushes: Surface-Initiated Rare Earth Metal Mediated Group Transfer Polymerization from a Poly(3-((2,6-dimethylpyridin-4-yl)-oxy)propyl methacrylate) Backbone. *Macromolecules* **2017**, *50*, 8456−8463.
(38) Wathier, M.; Polidori, A.; Ruiz, K.; Fabiano, A.-S.; Pucci, B. Stabilization of polymerized vesicular systems: an application of the dynamic molecular shape concept. *Chem. Phys. Lipids* **2002**, *115*, 17−37.
(39) Yan, H.; Oh, J.-S.; Song, C. E. A mild and efficient method for the selective deprotection of silyl ethers using KF in the presence of tetraethylene glycol. *Org. Biomol. Chem.* **2011**, *9*, 8119−8121.
(40) Macor, J. E.; Chenard, B. L.; Post, R. J. Use of 2,5-Dimethylpyrrole as an Amino-Protecting Group in an Efficient Synthesis of 5-Amino-3-[(N-methyl- pyrrolidin-2(R)-yl)methyl]-indole. *J. Org. Chem.* **1994**, *59*, 7496−7498.
(41) Riddles, P. W.; Blakeley, R. L.; Zerner, B. Ellman's reagent: 5,5′-dithiobis(2-nitrobenzoic acid)—a reexamination. *Anal. Biochem.* **1979**, *94*, 75−81.
(42) Ravasco, J. M. J. M.; Faustino, H.; Trindade, A.; Gois, P. M. P. Bioconjugation with Maleimides: A Useful Tool for Chemical Biology. *Chem. - Eur. J.* **2019**, *25*, 43−59.
(43) Renault, K.; Fredy, J. W.; Renard, P.-Y.; Sabot, C. Covalent Modification of Biomolecules through Maleimide-Based Labeling Strategies. *Bioconjugate Chem.* **2018**, *29*, 2497−2513.
(44) Stenzel, M. H. Bioconjugation Using Thiols: Old Chemistry Rediscovered to Connect Polymers with Nature's Building Blocks. *ACS Macro Lett.* **2013**, *2*, 14−18.
(45) Hultzsch, K. C.; Voth, P.; Beckerle, K.; Spaniol, T. P.; Okuda, J. Single-Component Polymerization Catalysts for Ethylene and Styrene: Synthesis, Characterization, and Reactivity of Alkyl and Hydrido Yttrium Complexes Containing a Linked Amido−Cyclopentadienyl Ligand. *Organometallics* **2000**, *19*, 228−243.
(46) Vaughn, G. D.; Krein, K. A.; Gladysz, J. A. Synthesis and reactivity of metallacyclic manganese.alpha.-(silyloxy)alkyl complexes [cyclic] (CO)4MnC(R)(OSi(CH3)3)P(C6H5)2. A new thermodynamic driving force for carbonyl insertion. *Organometallics* **1986**, *5*, 936−942.
(47) Cai, C.-X.; Toupet, L.; Lehmann, C. W.; Carpentier, J.-F. Synthesis, structure and reactivity of new yttrium bis(dimethylsilyl)-amido and bis(trimethylsilyl)methyl complexes of a tetradentate bis(phenoxide) ligand. *J. Organomet. Chem.* **2003**, *683*, 131−136.
(48) Salzinger, S. *Expansion of Rare Earth Metal-Mediated Group Transfer Polymerization to New Monomers, PhD*; Technical University of Munich, 2013.

https://dx.doi.org/10.1021/acs.macromol.0c00642
Macromolecules 2020, 53, 4345−4354

5.4 Reprint Permission Copyrighted Content

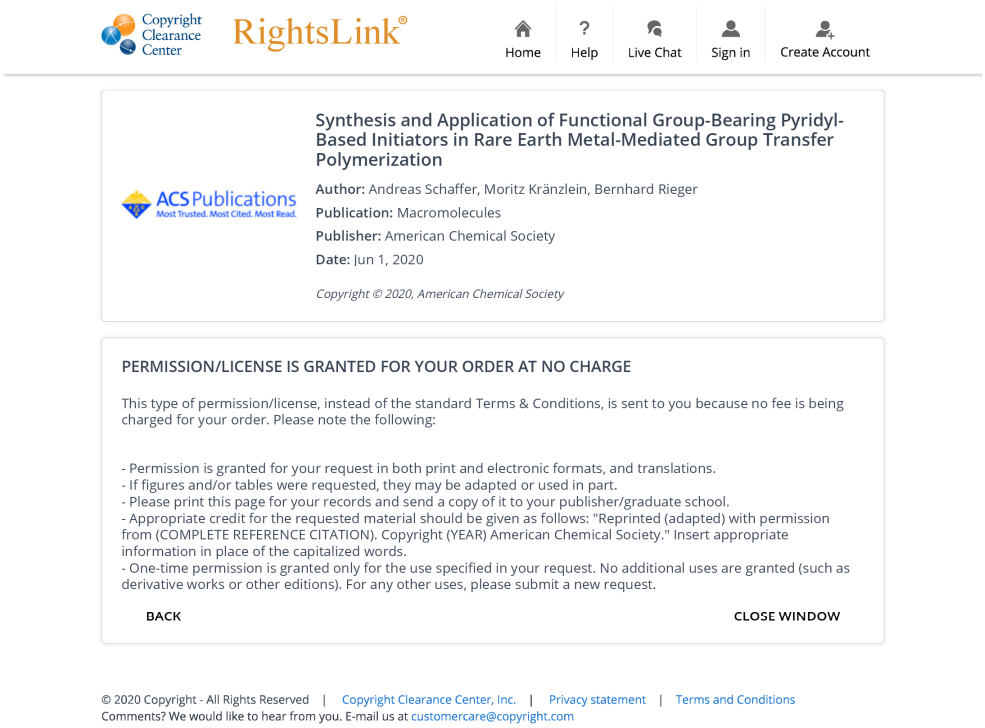

Copyright Clearance Center RightsLink®

Home | Help | Live Chat | Sign in | Create Account

ACS Publications
Most Trusted. Most Cited. Most Read.

Synthesis and Application of Functional Group-Bearing Pyridyl-Based Initiators in Rare Earth Metal-Mediated Group Transfer Polymerization

Author: Andreas Schaffer, Moritz Kränzlein, Bernhard Rieger
Publication: Macromolecules
Publisher: American Chemical Society
Date: Jun 1, 2020

Copyright © 2020, American Chemical Society

PERMISSION/LICENSE IS GRANTED FOR YOUR ORDER AT NO CHARGE

This type of permission/license, instead of the standard Terms & Conditions, is sent to you because no fee is being charged for your order. Please note the following:

- Permission is granted for your request in both print and electronic formats, and translations.
- If figures and/or tables were requested, they may be adapted or used in part.
- Please print this page for your records and send a copy of it to your publisher/graduate school.
- Appropriate credit for the requested material should be given as follows: "Reprinted (adapted) with permission from (COMPLETE REFERENCE CITATION). Copyright (YEAR) American Chemical Society." Insert appropriate information in place of the capitalized words.
- One-time permission is granted only for the use specified in your request. No additional uses are granted (such as derivative works or other editions). For any other uses, please submit a new request.

BACK CLOSE WINDOW

6 Precise Synthesis of Poly(dimethylsiloxane) Copolymers through C-H Bond Activated Macroinitiators in the Yttrium-mediated Group Transfer Polymerization and Ring-Opening Polymerization

6.1 Bibliographic Data

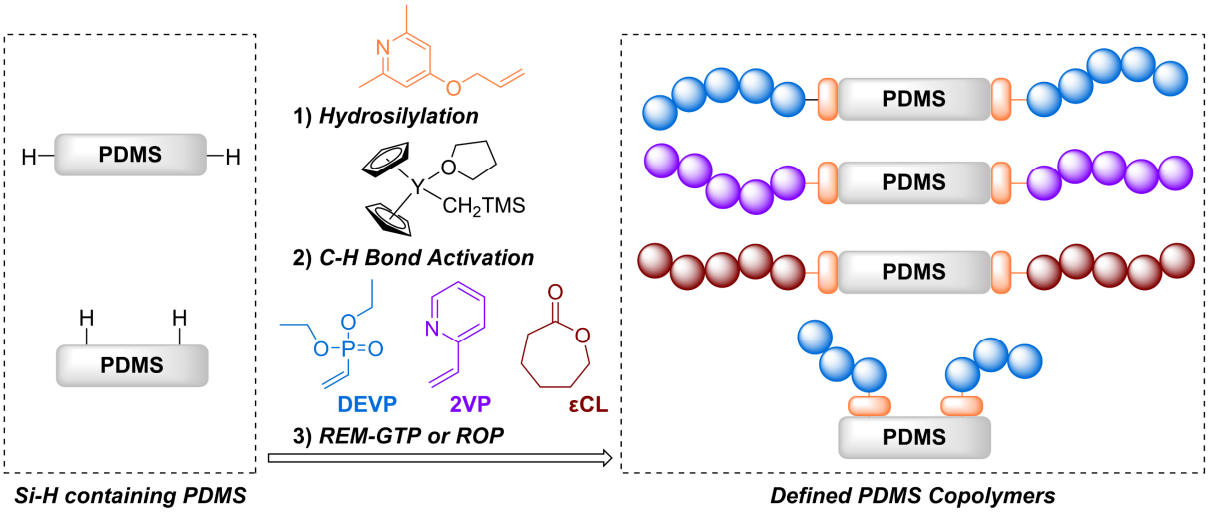

Title: "Precise Synthesis of Poly(dimethylsiloxane) Copolymers through C-H Bond Activated Macroinitiators in the Yttrium-mediated Group Transfer Polymerization and Ring-Opening Polymerization"

Status: Full paper, published online 25th September 2020

Journal: Macromolecules 2020, 53, 19, 8382–8392

Publisher: American Chemical Society

Link/DOI: https://pubs.acs.org/doi/10.1021/acs.macromol.0c01639

Authors: Andreas Schaffer, Moritz Kränzlein, and Bernhard Rieger[a]

[a]Andreas Schaffer conceptualized the experimental studies, carried out all experiments and wrote the manuscript. Moritz Kränzlein contributed with valuable ideas and discussions. All work was carried out under supervision of Bernhard Rieger.

6.2 Summary

Until today reports on the C-H bond activation with lanthanide complexes were limited to small initiating units, i.e. *sym*-collidine. In this study the substrate scope for the C-H bond activation with $Cp_2Y(CH_2TMS)(THF)$ was expanded towards polymer-sized initiators.

Herein, we initially focused on the combination of the highly hydrophobic PDMS with a hydrophilic PDEVP block as these opposing partners should result in copolymers with intriguing surface-active properties. Hence, preliminary studies were used to establish a functionalization route for the PDMS substrates and confirm the applicability of this approach in REM-GTP. Therefore, a binuclear initiator was synthesized from 1,1,3,3-tetramethyldisloxane and 4-(allyloxy)-2,6-dimethylpyridine via hydrosilylation. This model compound was successfully employed in the polymerization of DEVP which was confirmed by NMR spectroscopy, end-group analysis, and GPC-MALS. Next, two linear as well as one side group functionalized macroinitiator were generated from Si-H group bearing PDMS by hydrosilylation. In a similar fashion, the macroinitiators were successfully activated in the presence of $Cp_2Y(CH_2TMS)(THF)$ and converted into the respective graft and block copolymers with DEVP. Moreover, this approach was expanded towards 2-vinylpyridine and ε-caprolactone to investigate the versatility of this synthetic route. Here too, defined block copolymers were generated. Hence both, alternative *Michael*-type monomers as well as the ROP of εCL were accessible via this approach. In conclusion, the C-H bond activation of PDMS-based macroinitiators enables the utilization of a wide array of catalytic systems and monomers.

Characterization of the initial C-H bond activations were performed via NMR spectroscopy. Besides, the resulting copolymers were characterized by DOSY-NMR, which corroborated the covalent bonding of the polymer blocks. GPC and elemental analysis confirmed the compositions of the resulting copolymers calculated by ^{1}H-NMR spectroscopy. Furthermore, differential scanning calorimetry and dynamic light scattering in a variety of solvents gave fundamental insights into the material properties. Turbidity measurements of the PDEVP copolymers concluded an effect of the PDMS block length on the cloud point of PDEVP.

6.3 Manuscript

Macromolecules

pubs.acs.org/Macromolecules Article

Precise Synthesis of Poly(dimethylsiloxane) Copolymers through C−H Bond-Activated Macroinitiators via Yttrium-Mediated Group Transfer Polymerization and Ring-Opening Polymerization

Andreas Schaffer, Moritz Kränzlein, and Bernhard Rieger*

Cite This: *Macromolecules* 2020, 53, 8382−8392 Read Online

ACCESS | Metrics & More | Article Recommendations | Supporting Information

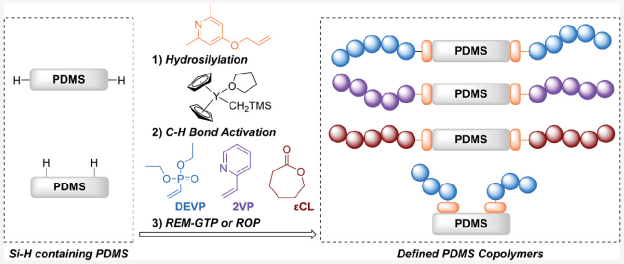

ABSTRACT: This article reports on the generation of copolymers from a hydrophobic poly(dimethylsiloxane) (PDMS) block, which was used as a macroinitiator in the formation of poly(diethyl vinylphosphonate) (PDEVP) and poly(2-vinylpyridine) (P2VP) by means of rare earth metal-mediated group transfer polymerization (REM-GTP) and the generation of poly(ε-caprolactone) via ring-opening polymerization (ROP). In preliminary studies, a binuclear initiator **3** was investigated as a model compound for ensuring the applicability of such siloxane-containing compounds in REM-GTP. Next, functionalization of the PDMS substrates with 2,6-dimethylpyridiyl units yielded the corresponding macroinitiators and enabled the C−H bond activation with $Cp_2Y(CH_2TMS)$-(THF) (**4**) as well as the subsequent REM-GTP and ROP. Two linear (**MI1**−**2**) and one side group (**MI3**)-functionalized macroinitiators were synthesized for the subsequent polymerization of diethyl vinylphosphonate, in order to elucidate the versatility of this route with different initiating substrates. In addition, 2-vinylpyridine was employed as an alternative Michael-type monomer, while the ROP of ε-caprolactone showed that this approach is not only limited to REM-GTP but also enables the utilization of a wide array of catalytic systems and monomers. The initial C−H bond activation process was tracked by nuclear magnetic resonance (NMR) spectroscopy. The resulting homo- and copolymers were characterized by NMR spectroscopy, gel permeation chromatography, and elemental analysis, which confirmed the compositions of the resulting copolymers calculated by ^{1}H-NMR spectroscopy. Differential scanning calorimetry and dynamic light scattering in a variety of solvents provided basic insights into the thermal and solution properties of these materials. Furthermore, turbidity measurements concluded an effect of the PDMS block length on the cloud point of PDEVP.

■ INTRODUCTION

Polydimethylsiloxane (PDMS) is the most widely used polymer among the group of silicones.[1,2] Due to the nature of the Si−O−Si linkage, PDMS exhibits intriguing properties. The high bond strength guarantees thermal stability and renders silicone networks chemically inert. A prolonged Si−O bond length compared to the carbon analog of 1.64 Å, a low torsion potential, and an elevated Si−O−Si bond angle of 143° result in flexible polymer chains with low glass transition temperatures.[2,3] Moreover, PDMS is characterized by high hydrophobicity[4,5] and unprecedented surface properties[2,3,6] and is generally considered to be nontoxic.[4,7] The applications of PDMS-based materials are diverse, ranging from antifoaming agents[8] and medicinal uses[9,10] to the application in soft lithography.[11,12] In addition, copolymer combinations of PDMS and hydrophilic counterparts were reported. Blends of PDMS and PDMS−polyethylene glycol (PEG) copolymers prevented the adsorption of proteins on the respective surface by reducing its hydrophobicity.[13] Nanocomposites comprising

Received: July 15, 2020
Revised: September 10, 2020
Published: September 25, 2020

https://dx.doi.org/10.1021/acs.macromol.0c01639
Macromolecules 2020, 53, 8382−8392

gold and PDMS−PEG copolymers were dispersed in water and used for the encapsulation of hypocrellin B.[14] Additionally, varying compositions of copolymers consisting of a *N*-isopropylacrylamide main chain and PDMS grafts enabled precise, temperature-dependent demixing.[15] Accordingly, we were interested in whether it was possible to combine polyvinylphosphonates with PDMS since poly(diethyl vinylphosphonate) (PDEVP) offers a set of attractive features for biomedical uses, for example, adjustable cloud points T_{LCST} (5−92 °C) through copolymerization[16,17] and high biocompatibility.[18−20] Common methods used to integrate new polymer blocks include polymer−polymer conjugations[21−24] or atom-transfer radical polymerization from functionalized PDMS substrates,[25,26] but ring-opening polymerization[27] or group transfer polymerization (GTP) was also reported.[28] However, such coupling reactions often lack sufficient coupling efficiencies due to dilution effects, and they require the introduction of specific, highly reactive end groups.[23,24,29] Moreover, polyvinylphosphonates are not available in a controlled fashion through radical or ionic polymerization techniques. Eventually, rare earth metal-mediated GTP (REM-GTP), which is a combination of living ionic and coordinative polymerizations, enabled the generation of a high-molecular weight PDEVP.[30−32] This polymerization technique emerged from the pioneering work of Webster et al., who used organosilicon initiators in the GTP of methylmethacrylate (MMA).[33] The groups of Yasuda and Collins and Ward refined this concept independently using either neutral samarocenes[34,35] or cationic zirconocene species.[36] In this context, the work of Mashima and coworkers must also be highlighted: the group employed yttrium ene-diamido species in the polymerization of 2-vinylpyridine that was initially activated by *N*-heteroaromatics through C−H bond activation.[37] Inspired by this approach and the work of Teuben et al.,[38] we were able to develop a catalyst through the activation of *sym*-collidine with $Cp_2Y(CH_2TMS)(THF)$ (**4**), thus allowing the defined and delay-free polymerization of Michael-type monomers such as DEVP.[39] This approach was also adopted in the polymerization of 2-vinylpyridine (2VP) with nonmetallocene lanthanides[40] and in the generation of pH-responsive micelles and nanoparticles for drug delivery applications.[20,41] Moreover, tailor-made initiators facilitated the incorporation of functional groups at the terminus of the polymer.[32,42,43] Recent studies in this field confirmed the successful ring-opening polymerization (ROP) of lactones after activation of yttrium-bis(phenolate) complexes with a variety of heteroaromatic compounds.[44]

In this study, we sought to combine these fundamentally different polymer types in one material. Consequently, PDMS had to be made compatible for the application in REM-GTP, which was preliminarily investigated with a model initiator comprising of a short siloxane linker. Based on the knowledge gained through these experiments, several macroinitiators were conceptualized and studied with respect to their applicability as C−H bond activation substrates and for the generation of block and graft copolymers. Furthermore, 2VP and *ε*-caprolactone (*ε*CL) were investigated to explore the flexibility of this polymerization strategy using weakly coordinating Michael-type monomers on the one hand and to examine the ring-opening polymerization as an alternative polymerization type on the other hand.

RESULTS AND DISCUSSION

Synthesis and Application of Initiator 3. A binuclear initiator **3** was synthesized from 4-(allyloxy)-2,6-dimethylpyridine (**1**) and 1,1,3,3-tetramethyldisiloxane (**2**) in a hydrosilylation reaction with a Karstedt's catalyst (Scheme 1, top).

Scheme 1. Two-Step Synthesis of the Model Initiator 3 and Application in the REM-GTP of DEVP Using $Cp_2Y(CH_2TMS)(THF)$ (4)

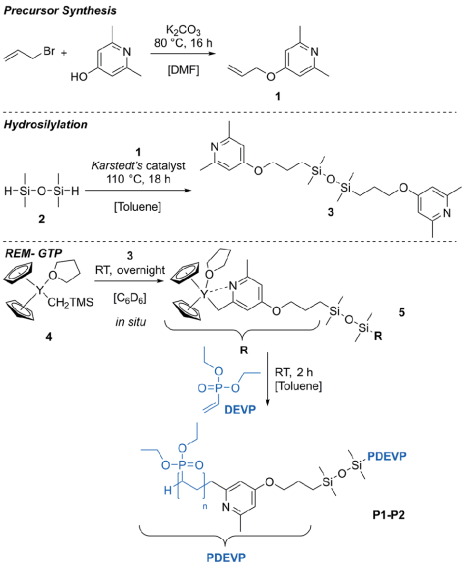

The initiator **3** was then converted in a C−H bond activation process with two equivalents of $Cp_2Y(CH_2TMS)(THF)$ (**4**), whereby the successful activation to **5** was monitored by ^{1}H- and ^{13}C-NMR spectroscopy (Figure 1; Figures S1 and S2). This reaction was characterized by a split of the four pyridine-related methyl groups (2.47 ppm, 12H) into two CH_2Y groups (2.34 ppm, 4H) and the remaining methyl groups (2.02 ppm, 6H). Moreover, the formation of the C−Y bond was detected in the ^{13}C-NMR spectra, exhibiting a signal at 41.2 ppm and a characteristic coupling constant of J_{CY} = 12.3 Hz. These values fell within a range which our previous works have shown to be typical.[42,43] In the next step, electrospray ionization mass spectrometry (ESI-MS) was performed with DEVP oligomers that were formed with the complex **5**. As shown in Figure S3, the oligomer pattern revealed the initiator ionized by H^+ (461 u) and $2H^+$ (231 u) and the respective oligomer signals ionized with H^+ (790 and 954 u) and $2H^+$ (395, 477, 559, 641, and 723 u), which confirmed the incorporation of **3** in the initiation step. This finding was corroborated by diffusion ordered spectroscopy (DOSY) (Figure S6). As shown in the corresponding DOSY spectrum of **P1**, only one polymer species was found, which comprised the signals of the initiator (0.11 ppm, 0.67 ppm) and phosphonate ester (1.38 ppm, 4.18 ppm) at the same diffusion level. Furthermore, a time-dependent polymerization

https://dx.doi.org/10.1021/acs.macromol.0c01639
Macromolecules 2020, 53, 8382−8392

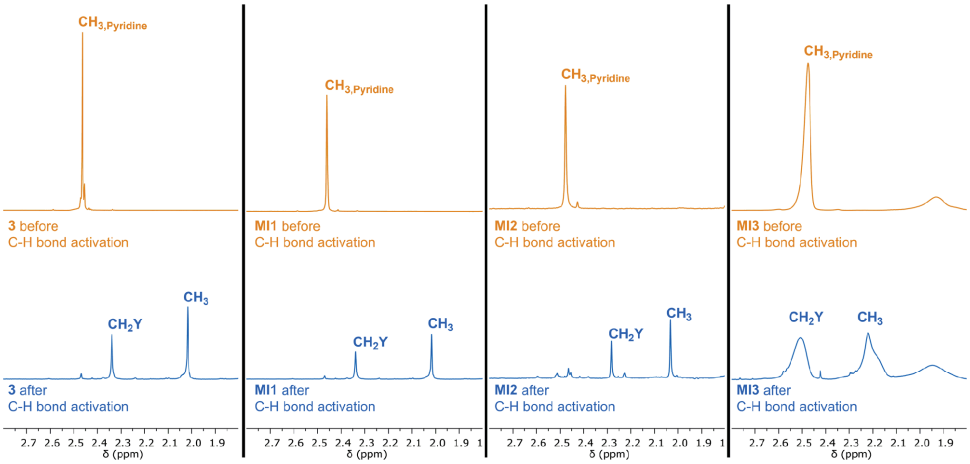

Figure 1. Comparison of the significant regions of the ^{1}H-NMR spectra of **3** and **MI1**−**MI3** (orange) before and (blue) after treatment with $Cp_2Y(CH_2TMS)(THF)$ (**4**) in C_6D_6.

Table 1. Monomer Feed Concentrations, Molecular Weights M_n, Polydispersities $Đ$, and Initiator Efficiencies *IE* of the Polymerizations

polymer	initiator	polymerization type	M_0/cat_0[a]	monomer	conv.[a]/%	$M_{n,NMR}$[b] /kg mol^{-1}	$M_{n,GPC}$ /kg mol^{-1}	$Đ$[c] /−	IE[g] /%
P1	**3**	GTP	100	DEVP	>99	39.7	39.0[c]	1.11[c]	85[h]
P2	**3**	GTP	300	DEVP	>99	132	139[c]	1.11[c,f]	71[h]
P3	**MI1**	GTP	100	DEVP	>99	57.5	n.d.	n.d.	64[i]
P4	**MI1**	GTP	300	DEVP	>99	164	n.d.	n.d.	62[i]
P5	**MI2**	GTP	100	DEVP	>99	50.6	n.d.	n.d.	88[i]
P6	**MI2**	GTP	300	DEVP	>99	237	n.d.	n.d.	40[i]
P7	**MI3**	GTP	20	DEVP	>99	61.0	47.0[c]	1.39[c]	27[i]
P8	**MI3**	GTP	60	DEVP	>99	171	129[c]	1.35[c]	28[i]
P9	**MI1**	GTP	100	2VP	>99	32.5	23.5[d]	1.13[d]	80[i]
P10	**MI1**	ROP	100	εCL	>99	30.5	37.8[d]	1.39[d,f]	94[i]

[a]Equivalent monomers per initiating unit. Polymerizations were monitored by ^{1}H- or ^{31}P-NMR and showed quantitative conversion after the respective reaction time. [b]Determined by ^{1}H-NMR by integral comparison of the PDMS signal (0.10 ppm) and the corresponding polymer signal (PDEVP: 4.38 ppm; P2VP: 7.93−8.46 ppm; PεCL: 4.05 ppm). [c]Determined via GPC-MALS in THF/water with added TBAB. [d]Determined via GPC in THF relative to a polystyrene standard. [e]Polydispersity indices $Đ$ were averaged over the entire peak. [f]Bimodal character of the peak region. [g]Initiator efficiency IE = $M_{n,theo}/M_{n,exp}$ with $M_{n,theo} = M_{PDMS}$ + n 163.22 g mol^{-1} + n $M_{Monomer}$ M_0/cat_0. [h]$M_{n,exp} = M_{n,GPC}$ [i]$M_{n,exp} = M_{n,NMR}$

experiment with DEVP and complex **5**, which was monitored by ^{31}P-NMR spectroscopy, revealed the living character of the polymerization (Figure S4). An analysis via gel permeation chromatography−multiangle light scattering (GPC-MALS) revealed the linear growth of the molecular weights M_n of PDEVP, while the corresponding polydispersity indices (PDIs) $Đ$ remained low ($Đ$ = 1.09−1.25) during the whole polymerization. As expected, complex **5** exhibited no initiation delay, meaning that the polymerization starts immediately upon the injection of the Michael-monomer (Figure S4). After verification of these key features, two PDEVP samples **P1** and **P2** were generated (Table 1, entries 1−2). Both polymerizations featured good initiator efficiencies (*IE*) and low polydispersities for the resulting polymers (**P1**: $Đ$ = 1.11, *IE* = 85%; **P2**: $Đ$ = 1.11, *IE* = 71%). However, it is also noteworthy that **P2** exhibited a bimodal character (Figure S10), which was caused by the formation of ABA- and AB-type polymers (A: PDEVP; B: disiloxane). Although the *IE* was directly affected by residual moisture that terminated a portion of the active yttrium centers, the initiation was necessarily viewed as a statistical process because of the binuclear character of species **5**. Consequently, the probability of forming an ABA-polymer is proportional to the square of the respective *IE* (**P1**: P_{ABA} = 0.85^2 = 72%; **P2**: P_{ABA} = 0.71^2 = 50%).[43]

Synthesis and Application of the Macroinitiators. Given the foundation laid by initiator **3**, we focused on the synthesis of macroinitiators **MI1**−**MI3**. Two linear, hydrogen-terminated PDMS substrates with different molar masses (M_n = 6000 g mol^{-1} and M_n = 17,500 g mol^{-1}) and an oligomer containing Si−H bonds as side groups (M_n = 950 g mol^{-1}, Si−H = 50 mol %) were selected for this task. In a manner similar to **3**, these polymers were modified by a hydrosilylation reaction with precursor **1** in order to yield the structures illustrated in Scheme 2 (top). For **MI1**, a quantitative conversion was determined by ^{1}H-NMR, whereas **MI2** and **MI3** were limited to 76 and 84% conversion, despite the

https://dx.doi.org/10.1021/acs.macromol.0c01639
Macromolecules 2020, 53, 8382−8392

Scheme 2. Macroinitiators MI1−MI3 Obtained After (Top) Hydrosilylation with 1, (Center) C−H Bond Activation with Complex 4, and (Left and Right) REM-GTP of DEVP

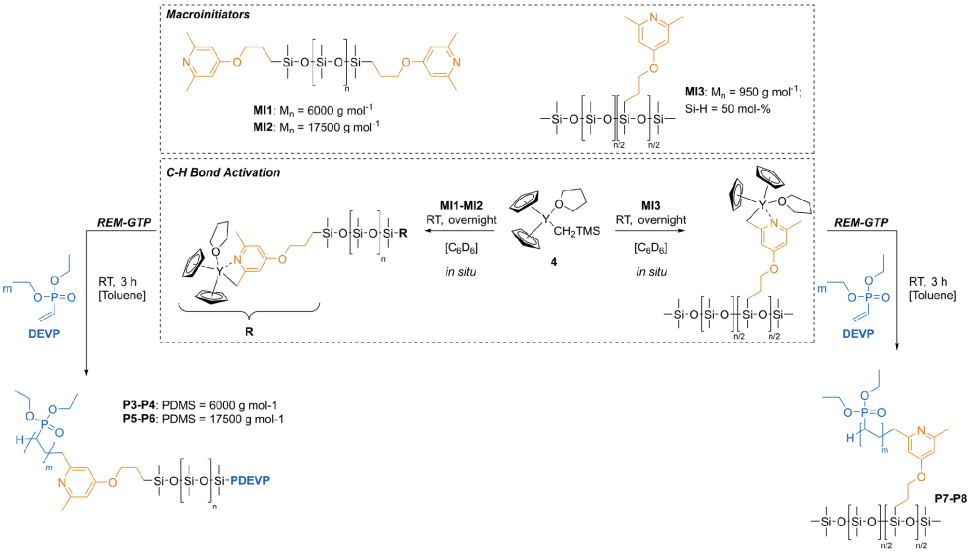

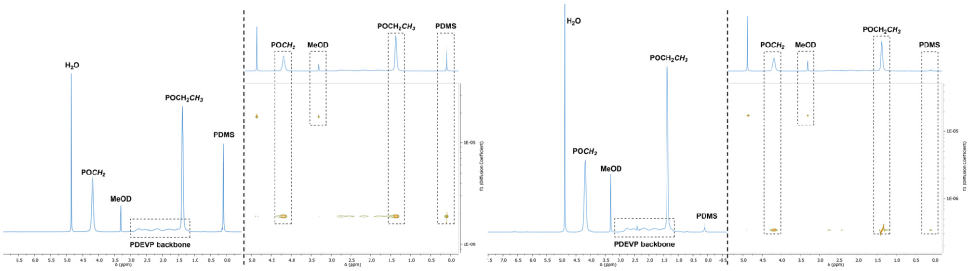

Figure 2. Exemplary illustration of the ^{1}H-NMR and DOSY spectra of (left) block copolymer **P3** and (right) graft copolymer **P7** in MeOD.

addition of extra educts during the reaction. We assume that the probability of reaching a free H-terminated chain end was reduced in the case of **MI2**, whereas the reactive Si−H sites of **MI3** might be sterically shielded by the previously conjugated initiating units, thus preventing further coupling reactions. Nevertheless, the initiator motifs were, in all cases, clearly visible in the ^{1}H-NMR spectra (2.47 ppm, $CH_{3,Pyridine}$; 6.43 ppm, $CH_{Pyridine}$). In addition, the corresponding DOSY spectra evidenced the attachment of the 2,6-methylpyridine unit to the PDMS backbone (Figures S13, S16, and S19). Concerning **MI3**, correlation spectroscopy also exhibited a cross peak of the PDMS backbone (0.31 ppm) and the silicon-conjugated CH_2 group (0.80 ppm) (Figure S20). Thereafter, **MI1−MI3** were investigated in the C−H bond activation experiments and were monitored by ^{1}H-NMR spectroscopy (Scheme 2, center).

Similar to **3**, **MI1** and **MI2** revealed the same distinct split toward CH_2Y and the remaining methyl groups (Figure 1). To further validate the successful activation, DOSY measurements were performed, which revealed that the PDMS backbone of both macroinitiators (**MI1** and **MI2**) shares the same diffusion unit with the Cp signals (Figures S23 and S26). The characterization of **MI3** turned out to be complex due to the statistical distribution of the Si−H bonds, thus resulting in broad and partially overlapping signals. Nevertheless, a successful conversion was substantiated by considering the integral values of the significant signals before and after the activation. By assuming a constant integral for the PDMS backbone (I = 70.8H), we observed a significant decrease of the CH_3 signal at 2.47 ppm from I = 30.8H to I = 25.6H, comprising two signals at 2.22 and 2.51 ppm (Figure 1).

Based on these results, the polymerizations of DEVP with varying feed concentrations were performed in order to generate the copolymers **P3−P8** (Scheme 2, Table 1, entries 3−8). In all cases, ^{31}P-NMR displayed the full conversion of DEVP. The analysis of **P3−P6** by means of ^{1}H-NMR exhibited the characteristic signals of the phosphonate esters (1.38 and

https://dx.doi.org/10.1021/acs.macromol.0c01639
Macromolecules 2020, 53, 8382−8392

Scheme 3. (Top) REM-GTP of 2VP and (Bottom) ROP of εCL After Activation of Complex 4 with the Macroinitiator MI1

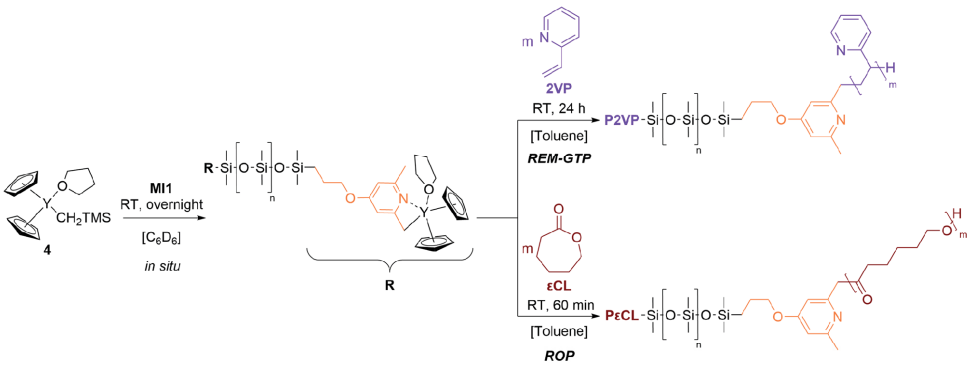

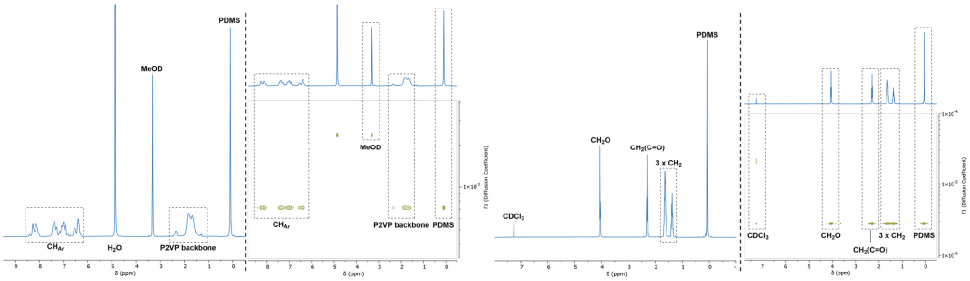

Figure 3. Illustration of the ^{1}H-NMR and DOSY spectra of (left) P2VP-*b*-PDMS-*b*-P2VP **P9** in MeOD and (right) PεCl-*b*-PDMS-*b*-PεCl **P10** in $CDCl_3$.

4.18 ppm) and the PDMS backbone (0.10 ppm), whereby the DOSY spectra of the substrates **P3**–**P6** corroborated the successful conjugation of PDEVP to the PDMS block (Figure 2; Figures S31, S33, S37, and S39). Moreover, ^{1}H-NMR enabled the determination of the molecular masses M_n, which ranged between 50.6 and 237 kg mol^{-1}, and an estimation of the *IE* (*IE* = 40–88%) (Table 1, entries 3–6). A verification of the polymeric nature via GPC-MALS was not possible because **P3**–**P6** formed micellar structures in the eluent THF/water, which was demonstrated by dynamic light scattering (DLS) (Figures S54–S57). The treatment of **P4** with HBr allowed the cleavage of the PDEVP block from the copolymer. An analysis by GPC-MALS exhibited a narrow molecular weight distribution (M_n = 76.0 kg mol^{-1}, $Đ$ = 1.08, Figure S35) and concluded a GTP-type polymerization mechanism. The initiator efficiency of 65% matches with the *IE* of **P4**, which was calculated via ^{1}H-NMR. Moreover, elemental analyses were performed to verify the composition of the block copolymers, which agreed well with the theoretical and experimental compositions (compare the Supporting Information data). The graft copolymers **P7** and **P8** were able to be characterized by GPC-MALS (**P7**: M_n = 46.0 kg mol^{-1}, $Đ$ = 1.39; **P8**: M_n = 129 kg mol^{-1}, $Đ$ = 1.35). These values were in the same range as those calculated by ^{1}H-NMR (**P7**: M_n = 61.0 kg mol^{-1}; **P8**: M_n = 171 kg mol^{-1}), but they also indicated comparatively low *IEs* (27–28%) (Table 1, entries 7–8). This finding might be explained by the steric crowding of the initiator side groups and the high rate of DEVP propagation. Because the initiator motifs are statistically distributed over the PDMS backbone in **MI3**, the active centers can be sterically hindered within the densely crowded macroinitiators. Consequently, the already growing PDEVP chains were more easily accessible than the active yttrium centers located at the PDMS backbone. These PDEVP chains can also form coil structures in solution and increase the shielding effect at the PDMS backbone. In addition, a previous study revealed the comparatively low initiator efficiencies at high catalyst loadings.[45] Hence, the monomer encounters a high concentration of active yttrium centers at the injection point and is consumed due to the fast initiation and a high propagation rate. Thus, a portion of the yttrium centers was excluded from the polymerization. The value for $Đ$ of approximately 1.40 was also satisfactory in consideration of the statistical character of the basic PDMS substrate. In this case as well, DOSY measurements concluded the formation of one polymeric species (Figure 2; Figures S41 and S44). In addition, an elemental analysis very precisely confirmed the composition of the polymers **P7** and **P8**.

To complement this synthetic approach, we decided to employ 2VP as an alternative Michael-type monomer in the REM-GTP with macroinitiator **MI1** (Scheme 3, top) and tested the capability of complex **4**, which was activated with

https://dx.doi.org/10.1021/acs.macromol.0c01639
Macromolecules 2020, 53, 8382–8392

Table 2. DLS Data of Polymers P1−P10 in Several Solvents, Glass Transition Temperatures T_g, Melting Points T_m, and Cloud Points T_{LCST} of PDMS-*co*-PDEVP Copolymers in Aqueous Solution

entry	polymer	d_{THF}[a] /nm (PDI)	d_{DMF}[a] /nm (PDI)	$d_{THF/Water}$[a] / nm (PDI)	d_{Water}[a] /nm (PDI)	T_g /°C	T_m /°C	T_{LCST} /°C
1	P1	n.d.	n.d.	n.d.	7.0 (0.65)	12.3		44.5
2	P2	n.d.	n.d.	n.d.	12.0 (0.35)	15.9		45.0
3	P3	8.0 (0.33)	n.d.	62.0 (0.25)	45.0 (0.47)	−108, 12.7		35.5
4	P4	13.0 (0.38)	n.d.	98.0 (0.25)	78.0 (0.20)	−107, 7.10		41.5
5	P5	16.0 (0.45)	n.d.	179 (0.16)	n.d.	−133, 11.9	−45.6	n.d.
6	P6	14.0 (0.42)	n.d.	248 (0.11)	88.0 (0.23)	−134, 10.6	−45.3	37.5
7	P7	7.0 (0.39)	n.d.	n.d.	12.0 (0.43)	−90.0, 8.80		42.5
8	P8	15.0 (0.18)	n.d.	n.d.	10.0 (0.42)	−104, 21.5		42.5
9	P9	7.0 (0.44)	20.0 (0.14)	n.d.	31.0 (0.19)[b]	−120, 98.7		n.a.
10	P10	10.0 (0.43)	36.0 (0.19)	n.d.	n.d.	−120, −65.7	55.5	n.a.

[a]The diameters were rounded to integer values. [b]Measured in hydrochloric acid (pH = 2).

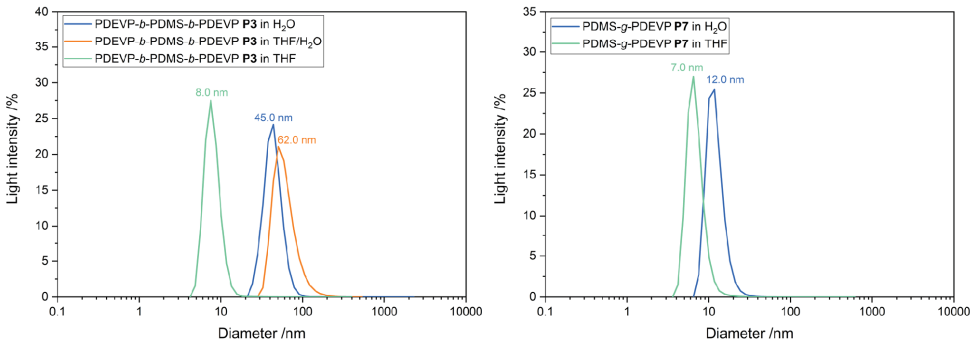

Figure 4. Illustration of the DLS data of the copolymers (left) **P3** and (right) **P7** in (turquoise) THF, (orange) THF/water, and (blue) water.

MI1, in the ring-opening polymerization of εCL (Scheme 3, bottom).

After the successful activation of the macroinitiator **MI1** with **4**, the catalyst was treated with 200 equivalents of the respective monomers (Table 1, entries 9−10). Full conversion of 2VP was detected after 24 h by proton NMR. After the isolation of **P9**, characterization by ^{1}H-NMR revealed the characteristic signals of P2VP (1.25−2.47 ppm and 6.26−8.46 ppm) and the PDMS backbone (0.10 ppm) (Figure 3). The comparison of the PDMS and P2VP signals concluded a molar mass $M_{n,NMR}$ of 32.5 kg mol^{-1} (*IE* = 80%), while the GPC analysis in THF revealed a molecular weight of 23.5 kg mol^{-1} relative to a polystyrene standard and a good polydispersity *Đ* of 1.13 (Figure S48). The DOSY-NMR spectra corroborated the covalent linkage of both the blocks (Figure 3). The ring-opening polymerization of εCL proceeded much faster and was finished after only 60 min. Likewise, the composition of **P10** was determined by proton NMR (Figure 3 (right)), which exhibited the characteristic CH_2 groups of PεCL (1.38, 1.64, 2.30, and 4.05 ppm). The molecular weight $M_{n,NMR}$ was calculated to be 30.5 kg mol^{-1} (*IE* = 94%). Here, too, an analysis by DOSY substantiated the presence of a single species and with that the successful copolymer formation (Figure 3). The corresponding analysis by GPC in THF reported a M_n of 37.8 kg mol^{-1} and a polydispersity *Đ* of 1.39 (Table 1, entry 10) (Figure S52), which is comparatively high. The broad molecular weight distribution of **P10** might be caused by an increase of the viscosity during the polymerization of εCL, which resulted in an irregular chain growth. Moreover, the polymerization of εCL even outperformed DEVP. Hence, it is conceivable that propagating and nonpropagating metal centers were present leading to a time-resolved initiation and a broader *Đ*.

Properties of the Block and Graft Copolymers. As mentioned in the previous section, **P3**−**P6** appeared to be highly surface-active due to the incorporation of the PDMS block. Therefore, DLS measurements were performed to analyze the micelle formation in various solvents. As expected, micelles were formed in water with diameters ranging between 44 and 88 nm with PDIs between 0.20 and 0.47. In the case of **P5**, a measurement was not possible due to its insolubility in water. Interestingly, the deviating block length of PDEVP in **P3** and **P4** affected the micelle diameter (Table 2, entries 3−4), thus leading to a larger diameter in the case of **P4**. The formation of micellar structures was also observed in a mixture of 50% THF and 50% water with diameters between 65 and 250 nm with narrow PDIs between 0.11 and 0.25 (Table 2, entries 3−6). In this case, both a prolonged PDMS chain and an elongated PDVEP block yielded larger structures. Control experiments in THF, however, provided no indication of the formation of aggregates. DLS measurements revealed that the graft-type polymers **P7** and **P8** in THF and water negated the formation of micelles as well (Table 2, entries 7−8). As shown in Table 2, the size values of **P7** (d = 12.0 nm) and **P8** (d = 7.0 nm) in water are within the range of the homopolymers **P1** and **P2**, which implies the presence of random coils in the

https://dx.doi.org/10.1021/acs.macromol.0c01639
Macromolecules 2020, 53, 8382−8392

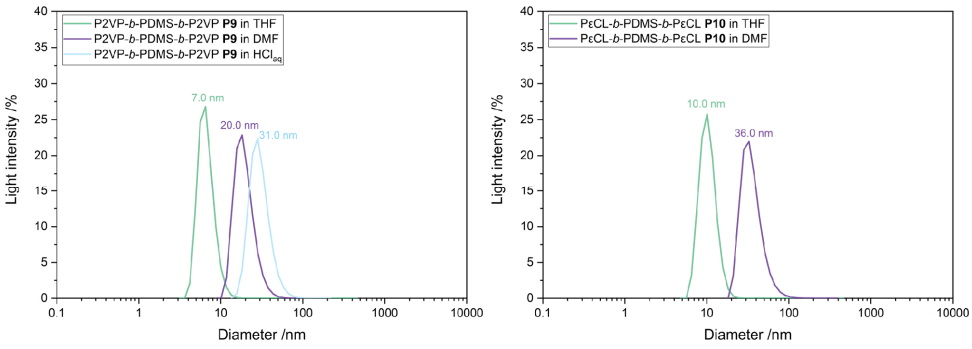

Figure 5. Illustration of the DLS data of (left) P2VP-*b*-PDMS-*b*-P2VP **P9** and (right) PεCl-*b*-PDMS-*b*-PεCl **P10** in (turquoise) THF, (purple) DMF, and (light blue) hydrochloric acid (pH = 2).

aqueous solution. In Figure 4, the size measurements of **P3** and **P7** are exemplified.

The DLS measurements of P2VP-*b*-PDMS-*b*-P2VP **P9** (Table 2, entry 9) were conducted in THF, DMF, and hydrochloric acid (pH = 2). While the analysis in THF concluded the absence of micelles, very defined objects were found in DMF (d = 20.0 nm, PDI = 0.14). Size measurements in hydrochloric acid attributed micelles with a diameter of 31.0 nm and a narrow PDI of 0.19 (Figure 5, left). In accordance with the data of **P9**, PεCl-*b*-PDMS-*b*-PεCl **P10** did not produce micelles in THF, while defined aggregates were observed in DMF as the solvent (36.0 nm, PDI = 0.19) (Figure 5, right).

Moreover, differential scanning calorimetry (DSC) provided the basic thermal properties of the copolymers (Figures S62–S71). As presented in Table 2, two glass transition temperatures T_g were determined, which corresponded to the respective polymer motifs. Hence, for both polymer architectures (block and graft), a T_g between −134 and −90 °C was able to be assigned to the PDMS block, while the T_g of PDEVP ranged between 8.80 and 21.5 °C. Copolymers **P5** and **P6** also exhibited a melting point T_m at −45 °C (Figures S66–S67), which is in agreement with the values found in the literature.[46] Likewise, the copolymers **P9** and **P10** were analyzed by DSC. While P2VP-*b*-PDMS-*b*-P2VP exhibited T_gs at −120 °C (PDMS) and 98.7 °C (P2VP) (Figure S70), the T_gs of PεCL-b-PDMS-*b*-PεCL were observed at −120 and − 65.7 °C. Additionally, the melting point of PεCL was observed at 55.5 °C (Figure S71). Eventually, turbidity measurements concluded an influence of the hydrophilic core on the lower critical solution temperature (LCST) of PDEVP (Figure S72). Hence, **P3** (T_{LCST} = 35.5 °C), **P4** (T_{LCST} = 41.5 °C), and **P6** (T_{LCST} = 37.5 °C) exhibited lower LCSTs (Table 2, entries 3, 4, and 6) than homopolymers **P1** and **P2** and graft polymers **P7** and **P8** with their comparably small PDMS block (T_{LCST} = 42.5–45.0 °C). The determination of the LCST of **P5** was not possible due to its insolubility in water. Studies on the stability of the linker revealed a high resilience toward irradiation with UV light and elevated temperatures.[47]

CONCLUSIONS

In conclusion, we were able to establish a synthesis strategy that combined hydrophobic PDMS with a polar PDEVP block, which was generated by REM-GTP. After the successful utilization of model initiator **3** in the REM-GTP of DEVP, macroinitiators **MI1**–**MI3** were synthesized via the hydrosilylation of several Si–H-containing PDMS substrates with 4-(allyloxy)-2,6-dimethylpyridine (**1**). These macroinitiators were successfully employed in the C–H bond activation with $Cp_2Y(CH_2TMS)(THF)$ (**4**) and the polymerization of DEVP in order to yield the corresponding copolymers. This approach was complemented by the utilization of 2VP as an alternative Michael-type monomer to form the corresponding P2VP-*b*-PDMS-*b*-P2VP copolymer. Furthermore, we were able to prove the high versatility of this approach and showed the controlled ROP of εCL toward PεCL-*b*-PDMS-*b*-PεCL. Apart from the ROP initiated by activated yttrium-bis(phenolate)s,[44] this is also the first report on an C–H bond-activated Cp_2Y system that was successfully employed in the rare earth metal-mediated ROP of lactones. The compositions of all copolymers were determined by ^{1}H-NMR spectroscopy and confirmed very precisely by elemental analysis. The DOSY-NMR spectra of the copolymers were able to prove the covalent conjugation of PDMS and the new polymer blocks. Moreover, DLS measurements demonstrated a solvent-dependent formation of micellar structures of PDEVP-*b*-PDMS-*b*-PDEVP in water and THF/water and attributed a high dependency of the diameter from the copolymer composition. Furthermore, P2VP-*b*-PDMS-*b*-P2VP and PεCL-*b*-PDMS-*b*-PεCL showed the formation of defined aggregates in DMF. The DSC analysis further corroborated the presence of two T_gs attributed to the PDMS and the newly introduced polymer block. The high versatility of the C–H bond activation enables the application of PDMS macroinitiators in a broad variety of complexes with different metal centers and opens the door to tailor-made hybrid materials having as yet unknown material properties consisting of either polar polyolefins (e.g., poly(2-isopropenyl-2-oxazoline), poly(4-vinylpyridine), and poly(*N*,*N*-dimethylacrylamide)), which are generated via GTP, or (co)polymers based on the ring opening of cyclic monomers (e.g., β-butyrolactone, lactide, and (−)-menthide).

https://dx.doi.org/10.1021/acs.macromol.0c01639
Macromolecules 2020, 53, 8382–8392

Precise Synthesis of Poly(dimethylsiloxane) Copolymers through C-H Bond Activated Macroinitiators in the Yttrium-mediated Group Transfer Polymerization and Ring-Opening Polymerization

EXPERIMENTAL SECTION

General. All reactions with air- and moisture-sensitive substances were carried out under an argon atmosphere using standard Schlenk techniques or in a glovebox. Prior to use, all glassware was heat-dried under a vacuum. Unless otherwise stated, all chemicals were purchased from Sigma-Aldrich, ABCR, or TCI Europe and used without further purification. Karstedt's catalyst was purchased from ABCR as a complex solution in xylene (2.1−2.4% Pt). Toluene, tetrahydrofuran (THF), pentane, and diethyl ether were dried using a MBraun SPS-800 solvent purification system and stored over 3 Å molecular sieves. LC-MS-grade acetonitrile and methanol were purchased from VWR. The precursor complexes $Y(CH_2Si(CH_3)_3)_3(THF)_2$ and $LiCH_2TMS$ and the catalyst $Cp_2Y(CH_2TMS)(THF)$ (**4**) were prepared according to the procedures found in the literature.[48−51] Diethyl vinylphosphonate was synthesized according to the procedures from the literature, dried over calcium hydride, and distilled prior to use.[52] Likewise, 2-vinylpyridine and ε-caprolactone were dried over calcium hydride and distilled prior to use.

NMR spectra were recorded on a Bruker AV-400HD and an AVIII-500 Cryo spectrometer. ^{1}H- and ^{13}C-NMR spectroscopy chemical shifts δ were reported in ppm relative to the residual proton signal of the solvent. δ (^{1}H) was calibrated to the residual proton signal and δ (^{13}C) to the carbon signal of the solvent. Unless otherwise stated, the coupling constants *J* are averaged values and refer to the couplings between two protons. All deuterated solvents (C_6D_6, $CDCl_3$, and MeOD-d_4) were obtained from Sigma-Aldrich. For the analysis of C−H bond activation products, C_6D_6 was dried and stored over 3 Å molecular sieves in a glovebox. DOSY-NMR measurements were performed for the characterization of the block and graft copolymers.

The ESI-MS spectra were measured using a Varian 500-MS spectrometer in acetonitrile or methanol. Elemental analyses were performed using a Vario EL (Elementar) at the Laboratory for Microanalysis at the Institute of Inorganic Chemistry at the Technical University of Munich.

Molecular Weight Determination Via GPC-MALS. Gel permeation chromatography was performed with samples of 5 mg mL^{-1} using a combination of a Shimadzu LC-10ADVP with a DGU-3A as the degasser (Shimadzu) and a column thermostat CTO-10A (Shimadzu) equipped with two PL PolarGel-M columns from Agilent Technologies. A mixture of 50% THF and 50% water with tetrabutylammonium bromide (TBAB) (9 g L^{-1}) and 340 mg L^{-1} of 3,5-di-*tert*-butyl-4-hydroxytoluene (BHT) as stabilizing agents was used as the eluent. The absolute molecular weights were determined by MALS analysis using a Wyatt Dawn Heleos II in combination with a Wyatt Optilab rEX as the concentration source. The dn/dc of PDEVP was determined experimentally (dn/dc = 0.0922 mL g^{-1}) at 40 °C.

THF-GPC. GPC of P2VP-*b*-PDMS-*b*-P2VP and PεCL-*b*-PDMS-*b*-PεCL was carried out using a Polymer Laboratories PL-GPC 50 Plus chromatograph with samples of 2.5 mg mL^{-1}. As an eluent, THF with 222 mg L^{-1} of BHT as the stabilizing agent was used. Polystyrene standards were used for calibration.

4-(Allyloxy)-2,6-dimethylpyridine (1). The reaction was adopted from a procedure found in the literature.[53] A mixture of 4-hydroxy-2,6-dimethylpyridine (7.00 g, 56.8 mmol, 1.00 equiv), allyl bromide (7.56 g, 62.5 mmol, 1.10 equiv.), and potassium carbonate (23.6 g, 171 mmol, 3.00 equiv) was treated with DMF (80 mL) and stirred at 80 °C for 16 h. After evaporation of the volatiles, DCM (100 mL) and deionized water (100 mL) were added to the residue. The organic phase was separated therefrom, the aqueous phase was extracted two times with DCM (100 mL each), and the combined organic phases were washed with brine and dried over Na_2SO_4. After filtration, the solvents were removed in vacuo and the residue was purified by column chromatography (SiO_2, H/EtOAc/NEt_3 = 5/5/1 → EtOAc/NEt_3 = 10/1). Compound **1** was obtained as a colorless solid (7.05 g, 43.2 mmol, 76%). **TLC**: R_f = 0.75 (EtOAc/NEt_3 = 10/1) [UV]. **^{1}H-NMR** (400 MHz, $CDCl_3$, 300 K): δ (ppm) = 6.48 (s, 2H, $CH_{Pyridine}$), 6.08−5.84 (m, 1H, CH_{Allyl}), 5.37 (d,^3J = 17.2 Hz, 1H, CH_{Allyl}), 5.28 (d,^3J = 10.5 Hz, 1H, CH_{Allyl}), 4.54−4.48 (m, 2H, CH_2O), 2.44 (s, 6H, $CH_{3,Pyridine}$). **^{13}C-NMR** (101 MHz, $CDCl_3$, 300 K): δ (ppm) = 165.4 (s, $C_{Pyridine}$), 159.3 (s, $C_{Pyridine}$), 132.4 (s, C_{Allyl}), 118.2 (s, C_{Allyl}), 106.9 (s, $C_{Pyridine}$), 68.3 (CH_2O), 24.7 (s, $CH_{3,Pyridine}$). **ESI-MS**: calculated: 164.11 $[M-H]^+$, found: 164.18 $[M-H]^+$.

1,3-Bis(3-((2,6-dimethylpyridin-4-yl)oxy)propyl)-1,1,3,3-tetramethyldisiloxane (3). To a solution of 4-(allyloxy)-2,6-dimethylpyridine (**1**) (2.00 g, 12.3 mmol, 3.00 equiv.) in absolute toluene (40 mL), 1,1,3,3-tetramethyldisiloxane (**2**) (722 μL, 4.08 mmol, 1.00 equiv) was added. Catalytic amounts of Karstedt's catalyst were added, and the reaction mixture was heated to 110 °C for 18 h. After the full conversion was confirmed by ^{1}H-NMR spectroscopy, toluene was evaporated under high vacuum and excess 4-(allyloxy)-2,6-dimethylpyridine was removed by recondensation. The residue was treated with DCM (30 mL) and washed with 1 M HCl (20 mL), deionized water (20 mL), and a saturated $NaHCO_3$ solution (20 mL). After extraction of the aqueous phase with DCM (2 × 20 mL), the combined organic phases were dried over Na_2SO_4 and filtrated. The residue was purified by column chromatography (SiO_2, H/EtOAc/NEt_3 = 5/5/1) to yield initiator **3** as a white, crystalline solid (261 mg, 566 μmol, 14%). **TLC**: R_f = 0.38 (H/EtOAc/NEt_3 = 5/5/1) [UV]. **^{1}H-NMR** (400 MHz, C_6D_6, 300 K): δ (ppm) = 6.42 (s, 4H, $CH_{Pyridine}$), 3.57 (t,^3J = 6.6 Hz, 4H, CH_2O), 2.46 (s, 12H, $CH_{3,Pyridine}$), 1.92−1.58 (m, 4H, CH_2), 0.62−0.53 (m, 4H, $SiCH_2$), 0.12 (s, 12H, $SiCH_3$). **^{13}C-NMR** (101 MHz, C_6D_6, 300 K): δ (ppm) = 166.1 (s, C_{Ar}), 159.6 (s, C_{Ar}), 106.7 (s, C_{Ar}), 69.9 (s, CH_2O), 24.8 (s, CH_3), 23.4 (s, CH_2), 14.6 (s, $SiCH_2$), 0.4 (s, $SiCH_3$). **^{29}Si-NMR** (99 MHz, C_6D_6, 300 K): δ (ppm) = 7.8. **ESI-MS**: calculated: 461.27 $[M-H]^+$, found: 461.82 $[M-H]^+$. **EA**: calculated: C 62.56, H 8.75, N 6.08; found: C 62.36, 8.82, N 6.02.

C−H Bond Activation. At room temperature, initiator **3** (26.4 μmol, 1.00 equiv.) was dissolved in dry C_6D_6 (550 μL) and added to $Cp_2Y(CH_2TMS)(THF)$ (**4**) (10.0 mg, 26.4 μmol, 1.00 equiv). Immediately after mixing, the solution showed an instant yellow color. The reaction was monitored by ^{1}H-NMR spectroscopy until full conversion was detected. The in situ generated compounds were analyzed by ^{1}H- and ^{13}C-NMR spectroscopy. Activation experiments with the macroinitiators were performed analogously. The compositions of the activation experiments with the macroinitiators are summarized in Table S1. If the C−H bond activation of the macroinitiators was not finished after the first period, an additional amount of the catalyst was added depending on the conversion calculated from the ^{1}H-NMR spectrum.

Oligomerization. Oligomeric PDEVP was generated to verify the incorporation of initiator **3** via the end-group analysis by ESI-MS measurements. A solution of $Cp_2Y(CH_2TMS)(THF)$ (**4**) (46.1 mg, 122 μmol, 2.00 equiv) in dry toluene (1.00 mL) was mixed with a solution of initiator **3** (60.9 μmol, 1.00 equiv) in toluene (1.00 mL). After the quantitative conversion was determined via ^{1}H-NMR spectroscopy, the solution was diluted with dry toluene (3.00 mL) and 5.00 equivalents of DEVP (100 mg, 609 μmol) were added. The full conversion of DEVP was confirmed by ^{31}P-NMR spectroscopy after 3 h. The reaction was terminated by the addition of 0.50 mL of methanol (LC−MS grade).

Polymerization Procedure for DEVP with Initiator 3. A solution of initiator **3** (30.4 μmol, 1.00 equiv) in absolute toluene (1.00 mL) was added to a solution of $Cp_2Y(CH_2TMS)(THF)$ (**4**) (23.1 mg, 60.9 μmol, 2.00 equiv) in absolute toluene (1.00 mL), resulting in instant coloration of the reaction mixture. After stirring at room temperature for 12 h, full conversion was verified by proton NMR and the mixture was diluted with additional toluene (8.00 mL). After this, DEVP (1.00 g, 6.09 mmol, 200 equiv) was added to the solution in one portion. After 3 h, the completion of the polymerization was detected by ^{31}P-NMR spectroscopy. The reaction was terminated by the addition of MeOH (500 μL), and the polymer was precipitated in pentane. The supernatant solvent was decanted off, and the residual polymer was dissolved in water and freeze-dried to yield the pure polymer as a colorless solid. Polymerizations with a feed of 600 equivalents of DEVP were performed analogously by

https://dx.doi.org/10.1021/acs.macromol.0c01639
Macromolecules 2020, 53, 8382−8392

reducing the initial amount of initiator **3** and $Cp_2Y(CH_2TMS)(THF)$ (**4**).

General Polymerization Procedure for DEVP with the Macroinitiators. A solution of the respective macroinitiator (1.00 equiv) in absolute C_6D_6 was added to a solution of $Cp_2Y(CH_2TMS)$-(THF) (**4**) (1.00 equiv per initiating unit) in absolute C_6D_6, resulting in instant coloration of the reaction mixture. After stirring at room temperature overnight, full conversion was verified by proton NMR. If the reaction was not yet completed, a desired amount of $Cp_2Y(CH_2TMS)(THF)$ was added to achieve full conversion. After this, the catalyst solution was divided into two portions and diluted with absolute toluene ($c \approx 1$ g DEVP/10 mL solvent). DEVP (**MI1** and **MI2**: 100 and 300 equiv per initiating unit; **MI3**: 20 and 60 equiv per initiating unit) was added to each solution in one portion. After 3 h, the completion of the polymerizations was detected by ^{31}P-NMR spectroscopy. The reaction was quenched by the addition of MeOH (500 μL), and the polymer was precipitated in pentane. The supernatant solvent was decanted off, and the residual polymer was dissolved in water and freeze-dried to yield the pure polymer as a colorless solid. Detailed compositions are summarized in Table S2.

Polymerization Procedure for 2VP with MI1. A solution of macroinitiator **MI1** (193 mg, 30.4 μmol, 1.00 equiv) in absolute C_6D_6 (1.00 mL) was added to a solution of $Cp_2Y(CH_2TMS)(THF)$ (**4**) (23.1 mg, 60.9 μmol, 2.00 equiv) in absolute C_6D_6 (1.00 mL), resulting in instant coloration of the reaction mixture. After stirring at room temperature overnight, full conversion was verified by proton NMR. If the reaction was not yet completed, a desired amount of $Cp_2Y(CH_2TMS)(THF)$ was added to achieve full conversion. After this, the solution was diluted by the addition of absolute toluene (8.00 mL), and 2VP (640 mg, 6.09 mmol, 200 equiv) was added in one portion. After 24 h, the completion of the polymerization was detected by ^{1}H-NMR spectroscopy. The reaction was terminated by the addition of MeOH (500 μL), and the polymer was precipitated in pentane. The supernatant solvent was decanted off after centrifugation, and the residual polymer was freeze-dried from benzene to yield the pure polymer as a colorless solid.

Polymerization Procedure for εCL with MI1. The C−H bond activation was performed analogously to the 2VP polymerization. After successful activation, the solution was diluted with absolute toluene (8.00 mL) and εCL (695 mg, 6.09 mmol, 200 equiv) was added in one portion. After 1 h, the quantitative conversion of εCL was detected by ^{1}H-NMR spectroscopy and the reaction was terminated by the addition of MeOH (500 μL). The viscous polymer mixture was diluted in DCM and precipitated in EtOH. The supernatant solvent was decanted off after centrifugation, and the residual polymer was freeze-dried from benzene to yield the pure polymer as a colorless solid.

■ ASSOCIATED CONTENT

Supporting Information

The Supporting Information is available free of charge at https://pubs.acs.org/doi/10.1021/acs.macromol.0c01639.

Detailed experimental procedures and analytical data for the macroinitiators **MI1**−**MI3**; ^{1}H-, ^{31}C-, and DOSY-NMR spectra of the C−H bond activation products; ESI-MS spectrum for end-group analysis of initiator **3**; procedure for the time-dependent polymerization of DEVP with complex **5**; ^{1}H-, ^{29}Si-, ^{31}P-, and DOSY-NMR spectra, GPC traces, LCST curves, DLS data, and DSC curves of (co)polymers **P1**−**P10**; composition of the C−H bond activation experiments with macroinitiators **MI1**−**MI3**; composition of the polymerization experiments with macroinitiators **MI1**−**MI3**; and overview of the heat- and light-treated copolymers (PDF)

■ AUTHOR INFORMATION

Corresponding Author

Bernhard Rieger − *WACKER-Chair of Macromolecular Chemistry, Catalysis Research Center, Technical University of Munich, Munich 85748, Germany;* orcid.org/0000-0002-0023-884X; Email: rieger@tum.de

Authors

Andreas Schaffer − *WACKER-Chair of Macromolecular Chemistry, Catalysis Research Center, Technical University of Munich, Munich 85748, Germany*

Moritz Kränzlein − *WACKER-Chair of Macromolecular Chemistry, Catalysis Research Center, Technical University of Munich, Munich 85748, Germany*

Complete contact information is available at: https://pubs.acs.org/10.1021/acs.macromol.0c01639

Author Contributions

The manuscript was written through contributions of all authors. All authors have given approval to the final version of the manuscript.

Funding

The authors are grateful to the Bundesministerium für Wirtschaft und Energie (BMWi) for the financial support of the SKETCH project.

Notes

The authors declare no competing financial interest.

■ ACKNOWLEDGMENTS

The authors thank Theresa Appleson for her support in performing the reactions and Alina Denk and Jonas Bruckmoser for revising the manuscript.

■ REFERENCES

(1) Kendrick, T. C.; Parbhoo, B. M.; White, J. W., Polymerization of Cyclosiloxanes. In *Comprehensive Polymer Science and Supplements*, Allen, G.; Bevington, J. C., Eds. Pergamon: Amsterdam, 1989; pp. 459−523.

(2) Mark, J. E. Some Interesting Things about Polysiloxanes. *Acc. Chem. Res.* **2004**, *37*, 946−953.

(3) Eduok, U.; Faye, O.; Szpunar, J. Recent developments and applications of protective silicone coatings: A review of PDMS functional materials. *Prog. Org. Coat.* **2017**, *111*, 124−163.

(4) Mata, A.; Fleischman, A. J.; Roy, S. Characterization of Polydimethylsiloxane (PDMS) Properties for Biomedical Micro/Nanosystems. *Biomed. Microdevices* **2005**, *7*, 281−293.

(5) Trantidou, T.; Elani, Y.; Parsons, E.; Ces, O. Hydrophilic surface modification of PDMS for droplet microfluidics using a simple, quick, and robust method via PVA deposition. *Microsyst. Nanoeng.* **2017**, *3*, 16091.

(6) Gohil, S. V.; Suhail, S.; Rose, J.; Vella, T.; Nair, L. S., Chapter 8 - Polymers and Composites for Orthopedic Applications. In *Materials for Bone Disorders*, Bose, S.; Bandyopadhyay, A., Eds. Academic Press: 2017; pp. 349−403.

(7) Zhang, H.; Chiao, M. Anti-fouling Coatings of Poly-(dimethylsiloxane) Devices for Biological and Biomedical Applications. *J. Med. Biol. Eng.* **2015**, *35*, 143−155.

(8) Chen, J.; Huang, X.; He, L.; Luo, X. Foaming of Oils: Effect of Poly(dimethylsiloxanes) and Silica Nanoparticles. *ACS Omega* **2019**, *4*, 6502−6510.

(9) Abbasi, F.; Mirzadeh, H.; Katbab, A.-A. Modification of polysiloxane polymers for biomedical applications: a review. *Polym. Int.* **2001**, *50*, 1279−1287.

(10) Abbasi, F.; Mirzadeh, H.; Simjoo, M. Hydrophilic interpenetrating polymer networks of poly(dimethyl siloxane) (PDMS) as

biomaterial for cochlear implants. *J. Biomater. Sci. Polym. Ed.* **2006**, *17*, 341−355.
(11) Xia, Y.; Rogers, J. A.; Paul, K. E.; Whitesides, G. M. Unconventional Methods for Fabricating and Patterning Nanostructures. *Chem. Rev.* **1999**, *99*, 1823−1848.
(12) Wu, H.; Odom, T. W.; Chiu, D. T.; Whitesides, G. M. Fabrication of Complex Three-Dimensional Microchannel Systems in PDMS. *J. Am. Chem. Soc.* **2003**, *125*, 554−559.
(13) Gökaltun, A.; Kang, Y. B.; Yarmush, M. L.; Usta, O. B.; Asatekin, A. Simple Surface Modification of Poly(dimethylsiloxane) via Surface Segregating Smart Polymers for Biomicrofluidics. *Sci. Rep.* **2019**, *9*, 7377.
(14) Li, D.; Li, C.; Wang, A.; He, Q.; Li, J. Hierarchical gold/copolymer nanostructures as hydrophobic nanotanks for drug encapsulation. *J. Mater. Chem.* **2010**, *20*, 7782−7787.
(15) Huber, R. O.; Beebe, J. M.; Smith, P. B.; Howell, B. A.; Ahn, D. Facile Synthesis of Thermoresponsive Poly(NIPAAm-g-PDMS) Copolymers Using Room Temperature Alkylborane Chemistry. *Macromolecules* **2018**, *51*, 4259−4268.
(16) Zhang, N.; Salzinger, S.; Rieger, B. Poly(vinylphosphonate)s with Widely Tunable LCST: A Promising Alternative to Conventional Thermoresponsive Polymers. *Macromolecules* **2012**, *45*, 9751−9758.
(17) Adams, F.; Altenbuchner, P. T.; Werz, P. D. L.; Rieger, B. Multiresponsive micellar block copolymers from 2-vinylpyridine and dialkylvinylphosphonates with a tunable lower critical solution temperature. *RSC Adv.* **2016**, *6*, 78750−78754.
(18) Schwarzenböck, C.; Schaffer, A.; Nößner, E.; Nelson, P. J.; Huss, R.; Rieger, B. Fluorescent Polyvinylphosphonate Bioconjugates for Selective Cellular Delivery. *Chem. − Eur. J.* **2018**, *24*, 2584−2587.
(19) Schwarzenböck, C.; Vagin, S. I.; Heinz, W. R.; Nelson, P. J.; Rieger, B. Studies on the Biocompatibility of Poly(diethyl vinylphosphonate) with a New Fluorescent Marker. *Macromol. Rapid Commun.* **2018**, *39*, 1800259.
(20) Schwarzenböck, C.; Nelson, P. J.; Huss, R.; Rieger, B. Synthesis of next generation dual-responsive cross-linked nanoparticles and their application to anti-cancer drug delivery. *Nanoscale* **2018**, *10*, 16062−16068.
(21) Razak, H. A. A.; Szabo, P.; Skov, A. L. Enhancement of dielectric permittivity by incorporating PDMS-PEG multiblock copolymers in silicone elastomers. *RSC Adv.* **2015**, *5*, 53054−53062.
(22) Xia, Y.; Yao, H.; Miao, Z.; Ma, Y.; Cui, M.; Yan, L.; Ling, H.; Qi, Z. Facile synthesis and self-assembly of amphiphilic polydimethylsiloxane with poly(ethylene glycol) moieties via thiol-ene click reaction. *RSC Adv.* **2015**, *5*, 50955−50961.
(23) Brendel, J. C.; Gody, G.; Perrier, S. Efficient click-addition sequence for polymer−polymer couplings. *Polym. Chem.* **2016**, *7*, 5536−5543.
(24) Fairbanks, B. D.; Love, D. M.; Bowman, C. N. Efficient Polymer-Polymer Conjugation via Thiol-ene Click Reaction. *Macromol. Chem. Phys.* **2017**, *218*, 1700073.
(25) Huan, K.; Bes, L.; Haddleton, D. M.; Khoshdel, E. Synthesis and properties of polydimethylsiloxane-containing block copolymers via living radical polymerization. *J. Polym. Sci., Part A: Polym. Chem.* **2001**, *39*, 1833−1842.
(26) Xu, J.; Qiu, M.; Ma, B.; He, C. "Near Perfect" Amphiphilic Conetwork Based on End-Group Cross-Linking of Polydimethylsiloxane Triblock Copolymer via Atom Transfer Radical Polymerization. *ACS Appl. Mater. Interfaces* **2014**, *6*, 15283−15290.
(27) Brogly, M.; Bistac, S.; Delaite, C.; Alzina, C. Influence of semi-crystalline poly(ε-caprolactone) and non-crystalline polylactide blocks on the thermal properties of polydimethylsiloxane-based block copolymers. *Polym. Int.* **2020**, DOI: 10.1002/pi.5964.
(28) Lim, K. T.; Webber, S. E.; Johnston, K. P. Synthesis and Characterization of Poly(dimethyl siloxane)−Poly[alkyl (meth)acrylic acid] Block Copolymers. *Macromolecules* **1999**, *32*, 2811−2815.
(29) Hiemenz, P. C.; Lodge, T. P., *Polymer Chemistry*. CRC Press: Boca Ratón, Florida, 2007, DOI: 10.1201/9781420018271.
(30) Salzinger, S.; Seemann, U. B.; Plikhta, A.; Rieger, B. Poly(vinylphosphonate)s Synthesized by Trivalent Cyclopentadienyl Lanthanide-Induced Group Transfer Polymerization. *Macromolecules* **2011**, *44*, 5920−5927.
(31) Seemann, U. B.; Dengler, J. E.; Rieger, B. High-Molecular-Weight Poly(vinylphosphonate)s by Single-Component Living Polymerization Initiated by Rare-Earth-Metal Complexes. *Angew. Chem., Int. Ed.* **2010**, *49*, 3567−3491.
(32) Soller, B. S.; Salzinger, S.; Rieger, B. Rare Earth Metal-Mediated Precision Polymerization of Vinylphosphonates and Conjugated Nitrogen-Containing Vinyl Monomers. *Chem. Rev.* **2016**, *116*, 1993−2022.
(33) Webster, O. W.; Hertler, W. R.; Sogah, D. Y.; Farnham, W. B.; RajanBabu, T. V. Group-transfer polymerization. 1. A new concept for addition polymerization with organosilicon initiators. *J. Am. Chem. Soc.* **1983**, *105*, 5706−5708.
(34) Yasuda, H.; Yamamoto, H.; Yokota, K.; Miyake, S.; Nakamura, A. Synthesis of monodispersed high molecular weight polymers and isolation of an organolanthanide(III) intermediate coordinated by a penultimate poly(MMA) unit. *J. Am. Chem. Soc.* **1992**, *114*, 4908−4910.
(35) Yasuda, H.; Yamamoto, H.; Yamashita, M.; Yokota, K.; Nakamura, A.; Miyake, S.; Kai, Y.; Kanehisa, N. Synthesis of high molecular weight poly(methyl methacrylate) with extremely low polydispersity by the unique function of organolanthanide(III) complexes. *Macromolecules* **1993**, *26*, 7134−7143.
(36) Collins, S.; Ward, D. G. Group-transfer polymerization using cationic zirconocene compounds. *J. Am. Chem. Soc.* **1992**, *114*, 5460−5462.
(37) Kaneko, H.; Nagae, H.; Tsurugi, H.; Mashima, K. End-Functionalized Polymerization of 2-Vinylpyridine through Initial C−H Bond Activation of N-Heteroaromatics and Internal Alkynes by Yttrium Ene−Diamido Complexes. *J. Am. Chem. Soc.* **2011**, *133*, 19626−19629.
(38) Duchateau, R.; van Wee, C. T.; Teuben, J. H. Insertion and C−H Bond Activation of Unsaturated Substrates by Bis(benzamidinato) yttrium Alkyl, [PhC(NSiMe3)2]2YR (R = CH2Ph·THF, CH(SiMe3)2), and Hydrido, {[PhC(NSiMe3)2]2Y(μ-H)}2, Compounds. *Organometallics* **1996**, *15*, 2291−2302.
(39) Soller, B. S.; Salzinger, S.; Jandl, C.; Pöthig, A.; Rieger, B. C−H Bond Activation by σ-Bond Metathesis as a Versatile Route toward Highly Efficient Initiators for the Catalytic Precision Polymerization of Polar Monomers. *Organometallics* **2015**, *34*, 2703−2706.
(40) Adams, F.; Machat, M. R.; Altenbuchner, P. T.; Ehrmaier, J.; Pöthig, A.; Karsili, T. N. V.; Rieger, B. Toolbox of Nonmetallocene Lanthanides: Multifunctional Catalysts in Group-Transfer Polymerization. *Inorg. Chem.* **2017**, *56*, 9754−9764.
(41) Altenbuchner, P. T.; Werz, P. D. L.; Schöppner, P.; Adams, F.; Kronast, A.; Schwarzenböck, C.; Pöthig, A.; Jandl, C.; Haslbeck, M.; Rieger, B. Next Generation Multiresponsive Nanocarriers for Targeted Drug Delivery to Cancer Cells. *Chem. − Eur. J.* **2016**, *22*, 14576−14584.
(42) Schwarzenbock, C.; Schaffer, A.; Pahl, P.; Nelson, P. J.; Huss, R.; Rieger, B. Precise synthesis of thermoresponsive polyvinylphosphonate-biomolecule conjugates via thiol-ene click chemistry. *Polym. Chem.* **2018**, *9*, 284−290.
(43) Pahl, P.; Schwarzenböck, C.; Herz, F. A. D.; Soller, B. S.; Jandl, C.; Rieger, B. Core-First Synthesis of Three-Armed Star-Shaped Polymers by Rare Earth Metal-Mediated Group Transfer Polymerization. *Macromolecules* **2017**, *50*, 6569−6576.
(44) Adams, F.; Pehl, T. M.; Kränzlein, M.; Kernbichl, S. A.; Kang, J.-J.; Papadakis, C. M.; Rieger, B. (Co)polymerization of (−)-menthide and β-butyrolactone with yttrium-bis(phenolates): tuning material properties of sustainable polyesters. *Polym. Chem.* **2020**, *11*, 4426−4437.
(45) Schaffer, A.; Kränzlein, M.; Rieger, B. Synthesis and Application of Functional Group-Bearing Pyridyl-Based Initiators in Rare Earth Metal-Mediated Group Transfer Polymerization. *Macromolecules* **2020**, *53*, 4345−4354.

https://dx.doi.org/10.1021/acs.macromol.0c01639
Macromolecules 2020, 53, 8382−8392

(46) Bosq, N.; Guigo, N.; Persello, J.; Sbirrazzuoli, N. Melt and glass crystallization of PDMS and PDMS silica nanocomposites. *Phys. Chem. Chem. Phys.* **2014**, *16*, 7830−7840.
(47) Copolymers **P4**, **P9**, and **P10** were stored at elevated temperatures (70 and 120 °C) under air for seven days to check the stability of the linker motif. Moreover, **P4** was irradiated at λ = 365 nm for 120 h in solid form and as a solution in benzene (Table S3). In all cases, the block structure remained intact after this period (shown by ^{1}H-NMR and DOSY-NMR). However, the phosphonate esters of **P4** degraded partially at 120 °C (occurrence of EtOH and Et_2O signals at 1.18, 3.49, and 3.60 ppm in MeOD), while the PεCL block of **P10** depolymerized significantly (from $M_{n,NMR}$ = 30.5 to 21.6 kg mol^{-1}) at 120 °C. According to the NMR analysis, **P9** remained intact after heat treatment at 120 °C; however, a slight color change was observed at 120 °C (Table S3).
(48) Hultzsch, K. C.; Voth, P.; Beckerle, K.; Spaniol, T. P.; Okuda, J. Single-Component Polymerization Catalysts for Ethylene and Styrene: Synthesis, Characterization, and Reactivity of Alkyl and Hydrido Yttrium Complexes Containing a Linked Amido−Cyclopentadienyl Ligand. *Organometallics* **2000**, *19*, 228−243.
(49) Vaughn, G. D.; Krein, K. A.; Gladysz, J. A. Synthesis and reactivity of metallacyclic manganese .alpha.-(silyloxy)alkyl complexes [cyclic] (CO)4MnC(R)(OSi(CH3)3)P(C6H5)2. A new thermodynamic driving force for carbonyl insertion. *Organometallics* **1986**, *5*, 936−942.
(50) Cai, C.-X.; Toupet, L.; Lehmann, C. W.; Carpentier, J.-F. Synthesis, structure and reactivity of new yttrium bis(dimethylsilyl)-amido and bis(trimethylsilyl)methyl complexes of a tetradentate bis(phenoxide) ligand. *J. Organomet. Chem.* **2003**, *683*, 131−136.
(51) Salzinger, S.; Soller, B. S.; Plikhta, A.; Seemann, U. B.; Herdtweck, E.; Rieger, B. Mechanistic Studies on Initiation and Propagation of Rare Earth Metal-Mediated Group Transfer Polymerization of Vinylphosphonates. *J. Am. Chem. Soc.* **2013**, *135*, 13030−13040.
(52) Leute, M. *Macromolecules with phosphorus functionalities*. PhD, University of Ulm, 2007.
(53) Wang, Q.; Chen, S.; Liang, Y.; Dong, D.; Zhang, N. Bottle-Brush Brushes: Surface-Initiated Rare Earth Metal Mediated Group Transfer Polymerization from a Poly(3-((2,6-dimethylpyridin-4-yl)-oxy)propyl methacrylate) Backbone. *Macromolecules* **2017**, *50*, 8456−8463.

https://dx.doi.org/10.1021/acs.macromol.0c01639
Macromolecules 2020, 53, 8382−8392

6.4 Reprint Permission Copyrighted Content

Copyright Clearance Center RightsLink®

Home | Help | Live Chat | Sign in | Create Account

ACS Publications
Most Trusted. Most Cited. Most Read.

Precise Synthesis of Poly(dimethylsiloxane) Copolymers through C–H Bond-Activated Macroinitiators via Yttrium-Mediated Group Transfer Polymerization and Ring-Opening Polymerization

Author: Andreas Schaffer, Moritz Kränzlein, Bernhard Rieger
Publication: Macromolecules
Publisher: American Chemical Society
Date: Oct 1, 2020

Copyright © 2020, American Chemical Society

PERMISSION/LICENSE IS GRANTED FOR YOUR ORDER AT NO CHARGE

This type of permission/license, instead of the standard Terms & Conditions, is sent to you because no fee is being charged for your order. Please note the following:

- Permission is granted for your request in both print and electronic formats, and translations.
- If figures and/or tables were requested, they may be adapted or used in part.
- Please print this page for your records and send a copy of it to your publisher/graduate school.
- Appropriate credit for the requested material should be given as follows: "Reprinted (adapted) with permission from (COMPLETE REFERENCE CITATION). Copyright (YEAR) American Chemical Society." Insert appropriate information in place of the capitalized words.
- One-time permission is granted only for the use specified in your request. No additional uses are granted (such as derivative works or other editions). For any other uses, please submit a new request.

BACK CLOSE WINDOW

© 2020 Copyright - All Rights Reserved | Copyright Clearance Center, Inc. | Privacy statement | Terms and Conditions
Comments? We would like to hear from you. E-mail us at customercare@copyright.com

7 Synthesis, Characterisation and Functionalisation of BAB-type Dual-Responsive Nanocarriers for Targeted Drug Delivery: Evolution of Nanoparticles based on 2-Vinylpyridine and Diethyl Vinylphosphonate

7.1 Bibliographic Data

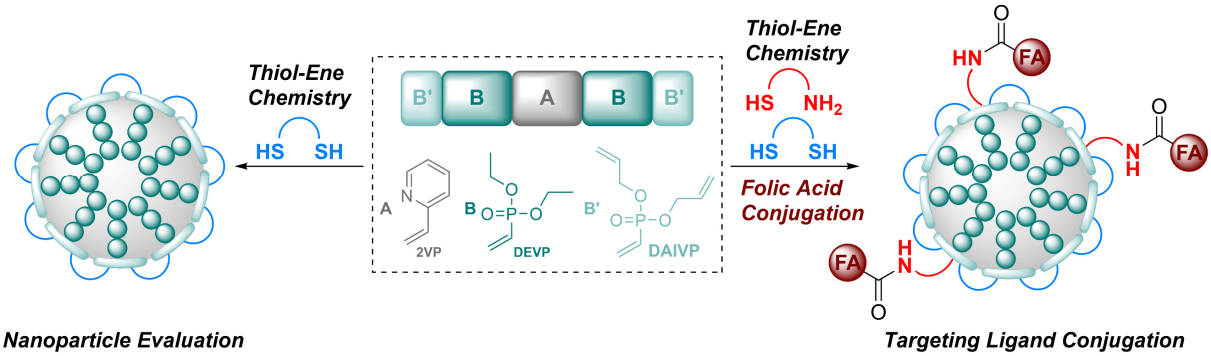

Title: "Synthesis, Characterisation and Functionalisation of BAB-type Dual-Responsive Nanocarriers for Targeted Drug Delivery: Evolution of Nanoparticles based on 2-Vinylpyridine and Diethyl Vinylphosphonate"

Status: Full Paper, published online

Journal: RSC Advances 2021, 11, 1586–1594

Publisher: The Royal Society of Chemistry

Link/DOI: https://doi.org/10.1039/D0RA08902H

Authors: Andreas Saurwein,[‡] Andreas Schaffer,[‡] Christina Wieser, and Bernhard Rieger[a]

[‡]These authors contributed equally. [a]Andreas Saurwein performed most of the experiments and gave advice on the manuscript. Andreas Schaffer performed some experiments and wrote the manuscript. Christina Wieser had the initial idea and contributed with valuable advice. All work was carried out under supervision of Bernhard Rieger.

7.2 Summary

The emerging field of nanomedicine provides new perspectives on diseases that are currently difficult to cure and, hence, represents a new opportunity for a more effective and patient-friendly treatment.

Herein, our previously published work, which explored ABB'-based nanoparticles as drug delivery vehicles, was expanded towards B'BABB' block copolymers (A: 2VP, B: DEVP, B': DAlVP). These copolymers were synthesized via REM-GTP with a binuclear catalyst **5** and used as substrates for the formation of stable nanocarriers. Complex **5** was characterized by ^{1}H- and ^{13}C-NMR spectroscopy and evaluated in kinetic experiments with 2VP. End-group analysis of the respective 2VP oligomers using electrospray ionization spectrometry confirmed the incorporation of 2,3,5,6-tetramethylpyrazine. Next, several feed compositions were adjusted for the copolymerizations. The obtained copolymers **BAB1-5** were analyzed by gel permeation chromatography as well as ^{1}H- and ^{31}P-NMR spectroscopy and cross-linked with three different dithiols via thiol-ene click chemistry to yield the corresponding nanocarriers. The cross-linking process was monitored via ^{1}H-NMR and the nanoparticles **NP1-7** were analyzed with regard to their size by DLS and TEM and were further characterized through zeta potential measurements. Hereby, higher amounts of 2VP and DAlVP resulted in particles with a smaller particle size Moreover, the stability of the particles was examined by DLS in chloroform. Most importantly, the release behavior was examined at varying conditions (pH and temperature) and exhibited higher releases in an acidic environment or at elevated temperatures.

Following this, a synthesis route towards active targeting vehicles which bear folic acid on their surface was established. For that purpose, the cross-linking procedure was turned into a two-step process which contained the addition of cysteamine followed by the cross-linking with dithiol **6**. Introduction of the amino groups enabled the conjugation of an activated folic acid derivative to yield the functionalized particle **NP-FA**. Likewise to the compounds **NP1-7**, **NP-FA** was analyzed by DLS, TEM and zeta potential measurements. ^{1}H-NMR exhibited the significant signals of the pteridine moiety while UV/Vis spectroscopy showed the characteristic absorption band of folic acid. Moreover, DOSY-NMR corroborated the covalent coupling of **NP-NH$_2$** with folic acid.

In conclusion, the combination of REM-GTP and thiol-ene chemistry represents a facile synthesis route towards tailor-made drug delivery vehicles with specific surface ligands for active drug targeting.

7.3 Manuscript

RSC Advances

ROYAL SOCIETY OF CHEMISTRY

PAPER

View Article Online
View Journal | View Issue

Check for updates

Cite this: *RSC Adv.*, 2021, **11**, 1586

Synthesis, characterisation and functionalisation of BAB-type dual-responsive nanocarriers for targeted drug delivery: evolution of nanoparticles based on 2-vinylpyridine and diethyl vinylphosphonate†

Andreas Saurwein,‡ Andreas Schaffer,‡ Christina Wieser and Bernhard Rieger *

Received 19th October 2020
Accepted 5th December 2020

DOI: 10.1039/d0ra08902h

rsc.li/rsc-advances

The emerging field of nanomedicine gives new opportunities in the treatment of cancer. Aspects such as dosage, bioavailability or the application to the patient can be drastically improved. Previously our group reported an efficient route towards cross-linked nanospheres based on ABB′ block copolymers made from 2-vinylpyridine (2VP), diethyl vinylphosphonate (DEVP) and diallyl vinylphosphonate (DAlVP). Followed by thiol–ene click chemistry stable nanoparticles were formed. Herein, this promising concept was extended to copolymers with the analogous B′BABB′ architecture. In this context the new yttrium complex **5** was investigated in the rare-earth metal-mediated group transfer polymerisation (REM-GTP) and used for the generation of copolymers with different monomer feeds (2VP: 100–300 equiv.; DEVP: 200–300 equiv.; DAlVP: 6–20 equiv.) to explore the influence of the copolymer compositon on the nanoparticle properties. After successful cross-linking with various cross-linking agents, all nanoparticles were characterised *via* DLS and TEM. These size measurements revealed defined, almost spherical particles (d_{DLS} = 17–52 nm; d_{TEM} = 17–43 nm) and were mainly affected by the 2VP content and the cross-linking density. Zeta potential measurements resulted in values in the range from −6 mV to −22 mV and revealed an influence of the cross-linking agent on the surface charge. Studies on the release behaviour exhibited the fastest release at pH = 4.5. Temperature-wise best results were achieved at 42 °C. Furthermore, we aimed for the conjugation of folic acid as a model compound for a potential application in active drug targeting. The consecutive couplings of cysteamine and dithiol **6** enabled the formation of an amine-modified precursor which was reacted with a folic acid derivative. Zeta potential measurements and analysis by NMR spectroscopy corroborated a successful conjugation while DLS and TEM (d_{DLS} = 44 nm; d_{TEM} = 38 nm) indicated defined nanoparticles.

Introduction

In the present-day cancer can be considered one of the biggest challenges to our modern society. Around 18 million new cancer cases and 9.6 million cancer-related deaths have been estimated for 2018 alone.[1] Common therapies can be divided into surgical removal, internal and external radiation and chemotherapy.[2] However, radiation and chemotherapy can be accompanied by severe side effects damaging normal tissue and organs as well as causing systemic toxicity owing to their inability to distinguish between healthy and cancer cells. Furthermore, the efficacy of the therapy can be highly individual despite a strictly identical treatment.[2–4]

Consequently, the treatment remains a complex task and demands improved, patient-friendly approaches since, for example, a study of Schiller *et al.* in 2002 implied that a therapeutic plateau was reached regarding the use of chemotherapeutics.[5,6] One promising development that aims to overcome this set of problems are nanosized drug-delivery vehicles. Currently, anticancer drugs are frequently limited owing to their high hydrophobicity and thus low solubility in aqueous media. Therefore, high tissue concentrations are required and can lead to systemic toxicity. Moreover, low molecular-weight agents are often eliminated by the liver or kidneys.[2,7] Drug-delivery vehicles allow the encapsulation of such hydrophobic substances, increase their bioavailability substantially and benefit from the enhanced permeability and retention (EPR)

WACKER-Chair of Macromolecular Chemistry, Catalysis Research Center, Technical University of Munich, Lichtenbergstraße 4, 85748 Garching Near Munich, Germany. E-mail: rieger@tum.de

† Electronic supplementary information (ESI) available: Synthetic procedures, NMR spectra, ESI analysis of the oligomers, GPC traces, release data for copolymers **BAB1–3**, DLS and TEM analysis of **NP1**, **NP3–7**, and **NP-FA**. See DOI: 10.1039/d0ra08902h

‡ These authors contributed equally.

effect which results in an improved accumulation at the tumour site. In addition, engineered nanoparticles are able to facilitate a controlled release of the drug.[2,8–13] One widely investigated approach focuses on polymeric micelles. These are usually composed of a hydrophilic shell such as poly(ethylene glycol) (PEG) or poly(*N*-vinyl pyrrolidone) (PVP) and a hydrophobic core (*e.g.* poly(propylene oxide) (PPO), poly(D,L-lactic acid) (PDLLA), poly(ε-caprolactone) (PεCL), poly(L-aspartate)) (PASA), which enable a loading of the pharmacologically active agent.[7,14] Exemplarily, the application of such a micellar carrier improved the concentration of paclitaxel significantly.[15]

From this broad basis, delivery vehicles made from smart materials emerge as next generation nanocarriers. Since cancerous tissue exhibits a slightly acidic environment (pH = 6.5–6.8) compared to healthy tissue (pH = 7.4) as well as elevated temperatures (hyperthermia), stimuli-responsive drug delivery vehicles can take advantage from the pathological conditions of the diseased tissue and use these triggers to enhance the drug release.[2,7] In this context formulations with poly(2-vinylpyridine) (P2VP) demonstrated a pH-stimulated degradation of the micellar system while P2VP-comprising polymerosomes showed the release of the encapsulated cargo upon protonation of the pyridine motifs.[16,17] Among the temperature-sensitive materials poly(*N*-isopropylacrylamide) (PNIPAAm) is commonly used and finds broad application in many biomedical fields. Consequently, PNIPAAm-based carriers were also investigated for their use as the hyperthermia-directed drug delivery vehicles.[18,19] However, PNIPAAm features a lower critical solution temperature (LCST) of 32 °C demanding copolymerisation to reach physiological range and it can show functional loss in biological fluids.[20,21] A rather new material class are polyvinylphosphonates, which are soluble in aqueous media, feature a tuneable LCST and exhibit high biocompatibility.[22,23] Our group was able to establish an efficient and precise route towards well-defined, high molecular-weight polyvinylphosphonates *via* rare earth metal-mediated group transfer polymerisation.[24–27] In 2016 this work concluded in the synthesis of BAB block copolymers consisting of P2VP and poly(diethyl vinylphosphonate) (PDEVP). These copolymers formed monodisperse and spherical micelles in aqueous solution and showed a pH as well as a temperature-triggered release of doxorubicin (DOX). Moreover *in vitro* studies revealed the internalisation of the DOX-loaded carriers into HeLa cells.[28] However, the self-assembly of micelles remains a concentration-dependent process and is always affected by the equilibrium with free, non-associated polymer chains. As a result, micelles are subjected to high dilution in the human body upon injection which shifts the equilibrium-state towards the free polymer resulting in the dissociation of the micellar structures.[29,30] This effect intensifies when the unimers bind to other constituents, *e.g.* proteins or membranes.[30]

To avoid this issue, the basic concept of these nanocarriers was optimised by the introduction of diallyl vinylphosphonate (DAlVP) as a third block resulting in copolymers with an ABB′ block structure. The allyl groups facilitated the cross-linking of the copolymers *via* thiol–ene click chemistry and yielded stable, monodisperse and spherical particles. Most importantly the stimuli-triggered release was retained after cross-linking. In addition *in vitro* experiments gave evidence for the internalisation of the carriers into the cells and a statistic insight on the uptake level.[31] In this context we adopted the cross-linking procedure for BAB-type block copolymers and investigated the effects of the changed polymer architecture on the particle formation and the release behaviour. Moreover, folic acid was conjugated to the particles as a targeting ligand.

Results and discussion

Complex synthesis

In order to change the copolymer architecture from the ABB′ structure (A: 2VP, B: DEVP, B′: DAlVP) to a B′BABB′ block structure, a binuclear catalyst is required. Such a structure can be achieved *via* performing C–H bond activations with bifunctional initiators such as 2,3,5,6-tetramethylpyrazine (TMPy) (**1**).[32] Besides TMPy, 2,3-dimethylpyrazine (**2**) and 2,5-dimethylpyrazine (**3**) were also considered as possible initiators (Scheme 1a). The two opposing methyl groups of **1** located next to the heteroaromatic nitrogen presumably allow the C–H bond activation with $Cp_2Y(CH_2TMS)(THF)$ (**4**) and resulted in a complex comprising two catalytically active sites. Surprisingly, the use of pyrazines **2** and **3** did not result in a successful activation and led only to the formation of degradation products. Fortunately, mixing of the Cp_2Y complex **4** with TMPy immediately resulted in an intense orange colouration of the solution that indicated the σ-bond metathesis (Scheme 1b). The respective ^{1}H-NMR spectrum of the isolated complex strongly suggests the presence of only one species (Fig. 1). Most importantly, the signals at 1.99 and 2.91 ppm can be attributed to the CH_2Y and CH_3 groups and exhibit a 4 : 6 ratio. Additionally, one THF molecule must be coordinated to each yttrium centre. These observations are supported by ^{13}C-NMR spectroscopy as well as elemental analysis (EA). Moreover, NOESY NMR supports the formation of a single species with both methyl groups being spatially adjacent to each other (Fig. S3†). The kinetic analysis of the C–H bond activation *via* NMR revealed the full conversion after 18 hours (Fig. S4†).

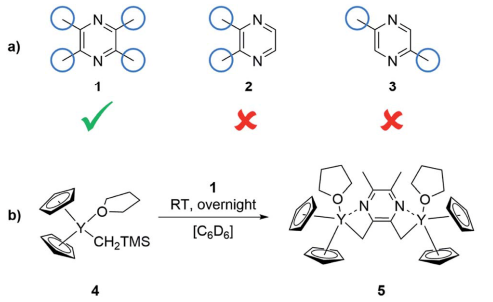

Scheme 1 (a) Screening of bifunctional pyrazines for the synthesis of a binuclear complex for REM-GTP. (b) Synthesis of the complex **5** with TMPy starting from $Cp_2Y(CH_2TMS)(THF)$ (**4**).

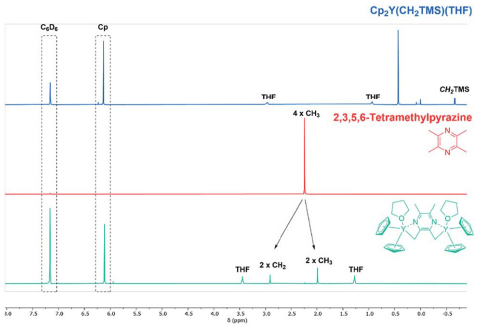

Fig. 1 Overview of C–H bond activation showing complex **4** (blue), TMPy (**1**) (red) and species **5** gained after completed C–H bond activation (green). ^{1}H-NMR spectra were recorded in benzene-d_6.

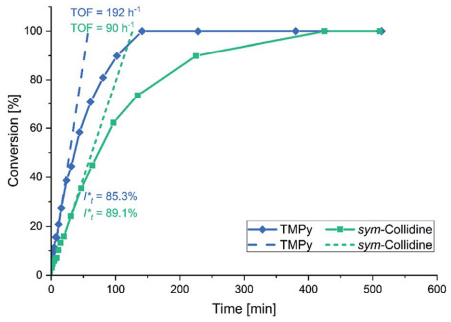

Fig. 2 Conversion-time plot for the polymerisation of 2VP with the TMPy activated complex **5** (blue) and with *sym*-collidine activated Cp_2Y (green).

End-group analysis

Since the lanthanide-based complexes activated with *sym*-collidine showed the incorporation of the initiator in the polymer chain, evidence was needed to prove the covalent integration of TMPy into the polymer chain.[25] By default, the characterisation of the end-group can be performed by electron spray ionisation mass spectrometry (ESI-MS) *via* analysis of the respective oligomer patterns. Three oligomer patterns were identified in the corresponding ESI-MS spectrum of the oligomers which were produced with complex **5** (Fig. S5†). The m/z values assigned to the first pattern show oligomer peaks ionised with H^+ (452 and 557 u) with a difference equal to the molecular mass of 2VP ($m_{2VP} = 105$ u). The second pattern with $z = 2$ was ionised by two protons and shows the respective oligomer signals (331, 384, 436, 489, and 541 u) with a difference of 52.5 u which is equivalent to the half of m_{2VP}. In addition, a third series of oligomer signals (291, 326, 361, and 396 u) can be attributed to $z - 3$. Thus, the mass difference was determined to be 35 u. For completeness, the ESI-MS spectrum generated with $Cp_2Y(CH_2(C_5H_2Me_2N))$ is illustrated in Fig. S6 in the ESI.†

Kinetic investigation of the TMPy-activated catalyst

In this context *sym*-collidine or TMPy were already employed as initiators in the polymerisation of 2VP with bisphenolate-based yttrium complexes by our group and alkyl yttrium complexes from Mashima *et al.*[33,34] As the C–H bond activated Cp_2Y complexes have not been evaluated in kinetic experiments with this monomer, the polymerisation of 2VP was investigated with the new complex **5**. Fig. 2 shows the conversion-time plot of complex **5** in blue. Hereby a turnover frequency (TOF) of 192 h^{-1} was determined while the corresponding initiator efficiencies (IE) were found to be 85% at the beginning and 88% at the end of the polymerisation. The living fashion of the polymerisation was able to be observed which is represented by the linear growth of the molecular weight. The corresponding polydispersites $Đ$ remained low with values $Đ < 1.10$ (Fig. 3). For a better classification, the kinetic measurements were also performed with the *sym*-collidine activated yttrium complex. The respective conversion-time plot is illustrated by the green curve in Fig. 2. In this case a TOF of 90 h^{-1} was determined. Concerning the initiator efficiency, a value of 89% was calculated at the start of the polymerisation and 72% at the end. As expected, the growth was found to be linear and showed low polydispersities between $Đ = 1.01$ and 1.12 (Fig. S7†). The kinetic data on the turnover frequencies appear to be in good agreement with the molecular structures of **5** and the complex with *sym*-collidine. Since **5** has two active sites attached to one initiator group after C–H bond activation the polymer chain can grow in two directions while *sym*-collidine can only bear one yttrium centre. This results in a TOF twice as high for complex **5**. Compared to the literature, the catalysts activated with TMPy or *sym*-collidine exhibit TOF values which are about three or 10 times lower than the bisphenolate system.[28,35] This finding might be explained by an improvement of the electronic properties of the metal centre induced by the bisphenolate ligand.

Copolymerisation results

Based on the complex analysis and kinetic findings a variety of copolymers were synthesised that were later conducted to the

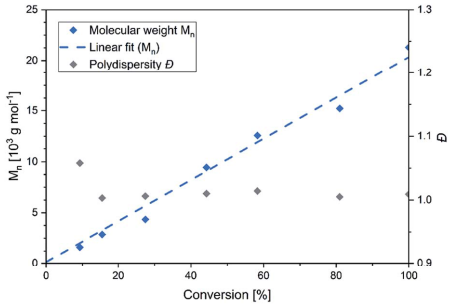

Fig. 3 Conversion-dependant plot of the molecular weights and corresponding polydispersities $Đ$ of P2VP generated with complex **5**.

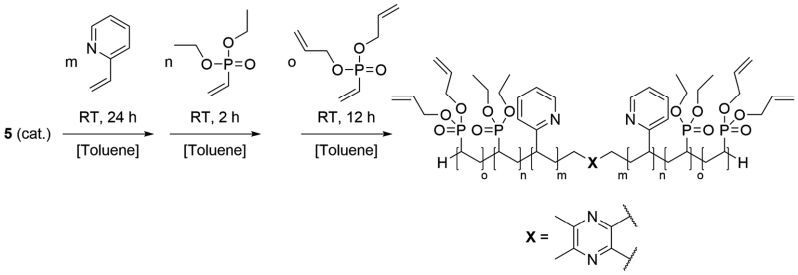

Scheme 2 Synthesis of the BAB block copolymers from 2VP, DEVP, and DAlVP *via* REM-GTP with catalyst **5**.

Table 1 Feed composition, monomer conversions, molecular weights M_n of block (A) and polydispersities $Đ$ for (A) and (BAB), initiator efficiencies IE of block (A) and composition of the copolymer

	Feed A/B/B′[a]/ equiv.	X (A)[b]/%	M_n (A)[c]/ 10^4 g mol^{-1}	$Đ$ (A)[c]/-	IE (A)[d]/%	X (B)[b]/%	Composition A/B [2VP/DEVP][b]	$Đ$ (BAB)[c]/—	M_n (B′BABB′)[b]/ 10^4 g mol^{-1}
BAB1	100/200/10	>99	1.21	1.05	94	>99	1.0/1.9	1.08	4.80
BAB2	200/200/10	>99	2.24	1.08	95	>99	1.0/1.1	1.10	5.90
BAB3	300/300/10	>99	2.97	1.04	>99	>99	1.0/1.1	1.07	8.12
BAB4	200/200/6	>99	2.76	1.06	80	>99	1.0/1.0	1.01	6.91
BAB5	200/200/20	>99	2.10	1.03	>99	>99	1.0/1.0	1.01	5.65

[a] By weighing the monomer, [M]/[cat.] = equiv. A: 2VP, B: DEVP, B′: DAlVP. [b] Conversions X were calculated from the corresponding ^{1}H-NMR or ^{31}P-NMR spectra. [c] Determined *via* GPC analysis in DMF. [d] Initiator efficiency IE was determined for block (A), IE = $M_{n,theo}/M_{n,exp}$.

cross-linking procedure (Scheme 2). In this work the monomer feed of 2VP and DEVP was varied between 100 equiv. and 300 equiv., while a feed ratio of 1 : 1 or 1 : 2 was adjusted. Furthermore, the DAlVP content was adjusted between six and 20 equiv. (Table 1). Each step of the copolymerisation was allowed to reach full conversion, which took approximately 24 hours in case of 2VP and two hours and 12 hours for DEVP and DAlVP, respectively (Scheme 2). Owing to the controlled nature of REM-GTP, all polymers showed narrow polydispersities ranging from $Đ$ = 1.01 to 1.10 and had molecular weights between 48.0 and 81.2 kg mol^{-1}, which exceeds the threshold for renal clearance of 40 kg mol^{-1}. The initiator efficiencies were calculated after determination of the P2VP block length and ranged around 90%. In addition, ^{1}H-NMR spectroscopy allowed the calculation of the experimental block ratios that match the theoretical block ratios very well. Here too, the signals of the allylic side groups were attributed *via* ^{1}H-NMR spectra between 4.50 and 6.00 ppm and are in good agreement with the previously published ABB′ based copolymers (Fig. 4, blue spectrum).

Nanoparticle formation *via* thiol–ene click chemistry

Cross-linking of the copolymers was performed *via* an established route using thiol–ene click chemistry with azobisisobutyronitrile (AIBN) as an initiator and 3,6-dioxa-1,8-octanedithiol (**6**),[31] 1,4-butanedithiol (**7**), or D,L-dithiothreitol (**8**) as a linking component (Scheme 3). As visualised in Fig. 4 the reaction was monitored *via* ^{1}H-NMR and was considered to reach full conversion after complete disappearance of the allylic protons. Since the cross-linking of the ABB′ copolymers was performed with an excess of dithiol **6**, we aimed for an optimisation by testing several dithiol amounts (3.0 equiv., 1.5 equiv., 1.0 equiv.) corresponding to the allyl group content of copolymer **BAB2**. As expected, an excess of three equivalents reached full conversion after 24 hours. But already a slight excess of the dithiol (1.5 equiv.) suffices to detect a complete reaction after the 24 hours. However, an amount of one equivalent appeared to be

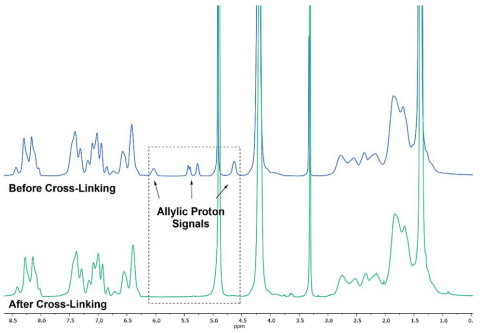

Fig. 4 Comparison of ^{1}H-NMR spectra before (**BAB2**) (blue) and after cross-linking (**NP2**) with 3,6-dioxa-1,8-octanedithiol (**6**) (green). Spectra were recorded in MeOD-d_4.

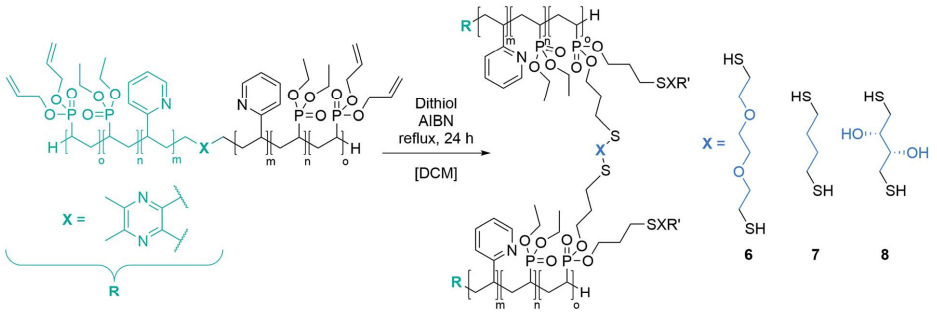

Scheme 3 Strategy for the cross-linking of the copolymers *via* thiol–ene click chemistry with dithiol **6**, **7** and **8**.

Table 2 Used copolymers and dithiols, diameters and polydispersities determined *via* DLS and TEM and zeta potential ζ of the nanoparticles

	Polymer	Dithiol	*d* (DLS)/nm	PDI (DLS)	ζ/mV	*d* (TEM)/nm	PDI (TEM)
NP1	**BAB1**	**6**	21.1 ± 0.9	0.17	−11 ± 0.3	17.1 ± 1.6	0.09
NP2	**BAB2**	**6**	32.6 ± 0.4	0.19	−13 ± 0.2	31.0 ± 4.7	0.15
NP3	**BAB3**	**6**	51.9 ± 3.9	0.16	−19 ± 1.0	42.7 ± 4.9	0.11
NP4	**BAB4**	**6**	41.7 ± 5.6	0.17	−16 ± 0.6	34.2 ± 2.3	0.08
NP5	**BAB5**	**6**	16.8 ± 0.6	0.22	−22 ± 0.5	26.1 ± 2.4	0.09
NP6	**BAB3**	**7**	47.4 ± 3.8	0.16	−9.8 ± 0.4	41.1 ± 5.6	0.14
NP7	**BAB3**	**8**	46.9 ± 1.8	0.13	−6.3 ± 0.2	41.0 ± 3.9	0.09

insufficient because traces of the allylic protons were still visible. After optimisation of the dithiol amount the successfully cross-linked samples were analysed *via* transmission electron microscopy (TEM) and dynamic light scattering (DLS) to verify the formation of the nanoparticles. Table 2 gives an overview of the experimental data of the generated nanoparticles. With the exception of **NP1** and **NP5**, all cross-linked particles exhibit diameters larger than 30 nm with particle sizes between 32.6 and 51.9 nm. These values match with data of earlier reports that recommend a size range of 30–100 nm for an optimised targeting of the cancerous tissue because nanocarriers of this size benefit from the EPR effect and they are too large for renal clearance.[36,37] Concerning the size distribution, PDIs ≤ 0.22 were found which slightly deviates from an optimal PDI below 0.10. Nevertheless, imaging *via* TEM indicates highly uniform and monodisperse, spherical particles. Furthermore, the size-related values gained with both methodologies are in good accordance with each other (Table 2). The DLS and TEM data of **NP2** are illustrated in Fig. 5. The remaining data are summarized in the ESI (Fig. S26, S29, S31, S33, S35, S38).† As shown by **NP1–3**, the particle size is mainly influenced by the P2VP block while a change of the DEVP block only has minor influence on the diameter. Moreover, a decrease of the DAlVP amount resulted in a larger diameter for **NP4** compared to **NP2**, while **NP5** exhibited a much smaller diameter. Therefore, it can be concluded that the spatial extent of the particles can be tuned by the cross-linking density. The type of cross-linker has no significant influence on the particle size. Additional zeta

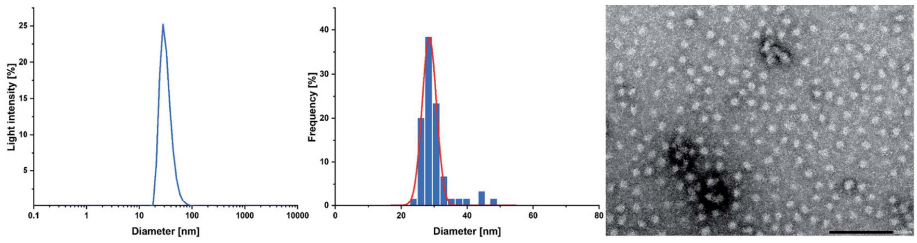

Fig. 5 Size distribution of **NP2** determined *via* DLS measurements at a concentration of 2.5 mg mL^{-1} in water (left); histogram plot with a Gaussian regression fit (middle); and a TEM image of **NP2** (right) with a scale bar of 200 nm.

potential measurements attribute a negative surface charge for the particles between −22 and −6.3 mV. A negative charge was also observed for the ABB′-type nanoparticles.[31] However, **NP6** and **NP7** tend to have potentials closer to zero than the ones with **6** as cross-linker. Generally speaking, a positive surface charge is preferable because of the anionic character of the cellular membrane. However, this is contradicted by an increasing cytotoxicity and a higher affinity towards vascular endothelial cells and other anionic species which leads to aggregation and a corruption of the potential therapeutic effects.[38–40] However, in 2008 Huang *et al.* demonstrated a slower clearance of neutral carriers compared to their anionic pendants, which indicated a surface charge near zero would be beneficial for drug delivery.[31,41] Additionally, measurements in $CHCl_3$ were performed to test the stability of the particles because both blocks are soluble in $CHCl_3$ (Fig. S41†). In case of **NP1**–**NP6** the particle diameters exceeded those values that were determined in water. Therefore, stable particles can be assumed since the free polymer chains should form random coils in solution which must be much smaller than the respective nanoparticles. However, the cross-linking of **BAB3** to **NP7** appeared not to be successful because a diameter of only 12.6 nm was determined compared to 46.9 nm in water.

Release behaviour of the nanoparticles

Eventually the loading and release behaviour of the nanoparticles was studied. After loading with fluorescein, the samples were analysed in respect of the cumulative release by dialysis. For this purpose, varying temperatures and pH-values were adjusted. For that purpose, room temperature and a neutral pH were adjusted as reference. A temperature of 37 °C was set to simulate the body temperature, while 42 °C was used to mimic hyperthermic conditions caused by cancer cells. With regard to the pH, acidic environments were adjusted to simulate the conditions in the endosomal environment (pH = 6.0) or the interior of the lysosome (pH = 4.5).[31,42] In Fig. 6 the cumulative fluorescein release of **BAB2** and **NP2** is visualised. Compared to the micelles formed from **BAB2** the release from the cross-linked nanoparticle **NP2** was improved by approximately 20% after 30 hours. In both cases elevated temperatures as well as acidic conditions stimulated the release compared to the standard scenario at room temperature and a neutral environment. Regarding the temperature, a coil-to-globule-transition triggers the collapse of the DEVP-based shell. Unfortunately, there is no

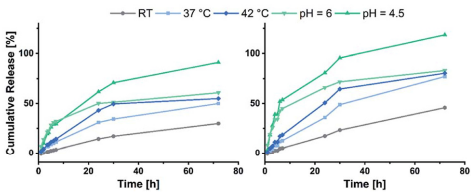

Fig. 6 Cumulative release of fluorescein from BAB2 (left) in comparison to NP2 (right).

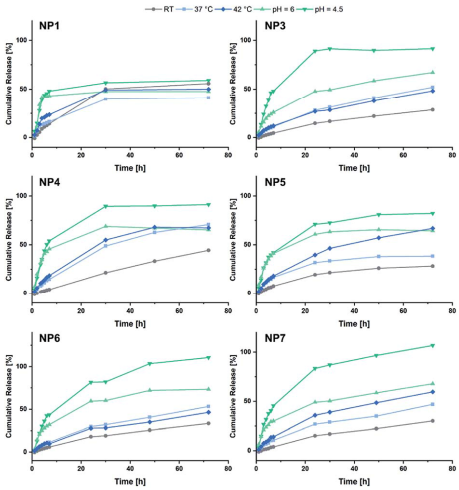

Fig. 7 Summary of the cumulative fluorescein release from NP1 and NP3–NP7.

significant differentiation between 37 °C and 42 °C. Overall best results were obtained at pH = 4.5. But whereas **BAB2** revealed a quantitative release after 70 hours, this was already achieved after 30 hours with **NP2**. The release data of nanoparticles **NP1** and **NP3**–**NP7** are illustrated in Fig. 7. Interestingly, **NP1** shows inferior characteristics with a cumulative release limited to approximately 50% in all scenarios after 30 hours. This might be attributed to a relatively rigid and inflexible structure of **BAB1** with its short P2VP core, which prevents the release of the cargo. **NP3** exhibited best results at acidic conditions and showed a quantitative release of fluorescein after 24 hours at pH = 4.5 and 60% after 70 hours at pH = 6.0. Hence, **NP3** must be most sensitive to conformational changes upon protonation of the pyridine units which promotes the release of the cargo as it has the largest P2VP block. **NP4** and **NP5** also showed best results at a pH of 4.5 with a cumulative release between 80 and 90%, but both nanoparticles also seem to be quite responsive to changes in temperature and outperform **NP3** in this category. **NP4** reaches a release of approximately 70% but shows no differentiation between 37 and 42 °C on the one hand. On the other hand, **NP5** features a distinctive gap of the releases at 37 °C (30%) and 42 °C (70%). Therefore, a tightly cross-linked particle shell might be beneficial in terms of a temperature-triggered release. The release behaviour of **NP6** and **NP7** corresponds with the results of **NP3** regarding the rate and extent of the release. However, the non-polar cross-linker 1,4-butanedithiol (7) seems to decrease the temperature-induced release of fluorescein.

Shell-functionalisation with folic acid

To broaden the scope of this concept the nanocarriers should be developed towards an application in active targeting. Such

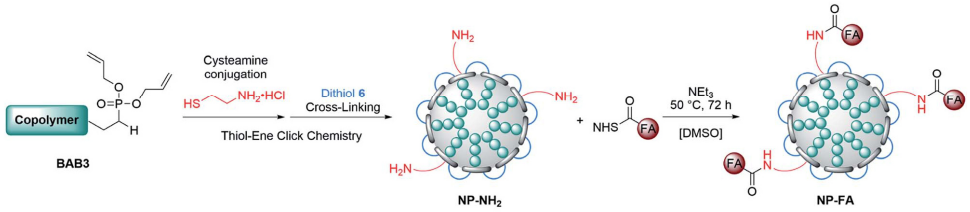

Scheme 4 Strategy for the introduction of shell-bound folic acid *via* partial conversion of the allyl groups with cysteamine hydrochloride. Folic acid was conjugated using an NHS-ester of folic acid after the cross-linking with dithiol **6**.

a type of nanoparticle requires the presence of superficial targeting ligands which can be recognised and bind to disease-specific cell features.[8] Folic acid is a prominent example for such a targeting ligand and shows high affinity to its folate-receptor ($K_d < 10^{-9}$) which is overexpressed on many cancer types,[43] and is therefore a beneficial targeting motif for the development of novel therapeutic concepts.[44–47] The conjugation of folic acid was achieved by the formation of a NH_2-bearing nanoparticle **NP-NH$_2$**. As depicted in Scheme 4 the allyl functions of **BAB3** were functionalised with cysteamine-hydrochloride first and cross-linked with dithiol **6** *via* thiol–ene chemistry to yield an amino-group containing surface. This reaction sequence was monitored *via* ^{1}H-NMR (Fig. S43†) and revealed a partial consumption of the allyl groups in the first step. Treatment of this precursor with the dithiol resulted in the quantitative conversion of the remaining allyl signals. With a zeta potential of −18 mV, **NP-NH$_2$** stayed in the same region as **NP3** (−19 mV). Subsequently, the particles were converted with the *N*-hydroxysuccinimide (NHS) ester of folic acid to form **NP-FA**. The NHS ester was employed in large excess to ensure a reaction with the surface-bound amino groups. After purification by dialysis, the ^{1}H-NMR exhibited characteristic signals of folic acid at 4.49 (CH_2NH), 6.64, 7.65 (both *p*-aminobenzoic acid) and 8.65 ppm (pteridine) (Fig. 8 and S45†). The zeta potential increased to −11 mV, which indicates a modification

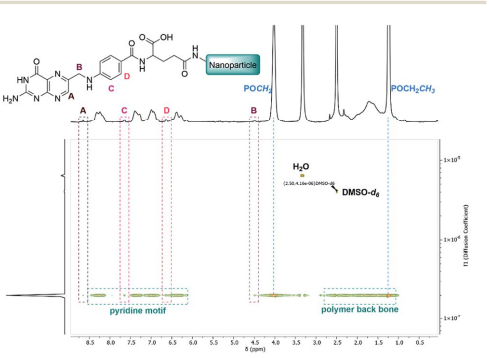

Fig. 8 DOSY-NMR spectrum of the folate-modified nanoparticle **NP-FA** in DMSO-d_6.

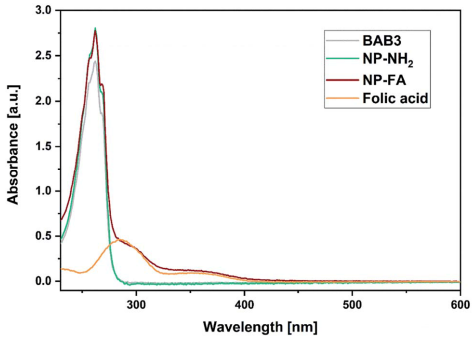

Fig. 9 UV/Vis spectra of **BAB3** (1.25 mg mL^{-1}), **NP-NH$_2$** (1.25 mg mL^{-1}), **NP-FA** (1.25 mg mL^{-1}), and free folic acid (100 μM) in methanol.

of the surface features of the particle shell. Diffusion-ordered spectroscopy (DOSY) was also performed to verify further the conjugation of folic acid. In the corresponding spectrum the folic acid related signals share the same diffusion coefficient ($D = 2.00 \times 10^{-7}$ m^2 s^{-1}) with the polymer-related signals from the polymer blocks. Additional characterisation by DLS and TEM confirmed the formation of spherical, almost uniform particles (Fig. S44†). The diameters were found to be 44.4 ± 0.9 (PDI = 0.11) for DLS and 38.2 ± 3.1 (PDI = 0.08) for TEM, respectively. In comparison to the non-modified analogues **NP3**, **NP6** or **NP7**, the diameters of **NP-FA** are slightly lower. Lastly, analysis by UV/Vis revealed the absorption band of folic acid at 360 nm, which was not visible for the copolymer **BAB3** and the precursor particle **NP-NH$_2$** (Fig. 9).

Conclusions

In summary, we expanded the scope of the ABB′-type (A: 2VP; B: DEVP, B′: DAlVP) nanoparticles towards a B′BABB′ architecture by using TMPy (**1**) as an initiator. The resulting complex **5** exhibited a TOF of 192 h^{-1} with 2VP and generated copolymers **BAB1**–**BAB5** with high precision by a GTP-type propagation mechanism. The copolymers were then cross-linked to **NP1**–**NP7** with three dithiols *via* thiol–ene click chemistry and formed defined particles in aqueous solution (d = 16.8–

51.9 nm, PDI = 0.13–0.22), which was confirmed by transmission electron microscopy. The particle diameters were mostly determined by the copolymer composition, while the choice of the cross-linker influenced the zeta potential of the shell. Elevated temperatures and acidic conditions improved the release of fluorescein as the corresponding release studies have revealed. Throughout all experiments, the strongest response was observed at a pH = 4.5. Temperature-wise **NP2**, **NP4** and **NP5** were most promising with respect to hyperthermia treatments. Moreover, we presented a facile synthesis approach towards nanoparticles with surface-bound folic acid, which was accomplished by the incorporation of cysteamine on the particle surface. As a result, the shell-located amino groups enabled the coupling of the activated folic acid derivative. The conjugation of such a ligand is a prerequisite for the application as targeted drug delivery vehicles. In addition, this synthetic strategy can be used to form tailor-made nanoparticles with selected targeting ligands that consider the molecular characteristics of the respective disease.

Conflicts of interest

There are no conflicts to declare.

Acknowledgements

The authors thank Laura Fuchs and Simone Poprawa for their support with the experiments and kinetic measurements, Dr Carsten Peters for his efforts to get the best TEM images, Dr Friederike Adams for the productive discussions and her helpful input and Alina Denk and Christopher Thomas for revising the manuscript.

Notes and references

1 F. Bray, J. Ferlay, I. Soerjomataram, R. L. Siegel, L. A. Torre and A. Jemal, *Ca-Cancer J. Clin.*, 2018, **68**, 394–424.
2 T. Sun, Y. S. Zhang, B. Pang, D. C. Hyun, M. Yang and Y. Xia, *Angew. Chem., Int. Ed.*, 2014, **53**, 12320–12364.
3 S. M. Bentzen, *Nat. Rev. Cancer*, 2006, **6**, 702.
4 D. Peer, J. M. Karp, S. Hong, O. C. Farokhzad, R. Margalit and R. Langer, *Nat. Nanotechnol.*, 2007, **2**, 751.
5 J. H. Schiller, D. Harrington, C. P. Belani, C. Langer, A. Sandler, J. Krook, J. Zhu and D. H. Johnson, *N. Engl. J. Med.*, 2002, **346**, 92–98.
6 J. Zugazagoitia, C. Guedes, S. Ponce, I. Ferrer, S. Molina-Pinelo and L. Paz-Ares, *Clin. Ther.*, 2016, **38**, 1551–1566.
7 C. Oerlemans, W. Bult, M. Bos, G. Storm, J. F. W. Nijsen and W. E. Hennink, *Pharm. Res.*, 2010, **27**, 2569–2589.
8 F. X. Gu, R. Karnik, A. Z. Wang, F. Alexis, E. Levy-Nissenbaum, S. Hong, R. S. Langer and O. C. Farokhzad, *Nano Today*, 2007, **2**, 14–21.
9 K. Cho, X. Wang, S. Nie, Z. Chen and D. M. Shin, *Clin. Cancer Res.*, 2008, **14**, 1310–1316.
10 S. Kalepu and V. Nekkanti, *Acta Pharm. Sin. B*, 2015, **5**, 442–453.
11 H. Maeda, J. Wu, T. Sawa, Y. Matsumura and K. Hori, *J. Controlled Release*, 2000, **65**, 271–284.
12 Y. Matsumura, *Adv. Drug Delivery Rev.*, 2008, **60**, 899–914.
13 O. C. Farokhzad and R. Langer, *ACS Nano*, 2009, **3**, 16–20.
14 D. Sutton, N. Nasongkla, E. Blanco and J. Gao, *Pharm. Res.*, 2007, **24**, 1029–1046.
15 K. M. Huh, S. C. Lee, Y. W. Cho, J. Lee, J. H. Jeong and K. Park, *J. Controlled Release*, 2005, **101**, 59–68.
16 A. Karanikolas, P. Tsolakis, G. Bokias and C. Tsitsilianis, *Eur. Phys. J. E*, 2008, **27**, 335–343.
17 U. Borchert, U. Lipprandt, M. Bilang, A. Kimpfler, A. Rank, R. Peschka-Süss, R. Schubert, P. Lindner and S. Förster, *Langmuir*, 2006, **22**, 5843–5847.
18 Y. Qu, J. Li, J. Ren, J. Leng, C. Lin and D. Shi, *Nanoscale*, 2014, **6**, 12408–12413.
19 H. Wei, S.-X. Cheng, X.-Z. Zhang and R.-X. Zhuo, *Prog. Polym. Sci.*, 2009, **34**, 893–910.
20 L. Zha, B. Banik and F. Alexis, *Soft Matter*, 2011, **7**, 5908–5916.
21 E. Roux, M. Francis, F. M. Winnik and J.-C. Leroux, *Int. J. Pharm.*, 2002, **242**, 25–36.
22 C. Schwarzenböck, A. Schaffer, P. Pahl, P. J. Nelson, R. Huss and B. Rieger, *Polym. Chem.*, 2018, **9**, 284–290.
23 N. Zhang, S. Salzinger and B. Rieger, *Macromolecules*, 2012, **45**, 9751–9758.
24 U. B. Seemann, J. E. Dengler and B. Rieger, *Angew. Chem.*, 2010, **122**, 3567–3569.
25 B. S. Soller, S. Salzinger, C. Jandl, A. Pöthig and B. Rieger, *Organometallics*, 2015, **34**, 2703–2706.
26 S. Salzinger, U. B. Seemann, A. Plikhta and B. Rieger, *Macromolecules*, 2011, **44**, 5920–5927.
27 S. Salzinger, B. S. Soller, A. Plikhta, U. B. Seemann, E. Herdtweck and B. Rieger, *J. Am. Chem. Soc.*, 2013, **135**, 13030–13040.
28 P. T. Altenbuchner, P. D. L. Werz, P. Schöppner, F. Adams, A. Kronast, C. Schwarzenböck, A. Pöthig, C. Jandl, M. Haslbeck and B. Rieger, *Chem.–Eur. J.*, 2016, **22**, 14576–14584.
29 A. Lavasanifar, J. Samuel and G. S. Kwon, *Adv. Drug Delivery Rev.*, 2002, **54**, 169–190.
30 C. F. van Nostrum, *Soft Matter*, 2011, **7**, 3246–3259.
31 C. Schwarzenböck, P. J. Nelson, R. Huss and B. Rieger, *Nanoscale*, 2018, **10**, 16062–16068.
32 F. Adams, P. T. Altenbuchner, P. D. L. Werz and B. Rieger, *RSC Adv.*, 2016, **6**, 78750–78754.
33 F. Adams, P. Pahl and B. Rieger, *Chem.–Eur. J.*, 2018, **24**, 509–518.
34 H. Kaneko, H. Nagae, H. Tsurugi and K. Mashima, *J. Am. Chem. Soc.*, 2011, **133**, 19626–19629.
35 F. Adams, M. R. Machat, P. T. Altenbuchner, J. Ehrmaier, A. Pöthig, T. N. V. Karsili and B. Rieger, *Inorg. Chem.*, 2017, **56**, 9754–9764.
36 Y. Matsumura and K. Kataoka, *Cancer Sci.*, 2009, **100**, 572–579.
37 J. Wang, W. Mao, L. L. Lock, J. Tang, M. Sui, W. Sun, H. Cui, D. Xu and Y. Shen, *ACS Nano*, 2015, **9**, 7195–7206.
38 R. Elul, *J. Physiol.*, 1967, **189**, 351–365.

39 A. Musyanovych, J. Dausend, M. Dass, P. Walther, V. Mailänder and K. Landfester, *Acta Biomater.*, 2011, **7**, 4160–4168.
40 E. Fröhlich, *Int. J. Nanomed.*, 2012, **7**, 5577–5591.
41 S.-D. Li and L. Huang, *Mol. Pharm.*, 2008, **5**, 496–504.
42 Y.-B. Hu, E. B. Dammer, R.-J. Ren and G. Wang, *Transl. Neurodegener.*, 2015, **4**, 18.
43 C. Chen, J. Ke, X. E. Zhou, W. Yi, J. S. Brunzelle, J. Li, E.-L. Yong, H. E. Xu and K. Melcher, *Nature*, 2013, **500**, 486–489.
44 C. M. Alexander, K. L. Hamner, M. M. Maye and J. C. Dabrowiak, *Bioconjugate Chem.*, 2014, **25**, 1261–1271.
45 B. Stella, S. Arpicco, M. T. Peracchia, D. Desmaële, J. Hoebeke, M. Renoir, J. D'Angelo, L. Cattel and P. Couvreur, *J. Pharm. Sci.*, 2000, **89**, 1452–1464.
46 X. Qiang, T. Wu, J. Fan, J. Wang, F. Song, S. Sun, J. Jiang and X. Peng, *J. Mater. Chem.*, 2012, **22**, 16078–16083.
47 S. Dong, H. J. Cho, Y. W. Lee and M. Roman, *Biomacromolecules*, 2014, **15**, 1560–1567.

7.4 Reprint Permission Copyrighted Content

Synthesis, characterisation and functionalisation of BAB-type dual-responsive nanocarriers for targeted drug delivery: evolution of nanoparticles based on 2-vinylpyridine and diethyl vinylphosphonate

A. Saurwein, A. Schaffer, C. Wieser and B. Rieger, *RSC Adv.*, 2021, **11**, 1586
DOI: 10.1039/D0RA08902H

8 Excursus: Synthesis of Poly(vinylphosphonate)-based Hydrogels

8.1 Polymerization

With their ability to swell in aqueous media, hydrogels are highly interesting materials for biomedical applications[116] and are used for drug delivery,[117] tissue engineering,[118, 119] wound dressing,[120] or the separation of biomolecules and cells.[121] Due to their high biocompatibility poly(vinylphosphonate)s appeared to be interesting candidates for such a material.[74, 77, 78] With the intention to synthesize PDEVP-based hydrogels, several copolymers with varying feed concentrations (100-600 equiv.) (**P1-P3**) and DAlVP contents (5-20%) (**P3-P5**) were synthesized to study the effects of the cross-linking density and the polymer length on the swelling behavior and stability of the swollen gel (Scheme 8.1). 2,6-Dimethyl-4-(4-vinylphenyl)pyridine (**4**) was used as initiator to allow the calculation of the molecular weight and determination of the polymer composition by referring to the initiator-bound vinyl group.

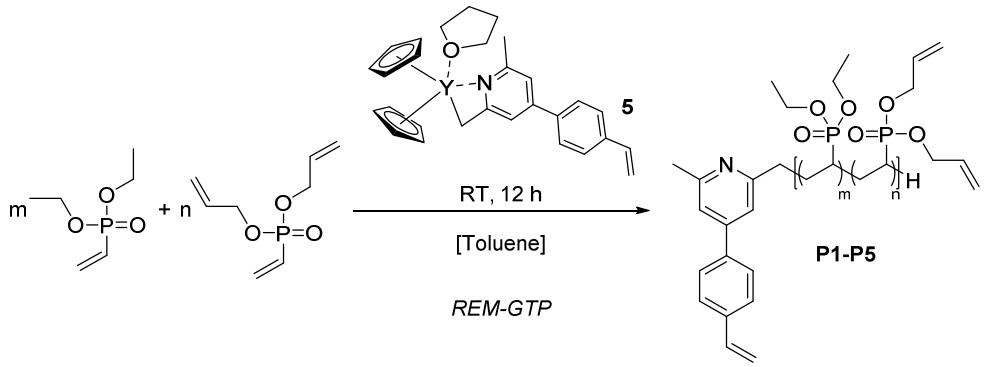

Scheme 8.1. Statistical copolymerization of DEVP and DAlVP with complex **5** generated after C-H bond activation with 2,6-dimethyl-4-(4-vinylphenyl)pyridine (**4**).

As depicted in Table 8.1, a constant feed ratio of 9/1 was adjusted for copolymers **P1-P3** (**P1**: 100 equiv., **P2**: 300 equiv., **P3**: 600 equiv.). The copolymers exhibited a DAlVP content of 9.85 to 12.5% which matched the target value of 10% quite well. The initiator efficiencies were calculated to be between 74 and 89% (Table 8.1, entries 1-3). **P4** also showed a good initiator efficiency of 72% and a DAlVP content of 25.6% which slightly exceeded the desired value of 20% (Table 8.1, entry 4). **P5** featured an *IE* of 63%. The determined DALVP proportion coincides with adjusted value of 5% (Table 8.1, entry 5). Moreover, the molecular weights of copolymers **P3-P5** have similar molecular masses (136-158 kg mol^{-1}; Table 8.1, entries 3-5), which ensures the comparability of the materials after cross-linking.

Table 8.1. Monomer feed, conversion, calculated ratio of the monomers in the polymer and the DAlVP fraction, molecular weights $M_{n,NMR}$, initiator efficiencies, and LCST of **P1-P5**

	$M_{DEVP,0}/M_{DALVP,0}/cat_0$[a] /-	Conversion[b] /%	Composition[c] /equiv.	DAlVP content[c] /%	$M_{n,NMR}$[c] /g mol^{-1}	*IE*[d] /%	T_{LCST} /°C
P1	90/10	>99	99/13	11.6	18 900	89	32.0
P2	270/30	>99	366/40	9.85	67 800	74	35.5
P3	540/60	>99	712/102	12.5	136 000	74	33.5
P4	480/120	>99	613/211	25.6	141 000	72	21.5
P5	570/30	>99	904/52	5.42	158 000	63	38.5

[a]Equivalents monomer per catalyst. [b]Polymerizations were monitored via ^{1}H- and ^{31}P-NMR and stopped after quantitative conversion was detected after the respective reaction time. [c]The monomer ratio in the polymer was calculated via ^{1}H-NMR by comparison of the vinyl signal of the initiator at 6.80 pmm (I = 1H) and the CH_2 signals of DEVP (4.18 ppm, m = I/4) and DAlVP (4.63 ppm, n = I/4). $IE = M_{n,theo}/M_{n,exp}$. $M_{n,exp} = 209.29$ g mol^{-1} + m · 164.14 g mol^{-1} + n · 188.16 g mol^{-1}.

8.2 Formation of the Hydrogels

The cross-linking of polymer **P3** was studied on the basis of three different reaction types. First, the hydrosilylation with *Karstedt's* catalyst and 1,1,3,3-tetramethyldisiloxane (**Si_2-H_2**) as cross-linking agent was investigated (Scheme 8.2).

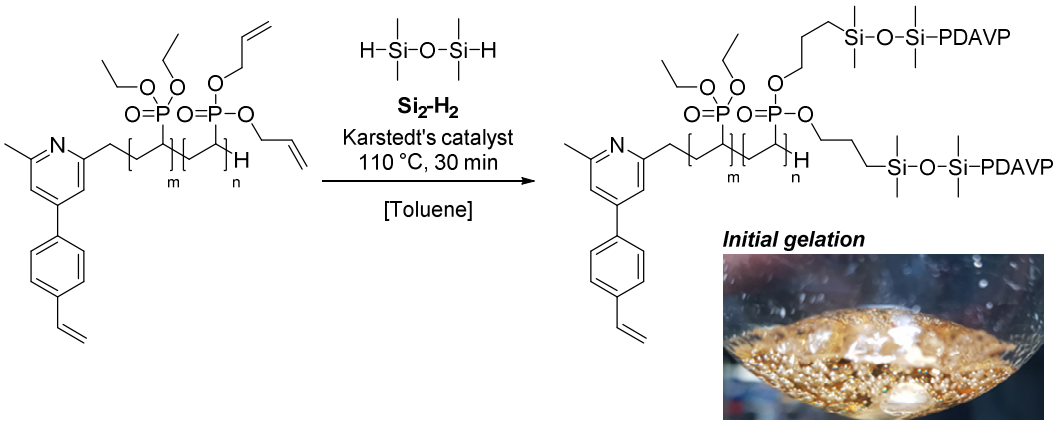

Scheme 8.2. Cross-linking of polymer **P3** via hydrosilylation and illustration of the gelled reaction solution (bottom right).

Hereby, polymer **P3** was dissolved in toluene and treated with both components. Immediately, the solution turned into a yellowish gel upon heating, indicating the successful formation of a polymer network. The resulting hydrogel featured a swelling factor of 158 in water (Table 8.2, entry 1). Unfortunately, it was not possible to differentiate between **HG3** and polymer **P3** by infrared (IR) spectroscopy as there was no characteristic band assignable to the hydrogel. Consequently, both spectra were congruent to each other (Figure 8.1).

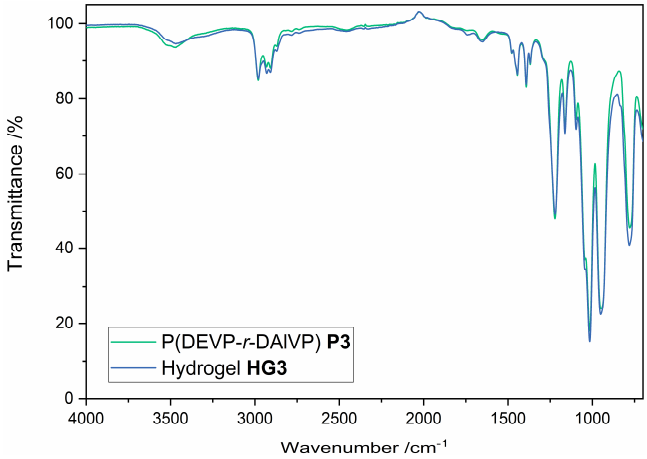

Figure 8.1. IR spectra of polymer **P3** prior to cross-linking and hydrogel **HG3** after purification.

A similar principle was adopted for the cross-linking with 3,6-dioxa-1,8-octanedithiol (**6**) via radical thiol-ene click chemistry (Scheme 8.3). Here too, the reaction solution gelled after reaching the degradation temperature of AIBN. However, the swelling behavior of **HG2** was inferior to **HG1** formed via hydrosilylation with a swelling ratio of only 7.03 (Table 8.2, entry 2).

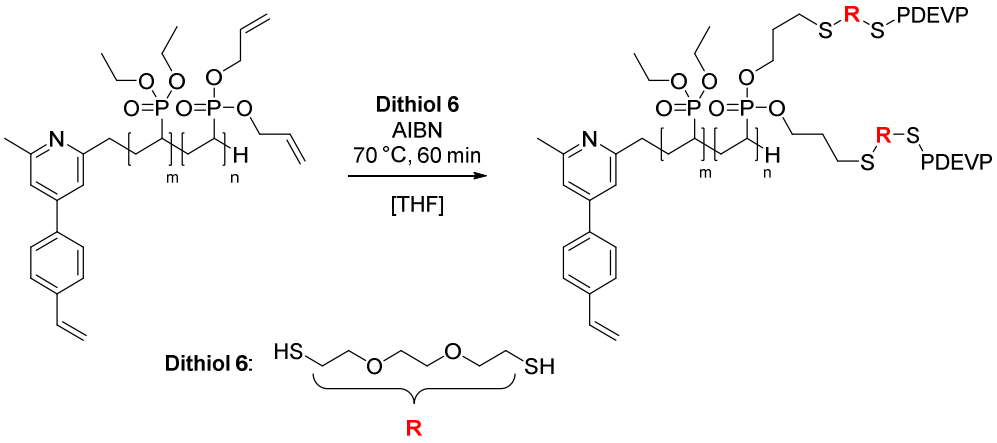

Scheme 8.3. Cross-linking of polymer **P3** via thiol-ene click chemistry.

Eventually, cross metathesis over the allyl groups was tested with a *Grubbs* I catalyst (Scheme 8.4) in dichloromethane. Likewise, a thickening of the solution was observed shortly after addition of the catalyst solution.

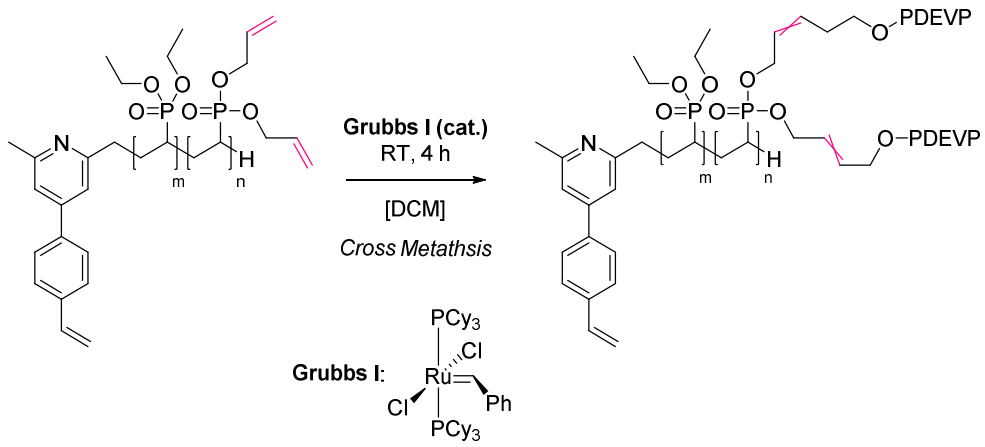

Scheme 8.4. Cross-linking of polymer **P3** via cross metathesis.

The reaction was monitored via ^{1}H-NMR spectroscopy in methanol-d_4. As shown in Figure 8.2 a new signal at 5.85 ppm representing the *cis*- and *trans*-linkage appeared in the course of the reaction, but traces of the allyl groups were also visible after the first reaction control. Hence, the solution was treated with additional catalyst but after purification some allyl signals were still visible. Though **HG3** was soluble in methanol-d_4, a satisfactory swelling factor of 19.9 was calculated. However, **HG3** lacked mechanical stability and was ruptured easily by the application of low force during the removal of excess water (Table 8.2, entry 3). It can be assumed that the intramolecular metathesis might be favored over the intermolecular reaction due to the steric hinderance of the catalyst and repulsion between the polymer chains and, thus, prevented an approximation of the "distant" allyl groups.

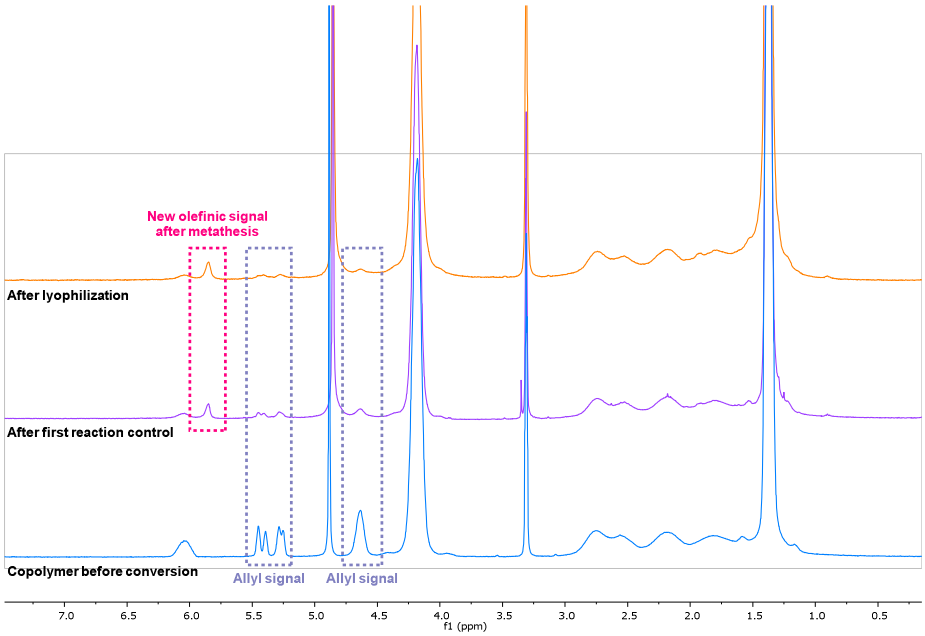

Figure 8.2. ^{1}H-NMR spectra in MeOD of polymer **P3** before and after cross metathesis.

Table 8.2. Overview on the hydrogels and the corresponding swelling ratio in varying solvents

	Polymer	Reaction type	Linker	Swelling ratio[a] H_2O /-	Swelling ratio[a] PBS /-	Swelling ratio[a] MeCN /-	Swelling ratio[a] Tol /-
HG1	**P3**	Hydrosilylation	**Si_2-H_2**	158	11.4	4.36	4.62
HG2	**P3**	Thiol-ene	**6**	7.03	n.d.	n.d.	n.d.
HG3	**P3**	Cross metathesis	-	19.9[b]	n.d.	n.d.	n.d.
HG4	**P1**	Hydrosilylation	**Si_2-H_2**	n.a.[b]	n.d.	n.d.	n.d.
HG5	**P2**	Hydrosilylation	**Si_2-H_2**	n.a.[b]	n.d.	n.d.	n.d.
HG6	**P4**	Hydrosilylation	**Si_2-H_2**	30.0	6.21	3.23	3.02
HG7	**P5**	Hydrosilylation	**Si_2-H_2**	5.00[c]	n.d.	n.d.	n.d.
HG8	**P3**	Hydrosilylation	**Si_3-H_2**	63.4	10.7	6.66	3.18
HG9	**P3**	Hydrosilylation	**Si_4-H_3**	50.2	13.5	9.80	4.77

[a]Determination of the swelling ratio by weight comparison of the swollen gel W_S and dry gel W_D. Swelling ratio (-) = $(W_S - W_D)/W_D$. [b]Very fragile. Dissolved in water or easily ruptured. [c]Fragile. Determination of the swelling ratio not accurate.

8.3 Characterization of the Swelling Behavior and Stability

Based on fundamental swelling experiments in water, the hydrogels generated from copolymers **P1**, **P2**, and **P5** (Table 8.2, entries 4, 5 and 7) showed no swelling behavior and degraded into small particles upon weighing or dissolution in water. A possible explanation for this observation might be led back to the polymer composition. While the short polymer chains of **P1** and **P2** might prevent a densely cross-linked network, **P5** lacks a sufficient amount of allyl groups and resulted an equally loose network.

Most promising candidates for the cross-linking were polymers **P3** and **P4** which exhibited swelling factors of 158 for **HG1** and 30 for **HG6**, respectively, which was explained by the higher cross-linking density. Additionally, these hydrogels were kept in PBS buffer, acetonitrile as a polar organic solvent, and toluene as an organic solvent. The swelling factors were drastically reduced in these solvents. However, this was expected especially for the PBS buffer containing several types of salt. Studies on the stability of the swollen gels exhibited only a slow release of water due to evaporation of the water into the surrounding volume (Figure 8.3).

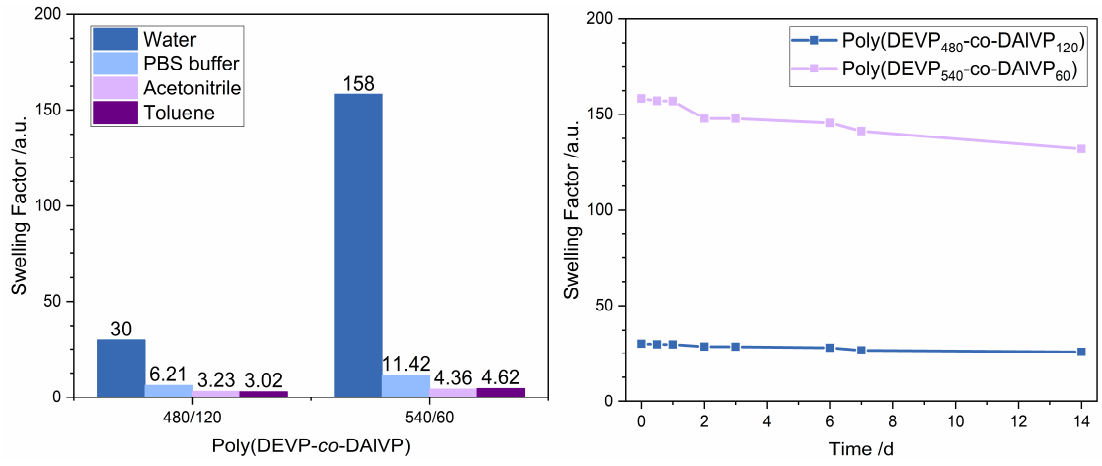

Figure 8.3. Swelling behavior in various solvents of the hydrogels based on **P3** and **P4** cross-linked with **Si_2-H_2** and monitored water swelling ratios over a period of 14 days.

Moreover, **P3** was cross-linked with two alternative silanes, namely 1,1,3,3,5,5-hexamethyltrisiloxane (**Si$_3$-H$_2$**) and 3-((dimethylsilyl)oxy)-1,1,3,5,5-pentamethyltrisiloxane (**Si$_4$-H$_3$**) (Figure 8.4; Table 8.2, entries 8-9). In comparison to **HG1** and **HG6**, lower swelling factors were determined for **HG8** and **HG9** in water. This behavior relates to a higher hydrophobicity introduced by the elongated siloxanes. Likewise, decreased swelling factors were observed in PBS buffer, MeCN, and toluene. **HG9** demonstrated the highest solvent capacity in PBS buffer and acetonitrile with a value of 13.5. Stability measurements showed only subordinate loss of water in a time frame of 14 days (Figure 8.4, right).

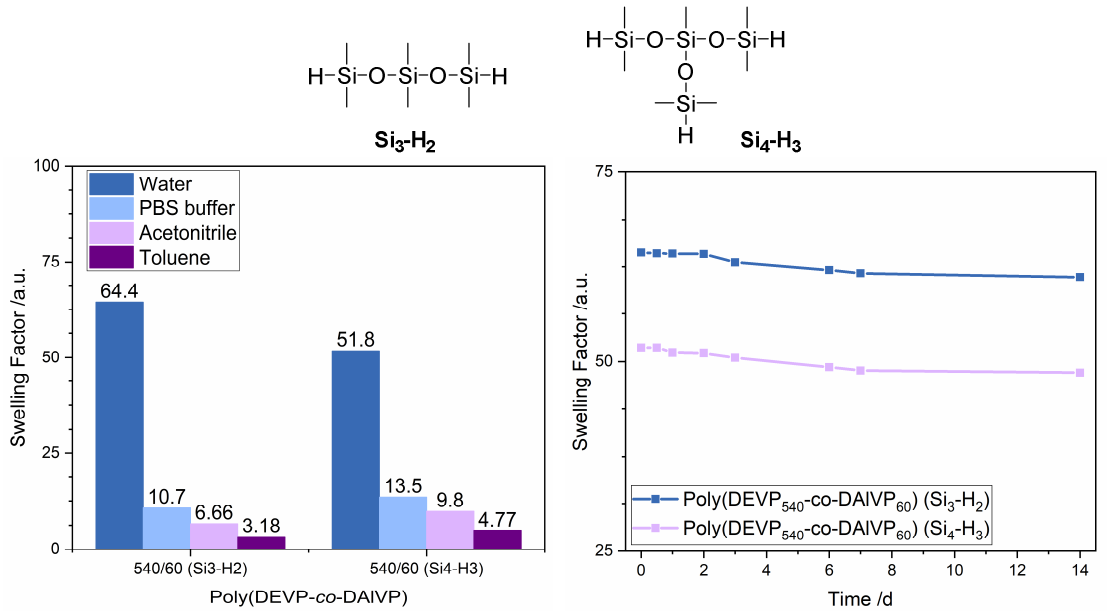

Figure 8.4. Swelling behavior in various solvents of the hydrogels based on **P3** cross-linked with **Si$_3$-H$_2$** (**HG8**) and **Si$_4$-H$_3$** (**HG9**) and monitored water swelling ratios over a period of 14 days.

As PDEVP shows thermoresponsive behavior we were interested if these hydrogels also behave sensitive to temperature changes. Therefore, the hydrogel samples were heated in regular temperature steps and equilibrated at this temperature for five minutes. Afterwards, the hydrogels were weighed after the removal of superficial water. In comparison to the sharp phase transition of **P3** and **P4**, the water release from the hydrogels appeared to happen in a linear fashion.

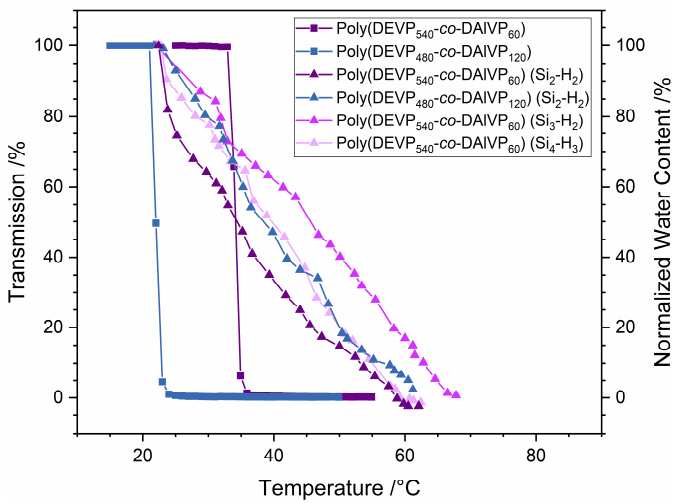

Figure 8.5. Determination of the cloud point of **P3** and **P4** and temperature-dependent release of water from the hydrogels.

9 Summary and Outlook

Emerging from the initial work of *Webster* and co-workers in 1983[44] and the advancements that were achieved by the groups of *Yasuda*[45] and *Collins* and *Ward*[46] in 1992, *Rieger et al.* were able to produce high molecular-weight PDEVP for the first time in 2010 via REM-GTP, using Yb metallocenes.[50] Since this year tremendous efforts were put into understanding the polymerization mechanism,[51, 52, 54] exploring a variety of monomers and catalytically active substrates for REM-GTP,[17, 51, 52, 54, 56, 122-125] and gaining insights on the polymer properties.[51, 53] Application-oriented studies led to halogen-free polymeric flame-retardants,[113] sophisticated drug delivery vehicles[64, 77, 79] or fluorescent, macromolecular conjugates for cell targeting[74, 78] and highlighted the potential for medicinal applications (e.g. tissue engineering or cell culture techniques) that demand for highly specialized materials.

To consider this factor, one objective of this thesis was dedicated to increasing the versatility of the functionalization strategy. Inspired by the structure of 2,6-dimethyl-4-(4-vinylphenyl)pyridine which was successfully employed in the REM-GTP of DEVP,[74] three complex initiators were designed which contained a 2,6-dimethylpyridyl motif for σ-bond metathesis and the functional groups (-OH, -NH_2, -SH) protected by an appropriate protection group. All initiators were successfully employed in the C-H bond activation. However, the complexes could not be crystallized due to the steric demand and flexible orientation of the protective groups, and thus required the activation to be *in situ*.

As shown by end-group analysis, all initiators were integrated in the polymers. The complexes generated with these initiators featured a fast conversion of DEVP (60-240 s) and exhibited a linear growth of the molecular weights and narrow polydisperities ($Đ < 1.30$). This basis enabled the generation of defined PDEVP with good initiator efficiencies (IE = 33-42%, 25 equiv. DEVP; IE = 61-82%, 100 equiv. DEVP) for the subsequent deprotection and functionalization studies. With exception of one pyrrole-bearing derivative, the protective groups were removed quantitatively under the chosen reaction conditions. Moreover, the integrity of PDEVP was verified by GPC analysis which revealed similar molecular weights and polydispersities compared to their protected pendants. Interestingly, the LCST of the short PDEVP derivates (25 equiv. DEVP) was heavily affected by the state of the end-group (protected vs. deprotected). Eventually, the released, functional groups of the short chain substrates were (re)functionalized with either cholesteryl chloroformate (-OH, -NH_2) or *N*-phenyl maleimide (-SH) (Scheme 9.1). Ultimately, the success of these reactions gives access to a plurality of new polymer conjugates which can take application-specific requirements into account. All data are presented in chapters 5 and 12.1.

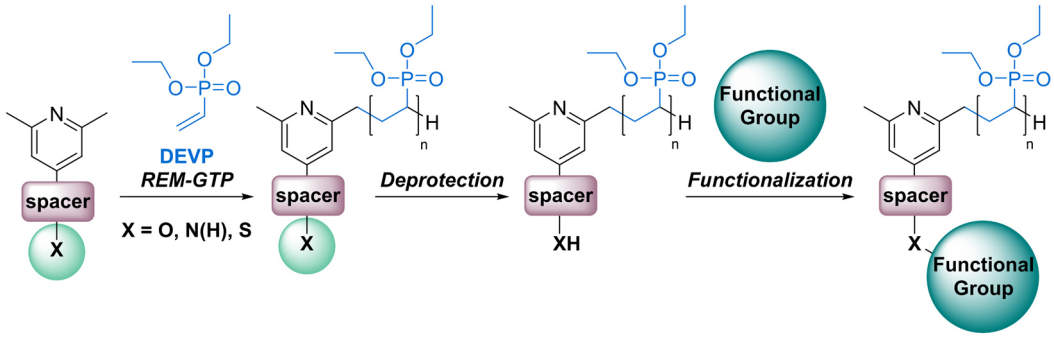

Scheme 9.1. Table of content of the publication presented in chapter 5 and 12.1: "Synthesis and Application of Functional Group-Bearing Pyridyl-Based Initiators in Rare Earth Metal-Mediated Group Transfer Polymerization".

With this new level of complexity, the question has risen if macromolecular initiators based on PDMS are applicable to REM-GTP as well. Similar approaches were already taken for ATRP,[103-107] ROP,[109, 110] as well as GTP[111] and gave access to new materials. Because PDMS is used in many medicinal fields[93-97] and PDEVP has proved its value in a variety of application-driven studies[64, 74, 77-79] it seemed logical to combine these two polymer types in one material class (Scheme 9.2).

To obtain basic insights into the polymerization procedure with such a siloxane system we investigated a binuclear model initiator comprising a disiloxane bridge. These preliminary studies revealed the C-H bond activation to be a quantitative and selective process. Time-dependent polymerization experiments confirmed a defined propagation ($Đ$ = 1.09-1.25; linear increase of M_n) while the end-group analysis by ESI-MS and NMR showed the covalent linkage of the initiator to the polymer chain. Subsequent REM-GTP of DEVP featured very good initiator efficiencies (IE = 71-85%) and low polydispersities ($Đ$ = 1.11). However, the GPC traces showed a bimodal character due to the binuclear structure of the initiator leading to the formation of AB- and ABA-type polymers in statistical fashion. On this basis three macroinitiators where synthesized from Si-H containing PDMS via hydrosilylation with 4-(allyloxy)-2,6-dimethylpyridine. In all cases, NMR and elemental analysis (EA) corroborated a successful conversion. C-H bond activation experiments were performed *in situ* and were found to proceed with high selectivity which was shown by ^{1}H-NMR through comparison of the macromolecular species with the small analogue, as well as by ^{13}C-NMR and DOSY. Likewise, REM-GTP yielded defined block and graft copolymers whose composition was analyzed by NMR, DOSY and EA. The *IE*s were found to be 40-88% for the block copolymers and 27-28% in case of the graft copolymers. However, only the graft copolymers were subjected to GPC analysis ($Đ \approx 1.40$) whereas the block copolymers formed micelles in THF/H_2O rendering GPC measurements impossible. This is why PDEVP-*b*-PDMS-*b*-PDEVP was treated with HBr to cleave the ether linkages and release the PDEVP block. Analysis by GPC-MALS corroborated a defined polymerization since the determined M_n matched the calculated mass of the respective PDEVP block. The polymerization studies were then complemented with the REM-GTP of 2VP and the ROP of εCL. Both polymerizations yielded defined block copolymers with good *IE*s and narrow molecular weight distributions (2VP: IE = 80%, $Đ$ =1.13; εCL: IE = 94%, $Đ$ =1.39). The formation of PεCL proceeded extremely fast and was terminated after only 60 minutes. All polymers were evaluated regarding their solution and thermal properties by DLS and DSC. Hereby, DLS revealed a strong dependence of the micelle formation from the copolymer architecture and the solvent. PDEVP block copolymers formed micellar structures in water (d = 45.0-88.0 nm) and THF/water (50/50) (d = 62.0-248 nm)

while the P2VP and PεCL copolymers were found to form micelles in aqueous HCl or DMF, respectively. In addition, the PDEVP-containing copolymers were also examined regarding their LCST behavior which was lowered in case of copolymers with a more dominant PDMS block. All data are presented in chapters 6 and 12.2.

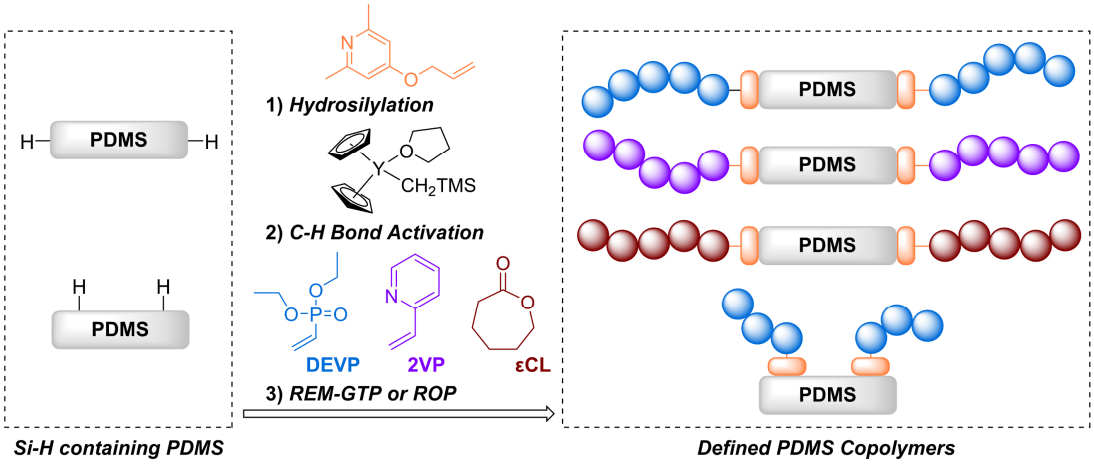

Scheme 9.2. Table of content of the publication presented in chapter 6 and 12.2: "Precise Synthesis of Poly(dimethylsiloxane) Copolymers through C-H Bond Activated Macroinitiators in the Yttrium-Mediated Group Transfer Polymerization and Ring-Opening Polymerization".

Not only the connection of two opposing polymer families provides access for novel material types, but also well-established approaches can be developed further into new directions. Hence, evolution of our cross-linked nanocarriers[77] resulted in the development of B'BABB' based carriers in style of the original work from 2016[64] as well as a simple, facile route towards folate-bearing nanoparticles (Scheme 9.3). To ensure comparability with the ABB' nanoparticles a new binuclear catalyst was investigated derived from the activation of TMPy with $Cp_2Y(CH_2TMS)(THF)$. Extensive evaluation of this complex by NMR confirmed the exclusive formation of a single, binuclear species. Subsequent analysis of 2VP oligomers by ESI-MS confirmed the incorporation of TMPy in the polymer chain, while kinetic experiments concluded a TOF of 192 h^{-1} for the polymerization of 2VP. This value was twice as high as the value calculated with *sym*-collidine (TOF = 90 h^{-1}) but both were slower than the related bisphenolate systems by a factor of three to ten.[64, 122] With the binuclear catalyst several defined copolymers with varying feed compositions (2VP: 100-300 equiv.; DEVP: 200-300 equiv.; DAlVP: 6-20 equiv.), high *IEs* (80-99%) and low polydispersities ($Đ \leq 1.10$) were prepared. In the following the polymers were cross-linked with three different dithiols via thiol-ene click chemistry. All nanoparticles were analyzed by DLS and TEM and revealed defined, almost spherical particles. Diameters ranged between 21.1 and 51.9 nm (PDI = 0.13-0.22) depending on the length of the 2VP block and the cross-linking density. Zeta potential measurements revealed a slight negative surface charge (-6.3 to -22 mV) which was seemingly affected by the polarity of the cross-linking agent. Consequently, release experiments with fluorescein evidenced a positive effect of elevated temperature and pH levels which accelerated the cargo release considerably. Overall, best results were achieved at pH = 4.5, especially in combination with a pronounced 2VP section. Temperature-wise, nanoparticles with a high DAlVP content (20 equiv.) exhibited a good differentiation of the release behavior between 37 °C and 42 °C. This study was complemented by introducing a synthetic route towards folate-bearing nanoparticle to fulfil a prerequisite for actively targeting drug carriers. Therefore, a part of the allyl groups was converted with cysteamine while the remaining allyl groups were saturated with 3,6-dioxa-1,8-octanedithiol. The superficial amine groups were then

reacted with an activated derivative of folic acid. Besides NMR spectroscopy, the reaction was able to be monitored by zeta potential measurements which showed a change from -18 mV (cysteamine conjugate) to -11 mV (with conjugated folic acid). Moreover, DOSY-NMR corroborated a covalent linkage between folic acid and the precursor particle. Analysis by DLS and TEM confirmed uniform particles.

In conclusion, the combination of this study with our previous work provides a facile synthetic fundament. It gives control over the particle size and its composition, can be used to tweak the release behavior, tune the surface charge, and gives access to ligand-modified particles for active drug targeting. All data are presented in chapters 7 and 12.3.

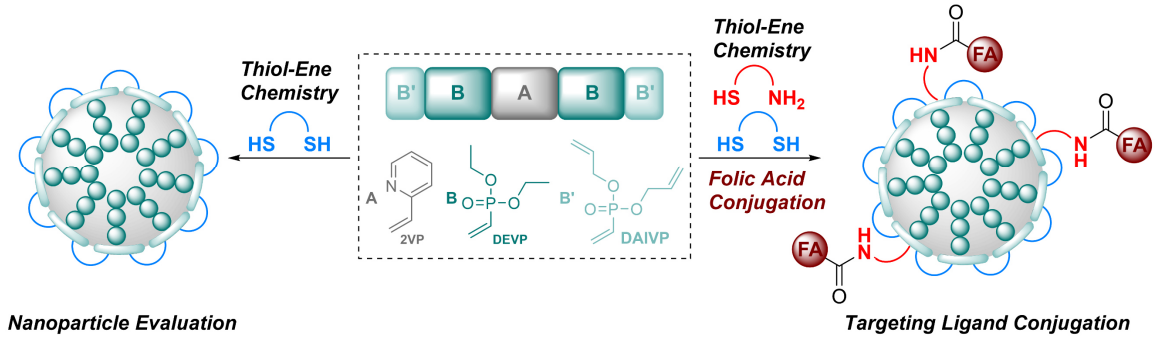

Scheme 9.3. Table of content of the publication presented in chapter 7 and 12.3: "Synthesis, Characterisation and Functionalisation of BAB-type Dual-Responsive Nanocarriers for Targeted Drug Delivery: Evolution of Nanoparticles based on 2-Vinylpyridine and Diethyl Vinylphosphonate".

These results underline how variable the generation process of poly(vinylphosphonate)s and other REM-GTP-derived polymers is. Functional motifs or reactive groups are introduced precisely during the initiation/polymerization via the (macro)initiator or the functional monomer and, thus, represents the prerequisite for a rich functionalization chemistry after polymerization (thiol-ene click chemistry, condensation reaction, *Michael*-addition, hydrosilylation). Altogether, this work implies the high potential of poly(vinylphosphonate)s for various biomedical applications. Besides the use as sophisticated macromolecular imaging probes or tailored drug delivery vehicles with specific targeting ligands, novel materials for bioseparation, tissue engineering, or as semipermeable membranes capable of islet encapsulation can be envisioned through the combination of respective post-polymerization functionalizations.

In the short run the horizon of this synthetic toolbox can be expanded to supramolecular materials, conjugation of complex biomolecules, or catalytically active hybrid-materials. Inspired by the helical structure of DNA nucleic acids and nucleotides are interesting coupling candidates for poly(vinylphosphonate)s as such modified polymers might self-assemble due to the formation of respective nucleobase interactions. These supramolecular structures might find application in molecular recognition,[126] aptamer-assisted delivery,[127, 128] or used as macromolecular binders.[129] In this context, the conjugation of more complex biomolecules appears logical. Currently, our group works on the incorporation of the RGD sequence (R: arginine, G: glycine, D: aspartic acid). Due to the binding properties of the RGD motif to extracellular receptors polymer-based materials for cell adhesion are conceivable.[130] Furthermore, an encapsulation of catalytically active substrates in micelles or nanoparticles is possible in which the catalyst is protected from environmental influences and the activity is controlled by a thermoresponsive block.

In the long run an in-depth evaluation of the nanocarriers should be of interest. Hereby, their biocompatibility and circulation times *in vivo*, or the renal clearance represent important pharmacokinetic parameters that have to be investigated. If those characteristics are found to be positive, the nanocarriers can be further optimized with regard to their potential application fields: *Hyperthermia* treatments can require a precisely adjusted LCSTs owing to the locally elevated temperatures of the malignant tissue. Formulations applied through local injections might demand an adjustment of the cross-linking stability since less stable particles are favored for this purpose. Besides, novel targeting ligands can be considered which are selective for certain disease-specific receptors.[131]

Clearly, this synthetic basis adds new levels of complexity to poly(vinylphosphonate)s and transforms this smart polymer class into multi-functional, application-tailored materials. Consequently, an employment of poly(vinylphosphonate)s in related biomedical fields is a given in the near future.

10 Zusammenfassung und Ausblick

Ausgehend von der Arbeit von *Webster* und Mitarbeitern im Jahr 1983[44] und den darauf aufbauenden Weiterentwicklungen, die durch die Gruppen von *Yasuda*[45] und von *Collins* und *Ward*[46] 1992 erzielt wurden, konnten *Rieger et al.* im Jahr 2010 zum ersten Mal hochmolekulares Poly(diethylvinylphosphonat) (PDEVP) mittels der seltenerdmetall-mediierten Gruppentransferpolymerisation (englisch: rare earth metal-mediated group transfer polymerization, REM-GTP) unter Zuhilfenahme von Yb-Metallocenen erzeugen.[50] Seitdem wurden enorme Anstrengungen unternommen, um ein besseres Verständnis über den Polymerisationsmechanismus zu erhalten[51, 52, 54], eine Vielzahl an Monomeren und katalytisch aktiven System für die REM-GTP untersucht[17, 51, 52, 54, 56, 122-125] und Erkenntnisse über Polymereigenschaften gewonnen.[51, 53] Anwendungsorientierte Studien führten zu halogenfreien, makromolekularen Flammschutzmittel,[113] komplexen Transportvehikeln für den Einsatz in der Wirkstoffverabreichung[64, 77, 79] oder fluoreszente, makromolekulare Konjugate zur Adressierung von Zellen.[74, 78] Entsprechend lässt sich das große Potential für medizinische Anwendungen (z.B. *Tissue Engineering* oder Zellkulturtechniken) erkennen, wofür hochspezialisierte Materialen notwendig sind.

Um diesen Umstand miteinzubeziehen, war ein Ziel dieser Arbeit, die Variabilität der Funktionalisierungsstrategie zu erhöhen. Inspiriert von der Struktur des Initiators 2,6-Dimethyl-4-(4-vinylphenyl)pyridin, welcher erfolgreich in der REM-GTP eingesetzt wurde,[74] wurden drei neue, komplexe Initiatoren entwickelt, die sowohl über eine 2,6-Dimethylpyridyl-Funktion für die σ-Bindungsmetathese als auch die mit passenden Schutzgruppen maskierten funktionellen Gruppen (-OH, -NH_2, -SH) verfügen. All diese Initiatoren konnten erfolgreich in der C-H-Bindungsaktivierung eingesetzt werden. Die dabei resultierenden Komplexe konnten jedoch aufgrund des hohen sterischen Anspruchs und der flexiblen Orientierung der Schutzgruppe im freien Raum nicht kristallisiert werden, weshalb die Aktivierung *in-situ* durchgeführt werden musste.

Alle Initiatoren wurden in die Polymerkette integriert, was mittels Endgruppenanalytik bewiesen worden ist. Die mit diesen Initiatoren erzeugten Komplexe zeichneten sich durch eine schnelle Umsetzung von DEVP (60-240 s) aus und sind durch ein lineares Wachstum des Molekulargewichts und geringe Polydispersitäten ($Đ < 1.30$) charakterisiert. Auf Basis dieses Fundaments wurde definiertes PDEVP mit guten Initiatoreffektivitäten erhalten (IE = 33-42%, 25 Äquiv. DEVP; IE = 61-82%, 100 Äquiv. DEVP), das in den darauffolgenden Entschützungstudien zum Einsatz kam. Mit Ausnahme eines pyrrol-modifizierten Substrates konnten die Schutzgruppen unter den gewählten Bedingungen in allen Fällen quantitativ abgespalten werden. Außerdem wurde mittels GPC-Analyse die Integrität der entschützten PDEVP-Substrate verifiziert, da diese im Vergleich zu ihren geschützten Gegenstücken ähnliche Molekulargewichte und Polydispersitäten vorweisen. Interessanterweise wurde die LCST der kurzkettigen PDEVP-Substrate (25 Äquiv. DEVP) in großem Maße durch die Art der Endgruppe (geschützt gegenüber entschützt) beeinflusst. Schließlich wurden die kurzkettigen Substrate über die freigesetzte, funktionelle Gruppe entweder mit Cholesterolchloroformat (-OH, -NH_2) oder *N*-Phenylmaleimid (-SH) (re-)funktionalisiert (Schema 10.1). Mit dem Erfolg dieser Funktionalisierungsreaktionen steht schlussendlich die Tür zu einer Vielzahl an neuartigen Polymer-Konjugaten offen, mit welchen anwendungsspezifische Anforderungen besser berücksichtigt werden können. Alle Daten wurden in den Kapiteln 5 und 12.1 präsentiert.

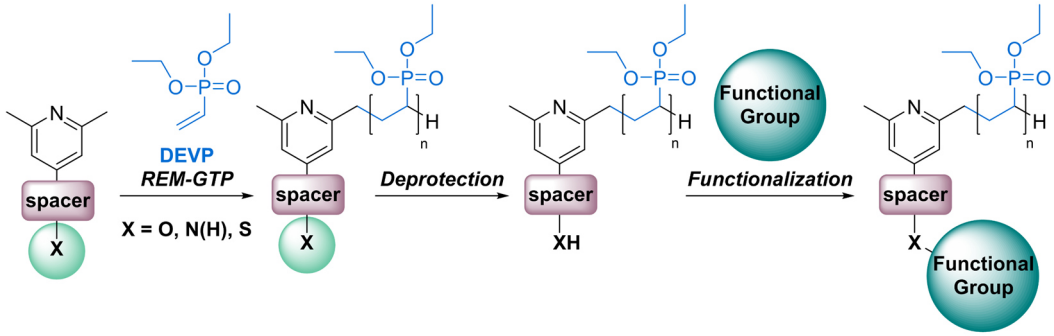

Schema 10.1. Graphische Zusammenfassung der Publikation mit dem Titel: "Synthesis and Application of Functional Group-Bearing Pyridyl-Based Initiators in Rare Earth Metal-Mediated Group Transfer Polymerization". Diese wird in den Kapiteln 5 und 12.1 präsentiert.

Dieses neue Komplexitätslevel warf die Frage auf, ob makromolekulare, PDMS-basierte Initiatoren ebenfalls für den Einsatz in der REM-GTP geeignet sind. Ähnliche Verfahren wurden schon über ATRP,[103-107] ROP,[109, 110] oder auch mittels GTP[111] durchgeführt und verschafften den Zugang zu neuen Materialien. Daher erschien es konsequent diese beiden Polymerarten in einem Material zu vereinen (Schema 10.2), da zum Einen PDMS in vielen medizinischen Bereichen verwendet wird[93-97] und zum Anderen PDEVP seinen Wert in einer Vielzahl an anwendungsorientieren Studien unter Beweis gestellt hat.[64, 74, 77-79]

Daher wurde ein binuklearer Initiator entwickelt, welcher über einer Disiloxan-Brücke verbunden ist, um grundlegende Einblicke in den Polymerisationsprozess mit siloxan-basierten Systemen zu erlangen. In hierzu gehörigen Vorstudien konnte eine quantitative wie auch selektive C-H-Bindungsaktivierung bestätigt werden. Zeitabhängige Polymerisationsexperimente demonstrierten außerdem einen definierten Propagationsprozess ($Đ$ = 1.09 -1.25; lineares Wachstum von M_n), während über die Endgruppenanalytik mittels ESI-MS und NMR die kovalente Verknüpfung zwischen Initiator und Polymerkette bestätigten. Hierauf folgend wurde die REM-GTP von DEVP durchgeführt, welche in Polymere mit guten Initiatoreffektivitäten (*IE* = 71-85%) und niedrigen Polydisperistäten ($Đ$ = 1.11) resultierte. Die zugehörigen GPC-Messungen zeigten jedoch eine bimodale Verteilung, was sich auf die binukleare Struktur des Initiators zurückführen lässt, was zur Bildung von AB- und ABA-artigen Polymeren führte. Basierend auf diesen Vorarbeiten wurden aus 4-(Allyloxy)-2,6-dimethylpyridin und drei entsprechenden Si-H-haltigen PDMS die Makroinitiatoren mittels Hydrosilylierung hergestellt. Für alle Makroinitiatoren konnte nach NMR-Analyse und Elementaranalyse eine erfolgreiche Umsetzung nachgewiesen werden. Die Experimente zur C-H-Bindungsaktivierung wurden *in-situ* durchgeführt und verliefen mit hoher Selektivität, was über einen ^{1}H-NMR-Vergleich der makromolekularen Spezies und dem Modelinitiator, sowie ^{13}C- und DOSY-NMR nachgewiesen wurde. Die REM-GTP mit den Makroinitiatoren führte ebenfalls zu definierten Block- und Pfropf-Copolymeren deren Zusammensetzung über NMR, DOSY und EA analysiert wurde. Die *IE*s lagen bei 40-88% für die Block-Copolymere und bei 27-28% im Fall der Pfropf-Copolymere. Eine Analyse mittels GPC war jedoch nur bei den Pfropf-Copolymeren möglich ($Đ \approx 1.40$), während die Block-Copolymere in THF/H_2O zur Bildung von Mizellen neigten. Über die Behandlung von PDEVP-*b*-PDMS-*b*-PDEVP mit HBr konnte außerdem die Etherverbrückung gespalten und damit der PDEVP-Block freigesetzt werden. Über die nachfolgende Analyse durch GPC-MALS konnte ein präziser Polymerisationsvorgang bewiesen werden, da das gemessene Molekulargewicht M_n genau mit der berechneten Masse des PDEVP-Blocks im Copolymer übereinstimmten. Die Polymerisationsstudien wurden noch durch REM-GTP von 2VP und der ROP von εCL komplementiert. Auch hier führten die Polymerisationen zu definierten Block-Copolymeren mit guten *IE*s und

engen Molekulargewichtsverteilungen (2VP: *IE* = 80%, *Đ* =1.13; εCL: *IE* = 94%, *Đ* =1.39). Die Bildung von PεCL verlief dabei sehr schnell und konnte schon nach 60 Minuten Reaktionszeit beendet werden. Alle Polymere wurden außerdem in Hinblick auf ihr Löslichkeitsverhalten und die thermischen Eigenschaften mittels DLS beziehungsweise DSC untersucht. Anhand der DLS-Messungen wurde ein großer Einfluss der Copolymer-Architektur und des Lösungsmittels auf die Mizellbildung verdeutlicht. PDEVP-Block-Copolymere bildeten mizellare Strukturen in Wasser (d = 45.0-88.0 nm) und THF/H_2O (50/50) (d = 62.0-248 nm) während die P2VP- und PεCL-Copolymere in wässriger Salzsäure beziehungsweise DMF als Mizellen vorlagen. Darüber hinaus wurde das LCST-Verhalten der PDEVP-haltigen Copolymere untersucht, wobei bei einem höheren Anteil des PDMS-Blocks eine Absenkung der LCST beobachtet werden konnte. Alle Daten sind in den Kapiteln 6 und 12.2 präsentiert.

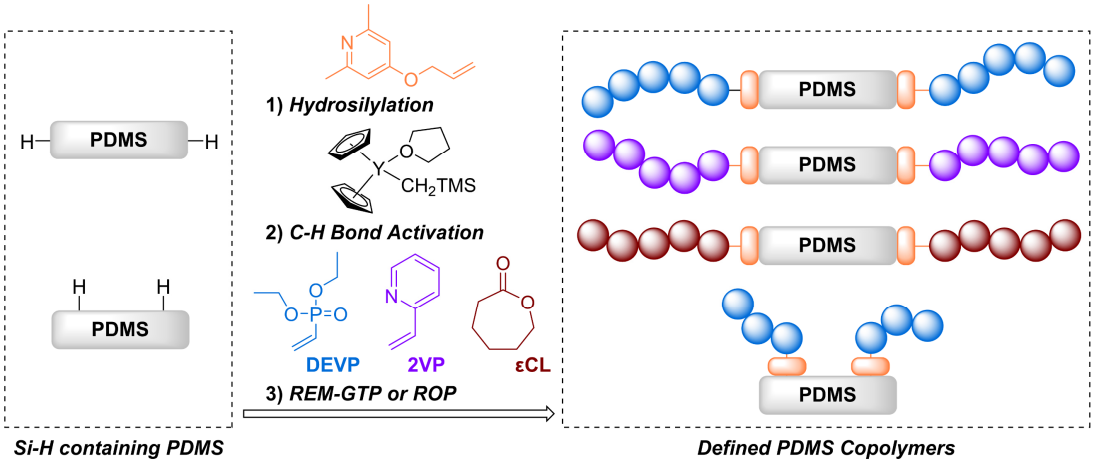

Schema 10.2. Graphische Zusammenfassung der Publikation mit dem Titel: "Precise Synthesis of Poly(dimethylsiloxane) Copolymers through C-H Bond Activated Macroinitiators in the Yttrium-Mediated Group Transfer Polymerization and Ring-Opening Polymerization". Diese wird in den Kapiteln 6 und 12.2 präsentiert.

Nicht nur die Vereinigung dieser gegensätzlichen Polymerklassen gewährt den Zugang zu neuen Materialien, sondern auch schon bei bestehenden Ansätzen können die Materialien in neue Richtungen weitergeführt werden. In Anlehnung an unsere Ursprungsstudien des Jahres 2016[64] resultierte die Weiterentwicklung der quervernetzten Nanoträger[77] in Trägervehikel, die aus B'BABB'-strukturierten Copolymeren aufgebaut sind, sowie einer einfach Syntheseroute hin zu folsäure-tragenden Nanopartikeln (Schema 10.3). Um hierbei die Vergleichbarkeit mit den ABB'-Nanopartikeln zu gewährleisten, wurde ein bifunktionaller Katalysator eingesetzt, der über die C-H-Bindungsaktivierung von TMPy mit $Cp_2Y(CH_2TMS)(THF)$ erhalten wurde. Die Untersuchug dieses Komplexes mittels NMR-Spektroskopie bescheinigte, dass sich ausschließlich eine bifunktionelle Spezies gebildet hatte. Durch die daran anschließende Endgruppenanalytik von 2VP-Oligomeren über ESI-MS konnte der Einbau des Initiators TMPy in die Polymerkette festgestellt werden. Indessen wurden kinetische Experimente zur 2VP-Polymerisation durchgeführt, wobei eine TOF von 192 h^{-1} bestimmt wurde. Dieser Wert ist damit zweimal so hoch wie die Aktivität, die mit *sym*-Collidin ermittelt wurde (TOF = 90 h^{-1}). Allerdings fallen die ermittelten Aktivitäten gegenüber den verwandten Bisphenolat-Systemen um einen Faktor von 3-10 niedriger aus als.[64, 122] Mit dem binuklearen Katalysator wurden definierte Copolymere mit verschiedenen Monomerzusammensetzungen (2VP: 100-300 Äquiv.; DEVP: 200-300 Äquiv.; DAlVP: 6-20 Äquiv.), bei gleichzeitig hohen *IEs* (80-99%) und niedrigen Molmassenverteilungen (*Đ* ≤ 1.10) hergestellt. Im Folgenden wurden die Polymere unter Verwendung

der Thiol-En-Klick-Chemie mit drei Dithiolen quervernetzt. Die herbei generierten Nanopartikel wurden mittels DLS und TEM analysiert, wobei definierte, beinahe sphärische Partikel nachgewiesen wurden. Die Durchmesser bewegten sich zwischen 21.1 und 51.9 nm (PDI = 0.13-0.22) und zeigten große Abhängigkeit von der Länge des 2VP-Blocks. Außerdem belegten Zeta-Potential-Messungen eine leicht negative Oberflächenladung (-6.3 bis -22 mV), welche anscheinend durch die Polarität des Quervernetzers beeinflusst werden kann. Unter erhöhten Temperaturen und pH-Werten ließ sich ein positiver Einfluss auf das Freisetzungsverhalten von Fluorescein nachgewiesen, wobei die Freigabe des transportierten Stoffes deutlich beschleunigt war gegenüber den Standardbedingungen. Dabei wurden die besten Resultate bei pH = 4.5 erzielt, insbesondere in Experimenten mit Partikeln, die einen hohen 2VP-Anteil vorweisen. Auf die Temperatur bezogen zeigten die Partikel mit einem hohen DAlVP-Anteil (20 Äquiv.) eine deutliche Abgrenzung beim Freisetzungsverhalten zwischen 37 °C und 42 °C. Die Etablierung einer Syntheseroute zu folsäure-modifizierten Nanopartikeln komplementierte diese Studie, um damit eine Grundvoraussetzung für die aktive-gerichtete Wirkstoffverabreichung zu erfüllen. Für diesen Zweck wurde zuerst ein Teil der Allylgruppen mit Cysteamin umgesetzt. Die übrigen Allylgruppen wurden anschließend mit 3,6-Dioxa-1,8-octandithiol gesättigt und die oberflächlichen Aminogruppen mit aktivierter Folsäure umgesetzt. Neben dem Einsatz der NMR-Spektroskopie wurde diese Reaktionssequenz über Zeta-Potential-Messungen nachvollzogen, die eine Änderung von -18 mV (Cysteamin-Konjugat) zu -11 mV (nach Folsäure-Kopplung) zeigten. Außerdem bekräftigten zugehörige DOSY-Messungen eine kovalente Bindung zwischen Folsäure und dem Vorläuferpartikel. Mit der Charakterisierung durch DLS und TEM wurde das Vorhandensein uniformer Partikel bestätigt.

In Kombination mit unseren vorangegangenen Arbeiten bietet diese Studie eine einfach zugängliche Synthesebasis. Folglich lässt sich die Partikelgröße und die Partikelzusammensetzung kontrollieren. Außerdem kann hiermit das Freisetzungsverhalten optimiert und das Oberflächenpotential eingestellt werden und macht zielmolekül-modifizierten Transportvehikeln für die aktive Wirkstoffverabreichung zugänglich. Alle Daten sind in den Kapiteln 7 und 12.3 präsentiert.

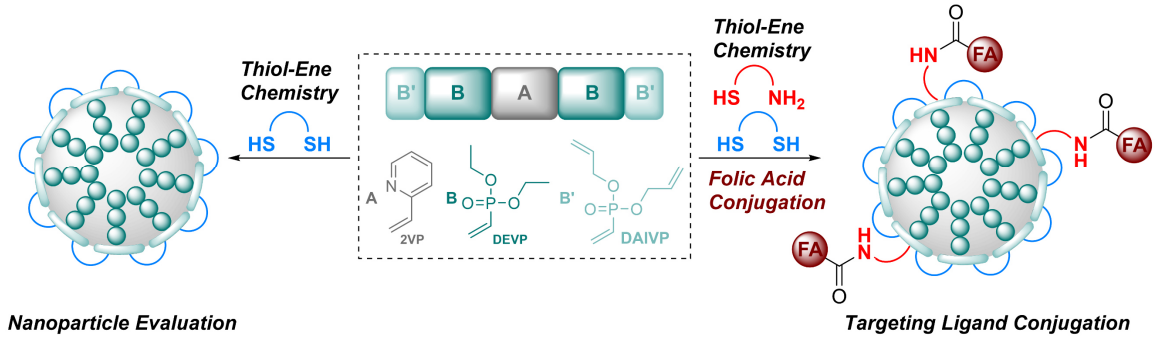

Schema 10.3. Graphische Zusammenfassung der Publikation mit dem Titel: "Synthesis, Characterisation and Functionalisation of BAB-type Dual-Responsive Nanocarriers for Targeted Drug Delivery: Evolution of Nanoparticles based on 2-Vinylpyridine and Diethyl Vinylphosphonate". Diese wird in den Kapiteln 7 und 12.3 präsentiert.

Diese Ergebnisse unterstreichen wie variabel der Erzeugungsprozess der Polyvinylphosphonate und anderer Polymere, die mittels REM-GTP erzeugt wurden, ist. Funktionelle oder reaktive Gruppen werden präzise während des Initiationsschritts beziehungsweise der Polymerisation über den (Makro-)Initiator oder das funktionelle Monomer eingeführt, welche somit die Grundvoraussetzung für die Funktionalisierungschemie nach der Polymerisation darstellen (Thiol-En-Klick-Chemie, Kondensationen, *Michael*-Additionen, Hydrosilylierung).

Zusammenfassend impliziert diese Arbeit das hohe Potential der Polyvinylphosphonate in verschiedenartigen biomedizinischen Anwendungen. Neben dem Einsatz als makromolekulare Bildgebungssonden oder maßgeschneiderte Transportvehikel für die Wirkstoffverabreichung mit zielspezifischen Liganden, sind neuartige Materialien für die Bioseparation, das *Tissue Engineering*, oder semipermeable Membranen (für die sogenannte *Islet Encapsulation*) durch Kombination entsprechender Post-Polymerisations-Funktionalisierungen vorstellbar.
Auf kurze Sicht kann der Horizont dieses synthetischen Instrumentariums in Richtung der supramolekularen Chemie, der Kopplung hochkomplexer Biomoleküle oder katalytisch aktiver Hybrid-Materialien erweitert werden. Bezogen auf die helikale Struktur der DNA erscheinen Nukleobasen oder auch Nukleotide als interessante Kopplungspartner für die Polyvinylphosphonate, da ein derartig modifiziertes Polymer aufgrund der Interaktionen entsprechender Nukleobasenpaare zur Selbstassemblierung neigen sollte. Solche supramolekularen Strukturen könnten in der molekularen Erkennung,[126] der aptamer-gestützten Wirkstoffverabreichung,[127, 128] oder als makromolekulare Bindungsmittel eine Anwendung finden.[129] In diesem Zusammenhang stellt die Kopplung komplexerer Biomoleküle ebenfalls eine Option dar. Unsere Arbeitsgruppe untersucht derzeit die synthetische Anbindung der RGD-Sequenz (R: Arginin, G: Glycin, D: Asparaginsäure) an die Polyvinylphosphonate. Wegen der Bindungseigenschaften der RGD-Funktionalität zu extrazellulären Rezeptoren sind polymer-basierte Materialien, die auf die Zelladhäsion abzielen, denkbar.[130] Darüber hinaus ist der Einschluss katalytisch aktiver Substrate in Mizellen oder Nanopartikeln möglich, die den Katalysator von äußeren Umwelteinflüssen abschirmen und dessen Aktivität über einen thermoresponsiven Block gesteuert werden kann.
Langfristig sollte eine tiefgehende Evaluierung der Nanoträger erfolgen. Hierunter fällt die Untersuchung wichtiger pharmakokinetische Kenngrößen wie der Biokompatibilität sowie den Zirkulationszeiten *in-vivo*, oder auch die Ausscheidung über die Nieren. Sollten sich diese Merkmale als positiv herausstellen, können die Nanoträger in Hinblick auf mögliche Anwendungszwecke optimiert werden: *Hyperthermia*-Behandlungen können nach einer präzise eingestellten LCST verlangen, welcher sich am lokal erhöhten Temperaturniveau des malignen Gewebes orientiert. Formulierungen, die über lokale Injektionen verabreicht werden, müssen unter Umständen hinsichtlich ihrer Vernetzungsstabilität angepasst werden, da für derartige Zwecke weniger stabile Partikel bevorzugt sind. Außerdem können neue zielgerichtete Moleküle in Betracht gezogen werden, welche selektiv mit bestimmten krankheitsspezifischen Rezeptoren interagieren.[131]
Dieses synthetische Fundament hievt die Polyvinylphosphonaten auf ein neues Komplexitätsniveau und verwandelt diese intelligente Polymerklasse in multi-funktionelle, anwendungsbezogene Materialien. Dementsprechend erscheint eine Anwendung der Polyvinylphosphonate in der nahen Zukunft in den entsprechenden biomedizinischen Feldern als gesichert.

11 Publications Beyond the Scope of this Thesis

11.1 Precise Synthesis of Thermoresponsive Polyvinylphosphonate-Biomolecule Conjugates via Thiol-Ene Click Chemistry

Title: "Precise Synthesis of Thermoresponsive Polyvinylphosphonate-Biomolecule Conjugates via Thiol-Ene Click Chemistry."

Status: Full Paper, First published 8th November 2017, Rewarded with Cover Page

Journal: Polymer Chemistry, 2018, 9, 284-290

Publisher: The Royal Society of Chemistry

Link/DOI: https://doi.org/10.1039/C7PY01796K

Authors: Christina Schwarzenböck, Andreas Schaffer, Philipp Pahl, Peter J. Nelson, Ralf Huss, and Bernhard Rieger

Abstract

A polymerisation type only recently attracting notice is the rare earth metal-mediated group transfer polymerisation (REM-GTP). This living-type polymerisation is able to conquer the limitations faced by classical anionic and radical polymerisations. REM-GTP enables the synthesis of biocompatible, water-soluble and thermoresponsive polymers with narrow polydispersities and controlled molecular weights. Furthermore, this technique renders the introduction of a functional end-group via the initiating molecule. Our group was able to synthesise a new multi-functional pyridine derivative and apply it as a highly active and efficient initiator in the polymerisation of diethylvinylphosphonate (DEVP). This novel end-group opens the door to various post-polymerisation modifications. In the present study, the thiol–ene click reaction, a fast, selective and well-established coupling method, was applied to link poly-DEVP and a biomolecule. The incentive for this investigation was to create a polymer platform, that can easily address a multiplicity of applications through facile alterations of the coupled biomolecule entities. Herein, we present for the first time the functionalisation of polyvinylphosphonates with biologically relevant motifs, namely cholesterol and folic acid.

Reprint Permission Copyrighted Content

Precise synthesis of thermoresponsive polyvinylphosphonate-biomolecule conjugates *via* thiol–ene click chemistry

C. Schwarzenböck, A. Schaffer, P. Pahl, P. J. Nelson, R. Huss and B. Rieger, *Polym. Chem.*, 2018, **9**, 284

DOI: 10.1039/C7PY01796K

11.2 Fluorescent Polyvinylphosphonate Bioconjugates for Selective Cellular Delivery

Title: "Fluorescent Polyvinylphosphonate Bioconjugates for Selective Cellular Delivery."

Status: Full Paper, Version of Record online: 25 January 2018

Journal: Chemistry – A European Journal, 2018, 24, 2584-2587

Publisher: John Wiley and Sons

Link/DOI: https://doi.org/10.1002/chem.201706034

Authors: Christina Schwarzenböck, Andreas Schaffer, Elfriede Nößner, Peter J. Nelson, Ralf Huss, and Bernhard Rieger

Abstract

To date, many poly(ethylene glycol) (PEG) and poly(*N*-isopropylacrylamide) (PNIPAAm) biomolecule conjugates have been described, but they often show long response times, are not bio-inert, or lose function in biological fluids. Herein, we present a modular synthetic approach to generate polyvinylphosphonate biomolecule conjugates. These conjugates exhibit a sharp phase transition temperature even under physiological conditions where few other examples with this property have been described to date. Furthermore, it was feasible to add biological functions to the polymers via the conjugation step. The polyvinylphosphonate cholesterol constructs are attached to the cellular membrane and the folic acid anchored polymers are shuttled into the cells. This is an exceptional finding through a straightforward synthetic approach.

Reprint Permission Copyrighted Content

Thank you for your order!

Dear Mr. Andreas Schaffer,

Thank you for placing your order through Copyright Clearance Center's RightsLink® service.

Order Summary

Licensee:	Technical University of Munich - WACKER-Chair of Macromolecular Chemistry
Order Date:	Nov 12, 2020
Order Number:	4946481234271
Publication:	Chemistry - A European Journal
Title:	Next Generation Multiresponsive Nanocarriers for Targeted Drug Delivery to Cancer Cells
Type of Use:	Dissertation/Thesis
Order Total:	0.00 EUR

View or print complete details of your order and the publisher's terms and conditions.

Sincerely,

Copyright Clearance Center

Tel: +1-855-239-3415 / +1-978-646-2777
customercare@copyright.com
https://myaccount.copyright.com

Copyright Clearance Center RightsLink®

11.3 Heteronuclear, Monomer-Selective Zn/Y Catalyst Combines Copolymerization of Epoxides and CO_2 with Group-Transfer Polymerization of *Michael*-Type Monomers

Title: "Heteronuclear, Monomer-Selective Zn/Y Catalyst Combines Copolymerization of Epoxides and CO_2 with Group-Transfer Polymerization of *Michael*-Type Monomers."

Status: Full Paper, Publication Date (Web): 27 March 2020, Awarded with Cover

Journal: ACS Macro Letters, 2020, 9, 571-575

Publisher: American Chemical Society

Link/DOI: https://doi.org/10.1021/acsmacrolett.9b01025

Authors: Alina Denk,‡ Sebastian Kernbichl,‡ Andreas Schaffer, Moritz Kränzlein, Thomas Pehl, and Bernhard Rieger

Abstract

Terpolymerizations of cyclohexene oxide (CHO), CO_2, and the Michael-type monomer 2-vinylpyridine (2VP) are presented. The combination of two distinct polymerization mechanisms was enabled by the synthesis of a heterobifunctional complex (**3**). Its β-diiminate zinc moiety allows the ring-opening copolymerization of CHO and CO_2, whereas the yttrium metallocene catalyzed the rare earth metal-mediated group-transfer polymerization of the polar vinyl monomer. Both units were connected via the CH-bond activation of a pyridyl-alkoxide linker. Matrix-assisted laser desorption/ionization time-of-flight mass spectrometry (MALDI-TOF-MS) revealed the successful transfer of the linker to the end-group of the respective homopolymers poly(cyclohexene carbonate) (PCHC) and poly(2VP) (P2VP) being the prerequisite for copolymer formation. Aliquot gel-permeation chromatography (GPC) analysis and solubility behavior tests confirmed the P2VP-*block*(*b*)-PCHC terpolymer formation via two pathways, a sequential and a one-pot procedure. Furthermore, the versatility of the method was demonstrated by introducing 2-isopropenyl-2-oxazoline (IPOx) as the second Michael-type monomer that yielded the terpolymer poly(IPOx)-*b*-PCHC.

‡These authors contributed equally.

Reprint Permission Copyrighted Content

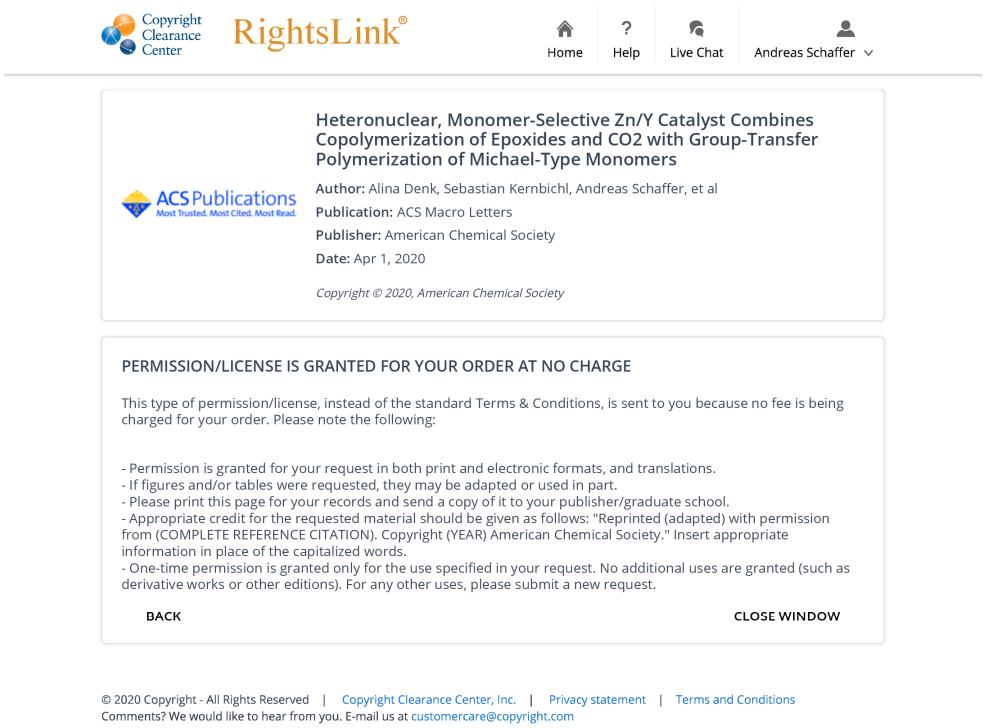

11.4 C–H Bond Activation of Silyl-Substituted Pyridines with Bis(Phenolate)Yttrium Catalysts as a Facile Tool towards Hydroxyl-Terminated Michael-Type Polymers

Title: "C–H Bond Activation of Silyl-Substituted Pyridines with Bis(Phenolate)Yttrium Catalysts as a Facile Tool towards Hydroxyl-Terminated Michael-Type Polymers."

Status: Full Paper, Published: 22 April 2020

Journal: Catalysts, 2020, 10, 448

Publisher: MPDI

Link/DOI: https://doi.org/10.3390/catal10040448

Authors: Thomas M. Pehl,‡ Moritz Kränzlein,‡ Friederike Adams,‡ Andreas Schaffer, and Bernhard Rieger

Abstract

Herein, silicon-protected, *ortho*-methylated hydroxy-pyridines were reported as initiators in 2-aminoalkoxy-bis(phenolate)yttrium complexes for rare earth metal-mediated group-transfer polymerization (REM-GTP) of Michael-type monomers. To introduce these initiators, C−H bond activation was performed by reacting [(ONOO)$^{t\text{Bu}}$Y(X)(thf)] (X = CH_2TMS, thf = tetrahydrofuran) with *tert*-butyl-dimethyl-silyl-functionalized α-methylpyridine to obtain the complex [(ONOO$^{t\text{Bu}}$Y(X)(thf)] (X = 4-(4′-(((*tert*-butyldimethylsilyl)oxy)methyl)phenyl)-2,6-di-methylpyridine). These initiators served as functional end-groups in polymers produced via REM-GTP. In this contribution, homopolymers of 2-vinylpyridine (2VP) and diethyl vinyl phosphonate (DEVP) were produced. Activity studies and end-group analysis via mass spectrometry, size-exclusion chromatography (SEC) and NMR spectroscopy were performed to reveal the initiator efficiency, the catalyst activity towards both monomers as well as the initiation mechanism of this initiator in contrast to commonly used alkyl initiators. In addition, 2D NMR studies were used to further confirm the end-group integrity of the polymers. For all polymers, different deprotection routes were evaluated to obtain hydroxyl-terminated poly(2-vinylpyridine) (P2VP) and poly(diethyl vinyl phosphonate) (PDEVP). Such hydroxyl groups bear the potential to act as anchoring points for small bioactive molecules, for post-polymerization functionalization or as macroinitiators for further polymerizations.

‡These authors contributed equally.

Reprint Permission Copyrighted Content

MDPI Open Access Information and Policy

All articles published by MDPI are made immediately available worldwide under an open access license. This means:

- everyone has free and unlimited access to the full-text of *all* articles published in MDPI journals;
- everyone is free to re-use the published material if proper accreditation/citation of the original publication is given;
- open access publication is supported by the authors' institutes or research funding agencies by payment of a comparatively low Article Processing Charge (APC) for accepted articles.

Permissions

No special permission is required to reuse all or part of article published by MDPI, including figures and tables. For articles published under an open access Creative Common CC BY license, any part of the article may be reused without permission provided that the original article is clearly cited. Reuse of an article does not imply endorsement by the authors or MDPI.

11.5 Allyl Group-Containing Polyvinylphosphonates as a Flexible Platform for the Selective Introduction of Functional Groups via Polymer-Analogous Transformations

Title: "Allyl Group-Containing Polyvinylphosphonates as a Flexible Platform for the Selective Introduction of Functional Groups via Polymer-Analogous Transformations."

Status: Manuscript in Preparation

Journal: -

Publisher: -

Link/DOI: -

Authors: Kerstin Halama,[‡] Andreas Schaffer,[‡] and Bernhard Rieger

Abstract

With their tunable lower critical solution temperature, high biocompatibility of homo- and copolymers, and a broad foundation for post-synthetic modifications, polyvinylphosphonates are highly promising candidates for (bio)medical applications. In contrast to our previous accomplishments which mainly focused on the selective introduction of single, terminal functionalities, we explored polymer-analogous transformations with statistical polyvinylphosphonates comprising diethyl vinylphosphonate (DEVP) and diallyl vinylphosphonate (DAlVP). The unsaturated C=C double bonds of **P1** were used as a starting point for a cascade of organic transformations. Initially, reactive functions were successfully introduced via bromination in **P2**, epoxidations with *OXONE* to **P5a** and *m*CPBA to **P5b**, or thiol-ene click chemistry with methyl thioglycolate (**6**) to form **P11**. The obtained substrates were then employed in a variety of consecutive reactions depending on the introduced functional motif: 1) The brominated substrates were converted with sodium azide to enable the copper-mediated alkyne-azide coupling with phenylacetylene (**1**). 2) The epoxides were reacted with sodium azide for an alkyne-azide click coupling with **1** as well as small nucleophilic compounds (phenol (**2**), benzylamine (**3**), and 4-amino-2,1,3-benzothiadiazol (**4**)). Afterwards the non-converted allyl groups of **P6b** and **P8** were converted with thiochloesterol (**5**) to form complex polymer conjugates. 3) An acid-labile hydrazone-linked conjugate **P13** was formed in a two-step approach starting from **P11**. The polymeric substrates were characterised by NMR, FTIR, and UV/Vis spectroscopy as well as elemental analysis and gel permeation chromatography to monitor the structural changes of the polymeric substrates and to prove the success of this modification approaches

[‡]These authors contributed equally.

12 Appendix

12.1 Supporting Information of the Manuscript "Synthesis and Application of Functional Group-Bearing Pyridyl-Based Initiators in Rare Earth Metal-Mediated Group Transfer Polymerization"

Supporting Information for the Manuscript Entitled *Synthesis and Application of Functional Group-Bearing Pyridyl-based Initiators in Rare Earth Metal-Mediated Group Transfer Polymerization*†

Andreas Schaffer,[a] Moritz Kränzlein,[a] and Bernhard Rieger*[a]

[a] *WACKER-Chair of Macromolecular Chemistry, Technical University of Munich, Lichtenbergstraße 4, 85748 Garching near Munich, Germany. E-mail: rieger@tum.de*

Table of Contents

1. Material and methods ... 2
2. Syntheses ... 3
2.1 Initiator synthesis ... 3
2.2 Complex synthesis ... 8
3. End-group analysis of oligomeric PDEVP by ESI-MS ... 13
4. Polymerization studies ... 15
4.1 Studies on the living characters of the DEVP polymerization with the active species 11-13 ... 15
4.2 Polymerization of PDEVP using the *in situ* generated complexes 11-13 ... 16
5. Deprotection experiments with the functional polymers ... 26
6. Refunctionalization of the polymers DP1, DP3 and DP5 ... 36
7. References ... 41

1. Material and methods

Thin-Layer Chromatography (TLC)

Thin-layer chromatography was performed on either silica coated aluminum plates (0.2 mm, F254) from *Macherey-Nagel* or aluminum oxide coated aluminum plates (0.2 mm, F254) from *Macherey-Nagel*. The compounds were detected by UV-light (λ = 254 nm, 366 nm).

Column Chromatography

Purification via column chromatography was performed on silica gel (grain size: 60-200 µm) from *Acros Organics* or aluminum oxide (activated, neutral; grain size: 50-150 µm) from *Sigma-Aldrich*. The eluent ratios are given for the corresponding procedures.

Dialysis

The purification via dialysis was performed with a Spectra/Por 1 dialysis membranes (regenerated cellulose) with a molecular weight cut-off (MWCO) of 6-8 kDa (*Spectrumlabs*). Prior to use, the membranes were treated with deionized water overnight and then rinsed with deionized water. A 100:1 ratio of dialysis fluid to sample volume was applied. Specific solvents used as dialysis fluid are given for the corresponding procedures.

UV/Vis Spectroscopy

UV/Vis spectra were recorded on a *Varian* Cary 50 UV/Vis spectrophotometer in 40 mm × 10 mm × 2 mm quartz glass cuvettes. Ethanol (absolute grade) was used as solvent.

2. Syntheses

2.1 Initiator synthesis

(4-(2,6-Dimethylpyridin-4-yl)phenyl)methanol (6)

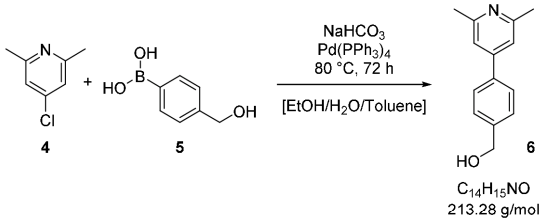

4-Chloro-2,6-dimethylpyridine (**4**) (2.48 g, 17.5 mmol, 1.00 equiv.) and 150 mL toluene were added to a suspension of 2.95 g 4-hydroxymethyl benzene boronic acid (**5**) (19.4 mmol, 1.10 equiv.) in EtOH (120 mL). Hereto a saturated $NaHCO_3$ solution (120 mL, 1.14 M) was added to obtain a basic pH value and the mixture was degassed by applying vacuum until evaporation started and argon (15 iterations). Afterwards, catalytic amounts of $Pd(PPh_3)_4$ (770 mg, 0.78 mmol, 0.04 equiv.) were added and the reaction mixture was heated to 80°C for 72 hours. After cooling to room temperature, black catalyst residues were removed by filtration and the phases were separated. The aqueous phase was extracted with EtOAc (2×80.0 mL) and $CHCl_3$ (100 mL). After the combined organic phases were dried over $MgSO_4$, the solvent was removed *in vacuo* and the crude product was purified by column chromatography (aluminum oxide, $CHCl_3$/MeOH = 95/5) and washing with ice-cold hexanes and ethyl acetate. Compound **6** was obtained as a white, crystalline solid (1.84 g, 8.60 mmol, 49%).

TLC: R_f = 0.47 ($CHCl_3$/MeOH = 95/5) [UV].

^{1}H-NMR (400 MHz, $CDCl_3$, 300 K): δ (ppm) = 7.60 (d, ^3J = 8.2 Hz, 2H, CH_{Ar}),7.46 (d, ^3J = 8.2 Hz, 2H, CH_{Ar}), 7.17 (s, 2H, $CH_{Pyridine}$), 4.76 (s, 2H, $CH_{2,Benzyl}$), 2.57 (s, 6H, CH_3),

^{13}C-NMR (101 MHz, $CDCl_3$, 300 K): δ (ppm) = 158.3 (s, $C_{Pyridine}$), 148.9 (s, $C_{Pyridine}$), 141.8 (s, C_{Ar}), 138.1 (s, C_{Ar}), 127.6 (s, CH_{Ar}), 127.3 (s, CH_{Ar}), 118.5 (s, $CH_{Pyridine}$), 65.0 (s, $CH_{2,Benzyl}$), 24.6 (s, $CH_{3,Pyridine}$).

ESI-MS: calculated: 213.12 $[M-H]^+$, found: 214.29 $[M-H]^+$.

EA:	calculated:	C 78.84	H 7.09	N 6.57
	found:	C 78.33	H 7.08	N 6.52

4-(4-(((*tert*-Butyldimethylsilyl)oxy)methyl)phenyl)-2,6-dimethylpyridine (1)

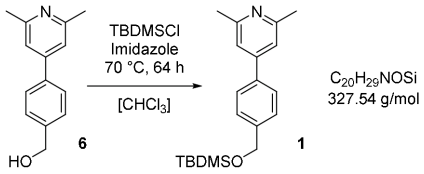

(4-(2,6-Dimethylpyridin-4-yl)phenyl)methanol (**6**) (2.00 g, 9.40 mmol, 1.00 equiv.) and 1*H*-imidazole (700 mg, 10.3 mmol, 1.10 equiv.) were dissolved in dry chloroform (100 mL). To this solution 1.55 g TBDMSCl (10.3 mmol, 1.10 equiv.) in dry chloroform (3.00 mL) were added dropwise. To ensure a quantitative protection, the reaction mixture was heated to 70°C and stirred for 64 hours under reflux before the solvent was removed *in vacuo*. Subsequently, the residue was suspended in water (100 mL) and treated with a saturated $NaHCO_3$ solution (100 mL). This mixture was stirred for 30 minutes at room temperature before extracting with benzene (3×150 mL). The combined organic phases were dried over $MgSO_4$ and the solvent was removed *in vacuo*, yielding initiator **1** as a yellow, viscous liquid (3.00 g, 9.20 mmol, 98%).

^{1}H-NMR (400 MHz, C_6D_6, 300 K): δ (ppm) = 7.41 (d, ^3J = 8.5 Hz, 2H, CH_{Ar}), 7.36 (d, ^3J = 8.5 Hz, 2H, CH_{Ar}), 6.97 (s, 2H, $CH_{Pyridine}$), 4.66 (s, 2H, $CH_{2,Benzyl}$), 2.52 (s, 6H, $CH_{3,Pyridine}$), 1.03 (s, 9H, $C(CH_3)_3$), 0.10 (s, 6H, $Si(CH_3)_2$).

^{13}C-NMR (101 MHz, C_6D_6, 300 K): δ (ppm) = 158.6 (s, $C_{Pyridine}$), 148.7 (s, $C_{Pyridine}$), 142.4 (s, C_{Ar}), 138.1 (s, C_{Ar}), 127.3 (s, CH_{Ar}), 126.91 (s, CH_{Ar}), 118.2 (s, $CH_{Pyridine}$), 64.9 ($CH_{2,Benzyl}$), 26.1 (s, $C(CH_3)_3$), 24.7 (s, $CH_{3,Pyridine}$), 18.6 (s, $C(CH_3)_3$), -5.10 (s, $Si(CH_3)_2$).

^{29}Si-NMR (80 MHz, C_6D_6, 300 K): δ (ppm) = 20.0.

ESI-MS: calculated: 327.20 $[M-H]^+$, found: 328.59 $[M-H]^+$.

EA:	calculated:	C 73.34	H 8.92	N 4.28
	found:	C 73.38	H 9.14	N 4.48

1-(2-Bromoethyl)-2,5-dimethyl-1*H*-pyrrole (7)[1]

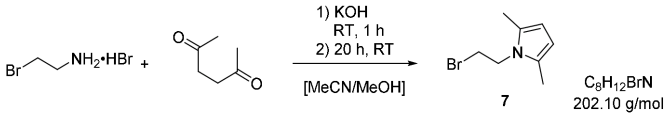

2-Bromoethylamine hydrobromide (4.50 g, 22.0 mmol, 1.00 equiv.) and potassium hydroxide (1.23 mg, 22.0 mmol, 1.00 equiv.) were suspended in acetonitrile (60 mL) and methanol (45 mL). After stirring for one hour at room temperature a solution of 2,5-hexanedione (2.75 mg, 24.1 mmol, 1.10 equiv.) in methanol (30 mL) was added and the mixture was stirred for additional 20 hours at room temperature. After a reaction control by TLC hydrochloric acid (2 M, 300 mL) was added and the mixture was extracted three times with diethyl ether (200 mL each). The organic phase was washed with hydrochloric acid (2 M, 150 mL), water (150 mL) and dried over $MgSO_4$. After filtration the volatiles were removed under

reduced pressure and the crude product was purified via column chromatography (aluminum oxide, H/EtOAc = 10/1) and product **7** was obtained as a red liquid in 41% (1.81 g, 8.96 mmol) yield.

TLC: R_f = 0.35 (H/EtOAc = 10/1) [UV].

^{1}H-NMR (400 MHz, $CDCl_3$, 300 K): δ (ppm) = 5.79 (s, 2H, $CH_{Pyrrole}$), 4.12 (dd, ^2J = 8.6 Hz, ^3J = 7.3 Hz, 2H, CH_2), 3.40 (dd, ^2J = 8.6 Hz, ^3J = 7.3 Hz, 2H, CH_2), 2.24 (s, 6H, $CH_{3,Pyrrole}$).

^{13}C-NMR (101 MHz, $CDCl_3$, 300 K): δ (ppm) = 127.5 (s, $C_{Pyrrole}$), 106.1 (s, $C_{Pyrrole}$), 45.2 (s, CH_2), 29.1 (s, CH_2), 12.6 (s, $CH_{3,Pyrrole}$).

EA: calculated: C 47.55 H 5.99 N 6.93
found: C 48.20 H 6.12 N 6.74

4-(2-(2,5-Dimethyl-1*H*-pyrrol-1-yl)ethoxy)-2,6-dimethylpyridine (2)

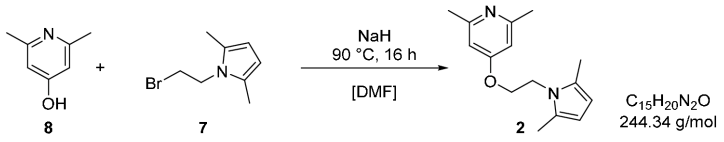

Sodium hydride (1.10 g, 60% in mineral oil, 13.4 mmol, 1.10 equiv.) was added to a solution of 4-hydroxy-2,6-dimethylpyridine (**8**) (1.50 g,12.2 mmol, 1.00 equiv.) in absolute DMF (30 mL) and the resulting mixture was stirred for 30 minutes at room temperature. Hereafter, 1-(2-Bromoethyl)-2,5-dimethyl-1*H*-pyrrole (**7**) (2.71 g, 13.4 mmol, 1.10 equiv.) in dry DMF (10 mL) was added dropwise and the reaction mixture was heated to 90°C. After stirring for 18 hours DMF was removed *in vacuo*, resulting in a brownish solid. The solid was treated with equal amounts of DCM and water (50 mL each) and the organic phase was separated subsequently. The aqueous phase was extracted with DCM (4 x 50 mL). The combined organic phases were washed with brine and dried over Na_2SO_4. After filtration, the solvent was removed under reduced pressure and the crude product was purified via column chromatography (SiO_2, H/EtOAc/NEt_3 = 10/10/1) yielding initiator **2** as yellowish needles (592 mg, 2.4 mmol, 20%).

TLC: R_f = 0.36 (H/EtOAc/NEt_3 = 10/10/1) [UV].

^{1}H-NMR (400 MHz, $CDCl_3$, 300 K): δ (ppm) = 6.42 (s, 2H, $CH_{Pyridine}$), 5.79 (s, 2H, $CH_{Pyrrole}$), 4.21 – 4.03 (m, 4H, 2 x CH_2), 2.45 (s, 6H, $CH_{3,Pyridine}$), 2.27 (s, 6H, $CH_{3,Pyrrole}$).

^{13}C-NMR (101 MHz, $CDCl_3$, 300 K): δ (ppm) = 165.3 (s, $C_{Pyridine}$), 159.5 (s, $C_{Pyridine}$), 127.9 (s, $C_{Pyrrole}$), 106.7 (s, $CH_{Pyridine}$), 105.9 (s, $CH_{Pyrrole}$l), 66.9 (s, CH_2), 42.7 (s, CH_2), 24.7 ($CH_{3,Pyridine}$), 12.8 (s, $CH_{3,Pyrrole}$).

ESI-MS: calculated: 245.16 $[M-H]^+$, found: 245.33 $[M-H]^+$.

EA: calculated: C 73.74 H 8.25 N 11.47
found: C 73.57 H 8.20 N 11.36

3-((2,6-Dimethylpyridin-4-yl)oxy)propan-1-ol[2]

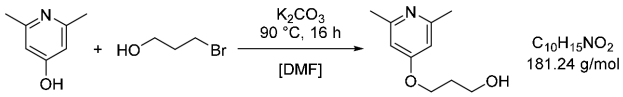

8

4-Hydroxy-2,6-dimethylpyridine (**8**) (5.00 g,40.6 mmol, 1.00 equiv.), 3-bromopropanol (6.21 g, 44.7 mmol, 1.10 equiv.) and potassium carbonate (16.8 g, 122 mmol, 3.00 equiv.) were suspended in DMF (50 mL) an stirred for six hours at 90°C. After this period, DMF was removed *in vacuo* and the resulting slurry was treated with water (100 mL) and DCM (100 mL) to dissolve the organic and inorganic components. The organic phase was separated, and the aqueous phase was extracted with DCM (3 x 100 mL). The combined organic phases were washed with brine (150 mL), dried over Na_2SO_4 and the solids were filtrated off. Volatiles were removed under reduced pressure and the crude product was purified using column chromatography (SiO_2, EtOAc/NEt_3 = 10/1 → EtOAc/MeOH/NEt_3 = 9/1/1) to yield the corresponding alcohol as a beige-colored solid (4.95 g, 27.3 mmol, 67%).

TLC: R_f = 0.33 (EtOAc/NEt_3 = 10/1) [UV].

^{1}H-NMR (400 MHz, $CDCl_3$, 300 K): δ (ppm) = 6.45 (s, 2H, $CH_{Pyridine}$), 4.10 (t, ^3J = 5.9 Hz, 2H, CH_2), 3.84 (t, ^3J = 5.9 Hz, 2H, CH_2), 2.44 (s, 6H, CH_3), 2.02 (p, ^3J = 5.9 Hz, 2H, CH_2).

^{13}C-NMR (101 MHz, $CDCl_3$, 300 K): δ (ppm) = 165.8 (s, $C_{Pyridine}$), 159.2 (s, $C_{Pyridine}$), 106.8 (s, $CH_{Pyridine}$), 64.9 (s, CH_2), 59.4 (s, CH_2), 31.9 (s, CH_2), 24.6 (s, CH_3).

ESI-MS: calculated: 182.12 $[M-H]^+$, found: 182.16 $[M-H]^+$.

4-(3-Bromopropoxy)-2,6-dimethylpyridine (9)[3]

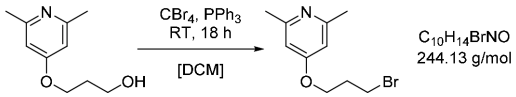

9

3-((2,6-Dimethylpyridin-4-yl)oxy)propan-1-ol (3.00 g, 16.6 mmol, 1.00 equiv.) and tetrabromomethane (7.14 g, 21.5 mmol, 1.30 equiv.) were dissolved in absolute DCM (75 mL). Afterwards, triphenylphosphine (5.64 g, 21.5 mmol, 1.30 equiv.) was added in small portions to the solution. The reaction was stirred for 18 hours at room temperature and monitored by ^{1}H NMR spectroscopy. After the full conversion was observed, solids were removed by filtration, DCM was removed *in vacuo* and the crude oil was purified by column chromatography (aluminum oxide, H/EtOAC = 10/1 → H/EtOAc = 1/1). Product **9** was obtained as yellowish oil in 58% yield (2.34 mg, 9.63 mmol).

TLC: R_f = 0.65 (H/EtOAc = 1/1) [UV].

^{1}H-NMR (400 MHz, $CDCl_3$, 300 K): δ (ppm) = 6.50 (s, 2H, $CH_{Pyridine}$), 4.12 (t, ^3J = 5.8 Hz, 2H, CH_2), 3.58 (t, ^3J = 6.4 Hz, 2H, CH_2), 2.47 (s, 6H, CH_3), 2.31 (virt. p, ^3J = 6.1 Hz, 2H, CH_2).

^{13}C-NMR (101 MHz, $CDCl_3$, 300 K): δ (ppm) = 165.6 (s, $C_{Pyridine}$), 159.4 (s, $C_{Pyridine}$), 106.8 (s, $CH_{Pyridine}$), 65.0 (s, CH_2), 32.1 (s, CH_2), 29.8 (s, CH_2), 24.8 (s, CH_3) .

ESI-MS: calculated: 244.03 $[M\text{-}H]^+$, found: 244.13 $[M_{^{79}Br}\text{-}H]^+$, 246.18 $[M_{^{81}Br}\text{-}H]^+$.

EA: calculated: C 49.20 H 5.78 N 5.74
found: C 48.55 H 5.96 N 5.57

2,6-Dimethyl-4-(3-(tritylthio)propoxy)pyridine (3)

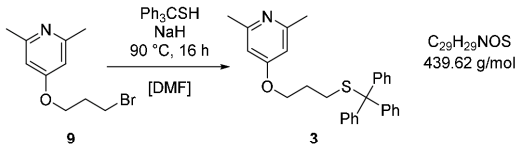

9 3

4-(3-Bromopropoxy)-2,6-dimethylpyridine (**9**) (1.00 g, 4.10 mmol, 1.00 equiv.) was dissolved in absolute DMF (20 mL) and added dropwise to a solution of sodium hydride (160 mg, 60% in mineral oil, 4.10 mmol, 1.00 equiv.) and triphenylmethanethiol (1.13 g, 4.10 mmol, 1.00 equiv.) in absolute DMF (10 mL) at 0°C. Afterwards the reaction mixture was heated to 90°C and stirred for 16 hours. After a reaction control by TLC, DMF was removed under reduced pressure and the resulting slurry was dissolved in DCM. The solution was then treated with a saturated $NaHCO_3$-solution (30 mL) and extracted with DCM (4 x 30 mL). The organic phase was dried over Na_2SO_4, filtrated and the solvent was removed under reduced pressure. Compound **3** was obtained after column chromatography (aluminum oxide, H/NEt_3 = 20/1 → H/EtOAc/NEt_3 =15/5/1) with a yield of 56% (1.00 g, 2.27 mmol)

TLC: R_f = 0.39 (H/EtOAc = 5/1) [UV].

^{1}H-NMR (400 MHz, $CDCl_3$, 300 K): δ (ppm) = 7.43 – 7.35 (m, 6H, CH_{Trityl}), 7.30 – 7.14 (m, 9H, CH_{Trityl}), 6.41 (s, 2H, $CH_{Pyridine}$), 3.91 (t, ^3J = 6.2 Hz, 2H, CH_2), 2.46 (s, 6H, CH_3), 2.35 (t, ^3J = 7.0 Hz, 2H, CH_2), 1.79 (p, ^3J = 6.6 Hz, 2H, CH_2).

^{13}C-NMR (101 MHz, $CDCl_3$, 300 K): δ (ppm) = 165.7 (s, $C_{Pyridine}$), 159.2 (s, $C_{Pyridine}$), 144.9 (s, C_{Trityl}), 129.7 (s, CH_{Trityl}), 128.0 (s, CH_{Trityl}), 126.8 (s, CH_{Trityl}), 106.9 (s, $CH_{Pyridine}$), 66.8 (s, $SCPh_3$), 66.0 (s, CH_2), 28.4 (s, CH_2), 28.2 (s, CH_2), 24.8 (s, CH_3).

ESI-MS: calculated: 440.20 $[M\text{-}H]^+$, found: 440.73 $[M\text{-}H]^+$.

EA: calculated: C 79.23 H 6.65 N 3.19 S 7.29
found: C 79.24 H 6.61 N 3.14 S 7.18

2.2 Complex synthesis

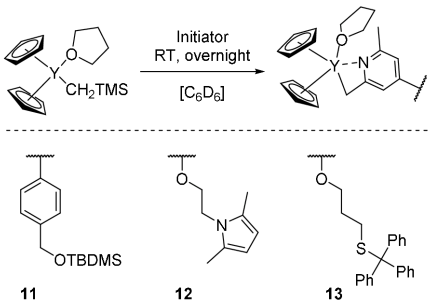

***In situ* activated complex 11**

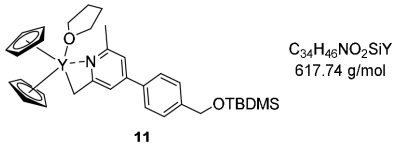

$C_{34}H_{46}NO_2SiY$
617.74 g/mol

11

Intense yellow color in solution.

^{1}H-NMR (400 MHz, C_6D_6, 300 K): δ (ppm) = 7.52 (d, ^{3}J = 8.0 Hz, 2H, CH_{Ar}), 7.34 (d, ^{3}J = 8.0 Hz, 2H, CH_{Ar}), 6.89 (s, 1H, $CH_{Pyridine}$), 6.36 (s, 1H, $CH_{Pyridiner}$), 6.06 (s, 10H, Cp), 4.64 (s, 2H, $CH_{2,Benzyl}$), 3.41 (m, 4H, THF), 2.40 (s, 2H, CH_2Y), 2.12 (s, 3H, CH_3), 1.26 (m, 4H, THF), 1.02 (s, 9H, $C(CH_3)_3$), 0.09 (s, 6H, $Si(CH_3)_2$).

^{13}C-NMR (101 MHz, C_6D_6, 300 K): δ (ppm) = 167.5 (s, C_{Ar}), 157.4 (s, C_{Ar}), 149.1 (s, C_{Ar}), 142.3 (s, C_{Ar}), 138.7 (s, C_{Ar}), 127.2 (s, CH_{Ar}), 126.9 (s, CH_{Ar}), 111.6 (s, CH_{Ar}), 110.5 (s, Cp), 108.6 (s, CH_{Ar}), 69.8 (s, THF), 65.0 (s, $CH_{2,Benzyl}$), 42.4 (d, J_{CY} = 11.0 Hz), 26.2 s, ($C(CH_3)_3$), 25.6 (s, THF), 24.1 (s, CH_3), 18.6 (s, $C(CH_3)_3$), -5.1 (s, $Si(CH_3)_2$).

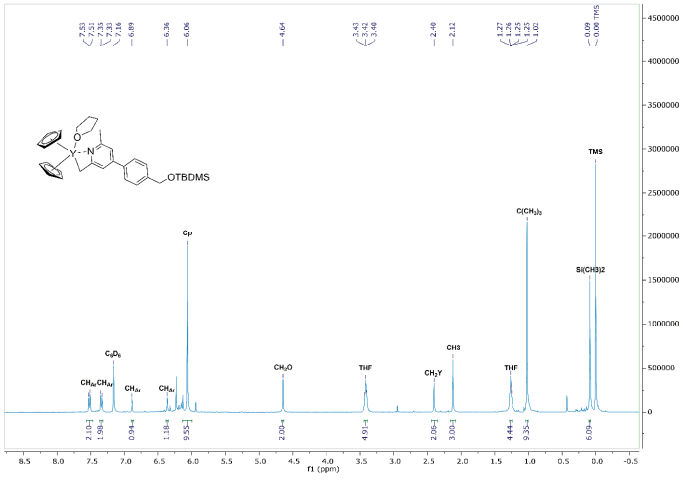

Figure S1. ^{1}H-NMR spectrum of complex **11** in C_6D_6.

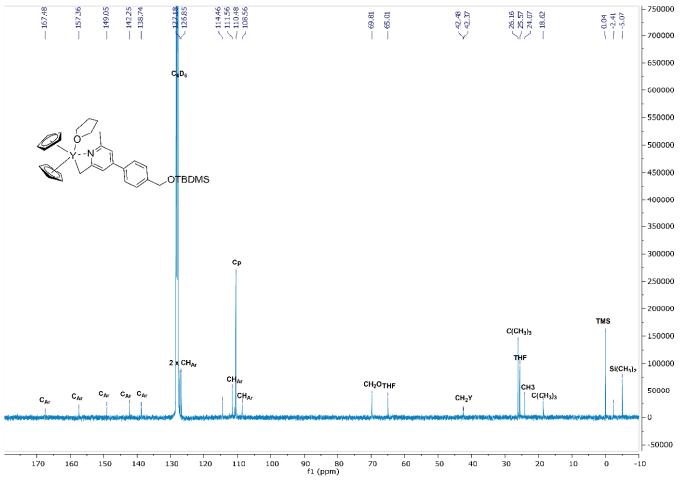

Figure S2. ^{13}C-NMR spectrum of complex **11** in C_6D_6.

***In situ* activated complex 12**

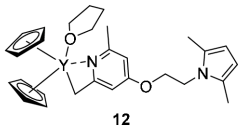

$C_{29}H_{37}N_2O_2Y$
534.53 g/mol

12

Intense orange color in solution.

^{1}H-NMR (400 MHz, C_6D_6, 300 K): δ (ppm) = 6.04 (s, 10H, Cp), 6.01 (s, 2H, $CH_{Pyrrole}$), 5.88 (d, ^{4}J = 2.2 Hz, 1H, $CH_{Pyridine}$), 5.84 (d, ^{4}J = 2.2 Hz, 1H, $CH_{Pyridine}$), 3.57 (s, 4H, 2 x CH_2), 3.49 – 3.30 (m, 5H, 1.2 x THF), 2.27 (s, 2H, CH_2Y), 2.02 (s, 9H, 2 x $CH_{3,Pyrrole}$, $CH_{3,Pyridine}$), 1.36 – 1.12 (m, 5H, 1.2 x THF).

^{13}C-NMR (101 MHz, C_6D_6, 300 K): δ (ppm) = 169.4 (s, C_{Ar}), 166.0 (s, C_{Ar}), 158.7 (s, C_{Ar}), 127.3 (s, $C_{Pyrrole}$), 110.3 (s, Cp), 106.6 (s, $CH_{Pyrrole}$), 101.1 (s, $CH_{Pyridine}$), 97.6 (s, $CH_{Pyridine}$), 70.2 (s, THF), 66.7 (s, CH_2), 42.5 (s, CH_2), 41.5 (d, J_{CY} = 11.6 Hz, CH_2Y), 25.6 (s, THF), 23.8 (s, $CH_{3,Pyridine}$), 12.7 (s, $CH_{3,Pyrrole}$).

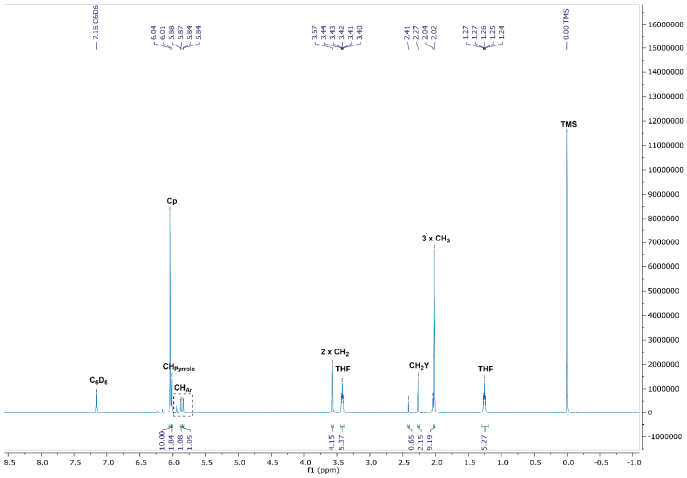

Figure S3. ^{1}H-NMR spectrum of complex **12** in C_6D_6.

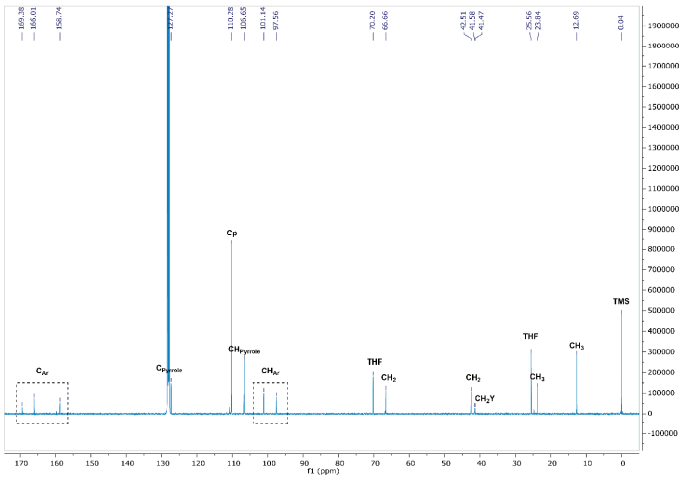

Figure S4. ^{13}C-NMR spectrum of complex **12** in C_6D_6.

***In situ* activated complex 13**

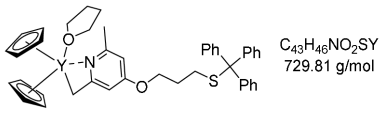

$C_{43}H_{46}NO_2SY$
729.81 g/mol

13

Light yellow color in solution.

^{1}H-NMR (400 MHz, C_6D_6, 300 K): δ (ppm) = δ 7.64 – 7.49 (m, 6H, CH_{Trityl}), 7.12 – 7.05 (m, 6H, CH_{Trityl}), 7.01 – 6.97 (m, 3H, CH_{Trityl}), 6.05 (s, 9H, Cp), 6.00 (d, ^4J = 2.2 Hz, 1H, $CH_{Pyridine}$), 5.90 (d, ^4J = 2.2 Hz, 1H, $CH_{Pyridine}$), 3.54 (t, ^3J = 6.3 Hz, 2H), 3.48 – 3.42 (m, 6H, 1.5 x THF), 2.32 (t,^3J = 7.1 Hz, 2H), 2.27 (s, 2H, CH_2Y), 2.03 (s, 3H, CH_3), 1.58 (virt. p, ^3J = 6.7 Hz, 2H, CH_2), 1.32 – 1.22 (m, 6H, 1.5 x THF).

^{13}C-NMR (101 MHz, C_6D_6, 300 K): δ (ppm) = 169.5 (s, C_{Ar}), 166.5 (s, C_{Ar}), 158.4 (s, C_{Ar}), 145.6 (s, C_{Trityl}), 130.1 (s, C_{Trityl}), 128.2 (s, C_{Trityl}), 126.9 (s, C_{Trityl}), 110.3 (s. Cp), 101.7 (s, $CH_{Pyridine}$), 97.9 (s, $CH_{Pyridine}$), 69.7 (s, THF), 67.1 (s, CPh_3), 65.8 (s, CH_2), 41.2 (d, J_{CY} = 12.1 Hz, CH_2Y), 28.7 (s, CH_2), 28.4 (s, CH_2), 25.6 (s, THF), 23.9 (s, CH_3).

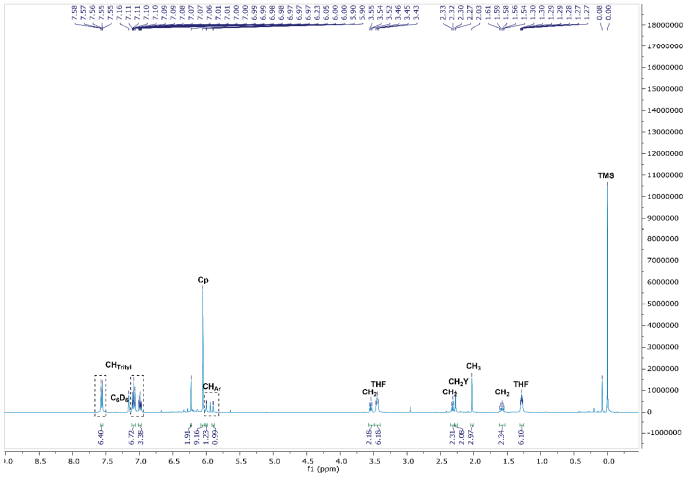

Figure S5. ^{1}H-NMR spectrum of complex **13** in C_6D_6.

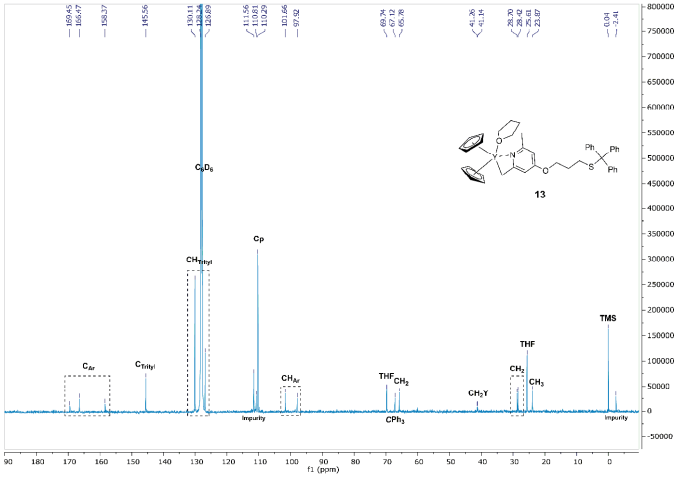

Figure S6. ^{13}C-NMR spectrum of complex **13** in C_6D_6.

3. End-group analysis of oligomeric PDEVP by ESI-MS

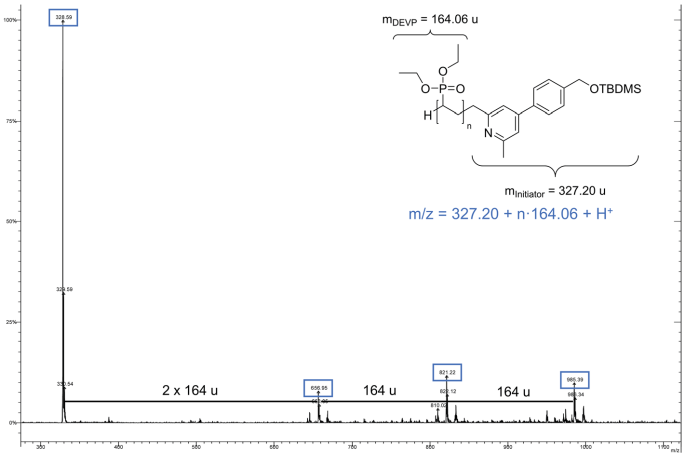

Figure S7. Oligomer pattern of PDEVP generated with active species **11**. ESI-MS measured in LC-MS acetonitrile.

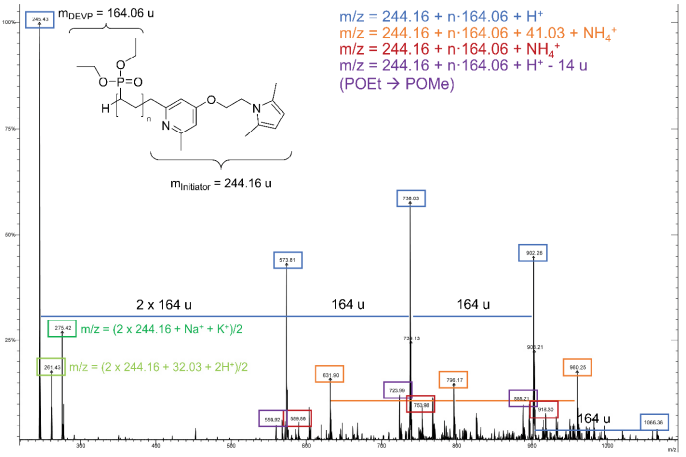

Figure S8. Oligomer pattern of PDEVP generated with active species **12**. ESI-MS measured in LC-MS acetonitrile. Low intensity signals were edited out for reasons of clarity.

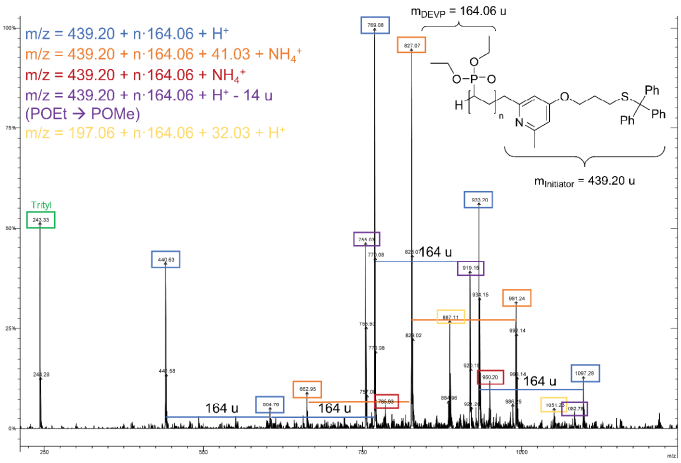

Figure S9. Oligomer pattern of PDEVP generated with active species **13**. ESI-MS measured in LC-MS acetonitrile.

4. Polymerization studies

4.1 Studies on the living characters of the DEVP polymerization with the active species 11-13

A solution of the corresponding initiator (21.7 µmol, 1.00 equiv.) in absolute toluene (5.00 mL) was added to a solution of 21.7 µmol $Cp_2Y(CH_2TMS)(THF)$ (8.21 mg, 1.00 equiv.) in 5.00 mL toluene resulting an instant coloration of the solution. The mixture was stirred overnight and the quantitative conversion of the C-H bond activation was confirmed by proton NMR. DEVP (2.13 g, 13.0 mmol, 600 equiv.) was added in one portion and aliquots were taken at regular time intervals, which were quenched by pouring into MeOD. The conversion of DEVP was monitored by ^{31}P-NMR spectroscopy. The molecular weights M_n and polydispersities $Đ$ of each polymer sample were determined via GPC-MALS after removal of the solvent.

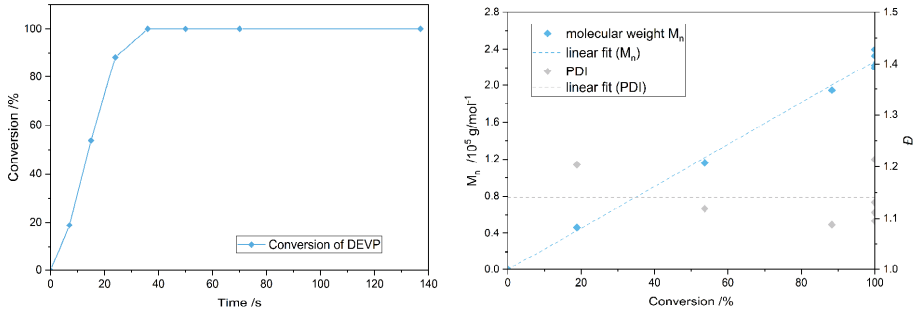

Figure S10. Conversion-time plot (left) and corresponding conversion-dependent plot of the molecular weights M_n and the corresponding polydispersities $Đ$ of PDEVP generated with species **12** (right).

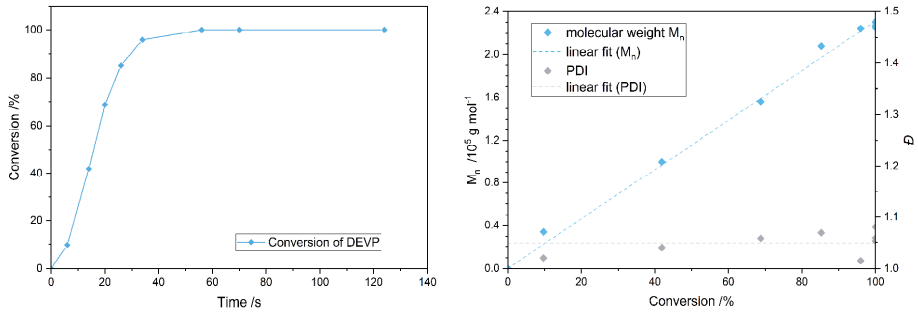

Figure S11 Conversion-time plot (left) and corresponding conversion-dependent plot of the molecular weights M_n and the corresponding polydispersities $Đ$ of PDEVP generated with species **13** (right).

4.2 Polymerization of PDEVP using the *in situ* generated complexes 11-13

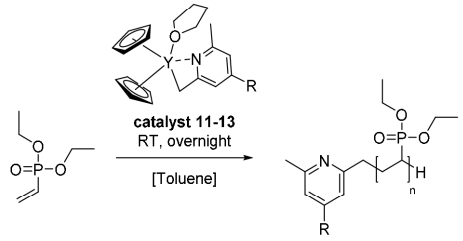

Characterization of poly(diethyl vinylphosphonates) P1-P2

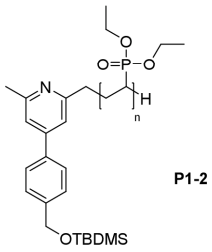

^{1}H-NMR (400 MHz, MeOD, 300 K): δ (ppm) = 7.80 – 7.36 (m, CH_{Ar}), 4.81 (s, $CH_{2,Benzyl}$), 4.18 (s, $POCH_2$), 2.56 (s, CH_3), 2.85 – 1.16 (m, polymer backbone), 1.38 (s, $POCH_2CH_3$), 0.97 (s, $C(CH_3)_3$), 0.13 (s, $Si(CH_3)_2$).

^{31}P-NMR (162 MHz, MeOD, 300 K): δ (ppm) = 33.1.

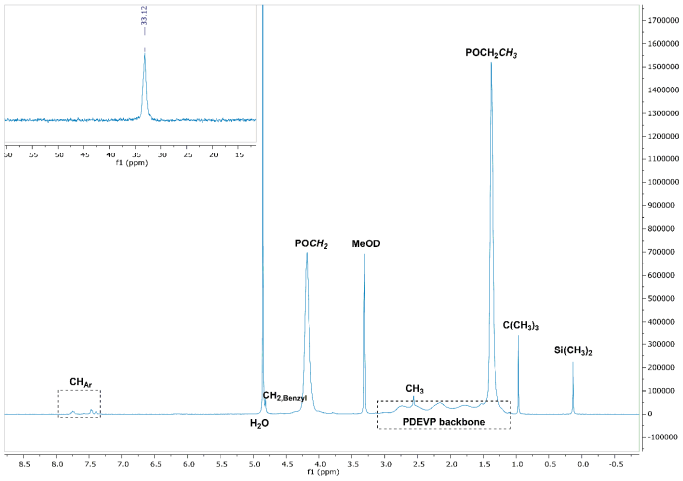

Figure S12. ^{1}H- and zoom of ^{31}P-NMR spectrum of PDEVP **P1** (25 equiv. DEVP) in MeOD.

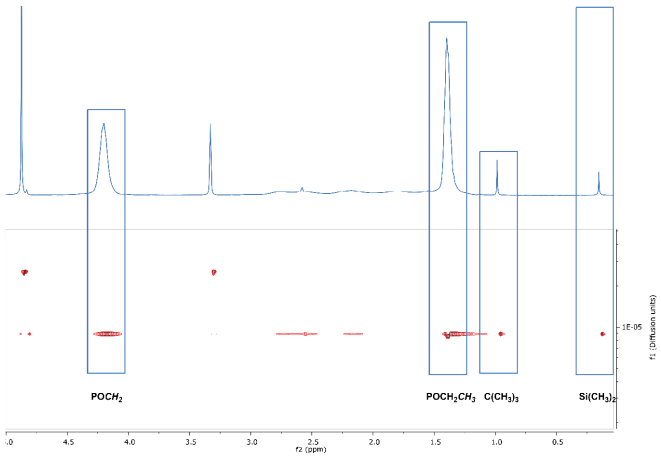

Figure S13. DOSY-NMR of PDEVP **P1** (25 equiv. DEVP) in MeOD.

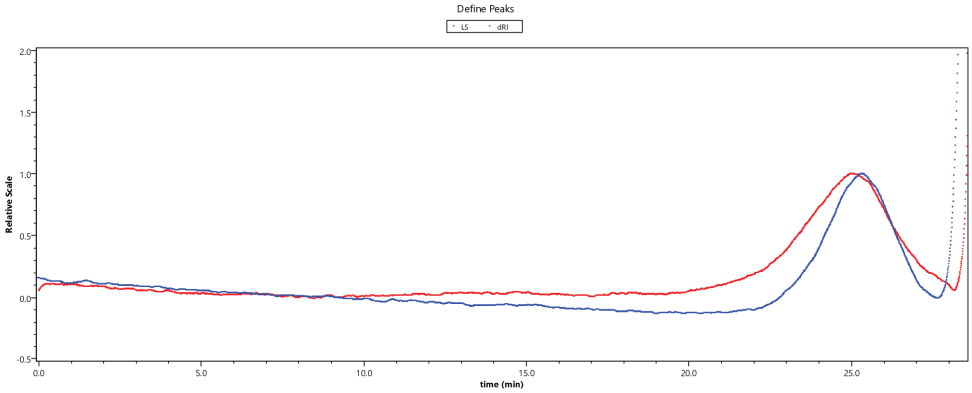

Figure S14. GPC trace of PDEVP **P1** (25 equiv. DEVP) generated with species **11**. Measured via GPC-MALS in THF/H_2O (on the right the washing artifact is visible).

^{1}H-NMR (500 MHz, MeOD, 300 K): δ (ppm) = 7.81 – 7.70 (m, CH_{Ar}), 7.61 – 7.36 (m, CH_{Ar}), 4.82 (s, $CH_{2,Benzyl}$), 4.18 (s, PO*CH_2*), 2.56 (s, CH_3), 2.89 – 1.20 (m, polymer backbone), 1.38 (s, $POCH_2$*CH_3*), 0.97 (s, $C(CH_3)_3$), 0.14 (s, $Si(CH_3)_2$).

^{31}P-NMR (203 MHz, MeOD, 300 K): δ (ppm) = 33.1.

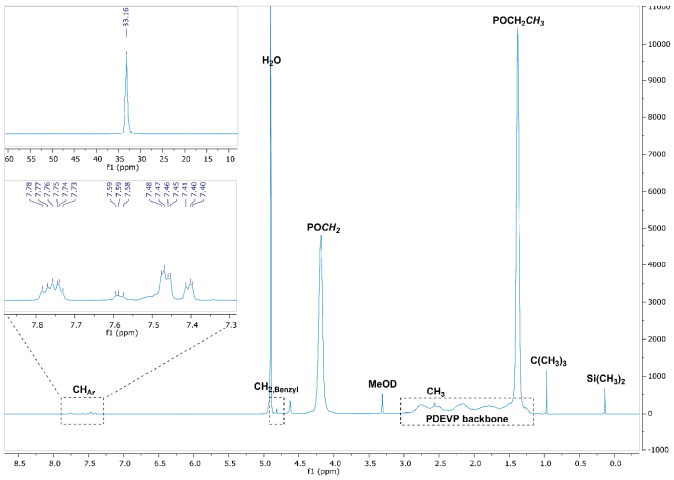

Figure S15. ^{1}H- and zoom of ^{31}P-NMR spectrum of PDEVP **P2** (100 equiv. DEVP) in MeOD.

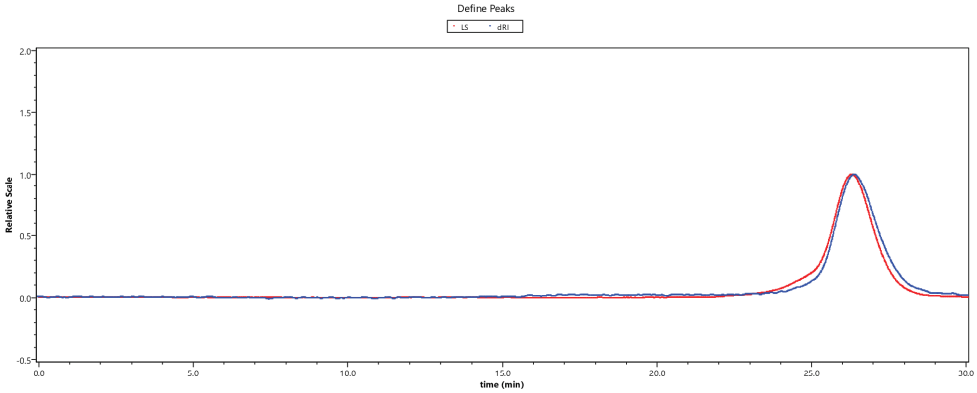

Figure S16. GPC trace of PDEVP **P2** (100 equiv. DEVP) generated with species **11**. Measured via GPC-MALS in THF/H_2O.

Characterization of poly(diethyl vinylphosphonates) P3-P4

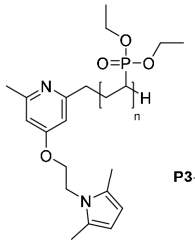

P3-4

^{1}H-NMR (400 MHz, MeOD, 300 K): δ (ppm) = 6.81 – 6.62 (m, $CH_{Pyridine}$), 6.57 (s, $CH_{Pyridine}$), 5.65 (s, $CH_{Pyrrole}$), 4.18 (s, $POCH_2$), 2.40 (s, CH_3), 2.24 (s, $CH_{3,Pyrrole}$), 2.92 – 1.11 (m, polymer backbone), 1.38 (s, $POCH_2CH_3$).

^{31}P-NMR (162 MHz, MeOD, 300 K): δ (ppm) = 33.1.

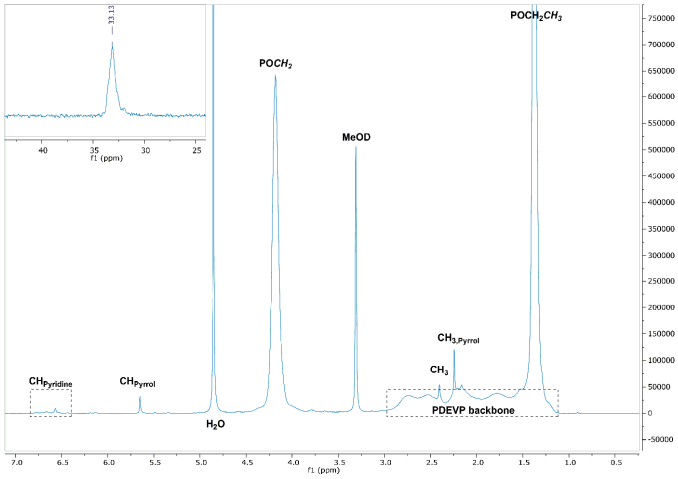

Figure S17. ^{1}H- and zoom of ^{31}P-NMR spectrum of PDEVP **P3** (25 equiv. DEVP) in MeOD.

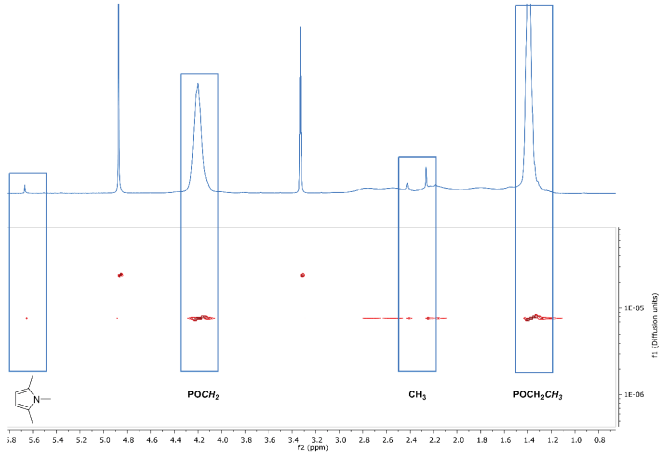

Figure S18. DOSY-NMR of PDEVP **P3** (25 equiv. DEVP) in MeOD.

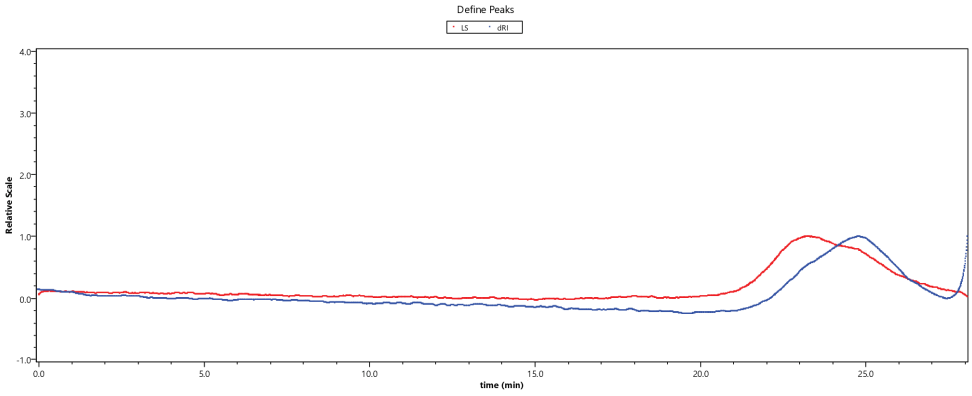

Figure S19. GPC trace of PDEVP **P3** (25 equiv. DEVP) generated with species **12**. Measured via GPC-MALS in THF/H_2O (on the right the washing artifact is visible).

^{1}H-NMR (500 MHz, MeOD, 300 K): δ (ppm) = 6.83 – 6.64 (m, $CH_{Pyridine}$), 6.57 (s, $CH_{Pyridine}$), 5.65 (s, $CH_{Pyrrole}$), 4.18 (s, $POCH_2$), 2.41 (s, CH_3), 2.25 (s, $CH_{3,Pyrrole}$), 2.96 – 1.09 (m, polymer backbone), 1.38 (s, $POCH_2CH_3$).

^{31}P-NMR (203 MHz, MeOD, 300 K): δ (ppm) = 33.2.

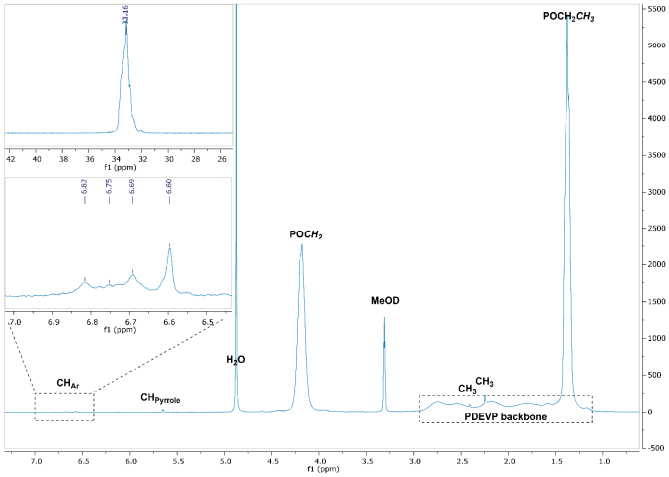

Figure S20. ^{1}H- and zoom of ^{31}P-NMR spectrum of PDEVP **P4** (100 equiv. DEVP) in MeOD.

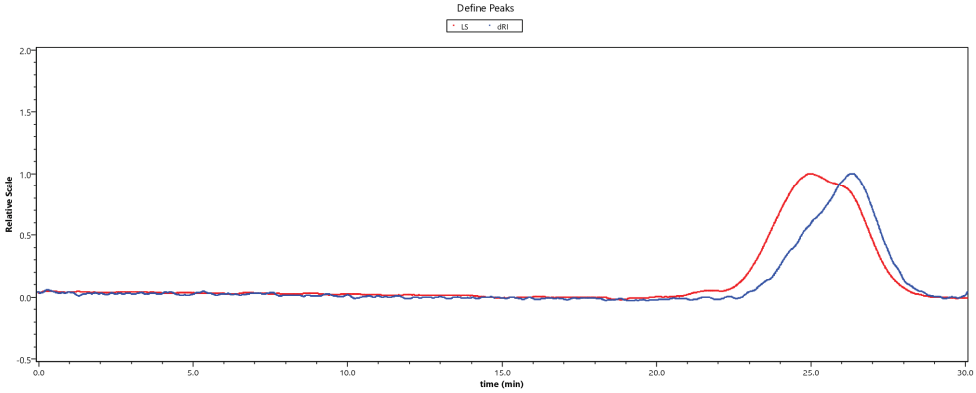

Figure S21. GPC trace of PDEVP **P4** (100 equiv. DEVP) generated with species **12**. Measured via GPC-MALS in THF/H_2O.

Characterization of poly(diethyl vinylphosphonates) P5-P6

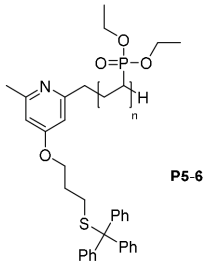

P5-6

^{1}H-NMR (400 MHz, MeOD, 300 K): δ (ppm) = 7.38 (dt, ^{3}J = 7.5 Hz, ^{4}J = 1.8 Hz, Trityl), 7.31 – 7.17 (m, Trityl), 6.81 – 6.50 (m, $CH_{Pyridine}$), 4.18 (s, $POCH_2$), 4.00 (m, $CH_{2,Initiator}$), 2.88 – 1.05 (m, polymer backbone), 1.38 (s, $POCH_2CH_3$).

^{31}P-NMR (162 MHz, MeOD, 300 K): δ (ppm) = 33.1.

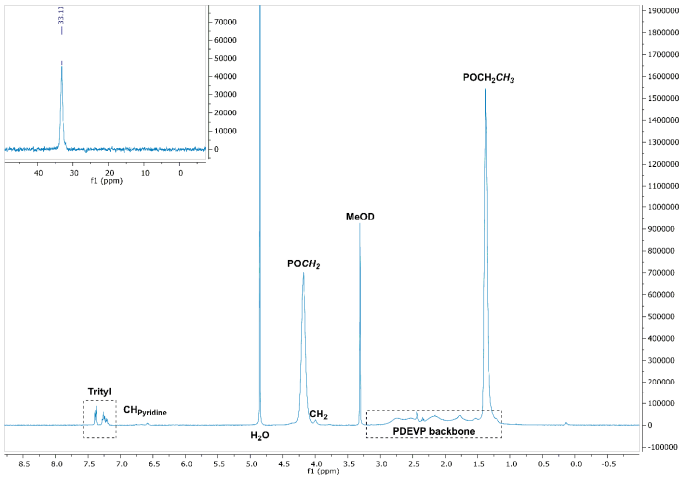

Figure S22. ^{1}H- and zoom of ^{31}P-NMR spectrum of PDEVP **P5** (25 equiv. DEVP) in MeOD.

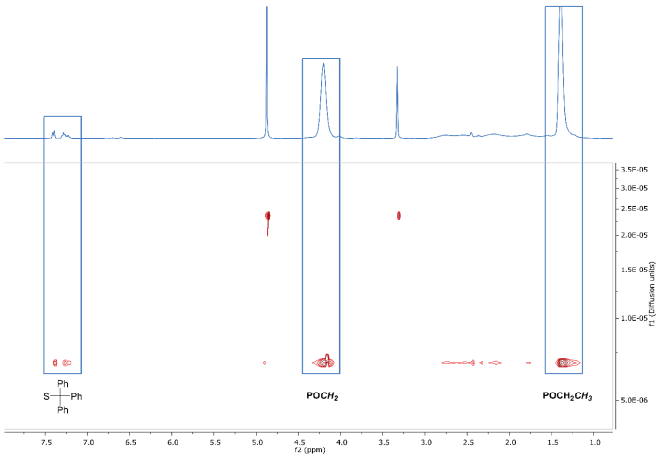

Figure S23. DOSY-NMR of PDEVP **P5** (25 equiv. DEVP) in MeOD.

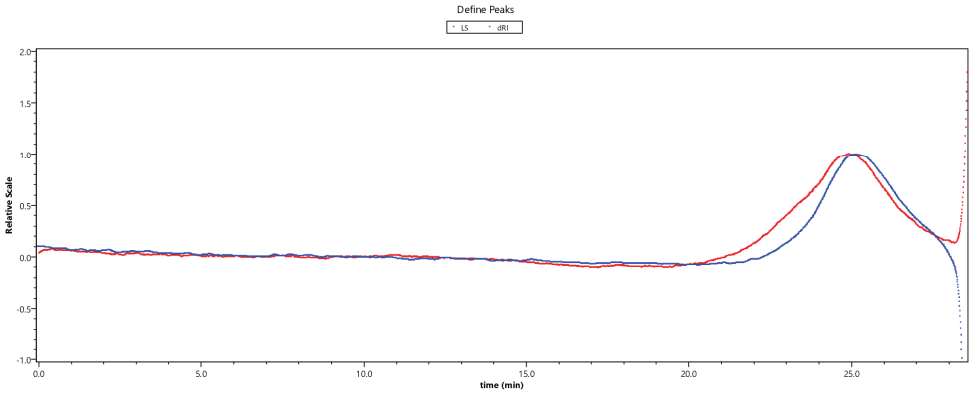

Figure S24. GPC trace of PDEVP **P5** (25 equiv. DEVP) generated with species **13**. Measured via GPC-MALS in THF/H_2O (on the right the washing artifact is visible).

^{1}H-NMR (500 MHz, MeOD, 300 K): δ (ppm) = 7.47 – 7.35 (m, CH_{Trityl}), 7.33 – 7.18 (m, CH_{Trityl}), 6.80 – 6.64 (m, $CH_{Pyridine}$), 6.62 – 6.56 (m, $CH_{Pyridine}$), 4.18 (s, $POCH_2$), 2.94 – 1.07 (m, polymer backbone), 1.38 (s, $POCH_2CH_3$).

^{31}P-NMR (203 MHz, MeOD, 300 K): δ (ppm) = 33.2.

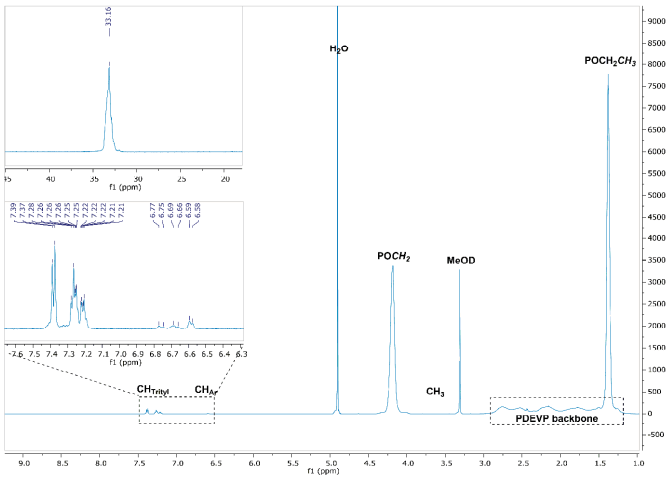

Figure S25. ^{1}H- and zoom of ^{31}P-NMR spectrum of PDEVP **P6** (100 equiv. DEVP) in MeOD.

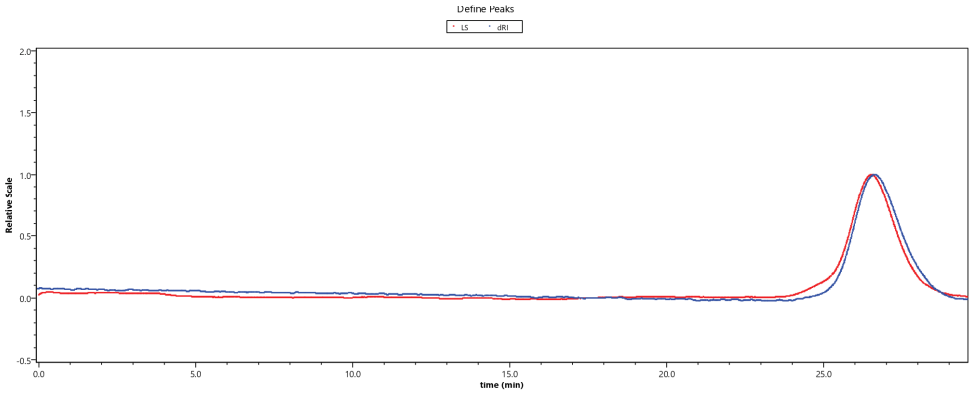

Figure S26. GPC trace of PDEVP **P6** (100 equiv. DEVP) generated with species **13**. Measured via GPC-MALS in THF/H_2O.

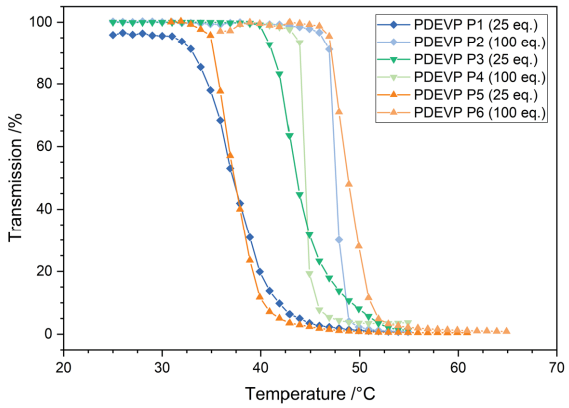

Figure S27. Determination of the LCST of the samples **P1-P6** in water (2.50 mg mL^{-1}). The cloud point was determined at 10% decrease of transmittance.

25

5. Deprotection experiments with the functional polymers

General procedure for the removal of the TBDMS protection group

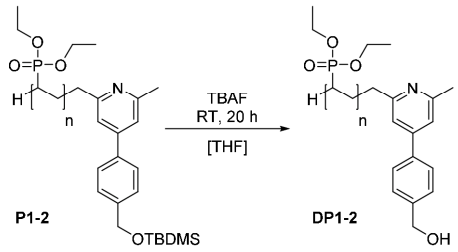

The experimental conditions were adopted in modified form from a procedure found in the literature.[4] Under argon atmosphere the TBDMS-protected poly(vinylphosphonate) (1.00 equiv.) is dissolved in absolute THF (4.00 mL per 100 mg polymer) and treated with tetrabutylammonium bromide (20.0 equiv., 1 M in THF). The resulting solution is stirred for 20 hours. After the removal of the protecting group was confirmed by ^{1}H NMR spectroscopy, the solvent was removed *in vacuo*, the residue was dissolved in water and the aqueous solution was purified by dialysis against water. The pure polymer was obtained after freeze-drying.

^{1}H-NMR (400 MHz, MeOD, 300 K): δ (ppm) = 7.91 – 7.42 (m, CH_{Ar}), 4.68 (s, CH_2OH), 4.18 (s, $POCH_2$), 2.87 – 1.13 (m, polymer backbone), 1.38 (s, $POCH_2CH_3$).

^{31}P-NMR (162 MHz, MeOD, 300 K): δ (ppm) = 33.2.

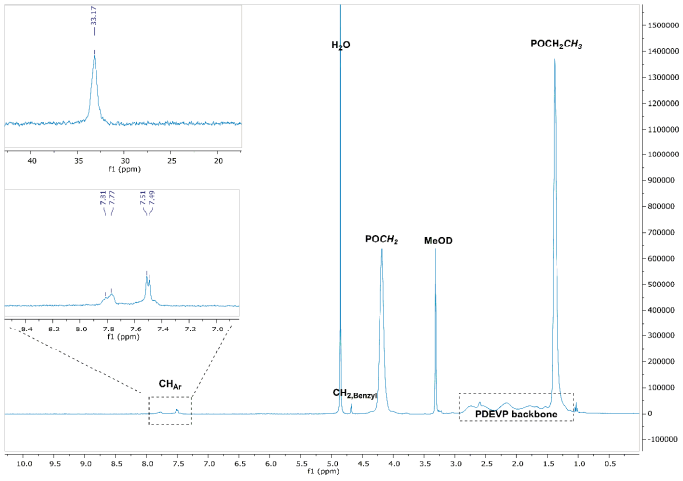

Figure S28. ^{1}H- and zoom of ^{31}P-NMR spectrum of PDEVP **DP1** (25 equiv. DEVP) in MeOD.

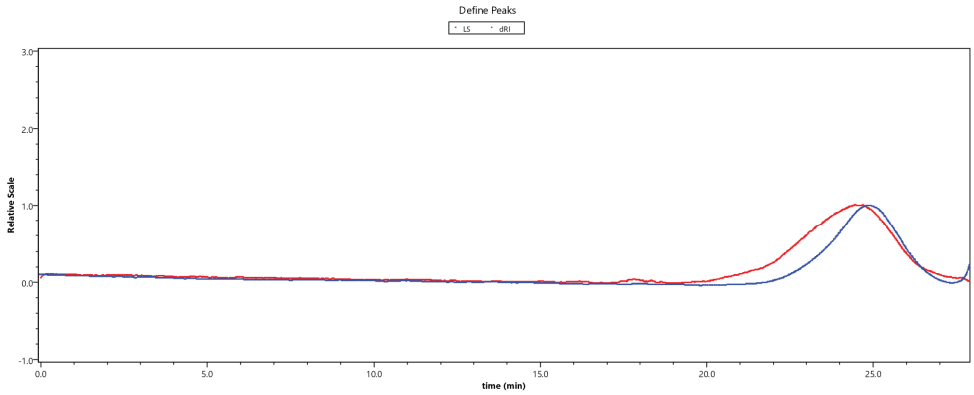

Figure S29. GPC trace of PDEVP **DP1** (25 equiv. DEVP). Measured via GPC-MALS in THF/H_2O (on the right the washing artifact is visible)

^{1}H-NMR (400 MHz, MeOD, 300 K): δ (ppm) = 7.83 – 7.71 (m, CH_{Ar}), 7.61 – 7.37 (m, CH_{Ar}), 4.67 (s, CH_2OH), 4.18 (s, $POCH_2$), 2.88 – 1.16 (m, polymer backbone), 1.38 (s, $POCH_2CH_3$).

^{31}P-NMR (162 MHz, MeOD, 300 K): δ (ppm) = 33.2.

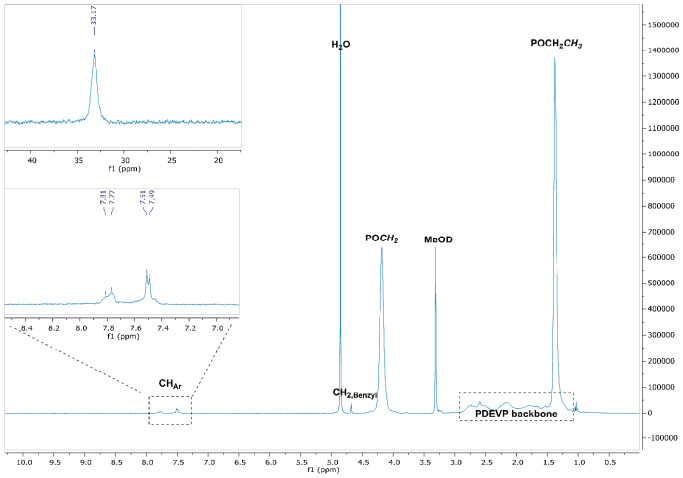

Figure S30. ^{1}H- and zoom of ^{31}P-NMR spectrum of PDEVP **DP2** (100 equiv. DEVP) in MeOD.

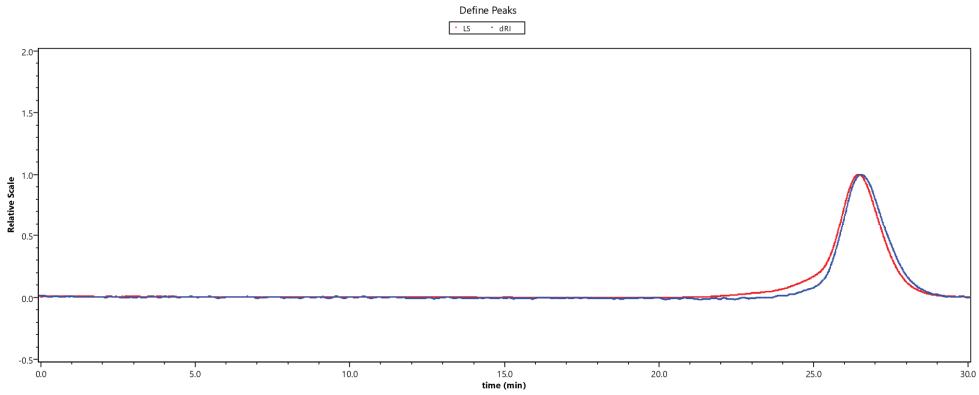

Figure S31. GPC trace of PDEVP **DP2** (100 equiv. DEVP). Measured via GPC-MALS in THF/H_2O.

General procedure for the removal of the pyrrole protection group

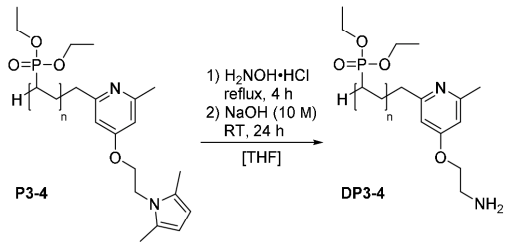

The decomposition of the pyrrole group was adopted from a published procedure.[5] Under argon atmosphere the pyrrole-bearing poly(vinylphosphonate) (1.00 equiv.) was dissolved in dry THF (10.0 mL per 150 mg polymer) and treated with triethylamine (20.0 equiv.) as well as hydroxylamine-hydrochloride (40.0 equiv.). The solution was heated under reflux for four hours, cooled to room temperature and treated with 10 M NaOH (20.0 equiv.). The reaction mixture was stirred for additional 24 hours at room temperature. The reaction was monitored via ^{1}H NMR spectroscopy until the quantitative conversion was able to be confirmed. The solvent was removed under reduced pressure and the crude product was dissolved in water. The purification was rendered via dialysis against water and the poly(vinylphosphonate) was obtained after lyophilization.

^{1}H-NMR (400 MHz, MeOD, 300 K): δ (ppm) = 6.78 – 6.49 (m, CH_{Ar}), 5.65 (s, residual signal of $CH_{Pyrrole}$), 4.18 (s, $POCH_2$), 2.98 – 1.08 (m, polymer backbone), 1.38 (s, $POCH_2CH_3$).

^{31}P-NMR (162 MHz, MeOD, 300 K): δ (ppm) = 33.1.

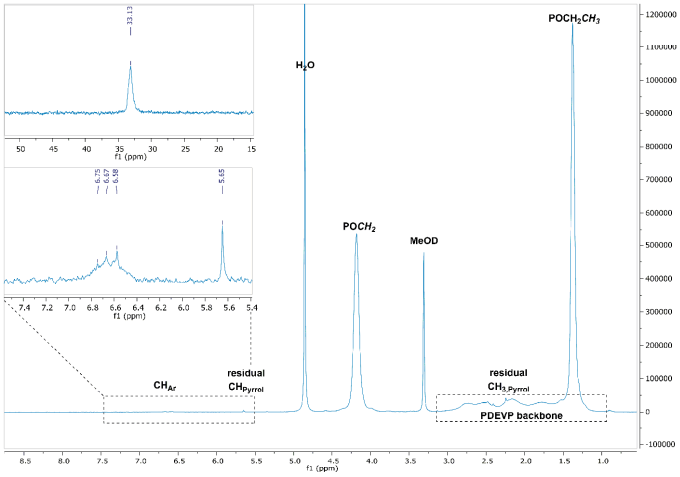

Figure S32. ^{1}H- and zoom of ^{31}P-NMR spectrum of PDEVP **DP3** (25 equiv. DEVP) in MeOD.

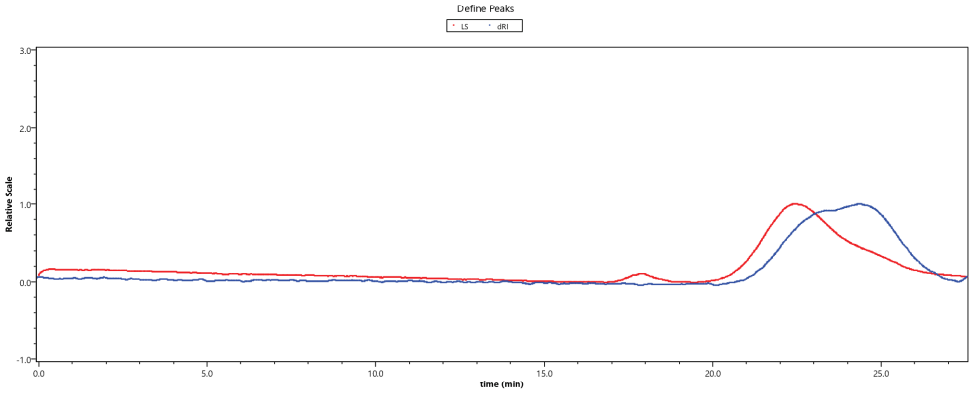

Figure S33. GPC trace of PDEVP **DP3** (25 equiv. DEVP). Measured via GPC-MALS in THF/H_2O.

^{1}H-NMR (500 MHz, MeOD, 300 K): δ (ppm) = 6.94 – 6.52 (m, CH_{Ar}), 4.18 (s, POCH_2), 2.96 – 1.16 (m, polymer backbone), 1.38 (s, $POCH_2CH_3$).

^{31}P-NMR (203 MHz, MeOD, 300 K): δ (ppm) = 33.2.

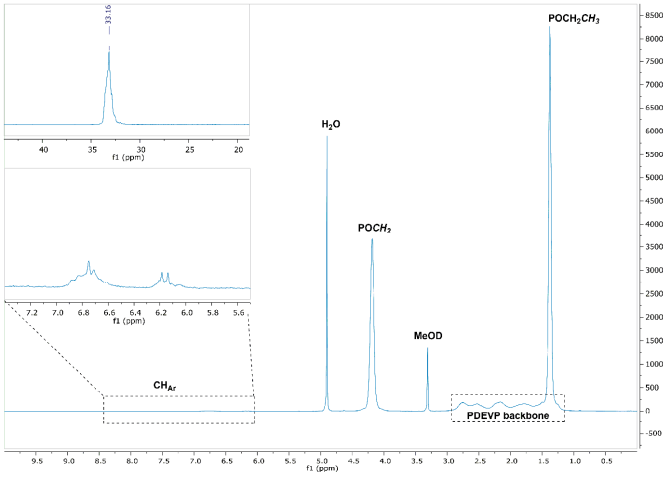

Figure S34. ^{1}H- and zoom of ^{31}P-NMR spectrum of PDEVP **DP4** (100 equiv. DEVP) in MeOD.

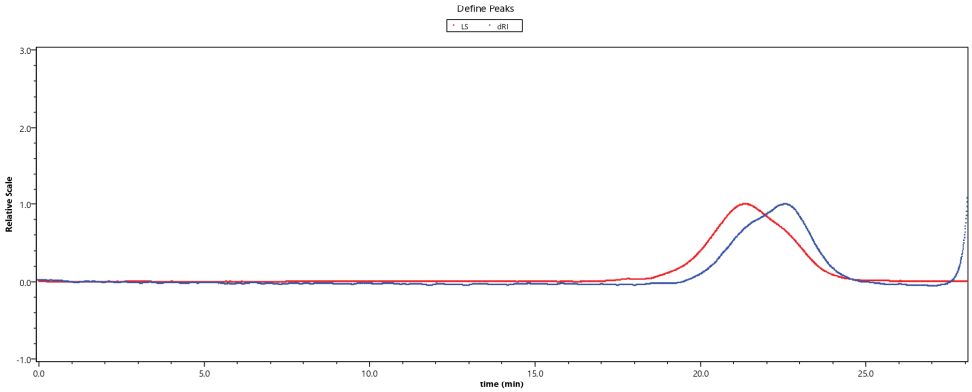

Figure S35. GPC trace of PDEVP **DP4** (100 equiv. DEVP). Measured via GPC-MALS in THF/H_2O (on the right the washing artifact is visible).

General procedure for the removal of the trityl protection group

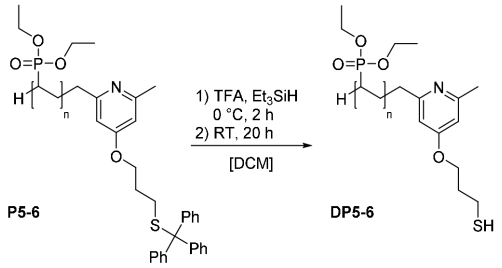

The experimental conditions were adopted in modified form from a procedure found in the literature.[6] Under argon atmosphere the trityl-protected poly(vinylphosphonate) (1.00 equiv.) was dissolved in dry DCM (10 mL per 200 mg polymer) and cooled to 0°C. At this temperature triethylsilane (10.0 equiv.) and trifluoroacetic acid (60.0 equiv.) were added and the mixture was stirred for two hours at 0°C and for 20 hours at room temperature. After the quantitative cleavage was confirmed by ^{1}H-NMR spectroscopy, volatiles were removed under reduced pressure and the residue was dissolved in a minimal amount of DCM. The polymer was precipitated in excess pentane, the supernatant solvent was decanted of and the crude polymer was dried at ambient temperature and dissolved in water. For the final purification the poly(vinylphosphonate) was dialyzed against water and freeze-dried.

^{1}H-NMR (400 MHz, MeOD, 300 K): δ (ppm) = 7.50 – 7.11 (m, CH_{Ar}), 4.46 (t, ^{3}J = 6.2 Hz, $CH_{2,Initiator}$), 4.19 (s, POCH_2), 2.92 – 1.21 (m, polymer backbone), 1.38 (s, POCH$_2CH_3$).

^{31}P-NMR (162 MHz, MeOD, 300 K): δ (ppm) = 33.1.

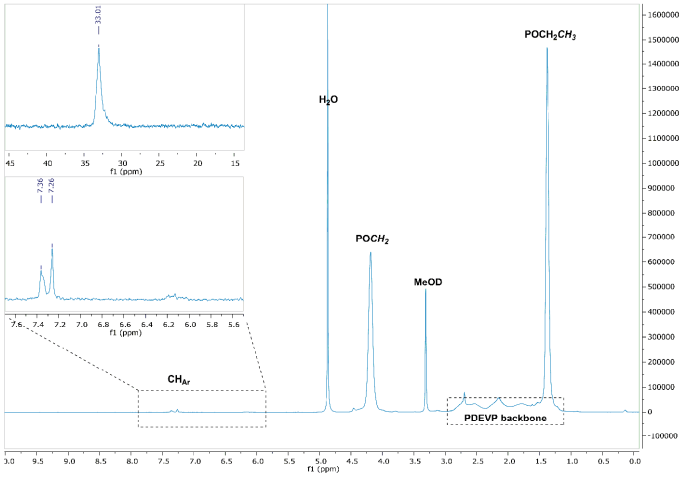

Figure S36. ^{1}H- and zoom of ^{31}P-NMR spectrum of PDEVP **DP5** (25 equiv. DEVP) in MeOD.

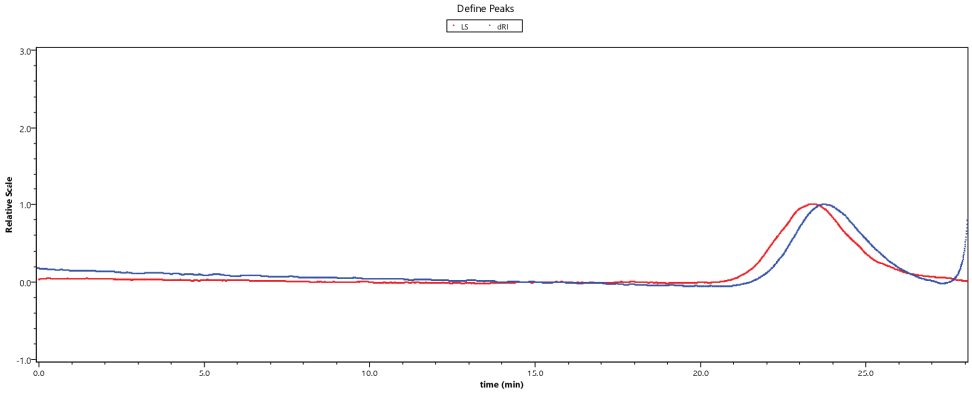

Figure S37. GPC trace of PDEVP **DP5** (25 equiv. DEVP). Measured *via* GPC-MALS in THF/H_2O (on the right the washing artifact is visible)

Detection of the thiol using *Ellman's* reagent

As blank sample 15.8 mg of 5,5'-dithiobis-(2-nitrobenzoic acid) (DTNB) (40.0 µmol) and two drops of triethylamine were dissolved in absolute ethanol (40.0 mL) to adjust a target concentration of 1.00 µmol mL^{-1}. Likewise, 15.0 mg of poly(vinylphosphonate) **DP5** (2.00 µol) were dissolved in absolute EtOH (2.00 mL) to adjust the target concentration of 1.00 µmol mL^{-1}. Absorption spectra were recorded of the blank sample (diluted to c_{DTNB} = 500 nM) and of the polymer

solution, treated with an equal volume of the DTNB solution (1.00 mL + 1.00 mL) to adjust the same concentration (c_{DP5} = c_{DTNB} = 500 nM).

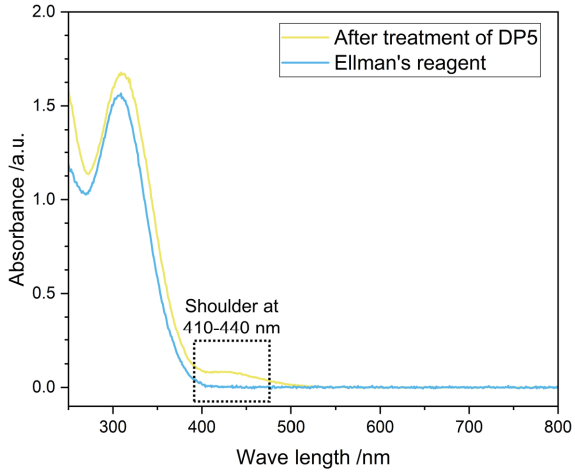

Figure S38. UV/Vis spectrum of DTNB (blue) and **DP5** after treatment with DTNB (yellow) in EtOH (c_{DP5} = c_{DTNB} = 500 nM).

^{1}H-NMR (500 MHz, MeOD, 300 K): δ (ppm) = 7.34 – 6.98 (m, CH_{Ar}), 4.18 (s, POCH_2), 2.95 – 1.09 (m, polymer backbone), 1.38 (s, POCH$_2$$CH_3$).

^{31}P-NMR (203 MHz, MeOD, 300 K): δ (ppm) = 33.2.

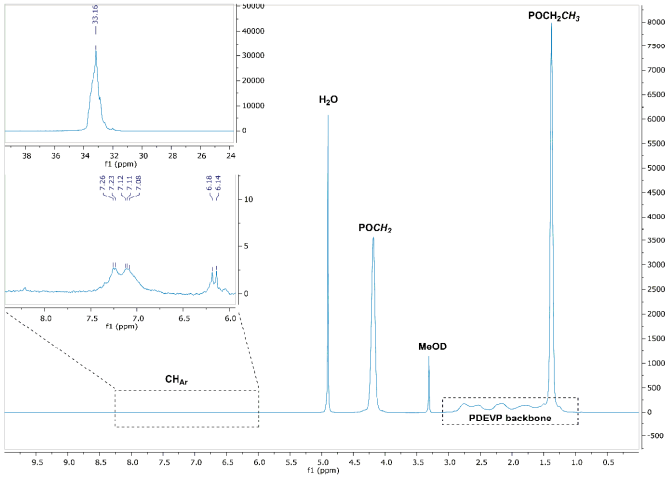

Figure S39. ^{1}H- and zoom of ^{31}P-NMR spectrum of PDEVP **DP6** (100 equiv. DEVP) in MeOD.

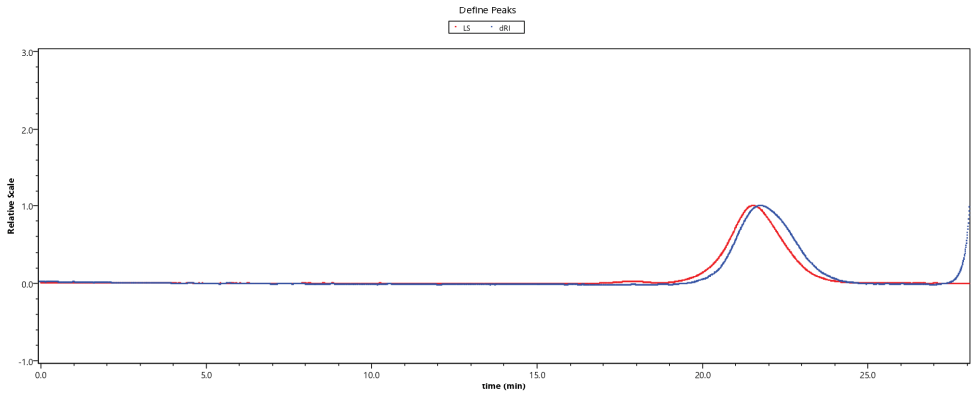

Figure S40. GPC trace of PDEVP **DP6** (100 equiv. DEVP). Measured *via* GPC-MALS in THF/H_2O (on the right the washing artifact is visible).

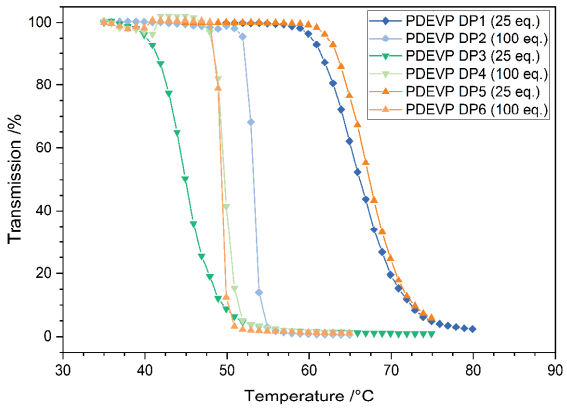

Figure S41. Determination of the LCST of the samples **DP1-DP6** in water (2.50 mg mL^{-1}). The cloud point was determined at 10% decrease of transmittance.

6. Refunctionalization of the polymers DP1, DP3 and DP5

Conversion of PDEVP DP1 with cholesteryl chloroformate

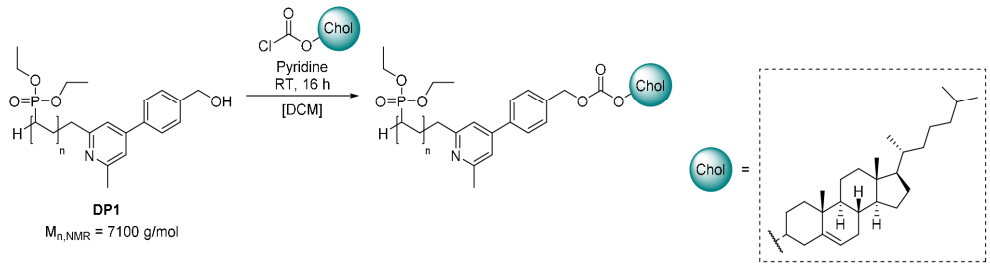

The experimental conditions were adopted in modified form from a procedure found in the literature.[7] Cholesteryl chloroformate (38.0 mg, 84.6 µmol, 6.00 equiv.) and pyridine (4.55 µL, 56.4 µmol, 4.00 equiv.) were added to a solution of **DP1** (100 mg, 14.1 µmol, 1.00 equiv.) in dry DCM (10 mL) under argon atmosphere and stirred for 16 hours at room temperature. The polymer was then precipitated in excess pentane, the solvent was decanted off and the crude polymer was purified by dialysis against water and lyophilized from water.

^{1}H-NMR (400 MHz, MeOD, 300 K): δ (ppm) = 5.35 (s, Chol), 4.18 (s, POCH_2), 2.88 – 1.15 (m, polymer backbone), 1.38 (s, POCH$_2CH_3$), 1.02 (s, $CH_{3,Chol}$), 0.95 (d, ^{3}J = 6.4 Hz, $CH_{3,Chol}$), 0.89 (s, $CH_{3,Chol}$), 0.87 (s, $CH_{3,Chol}$), 0.72 (s, Chol-CH_3).

^{31}P-NMR (162 MHz, MeOD, 300 K): δ (ppm) = 33.1.

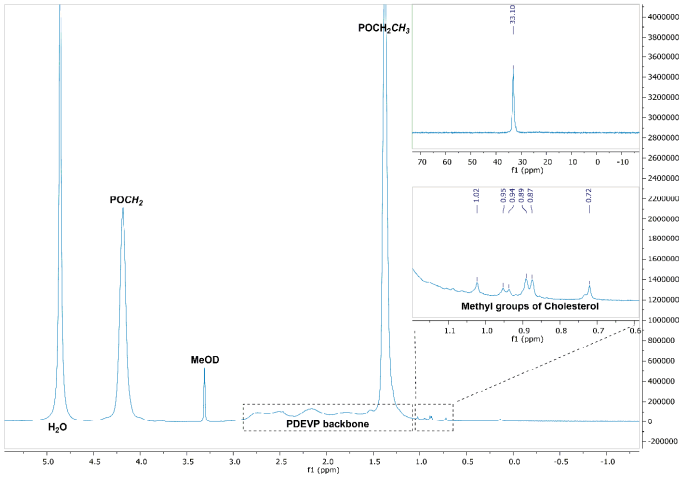

Figure S42. ^{1}H- and zoom of ^{31}P-NMR spectrum of PDEVP **DP1** (25 equiv. DEVP) in MeOD after conjugation of cholesteryl chloroformate.

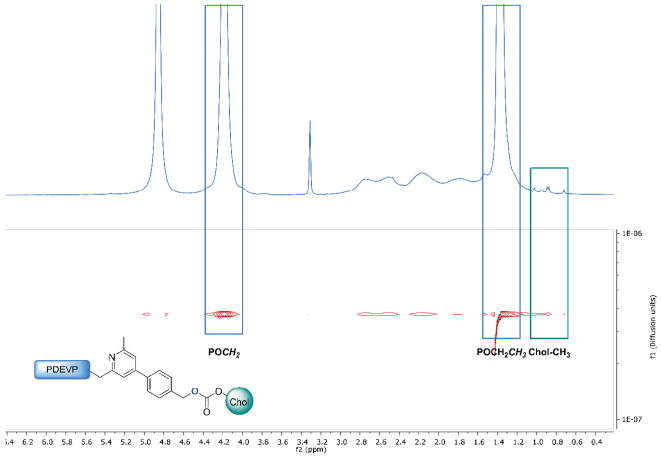

Figure S43. DOSY-NMR of PDEVP **DP1** (25 equiv. DEVP) after conjugation of cholesteryl chloroformate in MeOD.

Conversion of poly(vinylphosphonate) DP3 with cholesteryl chloroformate

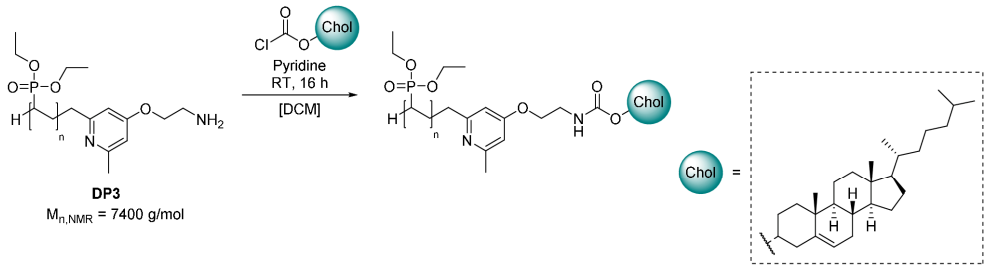

The procedure was adopted from a published procedure.[7] Cholesteryl chloroformate (36.4 mg, 81.1* µmol, 6.00 equiv.) and pyridine (4.35 µL, 54.1 µmol, 4.00 equiv.) were added to a solution of **DP3** (100 mg, 13.5 µmol, 1.00 equiv.) in dry DCM (10 mL) under an argon atmosphere and stirred for 16 hours at room temperature. The polymer was then precipitated in excess pentane, the solvent was decanted off and the crude polymer was purified by dialysis against water and lyophilized from water.

^{1}H-NMR (400 MHz, MeOD, 300 K): δ (ppm) = 5.35 (s, Chol), 4.18 (s, POCH_2), 2.88 – 1.17 (m, polymer backbone), 1.38 (s, POCH$_2$$CH_3$), 1.02 (s, $CH_{3,Chol}$), 0.95 (d, ^{3}J = 6.4 Hz, $CH_{3,Chol}$), 0.89 (d, ^{3}J = 6.6 Hz, $CH_{3,Chol}$), 0.88 (d, ^{3}J = 6.6 Hz, $CH_{3,Chol}$), 0.72 (s, $CH_{3,Chol}$).

^{31}P-NMR (162 MHz, MeOD, 300 K): δ (ppm) = 33.1.

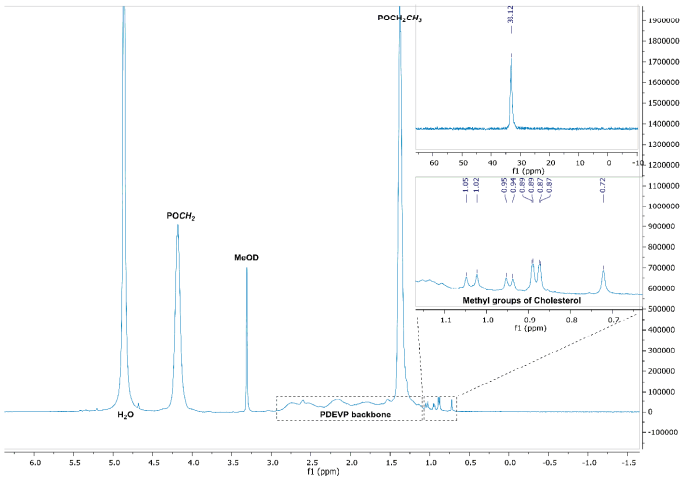

Figure S44. ^{1}H- and zoom of ^{31}P-NMR spectrum of PDEVP **DP3** (25 equiv. DEVP) in MeOD after conjugation of cholesteryl chloroformate.

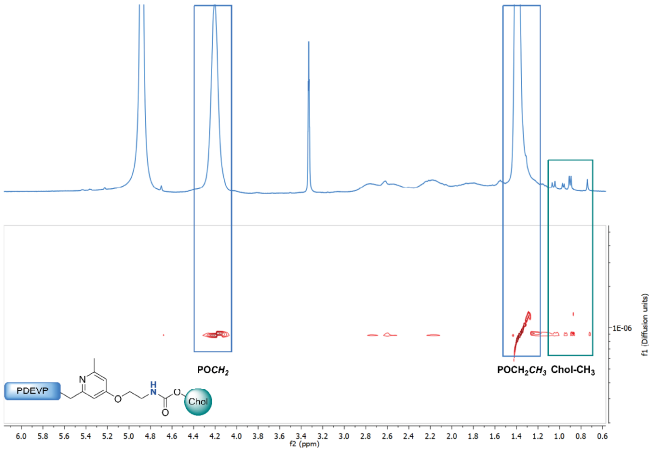

Figure S45. DOSY-NMR of PDEVP **DP3** (25 equiv. DEVP) after conjugation of cholesteryl chloroformate in MeOD.

***Michael* addition of poly(vinylphosphonate) DP5 to *N*-phenyl maleimide**

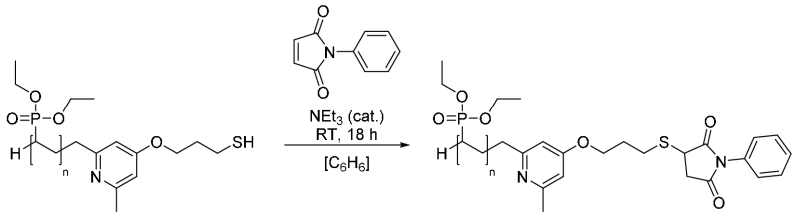

DP5
$M_{n,NMR}$ = 7500 g/mol

The procedure was adopted from a procedure found in the literature.[8] The deprotected poly(vinylphosphonate) **DP5** (100 mg, 13.3 µmol, 1.00 equiv.) was dissolved in benzene under an argon atmosphere. To the polymer solution *N*-phenyl maleimide (6.92 mg, 40.0 µmol, 3.00 equiv.) and a drop of triethylamine (catalyst) were added and the mixture was stirred for 18 hours at room temperature. The polymer was then precipitated in pentane, the solvent was decanted off and the polymer was freeze-dried from benzene to obtain die *Michael* adduct.

^{1}H-NMR (400 MHz, MeOD, 300 K): δ (ppm) = 7.61 – 7.16 (m, Phenyl), 4.19 (s, POCH_2), 2.97 – 1.05 (m, polymer backbone), 1.38 (s, POCH$_2CH_3$).

^{31}P-NMR (162 MHz, MeOD, 300 K): δ (ppm) = 33.1.

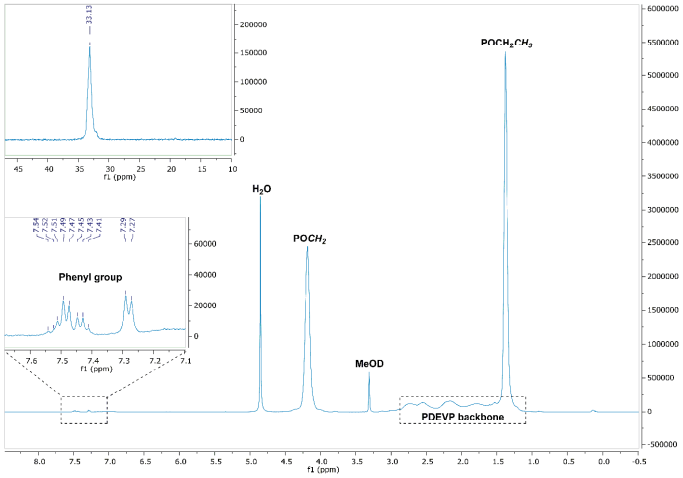

Figure S46. ^{1}H- and zoom of ^{31}P-NMR spectrum of PDEVP **DP5** (25 equiv. DEVP) after *Michael* addition to *N*-phenyl maleimide in MeOD.

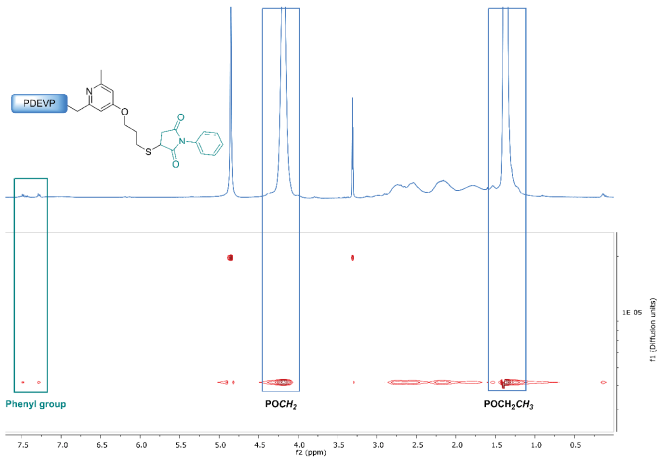

Figure S47. DOSY-NMR of PDEVP **DP5** (25 equiv. DEVP) after *Michael* addition to *N*-phenyl maleimide in MeOD.

7. References

1. Jacobi, N.; Lindel, T., Assembly of the Bis(imidazolyl)propene Core of Nagelamides C and S by Double Grignard Reaction. *European Journal of Organic Chemistry* **2010,** *2010* (28), 5415-5425.

2. Wang, Q.; Chen, S.; Liang, Y.; Dong, D.; Zhang, N., Bottle-Brush Brushes: Surface-Initiated Rare Earth Metal Mediated Group Transfer Polymerization from a Poly(3-((2,6-dimethylpyridin-4-yl)oxy)propyl methacrylate) Backbone. *Macromolecules* **2017,** *50* (21), 8456-8463.

3. Wathier, M.; Polidori, A.; Ruiz, K.; Fabiano, A.-S.; Pucci, B., Stabilization of polymerized vesicular systems: an application of the dynamic molecular shape concept. *Chemistry and Physics of Lipids* **2002,** *115* (1), 17-37.

4. Goodnow, R. A.; Hicks, A.; Sidduri, A.; Kowalczyk, A.; Dominique, R.; Qiao, Q.; Lou, J. P.; Gillespie, P.; Fotouhi, N.; Tilley, J.; Cohen, N.; Choudhry, S.; Cavallo, G.; Tannu, S. A.; Ventre, J. D.; Lavelle, D.; Tare, N. S.; Oh, H.; Lamb, M.; Kurylko, G.; Hamid, R.; Wright, M. B.; Pamidimukkala, A.; Egan, T.; Gubler, U.; Hoffman, A. F.; Wei, X.; Li, Y. L.; O'Neil, J.; Marcano, R.; Pozzani, K.; Molinaro, T.; Santiago, J.; Singer, L.; Hargaden, M.; Moore, D.; Catala, A. R.; Chao, L. C. F.; Hermann, G.; Venkat, R.; Mancebo, H.; Renzetti, L. M., Discovery of Novel and Potent Leukotriene B4 Receptor Antagonists. Part 1. *Journal of Medicinal Chemistry* **2010,** *53* (9), 3502-3516.

5. Macor, J. E.; Chenard, B. L.; Post, R. J., Use of 2,5-Dimethylpyrrole as an Amino-Protecting Group in an Efficient Synthesis of 5-Amino-3-[(N-methyl- pyrrolidin-2(R)-yl)methyl]indole. *The Journal of Organic Chemistry* **1994,** *59* (24), 7496-7498.

6. Trindade, A. F.; Frade, R. F. M.; Macoas, E. M. S.; Graca, C.; Rodrigues, C. A. B.; Martinho, J. M. G.; Afonso, C. A. M., "Click and go": simple and fast folic acid conjugation. *Organic & Biomolecular Chemistry* **2014,** *12* (20), 3181-3190.

7. Liu, J.-L.; Ma, Q.-P.; Huang, Q.-D.; Yang, W.-H.; Zhang, J.; Wang, J.-Y.; Zhu, W.; Yu, X.-Q., Cationic lipids containing protonated cyclen and different hydrophobic groups linked by uracil-PNA monomer: Synthesis and application for gene delivery. *European Journal of Medicinal Chemistry* **2011,** *46* (9), 4133-4141.

8. Jegelka, M.; Plietker, B., α-Sulfonyl Succinimides: Versatile Sulfinate Donors in Fe-Catalyzed, Salt-Free, Neutral Allylic Substitution. *Chemistry – A European Journal* **2011,** *17* (37), 10417-10430.

12.2 Supporting Information of the Manuscript "Precise Synthesis of Poly(dimethylsiloxane) Copolymers through C-H Bond Activated Macroinitiators in the Yttrium-Mediated Group Transfer Polymerization and Ring-Opening Polymerization"

Supporting Information for the Manuscript Entitled *Precise Synthesis of PDMS Copolymers through C-H Bond Activated Macroinitiators in the Yttrium-mediated Group Transfer Polymerization and Ring-Opening Polymerization*

Andreas Schaffer,[a] Moritz Kränzlein,[a] and Bernhard Rieger*[a]

[a] *WACKER-Chair of Macromolecular Chemistry, Catalysis Research Center, Technical University of Munich, Lichtenbergstraße 4, 85748 Garching near Munich, Germany. E-mail: rieger@tum.de*

Table of Contents

1. Material and Methods ... 2
2. Analysis of Initiator **3** in the C-H Bond Activation and Polymerization Process ... 3
2.1 Analysis of the C-H Bond Activation ... 3
2.2 End-group analysis of oligomeric PDEVP by ESI-MS ... 4
2.3 Studies on the living characters of the DEVP polymerization with the active species **5** ... 5
2.4 Polymerization of DEVP with Initiator **3** ... 5
3. Synthesis and Application of the Macroinitiators ... 9
3.1 Synthesis of the Macroinitiators ... 9
3.2 C-H Bond Activation of the Macroinitiators ... 16
4.3 Polymerization of DEVP using the Macroinitiators **MI1-3** ... 23
4.4 REM-GTP of 2VP and ROP of εCL with Macroinitiator **MI1** ... 34
4. Thermal and Size Analysis of the Copolymers ... 38
4.1 Characterization by Dynamic Light Scattering ... 38
4.2 Thermal Analysis by Differential Scanning Calorimetry ... 41
4.3 Thermoresponsive Behavior of Polymers **P1-P8** ... 46
4.4 Studies on the Structural Stability of the Copolymers ... 47

1. Material and Methods

Thin-Layer Chromatography (TLC)

Thin-layer chromatography was performed on silica coated aluminum plates (0.2 mm, F254) from *Macherey-Nagel*. The compounds were detected by UV-light (λ = 254 nm, 366 nm).

Column Chromatography

Purification via column chromatography was performed on silica gel (grain size: 60-200 µm) from *Acros Organics*. The eluent ratios are given for the corresponding procedures.

Turbidity Measurements

Turbidity measurements were performed on a Cary 50 UV-vis spectrophotometer (*Varian*). The cloud point of the aqueous polymer solutions was determined by spectrophotometric detection of the changes in transmittance at λ = 500 nm. The samples were heated/cooled at a rate of 1.0 K min^{-1} in steps of 1 K followed by a five minutes long period of constant temperature to ensure equilibration. The cloud point was defined as the temperature corresponding to a 10% decrease in optical transmittance.

Thermal Analysis via Differential Scanning Calorimetry

The thermal properties of the (co)polymers were analyzed with a Q2000 from *TA Instruments*. First, the samples were cooled to -150 °C (-50 °C in case of **P2**) and then heated or cooled at a rate of 10 K min^{-1} in alternating cycles (heating cycle: -150 °C to 100 °C/200 °C or -50 °C to 220 °C; cooling cycle: 100 °C/200 °C to -150 °C or 220 °C to -50 °C). The samples were kept at a constant temperature for one minute after reaching the end temperature of the respective cycle. The thermal properties were determined by analysis of the second cycle.

Analysis via Dynamic Light Scattering

DLS measurements were performed on Zetasizer Nano ZS from *Malvern*. The samples (2.5 mg mL^{-1}) were dissolved in water, THF, DMF, a mixture 50% THF and 50% water or hydrochloric acid (pH = 2).

2. Analysis of Initiator 3 in the C-H Bond Activation and Polymerization Process

2.1 Analysis of the C-H Bond Activation

***In situ* activated complex 5**

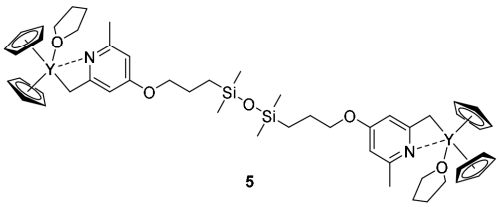

5

$C_{52}H_{74}N_2O_5Si_2Y_2$
1041.15 g/mol

Intense yellow color in solution.

^{1}H-NMR (400 MHz, C_6D_6, 300 K): δ (ppm) = 6.23 (s, 3H, Cp), 6.17 (d, ^{4}J = 2.2 Hz, 2H. $CH_{Pyridine}$), 6.07 (s, 17H, Cp), 6.04 (d, ^{4}J = 2.2 Hz, 2H, $CH_{Pyridine}$), 3.70 (t, ^{3}J = 6.7 Hz, 4H, CH_2O), 3.54 – 3.36 (m, 13H, 1.6 x THF), 2.34 (s, 4H, CH_2Y), 2.02 (s, 6H, $CH_{3,Pyridine}$), 1.79 – 1.66 (m, 4H, CH_2), 1.36 – 1.20 (m, 13H, 1.6 x THF), 0.66 – 0.49 (m, 4H, $SiCH_2$), 0.10 (s, 12H, $SiCH_3$).

^{13}C-NMR (101 MHz, C_6D_6, 300 K): δ (ppm) = 169.6 (s, C_{Ar}), 166.8 (s, C_{Ar}), 158.4 (s, C_{Ar}), 111.6 (s, Cp), 110.5 (s, Cp), 101.9 (s, C_{Ar}), 98.2 (s, C_{Ar}), 69.8 (s, CH_2O), 69.5 (s, THF), 41.19 (d, J_{CY} = 12.6 Hz), 25.6 (s, THF), 23.9 (s, $CH_{3,Pyridine}$), 23.4 (s, CH_2), 14.5 (s, $SiCH_2$), 0.5 (s, $SiCH_3$).

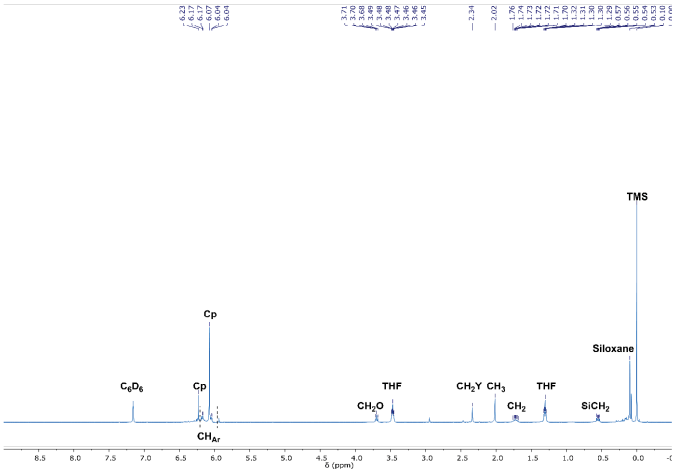

Figure S1. ^{1}H-NMR spectrum of complex **5** in C_6D_6.

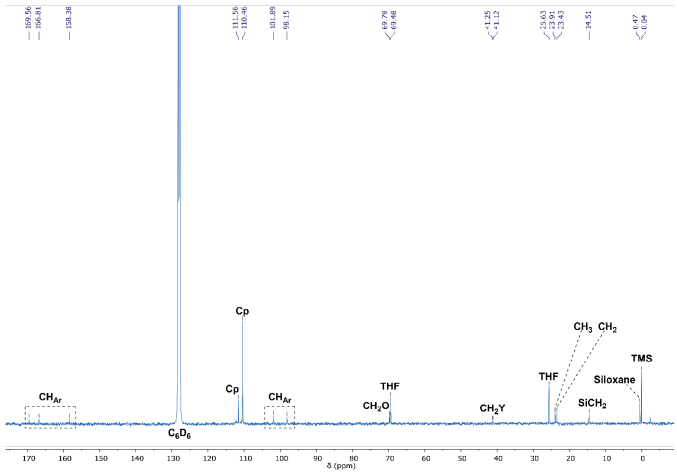

Figure S2. ^{13}C-NMR spectrum of complex **5** in C_6D_6.

2.2 End-group analysis of oligomeric PDEVP by ESI-MS

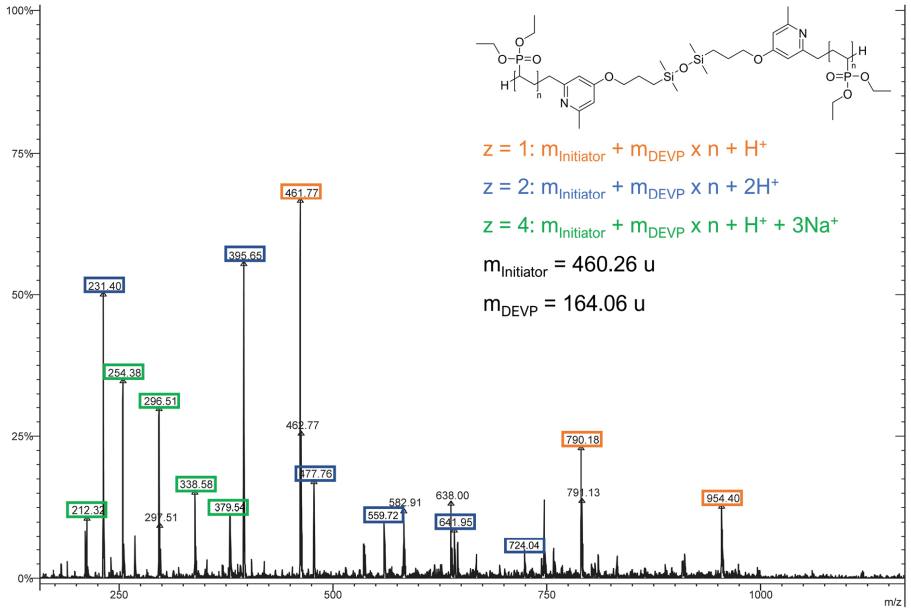

Figure S3. Oligomer pattern of PDEVP generated with active species **5**. ESI-MS measured in LC-MS acetonitrile.

2.3 Studies on the living characters of the DEVP polymerization with the active species 5

A solution of initiator **3** (10.9 µmol, 1.00 equiv.) in absolute toluene (5.00 mL) was added to a solution of 21.7 µmol $Cp_2Y(CH_2TMS)(THF)$ (**4**) (8.21 mg, 2.00 equiv.) in 5.00 mL toluene resulting in the instant coloration of the solution. The mixture was stirred overnight and the quantitative conversion of the C-H bond activation was confirmed by proton NMR. DEVP (2.13 g, 13.0 mmol, 600 equiv.) was added in one portion and aliquots were taken at regular time intervals, which were quenched by pouring into MeOD. The conversion of DEVP was monitored by ^{31}P-NMR spectroscopy, while the molecular weights M_n and polydispersities $Đ$ of each polymer sample were determined via GPC-MALS after removal of the solvent.

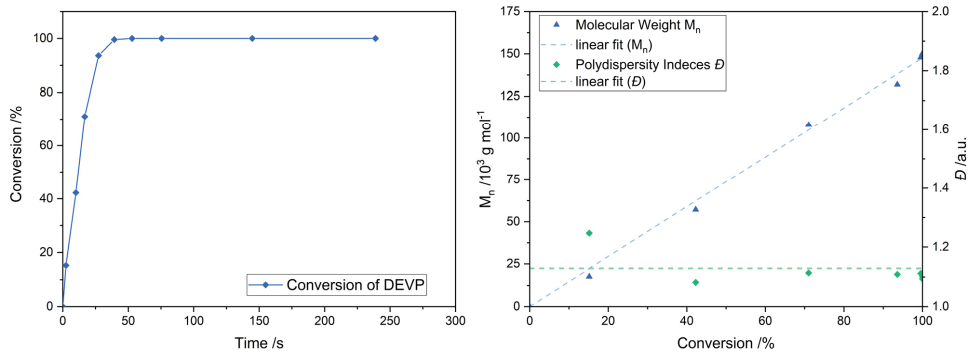

Figure S4. Conversion-time plot (left) and corresponding conversion-dependent plot of the molecular weights M_n and the corresponding polydispersities $Đ$ of PDEVP generated with species **5** (right).

2.4 Polymerization of DEVP with Initiator 3

Characterization of poly(diethyl vinylphosphonates) P1-P2

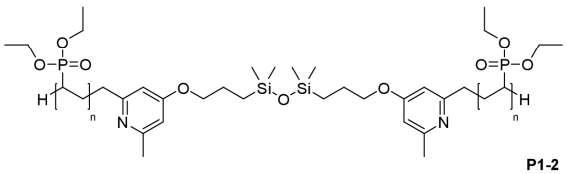

P1-2

^{1}H-NMR (400 MHz, MeOD, 300 K): δ (ppm) = 6.89 – 6.50 (m, $CH_{Pyridine}$), 4.18 (s, $POCH_2$), 2.93 – 1.18 (m, PDEVP backbone), 1.38 (s, $POCH_2CH_3$), 0.72 – 0.64 (m, $SiCH_2$), 0.26 – -0.15 (m, $SiCH_3$).

^{31}P-NMR (203 MHz, MeOD, 300 K): δ (ppm) = 33.2.

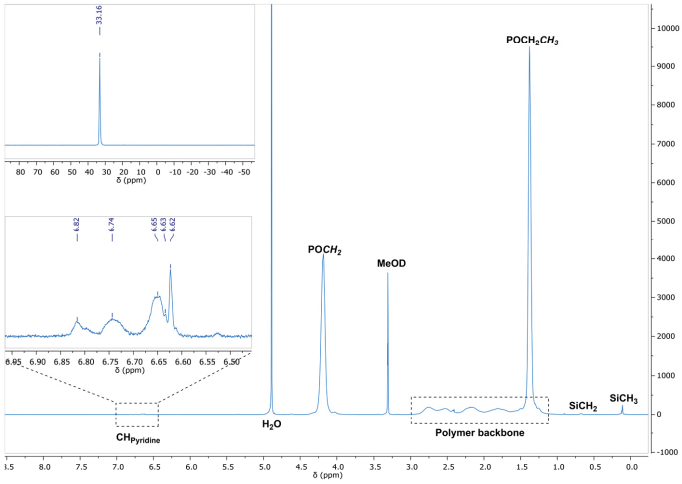

Figure S5. ^{1}H- and zoom of the ^{31}P-NMR spectrum of PDEVP **P1** (200 equiv. DEVP) in MeOD.

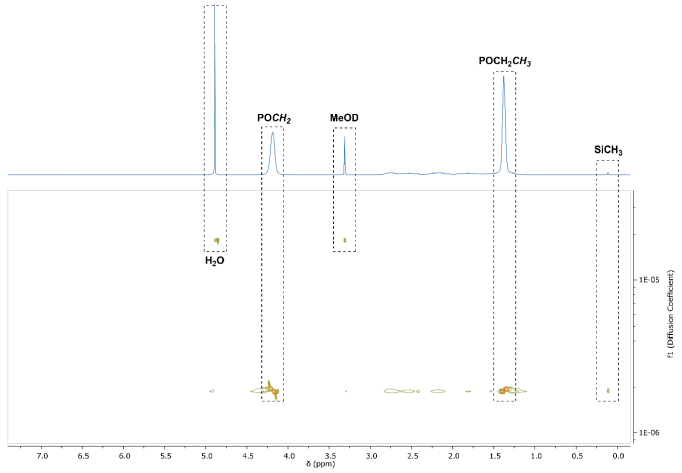

Figure S6. DOSY-NMR of PDEVP **P1** (200 equiv. DEVP) in MeOD.

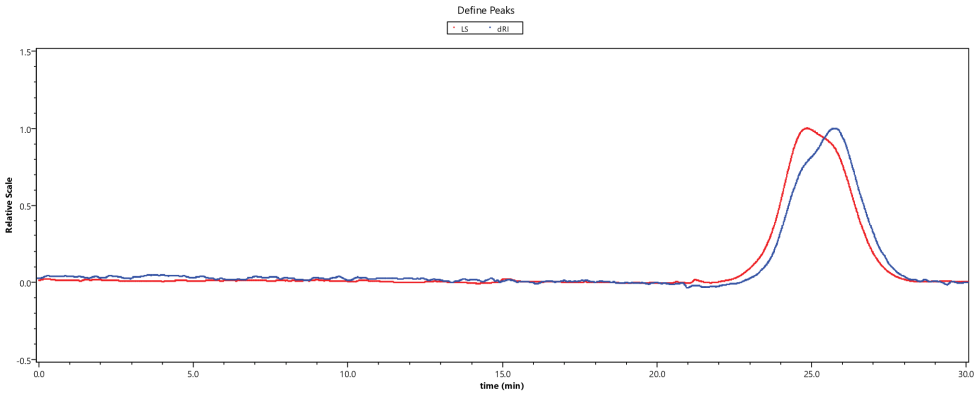

Figure S7. GPC trace of PDEVP **P1** (200 equiv. DEVP) generated with species **5**. Measured via GPC-MALS in THF/H_2O.

^{1}H-NMR (500 MHz, MeOD, 300 K): δ (ppm) = 6.87 – 6.50 (m, $CH_{Pyridine}$), 4.18 (s, POCH_2), 2.92 – 1.21 (m, PDEVP backbone), 1.38 (s, POCH$_2CH_3$), 0.77 – 0.56 (m, $SiCH_2$), 0.27 – 0.05 (m, $SiCH_3$).

^{31}P-NMR (203 MHz, MeOD, 300 K): δ (ppm) = 33.2.

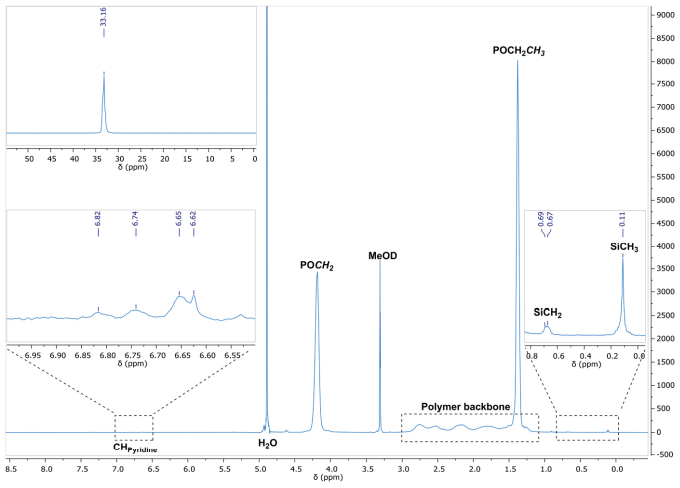

Figure S8. ^{1}H- and zoom of the ^{31}P-NMR spectrum of PDEVP **P2** (600 equiv. DEVP) in MeOD.

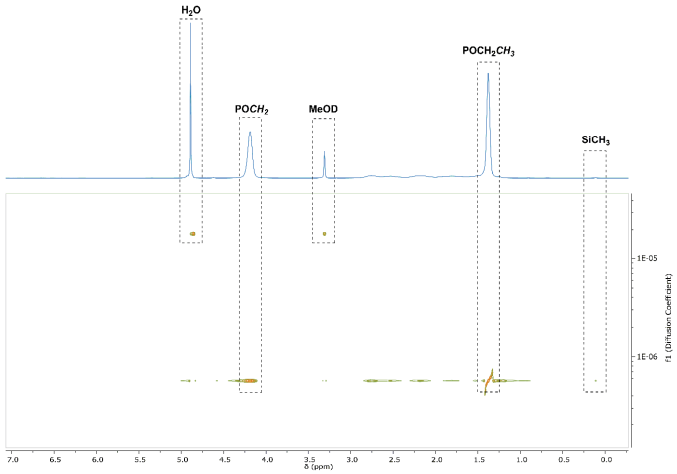

Figure S9. DOSY-NMR of PDEVP **P2** (600 equiv. DEVP) in MeOD.

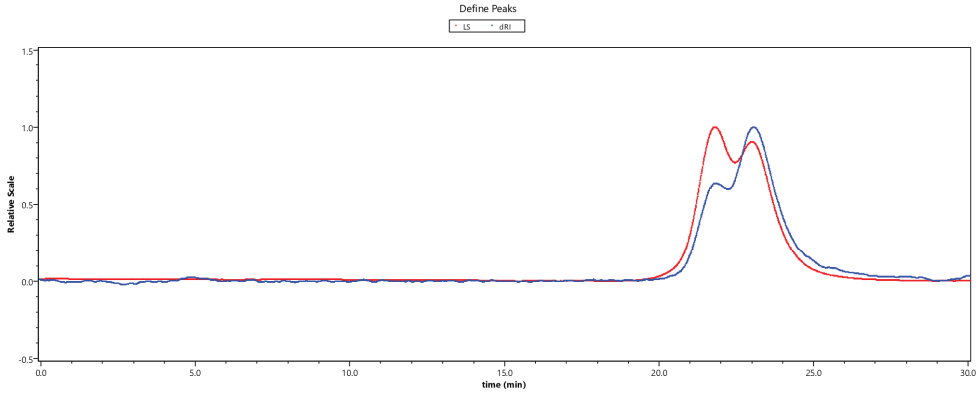

Figure S10. GPC trace of PDEVP **P2** (600 equiv. DEVP) generated with species **5**. Measured via GPC-MALS in THF/H_2O.

3. Synthesis and Application of the Macroinitiators

3.1 Synthesis of the Macroinitiators

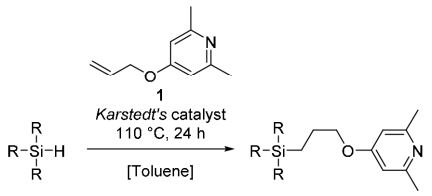

R = OPDMS or CH_3

General synthesis procedure for the linear macroinitiators. The respective amount of 4-(allyloxy)-2,6-dimethylpyridine (**1**) (3.00 equiv. per Si-H bond) was dissolved in absolute toluene (10 mL per 1.00 g of PDMS) and treated with the PDMS substrate (1.00 equiv.). Catalytic amounts of *Karstsedt's* catalyst were added, and the reaction mixture was heated to 110 °C and stirred for 24 hours. The progress of the reaction was checked by ^{1}H-NMR spectroscopy. If the conversion did not reach 100%, 3.00 equivalents of allyl compound **1** as well as new catalyst were added and the solution was stirred for another 24 hours at 110 °C. Hereafter, the reaction was terminated by evaporation of the solvent in high vacuum and removal of the excess allyl compound by recondensation. The residue was dissolved in pentane, treated with activated charcoal and filtrated through *Celite*. Volatiles were removed again, the PDMS residue put under argon, dried in high vacuum at 80 °C for several hours and stored over molecular sieves (3 Å) in a glove box.

General synthesis procedure for the side-group modified macroinitiator. The respective amount of 4-(allyloxy)-2,6-dimethylpyridine (**1**) (3.00 equiv. per Si-H bond) was dissolved in absolute toluene (10 mL per 200 mg of PDMS) and treated with the PDMS substrate (1.00 equiv.). Catalytic amounts of *Karstsedt's* catalyst were added, and the reaction mixture was heated to 110 °C and stirred for 24 hours. The progress of the reaction was checked by ^{1}H-NMR spectroscopy. If the conversion did not reach 100%, 3.00 equivalents of allyl compound **1** as well as new catalyst were added and the solution was stirred for another 24 hours at 110 °C. Hereafter, the reaction was terminated by evaporation of the solvent in high vacuum and removal of the excess allyl compound by recondensation. The residue was dissolved in diethyl ether, treated with activated charcoal and filtrated through *Celite*. Volatiles were removed again, the residue was put under argon, dried in high vacuum at 80 °C for several hours and stored over molecular sieves (3 Å) in a glove box.

Macroinitiator MI1

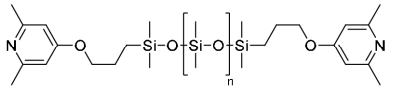

MI1: $M_{n,PDMS}$ = 6000 g mol^{-1}

^{1}H-NMR (400 MHz, C_6D_6, 300 K): δ (ppm) = 6.42 (s, $CH_{Pyridine}$), 3.60 (t, ^3J = 6.7 Hz, CH_2O), 2.47 (s, CH_3), 1.83 – 1.67 (m, CH_2), 0.67 – 0.59 (m, $SiCH_2$), 0.28 (s, PDMS).

^{13}C-NMR (101 MHz, C_6D_6, 300 K): δ (ppm) = 166.2 (s, C_{Ar}), 159.5 (s, C_{Ar}), 106.7 (s, C_{Ar}), 69.9 (s, CH_2O), 24.8 (s, CH_3), 23.4 (s, CH_2), 14.5 (s, $SiCH_2$), 1.43 (PDMS).

^{29}Si-NMR (99 MHz, C_6D_6, 300 K): δ (ppm) = 21.8.

EA: calculated: C 34.59 H 8.20 N 0.44
found: C 34.15 H 8.37 N 0.43

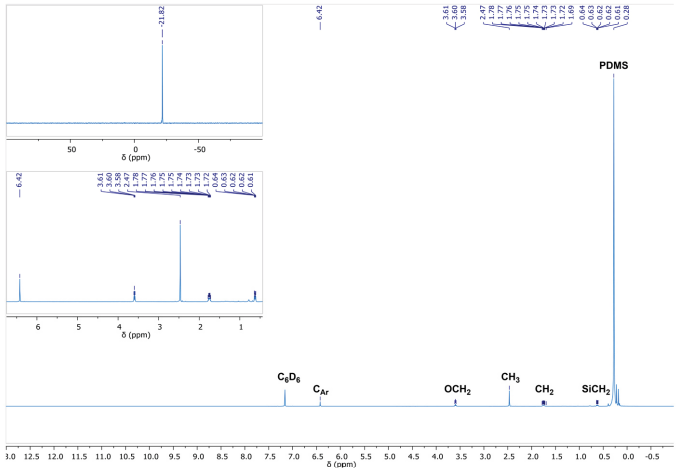

Figure S11. ^{1}H-NMR spectrum with zoomed-in region and ^{29}Si-NMR spectrum of macroinitiator **MI1** in C_6D_6.

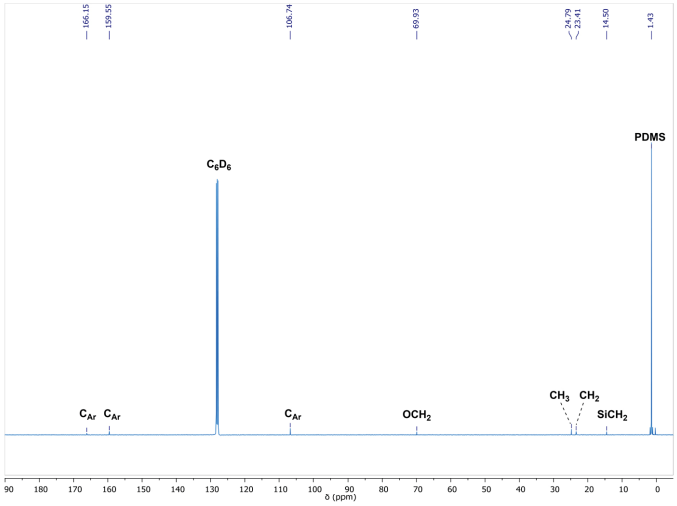

Figure S12. ^{13}C-NMR spectrum of macroinitiator **MI1** in C_6D_6.

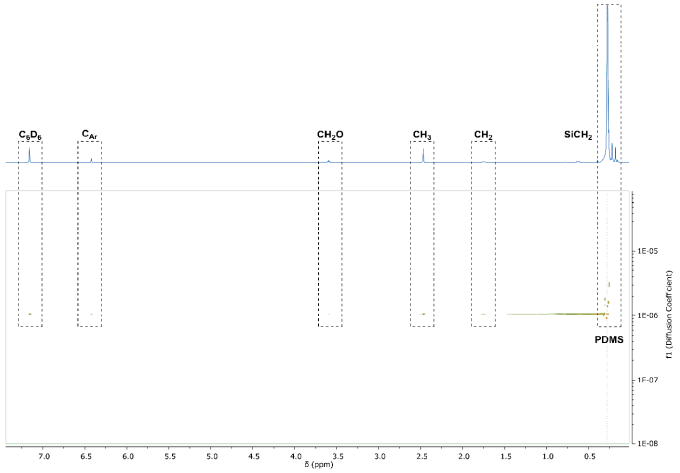

Figure S13. DOSY-NMR spectrum of macroinitiator **MI1** in C_6D_6.

Macroinitiator MI2

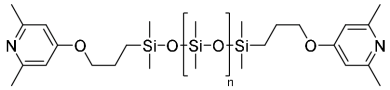

MI2: $M_{n,PDMS}$ = 17500 g mol^{-1}

^{1}H-NMR (400 MHz, C_6D_6, 300 K): δ (ppm) = 6.44 (s, $CH_{Pyridine}$), 3.61 (t, ^3J = 6.6 Hz, CH_2O), 2.48 (s, CH_3), 1.89 – 1.70 (m, CH_2), 0.67 – 0.60 (m, $SiCH_2$), 0.29 (s, PDMS).

^{13}C-NMR (101 MHz, C_6D_6, 300 K): δ (ppm) = 166.1 (s, C_{Ar}), 159.6 (s, C_{Ar}), 106.7 (s, C_{Ar}), 69.9 (s, CH_2O), 24.8 (s, CH_3), 23.4 (s, $SiCH_2$), 14.5 (s, CH_2), 1.43 (s, PDMS).

^{29}Si-NMR (99 MHz, C_6D_6, 300 K): δ (ppm) = -21.8.

EA:	calculated:	C 33.00	II 8.17	N 0.12
	found:	C 33.26	H 8.33	N 0.12

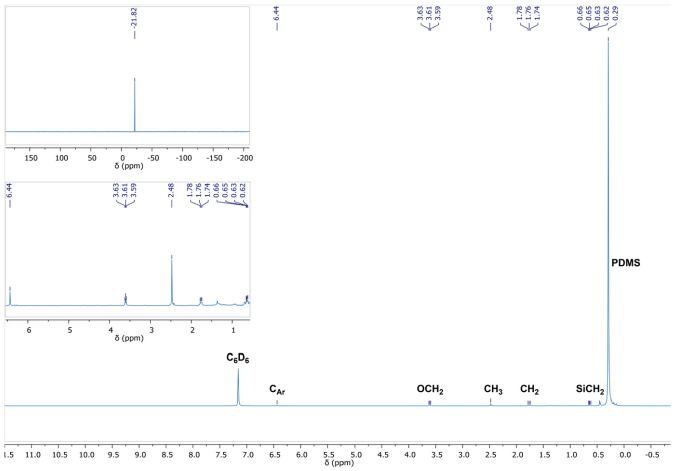

Figure S14. ^{1}H-NMR spectrum with zoomed-in region and ^{29}Si-NMR spectra of macroinitiator **MI2** in C_6D_6.

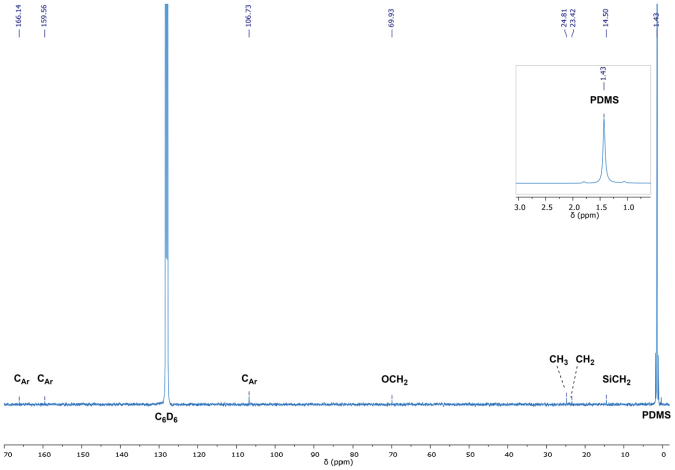

Figure S15. ^{13}C-NMR spectrum of macroinitiator **MI2** in C_6D_6.

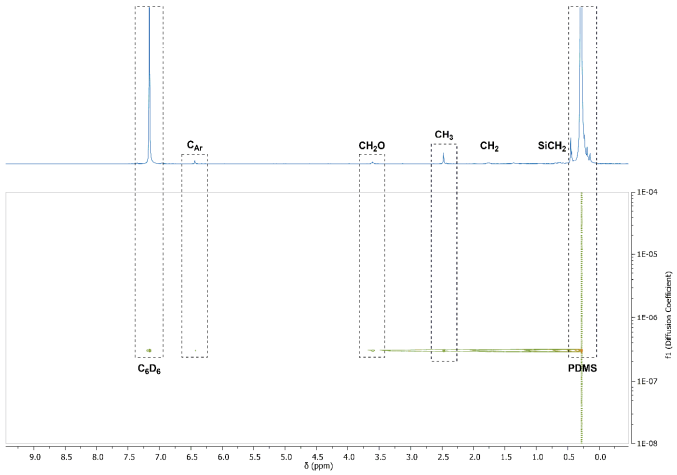

Figure S16. DOSY-NMR spectrum of macroinitiator **MI2** in C_6D_6.

Macroinitiator MI3

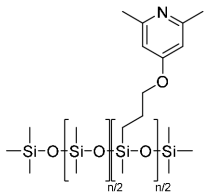

MI3: $M_{n,PDMS}$ = 950 g mol^{-1}; Si-H = 50 mol-%

^{1}H-NMR (400 MHz, C_6D_6, 300 K): δ (ppm) = 6.43 (br s, 9.2H, $CH_{Pyridine}$), 3.70 (br s, 9.1H, CH_2O), 2.48 (s, 30.8H, CH_3), 1.93 (br s, 9.2H, CH_2), 0.79 (br s, 10.6H, $SiCH_2$), 0.42 – 0.12 (m, 70.8H, PDMS).

^{13}C-NMR (101 MHz, C_6D_6, 300 K): δ (ppm) = 166.0 (s, C_{Ar}), 159.6 (s, C_{Ar}), 106.7 (s, C_{Ar}), 69.7 (s, CH_2O), 24.8 (s, CH_3), 23.3 (s, CH_2), 13.9 (s, $SiCH_2$), 2.55 – 0.69 (m, PDMS).

^{29}Si-NMR (99 MHz, C_6D_6, 300 K): δ (ppm) = -20.4 – -23.3 (m).

EA:	calculated:	C 49.84	H 8.08	N 3.92
	found:	C 48.51	H 7.91	N 3.89

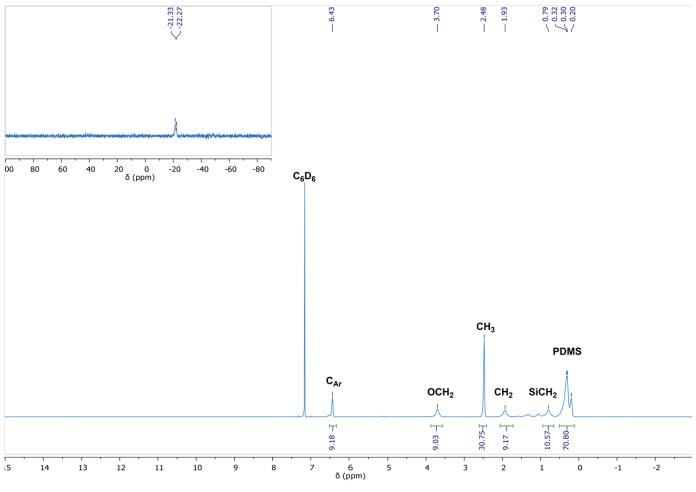

Figure S17. ^{1}H-NMR spectrum and ^{29}Si-NMR spectrum of macroinitiator **MI3** in C_6D_6.

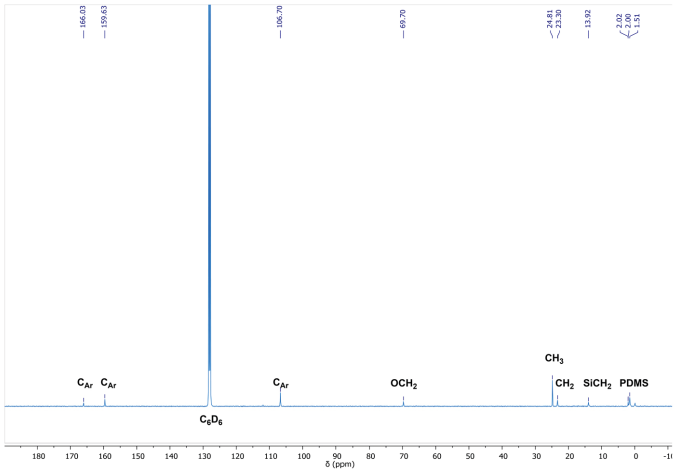

Figure S18. ^{13}C-NMR spectrum of macroinitiator **MI3** in C_6D_6.

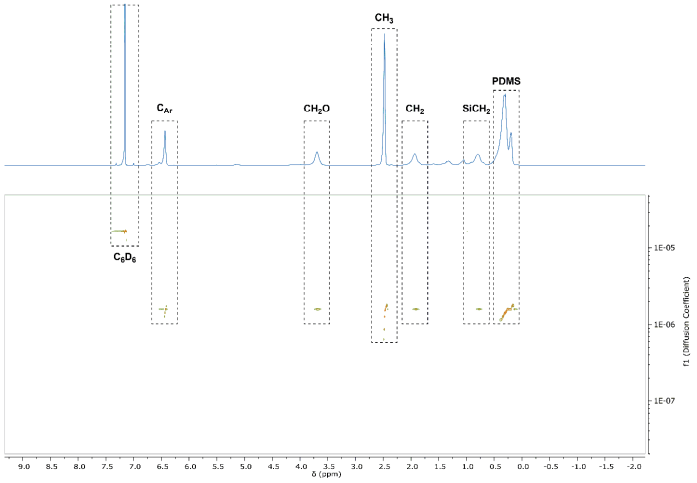

Figure S19. DOSY-NMR spectrum of macroinitiator **MI3** in C_6D_6.

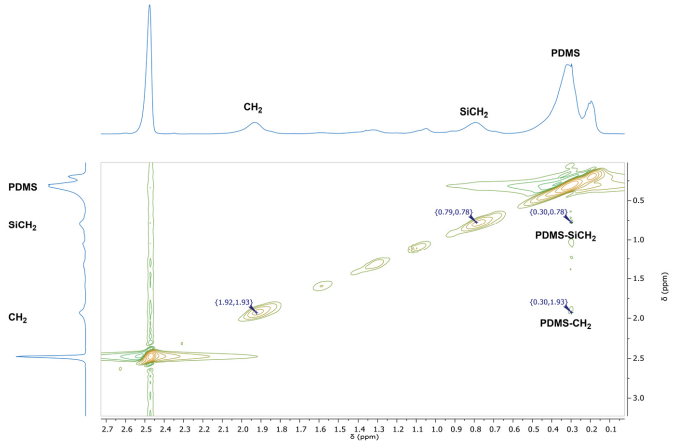

Figure S20. Zoomed-in region of the COSY-NMR spectrum of macroinitiator **MI3** in C_6D_6.

3.2 C-H Bond Activation of the Macroinitiators

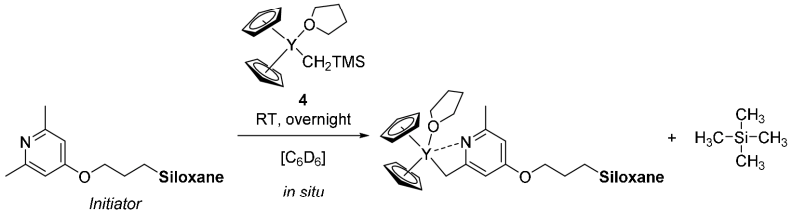

Table S1. Composition of the C-H bond activation experiments with macroinitiators **MI1-MI3**

Initiator	$m_{Initiator}$ /mg	$n_{Initiator}$ /µmol	$n_{Pyridiyl}$[a] /µmol	$m_{Catalyst}$ /mg	$n_{Catalyst}$ /µmol	Equivalents[a] /-	$V_{Benzene\text{-}d6}$ /mL
MI1	297	47.0	93.9	35.9	93.9	2.00	4.00
MI2	473	26.6	46.8	17.7	46.8	1.76	4.00
MI3	51.2	29.2	144	54.4	144	4.92	4.00

[a]Adjusted to the amount of pyridyl units being present in the ^{1}H-NMR spectrum.

***In situ* activated complex 4 with MI1**

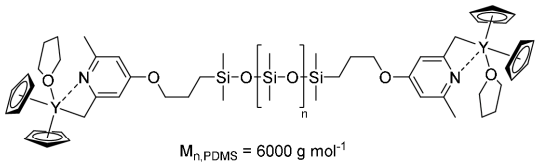

^{1}H-NMR (400 MHz, C_6D_6, 300 K): δ (ppm) = 6.36 (s, Cp), 6.17 (d, ^4J = 2.4 Hz, $CH_{Pyridine}$), 6.05 (s, Cp), 6.03 (d, ^4J = 2.4 Hz, $CH_{Pyridine}$), 3.70 (t, ^3J = 6.7 Hz, CH_2O), 3.53 – 3.46 (m, THF), 2.28 (s, CH_2Y), 2.06 (s, CH_3), 1.80 – 1.71 (m, CH_2O), 1.39 – 1.30 (m, THF), 0.65 – 0.56 (m, $SiCH_2$), 0.28 (s, PDMS).

^{13}C-NMR (101 MHz, C_6D_6, 300 K): δ (ppm) = 169.6 (s, C_{Ar}), 166.8 (s, C_{Ar}), 158.5 (s, C_{Ar}), 112.0 (s, Cp), 110.3 (s, Cp), 101.8 (s, C_{Ar}), 97.8 (s, C_{Ar}), 69.8 (s, CH_2O), 69.0 (s, THF), 41.1 (d, J_{CY} = 12.7 Hz, CH_2Y), 25.7 (s, THF), 23.9 (s, $CH_{3,Pyridine}$), 23.4 (s, CH_2), 14.5 (s, $SiCH_2$), 1.43 (s, PDMS).

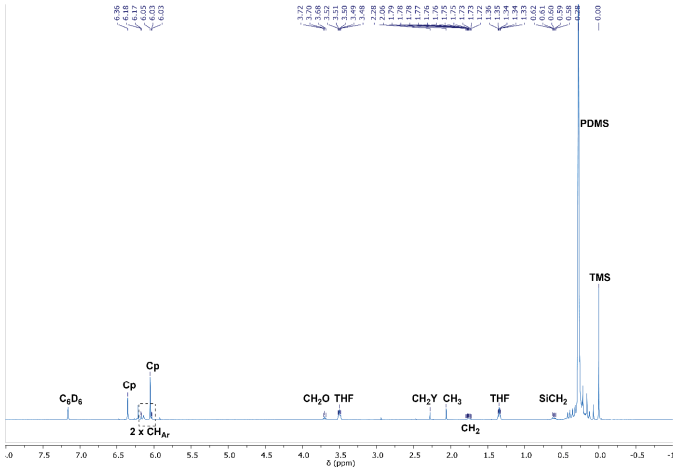

Figure S21. ^{1}H-NMR spectrum of **MI1** after treatment with $Cp_2Y(CH_2TMS)(THF)$ in C_6D_6.

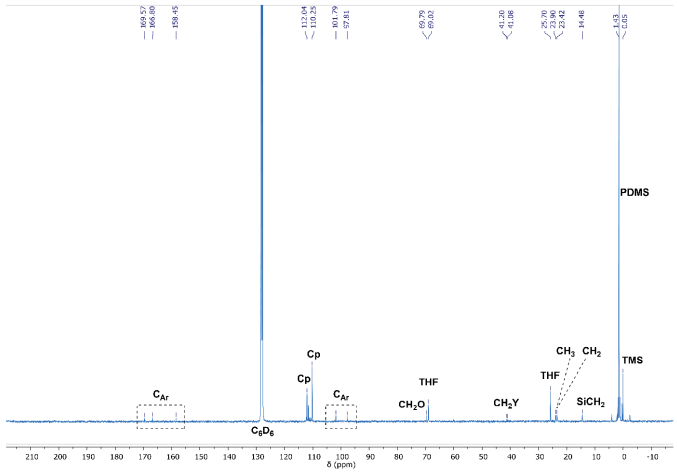

Figure S22. ^{13}C-NMR spectrum of **MI1** after treatment with $Cp_2Y(CH_2TMS)(THF)$ in C_6D_6.

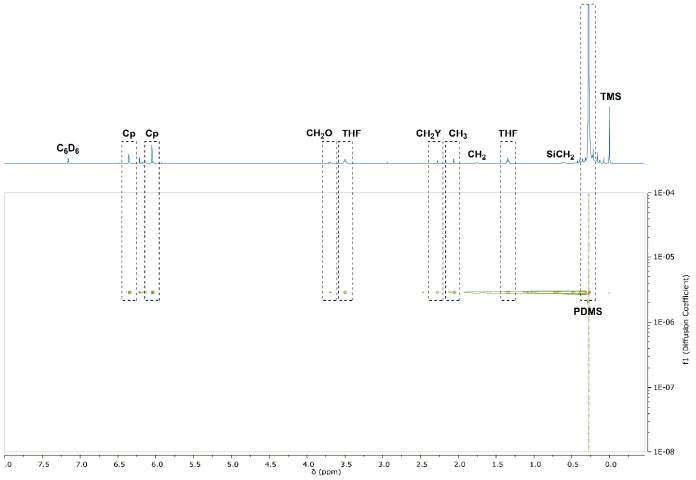

Figure S23. DOSY-NMR spectrum of **MI1** after treatment with $Cp_2Y(CH_2TMS)(THF)$ in C_6D_6.

***In situ* activated complex 4 with MI2**

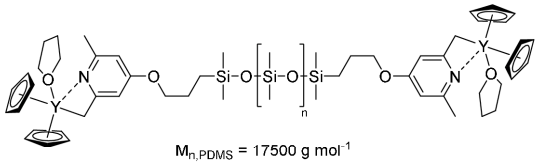

$M_{n,PDMS}$ = 17500 g mol^{-1}

^{1}H-NMR (400 MHz, C_6D_6, 300 K): δ (ppm) = 6.35 (s, Cp), 6.17 (d, ^4J = 2.7 Hz, $CH_{Pyridine}$), 6.04 (s, Cp), 6.01 (d, ^4J = 2.7 Hz, $CH_{Pyridine}$), 3.69 (t, ^3J = 6.7 Hz, CH_2O), 3.58 – 3.46 (m, THF), 2.28 (s, CH_2Y), 2.03 (s, $CH_{3,Pyridine}$), 1.75 (*virt*. p, ^3J = 6.6 Hz, CH_2), 1.42 – 1.35 (m, THF), 0.63 – 0.56 (m, $SiCH_2$), 0.27 (s, PDMS).

^{13}C-NMR (101 MHz, C_6D_6, 300 K): δ (ppm) 166.8 (s, C_{Ar}), 158.4 (s, C_{Ar}), 112.0 (s, Cp), 110.3 (s, Cp), 101.8 (s, C_{Ar}), 98.0 (s, C_{Ar}), 69.8 (s, CH_2O), 68.6 (s, THF), 25.8 (s, THF), 23.9 (s, $CH_{3,Pyridine}$), 23.4 (s, CH_2), 14.5 (s, $SiCH_2$), 1.43 (s, PDMS).

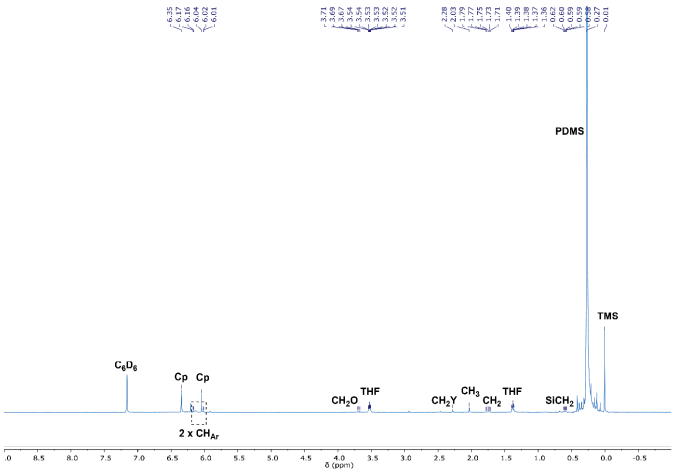

Figure S24. ^{1}H-NMR spectrum of **MI2** after treatment with $Cp_2Y(CH_2TMS)(THF)$ in C_6D_6.

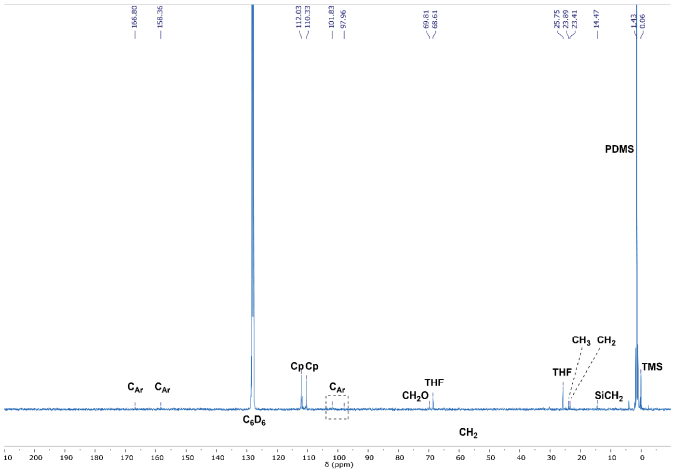

Figure S25. ^{13}C-NMR spectrum of **MI2** after treatment with $Cp_2Y(CH_2TMS)(THF)$ in C_6D_6.

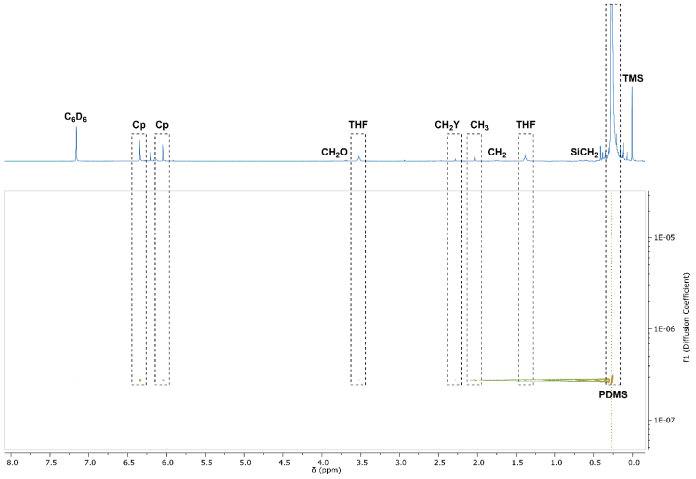

Figure S26. DOSY-NMR spectrum of **MI2** after treatment with $Cp_2Y(CH_2TMS)(THF)$ in C_6D_6.

***In situ* activated complex 4 with MI3**

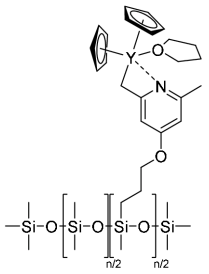

$M_{n,PDMS}$ = 950 g mol^{-1}

^{1}H-NMR (400 MHz, C_6D_6, 300 K): δ (ppm) = 6.52 – 6.01 (m, 60H, $CH_{Pyridine}$, Cp), 3.80 (br s, 9.4H, CH_2O), 3.49 (br s, 22H, THF), 2.63 – 2.14 (m, 25.6H, CH_2Y, $CH_{3,Pyridine}$), 1.95 (br s, 9.5H, CH_2), 1.34 (br s, 22H, THF), 0.79 (br s, 9.3H, $SiCH_2$), 0.50 – 0.17 (m, 73H, PDMS).

^{13}C-NMR (101 MHz, C_6D_6, 300 K): δ (ppm) = 169.5 (s, C_{Ar}), 166.7 (s, C_{Ar}), 159.6 (s, C_{Ar}), 111.6, 109.9, 101.5 (s, C_{Ar}), 97.2 (s, C_{Ar}), 69.5 (br s, CH_2O, THF), 41.4 (s, CH_2Y), 25.7 (s, THF), 23.9 (br s, $CH_{3,Pyridine}$), 23.4 (br s, CH_2), 13.9 (br s, $SiCH_2$), 2.68 – 1.25 (m, PDMS).

^{29}Si-NMR (80 MHz, C_6D_6, 300 K): δ (ppm) = -21.3 (br s)

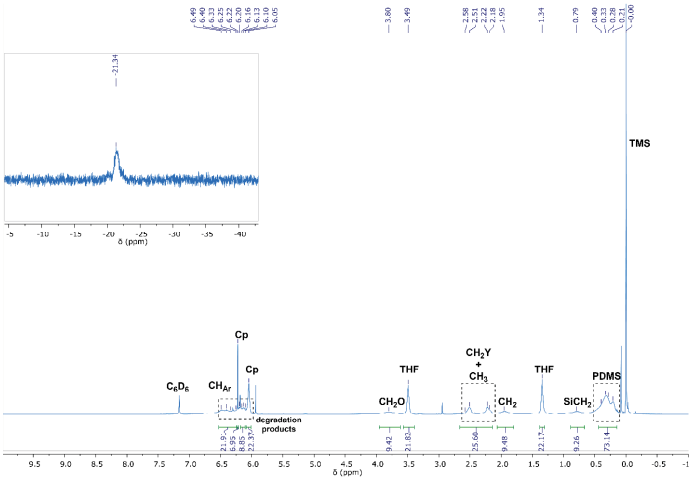

Figure S27. ^{1}H-NMR spectrum and significant region of the ^{29}Si-NMR spectrum of **MI3** after treatment with $Cp_2Y(CH_2TMS)(THF)$ in C_6D_6.

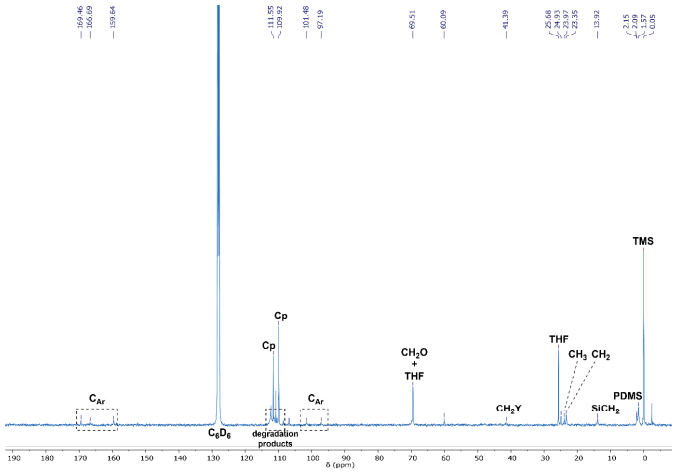

Figure S28. ^{13}C-NMR spectrum of **MI3** after treatment with $Cp_2Y(CH_2TMS)(THF)$ in C_6D_6.

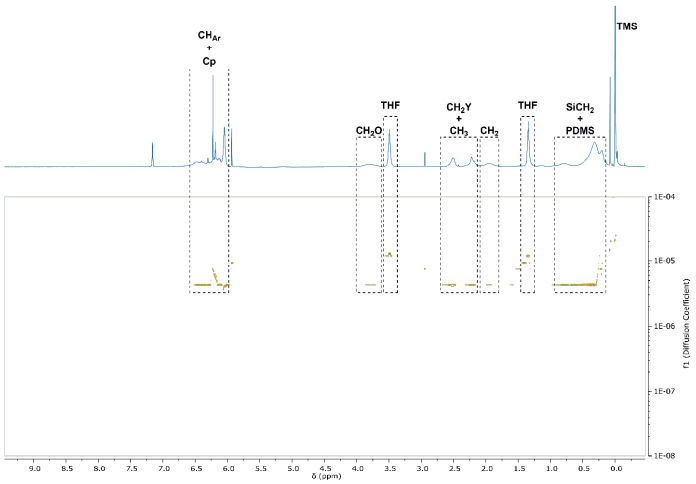

Figure S29. DOSY-NMR spectrum of **MI3** after treatment with $Cp_2Y(CH_2TMS)(THF)$ in C_6D_6.

4.3 Polymerization of DEVP using the Macroinitiators MI1-3

Table S2. Composition of the polymerization experiments with macroinitiators **MI1-MI3**

	$m_{Initiator}$ /mg	$n_{Initiator}$ /mmol	$m_{Catalyst}$ /mg	$n_{Catalyst}$[a] /mmol	$V_{Benzene\text{-}d6}$ /mL		$V_{Benzene\text{-}d6}$ /mL	$V_{Toluene}$ /mL	m_{DEVP} /mg	Equiv.[b] /-
MI1	259	41.0	31.0	82.0	3+1	**P3**	2.67	7.33	897	100
						P4	1.33	10.0	1346	300
MI2	434	24.4	16.2	42.9	4+1	**P5**	3.33	1.67	471	100
						P6	1.67	5.33	701	300
MI3	135	77.3	144	380	3+3	**P7**	5.00	5.00	987	20
						P8	1.00	6.00	740	60

[a]Adjusted to the amount of pyridyl units being present in the ^{1}H-NMR spectrum. [b]Equivalents of DEVP per initiating unit.

Characterization of PDEVP-*b*-PDMS-*b*-PDEVP Copolymers P3-P4

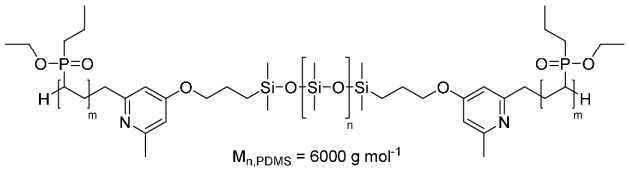

^{1}H-NMR (400 MHz, MeOD, 300 K): δ (ppm) = 6.83 – 6.59 (m, $CH_{Pyridine}$), 4.19 (s, PO*CH_2*), 2.43 (s, $CH_{3,Pyridine}$), 2.86 – 1.18 (m, PDEVP), 1.38 (s, $POCH_2$*CH_3*), 0.75 – 0.64 (m, $SiCH_2$), 0.10 (s, PDMS).

^{31}P-NMR (162 MHz, MeOD, 300 K): δ (ppm) = 33.2.

EA: PDEVP-*b*-PDMS-*b*-PDEVP copolymer containing 3.0 wt% water

calculated:	C 41.60	H 8.10	N 0.05	P 16.29
found:	C 41.41	H 8.10	N n.a.	P 16.05

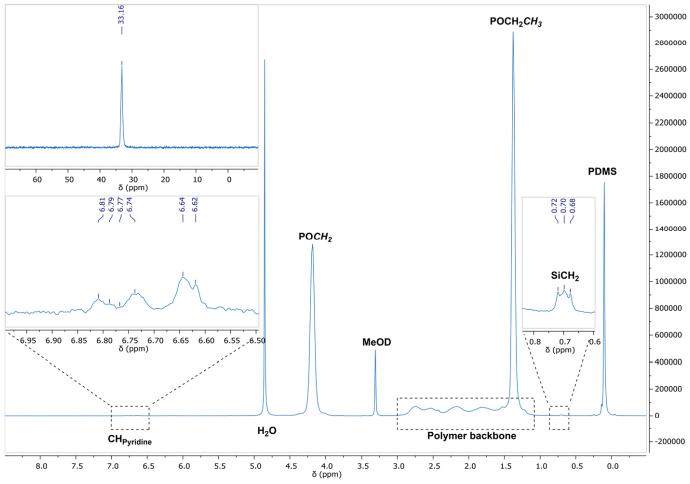

Figure S30. ^{1}H- and zoom of the ^{31}P-NMR spectrum of copolymer **P3** (100 equiv. DEVP per initiator unit) in MeOD.

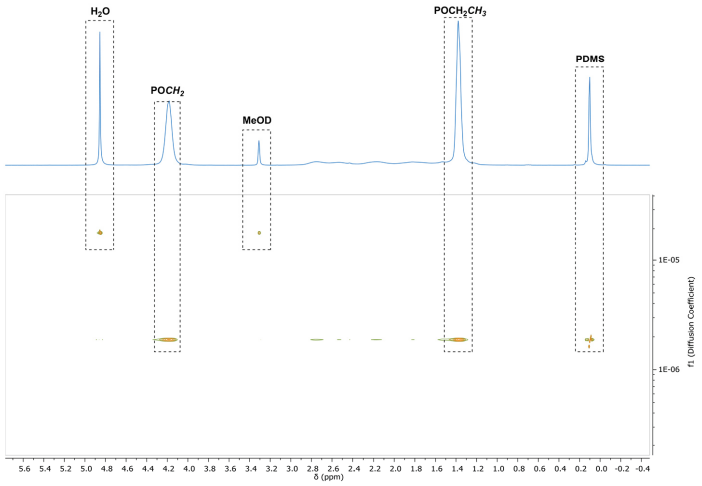

Figure S31. DOSY-NMR of copolymer **P3** (100 equiv. DEVP per initiator unit) in MeOD.

^{1}H-NMR (400 MHz, MeOD, 300 K): δ (ppm) = 4.18 (s, POCH_2), 2.90 – 1.18 (m, PDEVP), 1.38 (s, POCH$_2CH_3$), 0.76 – 0.65 (m, SiCH$_2$), 0.10 (s, PDMS).

^{31}P-NMR (162 MHz, MeOD, 300 K): δ (ppm) = 33.2.

EA: PDEVP-*b*-PDMS-*b*-PDEVP copolymer containing 3.0 wt% water

calculated:	C 42.24	H 8.09	N 0.02	P 17.60
found:	C 42.24	H 8.20	N n.a.	P 17.51

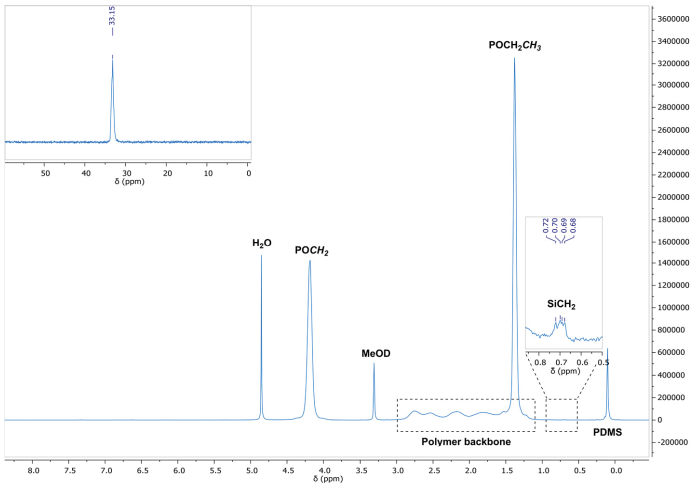

Figure S32. ^{1}H- and zoom of the ^{31}P-NMR spectrum of copolymer **P4** (300 equiv. DEVP per initiator unit) in MeOD.

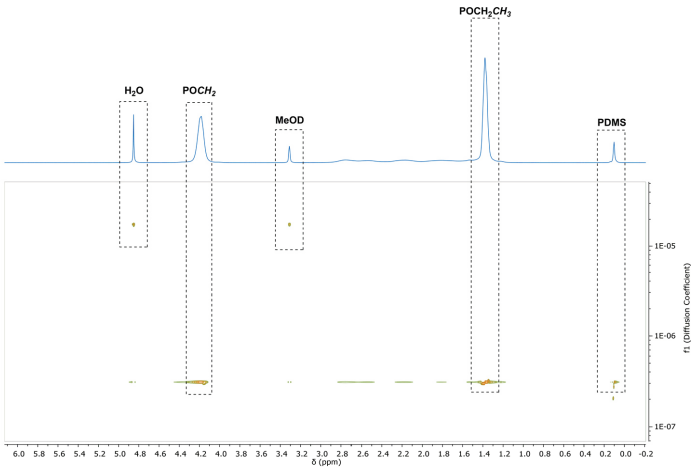

Figure S33. DOSY-NMR of copolymer **P4** (300 equiv. DEVP per initiator unit) in MeOD.

Cleavage of PDEVP from PDEVP-*b*-PDMS-*b*-PDEVP P4

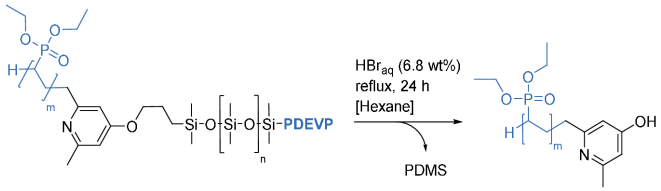

100 mg of copolymer **P4** were dissolved in deionized water (9.00 mL). This solution was treated with hydrobromic acid (1.00 mL, 48 wt%) and hexane (10.0 mL) and refluxed for 18 hours. The aqueous phase was neutralized with a sodium hydroxide solution, the phases were separated with a separatory funnel, and the aqueous phase was extracted three times with hexane. Water was removed *in vacuo* and the solid residue was extracted several times with methylene chloride to obtain PDEVP.

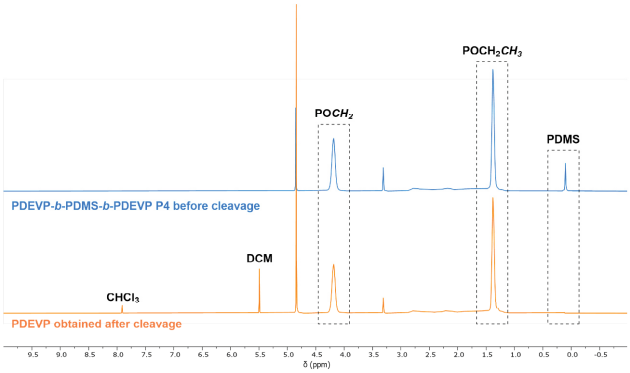

Figure S34. ^{1}H-NMR spectra in MeOD of copolymer **P4** before (top) and after (bottom) cleavage with HBr.

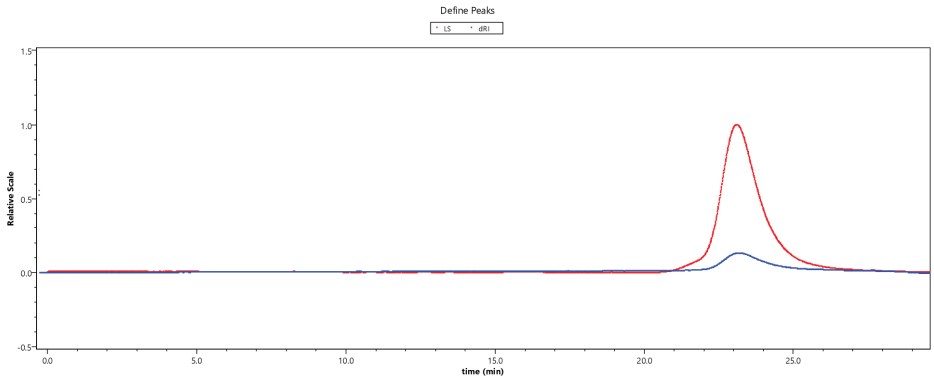

Figure S35. GPC trace of the PDEVP block of **P4** after cleavage with HBr. Measured via GPC-MALS in THF/H_2O.

Characterization of PDEVP-*b*-PDMS-*b*-PDEVP Copolymers P5-P6

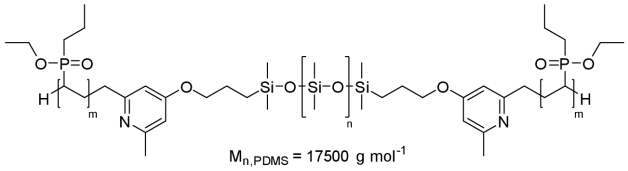

^{1}H-NMR (400 MHz, MeOD, 300 K): δ (ppm) = 4.18 (s, POCH_2), 2.41 (s, $CH_{3,Pyridine}$), 2.85 – 1.15 (m, PDEVP), 1.38 (s, POCH$_2CH_3$), 0.75 – 0.65 (m, $SiCH_2$), 0.11 (s, PDMS).

^{31}P-NMR (162 MHz, MeOD, 300 K): δ (ppm) = 33.2.

EA: PDEVP-*b*-PDMS-*b*-PDEVP copolymer containing 3.0 wt% water

calculated:	C 38.88	H 8.15	N 0.05	P 11.86
found:	C 39.06	H 8.00	N 0.05	P 11.82

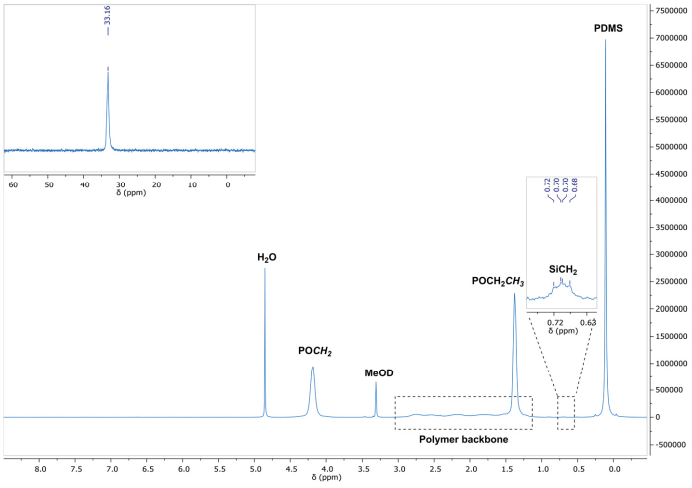

Figure S36. ^{1}H- and zoom of the ^{31}P-NMR spectrum of copolymer **P5** (100 equiv. DEVP per initiator unit) in MeOD.

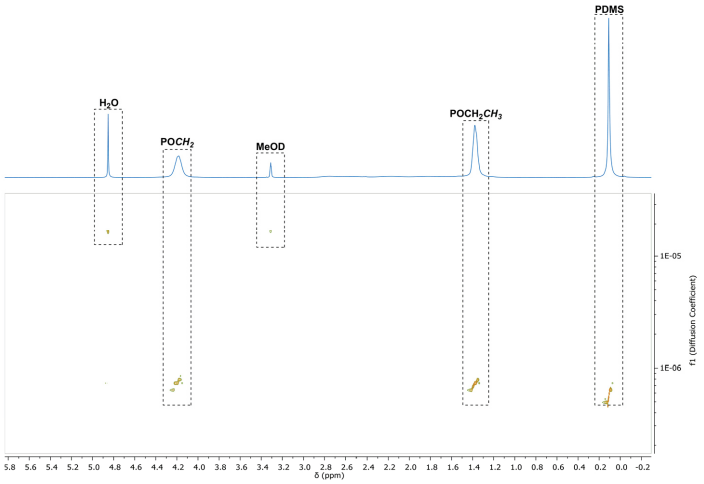

Figure S37. DOSY-NMR of copolymer **P5** (100 equiv. DEVP per initiator unit) in MeOD.

^{1}H-NMR (400 MHz, MeOD, 300 K): δ (ppm) = 4.18 (s, PO*CH*$_2$), 2.92 – 1.16 (m, PDEVP), 1.38 (s, POCH$_2$*CH*$_3$), 0.11 (s, PDMS).

^{31}P-NMR (162 MHz, MeOD, 300 K): δ (ppm) = 33.2.

EA: PDEVP-*b*-PDMS-*b*-PDEVP copolymer containing 3.0 wt% water

calculated:	C 41.80	H 8.09	N 0.01	P 16.93
found:	C 41.91	H 8.07	N n.a.	P 16.71

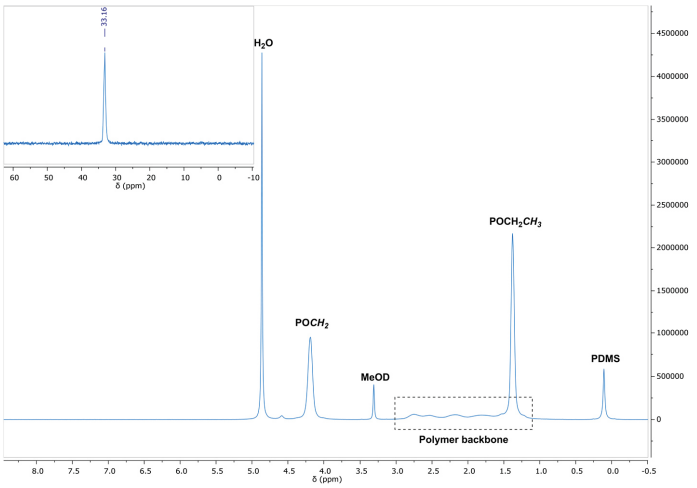

Figure S38. ^{1}H- and zoom of the ^{31}P-NMR spectrum of copolymer **P6** (300 equiv. DEVP per initiator unit) in MeOD.

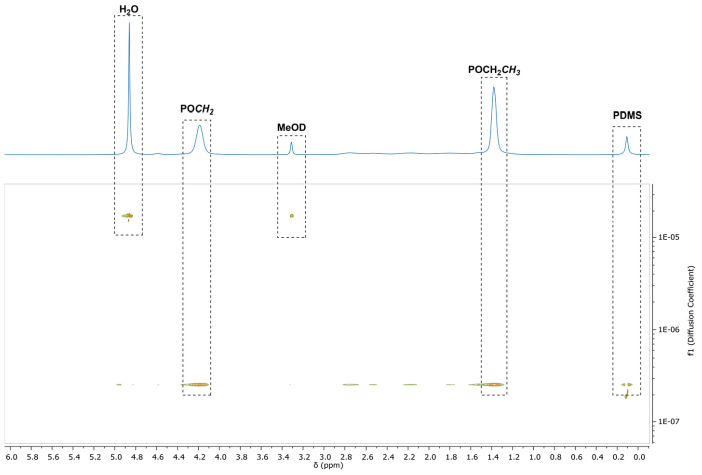

Figure S39. DOSY-NMR of copolymer **P6** (300 equiv. DEVP per initiator unit) in MeOD.

Characterization of PDMS-*g*-PDEVP Copolymers P7-P8

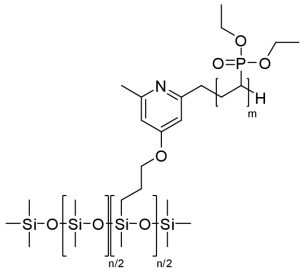

$M_{n,PDMS}$ = 950 g mol^{-1}

^{1}H-NMR (400 MHz, MeOD, 300 K): δ (ppm) = 6.63 (s, $CH_{Pyridine}$), 4.18 (s, POCH_2), 2.42 (s, $CH_{3,Pyridine}$), 2.86 – 1.17 (m, PDEVP), 1.38 (s, POCH$_2CH_3$), 0.77 – 0.64 (m, $SiCH_2$), 0.18 – 0.03 (m, PDMS).

^{31}P-NMR (162 MHz, MeOD, 300 K): δ (ppm) = 33.2.

EA: PDMS-*g*-PDEVP copolymer containing 3.5 wt% water

calculated:	C 42.64	H 8.08	N 0.11	P 17.66
found:	C 42.69	H 8.02	N 0.19	P 17.48

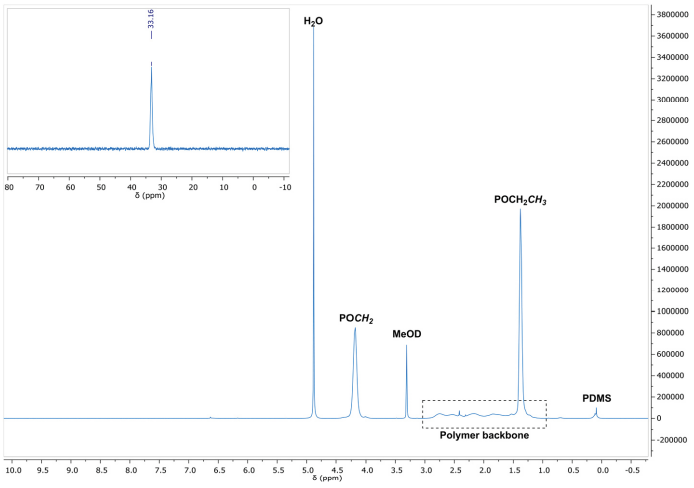

Figure S40. ^{1}H- and zoom of the ^{31}P-NMR spectrum of copolymer **P7** (20 equiv. DEVP per initiator unit) in MeOD.

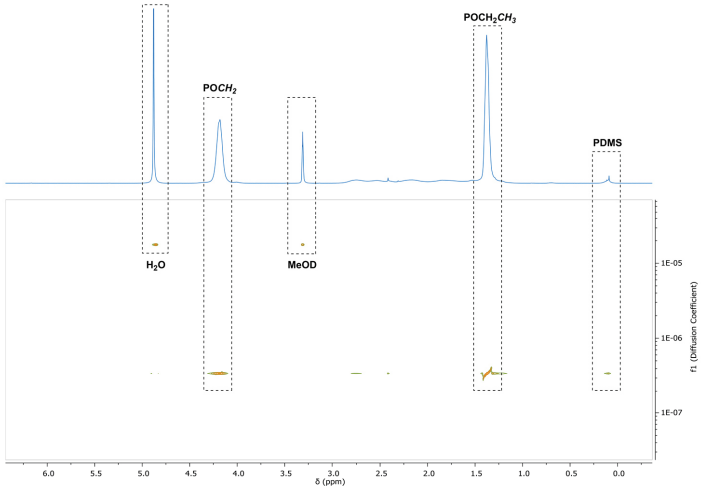

Figure S41. DOSY-NMR of copolymer **P7** (20 equiv. DEVP per initiator unit) in MeOD.

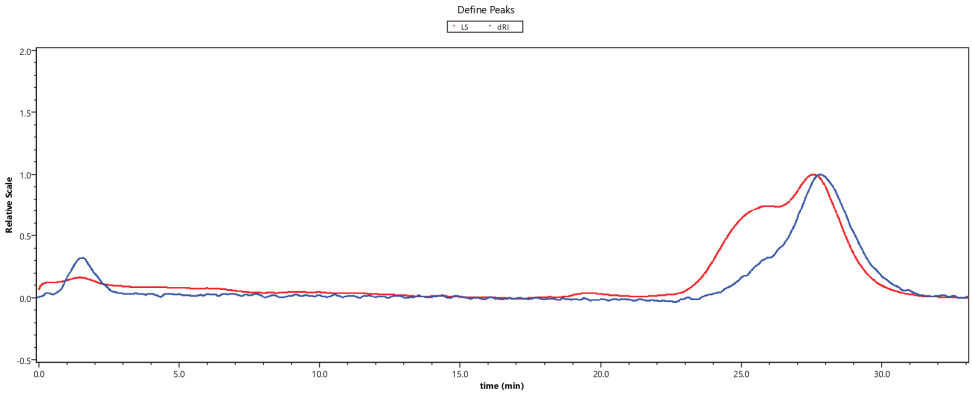

Figure S 42. GPC trace of PDEVP **P7** (20 equiv. DEVP per initiator unit) generated from **MI3**. Measured via GPC-MALS in THF/H_2O.

^{1}H-NMR (400 MHz, MeOD, 300 K): δ (ppm) = 6.63 (s, $CH_{Pyridine}$), 4.18 (s, $POCH_2$), 2.42 (s, $CH_{3,Pyridine}$), 2.89 – 1.19 (m, PDEVP), 1.38 (s, $POCH_2CH_3$), 0.76 – 0.64 (m, $SiCH_2$), 0.17 – 0.04 (m, PDMS).

^{31}P-NMR (162 MHz, MeOD, 300 K): δ (ppm) = 33.2.

EA: PDMS-*g*-PDEVP copolymer containing 3.5 wt% water

calculated:	C 42.43	H 8.10	N 0.04	P 18.02
found:	C 42.77	H 8.10	N 0.08	P 17.93

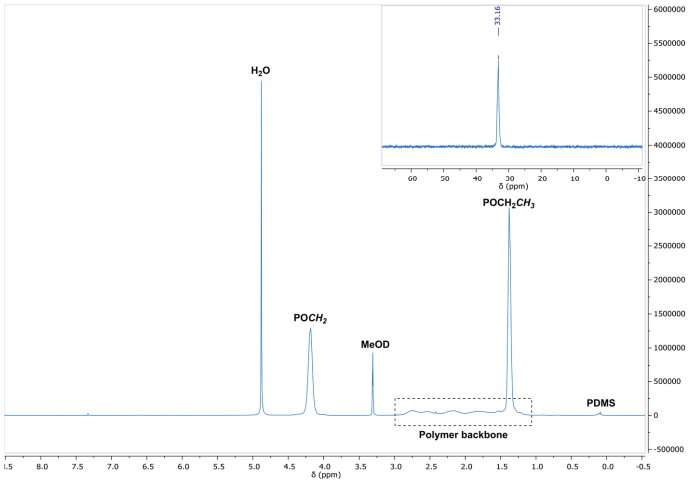

Figure S43. ^{1}H- and zoom of the ^{31}P-NMR spectrum of copolymer **P8** (60 equiv. DEVP per initiator unit) in MeOD.

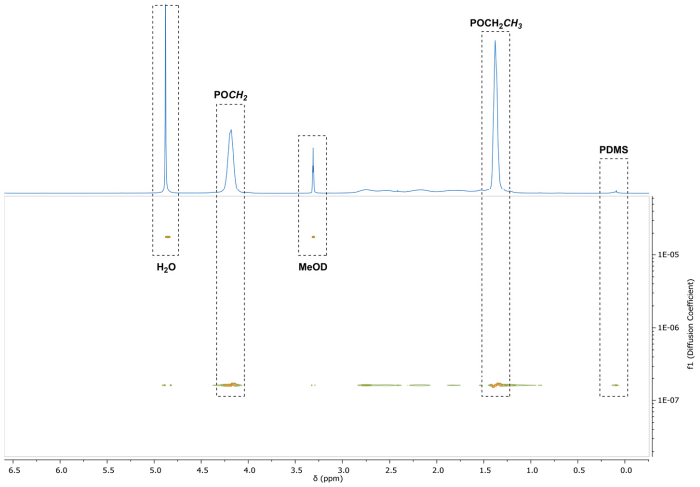

Figure S44. DOSY-NMR of copolymer **P8** (60 equiv. DEVP per initiator unit) in MeOD.

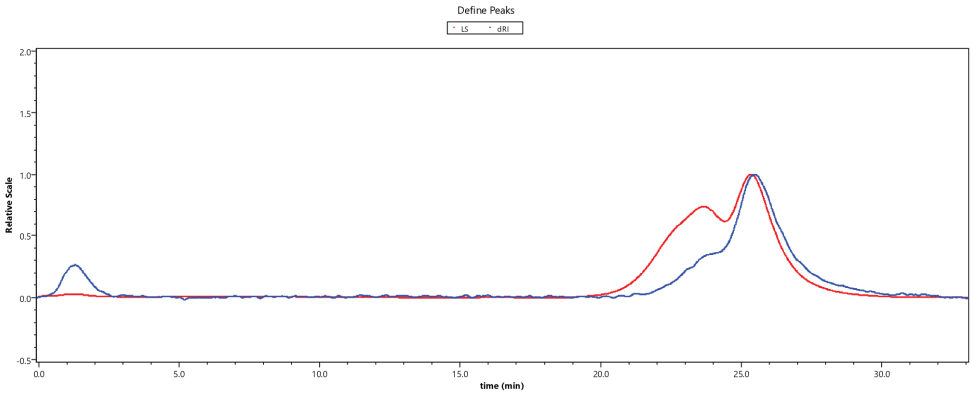

Figure S 45. GPC trace of PDEVP **P8** (60 equiv. DEVP per initiator unit) generated from **MI3**. Measured via GPC-MALS in THF/H_2O.

33

4.4 REM-GTP of 2VP and ROP of εCL with Macroinitiator MI1

Characterization of P2VP-*b*-PDMS-*b*-P2VP P9

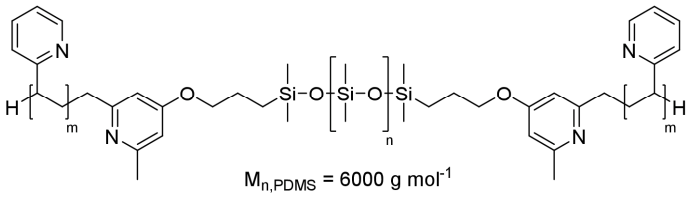

$M_{n,PDMS}$ = 6000 g mol^{-1}

^{1}H-NMR (400 MHz, MeOD, 300 K): δ (ppm) = 8.46 – 7.93 (m, $CH_{Pyridine}$), 7.52 – 6.80 (m, $CH_{Pyridine}$), 6.75 – 6.24 (m, $CH_{Pyridine}$), 2.47 – 1.25 (m, P2VP backbone), 0.74 – 0.62 (m, $SiCH_2$), 0.10 (br s, PDMS).

^{29}Si-NMR (80 MHz, MeOD, 300 K): δ (ppm) = -22.0.

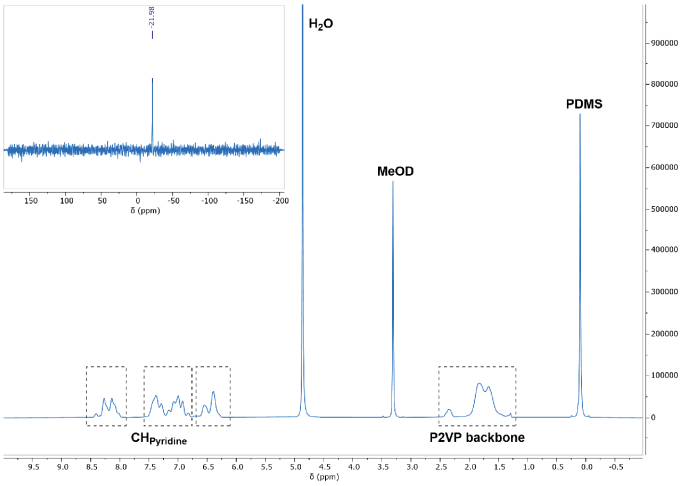

Figure S46. ^{1}H- and zoom of the ^{29}Si-NMR spectrum of copolymer **P9** (100 equiv. 2VP per initiator unit) in MeOD.

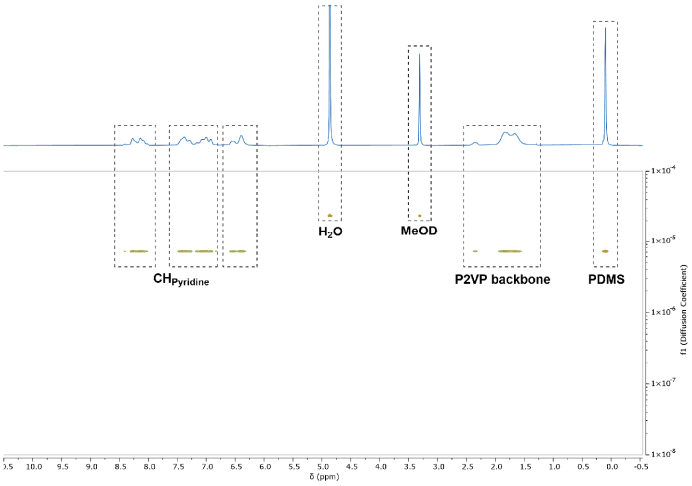

Figure S47. DOSY-NMR of copolymer **P9** (100 equiv. 2VP per initiator unit) in MeOD.

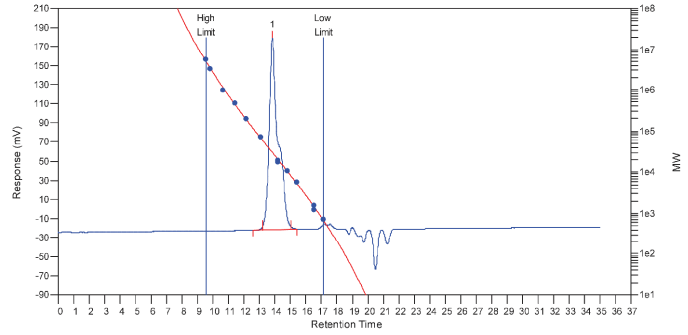

MW Averages

Peak No	Mp	Mn	Mw	Mz	Mz+1	Mv	PD
1	29834	23485	26502	29393	31970	26050	1.12846

Figure S48. GPC trace of **P9** (100 equiv. 2VP per initiator unit) generated from **MI1**. Measured via GPC in THF.

Characterization of PεCL-*b*-PDMS-*b*-PεCL P10

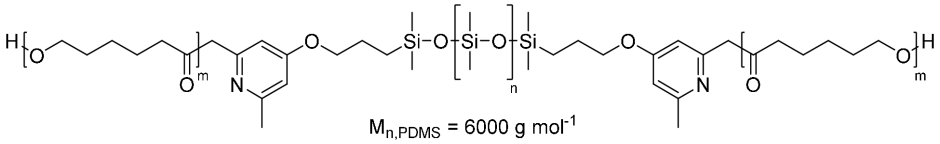

^{1}H-NMR (400 MHz, $CDCl_3$, 300 K): δ (ppm) = 4.05 (t, ^3J = 6.7 Hz, CH_2O), 2.30 (t, ^3J = 7.5 Hz, $CH_2C{=}O$), 1.74 – 1.57 (m, $CH_2CH_2CH_2$), 1.38 (*virt.* p, ^3J = 6.9, 7.6 Hz, $CH_2CH_2CH_2$), 0.71 – 0.56 (m, $SiCH_2$), 0.06 (br s, PDMS).

^{13}C-NMR (126 MHz, $CDCl_3$, 300 K): δ (ppm) = 173.7 (s), 64.3 (s), 34.3 (s), 28.5 (s), 25.7 (s), 24.7 (s), 1.16 (s).

^{29}Si-NMR (99 MHz, $CDCl_3$, 300 K): δ (ppm) = -21.9.

EA: PεCL-*b*-PDMS-*b*-PεCL copolymer

calculated:	C 57.23	H 8.70	N 0.09
found:	C 56.97	H 8.73	N 0.10

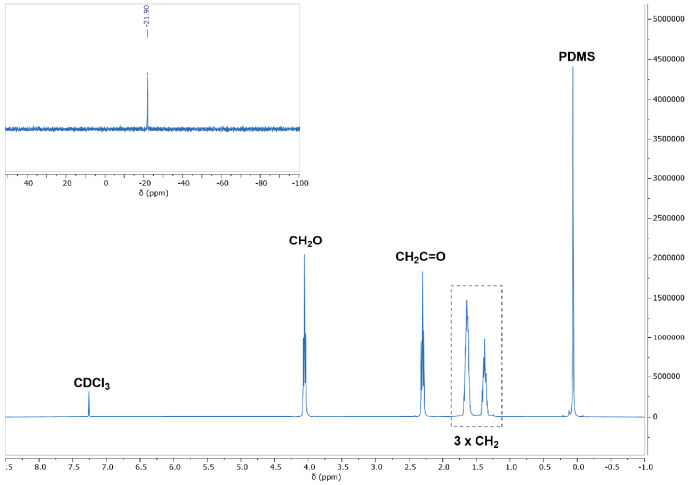

Figure S49. ^{1}H- and zoom of the ^{29}Si-NMR spectrum of copolymer **P10** (100 equiv. εCL per initiator unit) in $CDCl_3$.

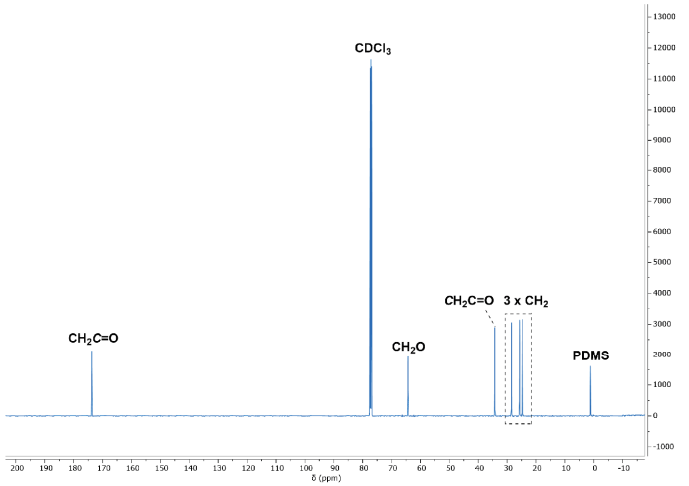

Figure S50. ^{13}C-NMR spectrum of copolymer **P10** (100 equiv. εCL per initiator unit) in $CDCl_3$.

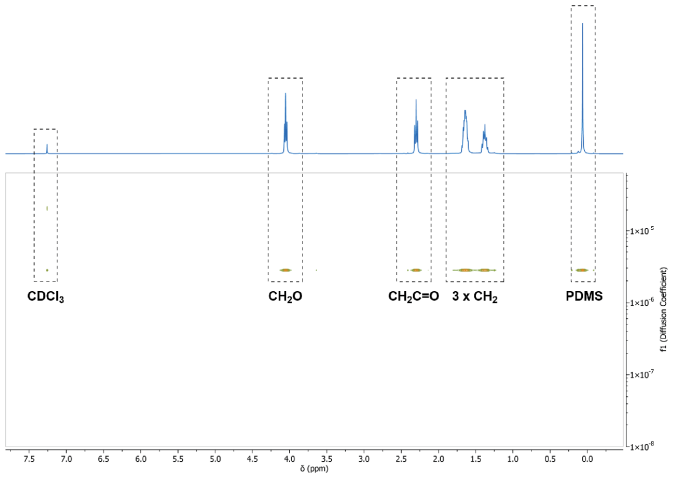

Figure S51. DOSY-NMR of copolymer **P10** (100 equiv. εCL per initiator unit) in $CDCl_3$.

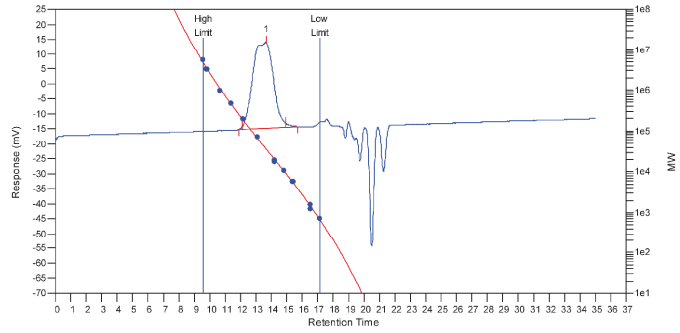

MW Averages

Peak No	Mp	Mn	Mw	Mz	Mz+1	Mv	PD
1	37625	37777	52505	70598	89000	50027	1.38987

Figure S52. GPC trace of **P10** (100 equiv. εCL per initiator unit) generated from **MI1**. Measured via GPC in THF.

4. Thermal and Size Analysis of the Copolymers

4.1 Characterization by Dynamic Light Scattering

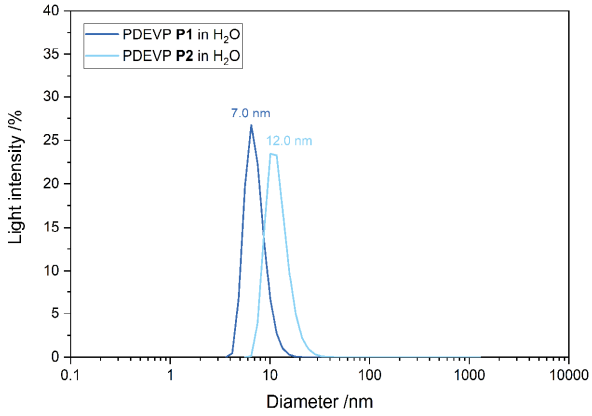

Figure S53. DLS data of PDEVP **P1** and **P2** in aqueous solution.

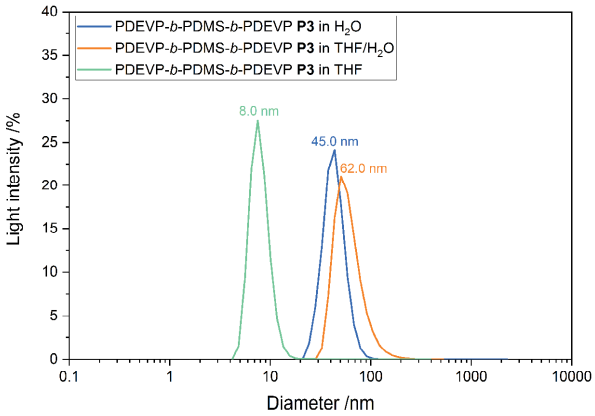

Figure S54. DLS data of copolymer **P3** in different solvents.

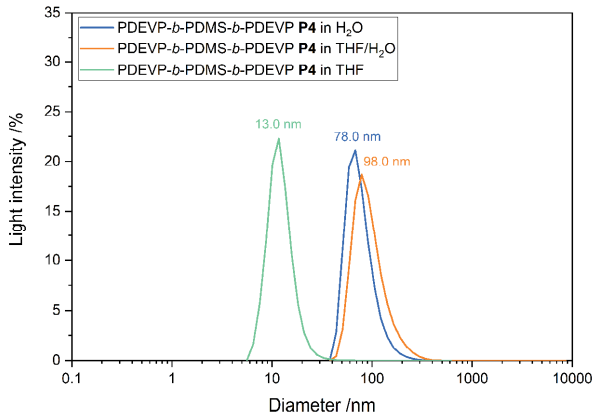

Figure S55. DLS data of copolymer **P4** in different solvents.

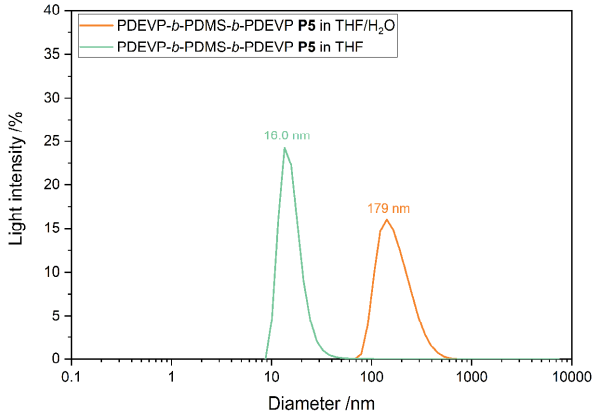

Figure S56. DLS data of copolymer **P5** in different solvents.

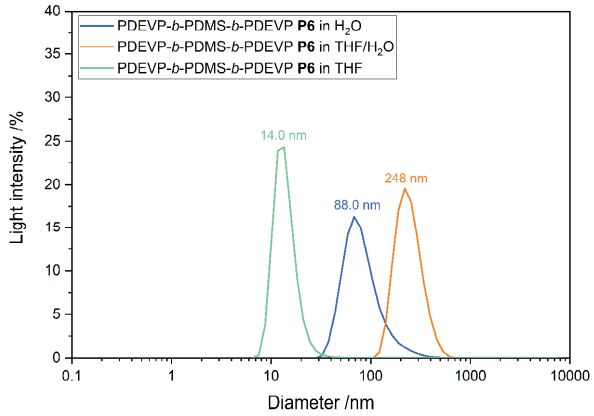

Figure S57. DLS data of copolymer **P6** in different solvents.

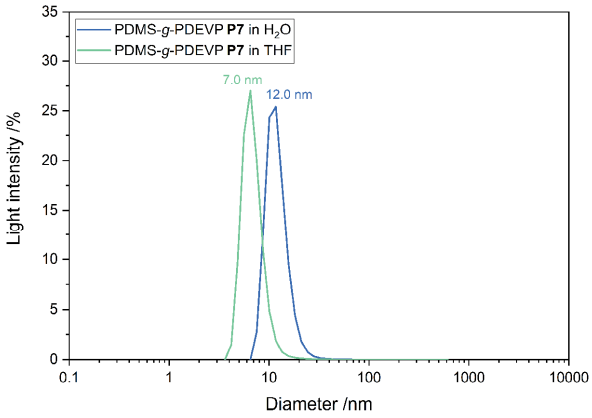

Figure S58. DLS data of copolymer **P7** in different solvents.

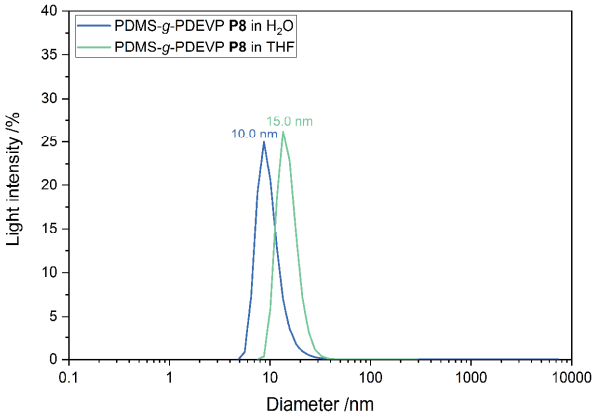

Figure S59. DLS data of copolymer **P8** in different solvents.

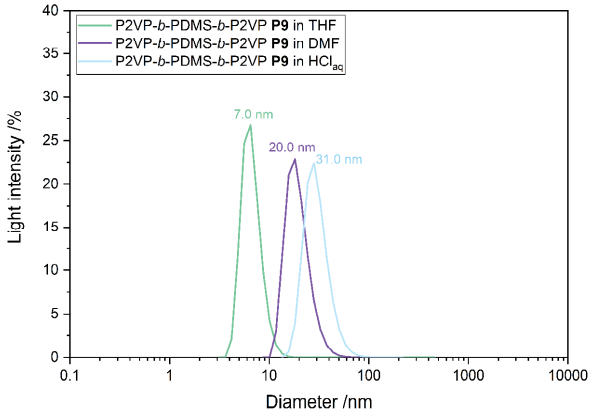

Figure S60. DLS data of copolymer **P9** in different solvents.

40

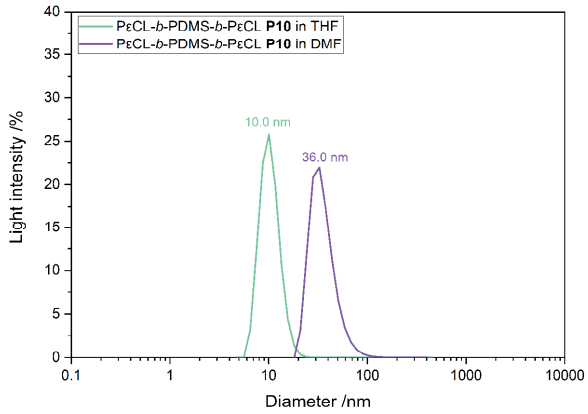

Figure S61. DLS data of copolymer **P10** in different solvents.

4.2 Thermal Analysis by Differential Scanning Calorimetry

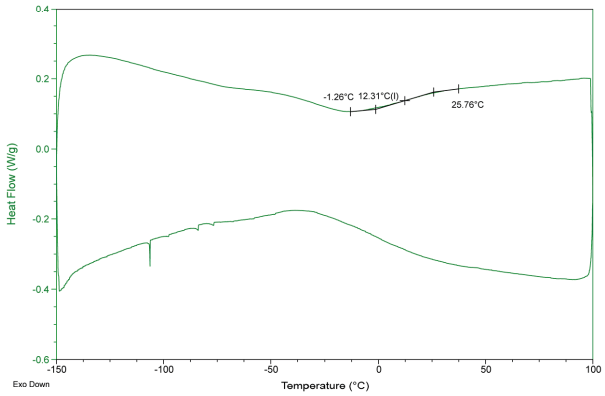

Figure S62. DSC curves of PDEVP **P1**.

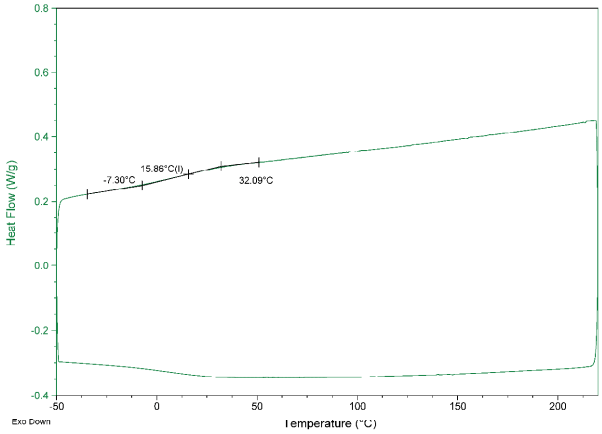

Figure S63. DSC curves of PDEVP **P2**.

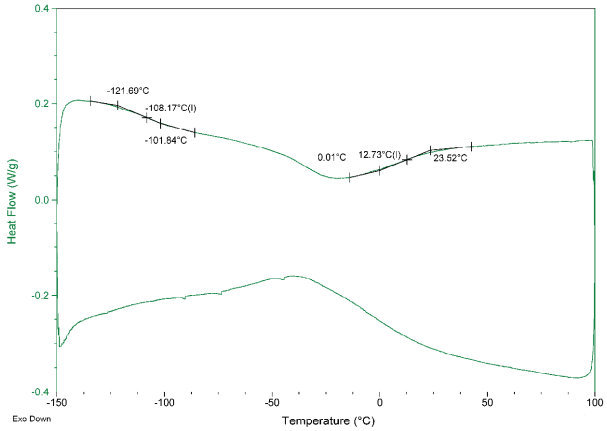

Figure S64. DSC curves of PDEVP-*b*-PDMS-*b*-PDEVP copolymer **P3**.

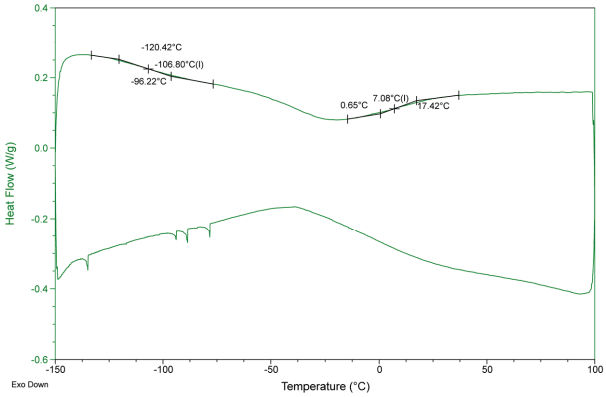

Figure S65. DSC curves of PDEVP-*b*-PDMS-*b*-PDEVP copolymer **P4**.

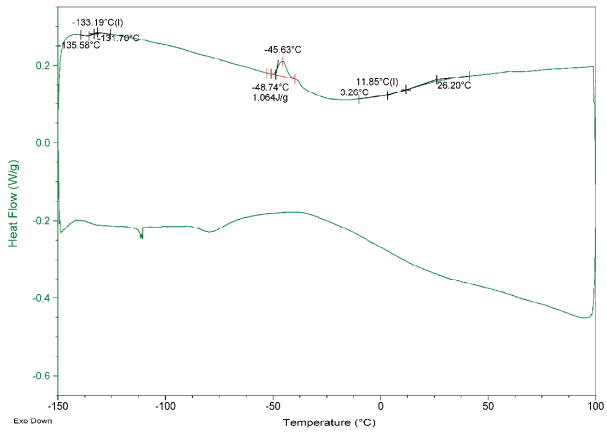

Figure S66. DSC curves of PDEVP-*b*-PDMS-*b*-PDEVP copolymer **P5**.

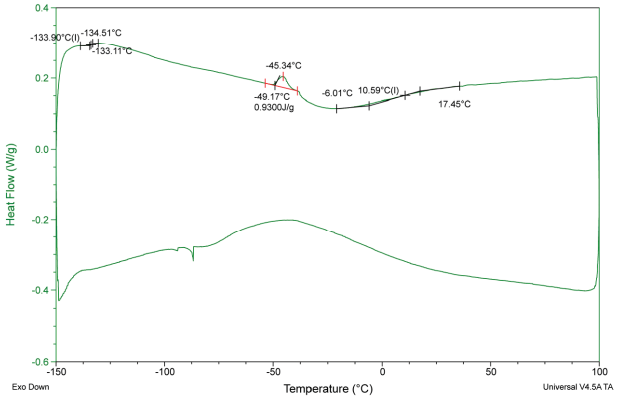

Figure S67. DSC curves of PDEVP-*b*-PDMS-*b*-PDEVP copolymer **P6**.

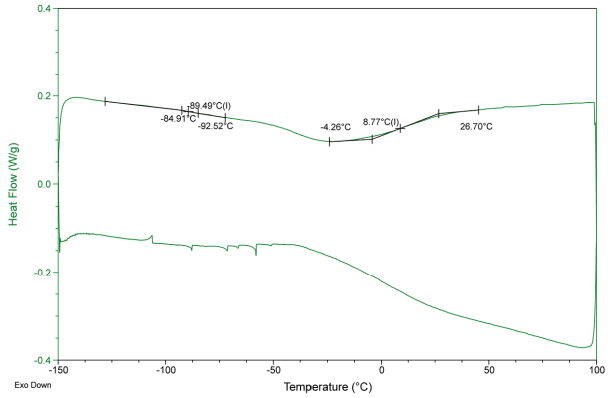

Figure S68. DSC curves of PDMS-*g*-PDEVP copolymer **P7**.

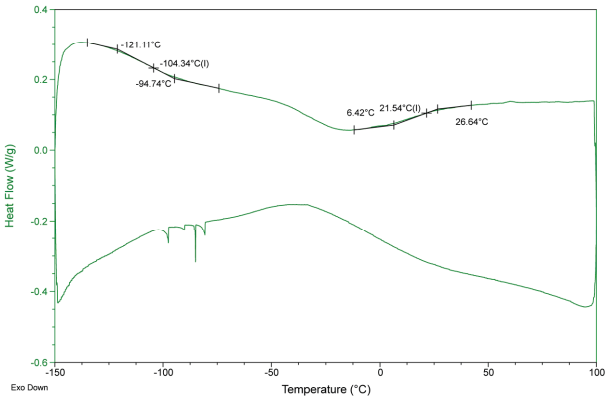

Figure S69. DSC curves of PDMS-*g*-PDEVP copolymer **P8**.

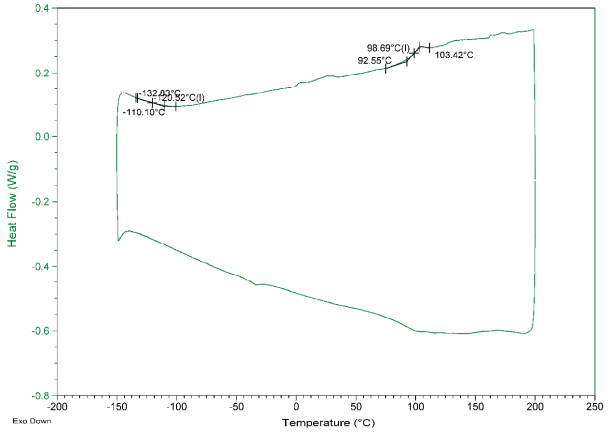

Figure S70. DSC curves of P2VP-*b*-PDMS-*b*-P2VP copolymer **P9**.

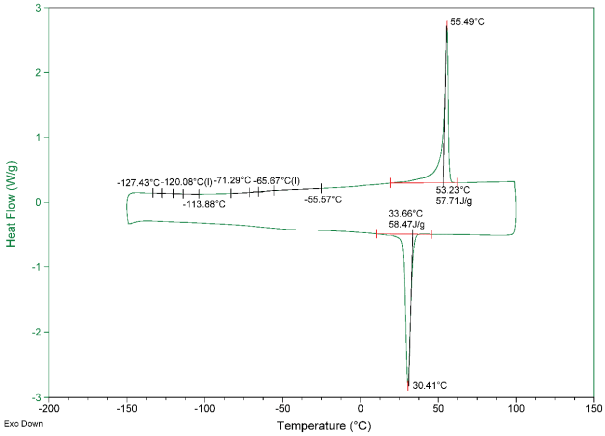

Figure S71. DSC curves of PεCL-*b*-PDMS-*b*-PεCL copolymer **P10**.

4.3 Thermoresponsive Behavior of Polymers P1-P8

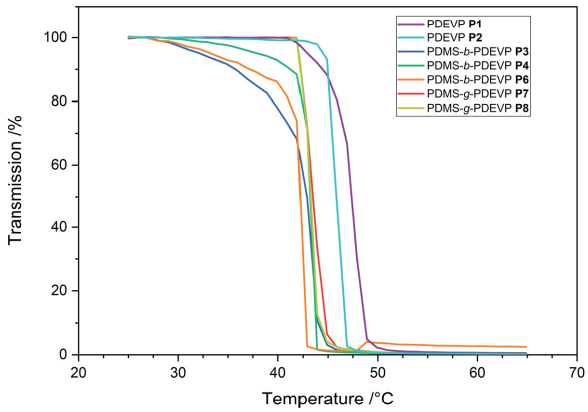

Figure S72. Determination of the LCST of the samples **P1-P8** in water (2.50 mg mL^{-1}). The cloud point was determined at 10% decrease of transmittance.

4.4 Studies on the Structural Stability of the Copolymers

Heat treatment: The polymer samples were stored under air at 70 °C or 120 °C for seven days. After this period ^{1}H-, ^{31}P-, and DOSY-NMR measurements were performed to elucidate the structural integrity.

Irradiation treatment: The polymers were irradiated in solid form or in solution (benzene as solvent) for 120 hours. After this period volatiles were removed if necessary and ^{1}H-, ^{31}P-, and DOSY-NMR measurements were performed to elucidate the structural integrity.

Table S3. Overview of the heat- and light-treated copolymers

PDEVP-*b*-PDMS-*b*-PDEVP **P4**				
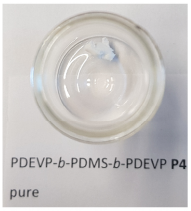	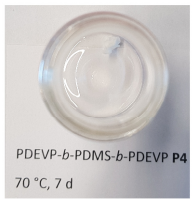	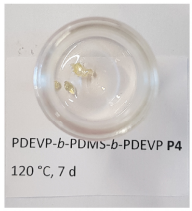	Irradiation, 365 nm, 120 h	Irradiation, 365 nm, 120 h [Benzene]
$M_{n,NMR}$ = 164 kg mol^{-1}	$M_{n,NMR}$ = 166 kg mol^{-1}; Intact block structure	Degradation of ethyl esters, color change	$M_{n,NMR}$ = 160 kg mol^{-1}; Intact block structure	$M_{n,NMR}$ = 163 kg mol^{-1}; Intact block structure
P2VP-*b*-PDMS-*b*-P2VP **P9**				
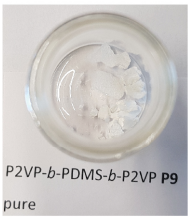	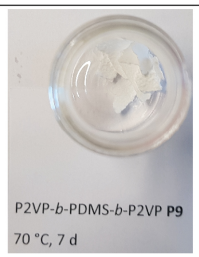		-	-
$M_{n,NMR}$ = 32.5 kg mol^{-1}	$M_{n,NMR}$ = 35.2 kg mol^{-1}; Intact block structure	$M_{n,NMR}$ = 36.2 kg mol^{-1}; Slight color change	-	-
PεCL-*b*-PDMS-*b*-PεCL **P10**				
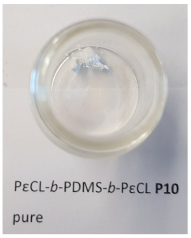	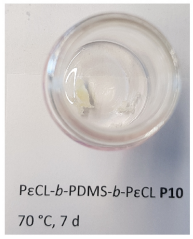	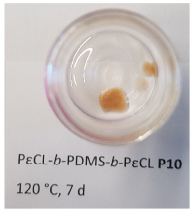	-	-
$M_{n,NMR}$ = 30.5 kg mol^{-1}	$M_{n,NMR}$ = 31.8 kg mol^{-1}; Intact block structure	$M_{n,NMR}$ = 21.6 kg mol^{-1}; Depolymerization, color change	-	-

12.3 Supporting Information of the Manuscript "Synthesis, Characterisation and Functionalisation of BAB-based Dual-Responsive Nanocarriers for Targeted Drug Delivery: Evolution of Nanoparticles based on 2-Vinylpyridine and Diethyl Vinylphosphonate"

Supporting information for the manuscript entitled *Synthesis, Characterisation and Functionalisation of BAB-type Dual-Responsive Nanocarriers for Targeted Drug Delivery: Evolution of Nanoparticles based on 2-Vinylpyridine and Diethyl Vinylphosphonate*

Andreas Saurwein,[‡a] Andreas Schaffer,[‡a] Christina Wieser,[a] and Bernhard Rieger[*a]

[a]WACKER-Chair of Macromolecular Chemistry, Catalysis Research Center, Technical University of Munich, Lichtenbergstraße 4, 85747 Garching near Munich, Germany. E-mail: rieger@tum.de.

Contents

1 Materials and Methods 2
2 Complex Synthesis 5
3 End-Group Analysis 8
4 Kinetic Investigation with Activated $Cp_2Y(CH_2TMS)(THF)$ 10
5 Synthesis and Characterisation of the Copolymers 11
6 Cross-Linking of the Copolymers and Characterisation of the Nanoparticles 22
7 Synthesis of Folate-Conjugated Nanoparticles 33
8 References 37

1 Materials and Methods

General Information

All moisture- or air-sensitive reactions were carried out under argon atmosphere using standard Schlenk technique or a glovebox. All glassware was heat dried under vacuum prior to use. Unless otherwise stated, all chemicals were purchased from *Sigma-Aldrich* or *TCI Chemicals* and used as received. Toluene were dried using a *MBraun* SPS-800 solvent purification system and stored of 3 Å molecular sieve. $Cp_2Y(THF)(CH_2TMS)$ (**4**)[1-4], $Cp_2Y(CH_2(C_5H_2Me_2N))$[5], diethyl vinylphosphonate (DEVP)[6] and diallyl vinylphosphonate (DAlVP)[7, 8] were prepared according to procedures found in the literature. The monomers 2-vinylpyridine (2VP), DEVP, and DAlVP were dried over calcium hydride and distilled prior to use. The folate-NHS active ester was synthesised according to a published procedure.[9, 10]

Dialysis

Purification of products via diaysis were rendered with *Spectra/Por 1* dialysis membranes (regenerated cellulose) from *VWR* against deionized water. The membranes used have a molecular weight cut-off of (MWCO) of 6-8 kDa and 3.3 mL cm^{-1} volume-length ratio. Loading and release experiments of the nanoparticles were rendered with *ZelluTrans T2* dialysis membranes (regenerated cellulose) from *Carl Roth*. These membranes have a molecular weight cut-off of (MWCO) of 6-8 kDa and 0.32 mL cm^{-1} volume-length ratio Prior to use the membranes were treated with deionized water over night.

Dynamic Light Scattering (DLS)

Hydrodynamic diameters of the particles were determined on a *Zetasizer Nona ZS* from *Malvern*. The samples were dissolved in *Millipore* water or HPLC chloroform at a concentration of 2.5 mg mL^{-1}. The DLS data were averaged from three measurements which for their part consisted of eleven single measurements.

Gel Permeation Chromatography (GPC)

For the determination of the molecular weight distributions polymer solutions with a concentration of 2.5 mg mL^{-1} were conducted to GPC measurements on a *PL-GPC 50* with two PL-Gel columns from *Agilent Technologies.* DMF with 2.17 g L^{-1} lithium bromide as additive was used as eluent. Absolute molar masses were determined *via* an integrated dual-angle light scattering detector and a RI detection unit for concentration calculation.

Elemental Analysis (EA)

Elemental analyses were performed on a *Vario EL* from *Elemetar* at the microanalytical lab of the inorganic-chemical institute at the Technical University Munich (TUM).

UV/Vis Spectroscopy

UV/vis spectra were recorded on a *Cary 50* UV/vis spectrophotometer from *Varian*. For the measurements quartz glass cuvettes were filled with samples dissolved in deionized water or methanol.

Photoluminescence Spectroscopy (PL)

Photoluminescence measurements were performed on *AVA-Spec 2048* from *Avantes*. For the excitation of the samples PS cuvettes were placed in a 90° cuvette holder consisting of *Prizmatix* current controller as light source irradiated with light of a wavelength of 365 nm.

Nuclear Magnetic Resonance Spectroscopy (NMR)

Nuclear magnetic resonance spectra were recorded on the devices *AVIII 300* (300 MHz), *AVIII 400 HD* (400 MHz) and a *AVIII 500 cryo* (500 MHz) from *Bruker*. Deuterated solvents were purchased from *Sigma-Aldrich*. For moisture-sensitive purposes the solvents were dried over 3 Å molecular sieve. ^{1}H and ^{13}C spectroscopic chemical shifts δ are reported in ppm and calibrated to the residual proton signals of the used solvents.

Benzene-d_6: δ (ppm) = 7.16 (^{1}H NMR); δ (ppm) = 128.1 (^{13}C NMR).

Dimethyl sulfoxide-d_6: δ (ppm) = 2.50 (^{1}H NMR); δ (ppm) = 39.5 (^{13}C NMR).

Methanol-d_4: δ (ppm) = 4.87 (^{1}H NMR); δ (ppm) = 49.0 (^{13}C NMR).

Unless otherwise stated coupling constants *J* are mean values and refer to coupling between two protons. For the assignment of the signals the signal multiplicities were abbreviated accordingly: s – singlet, d – doublet, t – triplet, m – multiplet.

Transmission Electron Microscopy (TEM)

Imaging via TEM was rendered with *JEM-1400 Plus* from *JEOL* with a magnification factor of 6 x 10^4. The *LaB6* filament was operated with an acceleration voltage of 120 kV. Aqueous nanoparticle solutions (2.5 mg mL^{-1}) were adsorbed on copper grid with a continuous film of charcoal for one minute and subsequently stained with uranylacetate (2 wt-%) solution. TEM images were used to determine an average diameter, a standard deviation and the polydispersity from 60 particles.

Turbidity Measurements

The determination of the cloud point was carried out on Cary *50* UV/vis spectrophotometer from *Varian* in 4 mL glass cuvettes using a peltier thermostat. Polymer or Nanoparticle solutions with a concentration of 2.5 mg mL^{-1} were used and heated/cooled with a rate of 1 K min^{-1} followed by a five-minute-long waiting period to establish a thermal equilibrium. The cloud point was detected by the changes in transmittance at λ = 500 nm. The lower critical solution temperature was defined as the temperature corresponding to a decrease of 10% in optical transmittance.

Zeta Potential Measurements

Zeta potentials ζ were measured on a *Zetasizer Nano ZS* from *Malvern* using aqueous solutions of the nanoparticles (2.5 mg mL^{-1}) and averaged from three measured values.

Loading of the Nanoparticles

For loading with fluorescein a solution of 6.96 mg nanoparticles was dissolved in 1.66 mL deionized water to adjust a concentration of 4.2 g mL^{-1}. To this solution a solution of fluorescein (580 mg) in DMSO (1.94 mL) was added dropwise at 0 °C. After stirring for 45 minutes at this temperature the mixture was stirred for additional 90 minutes at room temperature. Subsequently five dialysis membranes were filled with 600 µL each of this

solution and were dialysed against deionized water (500 mL) over night. Likewise, a sixth tubing was filled with 600 µL of the solution and dialysed against 100 mL deionized water over night. 1.5 mL were taken from the medium of the sixth dialysis and conducted to a photoluminescence measurement to obtain a reference value for the already released fluorescein.

Release Experiments

For the release studies the five dialysis tubes were placed in the corresponding media (60 mL) (deionized water for temperature-related measurements and citrate-buffer solutions with a pH of 4.5 or 6.0). Samples (1.5 mL) were taken at regular intervals (hourly during the first 7 hours, then after 24, 30, 48 and 72 hours) and the removed volume was backfilled with 1.5 mL of the related medium. Each sample taken was later conducted to photoluminescence spectroscopy. The amount of fluorescein was then determined from the relative irradiance at each measuring point using calibration curves. The calibration curves were generated *via* photoluminescence measurements using fluorescein solutions in water and the citrate-buffer solutions with varying concentrations. With help of the reference sample (*vide infra*, initial amount of fluorescein) the fraction of released fluorescein was calculated.

2 Complex Synthesis

C-H bond activation of TMPy (1) with $Cp_2Y(CH_2TMS)(THF)$ (4)

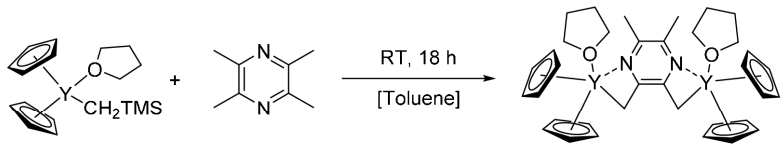

4 $C_{18}H_{29}OSiY$ 378.42 g/mol

1 $C_8H_{12}N_2$ 136.20 g/mol

5 $C_{36}H_{46}N_2O_2Y_2$ 716.59 g/mol

Complex **4** (83.4 mg, 220 µmol, 2.0 equiv.) was dissolved in absolute toluene (3.0 mL). 2,3,5,6-Tetramethylpyrazine (**1**) (15.0 mg, 110 µmol, 1.0 equiv.) was dissolved in absolute toluene (1.5 mL), added to the complex solution and rinsed with another 1.5 mL of dry toluene. Immediately after addition of the initiator a deeply orange solution could be observed. After four hours full conversion was detected *via* ^{1}H-NMR spectroscopy. Hereafter the solvent was removed under reduced pressure and the residue was washed with pentane. The supernatant solution was decanted of and the solid dried in high vacuum to afford complex **5** (84 %, 66.5 mg,92.8 µmol) as a red powder.

^{1}H NMR (500 MHz, Benzene-d_6, 300 K): δ (ppm) = 6.11 (s, 20H, Cp), 3.50 – 3.36 (m, 8H, THF), 2.91 (s, 4H, CH_2Y), 1.99 (s, 6H, CH_3), 1.35 – 1.17 (m, 8H, THF).

^{13}C NMR (126 MHz, Benzene-d_6, 300 K): δ (ppm) = 153.3 (s, $C_{Pyrazine}$), 127.2 (s, $C_{Pyrazine}$), 111.0 (d, Cp), 69.9 (t, THF), 45.5 (dt, J_{CY} = 5.0 Hz, CH_2Y), 25.6 (t, THF), 19.4 (q, CH_3).

EA: calculated: C 60.34 H 6.47 N 3.91
found: C 59.29 H 6.31 N 3.86

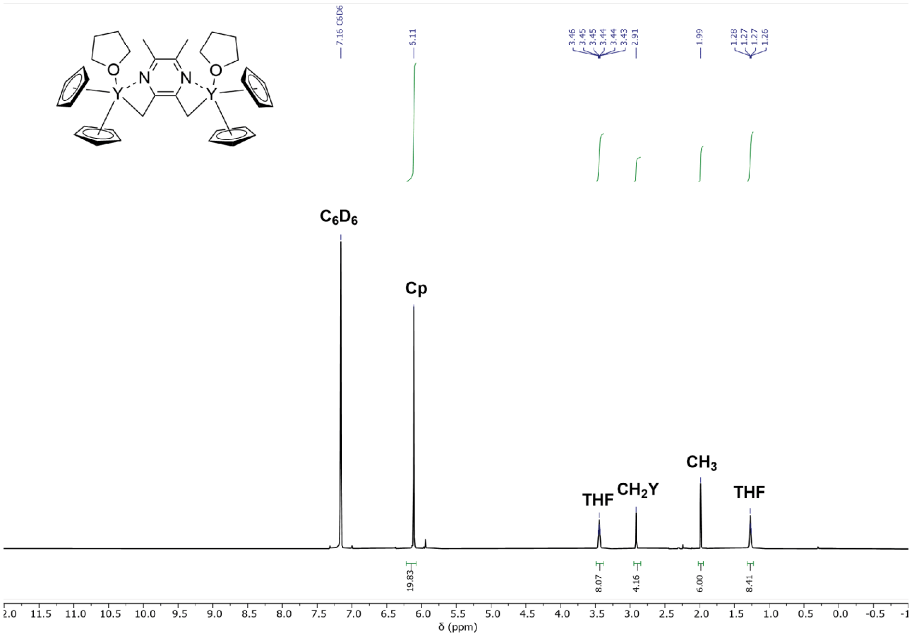

Fig. S1 ^{1}H-NMR spectrum of complex **5** recorded in benzene-d_6.

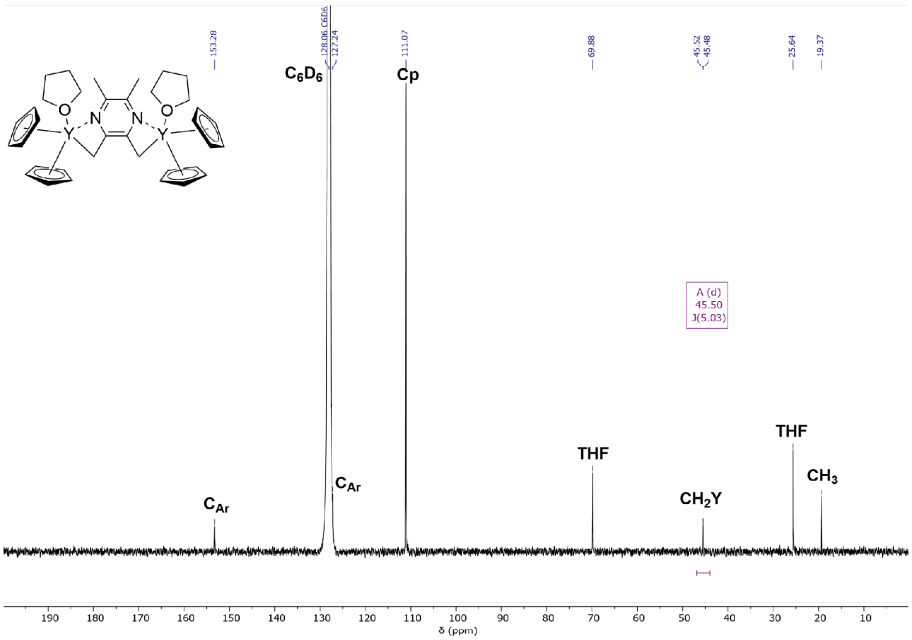

Fig. S2 ^{13}C-NMR spectrum of complex **5** recorded in benzene-d_6.

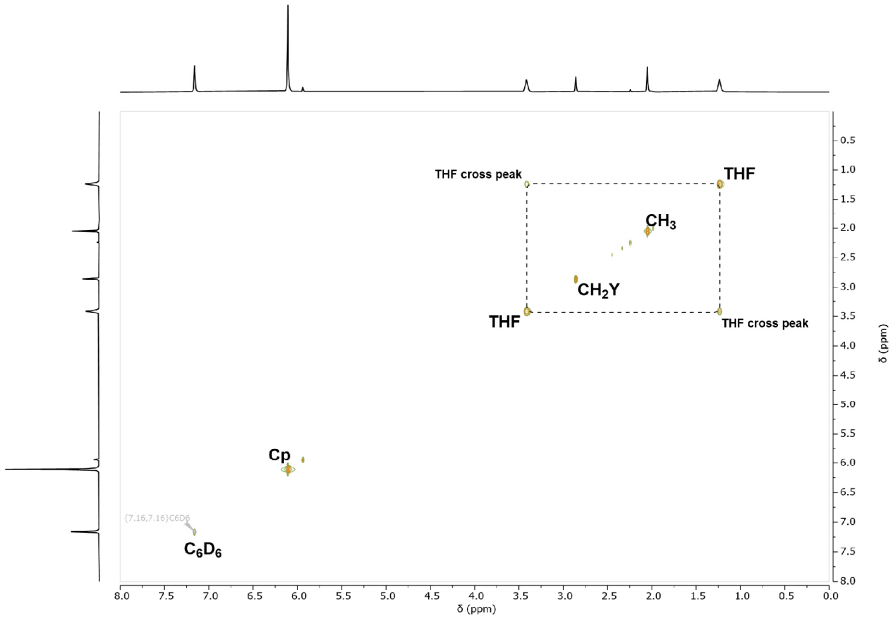

Fig. S3 NOESY spectrum of complex **5** recorded in benzene-d_6.

Kinetic investigation of the C-H bond activation of 2,3,5,6-Tetramethylpyrazine (1)

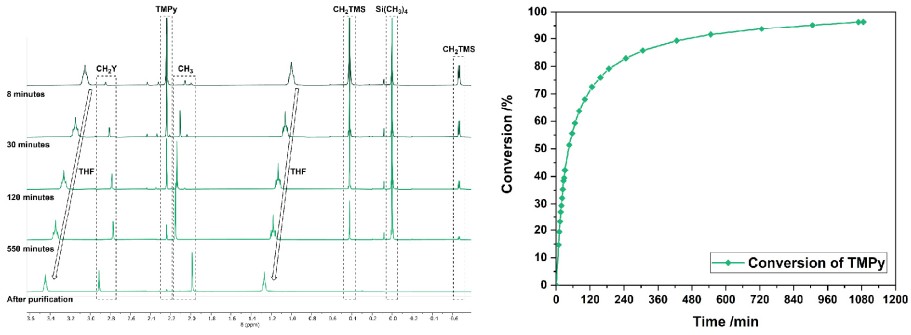

Fig. S4 Selected ^{1}H-NMR spectra of the kinetic analysis of the C-H bond activation of TMPy (**1**) recorded in benzene-d_6 (left) and time-dependent plot of the calculated conversions (right).

3 End-Group Analysis

Oligomerization with 2,3,5,6-tetramethylpyrazine and *sym*-collidine

A solution of $Cp_2Y(CH_2TMS)(THF)$ (**4**) (46.1 mg, 122 µmol, 2.00 equiv.) in absolute toluene (1.00 mL) was added to 2,3,5,6-tetramethylpyrazine (**1**) (8.29 mg, 60.9 µmol, 1.00 equiv.) in absolute toluene (1.00 mL) and resulted in the instant colouring of the reaction mixture. After the quantitative conversion was detected by ^{1}H-NMR spectroscopy, the mixture was diluted with 3.00 mL of toluene, and 2-vinylpyridine (64.0 mg, 609 µmol, 5.00 equiv.) was added in one portion. After 20 hours proton NMR confirmed the complete conversion of 2-vinylpyridine. The oligomerisation was terminated by addition of methanol and precipitated in pentane. The supernatant phase was decanted off and the oligomer was dried in vacuum. For the analysis by ESI-MS the oligomer was dissolved in LC-MS methanol at concentration of 0.10 mg mL^{-1}.

The oligomerisation of 2-vinylpyridine with *sym*-collidine as initiator was performed with a reduced amount of complex **4** (23.1 mg, 60.9 µmol, 1.00 equiv.).

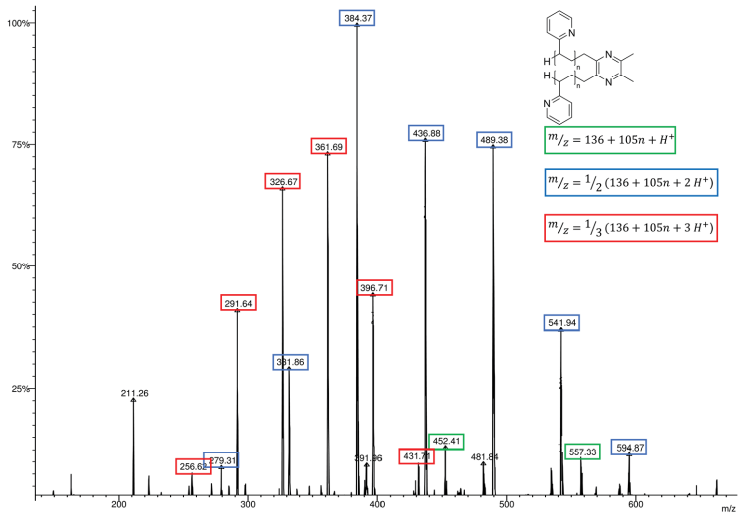

Fig. S5 ESI-MS spectrum of 2VP oligomers generated with complex **4** and 2,3,5,6-tetramethylpyrazine (**1**) as initiator.

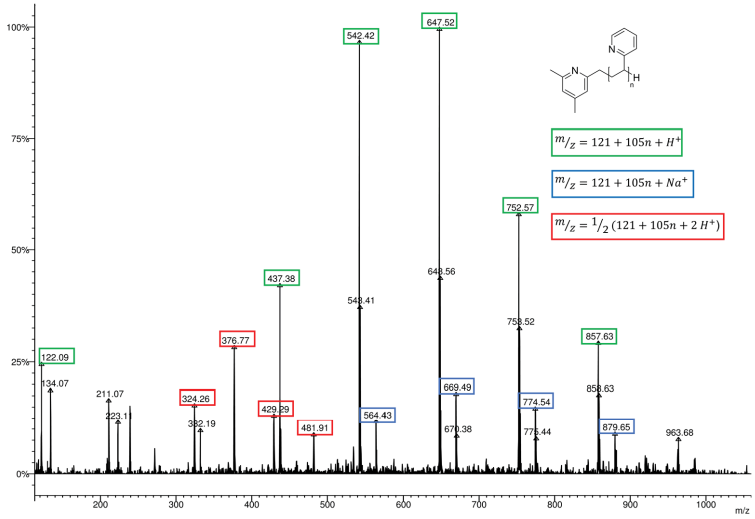

Fig. S6 ESI-MS spectrum of 2VP oligomers generated with complex **4** and *sym*-collidine as initiator.

4 Kinetic Investigation with Activated $Cp_2Y(CH_2TMS)(THF)$

Kinetic investigation with 2,3,5,6-Tetramethylpyrazine as initiator

102 mg $Cp_2Y(CH_2TMS)(THF)$ (**4**) (270 µmol, 2.00 equiv.) were dissolved in absolute toluene (4.00 mL) and treated with a solution of 2,3,5,6-tetramethylpyrazine (**1**) (135 µmol, 1.00 equiv.) in 2.00 mL absolute toluene. An instant orange colouration of the solution occurred, which indicated the successful C-H bond activation. After 16 hours ^{1}H-NMR spectroscopy confirmed the quantitative C-H bond activation. The solution was diluted with additional toluene (14.0 mL) and the polymerisation was started by addition of 2-vinylpyridine (2.84 g, 27.0 mmol, 200 equiv.) in one portion. Aliquots (circa 400 mg per sample) were taken in regular time intervals and poured into methanol (500 µL each). The aliquots were dried and then analysed by ^{1}H-NMR and GPC. After the complete conversion of 2-vinylpyridine, the reaction was terminated by addition of methanol (1.00 mL).

Kinetic investigation with *sym*-collidine as initiator

51.1 mg $Cp_2Y(CH_2TMS)(THF)$ (**4**) (135 µmol, 1.00 equiv.) were dissolved in absolute toluene (4.00 mL) and treated with a solution of *sym*-collidine (135 µmol, 1.00 equiv.) in 2.00 mL absolute toluene. An instant yellow colouration of the solution occurred, which indicated the successful C-H bond activation. After 16 hours ^{1}H-NMR spectroscopy confirmed the quantitative C-H bond activation. The solution was diluted with additional toluene (14.0 mL) and the polymerisation was started by addition of 2-vinylpyridine (2.84 g, 27.0 mmol, 200 equiv.) in one portion. Aliquots (circa 400 mg per sample) were taken in regular time intervals and poured into methanol (500 µL each). The aliquots were dried and then analysed by ^{1}H-NMR and GPC. After the complete conversion of 2-vinylpyridine, the reaction was terminated by addition of methanol (1.00 mL).

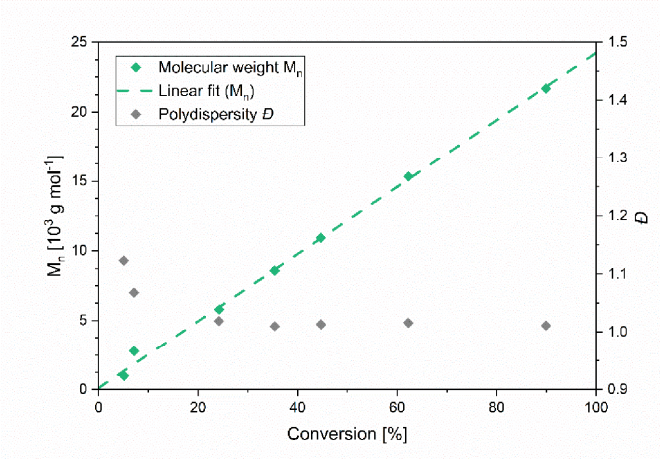

Fig. S7 Conversion-dependant plot of the molecular weights M_n and respective polydispersities $Đ$ of the P2VP aliquots generated with complex **4** and *sym*-collidine as initiator.

5 Synthesis and Characterisation of the Copolymers

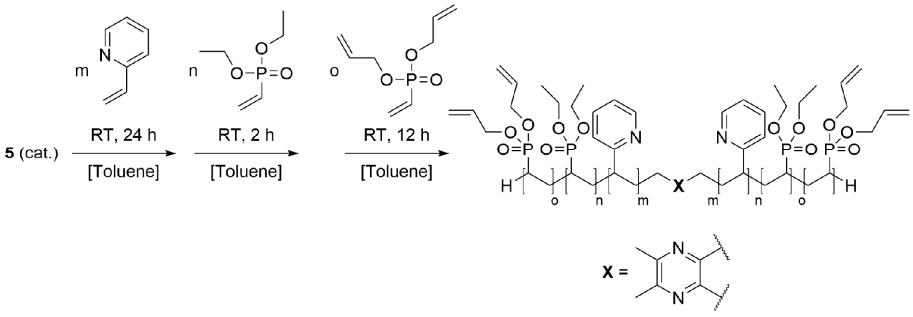

A solution of 2,3,5,6-tetramethylpyrazine (**1**) (1.00 equiv.) in dry toluene (1.00 mL) was added to a solution of $Cp_2Y(CH_2TMS)(THF)$ (**4**) (2.00 equiv.) in absolute toluene (1.00 mL). After the quantitative conversion was detected by ^{1}H-NMR spectroscopy, the reaction mixture was diluted with 8.00 mL of toluene and the respective amount of 2-vinylpyridine was added in one portion. After stirring overnight one aliquot was taken (0.1 mL quenched with 0.4 mL of MeOD-d_4), the conversion of 2-vinylpyridine was determined by ^{1}H-NMR and the calculated amount of DEVP was added to the solution in one portion. After two hours another aliquot was taken (0.1 mL quenched with 0.4 mL of MeOD-d_4) and the conversion of DEVP was determined *via* ^{31}P-NMR. For DAlVP the DEVP procedure was repeated. After ^{31}P-NMR had confirmed the full conversion of DAlVP, the reaction was quenched by addition of methanol (0.5 mL). After precipitation in pentane (200 mL) the clear solution was decanted off, volatiles were removed by drying at ambient temperature and the crude polymer was dissolved in water and freeze-dried.

Molecular weights M_n and the molecular weight distributions of the P2VP block were measured *via* GPC analysis of the first aliquot. The composition B'BABB' of the dried copolymer was determined *via* ^{1}H NMR spectroscopy. Molecular weights of the block copolymer were calculated on basis of the M_n of the P2VP block and the respective composition. The molecular weight distribution of the second sequence was also examined by GPC analysis.

Characterisation of BAB1 (100/200/10)

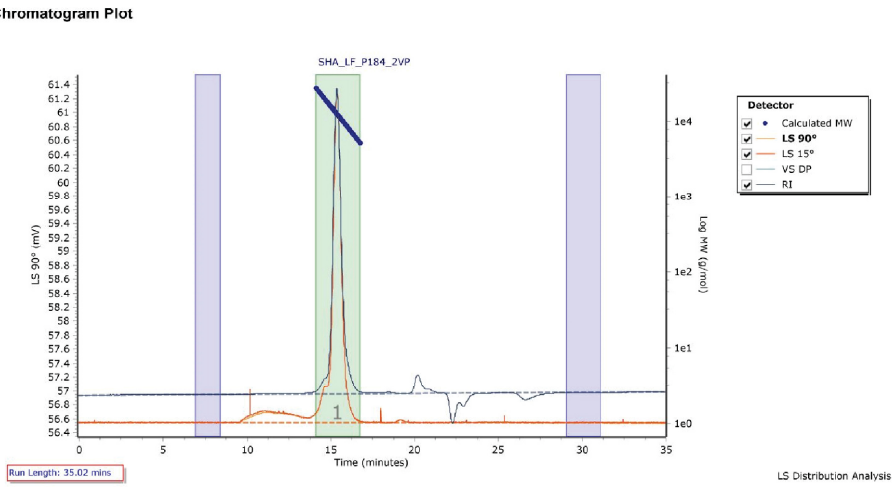

Fig. S8 GPC trace of P2VP block of **BAB1**.

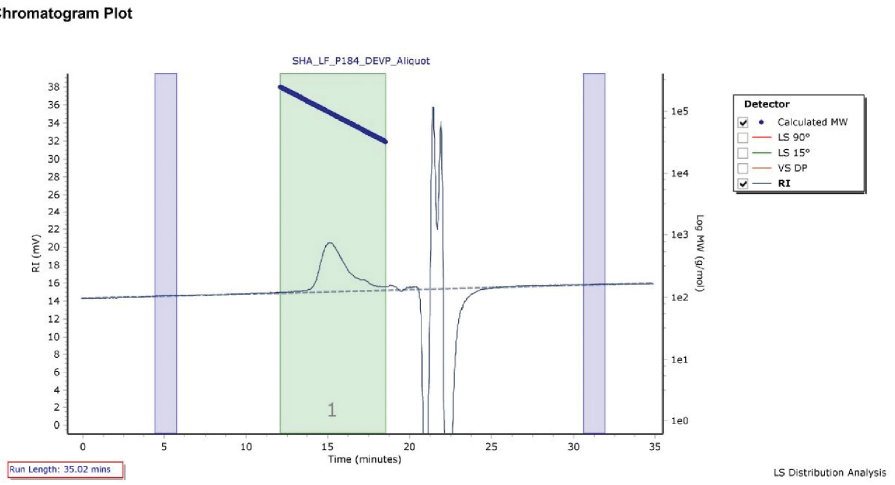

Fig. S9 GPC trace of P2VP-PDEVP blocks of **BAB1**.

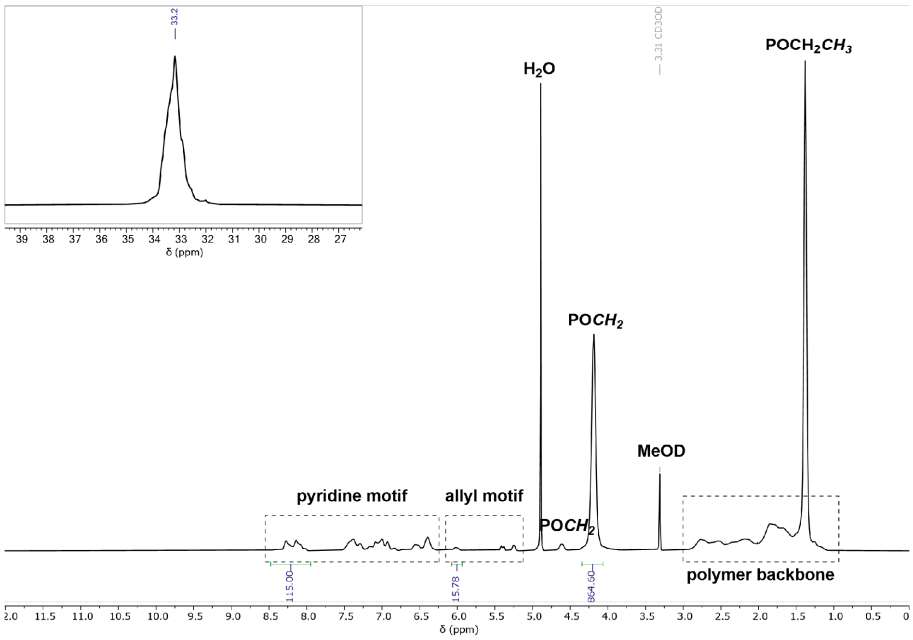

Fig. S10 ^{1}H-NMR and ^{31}P-NMR of **BAB1** in MeOD-d_4.

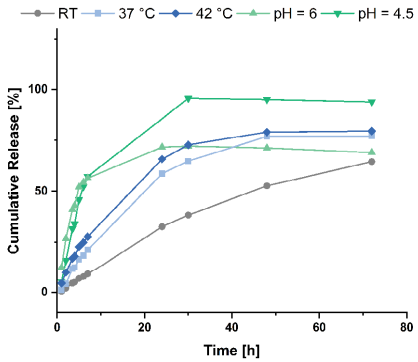

Fig. S11 Cumulative release of fluorescein from **BAB1** under varying conditions.

Characterisation of BAB2 (200/200/10)

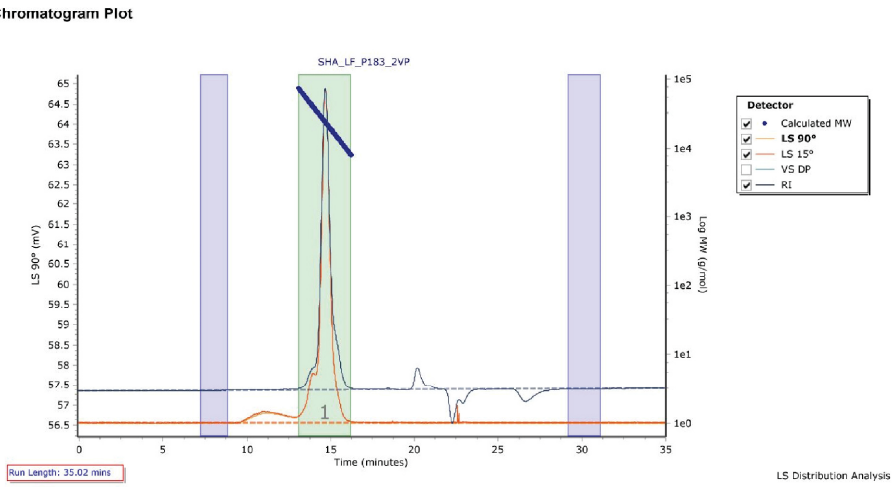

Fig. S12 GPC trace of P2VP block of **BAB2**.

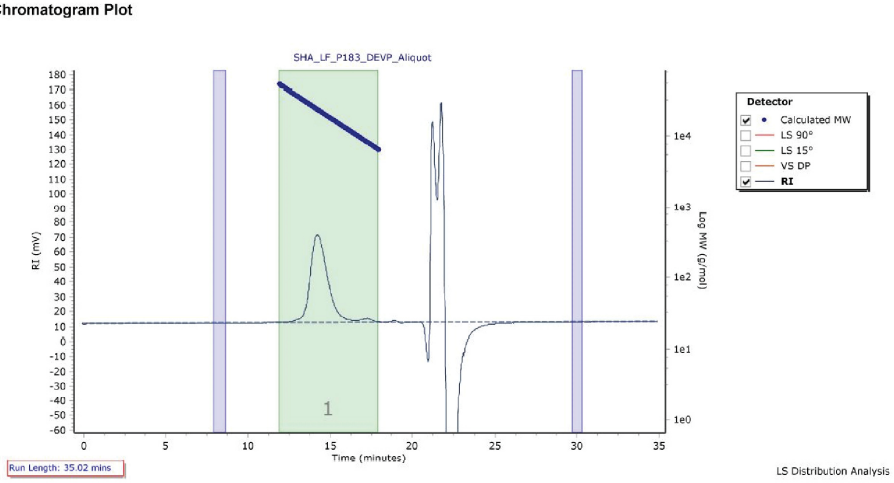

Fig. S13 GPC trace of P2VP-PDEVP blocks of **BAB2**.

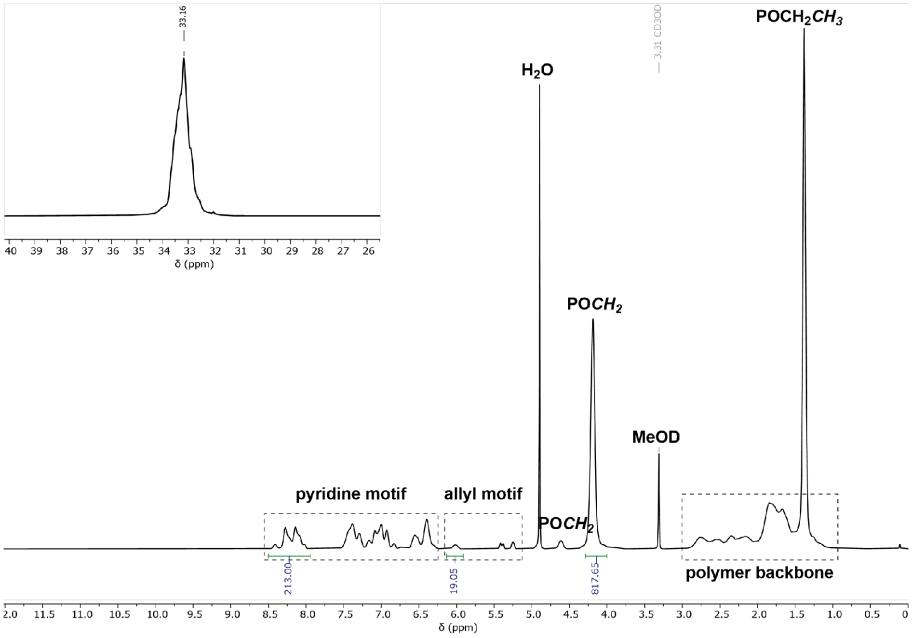

Fig. S14 ^{1}H-NMR and ^{31}P-NMR of **BAB2** in MeOD-d_4.

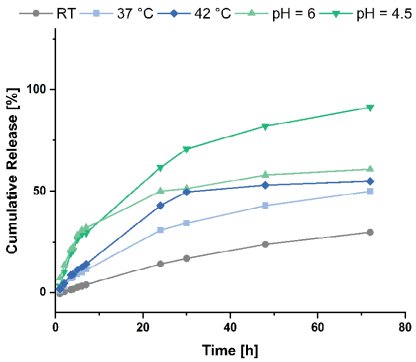

Fig. S15 Cumulative release of fluorescein from **BAB2** under varying conditions.

Characterisation of BAB3 (300/300/10)

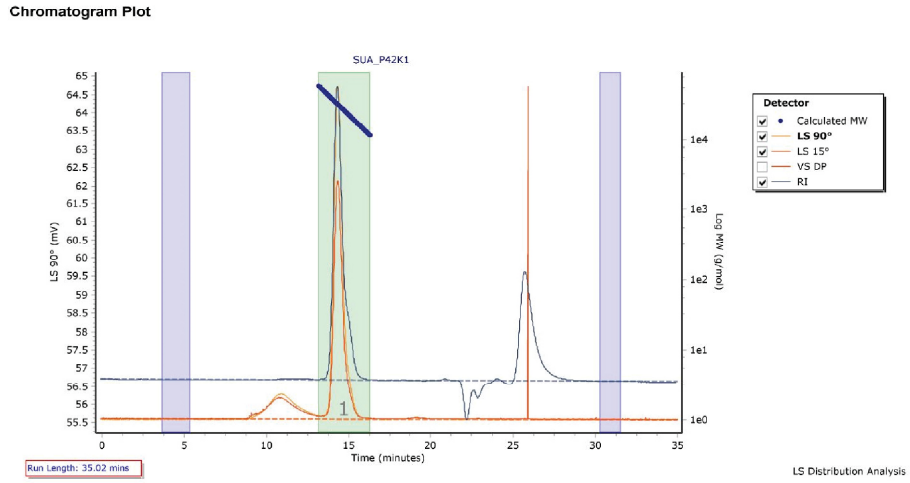

Fig. S16 GPC trace of P2VP block of **BAB3**.

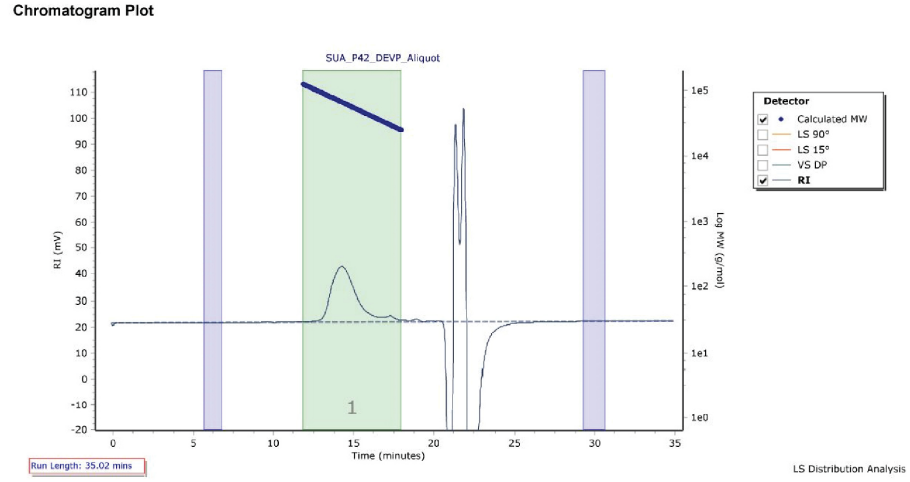

Fig. S17 GPC trace of P2VP-PDEVP blocks of **BAB3**.

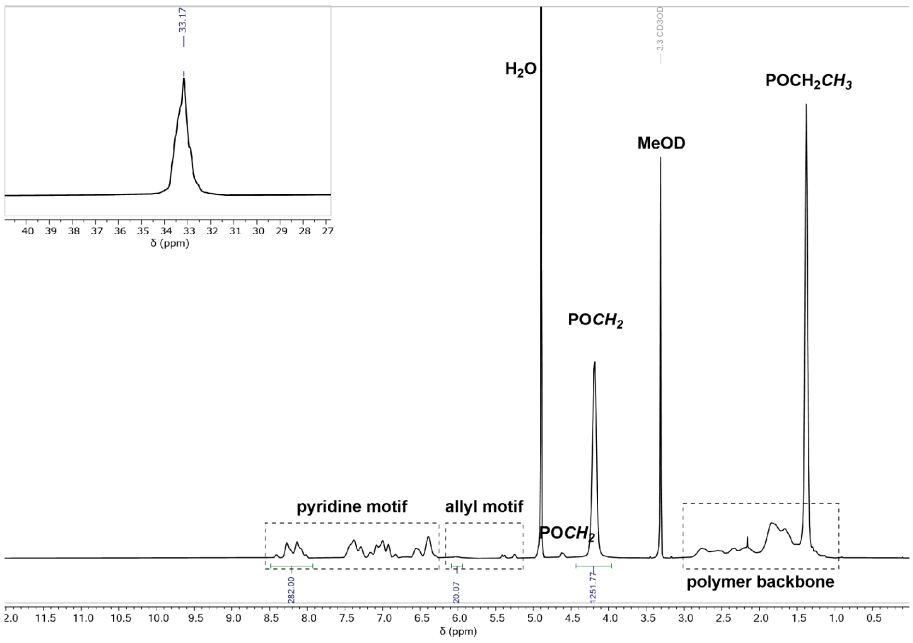

Fig. S18 ^{1}H-NMR and ^{31}P-NMR of **BAB3** in MeOD-d_4.

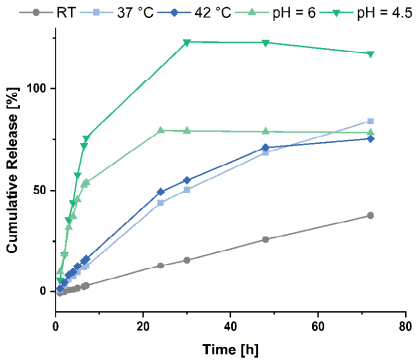

Fig. S19 Cumulative release of fluorescein from **BAB3** under varying conditions.

Characterisation of BAB4 (200/200/6)

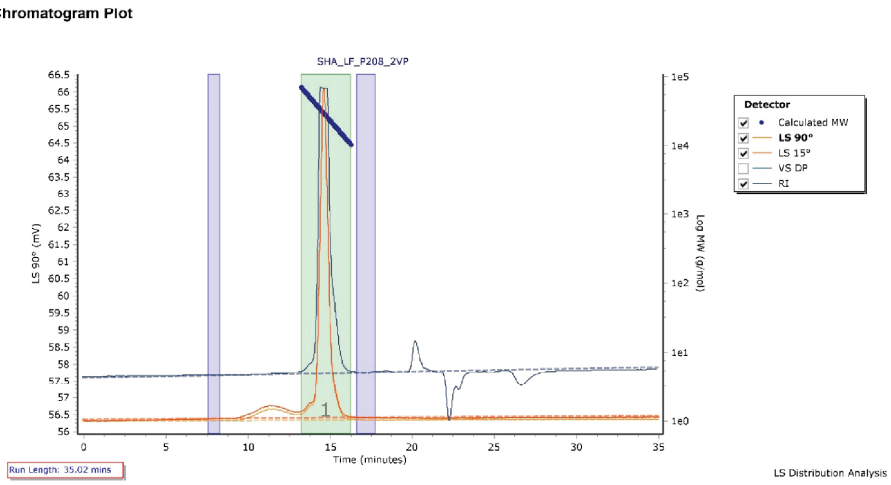

Fig. S20 GPC trace of P2VP blocks of **BAB4**.

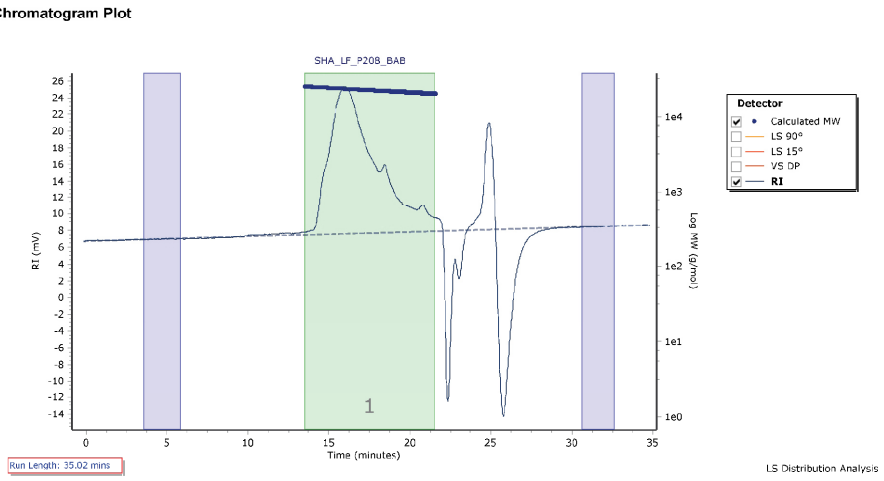

Fig. S21 GPC trace of P2VP-PDEVP blocks of **BAB4**.

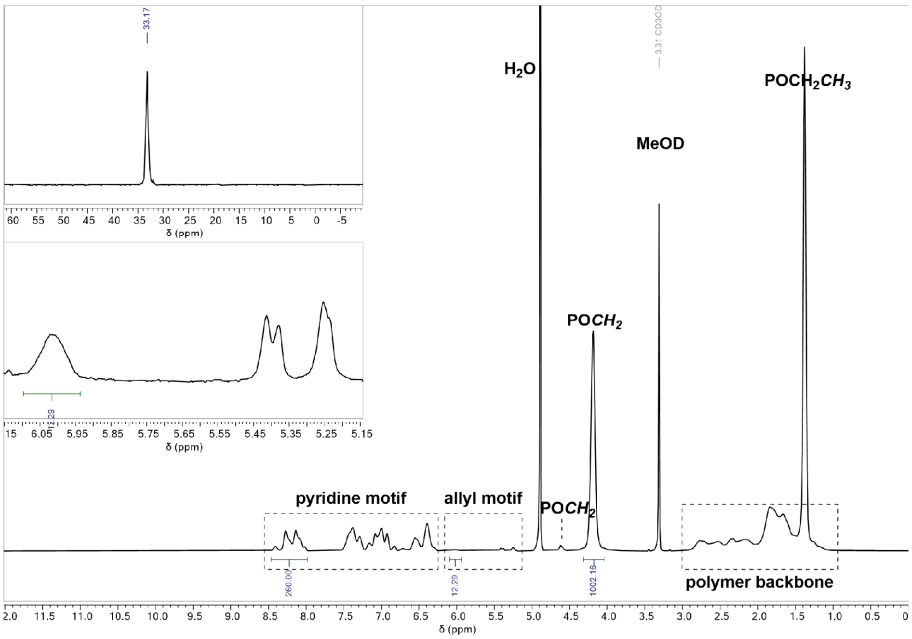

Fig. S22 ^{1}H-NMR and ^{31}P-NMR of **BAB4** in MeOD-*d*$_4$. Zoomed-in view of allylic protons.

Characterisation of BAB5 (200/200/20)

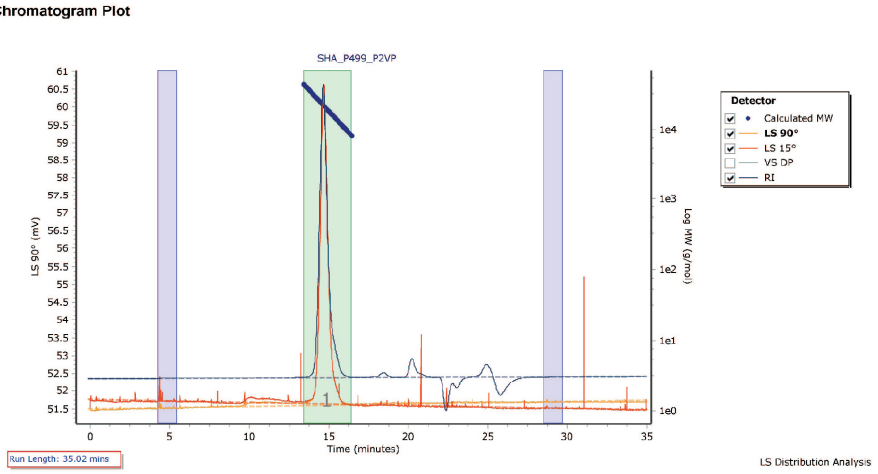

Fig. S23 GPC trace of P2VP block of **BAB5**.

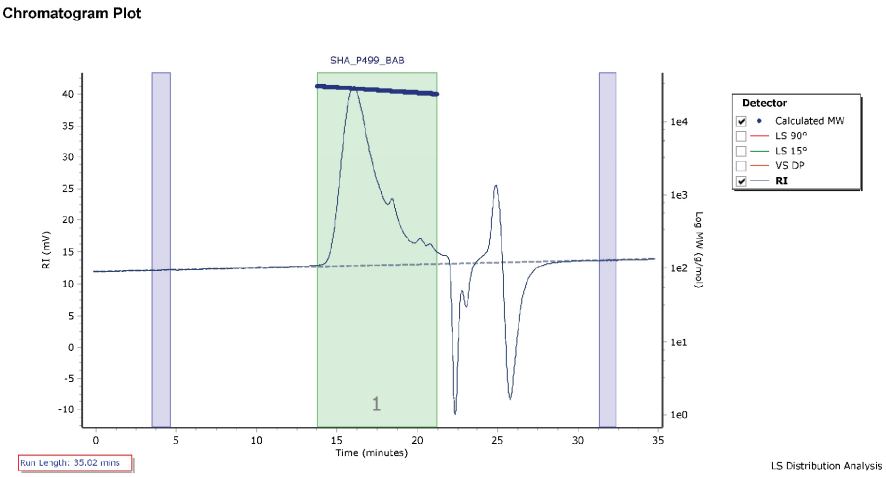

Fig. S24 GPC trace of P2VP-PDEVP block of **BAB5**.

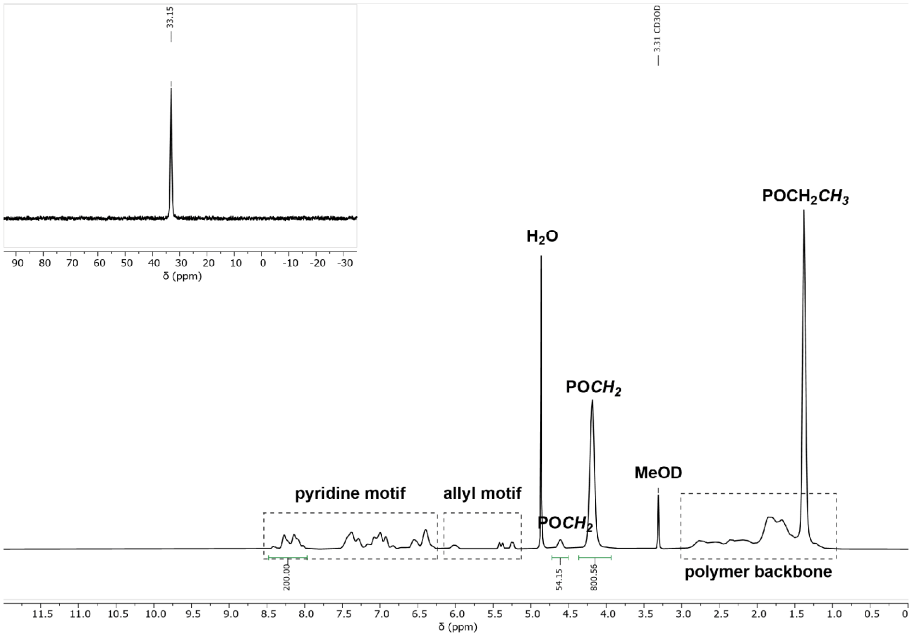

Fig. S25 ^{1}H-NMR and ^{31}P-NMR of **BAB5** in MeOD-*d*$_4$.

6 Cross-Linking of the Copolymers and Characterisation of the Nanoparticles

General procedure for the cross-linking with dithiols 6,7, and 8

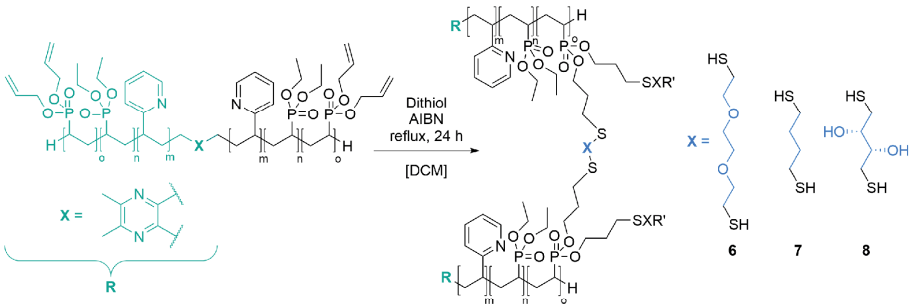

The corresponding copolymer was dissolved in methylene chloride (100 mg per 10 mL DCM) and treated with the respective dithiol (1.50 equiv. of dithiol per allyl group). It is recommended to prepare standard solutions of the dithiols. After addition of catalytic amounts of AIBN, the solution was degassed by the repeated evacuation of the reaction volume and filling with argon (20 iterations). The mixture was refluxed for 24 hours and the reaction progress was checked by proton NMR. After complete conversion of the allyl groups, volatiles were removed in vacuo, and the residue was dissolved in deionised water and purified by dialyses against water. Freeze-drying from water yielded the colourless product.

Characterisation of NP1 (100/200/10 - 3 6-dioxa-1,8-octanedithiol (6))

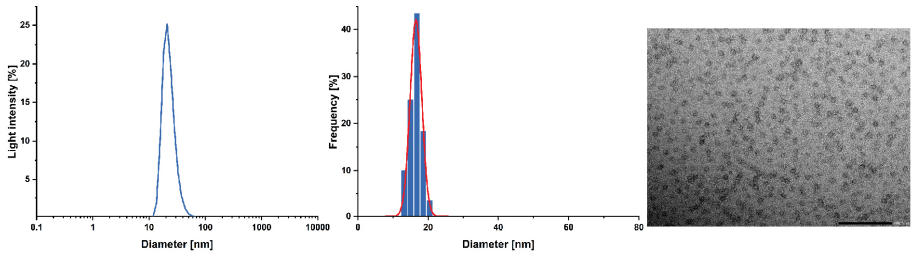

Fig. S26 Size distribution of **NP1** determined *via* DLS measurements at a concentration of 2.5 mg mL^{-1} in *Millipore* water (left); histogram plot with a gaussian regression fit (middle); and a TEM image of **NP1** (right) with a scale bar of 200 nm.

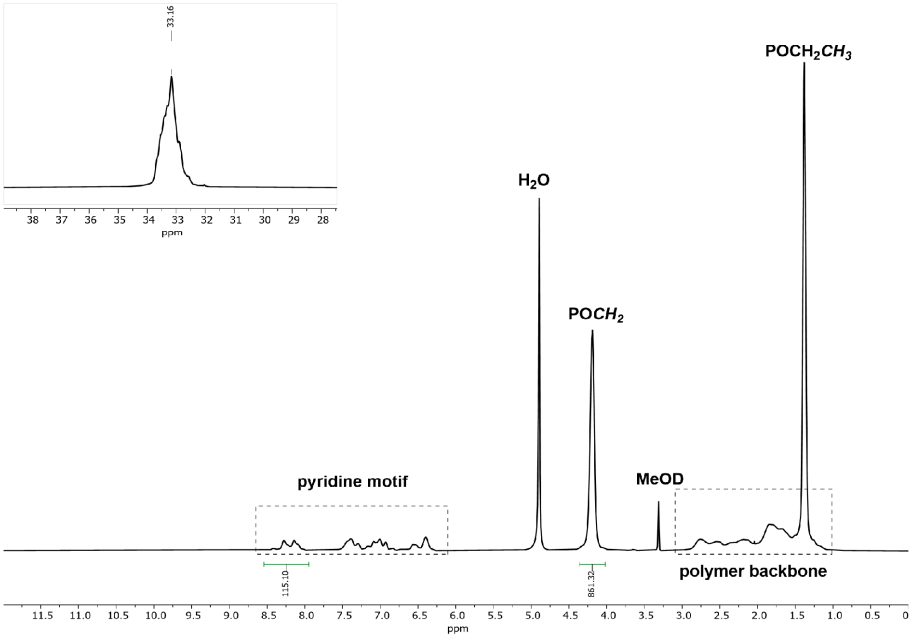

Fig. S27 ^{1}H-NMR and ^{31}P-NMR of **NP1** in MeOD-d_4.

Characterisation of NP2 (200/200/10 - 3 6-dioxa-1,8-octanedithiol (6))

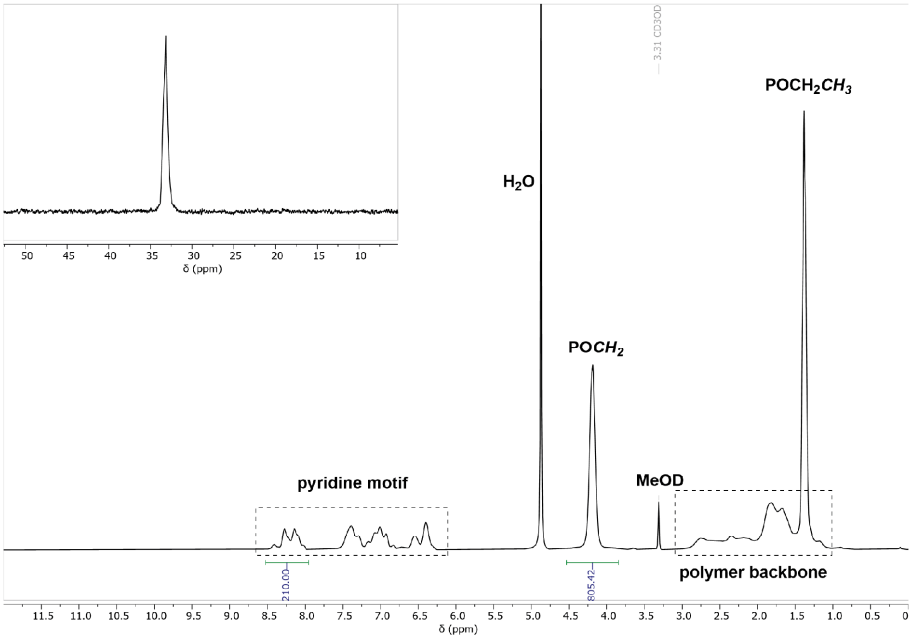

Fig. S28 ^{1}H-NMR and ^{31}P-NMR of **NP2** in MeOD-d_4.

Characterisation of NP3 (300/300/10 - 3 6-dioxa-1,8-octanedithiol (6))

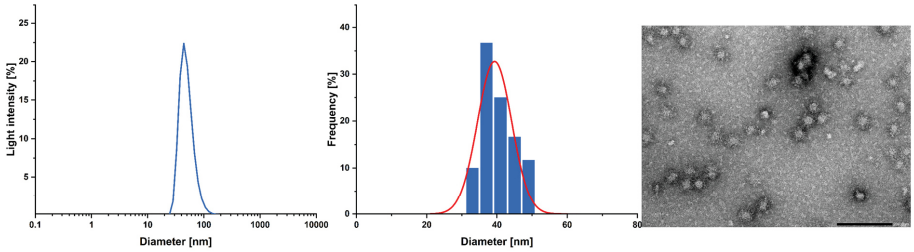

Fig. S29 Size distribution of **NP3** determined *via* DLS measurements at a concentration of 2.5 mg mL^{-1} in *Millipore* water (left); histogram plot with a gaussian regression fit (middle); and a TEM image of **NP3** (right) with a scale bar of 200 nm.

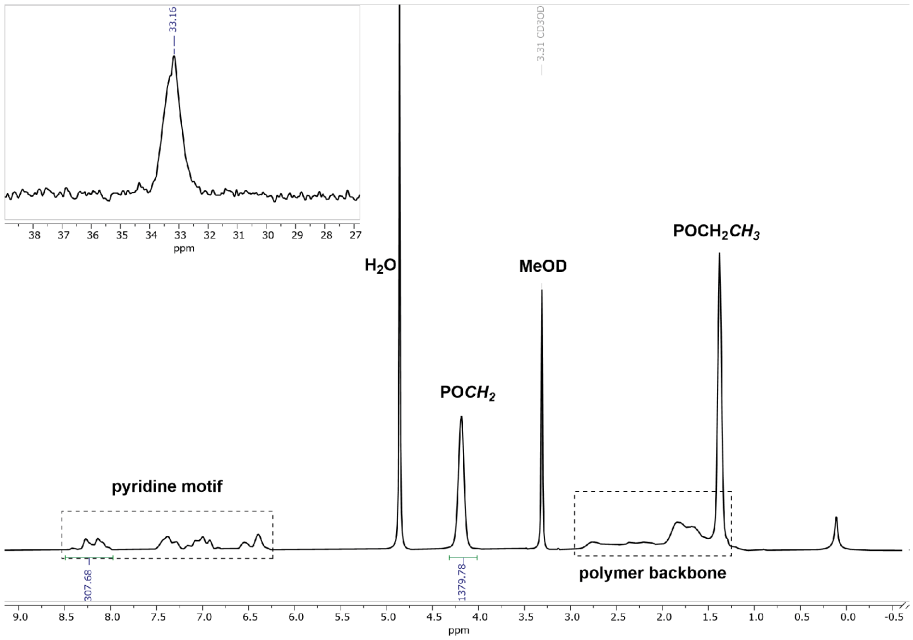

Fig. S30 ^{1}H-NMR and ^{31}P-NMR of **NP3** in MeOD-d_4.

Characterisation of NP4 (200/200/6 - 3 6-dioxa-1,8-octanedithiol (6))

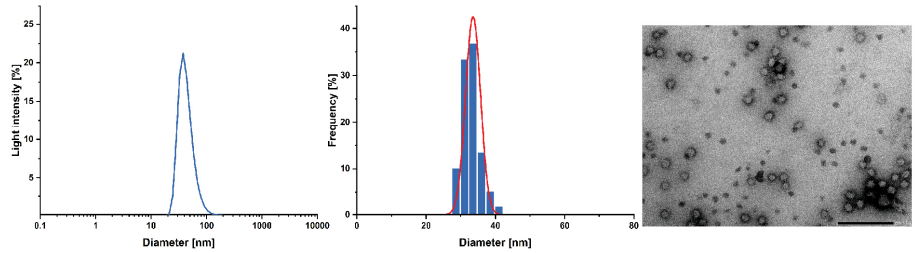

Fig. S31 Size distribution of **NP4** determined *via* DLS measurements at a concentration of 2.5 mg mL^{-1} in *Millipore* water (left); histogram plot with a gaussian regression fit (middle); and a TEM image of **NP4** (right) with a scale bar of 200 nm.

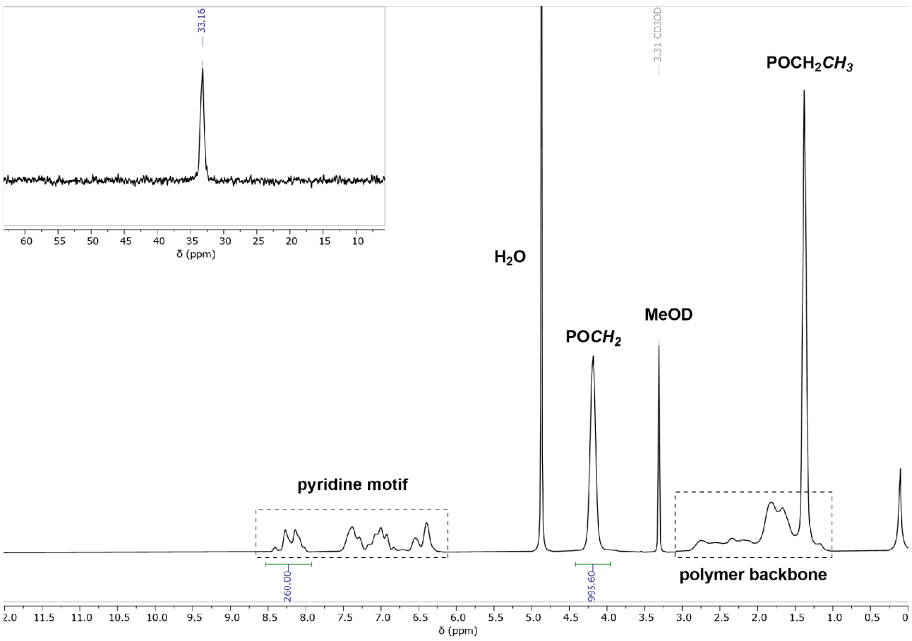

Fig. S32 ^{1}H-NMR and ^{31}P-NMR of **NP4** in MeOD-d_4.

Characterisation of NP5 (200/200/20 - 3 6-dioxa-1,8-octanedithiol (6))

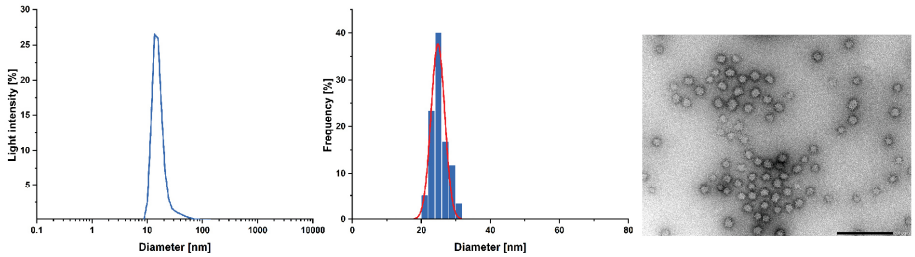

Fig. S33 Size distribution of **NP5** determined *via* DLS measurements at a concentration of 2.5 mg mL^{-1} in *Millipore* water (left); histogram plot with a gaussian regression fit (middle); and a TEM image of **NP5** (right) with a scale bar of 200 nm.

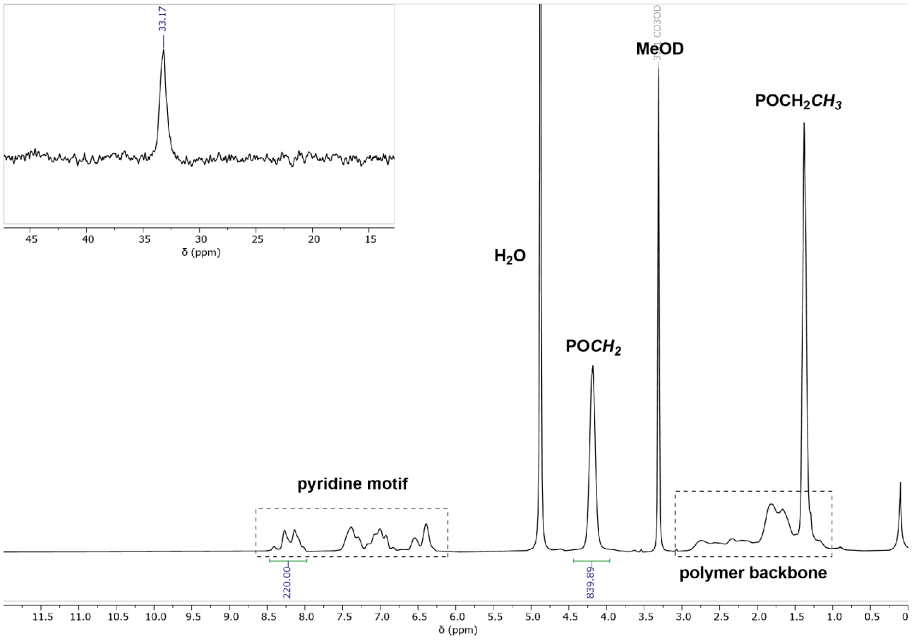

Fig. S34 ^{1}H-NMR and ^{31}P-NMR of **NP5** in MeOD-d_4.

Characterisation of NP6 (200/200/10 – 1,4-butanedithiol (7))

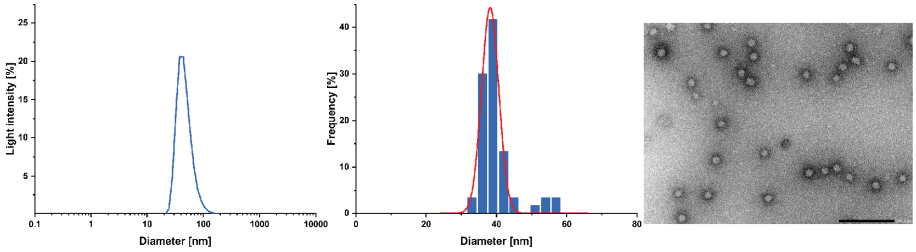

Fig. S35 Size distribution of **NP6** determined *via* DLS measurements at a concentration of 2.5 mg mL^{-1} in *Millipore* water (left); histogram plot with a gaussian regression fit (middle); and a TEM image of **NP6** (right) with a scale bar of 200 nm.

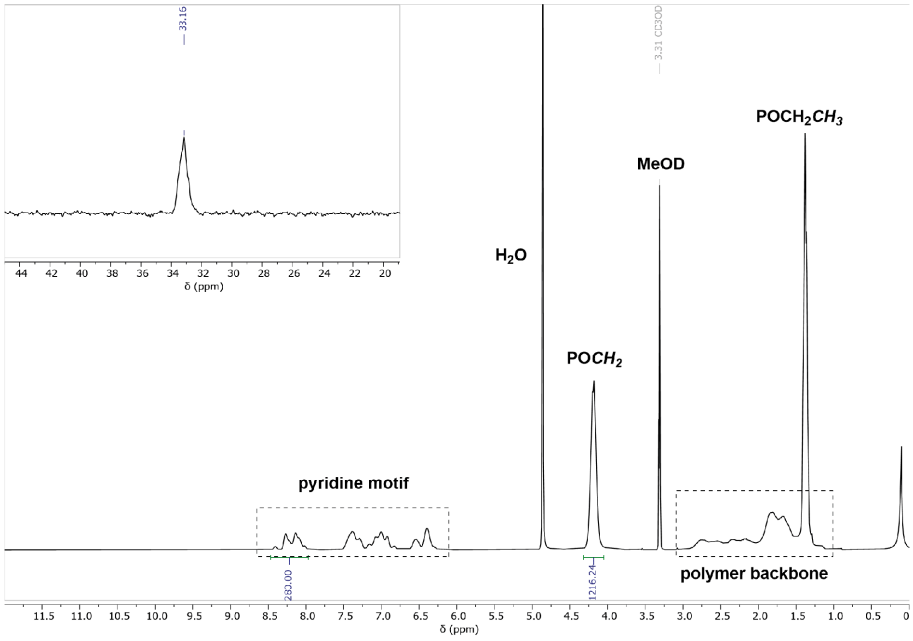

Fig. S36 ^{1}H-NMR and ^{31}P-NMR of **NP6** in MeOD-d_4.

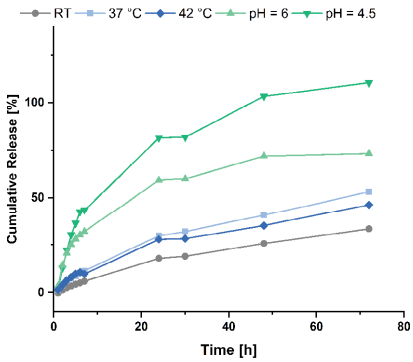

Fig. S37 Cumulative release of fluorescein from **NP6** under varying conditions.

Characterisation of NP7 (200/200/10 – D,L-dithiothreitol (8))

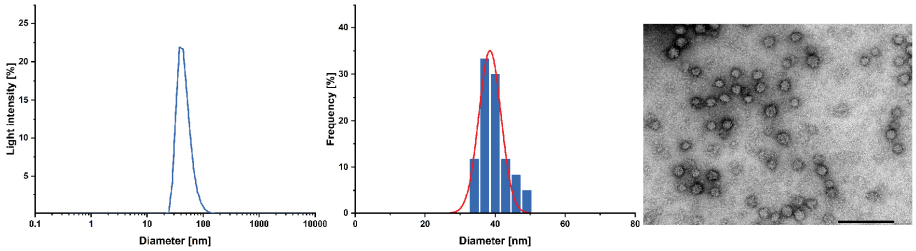

Fig. S38 Size distribution of **NP7** determined *via* DLS measurements at a concentration of 2.5 mg mL^{-1} in *Millipore* water (left); histogram plot with a gaussian regression fit (middle); and a TEM image of **NP7** (right) with a scale bar of 200 nm.

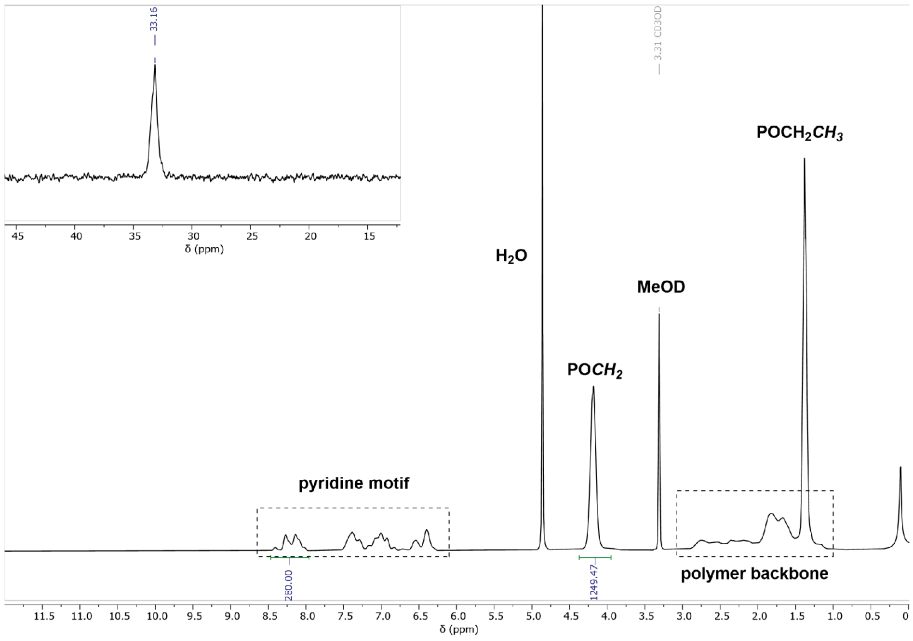

Fig. S39 ^{1}H-NMR and ^{31}P-NMR of **NP7** in MeOD-d_4.

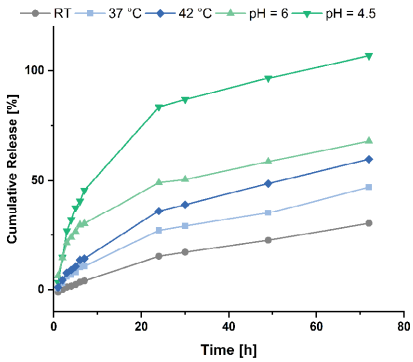

Fig. S40 Cumulative release of fluorescein from **NP7** under varying conditions.

Stability of NP1-NP7 in Chloroform

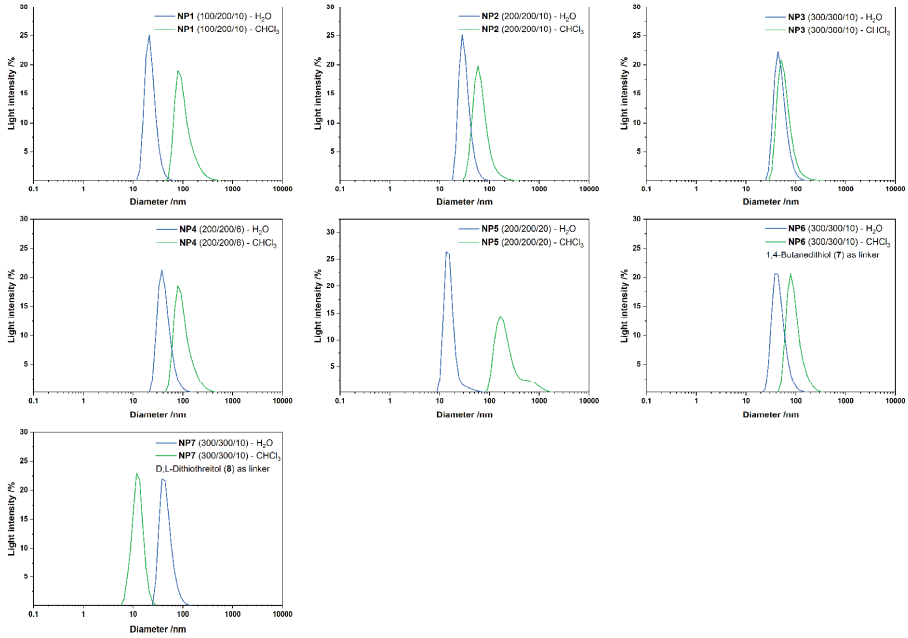

Fig. S41 Size distribution of **NP1-NP7** in *Millipore* water (blue) and chloroform (green) determined via DLS at a concentration of 2.5 mg mL^{-1}.

Determination of the LCST of NP1-NP7

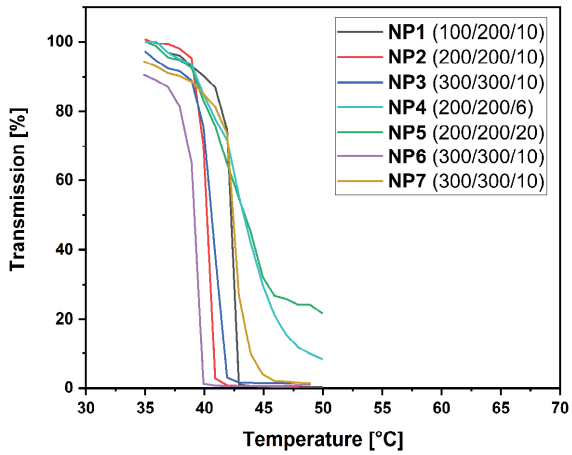

Fig. S42 Determination of the cloud points of the nanoparticles in aqueous solution (2.5 mg mL^{-1}).

7 Synthesis of Folate-Conjugated Nanoparticles

Synthesis of the cysteamine-containing nanoparticles

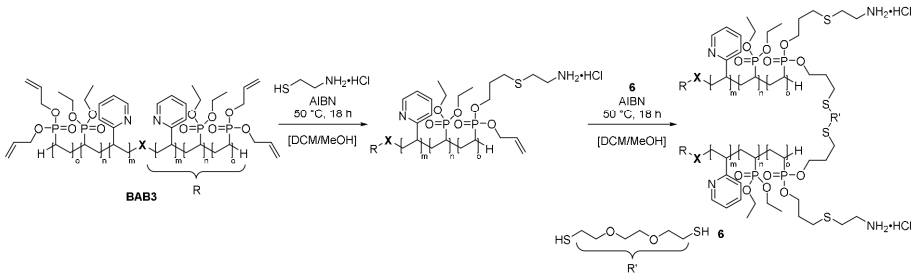

Copolymer **BAB3** (100 mg, 1.23 µmol) was dissolved in methylene chloride (20.0 mg) and treated with cysteamine-hydrochloride (980 µg, 8.62 µmol) in 2.00 mL methanol. After addition of catalytic amounts of AIBN, the solution was degassed, and stirred at 50 °C for 18 hours. The subsequent cross-linking was performed with dithiol **6** (4.90 mg, 26.9 µmol, 1.50 equiv. per allyl group). New AIBN was added and the reaction mixture was again stirred at 50 °C for 18 hours. The reaction progress was checked by proton NMR and after complete conversion of the allyl groups, the solvent was removed *in vacuo*, and the residue was dissolved in deionised water and purified by dialyses against water. Freeze-drying from water yielded the colourless solid (96.0 mg, 94 %).

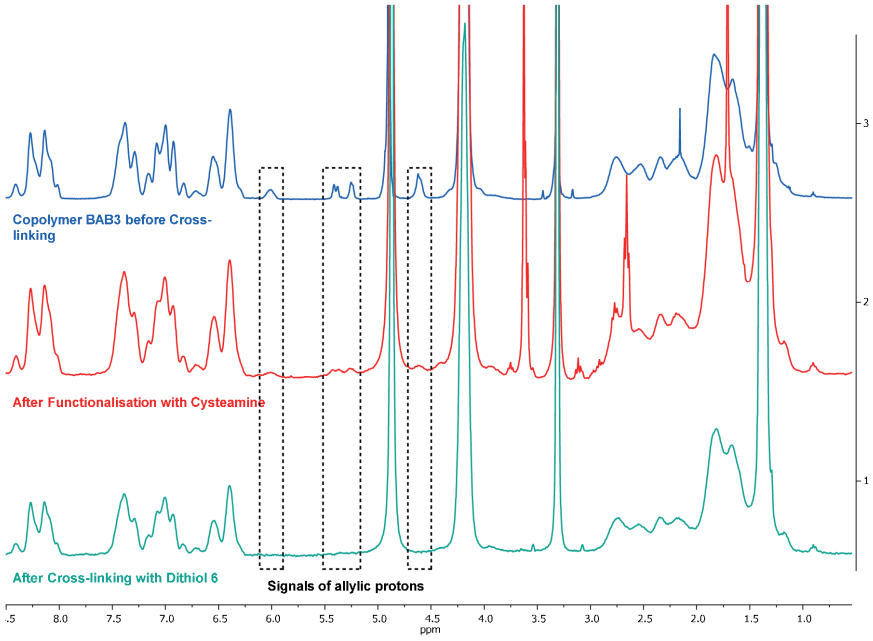

Fig. S43 Monitoring of the sequential functionalisation of **BAB3** (blue) with cysteamine-hydrochloride as linker unit (red) and cross-linking with dithiol **6** (turquoise) recorded in MeOD-d_4.

Conjugation of folate-NHS to the nanoparticle

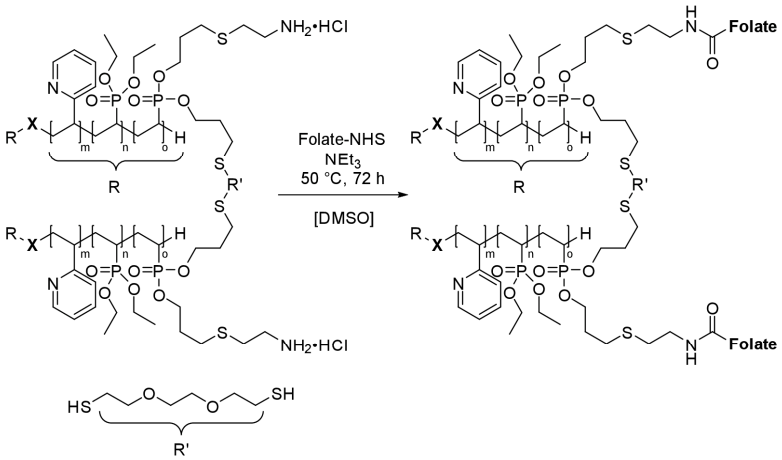

Folate-NHS (8.75 mg, 16.3 mg) and triethylamine (3.38 µL, 24.4 µmol) were added to a solution of the cysteamine-functionalised nanoparticles (96.0 mg, 1.16 µmol) in DMSO (20.0 mL). The solution was heated to 50°C and stirred for 72 hours. The reaction mixture was concentrated in high vacuum and purified by dialysis against water for 96 hours. The resulting, aqueous solution was lyophilised to yield the folate-containing substrate as a light-yellow solid (82.0 mg, 84 %).

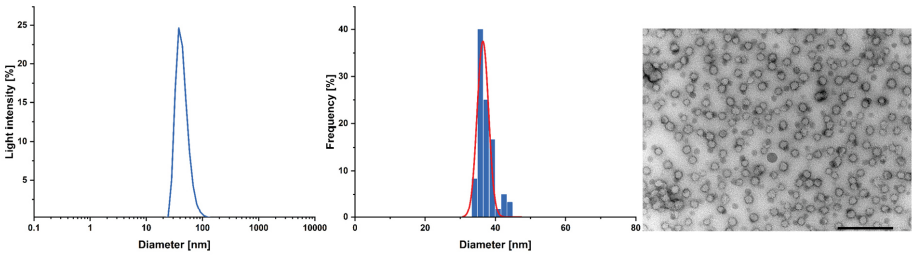

Fig. S44 Size distribution of the folate-functionalised nanoparticle ($2VP_{300}$-$DEVP_{300}$-$DAlVP_{10}$) determined *via* DLS measurements at a concentration of 2.5 mg mL^{-1} in *Millipore* water (left); histogram plot with a *gaussian* regression fit (middle); and a TEM image of folate-functionalised nanoparticle (right) with a scale bar of 200 nm.

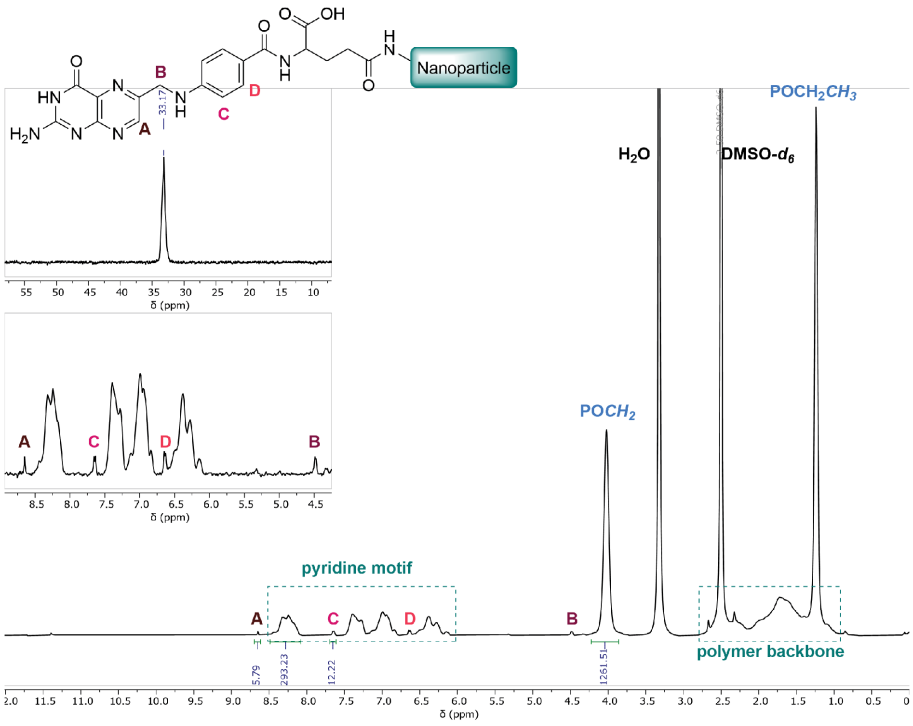

Fig. S45 ^{1}H- and ^{31}P-NMR of the folate functionalised nanoparticle recorded in DMSO-d_6. Detailed view on the region comprising folate corresponding signals between 4.25 and 8.90 ppm.

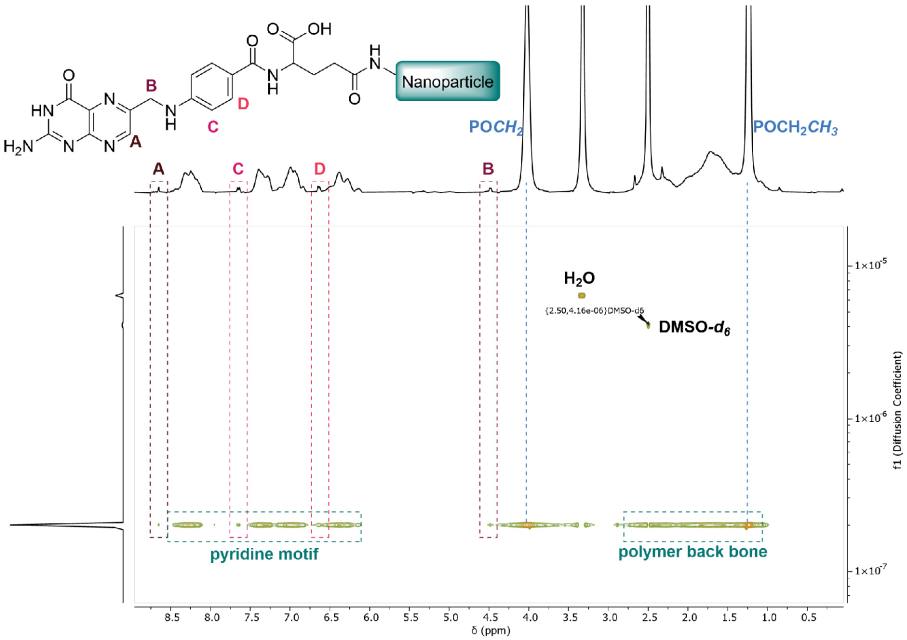

Fig. S46 DOSY-NMR of the folate functionalised nanoparticle recorded in DMSO-d_6.

8 References

1. K. C. Hultzsch, P. Voth, K. Beckerle, T. P. Spaniol and J. Okuda, *Organometallics*, 2000, **19**, 228-243.
2. G. D. Vaughn, K. A. Krein and J. A. Gladysz, *Organometallics*, 1986, **5**, 936-942.
3. C.-X. Cai, L. Toupet, C. W. Lehmann and J.-F. Carpentier, *J. Organomet. Chem.*, 2003, **683**, 131-136.
4. S. Salzinger, B. S. Soller, A. Plikhta, U. B. Seemann, E. Herdtweck and B. Rieger, *J. Am. Chem. Soc.*, 2013, **135**, 13030-13040.
5. B. S. Soller, S. Salzinger, C. Jandl, A. Pöthig and B. Rieger, *Organometallics*, 2015, **34**, 2703-2706.
6. M. Leute, DOI: 10.18725/OPARU-1106PhD, Universitity of Ulm, 2007.
7. C. Schwarzenböck, P. J. Nelson, R. Huss and B. Rieger, *Nanoscale*, 2018, **10**, 16062-16068.
8. L. Rigger, R. L. Schmidt, K. M. Holman, M. Simonović and R. Micura, *Chem. Eur. J.*, 2013, **19**, 15872-15878.
9. C. M. Alexander, K. L. Hamner, M. M. Maye and J. C. Dabrowiak, *Bioconjug. Chem.*, 2014, **25**, 1261-1271.
10. A. F. Trindade, R. F. M. Frade, E. M. S. Macoas, C. Graca, C. A. B. Rodrigues, J. M. G. Martinho and C. A. M. Afonso, *Org. Biomol. Chem.*, 2014, **12**, 3181-3190.

12.4 Experimental Section for Chapter 8

General Consideration

All air- and moisture sensitive reactions were carried out in heat dried glassware under an oxygen-free and dry argon atmosphere (Argon 4.6, *Westfalen AG*) using standard Schlenk or glovebox techniques. For that purpose, all glassware was heat-dried under high vacuum prior to use. Dichloromethane and toluene were dried using a SPS-800 solvent purification system (*MBraun*) and were stored over molecular sieves (3 Å). HPLC grade THF was purchased from *Sigma-Aldrich*. and were used without further purification steps. The precursors $Y(CH_2TMS)_3(THF)_2$, $LiCH_2TMS$, and complex the $Cp_2Y(CH_2TMS)(THF)$ (**1**) as well as the initiator 2,6-dimethyl-4-(4-vinylphenyl)pyridine (**4**) were synthesized according to published procedures.[52, 74, 132-134] C-H bond activations for the polymerizations were performed as described in the literature.[56, 74] DEVP and DAlVP were prepared according to procedures found in the literature.[77, 131, 135] The monomers were dried over CaH_2 and distilled prior to use.

Infrared Spectroscopy

Fourier transform infrared spectra (FTIR) were recorded a *Vertex 70 FTIR* (*Bruker*) equipped with a *Platinum ATR* from *Bruker*.

Nuclear Magnetic Resonance Spectroscopy

Nuclear magnetic resonance spectra were recorded on a *Bruker AVIII 400 HD* (400 MHz) or an *AVIII 500 cryo* (500 MHz). Deuterated solvents were purchased from *Sigma-Aldrich*. For moisture-sensitive substances the solvents were dried and stored over 3 Å molecular sieve. Spectroscopic chemical shifts δ are reported in ppm and calibrated to the residual proton signals of the used solvents.

Benzene-d_6: δ (ppm) = 7.16 (^{1}H-NMR).
Dimethyl sulfoxide-d_6: δ (ppm) = 2.50 (^{1}H-NMR).
Methanol-d_4: δ (ppm) = 3.31 (^{1}H-NMR)).

Unless otherwise stated coupling constants *J* are mean values and refer to coupling between two protons. For the assignment of the signals the signal multiplicities were abbreviated accordingly: s – singlet, d – duplet, t – triplet, m – multiplet.

Determination of the Lower Critical Solution Temperature

Lower critical solution temperatures were determined on a *Cary 50* UV/Vis spectrophotometer (*Varian*) equipped with a Peltier thermostat using conventional glass cuvettes (4 mL). The polymer solutions (2.5 mg mL^{-1} in deionized water) were heated at rate of 1 K min^{-1} followed by a five-minute-long equilibration period. The cloud points T_c was defined as a 10% decrease of transmittance at a wavelength of 500 nm.

Swelling Experiments

Swelling experiments were performed in water, PBS buffer, acetonitrile, and toluene. The mass of the dry hydrogel sample was determined, covered with the respective solvent, and kept in a sealed vial for 24 hours. Hereafter, the

swollen hydrogel was taken off the solvent, superficial solvent was removed, and the sample was weighed again. The swelling factor was calculated according to following formula: Swelling ratio = $(W_s\text{-}W_d)/(W_d) \cdot 100$ %.

Stability Experiments

In a similar manner to the swelling experiments, the hydrogels were swelled in water for 24 hours. Excess water was removed, and the swollen samples were freed from superficial water. Hereafter, the sample was weighed in a tared vial in regular time intervals to monitor the water loss.

Water Release Experiments

In a similar manner to the stability experiments, the hydrogels were swelled in water for 24 hours. Excess water was removed, and swollen samples were freed from superficial water. Hereafter, the samples were kept in a tared, sealed vial and the surrounding temperature was risen in regular steps until the dry mass was reached. The samples were equilibrated for five minutes for each temperature point and weighed after removing surface water.

General Procedure for the Statistical Copolymerization of DEVP and DAlVP

The polymerization procedure was adopted from reference [74].[74] When the C-H bond activation had reached full conversion, the reaction solution was diluted with absolute toluene (7.00 mL) and a solution of DEVP and DAlVP in absolute toluene (1.00 mL) was added in one portion. After 12 hours ^{31}P-NMR spectroscopy revealed full monomer conversion. The reaction was terminated with methanol (500 µL), the polymer was precipitated in excess pentane, and the supernatant solvent was decanted off. The crude polymer was dried, dissolved in water, and lyophilized thereof.

^{1}H-NMR (500 MHz, MeOD-*d_4*, 300 K): δ (ppm) = 7.76 (s, $CH_{Ar,Initiator}$), 7.61 – 7.30 (m, $CH_{Ar,\ Initiator}$), 6.80 (dd, ^{3}J = 10.8, 17.3 Hz, $CH_{Vinyl,Initiator}$), 6.04 (s, CH_{Allyl}), 5.88 (d, ^{3}J = 17.3 Hz, $CH_{Vinyl,Initiator}$), 5.42 (d, ^{3}J = 16.3 Hz, CH_{Allyl}), 5.28 (s, CH_{Allyl}), 4.62 (s, PO*CH_2*), 4.19 (s, PO*CH_2*), 2.92 – 1.19 (m, PDAVP backbone), 1.38 (s, $POCH_2$*CH_3*).

^{31}P-NMR (203 MHz, MeOD-*d_4*, 300 K) δ (ppm) = 33.2.

IR (ATR): $\tilde{\upsilon}$ (cm^{-1}) = 3476 (br m), 2982 (m, $\nu_{C\text{-}H}$), 2934 (m, $\nu_{C\text{-}H}$), 2907 (w, $\nu_{C\text{-}H}$), 2870 (w, $\nu_{C\text{-}H}$), 1655 (m), 1479 (w, $\delta_{C\text{-}H}$), 1443 (m, $\delta_{C\text{-}H}$), 1392 (m, $\delta_{C\text{-}H}$), 1369 (w, $\delta_{C\text{-}H}$), 1221 (st, $\nu_{P=O}$), 1161 (m, $\nu_{C\text{-}O}$), 1097 (w), 1044 (w, $\nu_{P\text{-}O}$), 1015 (st, $\nu_{P\text{-}O}$), 949 (st), 779 (st).

General Procedure for the Hydrosilylation

Prior to use the copolymer was kept under high vacuum for several minutes. The polymer was dissolved in absolute toluene (15 mL solvent per 500 mg polymer) after refilling the reaction flask with argon. The siloxane (one Si-H motif per allyl motif) and three drops of *Karstedt's* catalyst were added to the solution and heated to 110 °C. After the gel formation had started, the reaction was kept an additional hour at this temperature, cooled to room temperature and was separated from the solvent *in vacuo*. The residue was washed several times with pentane, diethyl ether and, *iso*-propanol to purify the hydrogel. Eventually, the crude hydrogel was treated with water and freeze-dried.

^{1}H-NMR (400 MHz, DMSO-d_6, 300 K): δ (ppm) = 4.03 (br s, POCH_2), 2.79 – 0.87 (m, PDAVP backbone), 1.24 (s, POCH$_2$$CH_3$), 0.16 – -0.14 (br m, Siloxane).

^{31}P-NMR (162 MHz, DMSO-d_6, 300 K) δ (ppm) = 33.1.

IR (ATR): $\tilde{\upsilon}$ (cm^{-1}) = 3466 (br m), 2979 (m, $\nu_{C\text{-}H}$), 2933 (m, $\nu_{C\text{-}H}$), 2911 (w, $\nu_{C\text{-}H}$), 2870 (w, $\nu_{C\text{-}H}$), 1714 (m), 1653 (m), 1479 (w, $\delta_{C\text{-}H}$), 1445 (m, $\delta_{C\text{-}H}$), 1392 (m, $\delta_{C\text{-}H}$), 1367 (w, $\delta_{C\text{-}H}$), 1221 (st, $\nu_{P=O}$), 1162 (m, $\nu_{C\text{-}O}$), 1096 (w), 1043 (w, $\nu_{P\text{-}O}$), 1015 (st, $\nu_{P\text{-}O}$), 950 (st), 781 (st).

Procedure for the Thiol-Ene Click Reaction

Prior to use the copolymer (250 mg, 1.83 µmol, n_{Allyl} = 187 µmol) was kept under high vacuum for several minutes. The polymer was dissolved in THF (7 mL) after refilling the reaction flask with argon. 3,6-Dioxa-1,8-octanedithiol (**6**) (34.1 mg, 187 µmol; one equivalent dithiol per DAlVP unit) and catalytic amounts of AIBN were added to the solution. The solution was degassed by repeatedly drawing vacuum and refilling with argon (20 iterations), heated to 70 °C, and was kept at this temperature for one hour. After the gel formation had started, the reaction was heated for an additional hour and then cooled to room temperature. The solvent was removed *in vacuo* and the residue was washed several times with pentane, diethyl ether, and *iso*-propanol to purify the hydrogel. Eventually, the crude hydrogel was treated with water and freeze-dried.

^{1}H-NMR (400 MHz, DMSO-d_6, 300 K): δ (ppm) = 4.01 (s, POCH_2), 2.88 – 1.03 (m, PDAVP backbone), 1.23 (s, POCH$_2$$CH_3$).

^{31}P-NMR (162 MHz, DMSO-d_6, 300 K) δ (ppm) = 33.2.

Procedure for the Cross Metathesis

Prior to use the copolymer (300 mg, 2.20 µmol, n_{Allyl} = 449 µmol) was kept under high vacuum for several minutes. The polymer was the dissolved in absolute dichloromethane (10 mL) and treated with the *Grubbs* I catalyst (5.00 mg, 6.08 µmol, 1.35 mol% respective to allyl groups). The reaction mixture was refluxed for 48 hours. The progress of the reaction was checked by ^{1}H- and ^{31}P-NMR in MeOD. New *Grubbs* I catalyst (2.50 mg) was added, and the mixture was refluxed for another 24 hours to reach full conversion of the allyl groups. Eventually, dichloromethane was removed by a rotary evaporator and the residue was washed several times with pentane, diethyl ether and *iso*-propanol to purify the hydrogel. The crude hydrogel was treated with benzene and freeze-dried.

^{1}H-NMR (400 MHz, MeOD-d_4, 300 K): δ (ppm) = 6.04 (s, CH_{Allyl}), 5.85 (s, CH=$CH_{cis/trans}$), 5.43 (dd, J = 18.4, 7.0 Hz, CH_{Allyl}), 5.27 (s, CH_{Allyl}), 4.63 (s, $CH_{2,Allyl}$), 4.18 (s, POCH_2), 2.92 – 1.00 (m, PDEVP backbone), 1.38 (s, POCH$_2$$CH_3$).

^{31}P-NMR (162 MHz, MeOD-d_4, 300 K) δ (ppm) = 33.2.

13 Copyright Licenses

Rightslink® by Copyright Clearance Center https://s100.copyright.com/AppDispatchServlet#formTop

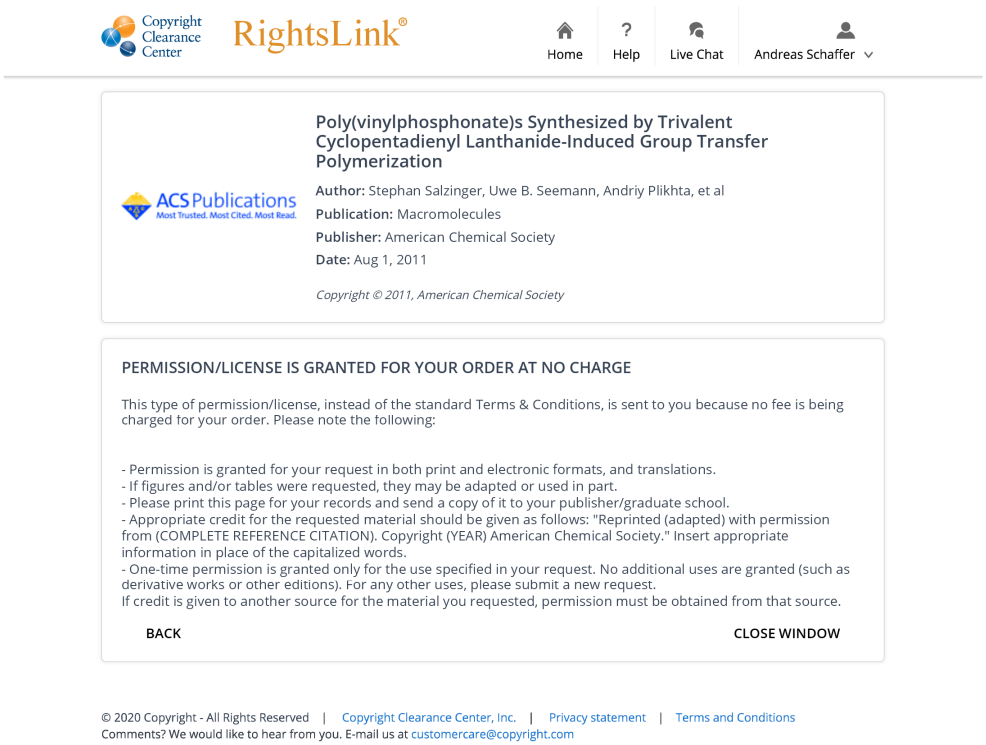

Rightslink® by Copyright Clearance Center https://s100.copyright.com/AppDispatchServlet#formTop

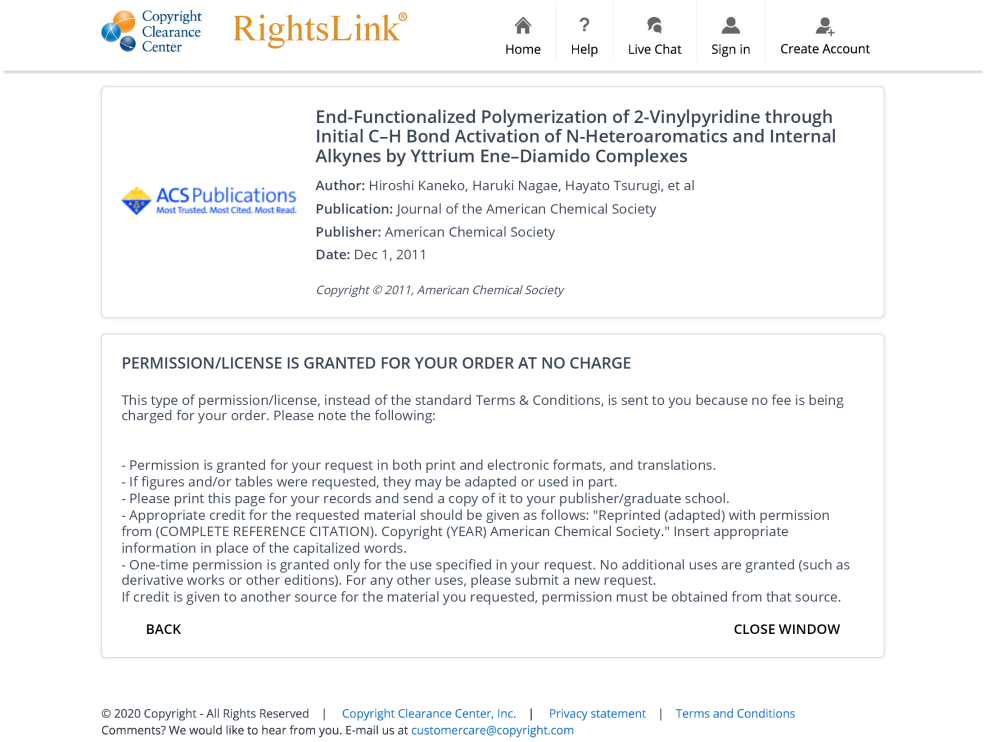

Copyright Licenses

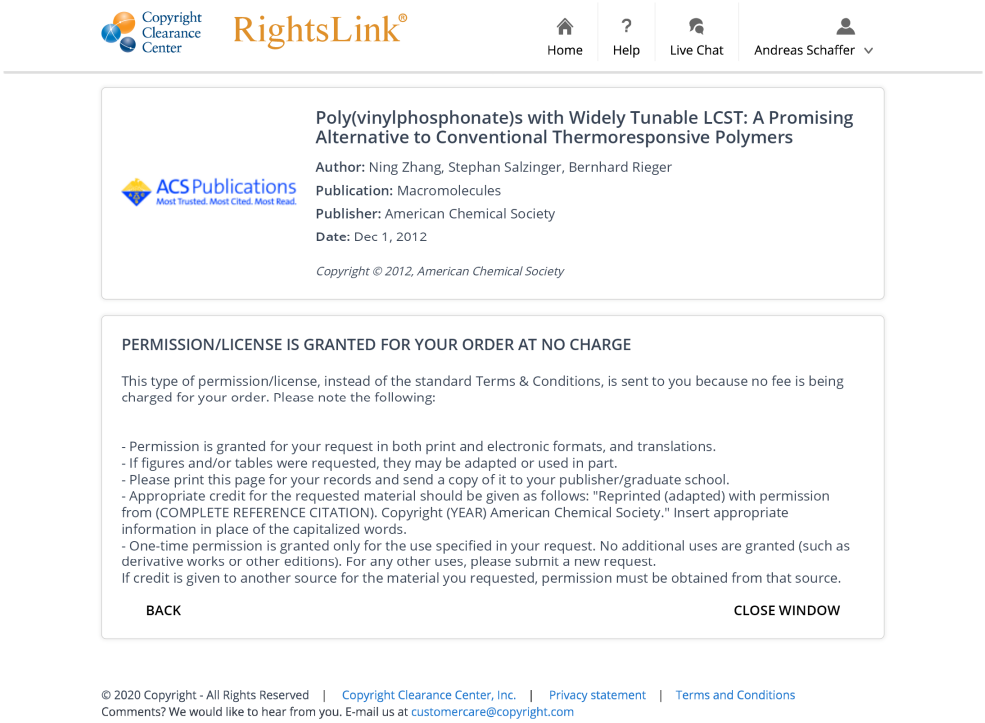

Copyright Clearance Center RightsLink®

Home | Help | Live Chat | Andreas Schaffer

ACS Publications Most Trusted. Most Cited. Most Read.

Poly(vinylphosphonate)s with Widely Tunable LCST: A Promising Alternative to Conventional Thermoresponsive Polymers

Author: Ning Zhang, Stephan Salzinger, Bernhard Rieger
Publication: Macromolecules
Publisher: American Chemical Society
Date: Dec 1, 2012

Copyright © 2012, American Chemical Society

PERMISSION/LICENSE IS GRANTED FOR YOUR ORDER AT NO CHARGE

This type of permission/license, instead of the standard Terms & Conditions, is sent to you because no fee is being charged for your order. Please note the following:

- Permission is granted for your request in both print and electronic formats, and translations.
- If figures and/or tables were requested, they may be adapted or used in part.
- Please print this page for your records and send a copy of it to your publisher/graduate school.
- Appropriate credit for the requested material should be given as follows: "Reprinted (adapted) with permission from (COMPLETE REFERENCE CITATION). Copyright (YEAR) American Chemical Society." Insert appropriate information in place of the capitalized words.
- One-time permission is granted only for the use specified in your request. No additional uses are granted (such as derivative works or other editions). For any other uses, please submit a new request.

If credit is given to another source for the material you requested, permission must be obtained from that source.

BACK CLOSE WINDOW

Rightslink® by Copyright Clearance Center https://s100.copyright.com/AppDispatchServlet#formTop

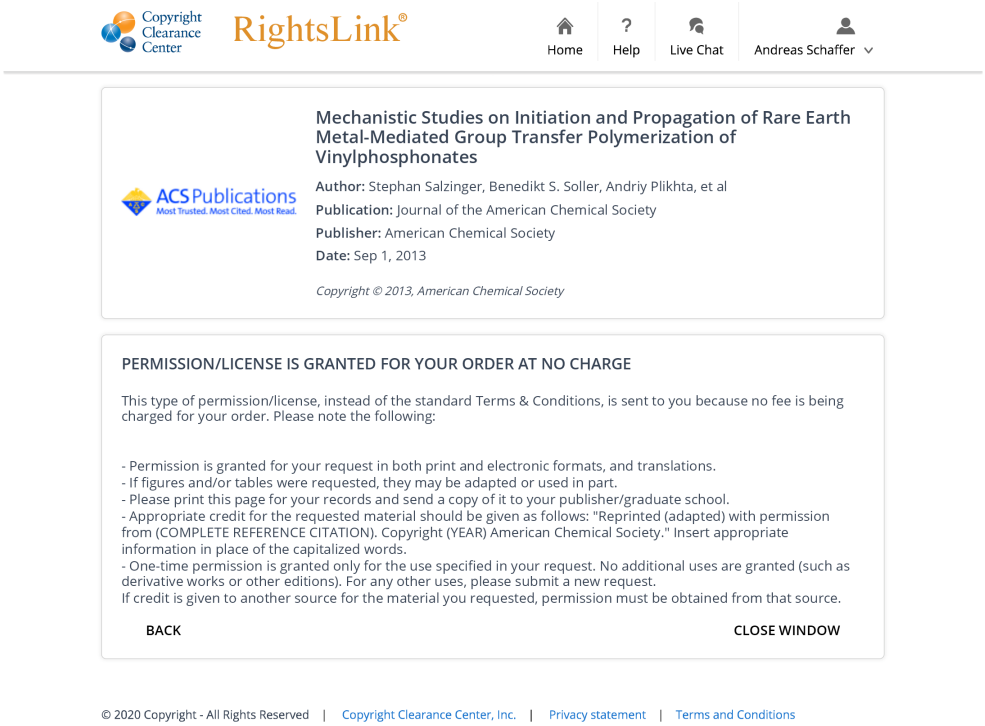

Copyright Clearance Center RightsLink®

Home | Help | Live Chat | Andreas Schaffer

ACS Publications Most Trusted. Most Cited. Most Read.

Mechanistic Studies on Initiation and Propagation of Rare Earth Metal-Mediated Group Transfer Polymerization of Vinylphosphonates

Author: Stephan Salzinger, Benedikt S. Soller, Andriy Plikhta, et al
Publication: Journal of the American Chemical Society
Publisher: American Chemical Society
Date: Sep 1, 2013

Copyright © 2013, American Chemical Society

PERMISSION/LICENSE IS GRANTED FOR YOUR ORDER AT NO CHARGE

This type of permission/license, instead of the standard Terms & Conditions, is sent to you because no fee is being charged for your order. Please note the following:

- Permission is granted for your request in both print and electronic formats, and translations.
- If figures and/or tables were requested, they may be adapted or used in part.
- Please print this page for your records and send a copy of it to your publisher/graduate school.
- Appropriate credit for the requested material should be given as follows: "Reprinted (adapted) with permission from (COMPLETE REFERENCE CITATION). Copyright (YEAR) American Chemical Society." Insert appropriate information in place of the capitalized words.
- One-time permission is granted only for the use specified in your request. No additional uses are granted (such as derivative works or other editions). For any other uses, please submit a new request.

If credit is given to another source for the material you requested, permission must be obtained from that source.

BACK CLOSE WINDOW

© 2020 Copyright - All Rights Reserved | Copyright Clearance Center, Inc. | Privacy statement | Terms and Conditions
Comments? We would like to hear from you. E-mail us at customercare@copyright.com

Copyright Licenses

Rightslink® by Copyright Clearance Center https://s100.copyright.com/AppDispatchServlet#formTop

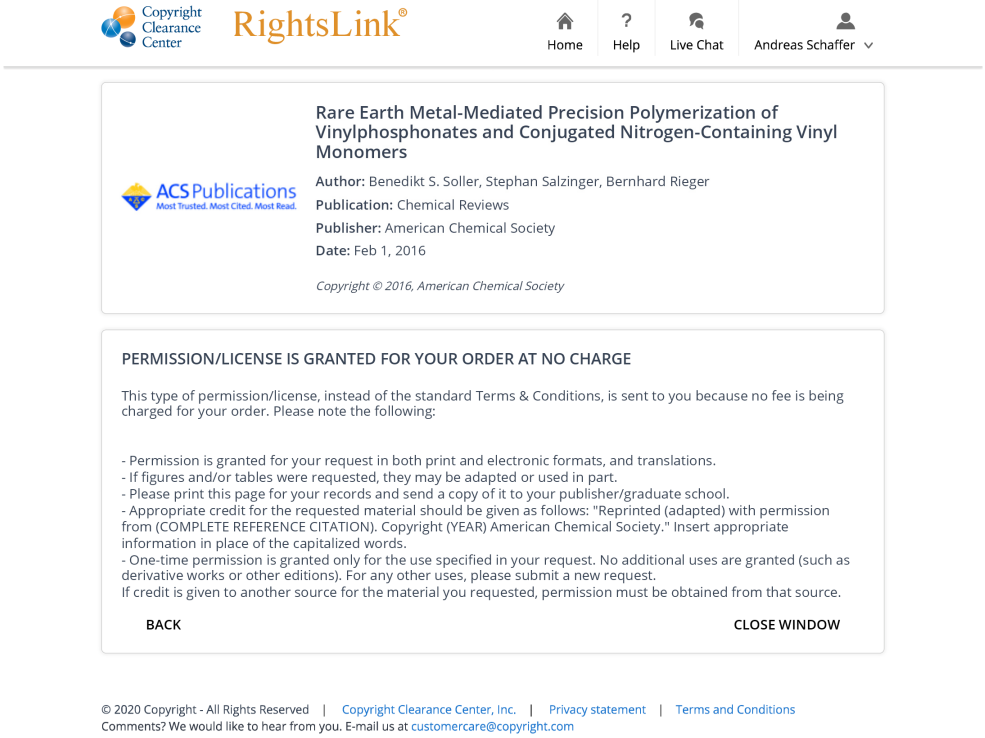

Copyright Licenses

Copyright Clearance Center RightsLink®

Home | Help | Live Chat | Sign in | Create Account

ACS Publications
Most Trusted. Most Cited. Most Read.

Ligand Induced Steric Crowding in Rare Earth Metal-Mediated Group Transfer Polymerization of Vinylphosphonates: Does Enthalpy Matter?

Author: Benedikt S. Soller, Qian Sun, Stephan Salzinger, et al
Publication: Macromolecules
Publisher: American Chemical Society
Date: Mar 1, 2016

PERMISSION/LICENSE IS GRANTED FOR YOUR ORDER AT NO CHARGE

This type of permission/license, instead of the standard Terms & Conditions, is sent to you because no fee is being charged for your order. Please note the following:

- Permission is granted for your request in both print and electronic formats, and translations.
- If figures and/or tables were requested, they may be adapted or used in part.
- Please print this page for your records and send a copy of it to your publisher/graduate school.
- Appropriate credit for the requested material should be given as follows: "Reprinted (adapted) with permission from (COMPLETE REFERENCE CITATION). Copyright (YEAR) American Chemical Society." Insert appropriate information in place of the capitalized words.
- One-time permission is granted only for the use specified in your request. No additional uses are granted (such as derivative works or other editions). For any other uses, please submit a new request.

If credit is given to another source for the material you requested, permission must be obtained from that source.

BACK CLOSE WINDOW

Copyright Clearance Center Marketplace™

Royal Society of Chemistry - License Terms and Conditions

This is a License Agreement between Andreas Schaffer ("You") and Royal Society of Chemistry ("Publisher") provided by Copyright Clearance Center ("CCC"). The license consists of your order details, the terms and conditions provided by Royal Society of Chemistry, and the CCC terms and conditions.

All payments must be made in full to CCC.

Order Date	13-Nov-2020	**Type of Use**	Republish in a thesis/dissertation
Order license ID	1077167-1		
ISSN	2040-3372	**Publisher**	RSC Pub
		Portion	Image/photo/illustration

LICENSED CONTENT

Publication Title	Nanoscale	**Country**	United Kingdom of Great Britain and Northern Ireland
Author/Editor	National Center for Nanoscience and Technology., Royal Society of Chemistry (Great Britain)	**Rightsholder**	Royal Society of Chemistry
		Publication Type	e-Journal
Date	01/01/2009	**URL**	http://www.rsc.org/Publishing/Journals/NR/index.asp
Language	English		

REQUEST DETAILS

Portion Type	Image/photo/illustration	**Distribution**	Worldwide
Number of images / photos / illustrations	5	**Translation**	Original language of publication
Format (select all that apply)	Print, Electronic	**Copies for the disabled?**	No
		Minor editing privileges?	Yes
Who will republish the content?	Academic institution	**Incidental promotional use?**	No
Duration of Use	Life of current edition	**Currency**	EUR
Lifetime Unit Quantity	Up to 499		
Rights Requested	Main product		

NEW WORK DETAILS

Title	C-H Bond Activation Brings Function: Novel Synthetic Strategies for the Generation of Functional Materials through Rare Earth Metal-Mediated Group Transfer Polymerization	**Institution name**	Technical University of Munich
		Expected presentation date	2021-02-28
Instructor name	Andreas Schaffer		

ADDITIONAL DETAILS

Order reference number	N/A	**The requesting person / organization to appear on the license**	Andreas Schaffer

REUSE CONTENT DETAILS

Title, description or numeric reference of the portion(s)	Scheme 2; Fig. 6; Fig. 7; Fig. 8; Fig. 9	**Title of the article/chapter the portion is from**	Synthesis of next generation dual-responsive cross-linked nanoparticles and their application to anti-cancer drug delivery†
Editor of portion(s)	The Royal Society of Chemistry	**Author of portion(s)**	National Center for Nanoscience and Technology.; Royal Society of Chemistry (Great Britain)
Volume of serial or monograph	Volume 10		
Page or page range of portion	16063-16066	**Issue, if republishing an article from a serial**	N/A
		Publication date of portion	2009-01-01

CCC Republication Terms and Conditions

1. Description of Service; Defined Terms. This Republication License enables the User to obtain licenses for republication of one or more copyrighted works as described in detail on the relevant Order Confirmation (the "Work(s)"). Copyright Clearance Center, Inc. ("CCC") grants licenses through the Service on behalf of the rightsholder identified on the Order Confirmation (the "Rightsholder"). "Republication", as used herein, generally means the inclusion of a Work, in whole or in part, in a new work or works, also as described on the Order Confirmation. "User", as used herein, means the person or entity making such republication.

2. The terms set forth in the relevant Order Confirmation, and any terms set by the Rightsholder with respect to a particular Work, govern the terms of use of Works in connection with the Service. By using the Service, the person transacting for a republication license on behalf of the User represents and warrants that he/she/it (a) has been duly authorized by the User to accept, and hereby does accept, all such terms and conditions on behalf of User, and (b) shall inform User of all such terms and conditions. In the event such person is a "freelancer" or other third party independent of User and CCC, such party shall be deemed jointly a "User" for purposes of these terms and conditions. In any event, User shall be deemed to have accepted and agreed to all such terms and conditions if User republishes the Work in any fashion.

3. Scope of License; Limitations and Obligations.

   3.1. All Works and all rights therein, including copyright rights, remain the sole and exclusive property of the Rightsholder. The license created by the exchange of an Order Confirmation (and/or any invoice) and payment by User of the full amount set forth on that document includes only those rights expressly set forth in the Order Confirmation and in these terms and conditions, and conveys no other rights in the Work(s) to User. All rights not expressly granted are hereby reserved.

   3.2. General Payment Terms: You may pay by credit card or through an account with us payable at the end of the month. If you and we agree that you may establish a standing account with CCC, then the following terms apply: Remit Payment to: Copyright Clearance Center, 29118 Network Place, Chicago, IL 60673-1291. Payments Due: Invoices are payable upon their delivery to you (or upon our notice to you that they are available to you for downloading). After 30 days, outstanding amounts will be subject to a service charge of 1-1/2% per month or, if less, the maximum rate allowed by applicable law. Unless otherwise specifically set forth in the Order Confirmation or in a separate written agreement signed by CCC, invoices are due and payable on "net 30" terms. While User may exercise the rights licensed immediately upon issuance of the Order Confirmation, the license is automatically revoked and is null and void, as if it had never been issued, if complete payment for the license is not received on a timely basis either from User directly or through a payment agent, such as a credit card company.

   3.3. Unless otherwise provided in the Order Confirmation, any grant of rights to User (i) is "one-time" (including the editions and product family specified in the license), (ii) is non-exclusive and non-transferable and (iii) is subject to any and all limitations and restrictions (such as, but not limited to, limitations on duration of use or circulation) included in the Order Confirmation or invoice and/or in these terms and conditions. Upon completion of the licensed use, User shall either secure a new permission for further use of the Work(s) or immediately cease any new use of the Work(s) and shall render inaccessible (such as by deleting or by

Thank you for your order!

Dear Mr. Andreas Schaffer,

Thank you for placing your order through Copyright Clearance Center's RightsLink® service.

Order Summary

Licensee:	Technical University of Munich - WACKER-Chair of Macromolecular Chemistry
Order Date:	Nov 12, 2020
Order Number:	4946510818460
Publication:	Progress in Polymer Science
Title:	Temperature responsive bio-compatible polymers based on poly(ethylene oxide) and poly(2-oxazoline)s
Type of Use:	reuse in a thesis/dissertation
Order Total:	0.00 USD

View or print complete details of your order and the publisher's terms and conditions.

Sincerely,

Copyright Clearance Center

Tel: +1-855-239-3415 / +1-978-646-2777
customercare@copyright.com
https://myaccount.copyright.com

Copyright Clearance Center RightsLink®

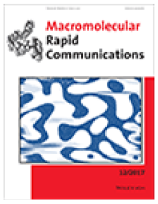

Thank you for your order!

Dear Mr. Andreas Schaffer,

Thank you for placing your order through Copyright Clearance Center's RightsLink® service.

Order Summary

Licensee:	Technical University of Munich - WACKER-Chair of Macromolecular Chemistry
Order Date:	Nov 12, 2020
Order Number:	4946570816624
Publication:	Macromolecular Rapid Communications
Title:	Rare Earth Metal-Mediated Group Transfer Polymerization of Vinylphosphonates
Type of Use:	Dissertation/Thesis
Order Total:	0.00 EUR

View or print complete details of your order and the publisher's terms and conditions.

Sincerely,

Copyright Clearance Center

Tel: +1-855-239-3415 / +1-978-646-2777
customercare@copyright.com
https://myaccount.copyright.com

Copyright Clearance Center RightsLink®

Thank you for your order!

Dear Mr. Andreas Schaffer,

Thank you for placing your order through Copyright Clearance Center's RightsLink® service.

Order Summary

Licensee:	Technical University of Munich - WACKER-Chair of Macromolecular Chemistry
Order Date:	Nov 12, 2020
Order Number:	4946481234271
Publication:	Chemistry - A European Journal
Title:	Next Generation Multiresponsive Nanocarriers for Targeted Drug Delivery to Cancer Cells
Type of Use:	Dissertation/Thesis
Order Total:	0.00 EUR

View or print complete details of your order and the publisher's terms and conditions.

Sincerely,

Copyright Clearance Center

Tel: +1-855-239-3415 / +1-978-646-2777
customercare@copyright.com
https://myaccount.copyright.com

Copyright Clearance Center RightsLink®

14 References

[1] L. Yan, B. Kasal, L. Huang, *Composites Part B: Engineering* **2016**, *92*, 94-132.
[2] R. Shamey, W. Sawatwarakul, *Textile Progress* **2014**, *46*, 323-450.
[3] J. S. S. B, *Nature* **1911**, *88*, 69-70.
[4] H. Offermanns, F. Retzlaff, *Nachrichten aus der Chemie* **2020**, *68*, 10-13.
[5] H. Staudinger, *Berichte der deutschen chemischen Gesellschaft (A and B Series)* **1926**, *59*, 3019-3043.
[6] H. Staudinger, J. Fritschi, *Helvetica Chimica Acta* **1922**, *5*, 785-806.
[7] R. Mülhaupt, *Angewandte Chemie International Edition* **2004**, *43*, 1054-1063.
[8] https://www.nobelprize.org/prizes/chemistry/1953/summary/, **2020**, Accessed: October 20, 2020.
[9] https://journals.openedition.org/factsreports/5071, **2019**, Accessed: October 20, 2020.
[10] https://www.vci.de/vci/downloads-vci/publikation/chemische-industrie-auf-einen-blick.pdf, **2019**, Accessed: October 20, 2020.
[11] https://www.grandviewresearch.com/industry-analysis/global-plastics-market, **2020**, Accessed: October 20, 2020.
[12] https://www.plasticseurope.org/application/files/1115/7236/4388/FINAL_web_version_Plastics_the_facts2019_14102019.pdf, **2019**, Accessed: October 20, 2020.
[13] https://www.statista.com/statistics/687717/plastic-material-demand-european-union-eu/, **2020**, Accessed: October 20, 2020.
[14] S.-A. Park, H. Jeon, H. Kim, S.-H. Shin, S. Choy, D. S. Hwang, J. M. Koo, J. Jegal, S. Y. Hwang, J. Park, D. X. Oh, *Nature Communications* **2019**, *10*, 2601.
[15] T. Sun, Y. S. Zhang, B. Pang, D. C. Hyun, M. Yang, Y. Xia, *Angew. Chem. Int. Ed.* **2014**, *53*, 12320-12364.
[16] N. Larson, H. Ghandehari, *Chem. Mat.* **2012**, *24*, 840-853.
[17] B. S. Soller, S. Salzinger, B. Rieger, *Chem. Rev.* **2016**, *116*, 1993-2022.
[18] F. H. Westheimer, *Science* **1987**, *235*, 1173.
[19] Y. H. Lim, G. S. Heo, S. Cho, K. L. Wooley, *ACS Macro Lett.* **2013**, *2*, 785-789.
[20] B. Clément, B. Grignard, L. Koole, C. Jérôme, P. Lecomte, *Macromolecules* **2012**, *45*, 4476-4486.
[21] Y. H. Lim, G. S. Heo, Y. H. Rezenom, S. Pollack, J. E. Raymond, M. Elsabahy, K. L. Wooley, *Macromolecules* **2014**, *47*, 4634-4644.
[22] Y. Iwasaki, E. Yamaguchi, *Macromolecules* **2010**, *43*, 2664-2666.
[23] S. Zhang, J. Zou, F. Zhang, M. Elsabahy, S. E. Felder, J. Zhu, D. J. Pochan, K. L. Wooley, *J. Am. Chem. Soc.* **2012**, *134*, 18467-18474.
[24] T. Steinbach, S. Ritz, F. R. Wurm, *ACS Macro Lett.* **2014**, *3*, 244-248.
[25] K. N. Bauer, L. Liu, D. Andrienko, M. Wagner, E. K. Macdonald, M. P. Shaver, F. R. Wurm, *Macromolecules* **2018**.
[26] K. Tauber, F. Marsico, F. R. Wurm, B. Schartel, *Polym. Chem.* **2014**, *5*, 7042-7053.
[27] M. Steinmann, J. Markwart, F. R. Wurm, *Macromolecules* **2014**, *47*, 8506-8513.
[28] T. Steinbach, E. M. Alexandrino, C. Wahlen, K. Landfester, F. R. Wurm, *Macromolecules* **2014**, *47*, 4884-4893.
[29] F. Marsico, M. Wagner, K. Landfester, F. R. Wurm, *Macromolecules* **2012**, *45*, 8511-8518.
[30] T. Steinbach, E. M. Alexandrino, F. R. Wurm, *Polym. Chem.* **2013**, *4*, 3800-3806.
[31] B. Bingöl, G. Hart-Smith, C. Barner-Kowollik, G. Wegner, *Macromolecules* **2008**, *41*, 1634-1639.
[32] C. L. Arcus, R. J. S. Matthews, *J. Chem. Soc.* **1956**, 4607-4612.
[33] Q. Wu, R. A. Weiss, *J. Polym. Sci. B Polym. Phys.* **2004**, *42*, 3628-3641.
[34] B. J. Muray, *J. Polym. Sci. C Polym. Symp.* **1967**, *16*, 1869-1886.
[35] M. Banks, J. R. Ebdon, M. Johnson, *Polymer* **1994**, *35*, 3470-3473.
[36] S. Jin, K. E. Gonsalves, *Macromolecules* **1998**, *31*, 1010-1015.
[37] S. Salzinger, B. Rieger, *Macromol. Rapid Commun.* **2012**, *33*, 1327-1345.
[38] D. M. Paisley, C. S. Marvel, *J. Polym. Sci.* **1962**, *56*, 533-538.
[39] J. Parvole, P. Jannasch, *Macromolecules* **2008**, *41*, 3893-3903.
[40] M. Leute, PhD thesis, Universitity of Ulm **2007**.
[41] B. Bingöl, PhD thesis, Johannes Gutenberg-Universität Mainz **2007**.
[42] R. Perrin, M. Elomaa, P. Jannasch, *Macromolecules* **2009**, *42*, 5146-5154.
[43] T. Wagner, A. Manhart, N. Deniz, A. Kaltbeitzel, M. Wagner, G. Brunklaus, W. H. Meyer, *Macromolecular Chemistry and Physics* **2009**, *210*, 1903-1914.
[44] O. W. Webster, W. R. Hertler, D. Y. Sogah, W. B. Farnham, T. V. RajanBabu, *J. Am. Chem. Soc.* **1983**, *105*, 5706-5708.

References

[45] H. Yasuda, H. Yamamoto, K. Yokota, S. Miyake, A. Nakamura, *J. Am. Chem. Soc.* **1992**, *114*, 4908-4910.
[46] S. Collins, D. G. Ward, *J. Am. Chem. Soc.* **1992**, *114*, 5460-5462.
[47] H. Yasuda, H. Yamamoto, M. Yamashita, K. Yokota, A. Nakamura, S. Miyake, Y. Kai, N. Kanehisa, *Macromolecules* **1993**, *26*, 7134-7143.
[48] E. Y. X. Chen, *Chem. Rev.* **2009**, *109*, 5157-5214.
[49] M. Nodono, T. Tokimitsu, T. Makino, *Macromol. Chem. Phys.* **2003**, *204*, 877-884.
[50] U. B. Seemann, J. E. Dengler, B. Rieger, *Angew. Chem. Int. Ed.* **2010**, *49*, 3489-3491.
[51] S. Salzinger, U. B. Seemann, A. Plikhta, B. Rieger, *Macromolecules* **2011**, *44*, 5920-5927.
[52] S. Salzinger, B. S. Soller, A. Plikhta, U. B. Seemann, E. Herdtweck, B. Rieger, *J. Am. Chem. Soc.* **2013**, *135*, 13030-13040.
[53] N. Zhang, S. Salzinger, B. Rieger, *Macromolecules* **2012**, *45*, 9751-9758.
[54] B. S. Soller, Q. Sun, S. Salzinger, C. Jandl, A. Pöthig, B. Rieger, *Macromolecules* **2016**, *49*, 1582-1589.
[55] H. Nguyen, A. P. Jarvis, M. J. G. Lesley, W. M. Kelly, S. S. Reddy, N. J. Taylor, S. Collins, *Macromolecules* **2000**, *33*, 1508-1510.
[56] B. S. Soller, S. Salzinger, C. Jandl, A. Pöthig, B. Rieger, *Organometallics* **2015**, *34*, 2703-2706.
[57] J. E. K. Huheey, Ellen A.; Keiter, Richard L., *Anorganische Chemie - Prinzipien von Struktur und Reaktivität, Vol. 4*, De Gruyter, Berlin, **2012**.
[58] L. Perrin, L. Maron, O. Eisenstein, in *Activation and Functionalization of C—H Bonds, Vol. 885*, American Chemical Society, **2004**, pp. 116-133.
[59] D. Steinborn, *Grundlagen der metallorganischen Komplexkatalyse, Vol. 2*, Vieweg+Teubner, Wiesbaden, **2010**.
[60] R. Waterman, *Organometallics* **2013**, *32*, 7249-7263.
[61] R. Duchateau, C. T. van Wee, J. H. Teuben, *Organometallics* **1996**, *15*, 2291-2302.
[62] H. Kaneko, H. Nagae, H. Tsurugi, K. Mashima, *J. Am. Chem. Soc.* **2011**, *133*, 19626-19629.
[63] F. Adams, M. Pschenitza, B. Rieger, *ChemCatChem* **2018**, *10*, 4309-4316.
[64] P. T. Altenbuchner, P. D. L. Werz, P. Schöppner, F. Adams, A. Kronast, C. Schwarzenböck, A. Pöthig, C. Jandl, M. Haslbeck, B. Rieger, *Chem. Eur. J.* **2016**, *22*, 14576-14584.
[65] P. Pahl, C. Schwarzenböck, F. A. D. Herz, B. S. Soller, C. Jandl, B. Rieger, *Macromolecules* **2017**, *50*, 6569-6576.
[66] C. E. Hoyle, C. N. Bowman, *Angew. Chem. Int. Ed.* **2010**, *49*, 1540-1573.
[67] H. C. Kolb, M. G. Finn, K. B. Sharpless, *Angew. Chem. Int. Ed.* **2001**, *40*, 2004-2021.
[68] A. B. Lowe, *Polym. Chem.* **2010**, *1*, 17-36.
[69] W. H. Binder, R. Sachsenhofer, *Macromol. Rapid Commun.* **2008**, *29*, 952-981.
[70] A. B. Lowe, *Polym. Chem.* **2014**, *5*, 4820-4870.
[71] T. M. Roper, C. A. Guymon, E. S. Jönsson, C. E. Hoyle, *J. Polym. Sci. A Polym. Chem.* **2004**, *42*, 6283-6298.
[72] L. M. Campos, K. L. Killops, R. Sakai, J. M. J. Paulusse, D. Damiron, E. Drockenmuller, B. W. Messmore, C. J. Hawker, *Macromolecules* **2008**, *41*, 7063-7070.
[73] I. Javakhishvili, W. H. Binder, S. Tanner, S. Hvilsted, *Polym. Chem.* **2010**, *1*, 506-513.
[74] C. Schwarzenböck, A. Schaffer, P. Pahl, P. J. Nelson, R. Huss, B. Rieger, *Polym. Chem.* **2018**, *9*, 284-290.
[75] F. Vidal, R. R. Gowda, E. Y. X. Chen, *J. Am. Chem. Soc.* **2015**, *137*, 9469-9480.
[76] Y. H. Lim, K. M. Tiemann, G. S. Heo, P. O. Wagers, Y. H. Rezenom, S. Zhang, F. Zhang, W. J. Youngs, D. A. Hunstad, K. L. Wooley, *ACS Nano* **2015**, *9*, 1995-2008.
[77] C. Schwarzenböck, P. J. Nelson, R. Huss, B. Rieger, *Nanoscale* **2018**, *10*, 16062-16068.
[78] C. Schwarzenböck, A. Schaffer, E. Nößner, P. J. Nelson, R. Huss, B. Rieger, *Chem. Eur. J.* **2018**, *24*, 2584-2587.
[79] F. Adams, P. T. Altenbuchner, P. D. L. Werz, B. Rieger, *RSC Adv.* **2016**, *6*, 78750-78754.
[80] C. Weber, R. Hoogenboom, U. S. Schubert, *Prog. Polym. Sci.* **2012**, *37*, 686-714.
[81] J.-F. Lutz, Ö. Akdemir, A. Hoth, *J. Am. Chem. Soc.* **2006**, *128*, 13046-13047.
[82] P. Greenspan, E. P. Mayer, S. D. Fowler, *J. Cell Biol.* **1985**, *100*, 965-973.
[83] A. Lavasanifar, J. Samuel, G. S. Kwon, *Adv. Drug Deliv. Rev.* **2002**, *54*, 169-190.
[84] C. F. van Nostrum, *Soft Matter* **2011**, *7*, 3246-3259.
[85] J. E. Mark, *Acc. Chem. Res.* **2004**, *37*, 946-953.
[86] R. J. Gillespie, S. A. Johnson, *Inorg. Chem.* **1997**, *36*, 3031-3039.
[87] U. Eduok, O. Faye, J. Szpunar, *Prog. Org. Coat.* **2017**, *111*, 124-163.
[88] A. Mata, A. J. Fleischman, S. Roy, *Biomed. Microdevices* **2005**, *7*, 281-293.
[89] T. Trantidou, Y. Elani, E. Parsons, O. Ces, *Microsyst. Nanoeng.* **2017**, *3*, 16091.
[90] S. V. Gohil, S. Suhail, J. Rose, T. Vella, L. S. Nair, in *Materials for Bone Disorders* (Eds.: S. Bose, A. Bandyopadhyay), Academic Press, **2017**, pp. 349-403.

References

[91] H. Zhang, M. Chiao, *J. Med. Biol. Eng.* **2015**, *35*, 143-155.
[92] J. Chen, X. Huang, L. He, X. Luo, *ACS Omega* **2019**, *4*, 6502-6510.
[93] F. Abbasi, H. Mirzadeh, A.-A. Katbab, *Polym. Int.* **2001**, *50*, 1279-1287.
[94] F. Abbasi, H. Mirzadeh, M. Simjoo, *J. Biomater. Sci. Polym. Ed.* **2006**, *17*, 341-355.
[95] Y. Xia, J. A. Rogers, K. E. Paul, G. M. Whitesides, *Chem. Rev.* **1999**, *99*, 1823-1848.
[96] H. Wu, T. W. Odom, D. T. Chiu, G. M. Whitesides, *J. Am. Chem. Soc.* **2003**, *125*, 554-559.
[97] C. Chen, B. T. Mehl, A. S. Munshi, A. D. Townsend, D. M. Spence, R. S. Martin, *Anal. Methods* **2016**, *8*, 6005-6012.
[98] B. D. Fairbanks, D. M. Love, C. N. Bowman, *Macromol. Chem. Phys.* **2017**, *218*, 1700073.
[99] Y. Xia, H. Yao, Z. Miao, Y. Ma, M. Cui, L. Yan, H. Ling, Z. Qi, *RSC Adv.* **2015**, *5*, 50955-50961.
[100] J. C. Brendel, G. Gody, S. Perrier, *Polym. Chem.* **2016**, *7*, 5536-5543.
[101] A. Hisyam A. Razak, P. Szabo, A. L. Skov, *RSC Adv.* **2015**, *5*, 53054-53062.
[102] D. Li, C. Li, A. Wang, Q. He, J. Li, *J. Mater. Chem.* **2010**, *20*, 7782-7787.
[103] S. Bas, M. D. Soucek, *Polym. J.* **2012**, *44*, 1087-1097.
[104] K. Huan, L. Bes, D. M. Haddleton, E. Khoshdel, *J. Polym. Sci. A Polym. Chem.* **2001**, *39*, 1833-1842.
[105] P. J. Miller, K. Matyjaszewski, *Macromolecules* **1999**, *32*, 8760-8767.
[106] J. Xu, M. Qiu, B. Ma, C. He, *ACS Appl. Mater. Interfaces* **2014**, *6*, 15283-15290.
[107] E. Martinelli, M. Suffredini, G. Galli, A. Glisenti, M. E. Pettitt, M. E. Callow, J. A. Callow, D. Williams, G. Lyall, *Biofouling* **2011**, *27*, 529-541.
[108] S. Zhang, Z. Hou, K. E. Gonsalves, *J. Polym. Sci. A Polym. Chem.* **1996**, *34*, 2737-2742.
[109] M. Brogly, S. Bistac, C. Delaite, C. Alzina, *Polym. Int.* **2019**, *, available online*.
[110] R. Rached, S. Hoppe, A. Jonquieres, P. Lochon, F. Pla, *J. Appl. Polym. Sci.* **2006**, *102*, 2818-2831.
[111] K. T. Lim, S. E. Webber, K. P. Johnston, *Macromolecules* **1999**, *32*, 2811-2815.
[112] M. Z. Yates, G. Li, J. J. Shim, S. Maniar, K. P. Johnston, K. T. Lim, S. Webber, *Macromolecules* **1999**, *32*, 1018-1026.
[113] D. Lanzinger, S. Salzinger, B. S. Soller, B. Rieger, *Ind. Eng. Chem. Res.* **2015**, *54*, 1703-1712.
[114] N. Zhang, S. Salzinger, B. S. Soller, B. Rieger, *J. Am. Chem. Soc.* **2013**, *135*, 8810-8813.
[115] Q. Wang, S. Chen, Y. Liang, D. Dong, N. Zhang, *Macromolecules* **2017**, *50*, 8456-8463.
[116] E. M. Ahmed, *J. Adv. Res.* **2015**, *6*, 105-121.
[117] M. Hamidi, A. Azadi, P. Rafiei, *Adv. Drug Deliv. Rev.* **2008**, *60*, 1638-1649.
[118] L. Zhang, K. Li, W. Xiao, L. Zheng, Y. Xiao, H. Fan, X. Zhang, *Carbohydr. Polym.* **2011**, *84*, 118-125.
[119] K. Y. Lee, D. J. Mooney, *Chem. Rev.* **2001**, *101*, 1869-1880.
[120] P. Sikareepaisan, U. Ruktanonchai, P. Supaphol, *Carbohydr. Polym.* **2011**, *83*, 1457-1469.
[121] F. Wang, Z. Li, M. Khan, K. Tamama, P. Kuppusamy, W. R. Wagner, C. K. Sen, J. Guan, *Acta Biomater.* **2010**, *6*, 1978-1991.
[122] F. Adams, M. R. Machat, P. T. Altenbuchner, J. Ehrmaier, A. Pöthig, T. N. V. Karsili, B. Rieger, *Inorg. Chem.* **2017**, *56*, 9754-9764.
[123] P. T. Altenbuchner, F. Adams, A. Kronast, E. Herdtweck, A. Pöthig, B. Rieger, *Polym. Chem.* **2015**, *6*, 6796-6801.
[124] P. T. Altenbuchner, B. S. Soller, S. Kissling, T. Bachmann, A. Kronast, S. I. Vagin, B. Rieger, *Macromolecules* **2014**, *47*, 7742-7749.
[125] A. Kronast, D. Reiter, P. T. Altenbuchner, S. I. Vagin, B. Rieger, *Macromolecules* **2016**, *49*, 6260-6267.
[126] T. Haino, *Polym. J.* **2013**, *45*, 363-383.
[127] S. S. Oh, B. F. Lee, F. A. Leibfarth, M. Eisenstein, M. J. Robb, N. A. Lynd, C. J. Hawker, H. T. Soh, *J. Am. Chem. Soc.* **2014**, *136*, 15010-15015.
[128] L. Yang, H. Sun, Y. Liu, W. Hou, Y. Yang, R. Cai, C. Cui, P. Zhang, X. Pan, X. Li, L. Li, B. S. Sumerlin, W. Tan, *Angew. Chem. Int. Ed.* **2018**, *57*, 17048-17052.
[129] N. Bertrand, M. A. Gauthier, C. Bouvet, P. Moreau, A. Petitjean, J.-C. Leroux, J. Leblond, *J. Control. Release* **2011**, *155*, 200-210.
[130] S. E. D'Souza, M. H. Ginsberg, E. F. Plow, *Trends Biochem. Sci.* **1991**, *16*, 246-250.
[131] C. E. Schwarzenböck, PhD thesis, Technische Universität München **2018**.
[132] K. C. Hultzsch, P. Voth, K. Beckerle, T. P. Spaniol, J. Okuda, *Organometallics* **2000**, *19*, 228-243.
[133] G. D. Vaughn, K. A. Krein, J. A. Gladysz, *Organometallics* **1986**, *5*, 936-942.
[134] C.-X. Cai, L. Toupet, C. W. Lehmann, J.-F. Carpentier, *J. Organomet. Chem.* **2003**, *683*, 131-136.
[135] L. Rigger, R. L. Schmidt, K. M. Holman, M. Simonović, R. Micura, *Chem. Eur. J.* **2013**, *19*, 15872-15878.

Anhang I

Eidesstattliche Erklärung

Ich erkläre an Eides statt, dass ich die bei der promotionsführenden Einrichtung
Fakultät für Chemie

der TUM zur Promotionsprüfung vorgelegte Arbeit mit dem Titel:

From C-H Bond Activation to Function: Diversification of Smart Materials Generated via Rare Earth Metal-Mediated Group Transfer Polymerization

in WACKER-Lehrstuhl für Makromolekulare Chemie
Fakultät, Institut, Lehrstuhl, Klinik, Krankenhaus, Abteilung

unter der Anleitung und Betreuung durch: Prof. Dr. Dr. h.c. Bernhard Rieger ohne sonstige Hilfe erstellt und bei der Abfassung nur die gemäß § 6 Ab. 6 und 7 Satz 2 angebotenen Hilfsmittel benutzt habe.

☒ Ich habe keine Organisation eingeschaltet, die gegen Entgelt Betreuerinnen und Betreuer für die Anfertigung von Dissertationen sucht, oder die mir obliegenden Pflichten hinsichtlich der Prüfungsleistungen für mich ganz oder teilweise erledigt.

☒ Ich habe die Dissertation in dieser oder ähnlicher Form in keinem anderen Prüfungsverfahren als Prüfungsleistung vorgelegt.

☐ Die vollständige Dissertation wurde in _____ veröffentlicht. Die promotionsführende Einrichtung

_____

hat der Veröffentlichung zugestimmt.

☒ Ich habe den angestrebten Doktorgrad noch nicht erworben und bin nicht in einem früheren Promotionsverfahren für den angestrebten Doktorgrad endgültig gescheitert.

☐ Ich habe bereits am _____ bei der Fakultät für _____

_____

der Hochschule _____

unter Vorlage einer Dissertation mit dem Thema _____

_____

die Zulassung zur Promotion beantragt mit dem Ergebnis: _____

_____

Die öffentlich zugängliche Promotionsordnung der TUM ist mir bekannt, insbesondere habe ich die Bedeutung von § 28 (Nichtigkeit der Promotion) und § 29 (Entzug des Doktorgrades) zur Kenntnis genommen. Ich bin mir der Konsequenzen einer falschen Eidesstattlichen Erklärung bewusst.

Mit der Aufnahme meiner personenbezogenen Daten in die Alumni-Datei bei der TUM bin ich

☒ einverstanden, ☐ nicht einverstanden.

Seefeld, 18.01.2021, Unterschrift